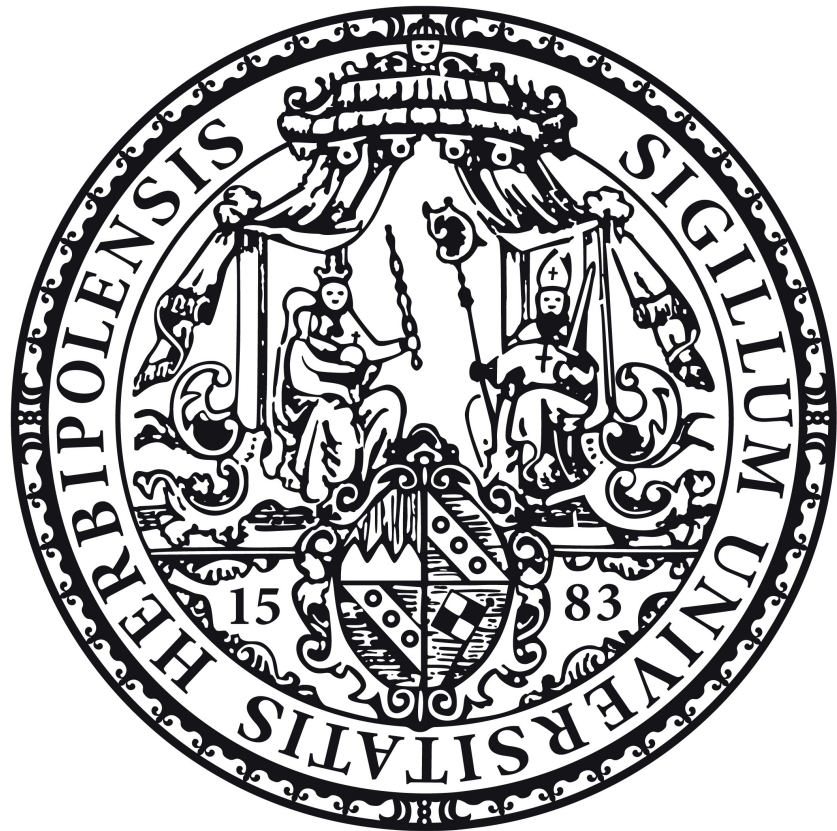


Modifying the Optoelectronic Properties of Polycyclic Aromatic Hydrocarbons and Linear Oligomers by Doping with Boron and Further Heteroatoms



Dissertation zur Erlangung des naturwissenschaftlichen Doktorgrades der
Julius-Maximilians-Universität Würzburg

vorgelegt von

Merian Crumbach

aus Heinsberg

Würzburg 2021

Eingereicht bei der Fakultät für Chemie und Pharmazie am

Gutachter der schriftlichen Arbeit

1. Gutachter: Prof. Dr. Holger Helten
2. Gutachter: Prof. Dr. Bernd Engels

Prüfer des öffentlichen Promotionskolloquiums

1. Prüfer: Prof. Dr. Holger Helten
2. Prüfer: Prof. Dr. Bernd Engels
3. Prüfer: Prof. Dr. Maik Finze

Datum des öffentlichen Promotionskolloquiums

Doktorurkunde ausgehändigt am

List of Publications

The publications listed below are reproduced in this dissertation with permission from The Royal Society of Chemistry and Wiley-VCH. The table itemizes at which position in this work the paper has been reproduced.

Publication	Position
M. Crumbach, O. Ayhan, L. Fritze, J.n A. P. Sprenger, L. Zapf, M. Finze, H. Helten, <i>Chem. Commun.</i> 2021 , <i>57</i> , 2408-2411.	Chapter 4.1
M. Crumbach, J. Bachmann, L. Fritze, A. Helbig, I. Krummenacher, H. Braunschweig, H. Helten, <i>Angew. Chem. Int. Ed.</i> 2021 , <i>60</i> , 9290-9295.	Chapter 4.2

Table of contents

1	Acknowledgements.....	2
2	List of Abbreviations	4
3	Introduction.....	7
3.1	Polycyclic Aromatic Hydrocarbons and Rylene Dyes.....	7
3.2	Boron-doped Materials.....	12
3.3	Boron-Nitrogen-Doped Materials	14
3.4	BNB-Doped Materials.....	17
3.5	Phosphinoboranes.....	18
3.6	Theoretical Methods.....	20
3.6.1	Nucleus Independent Chemical Shift.....	20
3.6.2	Anisotropy of the Induced Current Density.....	22
3.7	References	24
4	Results and Discussion	29
4.1	BNB-Doped phenalenyls – aromaticity switch upon one-electron reduction.....	29
4.1.1	Introduction.....	29
4.1.2	Results and Discussion	31
4.1.3	Conclusion	36
4.1.4	Experimental Section.....	36
4.1.5	References.....	43
4.2	Dithiophene-Fused Oxadiborepins and Azadiborepins: A New Class of Highly Fluorescent Heteroaromatics	47
4.2.1	Introduction.....	47
4.2.2	Results and Discussion	49
4.2.3	Conclusion	55
4.2.4	Experimental Section.....	55

4.2.5	References.....	66
4.3	First Molecular Model Compounds for a Boron-Phosphorus Analogue of Poly(<i>p</i> -phenylene vinylene).....	71
4.3.1	Introduction.....	71
4.3.2	Results and Discussion	72
4.3.3	Conclusion	83
4.3.4	Experimental Section.....	84
4.3.5	References.....	98
5	Conclusion	100
6	Zusammenfassung.....	108
7	Appendix.....	116
7.1	BNB-Doped phenalenyls – aromaticity switch upon one-electron reduction.....	116
7.2	Dithiophene-Fused Oxadiborepins and Azadiborepins: A New Class of Highly Fluorescent Heteroaromatics	145
7.3	First Molecular Model Compounds for a Boron-Phosphorus Analogue of Poly(<i>p</i> -phenylene vinylene).....	189

1 Acknowledgements

At first, I would like to thank Prof. Dr. Holger Helten for giving me the opportunity to do my PhD in his research group and for providing such an interesting research topic. Thank you for your continuous support, great advice and for inspiring and helpful discussions, as well as providing a kind and productive working atmosphere.

I also would like to thank Prof. Dr. Bernd Engels for taking over the second report on my thesis.

Furthermore, I would like to thank the whole Helten group for a very enjoyable working atmosphere and for being friends in and outside the lab. Dr. Ozan Ayhan and Dr. Artur Lik, thank you for the warm welcome several years ago and special thanks to Dr. Thomas Lorenz for the warm welcome, but also for being a great teacher, friend and my lab partner for the last few years. I also want to especially thank Lars Fritze and Dr. Nicolas Riensch who kept my company over the years through better or worse times. Thank you for your support, the helpful discussions, fun activities in and outside the lab and especially for being the great friends you are.

During my PhD I had the pleasure to work with some highly motivated and great students. I would like to thank Nicolas de la Vega Guerra, Sebastian Seidel and Jonas Bachmann for their supporting work during their internships, bachelor and master theses.

I would like to thank my in-house collaboration partners Prof. Dr. Maik Finze, Prof. Dr. Holger Braunschweig, Dr. Jan A. P. Sprenger and Dr. Ivo Krummenacher. I am grateful for the nice discussions and proof-reading of our joint publications.

Over the years a lot of people supported my work with analytical measurements, both at RWTH Aachen University and JMU Würzburg. Therefore I would like to thank Toni Gossen, Rachida Bohmarat, Dr. Gerhard Fink and Dr. Rüdiger Bertermann for NMR measurements, Brigitte Pütz and Christoph Mahler for MS measurements, Sabine Timmroth for elemental analysis, Lars Fritze and Tobias Bischof for X-ray diffraction experiments, Dr. Ivo Krummenacher and Ludwig Zapf for cyclic voltammetry measurements and Dr. Jan A. P. Sprenger for differential scanning calorimetry measurements. I thank Prof. Dr. Todd Marder for granting me access to UV-vis and fluorescence spectroscopy devices and Dr. Florian Rauch and Sarina Berger for the introduction and help with those.

Finally, I am extremely grateful for the continuous support and would therefore like to thank my parents Claudia and Edmund Hannot, my Brother Milius Liu, my girlfriend Marina Interwies and all the rest of my family. You supported me through all these years of my studies, endured my moods and encouraged me to keep on going. All this would not have been possible without you. I am dedicating this thesis to my grandparents Josef and Maria Donners.

2 List of Abbreviations

Å	angstrom
abs	absorbance
ACID	anisotropy of the induced current density
APCI	atmospheric-pressure chemical ionization
Ar	aryl substituent
BFI	bifuran imide
br	broad
BSeI	biselenophene imide
BTI	bithiophene imide
BzK	benzyl potassium
cm	centimeter
CV	cyclic voltammetry
D	debye
d	doublet
DCM	dichloromethane
DSC	differential scanning calorimetry
elem.	elemental
equiv.	equivalents
Et ₂ O	diethyl ether
eV	electron volt
^F Mes	Fluoromesityl, 2,4,6-tris(trifluoromethyl)phenyl
FWHM	full-width at half-maximum
g	gram
HOMO	highest occupied molecular orbital
HRMS	high-resolution mass spectrometry
Hz	hertz
<i>J</i>	coupling constant
LIFDI	liquid injection field desorption ionization
LUMO	lowest unoccupied molecular orbital
M	molar, mol per liter
m	multiplet

m/z	mass per charge
max	maximum
mbar	millibar
Mes	mesityl, 2,4,6-trimethylphenyl
Mes*	supermesityl, 2,4,6-tris- <i>tert</i> -butylphenyl
MO	molecular orbital
MS	mass spectrometry
NDI	naphthalene diimide
NICS	nucleus independent chemical shift
nm	nanometer
NMR	nuclear magnetic resonance
<i>o</i>	ortho
oct	octet
OFET	(organic) field-effect transistor
OLED	(organic) light-emitting diode
OPV	(organic) photovoltaic cell
<i>p</i>	para
PAH	polycyclic aromatic hydrocarbon
PDI	perylene diimide
Ph	phenyl
PLED	polymer light-emitting diode
ppm	parts per million
PPV	poly(<i>p</i> -phenylene vinylene)
PTCDA	perylene-3,4,9,10-tetracarboxylic dianhydride
R	organic substituent
r.t.	room temperature
s	singlet
sept	septet
t	fluorescence lifetime
TD-DFT	time-dependent density functional theory
THF	tetrahydrofuran
Tip	2,4,6-triisopropylphenyl
TMEDA	tetramethylethylenediamine

TMS	trimethylsilyl
UV-vis	ultraviolet-visible
δ	chemical shift
ε	extinction coefficient
Φ_f	fluorescence quantum yield
λ	wavelength

3 Introduction

The research in (semi)conducting π -conjugated organic materials and (doped) polycyclic aromatic hydrocarbons (PAHs), in particular, has attracted tremendous attention in recent years.^[1] The interest in such materials mainly comes from their applicability in electronic and optoelectronic devices, such as organic light-emitting diodes (OLED/PLED),^[2] organic photovoltaic cells (OPV)^[3] or organic field-effect transistors (OFET).^[3d, 3e, 4] Therein the replacement of established inorganic solid materials with organic compounds has been of great interest due to their significantly lower production costs and facile processability. Furthermore the possibility of incorporation in light-weight materials for flexible optoelectronic devices, electrodes in batteries,^[5] chemical sensing,^[6] bioimaging and drug delivery^[7] has been investigated.

3.1 Polycyclic Aromatic Hydrocarbons and Rylene Dyes

Polycyclic aromatic hydrocarbons (PAHs) and their derivatives have been widely used in the well explored area of dye chemistry. Especially rylene dyes, which are based on the rylene framework of naphthalene units linked in peri position have been utilized for a long time.^[8] The most famous type of rylene dyes are the perylene-3,4,9,10-tetracarboxylic acid diimides (perylene diimides, PDIs), which are derived from the PAH perylene. They have been extensively studied as industrial colorants, both as dyes (soluble) and pigments (insoluble). Figure 3.1.1 shows the structures of the PAH perylene, perylene-3,4,9,10-tetracarboxylic dianhydride (PTCDA) and of a generic PDI, showing the numbering of the positions in the ring system. PTCDA can be considered as the parental structure for all PDIs and was first obtained in 1912.^[8-9]

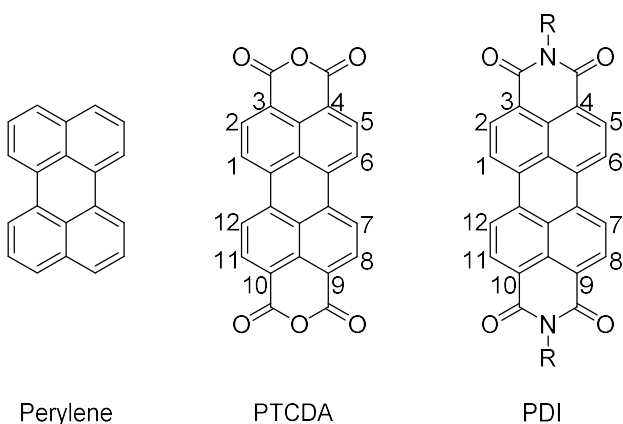
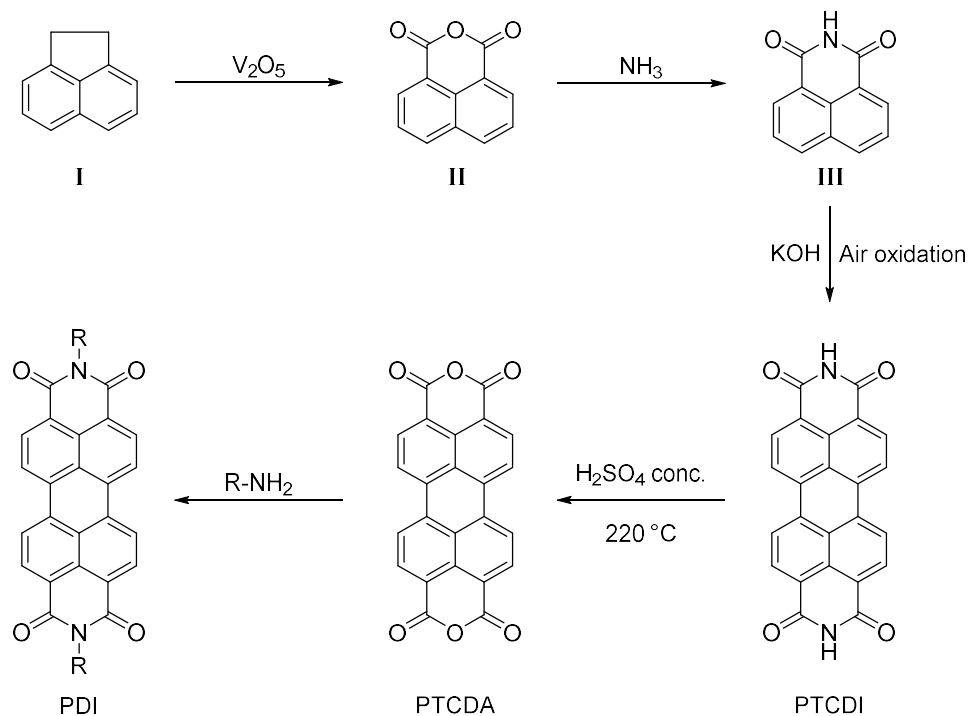


Figure 3.1.1. Structures of perylene, PTCDA and a generic PDI, showing the numbering of positions.

Every PDI is synthesized *via* condensation between PTCDA and a primary amine, usually resulting in high yields. PTCDA is industrially obtained by oxidation of acenaphthene (Scheme 3.1.1, **I**) to give 1,8-naphthalene dicarboxylic acid anhydride (**II**), which is subsequently treated with ammonia to provide naphthalene-1,8-dicarboxylic acid imide (**III**). Oxidative coupling *via* aerial oxidation in molten potassium hydroxide gives perylene-3,4,9,10-tetracarboxylic diimide (PTCDI), which can be converted into PTCDA by hydrolysis with concentrated sulfuric acid at high temperatures (scheme 3.1.1).^[8, 9b]



Scheme 3.1.1. Industrial synthetic approach for PDIs.

Although the substituent R does not take part in the chromophoric system, the colours of differently substituted PDI pigments vary from orange ($R = \text{ethyl}$) to red ($R = \text{xylyl}$) to black ($p\text{-methoxybenzyl}$). This is due to the different steric requirements of the substituent R, leading to different crystal structures and therefore changing the exciton interactions between neighbouring molecules. Due to their excellent chemical, thermal, photo and weather stability, PDI pigments are used as important industrial pigments.^[8, 9e]

In addition to their excellent stability, many PDIs exhibit other interesting properties, such as strong electron-accepting character, high photochemical stability and fluorescence quantum yields close to unity. Therefore PDIs, as well as naphthalene diimides (NDIs), have been used in (opto)electronic applications, such as dye lasers,^[10] optical sensors,^[11] organic field-effect transistors (OFETs)^[12] and organic photovoltaic cells (OPVs).^[12c, 12h, 13] The first two-layer

organic photovoltaic cell was reported by Tang in 1986 and incorporated a benzoimidazole PDI (Figure 3.1.2) as the acceptor and a copper phthalocyanine as donor, approaching a power conversion efficiency of 1%.^[14] In 1996 Horowitz and co-workers demonstrated the first PDI-based OFET, incorporating evaporated thin films of *N,N'*-diphenyl-3,4,9,10-perylene-tetracarboxylic-diimide.^[15]

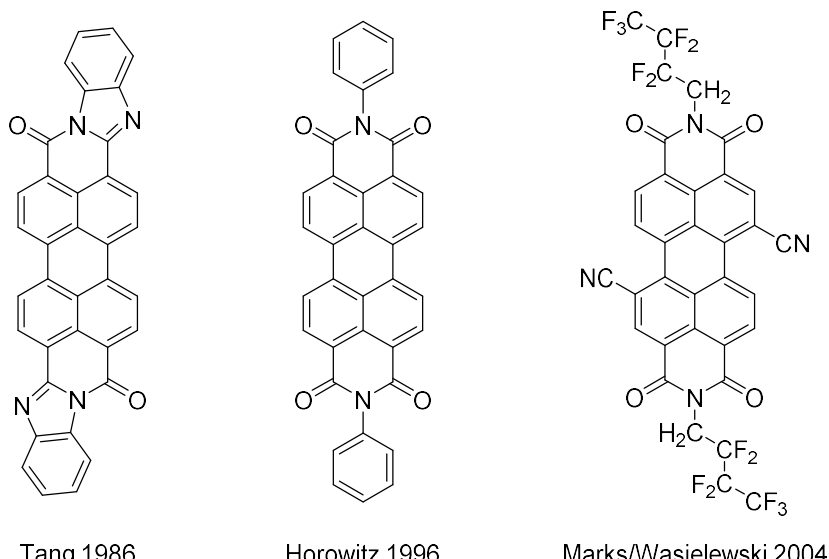
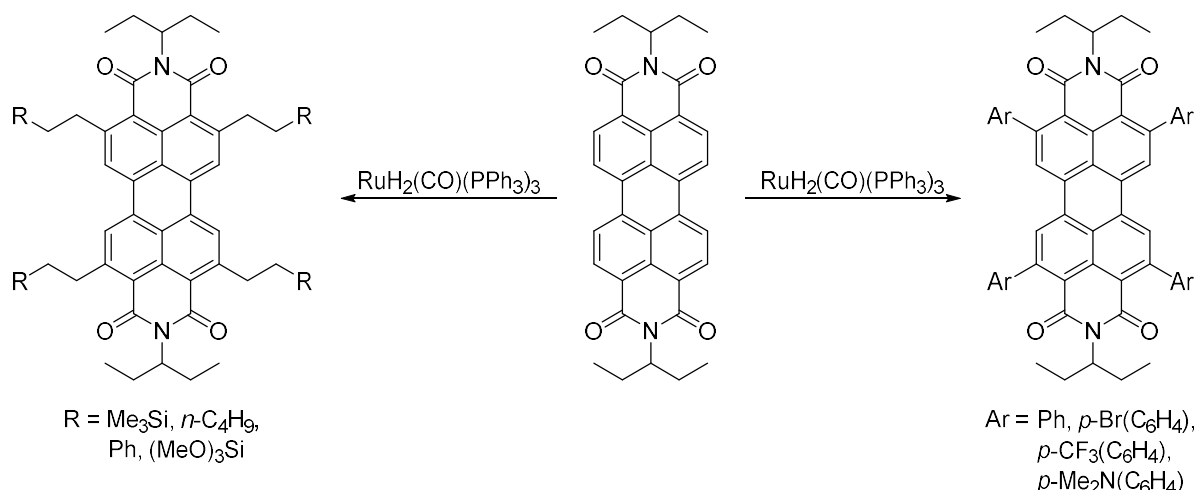


Figure 3.1.2. Selected examples of PDIs incorporated into organic electronics.

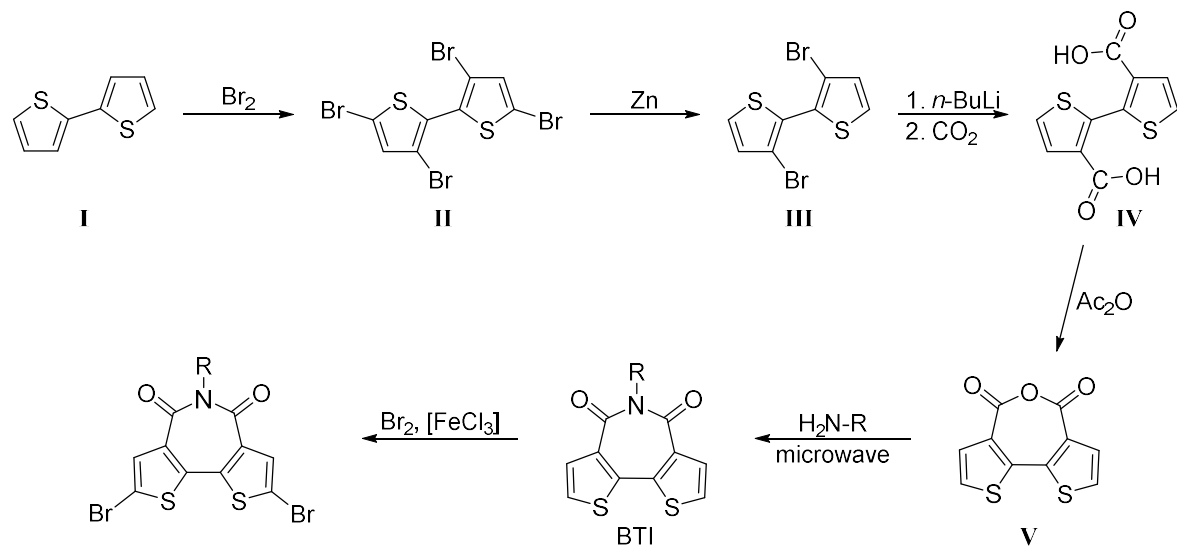
In order to increase the processability for such applications, enhanced solubility is often required. Therefore, solubility enhancing groups can be introduced during the imidization step, or the PDIs can be functionalized at the 1, 6, 7 and/or 12 (bay) positions, often resulting in twisting or bending of the perylene core, disrupting face-to-face π - π stacking. Marks, Wasielewski and co-workers reported dicyano-PDIs (Figure 3.1.2) as high carrier mobility materials with air-stable OFET operation.^[12b] The cyano functionalities in the bay-positions provide solubility for solution processing and stability of n-type charge carriers by increasing the stability towards ambient oxidation, but also induce a twist in the polycyclic core of about 5°. The electron-withdrawing *N*-functionalities also provide stability by further lowering the LUMO energies and may induce close molecular packing.

Functionalization at the 2, 5, 8 and/or 11 (peri) positions has not been reported until recently, when catalysed C-H bond activation was found to be effective for arylation and alkylation of perylene diimides (Scheme 3.1.2). Functionalization in the peri positions can also increase the solubility but in contrast to bay substitution, the PDI core remains undistorted, which may be beneficial for applications where strong π - π stacking is necessary (e.g. OFETs). [16]



Scheme 3.1.2. C-H bond activation of perylene diimides.

Another polycyclic organic building block featuring the effectively π -accepting imide moiety is 2,2'-bithiophene-3,3'-dicarboximide (BTI). Previously, thiophene-based polymeric semiconductors proved to be robust, air-stable materials for p-channel (hole transport) semiconductors.^[17] BTIs have therefore been investigated towards their efficiency in electron transport and electron affinity as n-channel materials in semiconductors or acceptor materials in organic photovoltaics.^[18] The first BTI was reported by Marks, Ratner, Facchetti and co-workers in 2008, Scheme 3.1.3 depicts the general synthetic approach.^[19]



Scheme 3.1.3. Synthetic approach to BTIs and postfunctionalization.

Starting from commercially available 2,2'-bithiophene (Scheme 3.1.3, I), elemental bromine is used for tetrabromination (II), followed by reduction with zinc to give 3,3'-dibromo-2,2'-bithiophene (III). Lithiation and subsequent reaction with carbon dioxide leads to the double carboxylic acid (IV), which undergoes a ring-closing reaction to give 2,2'-dithieno-3,3'-dicarboximide (V). Finally, BTI is synthesized via Br_2 and FeCl_3 , and postfunctionalization is achieved using $\text{H}_2\text{N}-\text{R}$ under microwave conditions.

carboxylic anhydride (**V**). Similar to PTCDA, a condensation with a primary amine leads to the imide moiety. The 5,5'-positions of the bithiophene core can be further functionalized via bromination and subsequent coupling reactions.

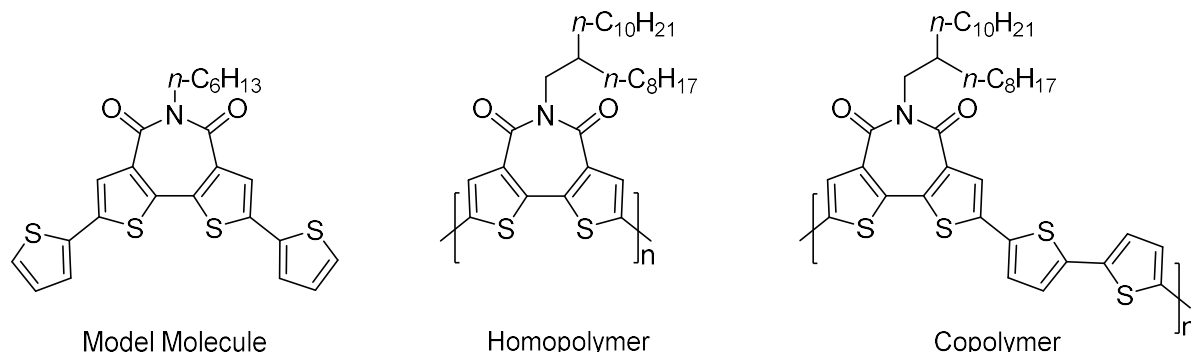


Figure 3.1.3. Structures of the first BTI polymers in OFETs.

High-performance polymeric semiconductors must maintain a delicate balance between solubility and close, efficient π - π stacking for efficient charge transport. Marks, Ratner, Facchetti and co-workers reported the homo- and copolymer, depicted in Figure 3.1.3, to provide those properties. The crystal structure of the model molecule revealed π -core planarity, antiparallel BTI packing, short π - π distance and favourable solubilizing group orientation. The homopolymer exhibits exceptional n-channel FET performance, while the copolymer exhibits air-stable p-channel FET operation. Due to the high degree of thin-film order, BTI polymer films exhibit FET performance predominately independent of film-casting conditions.^[19]

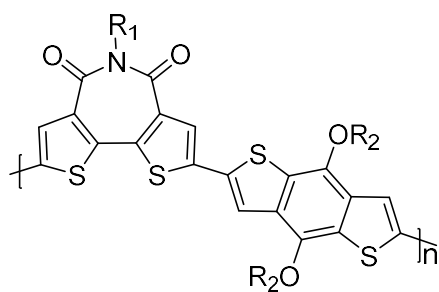


Figure 3.1.4. Structure of the first BTI polymer in OPVs.

The bithiophene imide and benzodithiophene copolymers reported by Marks, Facchetti, Chang and co-workers in 2012 were the first BTIs used in OPVs and show good solution processability and high molecular weights (Figure 3.1.4). The low-lying bithiophene imide HOMOs lead to high open circuit voltages and the reported devices exhibit up to 5.5 % power conversion efficiencies. Due to the inverted device structures and the low-lying HOMOs, the reported bithiophene imide-based polymers exhibit good device air and thermal

stability and therefore indicate bithiophene imide to be a very promising building block for polymer OPVs.^[3b]

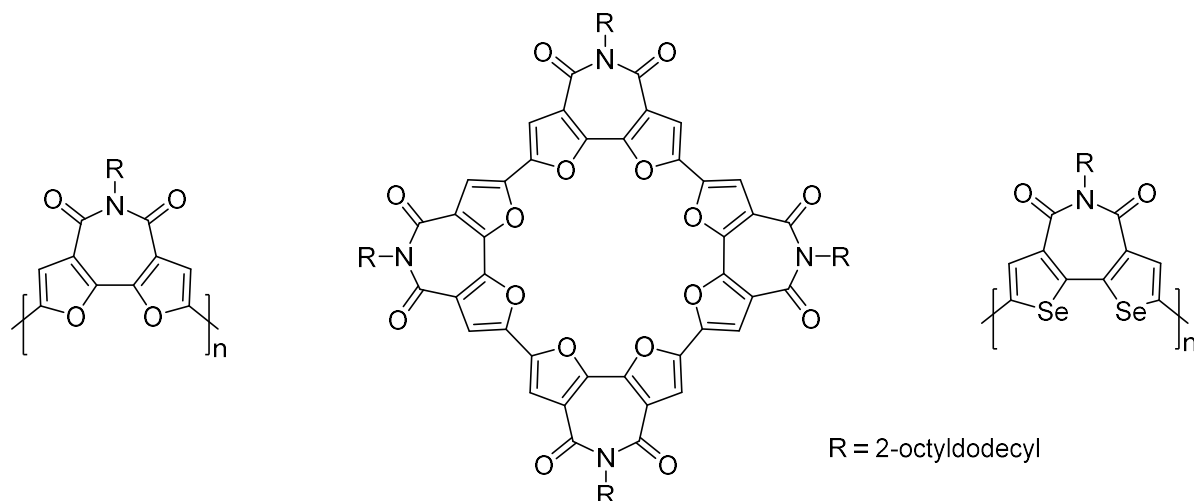


Figure 3.1.5. Structures of (poly)bifuran imides, Bifuran imide macrocycle and (poly)biselenophene imides.

Recently, other bichalcogenophene imides have been investigated as well.^[20] Bifuran imide (BFI) was used to synthesize homopolymers and a macrocycle (Figure 3.1.5). In comparison to BTI analogues, the BFI polymers display high solubility as well, but were accessible in higher molecular weights. Also the oligomers and polymers exhibit strong fluorescence with quantum yields up to 81% in solution. The monomeric BFI also exhibits strong blue emission in the solid state. Compared to their parent oligofurans, bifuran imides are significantly more stable under ambient conditions. Some of the macrocycles' characteristics include a planar backbone, fluorescence in solid state and p-type semiconducting behaviour.^[20a, 20b] With increasing size of the chalcogen-atom, the UV-vis absorption is gradually red-shifted and the optical band gap is narrowed, for both the monomers and polymers. Biselenophene imides (BSeI) have been synthesized and used to construct n-type organic thin-film transistors. Due to their narrowed band gap and good electron mobility, biselenophene imides should be highly promising in the construction of high-performance n-type photovoltaics.^[20c]

3.2 Boron-doped Materials

π -Conjugated organic materials with semiconducting properties have attracted tremendous attention in the past few decades, owing to their use as cost-effective, lightweight alternatives to inorganic solid-state materials in (opto)electronic devices. For such purposes, both molecular compounds and polymers were utilized.^[1] A promising strategy to tune the

(opto)electronic properties of such materials is to dope them with boron atoms. Trivalent boron has a vacant p-orbital and therefore can take part in π -conjugated systems, but it is also Lewis acidic and therefore many organoboron compounds are not stable towards water and air. Stabilizing such organoboron compounds can be achieved by either sterically shielding the boron atoms with bulky aryl groups or by incorporating the boron atoms into a structural constraint system.

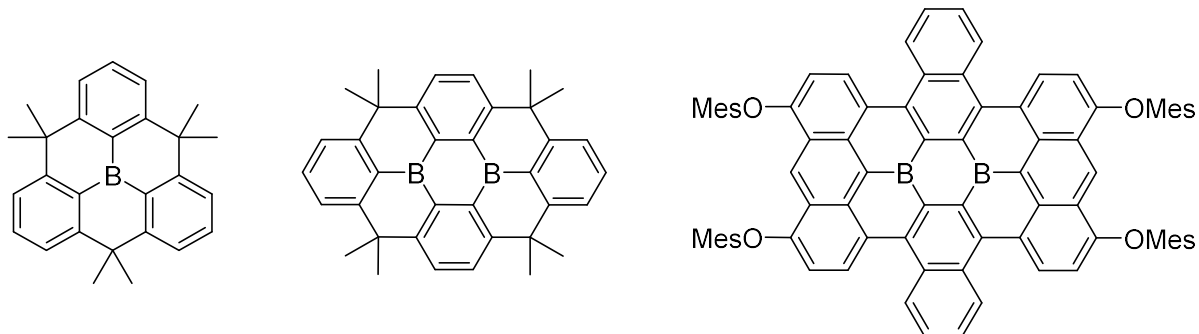


Figure 3.2.1. Polycyclic systems with boron stabilized via structural constraint.

In 2012 Yamaguchi *et al.* reported the synthesis of boron-doped polycyclic systems, in which the boron is stabilized via structural constraint (Figure 3.2.1). Due to the rigid structure around boron, the change into a tetrahedral structure upon coordination is prevented and therefore the systems are stable towards water and air.^[21] A boron-doped helicene was investigated by Wagner *et al.* and Hatakeyama *et al.*, at the same time, following different synthetic approaches. The reported boron-doped helicene showed high solubility, green emission and high stability towards water and air (Figure 3.2.2).^[22]

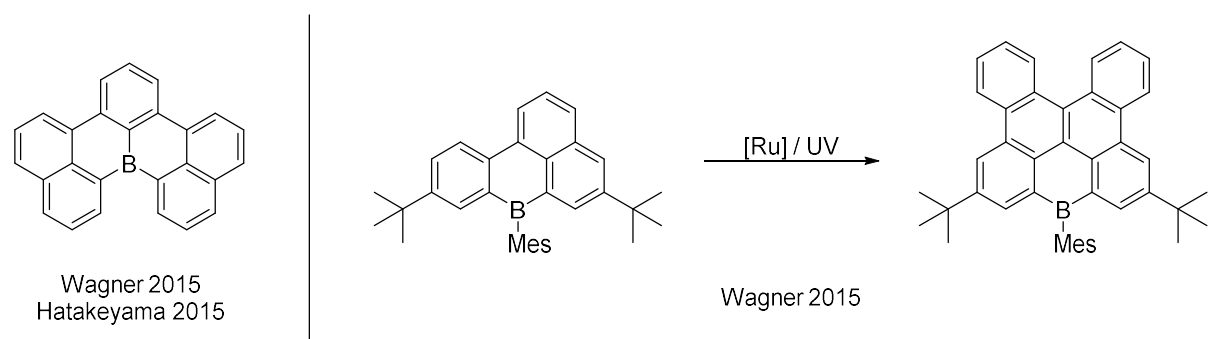


Figure 3.2.2. A boron-doped helicene and Ru-catalyzed benzannulation of boron-doped PAHs.

In 2015 Wagner *et al.* also reported syntheses of boron doped PAHs and the extension of the π -system thereof by Ru-catalyzed benzannulation.^[23] In order to stabilize the boron center towards water and air, bulky mesityl substituents were introduced to sterically shield the vacant p-orbital.

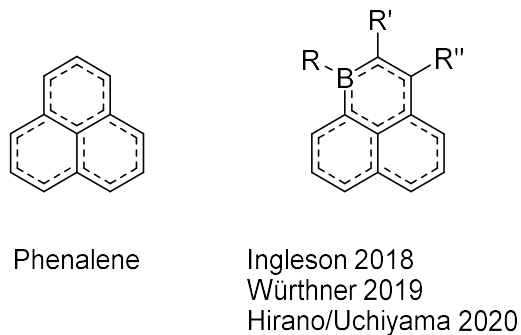


Figure 3.2.3. Structures of the PAH phenalene and its boron-only doped analogue.

The first boron-only doped derivatives of the PAH phenalene have been reported by Ingleson *et al.* in 2018, followed by further reports by Würthner *et al.* and Hirano, Uchiyama and co-workers in 2019 and 2020, respectively (Figure 3.2.3).^[24] The resulting derivatives are isoelectronic to the all-carbon phenalenyl cation and can be stabilized towards ambient conditions by incorporating a bulky mesityl substituent at the boron center, as reported by Ingleson *et al.*^[24a]

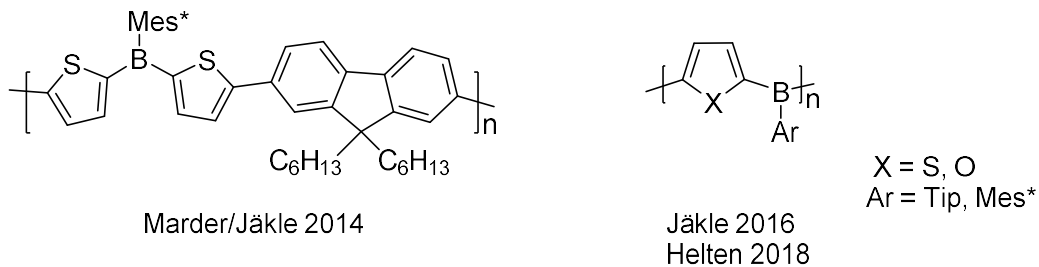


Figure 3.2.4. Selected examples of conjugated polymers with boron in their main-chain.

Boron can also be incorporated into the main chain of conjugated polymers, tuning their optoelectronic properties. Bulky aryl groups, such as 2,4,6-triisopropylphenyl (Tip) or 2,4,6-tri-*tert*-butylphenyl (Mes*), are used to stabilize such polymers towards ambient conditions. Figure 3.2.4 depicts examples for such polymers reported by Marder, Jäkle and co-workers, Jäkle *et al.* and Helten *et al.*^[25]

3.3 Boron-Nitrogen-Doped Materials

An emerging strategy to tune the optoelectronic properties of functional materials is to replace a C=C unit by a B=N unit, which results in a modified electronic situation while maintaining the basic structure.^[26] The B_{sp}²-N_{sp}² bond has significant double-bond character, as depicted in resonance form A (Figure 3.3.1). This π -bond contribution causes the necessity

to add a negative formal charge to boron and a positive charge to nitrogen, although the dipole moment of aminoborane is relatively small (1.844 D).^[27] The small dipole moment can be explained by two opposing forces resulting from σ and π contributions. Due to the large difference in electronegativity between B and N, the σ bond is strongly polarized towards nitrogen and therefore decreases the polarization induced by the π contribution towards the boron atom (Figure 3.3.1, C). Resonance form **B** does not reflect the double bond character, but also does not need the formal charges. Mostly resonance forms **B** or **A** with omitted formal charges are used in drawings.

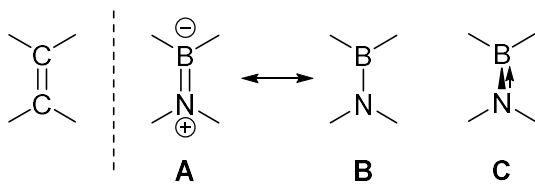


Figure 3.3.1. Isoelectronic relationship between C=C and B=N units.

The concept of BN/CC isosterism started with the discovery of borazine by Stock and Pohland in 1926.^[28] Borazine is commonly referred to as the “inorganic benzene”, but it has a significantly lower aromatic character.^[29] Dewar and co-workers reported the first derivative of 1,2-azaborinine (Figure 3.3.2) in 1962 and the first BN-doped phenalene in 1968.^[30] At the beginning of this century, the works by Piers, Paetzold and Ashe renewed the interest in such BN-doped materials.^[31] In 2011, Liu and co-workers reported the synthesis of the first 1,3-azaborinine derivative (Figure 3.3.2).^[32] In 2012, Braunschweig and co-workers managed to complete the series of structural isomers of azaborinine by synthesizing the first 1,4-azaborinine derivative.^[33]

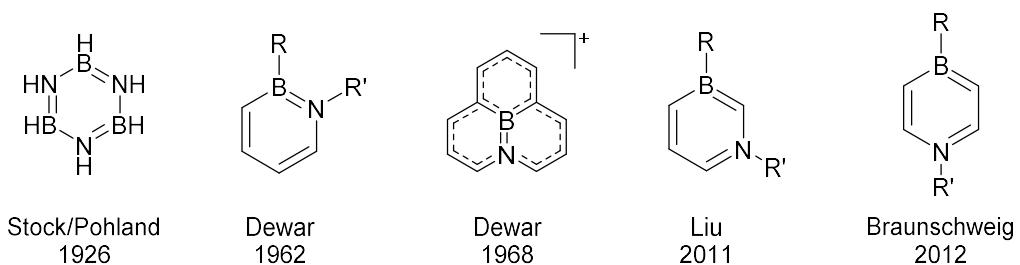


Figure 3.3.2. Structures of selected examples of BN/CC isosterism.

B=N units can also be incorporated into the main-chain of π -conjugated polymers,^[34] as first reported by Mulvaney *et al.* in 1962. These polymers feature the 1,3,2-benzodiazaboroline system as a building block, polymerized with another monomer into a copolymer (Figure 3.3.3).^[35]

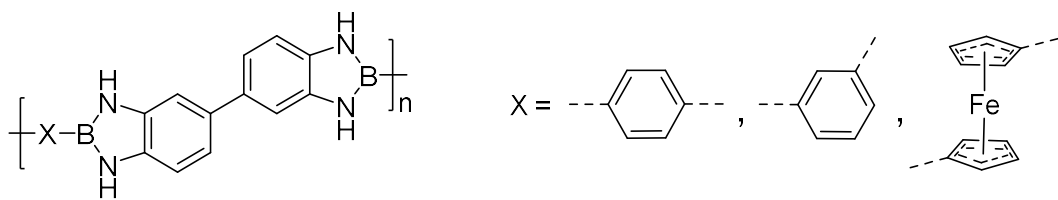


Figure 3.3.3. Polymers featuring 1,3,2-benzodiazaboroline in their main-chain.

Recently, Liu, Jäkle and co-workers reported the preparation of the first conjugated 1,2-azaborinine polymer (Figure 3.3.4). Single-crystal X-ray studies of a trimer revealed an almost perfectly coplanar *syn* arrangement of the heterocycles and spectroscopic investigations indicated a highly effective extension of conjugation upon chain elongation.^[36]

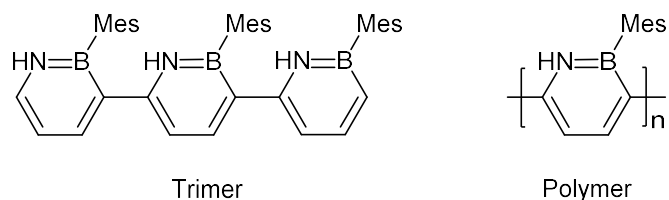


Figure 3.3.4. First 1,2-azaborinine trimer and polymer.

B=N units can also be used as linkages in conjugated polymers. Helten *et al.* reported the synthesis of the first BN analogue of poly(*p*-phenylene vinylene) (PPV) in 2017 (Figure 3.3.5). Boron/silicon exchange polycondensation was applied to access these organoboron polymers. Photophysical investigations and TD-DFT calculations revealed that the BN-PPV exhibits π -conjugation over the B=N units along the polymer backbone and extension of the π -system with increasing chain length.^[37]

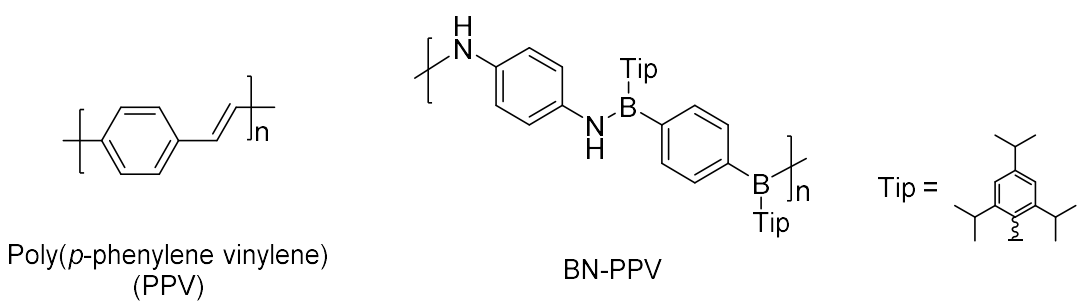
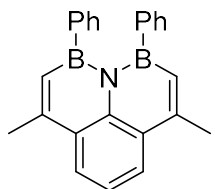


Figure 3.3.5. First BN analogue of PPV.

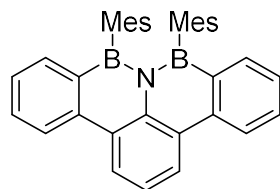
3.4 BNB-Doped Materials

In comparison to BN-doped materials, the incorporation of 3-center 2- π -electron B-N-B units has been scarcely explored so far.^[38] Borylene groups ($>\text{B}-\text{R}$) share common features with carbonyl groups ($>\text{C}=\text{O}$), both have a trigonal planar structure with bond angles of approximately 120° and pronounced π -acceptor character. Therefore, if the B-N-B moiety is incorporated at the outer rim of a PAH it can be considered as an analogue of the imide moiety.

Zeng *et al.* reported a neutral BNB isostere of the phenalenyl cation in 2017 (Figure 3.4.1). Steric congestion between the two B-bonded phenyl groups causes the tricyclic core to be significantly distorted from planarity. Upon chemical reduction the dianion is obtained, while attempts to generate the monoanion lead to an aromaticity driven rearrangement. Theoretical investigations revealed that the B-N-B moiety always participates in the π -conjugation in the neutral and anionic forms, but with a more localized character in comparison to the all-carbon analogues.^[38b]



Zeng 2017

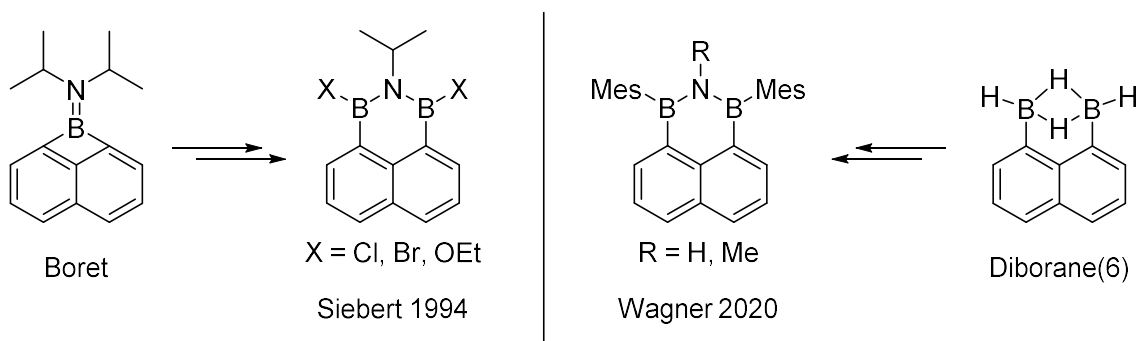


Bettinger 2017

Figure 3.4.1. Structures of PAHs with B-N-B units at the inner rim.

In 2017, Bettinger *et al.* presented the synthesis of a larger BNB-doped PAH, which shows distinct optical properties (Figure 3.4.1). The bulky mesityl substituents at boron provide stability under ambient conditions, but also cause clear distortion of the polycyclic plane.^[38c]

In 1994 Siebert *et al.* reported the first BNB-doped analogue of the phenalenyl cation (Scheme 3.4.1). Due to the B-N-B moiety being incorporated at the outer rim of the PAH, no steric stress between the B-substituents appears. The synthesis proceeds *via* ring expansion of the strained 1*H*-naphtho[1,8-*bc*]boret-1-amine with BX₃. Only derivatives with Cl, Br and OEt as boron substituents have been reported, hence, these azadiborinine derivatives are not stable towards ambient conditions and no further physical properties or chemical transformations are reported.^[38a]



Scheme 3.4.1. Structures of PAHs with B-N-B units at the outer rim.

Very recently Wagner *et al.* presented the synthesis of this ring system *via* a 1,8-naphthalenediyl-supported diborane(6) as the key intermediate. Due to the bulky mesityl substituents at boron, the resulting compounds are stable under ambient conditions. Reversible reduction by cyclic voltammetry (CV) has been reported, but also chemical reduction has been investigated, leading to a radical monoanion according to EPR spectroscopy. The latter, however underwent subsequent addition of an H atom to the naphthalene subunit. The azadiborinines exhibit bright fluorescence with fluorescence quantum yields of up to 51% and narrow full-width at half-maximum values down to 0.30 eV.^[38f]

3.5 Phosphinoboranes

The incorporation of phosphorus into π -conjugated materials has attracted some interest in the recent years.^[3e, 39] Incorporation of B=P units, which are valence isoelectronic to C=C and B=N units, however, have been investigated less extensively.^[40] Figure 3.5.1 depicts the two structural categories of $R_2BPR'_2$ compounds, so called borylphosphines (**A**) and phosphinoboranes (**B**). Borylphosphines feature a trivalent boron and pyramidal phosphorus connected by a single bond (**A**), whereas phosphinoboranes feature trivalent boron, double bonded to a planar phosphorus (**B**). To categorize structures as A-type or B-type, X-ray crystallography can be used. The stereoelectronic properties of the substituents R and R' determine the B-P bond order and chemistry of the B-P bond.^[40d] Planarized trivalent phosphorus is expected to have a significant π -donor effect, which may rival the π -donor ability of nitrogen.^[41]

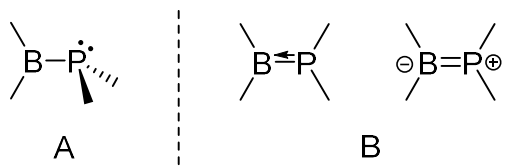
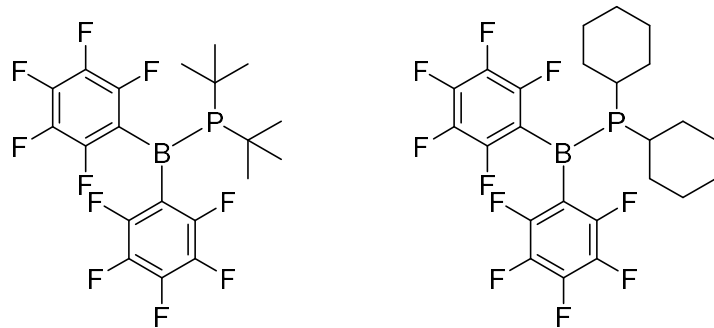


Figure 3.5.1. The two structural extremes of $R_2BPR'_2$ compounds.

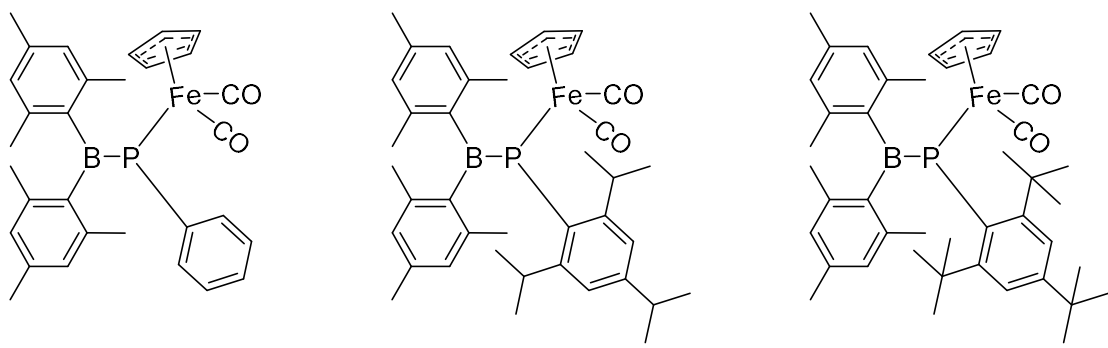
One possibility to planarize phosphorus in a BP unit is to exploit the electronic properties of the substituents R and R'. By substituting the boron center with electron withdrawing groups, while electron pushing groups are attached to the phosphorus, the P gets planarized and a significant π -bond character in the BP unit emerges, resulting in a shortened B-P bond.



Stephan 2011

Figure 3.5.2. Phosphinoboranes planarized by electronic effects.

In 2011, Stephan *et al.* reported the synthesis of phosphinoboranes, which exhibit highly planarized phosphorus and the shortest B-P bond lengths known so far. The compound featuring *t*-Bu-groups on phosphorus exhibits a sum of the angles around P of 359.1° and a B-P bond length of $1.786(4)$ Å (Figure 3.5.2, left). The structural analogue featuring mesityl substituents instead of C_6F_5 has a significantly longer B-P bond of 1.841 Å, suggesting that the electron-withdrawing effect of the C_6F_5 group shortens the B-P bond. The planarity of the P center in phosphinoborane $(C_6F_5)_2BPCy_2$ is even more pronounced (Figure 3.5.2, right), with a sum of the angles of 359.8° and the shortest B-P bond length known so far of $1.762(4)$ Å. Due to the large substituents on phosphorus, dimerization is prevented, and the B-P bond is still polarizable enough to react with H_2 , giving the possibility of application in hydrogen storage materials.^[42]



Mizuta 2012

Figure 3.5.3. Phosphinoboranes planarized by steric effects.

Another possibility to planarize a trivalent phosphorus atom is to introduce a sterically demanding substituent on phosphorus.^[40b] Kubo, Mizuta and co-workers reported the synthesis of P-iron-substituted phosphinoboranes in 2012. Due to the electrons in the d shell of the iron substituent, a repulsion with the lone pair of phosphorus was expected, but this appeared to be less severe, due to π -donation of the phosphorus into the vacant p orbital of boron. The phenyl substituted phosphinoborane (Figure 3.5.3, left) exhibits a sum of the angles around phosphorus of 350.4° , making it already quite planar, due to the electronic effect of the iron substituent. Upon increasing the steric demand of the substituent on phosphorus, an increased planarity of P was achieved. The Tip substituted phosphinoborane (Figure 3.5.3, middle) exhibits a sum of the angles around phosphorus of 356.8° , while the Mes* substituted analogue exhibits full planarity with a sum of the angles of 359.9° .^[43]

3.6 Theoretical Methods

3.6.1 Nucleus Independent Chemical Shift

The ability to sustain a diatropic ring current in response to an external magnetic field is a characteristic of aromatic species.^[44] By calculating the chemical shielding at certain points in space with nonchemical probes, the nucleus independent chemical shift (NICS) method allows assessment of aromaticity, antiaromaticity or nonaromaticity in single-ring systems or in individual rings of multi-ring systems. Upon applying an external magnetic field perpendicular to the ring, a ring current arises, which induces a magnetic field in the ring center. The strength of this field, and thus the chemical shift at this point, is related to the ring current density by the Biot-Savart law. The NICS method follows the chemical shift sign

convention, which is opposite to the shielding, meaning negative NICS values indicate upfield chemical shifts and therefore indicate aromaticity.^[45] Nowadays the NICS method is accepted as an indication for aromaticity and therefore it is widely used.^[46]

Initially, NICS values were calculated at the geometric center of the ring (NICS(0)), as first reported by Buhl and van Wüllen in 1995^[47] and then proposed as a general method by Schleyer *et al.* in 1996.^[48] After realization that the σ frame can influence the calculated values, it was suggested to calculate NICS at 1.0 Å above the center of the ring plane (NICS(1)).^[49] The NICS(1) values in some cases are misleading, for example in anthracene the central ring shows lower NICS(1) values, than the terminal rings.^[50] Following the idea of lower NICS values meaning higher aromaticity, this would suggest that the central ring of anthracene has a higher aromaticity than the terminal rings. This is contradictive to the observation that anthracene undergoes Diels-Alder reactions at the 9 and 10 position, which shows that the central ring is more reactive.^[51]

To avoid the estimation of aromaticity basing on a single value, Stanger suggested scanning the NICS values over distance (NICS-scan) in 2005. The NICS probes should be placed above the geometric center of the ring plane in 0.1 Å steps, ranging from 0.0 to 5.0 Å distance. The resulting NICS values should be separated into isotropic (Figure 3.6.1, green triangles), in-plane (red circles) and out-of-plane (black squares) values. Plotting these values against the distance from the geometric center of the ring plane results in a graph, which can be interpreted regarding aromaticity, antiaromaticity or nonaromaticity.^[52]

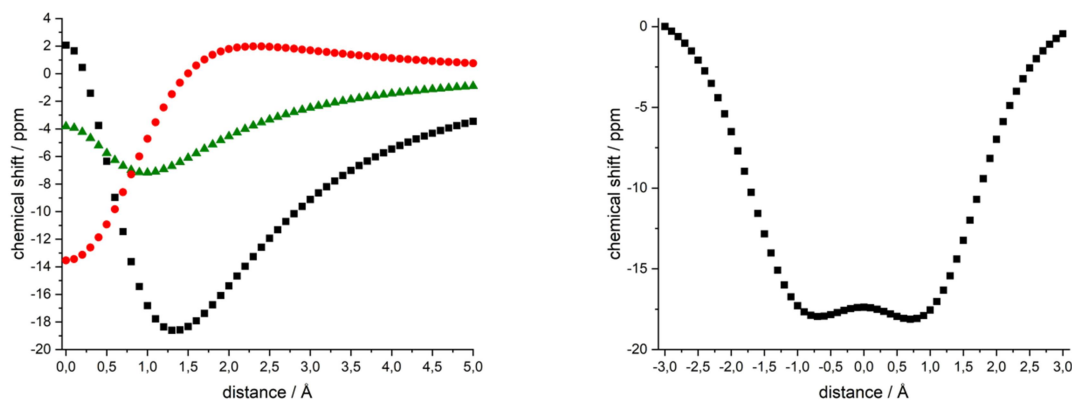


Figure 3.6.1. NICS-scan and NICS-XY-scan of phenalenyl cation (B3LYP-D3(BJ)/6-31+G*).

In 2014 Gershoni-Poranne and Stanger proposed a NICS based method to determinate local and global ring currents in conjugated multi-ring systems. The so called NICS-XY-scan involves placing the NICS probes across the system in a height of 1.7 Å. This distance above the ring plane proved to rule out almost every σ effect. Plotting the resulting NICS values against the distance from a geometric ring center produces a graph, which can be interpreted to give information about local and global ring currents (Figure 3.6.1, right). For example the previously mentioned ‘anthracene problem’ was solved. The NICS-XY-scan showed that the more negative NICS value of the central ring results from an addition of a global 3-ring current and a local benzene-like current (both induced magnetic fields are strongest in the center of the central ring), instead of only a strong local benzene-like ring current in the central ring. Therefore, the central ring seems not to be more aromatic than the terminal rings, which matches the experimental data.^[53]

3.6.2 Anisotropy of the Induced Current Density

In order to investigate delocalization and conjugation in molecules, Herges and Geuenich proposed to use the anisotropy of the induced current density (ACID) as a general method in 2001.^[54] Previously, it was applied by Diederich *et al.* in 1998 to investigate the aromaticity of a transition state in an electrocyclic reaction.^[55] The ACID method is based on a scalar field that is invariant with respect to the relative orientation of the applied magnetic field or the molecule and is not a simple function of the overall electron density. The scalar field has the same symmetry as the wave function and therefore as the molecule and can be plotted as an isosurface. The anisotropy of the induced current density is exclusively a function of the paramagnetic part of the current density, meaning it is only dependent on the perturbation of the wave function by the applied magnetic field. The ACID scalar fields are plotted as isosurfaces, onto which the current density vectors are plotted to distinguish between anisotropies caused by diatropic or paratropic ring currents (Figure 3.6.2).^[56]

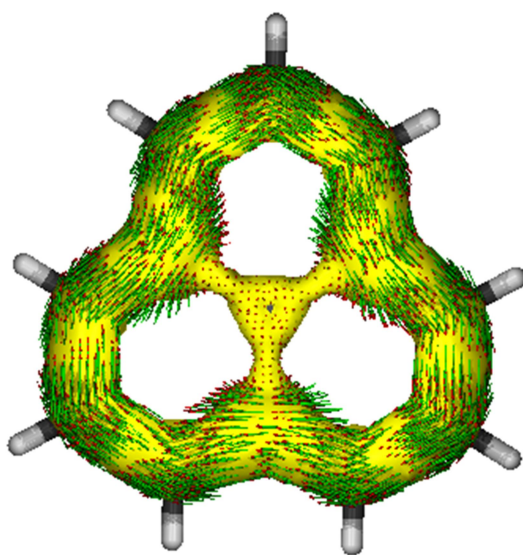


Figure 3.6.2. ACID map of phenalenyl cation (B3LYP-D3(BJ)/6-31+G*).

The ACID method is a generally applicable method for the investigation and visualization of delocalization and conjugation, both in linear and cyclic systems.^[54] The visualization gives an intuitive picture of the induced current, making the ACID method especially attractive for investigations towards aromaticity.^[56-57]

3.7 References

- [1] a) T. M. Swager, *Macromolecules* **2017**, *50*, 4867-4886; b) U. Scherf, A. Gutacker, N. Koenen, *Acc. Chem. Res.* **2008**, *41*, 1086-1097; c) Y. Wang, B. Liu, C. W. Koh, X. Zhou, H. Sun, J. Yu, K. Yang, H. Wang, Q. Liao, H. Y. Woo, X. Guo, *Adv. Energy Mat.* **2019**, *9*, 1803976; d) L. Dou, Y. Liu, Z. Hong, G. Li, Y. Yang, *Chem. Rev.* **2015**, *115*, 12633-12665; e) S. R. Forrest, *Nature* **2004**, *428*, 911-918; f) X.-Y. Wang, X. Yao, K. Müllen, *Sci. China Chem.* **2019**, *62*, 1099-1144; g) K. Takimiya, I. Osaka, M. Nakano, *Chem. Mater.* **2014**, *26*, 587-593.
- [2] a) J. Liang, L. Ying, F. Huang, Y. Cao, *J. Mater. Chem. C* **2016**, *4*, 10993-11006; b) A. C. Grimsdale, K. Leok Chan, R. E. Martin, P. G. Jokisz, A. B. Holmes, *Chem. Rev.* **2009**, *109*, 897-1091.
- [3] a) L. Dou, J. You, Z. Hong, Z. Xu, G. Li, R. A. Street, Y. Yang, *Adv. Mater.* **2013**, *25*, 6642-6671; b) N. Zhou, X. Guo, R. P. Ortiz, S. Li, S. Zhang, R. P. H. Chang, A. Facchetti, T. J. Marks, *Adv. Mater.* **2012**, *24*, 2242-2248; c) M. Saito, I. Osaka, Y. Suda, H. Yoshida, K. Takimiya, *Adv. Mater.* **2016**, *28*, 6921-6925; d) P. M. Beaujuge, J. M. J. Fréchet, *J. Am. Chem. Soc.* **2011**, *133*, 20009-20029; e) D. Joly, P. A. Bouit, M. Hissler, *J. Mater. Chem. C* **2016**, *4*, 3686-3698; f) C. Li, M. Liu, N. G. Pschirer, M. Baumgarten, K. Müllen, *Chem. Rev.* **2010**, *110*, 6817-6855; g) P.-L. T. Boudreault, A. Najari, M. Leclerc, *Chem. Mater.* **2011**, *23*, 456-469; h) H. Zhou, L. Yang, W. You, *Macromolecules* **2012**, *45*, 607-632; i) Y. Cai, L. Huo, Y. Sun, *Adv. Mater.* **2017**, *29*, 1605437.
- [4] a) H. Sirringhaus, *Adv. Mater.* **2014**, *26*, 1319-1335; b) J. Mei, Y. Diao, A. L. Appleton, L. Fang, Z. Bao, *J. Am. Chem. Soc.* **2013**, *135*, 6724-6746; c) S. Allard, M. Forster, B. Souharce, H. Thiem, U. Scherf, *Angew. Chem. Int. Ed.* **2008**, *47*, 4070-4098; d) C. Wang, H. Dong, W. Hu, Y. Liu, D. Zhu, *Chem. Rev.* **2012**, *112*, 2208-2267.
- [5] J. F. Mike, J. L. Lutkenhaus, *J. Polym. Sci., Part B: Polym. Phys.* **2013**, *51*, 468-480.
- [6] S. W. Thomas, G. D. Joly, T. M. Swager, *Chem. Rev.* **2007**, *107*, 1339-1386.
- [7] C. Zhu, L. Liu, Q. Yang, F. Lv, S. Wang, *Chem. Rev.* **2012**, *112*, 4687-4735.
- [8] K. Hunger, M. U. Schmidt, in *Industrial Organic Pigments*, Wiley-VCH, **2018**, pp. 425-611.
- [9] a) T. Weil, T. Vosch, J. Hofkens, K. Peneva, K. Müllen, *Angew. Chem. Int. Ed.* **2010**, *49*, 9068-9093; b) C. Huang, S. Barlow, S. R. Marder, *J. Org. Chem.* **2011**, *76*, 2386-2407; c) M. Al Kobaisi, S. V. Bhosale, K. Latham, A. M. Raynor, S. V. Bhosale, *Chem. Rev.* **2016**, *116*, 11685-11796; d) M. Stępień, E. Gońska, M. Żyła, N. Sprutta, *Chem. Rev.* **2017**, *117*, 3479-3716; e) A. Nowak-Król, F. Würthner, *Org. Chem. Front.* **2019**, *6*, 1272-1318.
- [10] a) M. Sadrai, G. R. Bird, *Opt. Commun.* **1984**, *51*, 62-64; b) G. S. R. Reisfeld, *Chimia* **1990**, *44*, 295-297; c) M. G. Ramírez, S. Pla, P. G. Boj, J. M. Villalvilla, J. A. Quintana, M. A. Díaz-García, F. Fernández-Lázaro, Á. Sastre-Santos, *Adv. Opt. Mater.* **2013**, *1*, 933-938.
- [11] a) L. Zang, R. Liu, M. W. Holman, K. T. Nguyen, D. M. Adams, *J. Am. Chem. Soc.* **2002**, *124*, 10640-10641; b) J. R. Siekierzycka, C. Hippius, F. Würthner, R. M.

Williams, A. M. Brouwer, *J. Am. Chem. Soc.* **2010**, *132*, 1240-1242; c) X. Feng, Y. An, Z. Yao, C. Li, G. Shi, *ACS Applied Materials & Interfaces* **2012**, *4*, 614-618; d) M. Xu, J.-M. Han, Y. Zhang, X. Yang, L. Zang, *Chem. Commun.* **2013**, *49*, 11779-11781.

- [12] a) M. J. Ahrens, M. J. Fuller, M. R. Wasielewski, *Chem. Mater.* **2003**, *15*, 2684-2686; b) B. A. Jones, M. J. Ahrens, M. H. Yoon, A. Facchetti, T. J. Marks, M. R. Wasielewski, *Angew. Chem. Int. Ed. Engl.* **2004**, *43*, 6363-6366; c) X. Zhan, Z. a. Tan, B. Domercq, Z. An, X. Zhang, S. Barlow, Y. Li, D. Zhu, B. Kippelen, S. R. Marder, *J. Am. Chem. Soc.* **2007**, *129*, 7246-7247; d) S. M. Lindner, N. Kaufmann, M. Thelakkat, *Org. Electron.* **2007**, *8*, 69-75; e) Á. J. Jiménez, F. Spänig, M. S. Rodríguez-Morgade, K. Ohkubo, S. Fukuzumi, D. M. Guldi, T. Torres, *Org. Lett.* **2007**, *9*, 2481-2484; f) H. Z. Chen, M. M. Ling, X. Mo, M. M. Shi, M. Wang, Z. Bao, *Chem. Mater.* **2007**, *19*, 816-824; g) B. J. Jung, N. J. Tremblay, M.-L. Yeh, H. E. Katz, *Chem. Mater.* **2011**, *23*, 568-582; h) X. Zhan, A. Facchetti, S. Barlow, T. J. Marks, M. A. Ratner, M. R. Wasielewski, S. R. Marder, *Adv. Mater.* **2011**, *23*, 268-284.
- [13] a) L. Schmidt-Mende, A. Fechtenkötter, K. Müllen, E. Moons, R. H. Friend, J. D. MacKenzie, *Science* **2001**, *293*, 1119-1122; b) Z. a. Tan, E. Zhou, X. Zhan, X. Wang, Y. Li, S. Barlow, S. R. Marder, *Appl. Phys. Lett.* **2008**, *93*, 073309; c) J. E. Anthony, *Chem. Mater.* **2011**, *23*, 583-590.
- [14] C. W. Tang, *Appl. Phys. Lett.* **1986**, *48*, 183-185.
- [15] G. Horowitz, F. Kouki, P. Spearman, D. Fichou, C. Nogues, X. Pan, F. Garnier, *Adv. Mater.* **1996**, *8*, 242-245.
- [16] a) S. Nakazono, Y. Imazaki, H. Yoo, J. Yang, T. Sasamori, N. Tokitoh, T. Cédric, H. Kageyama, D. Kim, H. Shinokubo, A. Osuka, *Chem. Eur. J.* **2009**, *15*, 7530-7533; b) S. Nakazono, S. Eswaramoorthi, D. Kim, H. Shinokubo, A. Osuka, *Org. Lett.* **2009**, *11*, 5426-5429.
- [17] a) Z. Bao, A. Dodabalapur, A. J. Lovinger, *Appl. Phys. Lett.* **1996**, *69*, 4108-4110; b) H. Sirringhaus, N. Tessler, R. H. Friend, *Science* **1998**, *280*, 1741-1744; c) J. Veres, S. Ogier, G. Lloyd, D. de Leeuw, *Chem. Mater.* **2004**, *16*, 4543-4555; d) B. S. Ong, Y. Wu, P. Liu, S. Gardner, *J. Am. Chem. Soc.* **2004**, *126*, 3378-3379; e) M. Heeney, C. Bailey, K. Genevicius, M. Shkunov, D. Sparrowe, S. Tierney, I. McCulloch, *J. Am. Chem. Soc.* **2005**, *127*, 1078-1079; f) I. McCulloch, M. Heeney, C. Bailey, K. Genevicius, I. MacDonald, M. Shkunov, D. Sparrowe, S. Tierney, R. Wagner, W. Zhang, M. L. Chabinyc, R. J. Kline, M. D. McGehee, M. F. Toney, *Nat. Mater.* **2006**, *5*, 328-333; g) H. Usta, G. Lu, A. Facchetti, T. J. Marks, *J. Am. Chem. Soc.* **2006**, *128*, 9034-9035; h) T. Umeda, S. Tokito, D. Kumaki, *J. Appl. Phys.* **2007**, *101*, 054517.
- [18] a) K. Feng, H. Guo, J. Wang, Y. Shi, Z. Wu, M. Su, X. Zhang, J. H. Son, H. Y. Woo, X. Guo, *J. Am. Chem. Soc.* **2021**, *143*, 1539-1552; b) Y. Wang, H. Guo, S. Ling, I. Arrechea-Marcos, Y. Wang, J. T. López Navarrete, R. P. Ortiz, X. Guo, *Angew. Chem. Int. Ed.* **2017**, *56*, 9924-9929; c) Y. Wang, Z. Yan, H. Guo, M. A. Uddin, S. Ling, X. Zhou, H. Su, J. Dai, H. Y. Woo, X. Guo, *Angew. Chem. Int. Ed.* **2017**, *56*, 15304-15308; d) Y. Wang, H. Guo, A. Harbuzaru, M. A. Uddin, I. Arrechea-Marcos, S. Ling, J. Yu, Y. Tang, H. Sun, J. T. López Navarrete, R. P. Ortiz, H. Y. Woo, X.

- Guo, *J. Am. Chem. Soc.* **2018**, *140*, 6095-6108; e) X. Guo, N. Zhou, S. J. Lou, J. W. Hennek, R. Ponce Ortiz, M. R. Butler, P.-L. T. Boudreault, J. Strzalka, P.-O. Morin, M. Leclerc, J. T. López Navarrete, M. A. Ratner, L. X. Chen, R. P. H. Chang, A. Facchetti, T. J. Marks, *J. Am. Chem. Soc.* **2012**, *134*, 18427-18439; f) X. Guo, R. P. Ortiz, Y. Zheng, Y. Hu, Y.-Y. Noh, K.-J. Baeg, A. Facchetti, T. J. Marks, *J. Am. Chem. Soc.* **2011**, *133*, 1405-1418.
- [19] J. A. Letizia, M. R. Salata, C. M. Tribout, A. Facchetti, M. A. Ratner, T. J. Marks, *J. Am. Chem. Soc.* **2008**, *130*, 9679-9694.
- [20] a) S. V. Mulay, B. Bogoslavky, I. Galanti, E. Galun, O. Gidron, *J. Mater. Chem. C* **2018**, *6*, 11951-11955; b) S. V. Mulay, O. Dishi, Y. Fang, M. R. Niazi, L. J. W. Shimon, D. F. Perepichka, O. Gidron, *Chem. Sci.* **2019**, *10*, 8527-8532; c) S. Shi, L. Tang, H. Guo, M. A. Uddin, H. Wang, K. Yang, B. Liu, Y. Wang, H. Sun, H. Y. Woo, X. Guo, *Macromolecules* **2019**, *52*, 7301-7312.
- [21] a) Z. Zhou, A. Wakamiya, T. Kushida, S. Yamaguchi, *J. Am. Chem. Soc.* **2012**, *134*, 4529-4532; b) C. Dou, S. Saito, K. Matsuo, I. Hisaki, S. Yamaguchi, *Angew. Chem. Int. Ed.* **2012**, *51*, 12206-12210.
- [22] a) K. Schickedanz, T. Trageser, M. Bolte, H.-W. Lerner, M. Wagner, *Chem. Commun.* **2015**, *51*, 15808-15810; b) F. Miyamoto, S. Nakatsuka, K. Yamada, K.-i. Nakayama, T. Hatakeyama, *Org. Lett.* **2015**, *17*, 6158-6161.
- [23] V. M. Hertz, H.-W. Lerner, M. Wagner, *Org. Lett.* **2015**, *17*, 5240-5243.
- [24] a) R. J. Kahan, D. L. Crossley, J. Cid, J. E. Radcliffe, M. J. Ingleson, *Angew. Chem. Int. Ed.* **2018**, *57*, 8084-8088; b) J. M. Farrell, C. Mütszel, D. Bialas, M. Rudolf, K. Menekse, A.-M. Krause, M. Stolte, F. Würthner, *J. Am. Chem. Soc.* **2019**, *141*, 9096-9104; c) K. Hirano, K. Morimoto, S. Fujioka, K. Miyamoto, A. Muranaka, M. Uchiyama, *Angew. Chem. Int. Ed. Engl.* **2020**, *59*, 21448-21453.
- [25] a) X. Yin, J. Chen, R. A. Lalancette, T. B. Marder, F. Jäkle, *Angew. Chem. Int. Ed.* **2014**, *53*, 9761-9765; b) A. Lik, S. Jenthra, L. Fritze, L. Müller, K.-N. Truong, H. Helten, *Chem. Eur. J.* **2018**, *24*, 11961-11972; c) X. Yin, F. Guo, R. A. Lalancette, F. Jäkle, *Macromolecules* **2016**, *49*, 537-546.
- [26] a) Z. Liu, T. B. Marder, *Angew. Chem. Int. Ed.* **2008**, *47*, 242-244; b) M. J. D. Bosdet, W. E. Piers, *Can. J. Chem.* **2009**, *87*, 8-29; c) P. G. Campbell, A. J. V. Marwitz, S.-Y. Liu, *Angew. Chem. Int. Ed.* **2012**, *51*, 6074-6092; d) D. Bonifazi, F. Fasano, M. M. Lorenzo-Garcia, D. Marinelli, H. Oubaha, J. Tasseroul, *Chem. Commun.* **2015**, *51*, 15222-15236; e) M. M. Morgan, W. E. Piers, *Dalton Transactions* **2016**, *45*, 5920-5924.
- [27] M. Sugie, H. Takeo, C. Matsumura, *Chem. Phys. Lett.* **1979**, *64*, 573-575.
- [28] A. Stock, E. Pohland, *Berichte der deutschen chemischen Gesellschaft (A and B Series)* **1926**, *59*, 2210-2215.
- [29] a) D. E. Bean, P. W. Fowler, *J. Phys. Chem. A* **2011**, *115*, 13649-13656; b) W. Wu, X. Li, L. Meng, S. Zheng, Y. Zeng, *J. Phys. Chem. A* **2015**, *119*, 2091-2097.
- [30] a) M. J. S. Dewar, P. A. Marr, *J. Am. Chem. Soc.* **1962**, *84*, 3782-3782; b) M. J. S. Dewar, R. Tones, *Tetrahedron Lett.* **1968**, *9*, 2707-2708.
- [31] a) D. J. H. Emslie, W. E. Piers, M. Parvez, *Angew. Chem. Int. Ed.* **2003**, *42*, 1252-1255; b) P. Paetzold, C. Stanescu, J. R. Stubenrauch, M. Bienmüller, U. Englert, Z.

- Anorg. Allg. Chem.* **2004**, *630*, 2632-2640; c) C. A. Jaska, D. J. H. Emslie, M. J. D. Bosdet, W. E. Piers, T. S. Sorensen, M. Parvez, *J. Am. Chem. Soc.* **2006**, *128*, 10885-10896; d) X. Fang, H. Yang, J. W. Kampf, M. M. Banaszak Holl, A. J. Ashe, *Organometallics* **2006**, *25*, 513-518; e) M. J. D. Bosdet, C. A. Jaska, W. E. Piers, T. S. Sorensen, M. Parvez, *Org. Lett.* **2007**, *9*, 1395-1398; f) M. J. D. Bosdet, W. E. Piers, T. S. Sorensen, M. Parvez, *Angew. Chem. Int. Ed.* **2007**, *46*, 4940-4943; g) C. A. Jaska, W. E. Piers, R. McDonald, M. Parvez, *J. Org. Chem.* **2007**, *72*, 5234-5243.
- [32] S. Xu, L. N. Zakharov, S.-Y. Liu, *J. Am. Chem. Soc.* **2011**, *133*, 20152-20155.
- [33] H. Braunschweig, A. Damme, J. O. C. Jimenez-Halla, B. Pfaffinger, K. Radacki, J. Wolf, *Angew. Chem. Int. Ed.* **2012**, *51*, 10034-10037.
- [34] H. Helten, *Chem. Eur. J.* **2016**, *22*, 12972-12982.
- [35] J. E. Mulvaney, J. J. Bloomfield, C. S. Marvel, *Journal of Polymer Science* **1962**, *62*, 59-72.
- [36] A. W. Baggett, F. Guo, B. Li, S.-Y. Liu, F. Jäkle, *Angew. Chem. Int. Ed.* **2015**, *54*, 11191-11195.
- [37] T. Lorenz, M. Crumbach, T. Eckert, A. Lik, H. Helten, *Angew. Chem. Int. Ed.* **2017**, *56*, 2780-2784.
- [38] a) A. Hergel, H. Pritzkow, W. Siebert, *Angew. Chem.* **1994**, *106*, 1342-1343; b) H. Wei, Y. Liu, T. Y. Gopalakrishna, H. Phan, X. Huang, L. Bao, J. Guo, J. Zhou, S. Luo, J. Wu, Z. Zeng, *J. Am. Chem. Soc.* **2017**, *139*, 15760-15767; c) M. Fingerle, C. Maichle-Mössmer, S. Schundelmeier, B. Speiser, H. F. Bettinger, *Org. Lett.* **2017**, *19*, 4428-4431; d) H. Noda, M. Furutachi, Y. Asada, M. Shibasaki, N. Kumagai, *Nature Chemistry* **2017**, *9*, 571-577; e) D. Prieschl, M. Arrowsmith, M. Dietz, A. Rempel, M. Müller, H. Braunschweig, *Chem. Commun.* **2020**, *56*, 5681-5684; f) A. S. Scholz, J. G. Massoth, M. Bursch, J.-M. Mewes, T. Hetzke, B. Wolf, M. Bolte, H.-W. Lerner, S. Grimme, M. Wagner, *J. Am. Chem. Soc.* **2020**, *142*, 11072-11083.
- [39] a) T. Hatakeyama, S. Hashimoto, M. Nakamura, *Org. Lett.* **2011**, *13*, 2130-2133; b) T. Baumgartner, *Acc. Chem. Res.* **2014**, *47*, 1613-1622; c) A. Lik, D. Kargin, S. Isenberg, Z. Kelemen, R. Pietschnig, H. Helten, *Chem. Commun.* **2018**, *54*, 2471-2474.
- [40] a) P. P. Power, *Angew. Chem. Int. Ed.* **1990**, *29*, 449-460; b) D. C. Pestana, P. P. Power, *J. Am. Chem. Soc.* **1991**, *113*, 8426-8437; c) R. T. Paine, H. Noeth, *Chem. Rev.* **1995**, *95*, 343-379; d) J. A. Bailey, P. G. Pringle, *Coord. Chem. Rev.* **2015**, *297-298*, 77-90.
- [41] a) L. Nyulászi, A. Belghazi, S. K. Szétsi, T. Veszprémi, J. Heinicke, *Journal of Molecular Structure: THEOCHEM* **1994**, *313*, 73-81; b) J. Kapp, C. Schade, A. M. El-Nahasa, P. von Ragué Schleyer, *Angew. Chem. Int. Ed.* **1996**, *35*, 2236-2238.
- [42] S. J. Geier, T. M. Gilbert, D. W. Stephan, *Inorg. Chem.* **2011**, *50*, 336-344.
- [43] K. Kubo, T. Kawanaka, M. Tomioka, T. Mizuta, *Organometallics* **2012**, *31*, 2026-2034.
- [44] J. A. Elvidge, L. M. Jackman, *J. Chem. Soc.* **1961**, 859-866.
- [45] C. Corminboeuf, T. Heine, J. Weber, *Phys. Chem. Chem. Phys.* **2003**, *5*, 246-251.
- [46] a) R. Ayub, O. E. Bakouri, K. Jorner, M. Solà, H. Ottosson, *J. Org. Chem.* **2017**, *82*, 6327-6340; b) J. I. Wu, I. Fernández, P. v. R. Schleyer, *J. Am. Chem. Soc.* **2013**, *135*,

- 315-321; c) J. V. Milić, C. Schaack, N. Hellou, F. Isenrich, R. Gershoni-Poranne, D. Neshchadin, S. Egloff, N. Trapp, L. Ruhlmann, C. Boudon, G. Gescheidt, J. Crassous, F. Diederich, *J. Phys. Chem. C* **2018**, *122*, 19100-19109; d) Z. Chen, C. S. Wannere, C. Corminboeuf, R. Puchta, P. v. R. Schleyer, *Chem. Rev.* **2005**, *105*, 3842-3888; e) P. Biegger, M. Schaffroth, O. Tverskoy, F. Rominger, U. H. F. Bunz, *Chem. Eur. J.* **2016**, *22*, 15896-15901; f) D. Moran, F. Stahl, H. F. Bettinger, H. F. Schaefer, P. v. R. Schleyer, *J. Am. Chem. Soc.* **2003**, *125*, 6746-6752; g) T. M. Krygowski, M. K. Cyrański, *Phys. Chem. Chem. Phys.* **2004**, *6*, 249-255.
- [47] M. Bühl, C. van Wüllen, *Chem. Phys. Lett.* **1995**, *247*, 63-68.
- [48] N. J. R. van Eikema Hommes, H. Jiao, A. Dransfeld, C. Maerker, P. v. R. Schleyer, *J. Am. Chem. Soc.* **1996**, *118*, 6317-6318.
- [49] M. Manoharan, Z.-X. Wang, B. Kiran, H. Jiao, R. Puchta, N. J. R. van Eikema Hommes, P. v. R. Schleyer, *Org. Lett.* **2001**, *3*, 2465-2468.
- [50] P. v. R. Schleyer, M. Manoharan, H. Jiao, F. Stahl, *Org. Lett.* **2001**, *3*, 3643-3646.
- [51] P. Yates, P. Eaton, *J. Am. Chem. Soc.* **1960**, *82*, 4436-4437.
- [52] A. Stanger, *J. Org. Chem.* **2006**, *71*, 883-893.
- [53] R. Gershoni-Poranne, A. Stanger, *Chem. Eur. J.* **2014**, *20*, 5673-5688.
- [54] D. Geuenich, R. Herges, *J. Phys. Chem. A* **2001**, *105*, 3214-3220.
- [55] E.-U. Wallenborn, R. F. Haldimann, F.-G. Klärner, F. Diederich, *Chem. Eur. J.* **1998**, *4*, 2258-2265.
- [56] D. Geuenich, K. Hess, F. Köhler, R. Herges, *Chem. Rev.* **2005**, *105*, 3758-3772.
- [57] a) Chaolumen, M. Murata, A. Wakamiya, Y. Murata, *Org. Lett.* **2017**, *19*, 826-829; b) N. Halder, M. Sangeetha, D. Usharani, H. Rath, *J. Org. Chem.* **2020**, *85*, 2059-2067; c) Y. Mitsushige, S. Yamaguchi, B. S. Lee, Y. M. Sung, S. Kuhri, C. A. Schierl, D. M. Guldi, D. Kim, Y. Matsuo, *J. Am. Chem. Soc.* **2012**, *134*, 16540-16543.

4 Results and Discussion

4.1 BNB-Doped phenalenyls – aromaticity switch upon one-electron reduction

The following section is slightly modified and reproduced from published article^[†] with permission from The Royal Society of Chemistry.

Fully aromatic, luminescent, and highly robust BNB-doped phenalenyls have been prepared, which are isoelectronic to the phenalenyl cation. B-Fluoromesityl-substitution leads to fluorescence in an extremely narrow range and significant increase in the reduction potential. Detailed theoretical investigations revealed an intramolecular aromaticity switch upon one-electron reduction.

4.1.1 Introduction

The archetypal phenalenyl system (**A**, Fig. 4.1.1) is of particular fundamental importance due to its unique electronic properties.^[1] It can exist in the neutral radical (13 π electrons), the cationic (12 π electrons), or the anionic state (14 π electrons) – all having the same Hückel MO π-electron delocalization energy. Consequently, phenalenyl-based materials have been fruitfully exploited for a range of applications (including organic electronics, energy storage, information processing).^[2,3] Incorporating main group elements in organic scaffolds has proved to be a promising strategy to effectively expand the chemical space for PAHs^[4-6] (e.g., B-doping of **A** gives the phenalenyl cation analogue **B**^[7-9]). The doping of organic compounds with BN couples is currently of particular interest.^[6,10] Substitution of selected C=C units in aromatic compounds by their isoelectronic and isosteric dipolar B=N units often leads to significantly altered electronic properties but little structural perturbation. This may also cause a modification of the intermolecular interactions, resulting in altered solid-state packing motifs, as well as modified reactivity. The BN/CC isosterism concept was first applied to the phenalenyl system by Dewar in 1968 with the synthesis of the cation **C**.^[11] Indeed, the incorporation of 3-center 2-π-electron B–N–B units in PAHs has been hardly explored thus far.^[12-16]

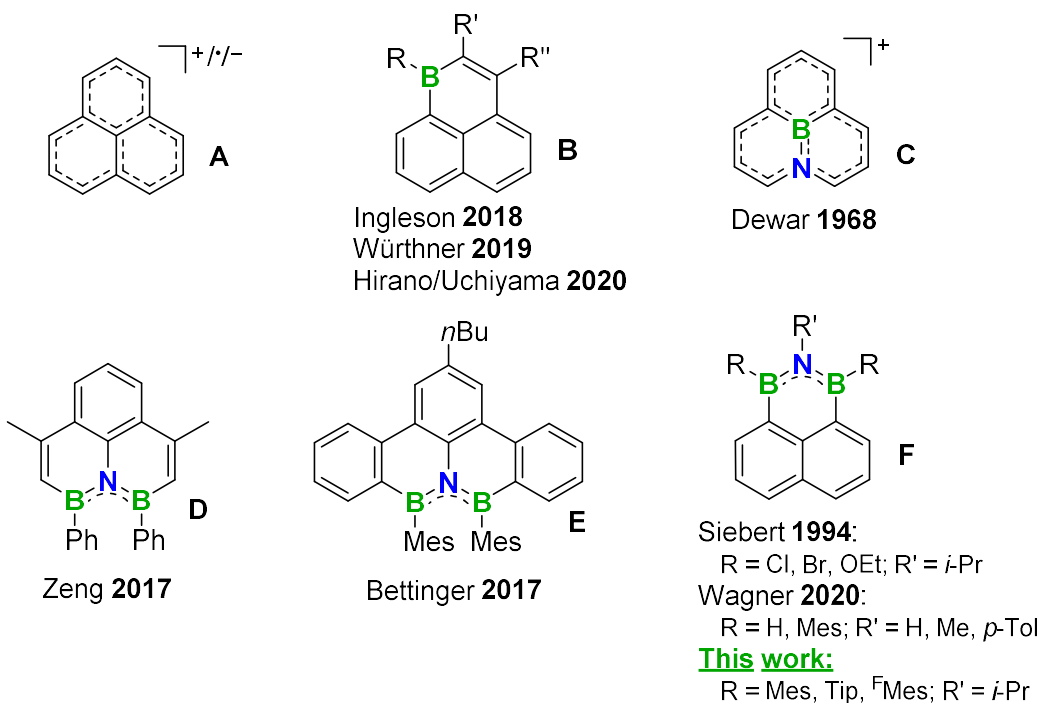
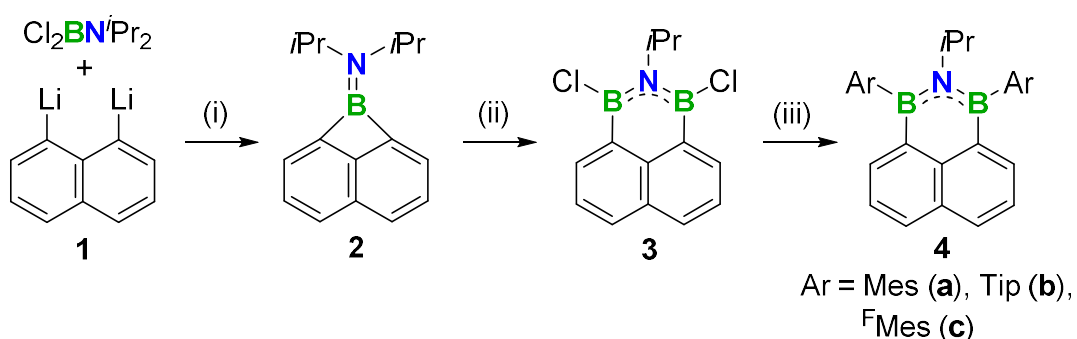


Figure 4.1.1. Phenalenyl cation/radical/anion (**A**), 1-boraphenalenes (**B**), and BN-doped phenalenyl derivatives (**C – F**).

In 2017, Zeng *et al.* presented the species **D**,^[13] which is a neutral BNB isostere of the phenalenyl cation. Steric congestion between the two B-bonded phenyl groups, however, causes the tricyclic scaffold to distort significantly from planarity. Chemical reduction of **D** generated its dianion, while an attempt to obtain the monoanion resulted in an aromaticity driven rearrangement. Bettinger and co-workers presented the related BNB-doped PAH **E**,^[14] which has distinct electronic properties. In this case, too, the substituents on boron (here Mes = mesityl) cause a substantial distortion of the polycyclic plane. Such steric stress between the *B*-substituents is effectively avoided if the BNB moiety is positioned at the outer rim of the phenalenyl system, as is the case in structure **F**. In 1994, Siebert and co-workers reported the first synthesis of derivatives of **F** with R = Cl, Br, or OEt and R' = N*i*Pr₂ via ring expansion of the strained 1*H*-naphtho[1,8-*bc*]boret-1-amine **2** with BX₃ (Scheme 4.1.1).^[15] Apart from basic analytical data to ascertain the constitution of the products, no physical properties and no further chemical transformations were reported. Very recently, Wagner *et al.* presented a new route to this ring system, via a 1,8-naphthalenediyl-supported diborane(6) as the key intermediate.^[16] Upon chemical reduction of the BMes/NMe derivative, the formation of its radical anion **F**[–] was suggested by EPR spectroscopy, however, it underwent subsequent addition of an H atom to its naphthalene subunit.

4.1.2 Results and Discussion

In parallel, we re-examined Siebert's route to this system and found that it provides facile and scalable access to very robust derivatives of **F** with different kinetically stabilizing aryl substituents on boron (*Mes* = mesityl, *Tip* = 2,4,6-triisopropylphenyl, and $^{\text{F}}\text{Mes}$ = 2,4,6-tris(trifluoromethyl)phenyl). Along with these studies, we herein present an in-depth theoretical investigation that sheds light on the aromaticity of **F** and its radical anion F^- and provides an explanation for the observed reactivity of F^- .



Scheme 4.1.1. Synthesis of **4a-c**. Reagents and conditions: (i) *n*-hexane/ Et_2O , $-30\text{ }^\circ\text{C}$. (ii) BCl_3 , CH_2Cl_2 , $-78\text{ }^\circ\text{C}$ to r.t. (iii) ArLi , toluene, $-78\text{ }^\circ\text{C}$ to r.t.

Compound **2**, prepared from **1** and $\text{Cl}_2\text{BN}^i\text{Pr}_2$ (Scheme 4.1.1), is conveniently obtained in gram quantities and in high yield and purity after vacuum sublimation.^[15] We found that the ring expansion of **2** with BCl_3 and the introduction of the kinetically stabilizing aryl groups on boron can be performed sequentially without the need to isolate the intermediate **3**. In this way, we succeeded in the synthesis and isolation by column chromatography of **4a-c**. They were unambiguously identified by multinuclear NMR spectroscopy and mass spectrometry (see appendix 7.1). The structures of **4b** and **4c** in the solid state were additionally determined by single-crystal X-ray diffractometry (Fig. 4.1.2). Despite the increased steric bulk of the substituents (BTip or $\text{B}^{\text{F}}\text{Mes}$ and N^iPr) compared to the BMes/NMe and BMes/NH derivatives structurally investigated by Wagner *et al.*,^[16] the tricyclic system in both **4b** and **4c** is fully planar and essentially unstrained, having $\text{B}-\text{N}-\text{B}$ bond angles close to 120° . The aryl planes of the bulky *B*-substituents are oriented almost perpendicularly to the phenalenyl plane. The $\text{B}-\text{N}$ bonds in **4b** (av. 1.445 \AA) are slightly longer than those in the BMes/NMe derivative ($1.431(2)\text{ \AA}$),^[16] but still in the same range with those in typical BN aromatics^[6] and shorter than in **D** ($1.463(1)\text{ \AA}$)^[13] and **E** (1.46 \AA).^[14] The $\text{B}-\text{N}$ bond in **4c** is slightly shorter (av. 1.433 \AA , i.e., close to that of the BMes/NMe derivative), as an effect of the electron withdrawing character of the $^{\text{F}}\text{Mes}$ group on boron. Compounds **4a-c** proved to be

fully stable towards air and moisture. They showed no sign of decomposition for at least 14 days in moist solution or for more than two years when stored in air in the solid state (appendix 7.1, Figs. 7.1.4, 7.1.8, and 7.1.13). They also exhibited excellent thermal stability. Differential scanning calorimetry (DSC) measurements revealed no sign of decomposition up to 376 (**4a**), 452 (**4b**), and 378 °C (**4c**) (appendix 7.1, Fig. 7.1.29).

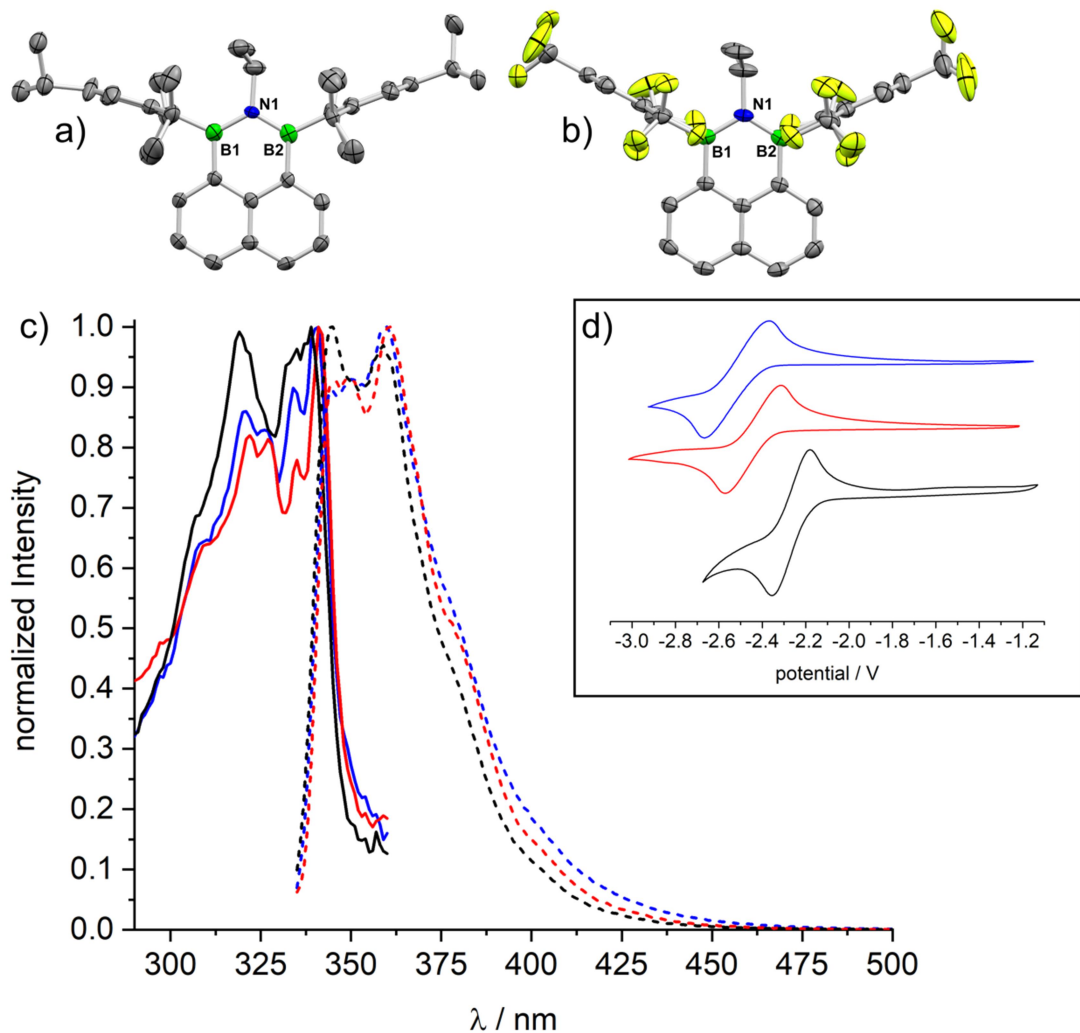


Figure 4.1.2. Molecular structures of **4b** (a) and **4c** (b) by single-crystal X-ray diffraction (H atoms omitted for clarity). UV-vis absorption (solid lines) and fluorescence spectra (dashed lines) (c) (in *n*-hexane) and cyclic voltammograms (d) (vs. $[\text{Cp}_2\text{Fe}]^{0+}$, scan rate: 100 mVs⁻¹, in THF) of **4a** (blue), **4b** (red) and **4c** (black).

The UV-vis absorption spectra for **4a-c** in *n*-hexane display one structured low-energy band with two maxima, assigned to a $\pi-\pi^*$ transition in the BNB-phenalenyl system (Fig. 4.1.2c and Table 4.1.1). Compounds **4a-c** show blue fluorescence with small Stokes shifts (513 – 754 cm⁻¹, in *n*-hexane), vibrational fine structure, and solvatochromism, pointing to some extent of charge transfer upon excitation. The emission bandwidths of **4a-c** are relatively narrow – a feature that is of great interest for the generation of pure luminescence colors.

Comparison of **4a** with Wagner's BMes/NMe derivative^[16] reveals that an exchange of Me by *i*-Pr at N causes a decrease in the quantum efficiency (by 17%) along with a slight broadening of the bandwidth (by 0.08 eV), due to additional rotational and vibrational degrees of freedom in the *i*-Pr group, thus, promoting non-emissive decay pathways. Variation of the *B*-substituent from Mes to Tip to ^FMes, on the other hand, leads to an increase of the quantum yield and a narrowing of the bandwidth in this order. The B^FMes/-NiPr derivative **4c** shows values in a similar range with that of the BMes/NMe derivative ($\Phi_{fl} = 51\%$, FWHM = 0.30 eV).^[16] Cyclic voltammetry (CV) investigations (Fig. 4.1.2d) revealed reversible reductions at $E_{1/2} = -2.52$ (**4a**) and -2.44 V (**4b**), respectively. Incorporating ^FMes at boron facilitates electron injection and results in a reversible reduction at $E_{1/2} = -2.27$ V for **4c**.

Table 4.1.1. Photophysical data for **4a**, **4b** and **4c**.^[a]

	λ_{abs} ^[b] / nm	λ_{em} ^[b,c] / nm	Φ_{fl} ^[d]	τ / ns	FWHM / cm ⁻¹ (eV)
4a	321	344	34 %	1.11 (12 %)	3096 (0.38)
	<u>341</u>	<u>360</u>		3.74 (88%)	
4b	322	345	36 %	1.17 (11 %)	2870 (0.36)
	<u>341</u>	<u>361</u>		3.20 (89 %)	
4c	319	<u>345</u>	47 %	1.40 (5 %)	2689 (0.33)
	<u>339</u>	359		5.26 (95 %)	

[a] In hexane. [b] Absorption and emission maxima underscored. [c] Excited at the wavelength of the respective absorption maximum. [d] Fluorescence quantum yield determined absolutely with an integrating sphere.

With a view to elucidate the possible aromaticity of the BNB-phenalenyl system **F** and its putative radical anion **F**⁻, suggested through the studies by Wagner *et al.*,^[16] we conducted comprehensive theoretical investigations on **4a** and **4a**⁻. We performed NICS scans,^[17a,b] considering the heteroatomic ring and the naphthalenic part separately, which provides a more detailed picture than merely regarding single NICS(0)/NICS(1) values. Additionally, we applied the Anisotropy of the Induced Current Density (ACID) method^[17c,d] to visualize possible aromatic and/or antiaromatic ring currents in **4a** and **4a**⁻. The plot of the NICS-Z-scan for the naphthalenic part of **4a**, perpendicular to the PAH plane from the geometric center of that part of the molecule up to 5 Å above the plane, shows the typical shape of an aromatic system (Fig. 4.1.3a); it is actually very similar to that of naphthalene itself.^[17a]

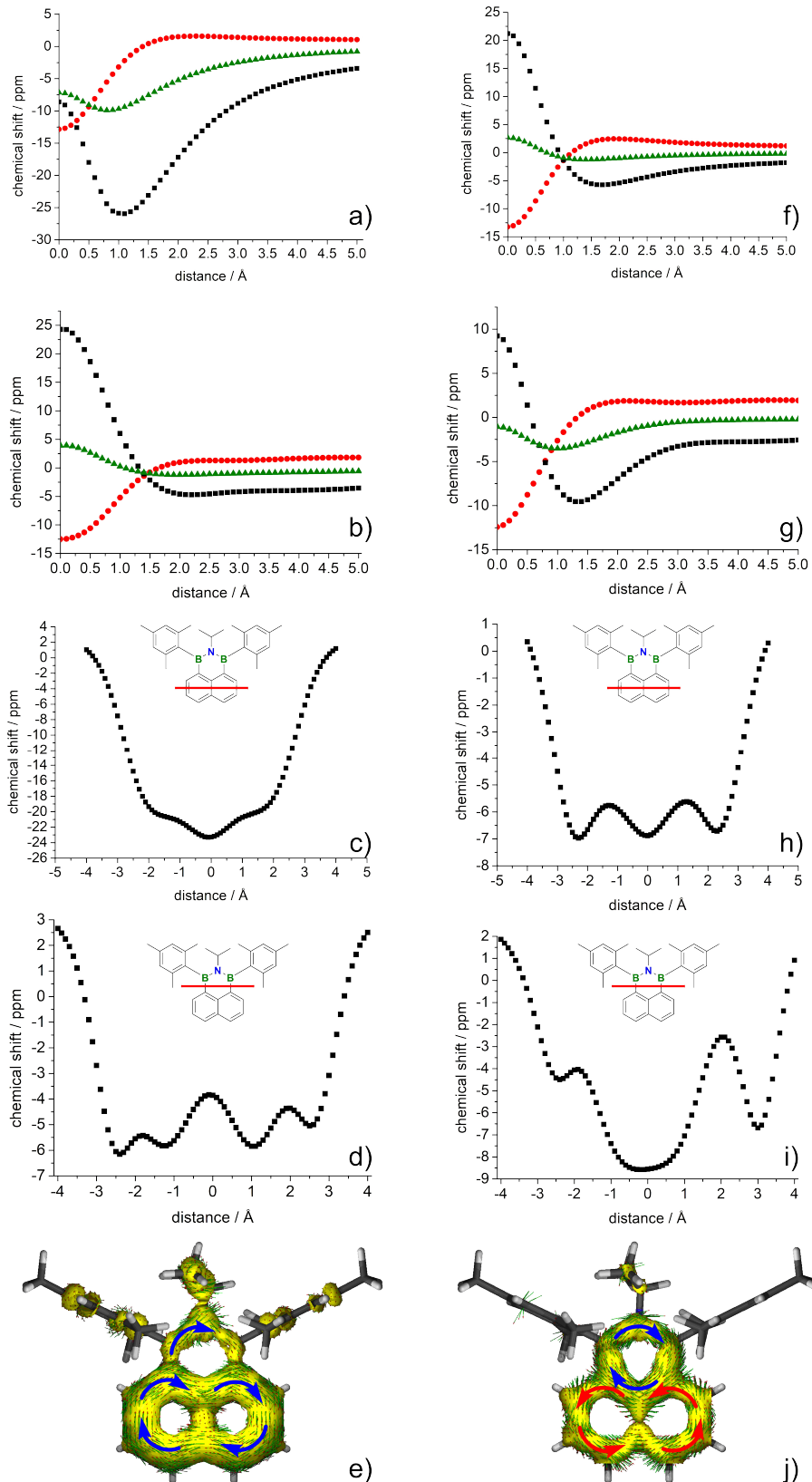


Figure 4.1.3. NICS-scans (for **4a**: naphthalenic part (a), hetero ring (b); **4a⁻**: naphthalenic part (f), hetero ring (g); out-of-plane (black), in-plane (red) and isotropic (green)), NICS-X-scans (for **4a**: naphthalenic part (c), hetero ring (d); **4a⁻**: naphthalenic part (h); hetero ring (i)) and ACID plots (for **4a** (e), for **4a⁻** (j)); isovalue 0.015); B3LYP-D3(BJ)/6-31+G*.

The isotropic chemical shift is mainly controlled by the out-of-plane component and both curves display a clear minimum. The NICS-scan for the hetero ring of **4a** (b) shows these features as well, but with significantly less negative values and shallow minima. This points to aromaticity in this ring, though to a much lower degree, however, it is not decisive enough as such. Therefore, we additionally performed NICS-X-scans^[17b] at 1.7 Å above the ring plane along the red lines drawn in the respective formulae in Fig. 4.1.3. For the naphthalenic system of **4a** the resulting plot (c) showed a shape characteristic of that for naphthalene. All NICS values are negative throughout the scan. Two plateaus, at -1.2 and 1.2 Å, are due to diatropic benzenic currents in each of the constituent six-membered rings, and the global minimum at the center results from the additional diatropic naphthalenic ring current, which enhances the external magnetic field even further. The NICS-X-scan for the hetero ring (d) also shows throughout negative but smaller values, thus supporting the assignment of a low degree of aromaticity to this ring system. The local maximum at the center results from σ -effects, and the shallow maxima at -2.0 and 2.0 Å are caused by perturbation from the *ortho*-methyl groups of the mesityl substituents (see appendix 7.1, Fig. 7.1.40). The ACID plot (e) unambiguously shows a strong diatropic ring current in the naphthalenic rings and a weaker one in the hetero ring, leading to a global diatropic (i.e. aromatic) ring current.

In the radical anion, **4a**⁻, the situation is switched to an extent. The NICS-Z-scan for the naphthalenic system (f) still shows minima in the isotropic chemical shift and the out-of-plane component, which are, however, rather shallow and the values are significantly less negative compared to those for the neutral form. The latter statement is also true for the NICS-X-scan (h). Overall, it shows small negative values, with a minimum at the center, but maxima at the center of each of the six-membered rings (-1.2 and 1.2 Å). This can be explained by a weak diatropic naphthalenic ring current superimposed by two paratropic benzenic circuits. For the hetero ring of **4a**⁻ (g), on the other hand, the NICS-Z-scan exhibits clearer minima and more negative values compared to the neutral form. The same is true for the NICS-X-scan (i), which has a clear minimum at the ring center.^[18] This indicates that this ring has gained aromaticity upon reduction. In accordance with our interpretation, the ACID plot (j) shows a strong diatropic ring current in the hetero ring and a slightly weaker paratropic ring current in the naphthalenic rings. This shows that the hetero ring is clearly aromatic and the rings of the naphthalene subsystem are at least partially antiaromatic.

4.1.3 Conclusion

In conclusion, we have prepared three robust BNB-doped phenalenyl derivatives with favorable optoelectronic properties via a highly efficient ring expansion–substitution procedure. This method provides a convenient synthesis, facile scalability, and the possibility to introduce different *B*-substituents at a late stage. Our theoretical investigations suggest an aromaticity switch within the molecule upon one-electron reduction. Consistent with the follow-up reaction of the radical anion at the naphthalene moiety observed by Wagner *et al.*,^[16] our calculations reveal that the reduction comes along with a loss of aromaticity in the naphthalenic subsystem.

4.1.4 Experimental Section

General procedures. All manipulations before the aqueous work-up were performed under an atmosphere of dry argon using standard Schlenk techniques or in an MBraun glovebox. Solvents (dichloromethane, *n*-pentane, *n*-hexane, toluene, THF, and diethylether) were dried and degassed by means of an MBraun SPS-800 solvent purification system. CDCl₃ and C₆D₆ for NMR spectroscopy were dried and degassed at reflux over CaH₂ or Na, respectively, and freshly distilled prior to use. *n*-Butyllithium solutions (1.6 M and 2.5 M in hexanes), trichloroborane, 1-bromonaphthalene, 2,4,6-trimethylphenyl bromide, 2,4,6-triisopropylphenyl bromide and 1,3,5-tris(trifluoromethyl)benzene were commercially purchased and used as received. Triethylamine and diisopropylamine were dried and degassed at reflux over Na and freshly distilled prior to use. Trimethylsilyl chloride and TMEDA were purified by inert-gas distillation. Dichloro(diisopropylamino)borane,^[19] 1,8-dilithionaphthalene,^[20] naphtho[1,8-*cd*]-*N*-isopropyl-*B,B'*-dichloro-[1,2,6]-azadiborinine,^[21] 2,4,6-trimethylphenyl-lithium,^[22] 2,4,6-triisopropylphenyllithium,^[23] and 2,4,6-tris(trifluoromethyl)phenyllithium^[24] were prepared according to literature procedures. NMR spectra were recorded at 25 °C on a Bruker Avance III HD spectrometer operating at 300 MHz or on a Bruker Avance 500 spectrometer operating at 500 MHz. Chemical shifts were referenced to residual protic impurities in the solvent (¹H) or the deuterio solvent itself (¹³C) and reported relative to external SiMe₄ (¹H, ¹³C, ²⁹Si), BF₃·OEt₂ (¹¹B), or CFCl₃ (¹⁹F) standards. Mass spectra were obtained with the use of a Thermo Scientific Exactive Plus Orbitrap MS system employing atmospheric pressure chemical ionization (APCI). UV-vis spectra were obtained using a Jasco V-630 spectrophotometer. Emission spectra were recorded using an Edinburgh

Instruments FLSP920 spectrometer equipped with a double monochromator for both excitation and emission, operating in right-angle geometry mode, and all spectra were fully corrected for the spectral response of the instrument. Fluorescence quantum yields were measured using a calibrated integrating sphere from Edinburgh Instruments combined with the FLSP920 spectrometer described above. Elemental analyses were performed on an Elementar vario MICRO cube elemental analyzer. Cyclic voltammetry experiments were performed using a Gamry Instruments Reference 600 potentiostat. The scans were referenced after the addition of a small amount of ferrocene as internal standard. The potentials are reported relative to the ferrocene/ferrocenium couple. Differential scanning calorimetry (DSC) was performed using a DSC 204 F1 Phoenix calorimeter. Crystals suitable for single-crystal X-ray diffraction were selected, coated in perfluoropolyether oil, and mounted on MiTeGen sample holders. Diffraction data were collected on Bruker X8 Apex II 4-circle diffractometers with CCD area detectors using Mo-K α radiation. The crystals were cooled using an Oxford Cryostreams low-temperature device. Data were collected at 100 K. The images were processed and corrected for Lorentz-polarization effects and absorption as implemented in the Bruker software packages. The structures were solved using the intrinsic phasing method (SHELXT)^[25] and Fourier expansion technique. All non-hydrogen atoms were refined in anisotropic approximation, with hydrogen atoms ‘riding’ in idealized positions, by full-matrix least squares against F2 of all data, using SHELXL^[26] software and the SHELXLE graphical user interface.^[27] Other structural information was extracted using OLEX2 software.^[28]

Spectra. All spectra and other result figures are shown in Appendix 7.1.

Synthesis of naphtho[1,8-cd]-N-isopropyl-B,B'-bis(2,4,6-trimethylphenyl)-[1,2,6]-azadi-borinine (4a). To a solution of 1*H*-naphtho[1,8-*bc*]boret-1-amine **2** (2.00 mmol) in DCM (4 mL) was added a solution of BCl₃ (17.6 mmol) in DCM (5 mL) at -78 °C. The mixture was stirred for 5 days and all volatile components were removed *in vacuo*. The residue was dissolved in toluene (10 mL) and a solution of 2,4,6-trimethylphenyllithium (4.64 mmol) in toluene (25 mL) was added at -78 °C. The mixture was subsequently warmed to ambient temperature and stirred overnight. All volatile components were removed *in vacuo* and the residue was dissolved in DCM. It was washed with water and the organic phase was

evaporated to dryness using a rotary evaporator. The product was received as colourless crystals after purification *via* column chromatography (silica; *n*-hexane) and crystallization from CHCl₃/MeOH. Yield: 0.3622 g (0.82 mmol, 41%). ¹H NMR (400 MHz, CDCl₃): δ = 8.07 (d, ³J_{HH} = 8.2 Hz, 2 H, C^{4/5}H Naph), 7.64 (d, ³J_{HH} = 6.9 Hz, 2 H, C^{2/7}H Naph), 7.52 (pseudo t, ³J_{HH} = 8.1 Hz, 2 H, C^{3/6}H), 6.97 (s, 4 H, CH Mes), 4.21 (sept, ³J_{HH} = 7.0 Hz, 1 H, CH-(CH₃)₂), 2.43 (s, 6 H, *p*-CH₃ Mes), 2.23 (s, 12 H, *o*-CH₃ Mes), 1.23 ppm (d, ³J_{HH} = 7.0 Hz, 6 H, CH-(CH₃)₂) ppm; ¹¹B{¹H} NMR (128 MHz, CDCl₃): δ = 50.8 ppm (s); ¹³C{¹H} NMR (101 MHz, CDCl₃): δ = 140.2 (*ipso*-C Mes), 139.9 (C^{2/7} Naph), 138.8 (*p*-C Mes), 136.9 (C^{8a} Naph), 136.7 (*o*-C Mes), 135.2 (C^{1/8} Naph), 132.6 (C^{4/5} Naph), 131.1 (C^{4a} Naph), 127.0 (CH Mes), 126.1 (C^{3/6} Naph), 53.3 (NCH(CH₃)₂), 23.7 (NCH(CH₃)₂), 23.5 (*o*-CH₃ Mes), 21.3 (*p*-CH₃ Mes) ppm; HR-MS (APCI): m/z = 444.3029 [M+H⁺], calcd. for C₃₁H₃₅B₂N: 443.2956; UV/vis (DCM): $\lambda_{\text{abs,max}}$ = 234 (ε = 66539 L mol⁻¹ cm⁻¹), 321 (ε = 13129 L mol⁻¹ cm⁻¹), 341 nm (ε = 13891 L mol⁻¹ cm⁻¹); fluorescence (DCM): $\lambda_{\text{ex}} = 321$, $\lambda_{\text{em1}} = 352$, $\lambda_{\text{em2}} = 370$, $\lambda_{\text{em3}} = 386$ nm ($\Phi_f = 17\%$).

Synthesis of naphtho[1,8-*cd*]-*N*-isopropyl-*B,B'*-bis(2,4,6-triisopropylphenyl)-[1,2,6]-azadiborinine (4b). To a solution of 1*H*-naphtho[1,8-*bc*]boret-1-amine **2** (2.04 mmol) in DCM (4 mL) was added a solution of BCl₃ (17.6 mmol) in DCM (5 mL) at -78 °C. The mixture was stirred for 5 days and all volatile components were removed *in vacuo*. The residue was dissolved in toluene (10 mL) and a solution of 2,4,6-triisopropylphenyllithium (4.03 mmol) in toluene (15 mL) was added at -78 °C. The mixture was subsequently warmed to ambient temperature and stirred overnight. All volatile components were removed *in vacuo* and the residue was dissolved in *n*-hexane. It was washed with water and the organic phase was evaporated to dryness using a rotary evaporator. The product was received as colourless crystals after purification *via* column chromatography (silica; *n*-hexane) and crystallization from CHCl₃/MeOH. Yield: 0.4778 g (0.78 mmol, 38%). ¹H NMR (400 MHz, CDCl₃): δ = 8.05 (d, ³J_{HH} = 8.2 Hz, 2 H, C^{4/5}H Naph), 7.63 (d, ³J_{HH} = 6.9 Hz, 2 H, C^{2/7}H Naph), 7.52 (pseudo t, ³J_{HH} = 8.1 Hz, 2 H, C^{3/6}H Naph), 7.08 (s, 4 H, CH Tip), 4.38 (sept, ³J_{HH} = 6.9 Hz, 1 H, NCH(CH₃)₂), 3.01 (sept, ³J_{HH} = 6.9 Hz, 2 H, *p*-CH(CH₃)₂ Tip), 2.67 (sept, ³J_{HH} = 6.7 Hz, 4 H, *o*-CH(CH₃)₂ Tip), 1.37 (d, ³J_{HH} = 6.9 Hz, 12 H, *p*-CH(CH₃)₂ Tip), 1.30 (d, ³J_{HH} = 6.7 Hz, 12 H, *o*-CH(CH₃)₂ Tip), 1.24 (d, ³J_{HH} = 6.9 Hz, 6 H, NCH(CH₃)₂), 0.96 ppm (d, ³J_{HH} = 6.6 Hz, 12 H, *o*-CH(CH₃)₂ Tip) ppm; ¹¹B{¹H} NMR (128 MHz, CDCl₃): δ = 50.8 ppm (s); ¹³C{¹H} NMR (101 MHz, CDCl₃): δ = 149.7 (*o*-C Tip), 148.4 (*p*-C Tip), 141.9 (C^{2/7} Naph), 138.3 (*ipso*-C Tip), 136.5 (C^{8a} Naph), 136.2 (C^{1/8}

Naph), 132.6 ($C^{4/5}$ Naph), 130.9 (C^{4a} Naph), 125.2 ($C^{3/6}$ Naph), 120.1 (CH Tip), 52.8 (NCH(CH₃)₂), 35.0 (*o*-CH(CH₃)₂ Tip), 34.2 (*p*-CH(CH₃)₂), 25.5/23.5 (*o*-CH(CH₃)₂ Tip), 24.9 (NCH(CH₃)₂), 24.2 ppm (*p*-CH(CH₃)₂ Tip); HR-MS (APCI): m/z = 612.4897 [M+H⁺], calcd. for C₄₃H₅₉B₂N: 611.4834; UV/vis (DCM): $\lambda_{abs,max} = 236$ ($\epsilon = 68240$ L mol⁻¹ cm⁻¹), 326 ($\epsilon = 12397$ L mol⁻¹ cm⁻¹), 342 nm ($\epsilon = 13846$ L mol⁻¹ cm⁻¹); fluorescence (DCM): $\lambda_{ex} = 326$, $\lambda_{em1} = 353$, $\lambda_{em2} = 369$, $\lambda_{em3} = 382$ nm ($\Phi_f = 26\%$).

Synthesis of naphtho[1,8-*cd*]-*N*-isopropyl-*B,B'*-bis(2,4,6-tris(trifluoromethyl)phenyl)-[1,2,6]azadiborinine (4c). To a solution of 1*H*-naphtho[1,8-*bc*]boret-1-amine **2** (4.00 mmol) in DCM (8 mL) was added a solution of BCl₃ (35.2 mmol) in DCM (10 mL) at -78 °C. The mixture was stirred for 5 days and all volatile components were removed *in vacuo*. The residue was dissolved in toluene (10 mL) and a solution of freshly prepared 2,4,6-tris(trifluoromethyl)phenyllithium (ca. 9 mmol) in toluene (15 mL) was added at -78 °C. The mixture was subsequently warmed to ambient temperature and stirred for 5 days. All volatile components were removed *in vacuo* and the residue was dissolved in *n*-hexane. It was washed with water and the organic phase was evaporated to dryness using a rotary evaporator. The product was received as yellowish crystals after purification *via* column chromatography (silica; *n*-hexane/ethyl acetate, 90:10) and crystallization from CHCl₃/MeOH. Yield: 0.5166 g (0.67 mmol, 17%). ¹H NMR (400 MHz, CDCl₃): $\delta = 8.21$ (s, 4H, CH ^FMes), 8.12 (d, ³J_{HH} = 8.3 Hz, 2H, C^{4/5}H Naph), 7.52 (pseudo t, ³J_{HH} = 7.0 Hz, 2H, C^{3/6}H Naph), 7.21 (d, ³J_{HH} = 7.0 Hz, 2H, C^{2/7}H Naph), 3.73 (sept, ³J_{HH} = 6.9 Hz, 1H, NCH(CH₃)₂), 1.04 (d, ³J_{HH} = 6.8 Hz, 6H, NCH(CH₃)₂) ppm; ¹¹B{¹H} NMR (128 MHz, CDCl₃): $\delta = 47.5$ ppm (s); ¹³C{¹H} NMR (101 MHz, CDCl₃): $\delta = 142.8$ (*ipso*-C ^FMes), 139.1 (C^{2/7} Naph), 135.9 (C^{4a} Naph), 135.2 (q, ¹J_{CF} = 31.5 Hz, *o*-C ^FMes), 133.9 (C^{1/8} Naph), 133.6 (C^{4/5} Naph), 132.2 (q, ¹J_{CF} = 34.5 Hz, *p*-C ^FMes), 130.9 (C^{8a} Naph), 126.5 (*m*-C Naph), 126.0 (C^{3/6} Naph), 123.7 (q, ¹J_{CF} = 275.8 Hz, *o*-CF₃), 122.8 (q, ¹J_{CF} = 272.2 Hz, *p*-CF₃), 54.4 (NCH(CH₃)₂), 23.8 (NCH(CH₃)₂) ppm; ¹⁹F{¹H} NMR (376 MHz, CDCl₃): $\delta = -56.7$ (s, 12F, *o*-CF₃), -63.2 (s, 6F, *p*-CF₃) ppm; HR-MS (APCI): m/z = 768.1322 [M+H⁺], calcd. for C₃₁H₁₇B₂F₁₈N: 767.1260; UV/vis (DCM): $\lambda_{abs,max} = 231$ ($\epsilon = 45827$ L mol⁻¹ cm⁻¹), 320 ($\epsilon = 14312$ L mol⁻¹ cm⁻¹), 339 nm ($\epsilon = 13654$ L mol⁻¹ cm⁻¹); fluorescence (DCM): $\lambda_{ex} = 320$, $\lambda_{em1} = 349$, $\lambda_{em2} = 363$ nm ($\Phi_f = 30\%$).

Crystallographic data

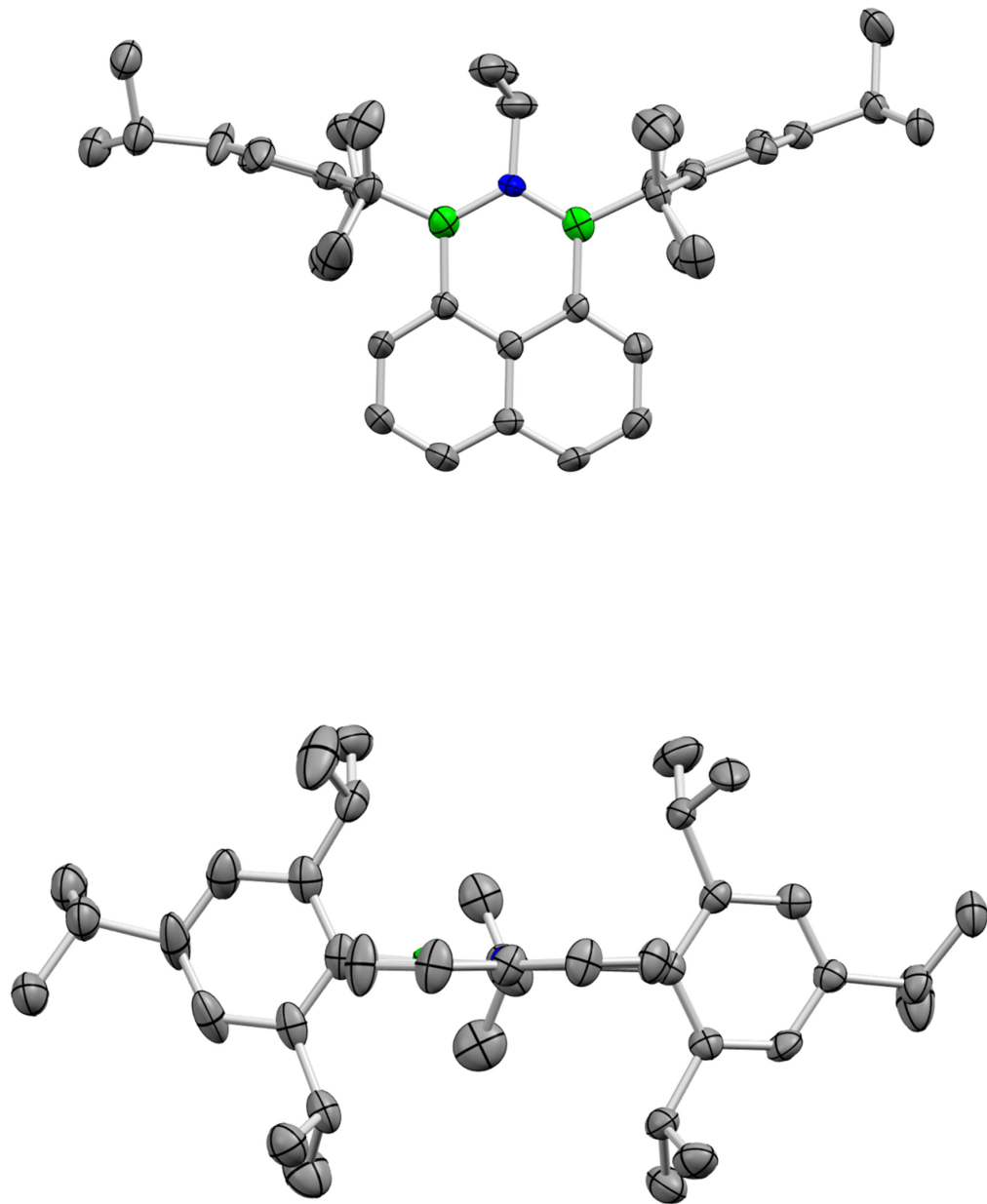


Figure 4.1.4. Molecular structure of **4b** (with views perpendicular and parallel to the polycyclic plane) in the solid state by single-crystal X-ray diffraction.

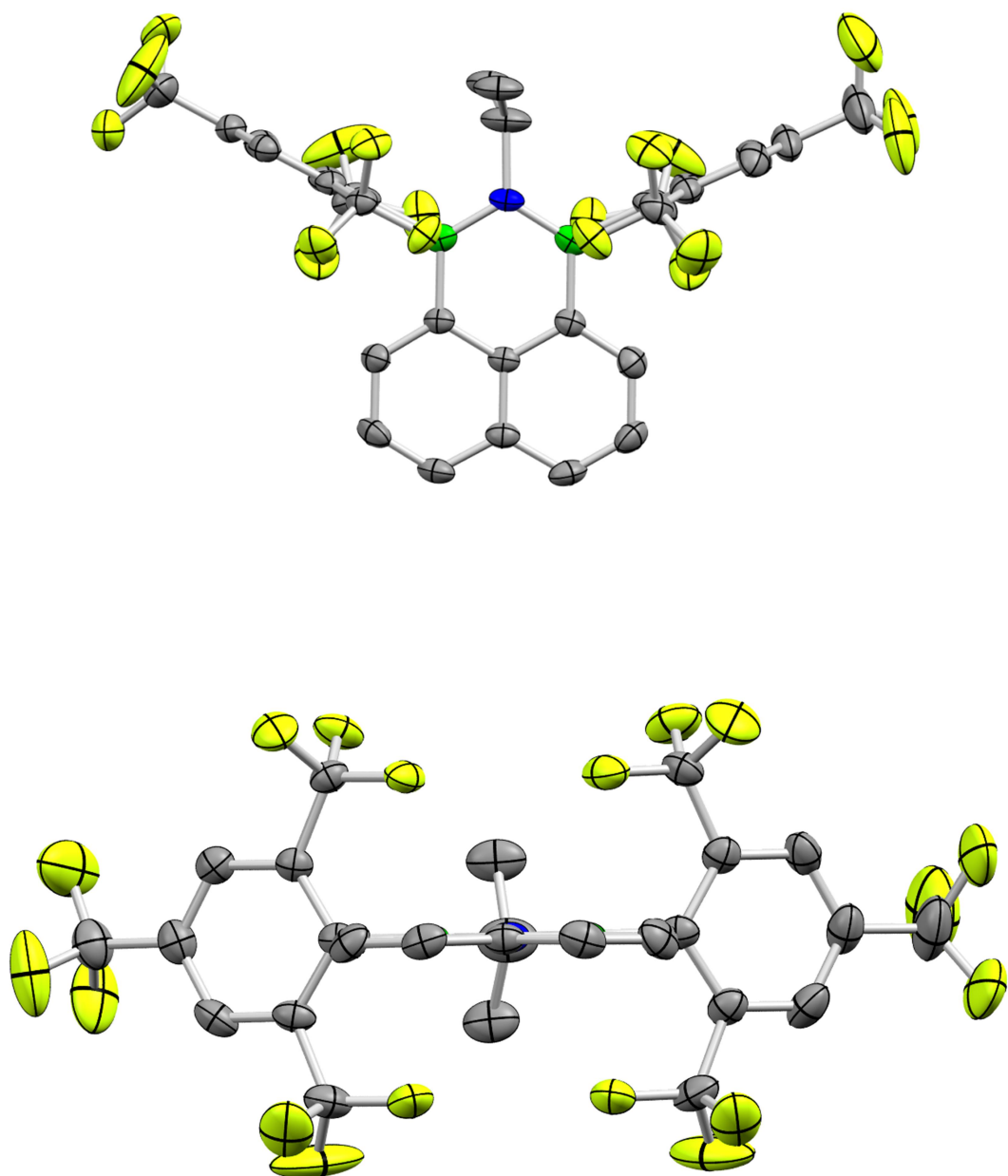


Figure 4.1.5. Molecular structure of **4c** (with views perpendicular and parallel to the polycyclic plane) in the solid state by single-crystal X-ray diffraction.

Table 4.1.2. Crystallographic data of **4b** and **4c**.

No.	4b	4c
CCDC number	2023745	2031332
Size / mm	0.22 x 0.17 x 0.07	0.41 x 0.21 x 0.15
Empiric Formula	C ₄₃ H _{58.68} B ₂ N	C ₃₁ H ₁₇ B ₂ F ₁₈ N, 0.46(C ₁ H ₁ Cl ₃)
M / g mol⁻¹	611.21	821.34
Crystal system	monoclinic	monoclinic
Space group	P 21/c	P 1 21/n 1
a / Å	25.774(3)	20.0781(7)
b / Å	17.2923(18)	7.6006(3)
c / Å	17.0060(18)	22.0644(7)
α / deg	90	90
β / deg	92.749(3)	100.5340(10)
γ / deg	90	90
V / Å³	7570.7(14)	3310.4(2)
Z	8	4
μ / mm⁻¹	0.060	0.273
T / K	173	100
θ_{min,max}	0.79, 25.37	2.52, 25.88
Completeness	99.8	99.8
Reflections: total / independent	13877, 7180	7036, 5352
R_{int}	0.1480	0.0374
Final R1 and wR2	0.0694, 0.1824	0.0663, 0.1801
Largest peak and hole / e Å⁻³	0.386, -0.291	1.366, -0.731
ρ_{calc} / g cm⁻³	1.072	1.648

Computational methods. Optimizations were carried out with the TURBOMOLE V7.0.1 program package.^[29] NICS Scan,^[30] NICS XY-Scan^[31] and ACID^[32] calculations were carried out using the Gaussian 09 program package, revision D.01.^[33] Becke's three parameter exchange-correlation hybrid functional B3LYP^[34] was used in combination with the 6-31+G* basis set in Gaussian 09 and the valence-double- ζ basis set def2-SV(P)^[35] in TURBOMOLE. The empirical dispersion correction DFT-D3 by Grimme was used including the three-body term and with Becke-Johnson (BJ) damping.^[36] The stationary points were

characterized as minima by an analytical vibrational frequency calculation,^[37] which revealed the absence of imaginary frequencies. Vertical singlet excitations were calculated by means of time-dependent DFT.^[38]

4.1.5 References

- [‡] M. Crumbach, O. Ayhan, L. Fritze, J.n A. P. Sprenger, L. Zapf, M. Finze, H. Helten, *Chem. Commun.* **2021**, *57*, 2408-2411.
- [1] D. H. Reid, *Q. Rev. Chem. Soc.*, 1965, **19**, 274; (b) K. Goto, T. Kubo, K. Yamamoto, K. Nakasuji, K. Sato, D. Shiomi, T. Takui, M. Kubota, T. Kobayashi, K. Yakusi and J. Ouyang, *J. Am. Chem. Soc.*, 1999, **121**, 1619; (c) K. Kamada, K. Ohta, T. Kubo, A. Shimizu, Y. Morita, K. Nakasuji, R. Kishi, S. Ohta, S.-i. Furukawa, H. Takahashi and M. Nakano, *Angew. Chem. Int. Ed.*, 2007, **46**, 3544; (d) Y. Morita, S. Suzuki, K. Sato and T. Takui, *Nat. Chem.*, 2011, **3**, 197; (e) Z. Mou, K. Uchida, T. Kubo and M. Kertesz, *J. Am. Chem. Soc.*, 2014, **136**, 18009; (f) T. Kubo, *Chem. Rec.*, 2015, **15**, 218; (g) K. Uchida, S. Ito, M. Nakano, M. Abe and T. Kubo, *J. Am. Chem. Soc.*, 2016, **138**, 2399; (h) K. Uchida, Z. Mou, M. Kertesz and T. Kubo, *J. Am. Chem. Soc.*, 2016, **138**, 4665; (i) A. Mukherjee, S. C. Sau and S. K. Mandal, *Acc. Chem. Res.*, 2017, **50**, 1679.
- [2] R. C. Haddon, *Nature*, 1975, **256**, 394; (b) K. Tagami, L. Wang and M. Tsukada, *Nano Lett.*, 2004, **4**, 209; (c) S. K. Pal, M. E. Itkis, F. S. Tham, R. W. Reed, R. T. Oakley and R. C. Haddon, *Science*, 2005, **309**, 281; (d) S. K. Mandal, M. E. Itkis, X. Chi, S. Samanta, D. Lidsky, R. W. Reed, R. T. Oakley, F. S. Tham and R. C. Haddon, *J. Am. Chem. Soc.*, 2005, **127**, 8185; (e) Y. Morita, S. Suzuki, K. Fukui, S. Nakazawa, H. Kitagawa, H. Kishida, H. Okamoto, A. Naito, A. Sekine, Y. Ohashi, M. Shiro, K. Sasaki, D. Shiomi, K. Sato, T. Takui and K. Nakasuji, *Nat. Mater.*, 2008, **7**, 48; (f) Y. Morita, S. Nishida, T. Murata, M. Moriguchi, A. Ueda, M. Satoh, K. Arifuku, K. Sato and T. Takui, *Nat. Mater.*, 2011, **10**, 947; (g) I. Ratera and J. Veciana, *Chem. Soc. Rev.*, 2012, **41**, 303; (h) K. V. Raman, A. M. Kamerbeek, A. Mukherjee, N. Atodiresei, T. K. Sen, P. Lazić, V. Caciuc, R. Michel, D. Stalke, S. K. Mandal, S. Blügel, M. Münzenberg and J. S. Moodera, *Nature*, 2013, **493**, 509; (i) A. Ueda, S. Suzuki, K. Yoshida, K. Fukui, K. Sato, T. Takui, K. Nakasuji and Y. Morita, *Angew. Chem. Int. Ed.*, 2013, **52**, 4795.
- [3] For azaphenalene derivatives, see, e.g.: (a) Y. Morita, T. Aoki, K. Fukui, S. Nakazawa, K. Tamaki, S. Suzuki, A. Fuyuhiro, K. Yamamoto, K. Sato, D. Shiomi, A. Naito, T. Takui and K. Nakasuji, *Angew. Chem. Int. Ed.*, 2002, **41**, 1793; (b) S. Zheng, J. Lan, S. I. Khan and Y. Rubin, *J. Am. Chem. Soc.*, 2003, **125**, 5786; (c) R. Berger, A. Giannakopoulos, P. Ravat, M. Wagner, D. Beljonne, X. Feng and K. Müllen, *Angew. Chem. Int. Ed.*, 2014, **53**, 10520; (d) J. Y. Koo, Y. Yakiyama, G. R. Lee, J. Lee, H. C. Choi, Y. Morita and M. Kawano, *J. Am. Chem. Soc.*, 2016, **138**, 1776.

- [4] A. Narita, X.-Y. Wang, X. Feng and K. Müllen, *Chem. Soc. Rev.*, 2015, **44**, 6616; (b) M. Stępień, E. Gońska, M. Żyła and N. Sprutta, *Chem. Rev.*, 2017, **117**, 3479.
- [5] For reviews on B-doped organic compounds, see: (a) H. Zhao, L. A. Leamer and F. P. Gabbaï *Dalton Trans.*, 2013, **42**, 8164–8178; (b) A. Wakamiya and S. Yamaguchi, *Bull. Chem. Soc. Jpn.*, 2015, **88**, 1357–1377; (c) A. Escande and M. J. Ingleson, *Chem. Commun.*, 2015, **51**, 6257–6274; (d) L. Ji, S. Griesbeck and T. B. Marder, *Chem. Sci.*, 2017, **8**, 846–863; (e) E. von Grotthuss, A. John, T. Kaese and M. Wagner, *Asian J. Org. Chem.*, 2018, **7**, 37–53; (f) H. Helten, *Chem. Asian J.*, 2019, **14**, 919–935; (g) S. K. Mellerup and S. Wang, *Chem. Soc. Rev.*, 2019, **48**, 3537–3549; (h) X. Yin, J. Liu and F. Jäkle, *Chem. Eur. J.*, 2020, DOI: 10.1002/chem.202003481.
- [6] See for BN-doping: (a) Z. Liu and T. B. Marder, *Angew. Chem. Int. Ed.*, 2008, **47**, 242; (b) M. J. D. Bosdet and W. E. Piers, *Can. J. Chem.*, 2009, **87**, 8; (c) P. G. Campbell, A. J. V. Marwitz and S.-Y. Liu, *Angew. Chem. Int. Ed.*, 2012, **51**, 6074; (d) X.-Y. Wang, J.-Y. Wang and J. Pei, *Chem. Eur. J.*, 2015, **21**, 3528; (e) D. Bonifazi, F. Fasano, M. M. Lorenzo-Garcia, D. Marinelli, H. Oubaha and J. Tasserou, *Chem. Commun.*, 2015, **51**, 15222; (f) M. M. Morgan and W. E. Piers, *Dalton Trans.*, 2016, **45**, 5920; (g) H. Helten, *Chem. Eur. J.*, 2016, **22**, 12972; (h) G. Bélanger-Chabot, H. Braunschweig and D. K. Roy, *Eur. J. Inorg. Chem.*, 2017, 4353; (i) Z. X. Giustra and S.-Y. Liu, *J. Am. Chem. Soc.*, 2018, **140**, 1184; (j) C. R. McConnell and S.-Y. Liu, *Chem. Soc. Rev.*, 2019, **48**, 3436; for non-aromatic BN isosteres, see: (k) A. Staibitz, A. P. M. Robertson, M. E. Sloan and I. Manners, *Chem. Rev.*, 2010, **110**, 4023.
- [7] R. J. Kahan, D. L. Crossley, J. Cid, J. E. Radcliffe and M. J. Ingleson, *Angew. Chem. Int. Ed.*, 2018, **57**, 8084; (b) J. M. Farrell, C. Mützel, D. Bialas, M. Rudolf, K. Menekse, A.-M. Krause, M. Stolte and F. Würthner, *J. Am. Chem. Soc.*, 2019, **141**, 9096; (c) K. Hirano, K. Morimoto, S. Fujioka, K. Miyamoto, A. Muranaka and M. Uchiyama, *Angew. Chem. Int. Ed.*, 2020, **59**, 21448.
- [8] For larger PAHs containing boraphenalene subunits, see: (a) K. Schickedanz, T. Trageser, M. Bolte, H.-W. Lerner and M. Wagner, *Chem. Commun.*, 2015, **51**, 15808; (b) V. M. Hertz, H.-W. Lerner and M. Wagner, *Org. Lett.*, 2015, **17**, 5240; (c) F. Miyamoto, S. Nakatsuka, K. Yamada, K.-I. Nakayama and T. Hatakeyama, *Org. Lett.*, 2015, **17**, 6158.
- [9] For boraphenalene derivatives with further heteroatoms incorporated, see: (a) T. Katayama, S. Nakatsuka, H. Hirai, N. Yasuda, J. Kumar, T. Kawai and T. Hatakeyama, *J. Am. Chem. Soc.*, 2016, **138**, 5210; (b) X.-Y. Wang, A. Narita, W. Zhang, X. Feng and K. Müllen, *J. Am. Chem. Soc.*, 2016, **138**, 9021; (c) M. Numano, N. Nagami, S. Nakatsuka, T. Katayama, K. Nakajima, S. Tatsumi, N. Yasuda and T. Hatakeyama, *Chem. Eur. J.*, 2016, **22**, 11574; (d) X. Wang, F. Zhang, K. S. Schellhammer, P. Machata, F. Ortmann, G. Cuniberti, Y. Fu, J. Hunger, R. Tang, A. A. Popov, R. Berger, K. Müllen and X. Feng, *J. Am. Chem. Soc.*, 2016, **138**, 11606; (e) X.-Y. Wang, J. I. Urgel, G. B. Barin, K. Eimre, M. Di Giovannantonio, A. Milani, M. Tommasini, C. A. Pignedoli, P. Ruffieux, X. Feng, R. Fasel, K. Müllen and A. Narita, *J. Am. Chem. Soc.*, 2018, **140**, 9104; (f) D.-T. Yang, T. Nakamura, Z. He, X.

- Wang, A. Wakamiya, T. Peng and S. Wang, *Org. Lett.*, 2018, **20**, 6741; (g) Y. Fu, K. Zhang, E. Dmitrieva, F. Liu, J. Ma, J. J. Weigand, A. A. Popov, R. Berger, W. Pisula, J. Liu and X. Feng, *Org. Lett.*, 2019, **21**, 1354; (h) P. Qiang, Z. Sun, M. Wan, X. Wang, P. Thiruvengadam, C. Bingi, W. Wei, W. Zhu, D. Wu and F. Zhang, *Org. Lett.*, 2019, **21**, 4575; (i) Z. Sun, C. Yi, Q. Liang, C. Bingi, W. Zhu, P. Qiang, D. Wu and F. Zhang, *Org. Lett.*, 2020, **22**, 209; (j) Y. Fu, H. Yang, Y. Gao, L. Huang, R. Berger, J. Liu, H. Lu, Z. Cheng, S. Du, H.-J. Gao and X. Feng, *Angew. Chem. Int. Ed.*, 2020, **59**, 8873; (k) J. Tasseroul, M. M. Lorenzo-Garcia, J. Dosso, F. Simon, S. Velari, A. de Vita, P. Tecilla and D. Bonifazi, *J. Org. Chem.*, 2020, **85**, 3454.
- [10] For our work on BN-containing polymers, see: (a) T. Lorenz, A. Lik, F. A. Plamper and H. Helten, *Angew. Chem. Int. Ed.*, 2016, **55**, 7236; (b) O. Ayhan, T. Eckert F. A. Plamper and H. Helten, *Angew. Chem. Int. Ed.*, 2016, **55**, 13321; (c) T. Lorenz, M. Crumbach, T. Eckert, A. Lik and H. Helten, *Angew. Chem. Int. Ed.*, 2017, **56**, 2780.
- [11] M. J. S. Dewar and R. Jones, *Tetrahedron Lett.*, 1968, **9**, 2707.
- [12] H. Noda, M. Furutachi, Y. Asada, M. Shibasaki and N. Kumagai, *Nat. Chem.*, 2017, **9**, 571; (b) D. Prieschl, M. Arrowsmith, M. Dietz, A. Rempel, M. Müller and H. Braunschweig, *Chem. Commun.*, 2020, **56**, 5681.
- [13] H. Wei, Y. Liu, T. Y. Gopalakrishna, H. Phan, X. Huang, L. Bao, J. Guo, J. Zhou, S. Luo, J. Wu and Z. Zeng, *J. Am. Chem. Soc.*, 2017, **139**, 15760.
- [14] M. Fingerle, C. Maichle-Mössmer, S. Schundelmeier, B. Speiser and H. F. Bettinger, *Org. Lett.*, 2017, **19**, 4428.
- [15] Hergel, H. Pritzkow and W. Siebert, *Angew. Chem. Int. Ed.*, 1994, **33**, 1247.
- [16] S. Scholz, J. G. Massoth, M. Bursch, J.-M. Mewes, T. Hetzke, B. Wolf, M. Bolte, H.-W. Lerner, S. Grimme and M. Wagner, *J. Am. Chem. Soc.*, 2020, **142**, 11072.
- [17] A. Stanger, *J. Org. Chem.*, 2006, **71**, 883; (b) R. Gershoni-Poranne and A. Stanger, *Chem. Eur. J.*, 2014, **20**, 5673; (c) R. Herges and D. Geuenich, *J. Phys. Chem. A*, 2001, **105**, 3214; (d) D. Geuenich, K. Hess, F. Köhler and R. Herges, *Chem. Rev.*, 2005, **105**, 3758.
- [18] The maxima at -2.0 and 2.0 Å are caused by the Mes-*o*-methyl groups.
- [19] W. Gerrard, H. R. Hudson, E. F. Mooney, *J. Chem. Soc.* **1960**, 5168–5172.
- [20] J. van Soolingen, R.-J. de Lang, R. den Besten, P. A. A. Klusener, N. Veldman, A. L. Spek, L. Brandsma, *Synth. Commun.* **1995**, **25**, 1741–1744.
- [21] A. Hergel, H. Pritzkow, W. Siebert, *Angew. Chem. Int. Ed.* **1994**, **33**, 1247–1248; *Angew. Chem.* **1994**, **106**, 1342–1343.
- [22] B. M. Lindkey, B. P. Jacobs, S. N. MacMillan, P. T. Wolczanski, *Chem. Commun.* **2016**, **52**, 3891–3894.
- [23] K. Ruhlandt-Senge, J. J. Ellison, R. J. Wehmschulte, F. Pauer, P. P. Power, *J. Am. Chem. Soc.* **1993**, **115**, 11353–11357.
- [24] G. E. Carr, R. D. Chambers, T. F. Holmes, D. G. Parker, *J. Organomet. Chem.* **1987**, **325**, 13–23.
- [25] G. M. Sheldrick, *Acta Crystallogr. A* **2015**, **71**, 3–8.
- [26] G. M. Sheldrick, *Acta Crystallogr. A* **2008**, **64**, 112–122.
- [27] C. B. Hubschle, G. M. Sheldrick, B. Dittrich, *J. Appl. Crystallogr.* **2011**, **44**, 1281–1284.

- [28] O. V. Dolomanov, L. J. Bourhis, R. J. Gildea, J. A. K. Howard, H. Puschmann, *J. Appl. Crystallogr.* **2009**, *42*, 339–341.
- [29] R. Ahlrichs, M. Bär, M. Häser, H. Horn, C. Kölmel, *Chem. Phys. Lett.* **1989**, *162*, 165–169.
- [30] A. Stanger, *J. Org. Chem.* **2006**, *71*, 883–893.
- [31] R. Gershoni-Poranne, A. Stanger, *Chem. Eur. J.* **2014**, *20*, 5673–5688.
- [32] D. Geuenich, K. Hess, F. Köhler, R. Herges, *Chem. Rev.* **2005**, *105*, 3758–3772.
- [33] Gaussian 09, Revision D.01, M. J. Frisch, G. W. Trucks, H. B. Schlegel, G. E. Scuseria, M. A. Robb, J. R. Cheeseman, G. Scalmani, V. Barone, G. A. Petersson, H. Nakatsuji, X. Li, M. Caricato, A. Marenich, J. Bloino, B. G. Janesko, R. Gomperts, B. Mennucci, H. P. Hratchian, J. V. Ortiz, A. F. Izmaylov, J. L. Sonnenberg, D. Williams-Young, F. Ding, F. Lipparini, F. Egidi, J. Goings, B. Peng, A. Petrone, T. Henderson, D. Ranasinghe, V. G. Zakrzewski, J. Gao, N. Rega, G. Zheng, W. Liang, M. Hada, M. Ehara, K. Toyota, R. Fukuda, J. Hasegawa, M. Ishida, T. Nakajima, Y. Honda, O. Kitao, H. Nakai, T. Vreven, K. Throssell, J. A. Montgomery, Jr., J. E. Peralta, F. Ogliaro, M. Bearpark, J. J. Heyd, E. Brothers, K. N. Kudin, V. N. Staroverov, T. Keith, R. Kobayashi, J. Normand, K. Raghavachari, A. Rendell, J. C. Burant, S. S. Iyengar, J. Tomasi, M. Cossi, J. M. Millam, M. Klene, C. Adamo, R. Cammi, J. W. Ochterski, R. L. Martin, K. Morokuma, O. Farkas, J. B. Foresman, D. J. Fox, *Gaussian Inc., Wallingford CT*, **2016**.
- [34] a) P. A. M. Dirac, *Proc. R. Soc. London, Ser. A* **1929**, *123*, 714–733; b) J. C. Slater, *Phys. Rev.* **1951**, *81*, 385–390; c) A. D. Becke, *Phys. Rev. A* **1988**, *38*, 3098–3100; d) C. Lee, W. Yang, R. G. Parr, *Phys. Rev. B* **1988**, *37*, 785–89; e) A. D. Becke, *J. Chem. Phys.* **1993**, *98*, 5648–5652.
- [35] A. Schäfer, H. Horn, R. Ahlrichs, *J. Chem. Phys.* **1992**, *97*, 2571–2577.
- [36] a) S. Grimme, J. Antony, S. Ehrlich, H. Krieg, *J. Chem. Phys.* **2010**, *132*, 154104; b) S. Grimme, S. Ehrlich, L. J. Goerigk, *J. Comput. Chem.* **2011**, *32*, 1456–1465.
- [37] a) P. Deglmann, F. Furche, R. Ahlrichs, *Chem. Phys. Lett.* **2002**, *362*, 511–518; b) P. Deglmann, F. Furche, *J. Chem. Phys.* **2002**, *117*, 9535–9538.
- [38] a) R. Bauernschmitt, R. Ahlrichs, *Chem. Phys. Lett.* **1996**, *256*, 454–464; b) R. Bauernschmitt, R. Ahlrichs, *J. Chem. Phys.* **1996**, *104*, 9047–9052; c) F. Furche, D. Rappoport, *Density functional methods for excited states: equilibrium structure and electronic spectra*. In M. Olivucci, Ed., *Computational Photochemistry*, Vol. 16 of *Computational and Theoretical Chemistry*, ch. III., Elsevier, Amsterdam, **2005**.

4.2 Dithiophene-Fused Oxadiborepins and Azadiborepins: A New Class of Highly Fluorescent Heteroaromatics

The following section is slightly modified and reproduced from published article^[‡] with permission from Wiley-VCH.

Access to dithiophene-fused oxadiborepins and the first azadiborepins via a modular synthesis route is presented. The new compounds emit intense blue light, some of which with fluorescence quantum yields close to unity. Cyclic voltammetry (CV) revealed electrochemically reversible one-electron reduction processes. Via in-depth theoretical investigations using nucleus-independent chemical shift (NICS) scans and anisotropy of the induced current density (ACID) calculations, we demonstrate that the novel 1,2,7-azadiborepin ring has weak aromatic character.

4.2.1 Introduction

π -Conjugated organic materials have received tremendous attention in the past decades due to applications thereof in organic (opto)electronics, sensors, and biomedicine.^[1] The current focus in the design of new materials for such purposes has shifted towards electron-deficient building blocks, which, in the past, have been markedly less well developed compared with their electron-rich counterparts.^[2] The doping of π -conjugated frameworks with trivalent boron has recently emerged as a powerful tool for producing strongly electron-accepting materials; a result of the incorporation of the vacant p orbital of boron in the π system.^[3] 2,2'-Bithiophene-3,3'-dicarboximide (**BTI**, **A**, Figure 4.2.1) is a representative example of an electron-deficient polycyclic organic building block that has been successfully used in electron-transporting materials.^[4-6] It features the effectively π -accepting imide moiety $[-\text{C}(=\text{O})-\text{NR}-\text{C}(=\text{O})-]$.^[7] Borylene groups ($>\text{B}-\text{R}$) share some common features with carbonyl groups ($>\text{C}=\text{O}$): both of them constitute a trigonal-planar linking site with bond angles of approximately 120° , and they both have pronounced π -acceptor character. Considering this analogy, we decided to target the dithiophene-fused azadiborepin system **B**, which is formally derived from **A** by substitution of the $\text{C}=\text{O}$ with $\text{B}-\text{Ar}$ units. The latter should offer the additional opportunity of fine-tuning of the compound's properties through the variable aryl group (Ar). The substance class **B** is unknown thus far, and so is the parent seven-membered azadi-

borepin ring system **D**. It contains six π electrons in the cycle and is therefore potentially aromatic. Heteroaromaticity in boron-containing heterocycles has fascinated experimental and theoretical researchers for a long time.^[8,9] Borepin (**E**), for example, comprises a seven-membered ring with one boron atom and six π electrons. It has been ascribed substantial aromaticity.^[9] Replacing one or more C=C pairs in mono- or polycyclic aromatic hydrocarbons (PAHs) by their isoelectronic and isosteric B=N units has brought about a wide range of novel heteroaromatic compounds, many of which show intriguing properties and functions.^[10-11] Surprisingly, PAHs comprising 3-center 2- π -electron B–N–B moieties have been explored rather scarcely thus far.^[12-15] Zeng *et al.* recently presented the BNB-phenalenyl analogue **F**.^[12] Steric congestion between the two *B*-bonded phenyl groups causes significant distortion of its tricyclic scaffold from planarity. Detailed theoretical investigations revealed that the NBC₄ rings in **F** are weakly aromatic. Bettinger and co-workers reported the π -extended BNB-doped PAH **G**.^[13] Computations on this species showed that its BN-containing rings are nonaromatic, while aromatic character is confined to the three peripheral carbonaceous rings (also here, the two *B*–Mes groups induce some distortion of the PAH plane).

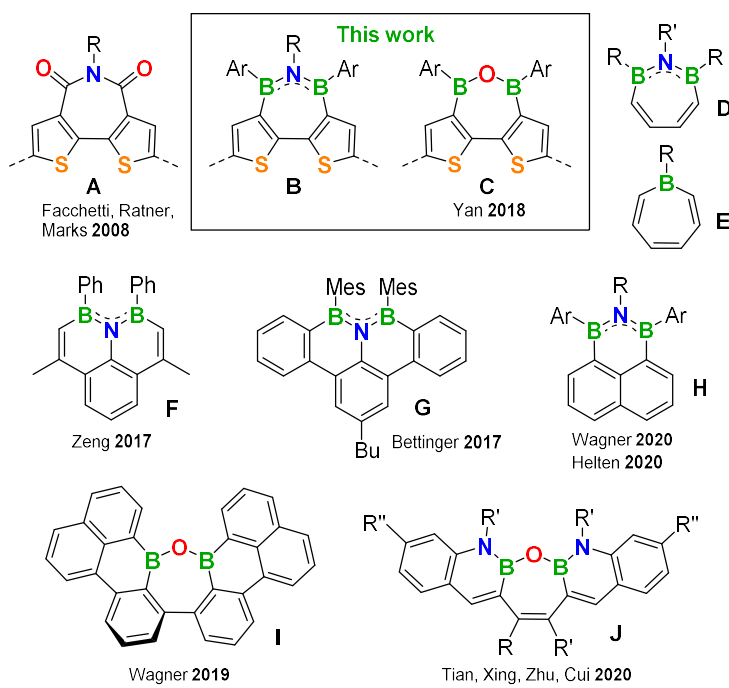


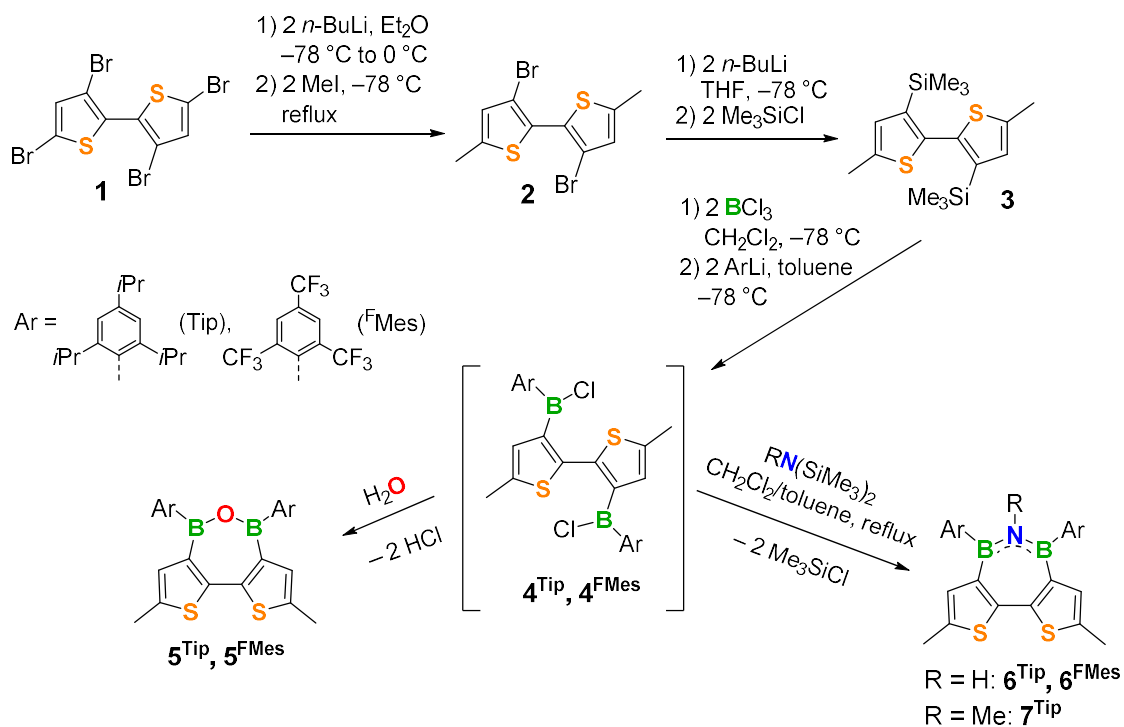
Figure 4.2.1. 2,2'-Bithiophene-3,3'-dicarboximide (BTI, **A**), dithieno[3,2-*c*:2',3'-*e*][1,2,7]azadiborepin (**B**), and dithieno[3,2-*c*:2',3'-*e*][1,2,7]oxadiborepin building blocks (**C**), the parent 1,2,7-azadiborepin (**D**) and borepin (**E**) ring systems, BNB-doped PAHs (**F** – **H**), and oxadiborepin-containing PAHs (**I** and **J**).

Wagner's and our group independently explored the BNB-doped phenalenyl system **H**, wherein such steric stress is effectively prevented.^[14,15] Via in-depth theoretical studies using

nucleus-independent chemical shift (NICS) scans and anisotropy of the induced current density (ACID) calculations, we showed that the B_2NC_3 -ring in **H** is slightly aromatic.^[15] Recently, Yan *et al.* reported the synthesis of dithiophene-fused oxadiborepin derivatives **C**.^[16] The tricyclic compound with $\text{Ar} = {}^{\text{F}}\text{Mes}$ (2,4,6-tris(trifluoromethyl)phenyl) was serendipitously obtained in an attempt to prepare a dithienoborole from 3,3'-dilithio-2,2'-bithiophene and BCl_3 and subsequent reaction with ${}^{\text{F}}\text{MesLi}$. The unexpected product **C** formed through hydrolysis during the workup procedure. Only few further examples of compounds featuring oxadiborepin as a substructure have been reported in the literature.^[17-20] The first one, described by Wagner and co-workers in 2011, was a bisboronic acid anhydride.^[17] Recently, they presented the BOB-doped PAH **I**.^[18] Due to steric congestion between the annulated benzene rings, this species deviates significantly from planarity. Tian, Xing, Zhu, Cui *et al.* recently presented BNO-doped PAHs **J**,^[20] which feature a planar framework. This system is actually described as a bis-BN-naphthalene-fused oxepin.

4.2.2 Results and Discussion

Herein, we present the systematic synthesis of dithiophene-fused oxadiborepin and the first azadiborepin derivatives from a common precursor. Extensive theoretical investigations aid in elucidating the aromatic character of the individual rings of these strongly blue light emitting species. As we were unable to obtain a selective reaction towards the desired products if the bithiophene starting material was unsubstituted in the positions 5 and 5', we decided to block these positions with methyl groups. Selective 5,5'-dilithiation of 3,3',5,5'-tetrabromo-2,2'-bithiophene (**1**) was accomplished with *n*-BuLi in Et_2O , and subsequent reaction with MeI afforded compound **2** in nearly quantitative yield (Scheme 4.2.1). Treating **2** with two equivalents of *n*-BuLi, followed by addition of Me_3SiCl , resulted in formation of the disilylated compound **3**, which served as the precursor for all further transformations. Bisborylation of **3** with BCl_3 and mono-arylation of both introduced dichloroboryl groups with ArLi ($\text{Ar} = \text{Tip}$, ${}^{\text{F}}\text{Mes}$) was performed sequentially without isolating the intermediates. Further *in situ* reaction of **4^{Tip}** and **4^{FMes}** with H_2O gave dithienooxadiborepins **5^{Tip}** and **5^{FMes}** in 75% yield each. For the synthesis of dithienoazadiborepins **6^{Tip}**, **6^{FMes}**, and **7^{Tip}**, toluene solutions of **4^{Tip}** and **4^{FMes}** were treated with $\text{HN}(\text{SiMe}_3)_2$ or $\text{MeN}(\text{SiMe}_3)_2$, respectively; CH_2Cl_2 was added to increase the polarity, and refluxing the resulting mixtures for about one day gave the novel dithienoazadiborepins **6^{Tip}**, **6^{FMes}**, and **7^{Tip}** in moderate yields.



Scheme 4.2.1. Synthesis of dithienooxa- and azadiborepins **5**, **6** and **7**.

All products proved to be fully stable towards air and moisture and could be purified by column chromatography at standard ambient conditions. They were unambiguously identified by multinuclear NMR spectroscopy and mass spectrometry, and elemental analyses gave satisfactory results. Compounds **5^{Tip}** and **7^{Tip}** were additionally characterized by single-crystal X-ray diffractometry (Figure 4.2.2). In the solid-state structure, both species feature a quasi-planar tricycle, with the Tip groups being almost perpendicularly oriented to that plane. The seven-membered rings are close to planar, as suggested by the sums of their interior angles, which are 898.1° (**5^{Tip}**) and 899.3° (**7^{Tip}**), respectively. The oxadiborepin shows a slight twist of 7.2(3)° between the B-O-B moiety and the best plane through the ring carbon atoms C(4)-C(5)-C(6)-C(7). The B-O-B bond angle in **5^{Tip}** amounts to 137.05(17)° (cf. 134.8(10)° in **I**),^[18] and is much larger than the B-N-B angle in **7^{Tip}** (129.7(3)°). This is accompanied by a slightly shorter distance between the thiophene units in the latter [C(2)-C(3), 1.432(5) Å in **7^{Tip}** vs. C(5)-C(6), 1.449(3) Å in **5^{Tip}**]. The twist angles between the thiophene rings are 7.00(10) (**5^{Tip}**) and 11.4(2)° (**7^{Tip}**), respectively. The B-N bond lengths in **7^{Tip}** are 1.434(5) and 1.445(5) Å, which is in the same range with those in derivatives of **H**^[14,15] and typical BN aromatics,^[10] but shorter than in **F** (1.463(1) Å)^[12] and **G** (1.46 Å).^[13]

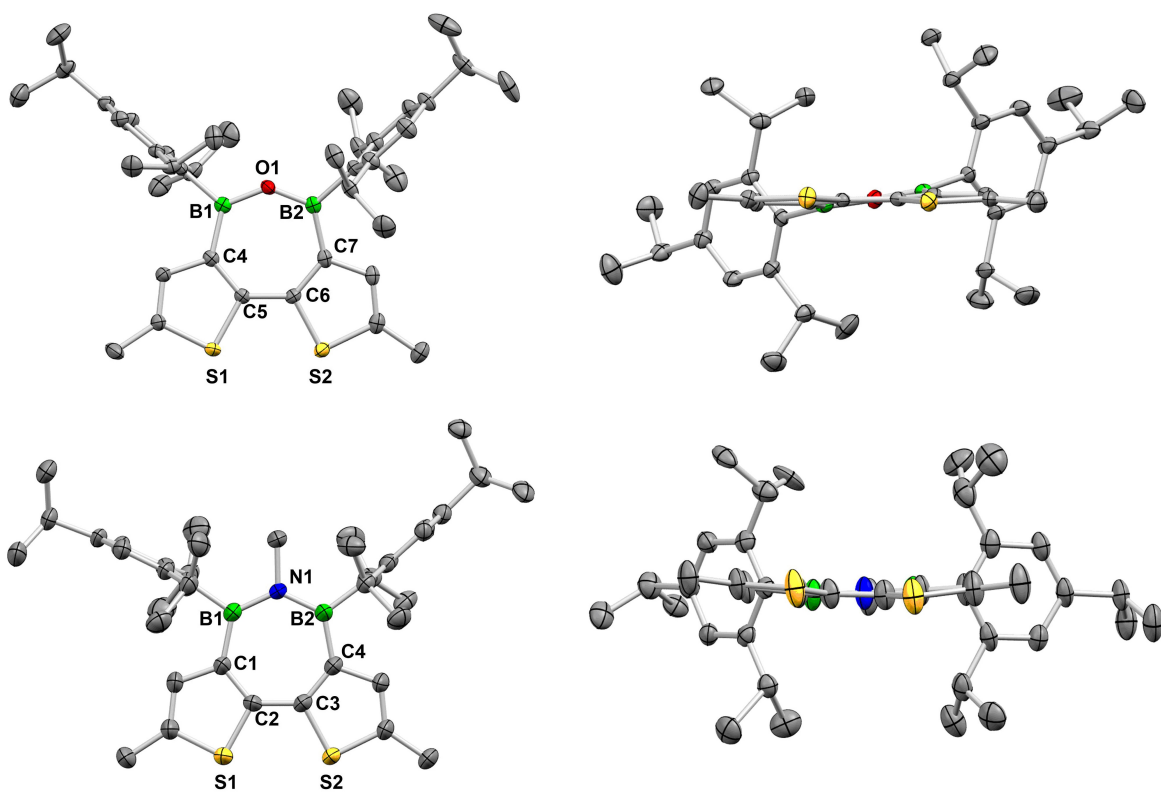


Figure 4.2.2: Molecular structures of $\mathbf{5}^{\text{Tip}}$ and $\mathbf{7}^{\text{Tip}}$ (with views perpendicular and parallel to the polycyclic plane) in the solid state by single-crystal X-ray diffraction (H-atoms and disorder of a Tip group in $\mathbf{7}^{\text{Tip}}$ omitted for clarity).

The UV-vis absorption spectra for $\mathbf{5}^{\text{Tip}}$, $\mathbf{6}^{\text{Tip}}$, $\mathbf{7}^{\text{Tip}}$, $\mathbf{5}^{\text{FMeS}}$ and $\mathbf{6}^{\text{FMeS}}$ in CH_2Cl_2 display one structured low-energy band each with a maximum at 366 – 376 nm (Figure 4.2.3a and Table 4.2.1). According to our TD-DFT calculations (level: B3LYP-D3(BJ)/def2-SV(P)), this is assigned to a $\pi-\pi^*$ transition involving the HOMO and the LUMO of the molecules (Figure 4.2.3c). Both orbitals are fully delocalized over the tricyclic plane, and both include the two boron centers. The O or N atoms contribute to the LUMOs, while in the HOMOs there is a nodal plane at the same position. The calculated excitation wavelengths are in excellent agreement with the experimental data. These show a marginal bathochromic shift of the absorption maximum (by 6 – 8 nm) upon exchanging N(H/Me) by O (cf. $\mathbf{5}^{\text{Tip}}$ vs. $\mathbf{6}^{\text{Tip}}/\mathbf{7}^{\text{Tip}}$, and $\mathbf{5}^{\text{FMeS}}$ vs. $\mathbf{6}^{\text{FMeS}}$). Our calculations reveal that this modification results in a decrease of the frontier orbital energies to a similar extent. Exchange of Tip by ${}^{\text{F}}\text{MeS}$ leads to virtually no shift of the absorption wavelength. This substitution causes an even more pronounced lowering of the energies of both frontier orbitals, to approximately the same extent. All compounds show intense blue fluorescence with exceptionally high quantum efficiencies. Especially in the series of Tip-substituted derivatives, the quantum yields are close to unity.

The Φ_{fl} values for the azadiborepin species are slightly higher than those for their respective oxadiborepin congeners (4 % for $\mathbf{5}^{\text{Tip}}$ vs. $\mathbf{6}^{\text{Tip}}$, and 10 % for $\mathbf{5}^{\text{FMes}}$ vs. $\mathbf{6}^{\text{FMes}}$).

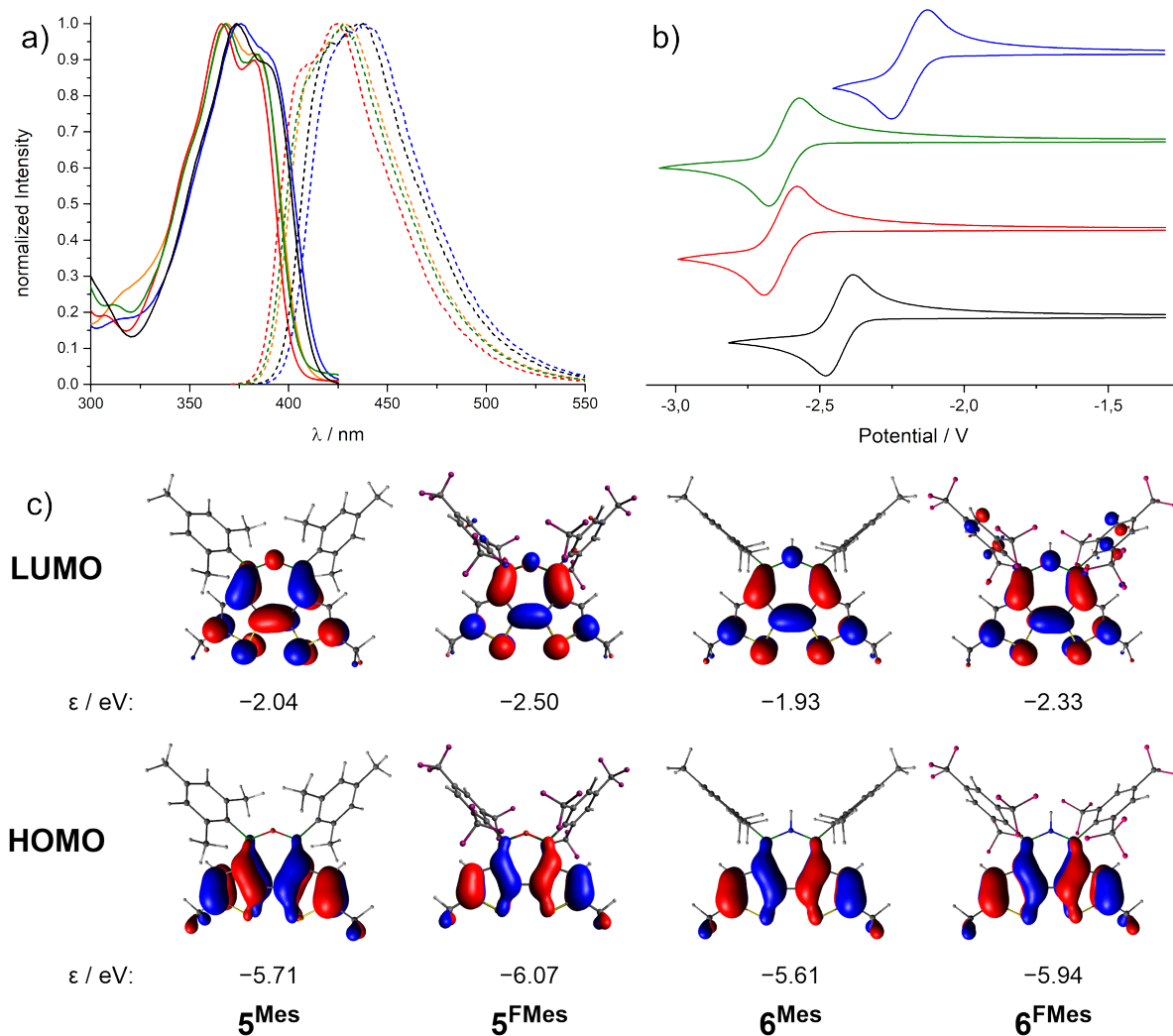


Figure 4.2.3: a) UV-vis absorption (solid lines) and fluorescence (dashed lines) spectra of $\mathbf{5}^{\text{Tip}}$ (black), $\mathbf{6}^{\text{Tip}}$ (red), $\mathbf{7}^{\text{Tip}}$ (green), $\mathbf{5}^{\text{FMes}}$ (blue) and $\mathbf{6}^{\text{FMes}}$ (orange) in CH_2Cl_2 . b) Cyclic voltammograms of $\mathbf{5}^{\text{Tip}}$ (black), $\mathbf{6}^{\text{Tip}}$ (red), $\mathbf{7}^{\text{Tip}}$ (green), and $\mathbf{5}^{\text{FMes}}$ (blue) in THF (vs. $[\text{Cp}_2\text{Fe}]^{0+/+}$, scan rate: 250 mVs⁻¹). c) B3LYP-D3(BJ)/def2-SV(P) calculated frontier orbitals of $\mathbf{5}^{\text{Mes}}$, $\mathbf{5}^{\text{FMes}}$, $\mathbf{6}^{\text{Mes}}$, and $\mathbf{6}^{\text{FMes}}$ (isovalue 0.035).

To the best of our knowledge, it has not been reported if the parent 2,2'-bithiophene-3,3'-dicarboximide (BTI) or the corresponding anhydride show any luminescence; absorption data are available for *N*-substituted derivatives.^[4a] In order to get an estimate of how the optoelectronic properties of our new diborepins compare with those of their organic congeners, we performed TD-DFT calculations additionally for the latter. This revealed that the excitations for BTI and its anhydride are blue-shifted compared to those of **5 – 7** (by 16 – 29 nm). Their frontier orbital energies are slightly lower, but those of the *B*-^FMes derivatives $\mathbf{5}^{\text{FMes}}$ and $\mathbf{6}^{\text{FMes}}$ fall roughly in the same range (cf. Table 4.2.3 and Figures 4.2.7 and 4.2.8).

Table 4.2.1. Photophysical data for **5^{Tip}**, **6^{Tip}**, **7^{Tip}**, **5^{FMes}** and **6^{FMes}**.^[a]

compound	λ_{abs} [nm] ^[b] (calcd. ^[c])	λ_{em} [nm] ^[b,d]	Φ_{fl} ^[e]
5^{Tip}	<u>374</u> , 391 ^[f] (365) ^[g]	421, ^[f] <u>436</u>	0.92
6^{Tip}	<u>366</u> , 382 (360) ^[g]	410, ^[f] <u>424</u>	0.96
7^{Tip}	<u>368</u> , 384 (364) ^[g]	413, ^[f] <u>428</u>	0.94
5^{FMes}	<u>376</u> , 392 ^[f] (373)	428, ^[f] <u>439</u>	0.70
6^{FMes}	<u>369</u> , 383 (370)	417, ^[f] <u>429</u>	0.80

^[a] In CH₂Cl₂. ^[b] Absorption and emission maxima underscored. ^[c] Data from TD-DFT calculations in parentheses. ^[d] Excited at the wavelength of the respective absorption maximum. ^[e] Fluorescence quantum yield determined absolutely with an integrating sphere. ^[f] Shoulder. ^[g] B-Mes- instead of Tip-substituted derivatives were calculated for computational convenience.

Cyclic voltammetry (CV) in THF (Figure 4.2.3b) using [n-Bu₄N][PF₆] as the supporting electrolyte revealed for compounds **5^{Tip}**, **6^{Tip}**, **7^{Tip}**, and **5^{FMes}** one reversible one-electron reduction wave each [$E_{1/2} = -2.43$ (**5^{Tip}**), -2.63 (**6^{Tip}**), -2.62 V (**7^{Tip}**), -2.19 V (**5^{FMes}**)], whereas **6^{FMes}** undergoes an irreversible reduction at $E_{pc} = -2.50$ V. All compounds also show a second reduction process [$E_{pc} = -3.10$ (**5^{Tip}**), -3.32 (**6^{Tip}**), -3.34 (**7^{Tip}**), -2.91 (**5^{FMes}**), and -2.87 V (**6^{FMes}**)], which, however, is irreversible (see Figures 7.2.32 – 7.2.36, appendix 7.2). Consistent with our MO calculations mentioned above, the reduction waves show an anodic shift upon the transition from N(H/Me) to O (**5^{Tip}** vs. **6^{Tip}/7^{Tip}**) and an even stronger shift upon exchanging Tip through ^FMes (cf. **5^{FMes}** vs. **5^{Tip}**). Of special interest was to assess the aromatic character of the novel azadiborepin ring system. First evidence comes from ¹H NMR spectroscopy. The resonance for the NH proton of **6^{Tip}** and **6^{FMes}** was detected at 7.11 and 6.67 ppm, respectively, which is at relatively low field, thus pointing to some degree of aromaticity in this ring. For comparison, the NH proton of the weakly aromatic BNB-phenalenyl **H** with R = H and Ar = Mes by Wagner *et al.* (Figure 4.2.1) resonated at 6.15 ppm.^[14]

To gain deeper insight, we performed NICS-scans^[21a] through the centers of the constituent ring systems (perpendicular to the respective ring, from its center up to 5 Å above the plane; Figures 4.2.4a,c) as well as NICS-X-scans^[21b] (at 1.7 Å above the rings, along the red lines drawn in the respective formulae in Figures 4.2.4b,d). Such calculations provide more

detailed information than NICS(0)/NICS(1) values alone. For computational convenience, we used a model compound, **6^{Mes}**, that carries mesityl (Mes) instead of Tip or ^FMes substituents.

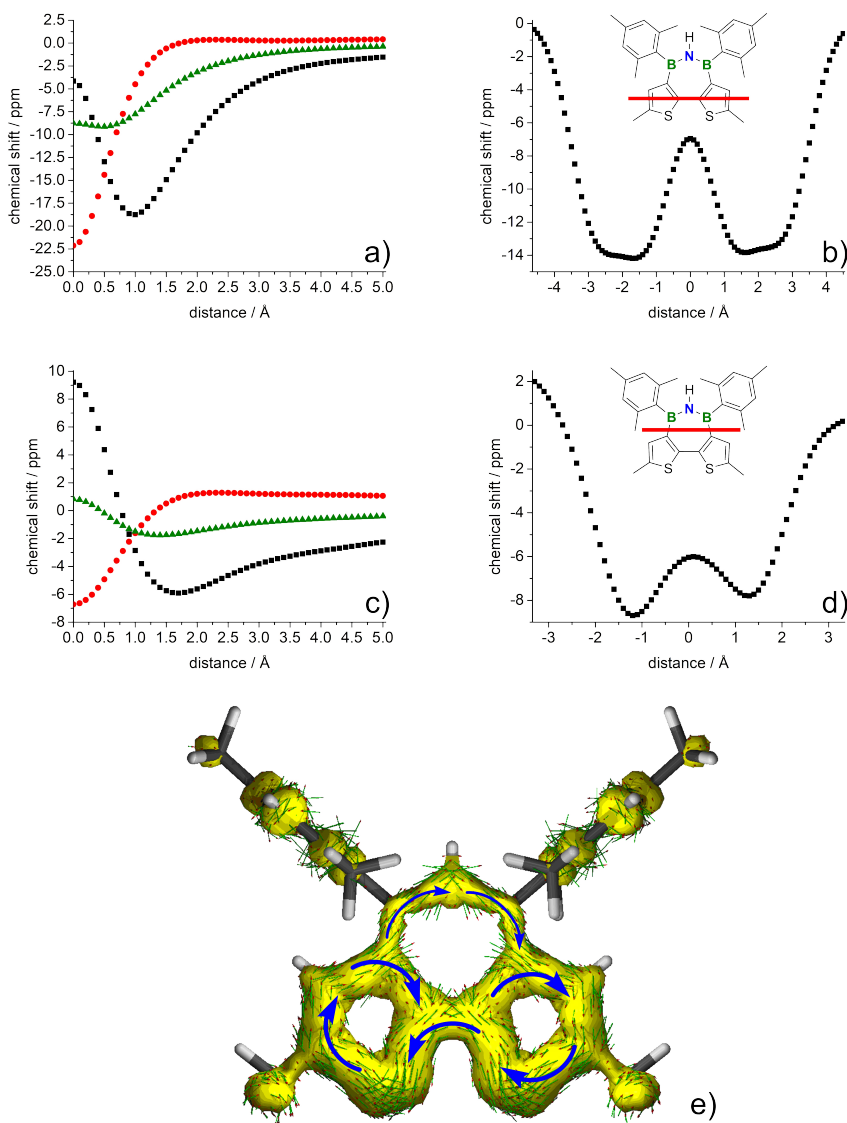


Figure 4.2.4. NICS-scan (thiophene ring (a); hetero ring (c); out-of-plane (black), in-plane (red) component, and isotropic chemical shift (green)), NICS-X-scan (bithiophene (b); hetero ring (d)) and ACID plot (e) (isovalue 0.02) of **6^{Mes}**.

The plot for the NICS-scan through one of the thiophene rings of **6^{Mes}** (a) shows the typical shape of an aromatic system. The isotropic chemical shift is mainly controlled by the out-of-plane component, and both curves show a clear minimum. The NICS-X-scan through the bi-thiophene subunit (b) shows negative chemical shifts throughout the scan. The local maximum at the center results from the C–C-bond connecting the two thiophene rings. Indeed, the corresponding graphs for the azadiborepin ring show similar shapes. In the NICS-scan through this ring (c), the isotropic value is also mainly controlled by the out-of-plane com-

ponent, and both curves show a distinct minimum. In this case, the minima are shallower than in the plot for the thiophene ring, and the values are overall less negative. Also in the NICS-X-scan (d), the chemical shifts are negative throughout.^[22] Overall, these results suggest that the azadiborepin system is weakly aromatic. This interpretation is further substantiated by ACID calculations.^[21c,d] The plot for **6^{Mes}** (e) shows an overall diatropic ring current, which is somewhat more pronounced in the bithiophene subunit.

To learn more about the electronic situation of the novel azadiborepin and the oxadiborepin system, we additionally performed analogous calculations on the parental heterocycles without dithiophene fused. This revealed that these rings are slightly aromatic as such, though the conjugation between boron and carbon is somewhat less effective compared to the dithiophene-fused systems (see appendix 7.2, Figures 7.2.45 – 7.2.50). As anticipated, the aromaticity is more pronounced in the azadiborepin than in the oxadiborepin system (cf. Figure 7.2.45 vs. 7.2.48). For borepin (**E**, R = Mes; Figure 4.2.1), our calculations indicate significantly stronger aromaticity (appendix 7.2, Figures 7.2.51 – 7.2.53), consistent with previous studies on this ring system.^[9]

4.2.3 Conclusion

In conclusion, we have devised a modular synthesis of highly fluorescent dithienooxa- and azadiborepins from a common precursor. Our calculations show that the novel azadiborepin ring system exhibits weak aromatic character. Currently, we are working on the incorporation of the new heterocycles into π -extended materials and exploring the potential thereof for the use in optoelectronic and related applications.

4.2.4 Experimental Section

General procedures. All manipulations before the aqueous workup were performed under an atmosphere of dry argon using standard Schlenk techniques or in an MBraun glovebox. Solvents (dichloromethane, *n*-pentane, *n*-hexane, toluene, THF, and diethylether) were dried and degassed by means of an MBraun SPS-800 solvent purification system. CDCl₃ and C₆D₆ for NMR spectroscopy were dried and degassed at reflux over CaH₂ or Na, respectively, and freshly distilled prior to use. *n*-Butyllithium solutions (1.6 M and 2.5 M in hexanes),

trichloroborane, 2,4,6-triisopropylphenyl bromide, 1,3,5-tris(trifluoromethyl)benzene, 2-bromothiophene, dimethylformamide, iodomethane, heptamethyldisilazane, hexamethyldisilazane, bromine, acetic acid and chloroform were commercially purchased and used as received. Trimethylsilyl chloride was purified by inert-gas distillation. 2,4,6-triisopropylphenyllithium,^[23] 2,4,6-tris-(trifluoromethyl)phenyllithium,^[24] 2,2'-bithiophene,^[25] and 3,3',5,5'-tetrabromo-2,2'-bithiophene^[26] were prepared according to literature procedures. NMR spectra were recorded at 25 °C on a Bruker Avance III HD spectrometer operating at 300 MHz or on a Bruker Avance 500 spectrometer operating at 500 MHz. Chemical shifts were referenced to residual protic impurities in the solvent (¹H) or the deuterio solvent itself (¹³C) and reported relative to external SiMe₄ (¹H, ¹³C, ²⁹Si), BF₃·OEt₂ (¹¹B) or CFCl₃ (¹⁹F) standards. Mass spectra were obtained with the use of a Thermo Scientific Exactive Plus Orbitrap MS system employing atmospheric pressure chemical ionization (APCI). UV-vis spectra were obtained using a Jasco V-630 spectrophotometer. Emission spectra were recorded using an Edinburgh Instruments FLSP920 spectrometer equipped with a double monochromator for both excitation and emission, operating in right-angle geometry mode, and all spectra were fully corrected for the spectral response of the instrument. Fluorescence quantum yields were measured using a calibrated integrating sphere from Edinburgh Instruments combined with the FLSP920 spectrometer described above. Elemental analyses were performed on an Elementar vario MICRO cube elemental analyzer. Cyclic voltammetry experiments were performed using a Gamry Instruments Reference 600 potentiostat. The scans were referenced after the addition of a small amount of ferrocene as internal standard. The potentials are reported relative to the ferrocene/ferrocenium couple.

Crystals suitable for single-crystal X-ray diffraction were selected, coated in perfluoropolyether oil, and mounted on MiTeGen sample holders. Diffraction data were collected on Bruker X8 Apex II 4-circle diffractometers with CCD area detectors using Mo-K α radiation. The crystals were cooled using an Oxford Cryostreams low-temperature device. Data were collected at 100 K. The images were processed and corrected for Lorentz-polarization effects and absorption as implemented in the Bruker software packages. The structures were solved using the intrinsic phasing method (SHELXT)^[27] and Fourier expansion technique. All non-hydrogen atoms were refined in anisotropic approximation, with hydrogen atoms ‘riding’ in idealized positions, by full-matrix least squares against F2 of all data, using SHELXL^[28] software and the SHELXLE graphical user interface.^[29] Other structural information was extracted using OLEX2 software.^[30]

Spectra. All spectra and other result figures are shown in Appendix 7.2.

Synthesis of 3,3'-dibromo-5,5'-dimethyl-2,2'-bithiophene (2). To a solution of 3,3',5,5'-tetrabromo-2,2'-bithiophene (2.39 g, 4.96 mmol) in diethylether (10 mL) was added *n*-butyllithium (1.6 M in hexanes, 6.38 mL, 10.21 mmol) at -78 °C. The mixture was subsequently warmed to 0 °C and stirred for 3 h. Then, neat iodomethane (1.4592 g, 10.28 mmol) was added at -78 °C. The mixture was stirred at ambient temperature overnight, followed by refluxing for 8 h. All volatile components were removed *in vacuo* and the residue was dissolved in DCM. It was washed with water and the organic phase was evaporated to dryness using a rotary evaporator. The product was received as light brownish solid (yield: 98%). ¹H NMR (400 MHz, CDCl₃): δ = 6.74 (s, 2H, 4/4'-CH arom.), 2.49 (s, 6H, 5/5'-CH₃) ppm.

Synthesis of 3,3'-bis(trimethylsilyl)-5,5'-dimethyl-2,2'-bithiophene (3). To a solution of 3,3'-dibromo-5,5'-dimethyl-2,2'-bithiophene (1.3220 g, 3.75 mmol) in THF (10 mL) was added *n*-butyllithium (1.6 M in hexanes, 4.80 mL, 7.68 mmol) at -78 °C. After stirring for 45 min at -78 °C, trimethylsilyl chloride (0.9743 g, 8.97 mmol) was added and stirred for 10 min at -78 °C. The mixture was subsequently warmed to ambient temperature and stirred overnight. Water (10 mL) was added to stop the reaction. The mixture was extracted with water and DCM, the combined organic phases were dried over MgSO₄ and evaporated to dryness using a rotary evaporator. The product was obtained as light yellowish crystals after purification *via* column chromatography (*n*-hexane) (yield: 73%). ¹H NMR (500 MHz, CDCl₃): δ = 6.70 (q, J = 1.00 Hz, 2H, CH arom.), 2.48 (d, J = 1.25 Hz, 6H, 5/5'-CH₃), 0.08 (s, 18H, Si(CH₃)₃) ppm. ¹³C{¹H} NMR (126 MHz, CDCl₃): δ = 141.78 (s, 3/3'-C), 140.62 (s, 2/2'-C), 140.09 (s, 5/5'-C), 130.78 (s, 4/4'-C), 14.90 (s, 5/5'-CH₃), 0.00 (s, Si(CH₃)₃) ppm.

Synthesis of dithieno[3,2-*c*:2',3'-*e*]-*B,B'*-bis(2,4,6-triisopropylphenyl)-[1,2,7]oxadiborepine (5^{Tip}). To a solution of 3,3'-bis(trimethylsilyl)-5,5'-dimethyl-2,2'-bithiophene (0.683 g, 2.02 mmol) in DCM (4 mL) was added trichloroborane (3.34 M in DCM, 3.50 mL, 11.69 mmol) at -78 °C. The mixture was subsequently warmed to ambient temperature and stirred overnight. All volatile components were removed *in vacuo* and the residue was dissolved in toluene (20 mL). A solution of 2,4,6-triisopropylphenyllithium (0.8734 g, 4.15 mmol) in toluene (20 mL) was added at -78 °C. The mixture was subsequently warmed to ambient temperature and stirred for 7 days. After adding water (25 mL) all volatile

components were removed *in vacuo* and the residue was dissolved in DCM. It was washed with water and the organic phase was evaporated to dryness using a rotary evaporator. The product was obtained as colourless crystals after column chromatography (*n*-hexane) and crystallization from DCM/MeOH (yield: 75%). ^1H NMR (500 MHz, CDCl_3): δ = 6.97 (s, 4H, Tip-*CH* arom.), 6.77 (s, 2H, 4/4'-*CH* arom. thiophene), 2.91 (sept, J = 6.94 Hz, 2H, *p*-*CH(CH*₃)₂), 2.69 (sept, J = 6.78 Hz, 4H, *o*-*CH(CH*₃)₂), 2.44 (s, 6H, 5/5'-*CH*₃), 1.30 (d, J = 6.94 Hz, 12H, *p*-*CH(CH*₃)₂), 1.19 (d, J = 6.78 Hz, 12H, *o*-*CH(CH*₃)₂), 1.12 ppm (d, J = 6.78 Hz, 12H, *o*-*CH(CH*₃)₂); $^{11}\text{B}\{\text{H}\}$ NMR (160 MHz, CDCl_3): δ = 45.7 ppm; $^{13}\text{C}\{\text{H}\}$ NMR (126 MHz, CDCl_3): δ = 149.5 (s, quart. *o*-Tip-*C*), 148.9 (s, quart. 2/2'-*C*), 148.4 (s, quart. *p*-Tip-*C*), 139.3 (br, 3/3'-*C-B*), 138.2 (br, Tip-*C-B*), 137.9 (s, quart. 5/5'-*C*), 136.8 (s, 4/4'-*C*), 119.8 (s, *m*-Tip-*C*), 35.0 (s, *o*-*CH(CH*₃)₂), 34.3 (s, *p*-*CH(CH*₃)₂), 24.7 (s, *o*-*CH(CH*₃)₂), 24.6 (s, *o*-*CH(CH*₃)₂), 24.1 (s, *p*-*CH(CH*₃)₂), 14.9 ppm (s, 5/5'-*CH*₃) MS (APCI): m/z (%) = 637.38 ([M+H⁺], 100); elem. anal. calc. (%): C 75.47, H 8.55, S 10.07; found: C 75.61, H 8.72, S 10.07; UV/vis (DCM): $\lambda_{\text{abs,max}} = 265$ ($\varepsilon = 31470$ L mol⁻¹ cm⁻¹), 374 ($\varepsilon = 22341$ L mol⁻¹ cm⁻¹), 391 nm ($\varepsilon = 19628$ L mol⁻¹ cm⁻¹); fluorescence (DCM): $\lambda_{\text{em}1} = 421$, 436 nm (for $\lambda_{\text{ex}1} = 265$, $\lambda_{\text{ex}2} = 374$ or $\lambda_{\text{ex}3} = 391$ nm; $\Phi_f = 92\%$).

Synthesis of dithieno[3,2-*c*:2',3'-*e*]-*B,B'*-bis(2,4,6-triisopropylphenyl)-[1,2,7]aza-diborepine (6^{Tip}**).** To a solution of 3,3'-bis(trimethylsilyl)-5,5'-dimethyl-2,2'-bithiophene (0.674 g, 1.99 mmol) in DCM (4 mL) was added trichloroborane (3.34 M in DCM, 3.50 mL, 11.69 mmol) at -78 °C. The mixture was subsequently warmed to ambient temperature and stirred overnight. All volatile components were removed *in vacuo* and the residue was dissolved in toluene (20 mL). A solution of 2,4,6-triisopropylphenyllithium (0.8768 g, 4.17 mmol) in toluene (20 mL) was added at -78 °C. The mixture was subsequently warmed to ambient temperature and stirred for 7 days. All volatile components were removed *in vacuo* and the residue was dissolved in *n*-pentane (20 mL). The suspension was filtered, all volatile components were removed *in vacuo* and the residue was dissolved in a mixture of DCM and toluene (1:1, 80 mL). Neat hexamethyldisilazane (0.3168 g, 1.96 mmol) was added dropwise and the mixture was stirred for 19 days. All volatile components were removed *in vacuo* and the residue was dissolved in DCM. It was washed with water and the organic phase was evaporated to dryness using a rotary evaporator. The product was obtained as colourless crystals after column chromatography (*n*-hexane) and crystallization from DCM/MeOH (yield: 19 %). ^1H NMR (500 MHz, CDCl_3): δ = 7.11 (br, 1H, NH), 6.99 (s, 4H, Tip-*CH*

arom.), 6.75 (s, 2H, 4/4'-*CH* arom. thiophene), 2.91 (sept, *J* = 6.94 Hz, 2H, *p*-*CH(CH*₃)₂), 2.70 (sept, *J* = 6.78 Hz, 4H, *o*-*CH(CH*₃)₂), 2.44 (s, 6H, 5/5'-*CH*₃), 1.29 (d, *J* = 6.94 Hz, 12H, *p*-*CH(CH*₃)₂), 1.16 (d, *J* = 6.78 Hz, 12H, *o*-*CH(CH*₃)₂); ¹¹B{¹H} NMR (160 MHz, CDCl₃): δ = 43.8 ppm; ¹³C{¹H} NMR (126 MHz, CDCl₃): δ = 149.5 (s, quart. *p*-Tip-*C*), 148.5 (s, quart. *o*-Tip-*C*), 148.3 (s, quart. 2/2'-*C*), 140.2 (br, Tip-*C*-B), 140.1 (br, 3/3'-*C*-B), 137.1 (s, 4/4'-*C*), 120.0 (s, *m*-Tip-*C*), 34.6 (s, *o*-*CH(CH*₃)₂), 34.3 (s, *p*-*CH(CH*₃)₂), 24.7 (s, *o*-*CH(CH*₃)₂), 24.6 (s, *o*-*CH(CH*₃)₂), 24.1 (s, *p*-*CH(CH*₃)₂), 14.9 ppm (s, 5/5'-*CH*₃); MS (APCI): m/z (%) = 636.40 ([M+H⁺], 100); elem. anal. calc. (%): C 75.59, H 8.72, N 2.20, S 10.09; found: C 75.65, H 9.01, N 2.26, S 9.75; UV/vis (DCM): $\lambda_{\text{abs,max}} = 265$ (ε = 34021 L mol⁻¹ cm⁻¹), 366 (ε = 20569 L mol⁻¹ cm⁻¹), 382 nm (ε = 18434 L mol⁻¹ cm⁻¹); fluorescence (DCM): $\lambda_{\text{em1}} = 410$, 424 nm (for $\lambda_{\text{ex1}} = 265$, $\lambda_{\text{ex2}} = 366$ or $\lambda_{\text{ex3}} = 382$ nm; $\Phi_f = 96\%$).

Synthesis of dithieno[3,2-*c*:2',3'-*e*]-*N*-methyl-*B,B'*-bis(2,4,6-triisopropylphenyl)-[1,2,7]-azadiborepine (7^{Tip}). To a solution of 3,3'-bis(trimethylsilyl)-5,5'-dimethyl-2,2'-bithiophene (0.679 g, 2.00 mmol) in DCM (4 mL) was added trichloroborane (3.34 M in DCM, 3.50 mL, 11.69 mmol) at -78 °C. The mixture was subsequently warmed to ambient temperature and stirred overnight. All volatile components were removed *in vacuo* and the residue was dissolved in toluene (20 mL). A solution of 2,4,6-triisopropylphenyllithium (0.8871 g, 4.22 mmol) in toluene (20 mL) was added at -78 °C. The mixture was subsequently warmed to ambient temperature and stirred for 7 days. All volatile components were removed *in vacuo* and the residue was dissolved in *n*-pentane (20 mL). The suspension was filtered, all volatile components were removed *in vacuo* and the residue was dissolved in a mixture of DCM and toluene (1:1, 80 mL). Neat heptamethyldisilazane (0.3168 g, 1.96 mmol) was added dropwise and the mixture was refluxed for 12 h. All volatile components were removed *in vacuo* and the residue was dissolved in DCM. It was washed with water and the organic phase was evaporated to dryness using a rotary evaporator. The product was obtained as colourless crystals after column chromatography (*n*-hexane) and crystallization from DCM/MeOH (yield: 12%). ¹H NMR (500 MHz, CDCl₃): δ = 7.01 (s, 4H, Tip-*CH* arom.), 6.48 (s, 2H, 4/4'-*CH* arom. thiophene), 2.96 (s, 3H, N-*CH*₃), 2.95 (sept, *J* = 6.94 Hz, 2H, *p*-*CH(CH*₃)₂), 2.55 (sept, *J* = 6.78 Hz, 4H, *o*-*CH(CH*₃)₂), 2.37 (s, 6H, 5/5'-*CH*₃), 1.32 (d, *J* = 6.94 Hz, 12H, *p*-*CH(CH*₃)₂), 1.18 (d, *J* = 6.78 Hz, 12H, *o*-*CH(CH*₃)₂); ¹¹B{¹H} NMR (160 MHz, CDCl₃): δ = 47.0 ppm; ¹³C{¹H} NMR (126 MHz,

CDCl_3): $\delta = 148.0$ (s, quart. *p*-Tip-C), 147.8 (s, quart. *o*-Tip-C), 147.7 (s, quart. 2/2'-C), 141.7 (br, Tip-C-B), 139.8 (br, 3/3'-C-B), 138.6 (s, 4/4'-C), 135.7 (s, quart. 5/5'-C), 120.2 (s, *m*-Tip-C), 43.9 (s, N-CH₃), 34.9 (s, *o*-CH(CH₃)₂), 34.2 (s, *p*-CH(CH₃)₂), 24.7 (s, *o*-CH(CH₃)₂), 24.3 (s, *o*-CH(CH₃)₂), 24.2 (s, *p*-CH(CH₃)₂), 15.0 ppm (s, 5/5'-CH₃); MS (APCI): m/z (%) = 650.41 ([M+H⁺], 100); Elem. anal. calc. (%): C 75.80, H 8.84, N 2.16, S 9.87; found: C 75.72, H 9.01, N 2.21, S 9.83; UV/vis (DCM): $\lambda_{\text{abs,max}} = 267$ ($\varepsilon = 36038$ L mol⁻¹ cm⁻¹), 368 ($\varepsilon = 20516$ L mol⁻¹ cm⁻¹), 384 nm ($\varepsilon = 18640$ L mol⁻¹ cm⁻¹); fluorescence (DCM): $\lambda_{\text{em1}} = 413$, 428 nm (for $\lambda_{\text{ex1}} = 267$, $\lambda_{\text{ex2}} = 368$ or $\lambda_{\text{ex3}} = 384$ nm; $\Phi_f = 94\%$).

Synthesis of dithieno[3,2-*c*:2',3'-*e*]-*B,B'*-bis(2,4,6-tris(trifluoromethyl)phenyl)-[1,2,7]-oxadiborepine (5^{F_{Mes}}). To a solution of 3,3'-bis(trimethylsilyl)-5,5'-dimethyl-2,2'-bithiophene (0.663 g, 1.96 mmol) in DCM (4 mL) was added trichloroborane (3.34 M in DCM, 3.50 mL, 11.69 mmol) at -78 °C. The mixture was subsequently warmed to ambient temperature and stirred overnight. All volatile components were removed *in vacuo* and the residue was dissolved in toluene (20 mL). A solution of 2,4,6-tris(trifluoromethyl)phenyl (ca. 5.40 mmol) in toluene (20 mL) was added at -78 °C. The mixture was subsequently warmed to ambient temperature and stirred for 7 days. After adding water (20 mL) all volatile components were removed *in vacuo* and the residue was dissolved in DCM. It was washed with water and the organic phase was evaporated to dryness using a rotary evaporator. The product was obtained as light yellowish crystals after column chromatography (*n*-hexane) and crystallization from DCM/MeOH (yield: 75%). ¹H NMR (500 MHz, CDCl₃): $\delta = 8.10$ (s, 4H, ^{F_{Mes}}-CH arom.), 6.43 (s, 2H, 4/4'-CH arom. thiophene), 2.44 ppm (s, 6H, 5/5'-CH₃); ¹¹B{¹H} NMR (160 MHz, CDCl₃): $\delta = 41.3$ ppm; ¹⁹F{¹H} NMR (470 MHz, CDCl₃): $\delta = -58.1$ (s, *o*-CF₃), -63.2 ppm (s, *p*-CF₃); ¹³C{¹H} NMR (126 MHz, CDCl₃): $\delta = 150.4$ (s, quart. 2/2'-C), 141.5 (br, ^{F_{Mes}}-C-B), 139.4 (s, quart. 5/5'-C), 135.1 (br, 3/3'-C-B), 134.4 (q, J = 32.9 Hz, quart. *p*-^{F_{Mes}}-C), 134.2 (s, 4/4'-C), 132.0 (q, J = 34.5 Hz, quart. *o*-^{F_{Mes}}-C), 126.0 (s, *m*-^{F_{Mes}}-C), 123.5 (q, J = 275.0 Hz, *o*-CF₃), 122.7 (q, J = 272.8 Hz, *p*-CF₃), 15.0 ppm (s, 5/5'-CH₃); MS (APCI): m/z (%) = 793.02 ([M+H⁺], 100); elem. anal. calc. (%): C 42.46, H 1.53, S 8.09; found: C 42.62, H 1.71, S 8.23; UV/vis (DCM): $\lambda_{\text{abs,max}} = 262$ ($\varepsilon = 27730$ L mol⁻¹ cm⁻¹), 376 ($\varepsilon = 22975$ L mol⁻¹ cm⁻¹), 392 nm ($\varepsilon = 20667$ L mol⁻¹ cm⁻¹); fluorescence (DCM): $\lambda_{\text{em1}} = 428$, 439 nm (for $\lambda_{\text{ex1}} = 262$, $\lambda_{\text{ex2}} = 376$ or $\lambda_{\text{ex3}} = 392$ nm; $\Phi_f = 70\%$).

Synthesis of dithieno[3,2-*c*:2',3'-*e*]-*B,B'*-bis(2,4,6-tris(trifluoromethyl)phenyl)-[1,2,7]-azadiborepine (6^{F_{Mes}}**).** To a solution of 3,3'-bis(trimethylsilyl)-5,5'-dimethyl-2,2'-bithiophene (0.679 g, 2.00 mmol) in DCM (4 mL) was added trichloroborane (3.34 M in DCM, 3.50 mL, 11.69 mmol) at -78 °C. The mixture was subsequently warmed to ambient temperature and stirred overnight. All volatile components were removed *in vacuo* and the residue was dissolved in toluene (20 mL). A solution of 2,4,6-tris(trifluoromethyl)phenyl (ca. 5.40 mmol) in toluene (20 mL) was added at -78 °C. The mixture was subsequently warmed to ambient temperature and stirred for 7 days. All volatile components were removed *in vacuo* and the residue was dissolved in *n*-pentane (20 mL). The suspension was filtered, all volatile components were removed *in vacuo* and the residue was dissolved in a mixture of DCM and toluene (1:1, 80 mL). Neat hexamethyldisilazane (0.3240 g, 2.01 mmol) was added dropwise and the mixture was refluxed for 22 h. All volatile components were removed *in vacuo* and the residue was dissolved in DCM. It was washed with water and the organic phase was evaporated to dryness using a rotary evaporator. The product was obtained as light yellowish crystals after column chromatography (*n*-hexane) and crystallization from DCM/MeOH (yield: 21%). ¹H NMR (500 MHz, CDCl₃): δ = 8.14 (s, 4H, ^{F_{Mes}}-CH arom.), 6.67 (br, 1H, N-H), 6.32 (s, 2H, 4/4'-CH arom. thiophene), 2.43 ppm (s, 6H, 5/5'-CH₃); ¹¹B{¹H} NMR (160 MHz, CDCl₃): δ = 41.5 ppm; ¹⁹F{¹H} NMR (470 MHz, CDCl₃): δ = -57.8 (s, *o*-CF₃), -63.2 ppm (s, *p*-CF₃); ¹³C{¹H} NMR (126 MHz, CDCl₃): δ = 149.9 (s, quart. 2/2'-C), 144.4 (br, ^{F_{Mes}}-C-B), 138.4 (s, quart. 5/5'-C), 136.6 (br, 3/3'-C-B), 134.8 (s, 4/4'-C), 134.7 (q, J = 32.5 Hz, quart. *p*-^{F_{Mes}}-C), 131.7 (q, J = 34.5 Hz, quart. *o*-^{F_{Mes}}-C), 125.9 (s, *m*-^{F_{Mes}}-C), 123.3 (q, J = 275.1 Hz, *o*-CF₃), 122.8 (q, J = 272.8 Hz, *p*-CF₃), 14.9 ppm (s, 5/5'-CH₃); MS (APCI): m/z (%) = 792.04 ([M+H⁺], 100); elem. anal. calc. (%): C 42.51, H 1.66, N 1.77, S 8.10; found: C 41.98, H 1.60, N 1.70, S 7.63; UV/vis (DCM): λ_{abs,max} = 264 (ε = 24428 L mol⁻¹ cm⁻¹), 369 (ε = 17295 L mol⁻¹ cm⁻¹), 383 nm (ε = 15743 L mol⁻¹ cm⁻¹); fluorescence (DCM): λ_{em1} = 417, 429 nm (for λ_{ex1} = 264, λ_{ex2} = 369 or λ_{ex3} = 383 nm; Φ_f = 80%).

Crystallographic Data

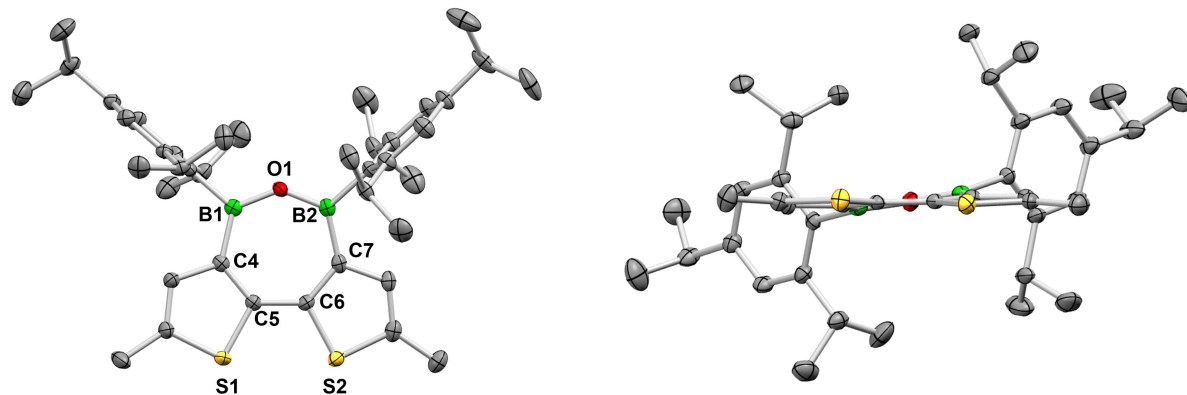


Figure 4.2.5. Molecular structure of $\mathbf{5}^{\text{Tip}}$ (with views perpendicular and parallel to the polycyclic plane) in the solid state by single-crystal X-ray diffraction (H-atoms omitted for clarity).

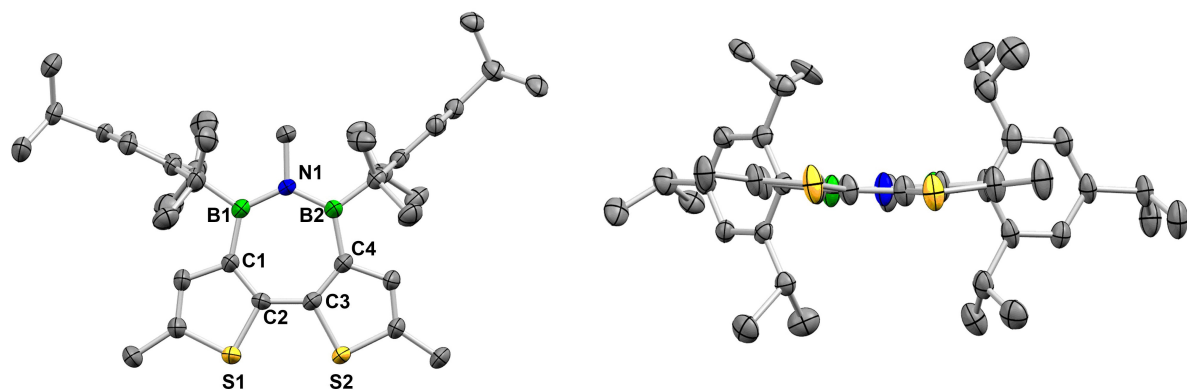


Figure 4.2.6. Molecular structure of $\mathbf{7}^{\text{Tip}}$ (with views perpendicular and parallel to the polycyclic plane) in the solid state by single-crystal X-ray diffraction (H-atoms and disorder of a Tip group omitted for clarity).

Table 4.2.2. Crystallographic data of $\mathbf{5}^{\text{Tip}}$ and $\mathbf{7}^{\text{Tip}}$.

No.	$\mathbf{5}^{\text{Tip}}$	$\mathbf{7}^{\text{Tip}}$
CCDC number	2022909	2022908
Size / mm	0.18 x 0.11 x 0.09	0.37 x 0.22 x 0.16
Empiric Formula	C40H54B2OS2	C82 H113.22 B4 N2 S4
M	636.57	1298.43
Crystal system	triclinic	monoclinic

Space group	P -1	P 1 21/n 1
$a/\text{\AA}$	12.3730(16)	16.0326(19)
$b/\text{\AA}$	13.0366(17)	14.1619(17)
$c/\text{\AA}$	14.401(2)	18.545(2)
α°	73.787(4)	90
β°	65.470(4)	113.321(4)
γ°	64.055(3)	90
$V/\text{\AA}^3$	1886.7(4)	3866.7(8)
Z	2	2
μ/mm^{-1}	0.170	0.166
T/K	100	100
$\theta_{\min,\max}$	2.48, 26.89	2.392, 26.021
Completeness	99.4	99.7
Reflections: total/independent	8141, 6630	7594, 6317
R_{int}	0.0855	0.0847
Final $R1$ and $wR2$	0.0581, 0.1609	0.0967, 0.2285
Largest peak, hole/e \AA^{-3}	0.472, -0.456	0.7, -0.7
$\rho_{\text{calc}}/\text{g cm}^{-3}$	1.120	1.115

Computational methods. Optimization and TD-DFT calculations were carried out with the TURBOMOLE V7.0.1 program package.^[31] NICS Scan,^[32] NICS XY-Scan^[33] and ACID^[34] calculations were carried out using the Gaussian 09 program package, revision D.01.^[35] Becke's three parameter exchange-correlation hybrid functional B3LYP^[36] was used in combination with the 6-31+G* basis set. The empirical dispersion correction DFT-D3 by Grimme was used including the three-body term and with Becke-Johnson (BJ) damping.^[37]

The stationary points were characterized as minima by an analytical vibrational frequency calculation,^[38] which revealed the absence of imaginary frequencies. Vertical singlet excitations were calculated by means of time-dependent DFT^[39] using the same density functional and the valence-double- ζ basis set def2-SV(P).^[40]

Table 4.2.3. Results from TD-DFT calculations for compounds **5** – **7** as well as 2,2‘-bithiophene-3,3‘-dicarboxylic anhydride and 2,2‘-bithiophene-3,3‘-dicarboximide.

Compound	λ / nm	Oscillator strength f	Orbital contributions	$ \mathbf{c} ^2 / \%$
5^{Mes}	365	0.4116	HOMO → LUMO	96.3
5^{FMes}	373	0.3896	HOMO → LUMO	96.4
6^{Mes}	360	0.4141	HOMO → LUMO	96.7
6^{FMes}	370	0.2815	HOMO → LUMO	92.0
7^{Mes}	364	0.3927	HOMO → LUMO	96.6
2,2‘- bithiophene- 3,3‘-dicarboxylic anhydride	344	0.3048	HOMO → LUMO	97.0
2,2‘- bithiophene- 3,3‘- dicarboximide	346	0.2903	HOMO → LUMO	96.4

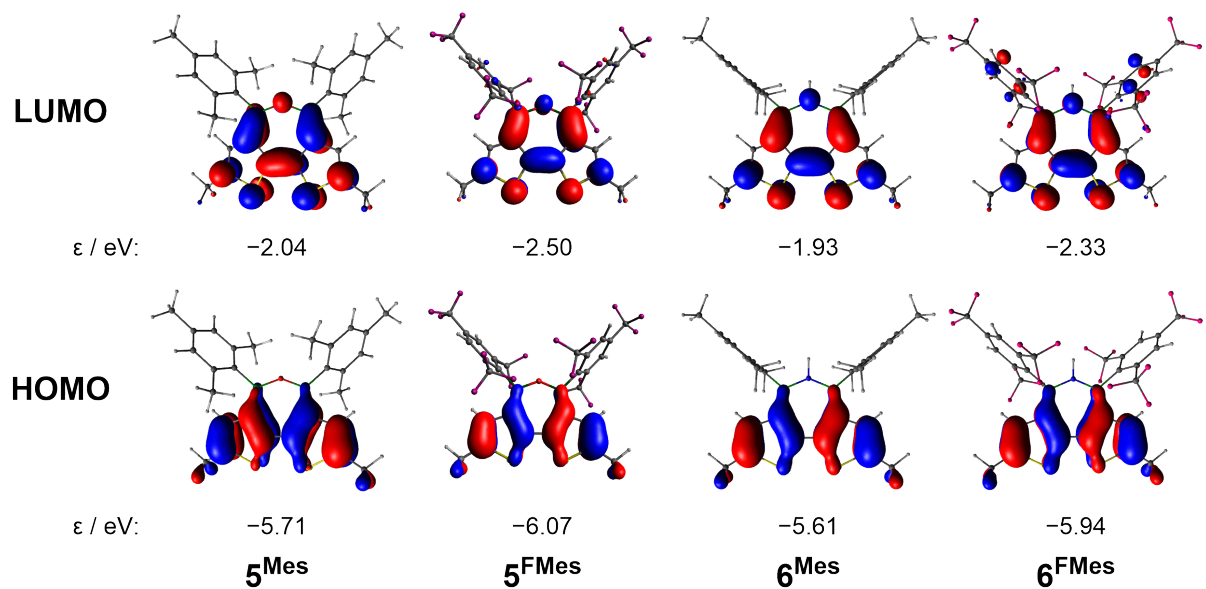


Figure 4.2.7. B3LYP-D3(BJ)/def2-SV(P) calculated frontier orbitals of 5^{Mes} , 5^{FMes} , 6^{Mes} and 6^{FMes} (isovalue 0.035).

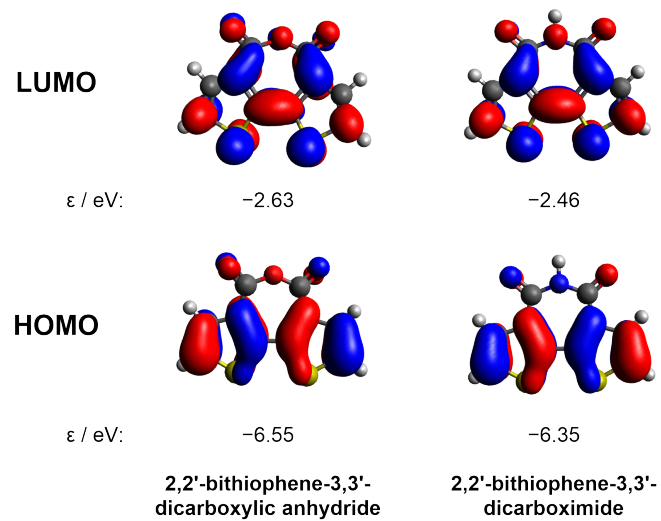


Figure 4.2.8. B3LYP-D3(BJ)/def2-SV(P) calculated frontier orbitals of 2,2'-bithiophene-3,3'-dicarboxylic anhydride and 2,2'-bithiophene-3,3'-dicarboximide (isovalue 0.035).

4.2.5 References

- [‡] M. Crumbach, J. Bachmann, L. Fritze, A. Helbig, I. Krummenacher, H. Braunschweig, H. Helten, *Angew. Chem. Int. Ed.* **2021**, *60*, 9290–9295.
- [1] a) C. Wang, H. Dong, W. Hu, Y. Liu, D. Zhu, *Chem. Rev.* **2012**, *112*, 2208–2267; b) J. Mei, Y. Diao, A. L. Appleton, L. Fang, Z. Bao, *J. Am. Chem. Soc.* **2013**, *135*, 6724–6746; c) T. M. Swager, *Macromolecules* **2017**, *50*, 4867–4886.
- [2] a) M. Stolar, T. Baumgartner, *Phys. Chem. Chem. Phys.* **2013**, *15*, 9007–9024; b) J. Dhar, U. Salzner, S. Patil, *J. Mater. Chem. C* **2017**, *5*, 7404–7430.
- [3] a) C. R. Wade, A. E. J. Broomsgrove, S. Aldridge, F. P. Gabbaï, *Chem. Rev.* **2010**, *110*, 3958–3984; b) F. Jäkle, *Chem. Rev.* **2010**, *110*, 3985–4022; c) H. Zhao, L. A. Leamer, F. P. Gabbaï, *Dalton Trans.* **2013**, *42*, 8164–8178; d) A. Wakamiya, S. Yamaguchi, *Bull. Chem. Soc. Jpn.* **2015**, *88*, 1357–1377; e) S. Mukherjee, P. Thilagar, *J. Mater. Chem. C* **2016**, *4*, 2647–2662; f) L. Ji, S. Griesbeck, T. B. Marder, *Chem. Sci.* **2017**, *8*, 846–863; g) E. von Grothuss, A. John, T. Kaese, M. Wagner, *Asian J. Org. Chem.* **2018**, *7*, 37–53; h) H. Helten, *Chem. Asian J.* **2019**, *14*, 919–935; i) S. K. Mellerup, S. Wang, *Chem. Soc. Rev.* **2019**, *48*, 3537–3549; j) S. A. Iqbal, J. Pahl, K. Yuan, M. J. Ingleson, *Chem. Soc. Rev.* **2020**, *49*, 4564–4591; k) Z. Huang, S. Wang, R. D. Dewhurst, N. V. Ignat'ev, M. Finze, H. Braunschweig, *Angew. Chem. Int. Ed.* **2020**, *59*, 8800–8818; *Angew. Chem.* **2020**, *132*, 8882–8900; l) X. Yin, J. Liu, F. Jäkle, *Chem. Eur. J.* **2020**, DOI: 10.1002/chem.202003481.
- [4] a) J. A. Letizia, M. R. Salata, C. M. Tribout, A. Facchetti, M. A. Ratner, T. J. Marks, *J. Am. Chem. Soc.* **2008**, *130*, 9679–9694; b) X. Guo, R. P. Ortiz, Y. Zheng, Y. Hu, Y.-Y. Noh, K.-J. Baeg, A. Facchetti, T. J. Marks, *J. Am. Chem. Soc.* **2011**, *133*, 1405–1418; c) X. Guo, N. Zhou, S. J. Lou, J. W. Hennek, R. P. Ortiz, M. R. Butler, P.-L. T. Boudreault, J. Strzalka, P.-O. Morin, M. Leclerc, J. T. López Navarrete, M. A. Ratner, L. X. Chen, R. P. H. Chang, A. Facchetti, T. J. Marks, *J. Am. Chem. Soc.* **2012**, *134*, 18427–18439; d) N. Zhou, X. Guo, R. P. Ortiz, S. Li, S. Zhang, R. P. H. Chang, A. Facchetti, T. J. Marks, *Adv. Mater.* **2012**, *24*, 2242–2248; e) X. Guo, N. Zhou, S. J. Lou, J. Smith, D. B. Tice, J. W. Hennek, R. P. Ortiz, J. T. López Navarrete, S. Li, J. Strzalka, *Nat. Photonics* **2013**, *7*, 825–833; f) M. Saito, I. Osaka, Y. Suda, H. Yoshida, K. Takimiya, *Adv. Mater.* **2016**, *28*, 6921–6925; g) Y. Wang, H. Guo, S. Ling, I. Arrechea-Marcos, Y. Wang, J. T. López Navarrete, R. P. Ortiz, X. Guo, *Angew. Chem. Int. Ed.* **2017**, *56*, 9924–9929; *Angew. Chem.* **2017**, *129*, 10056–10061; h) Y. Wang, Z. Yan, H. Guo, M. A. Uddin, S. Ling, X. Zhou, H. Su, J. Dai, H. Y. Woo, X. Guo, *Angew. Chem. Int. Ed.* **2017**, *56*, 15304–15308; *Angew. Chem.* **2017**, *129*, 15506–15510; i) Y. Wang, H. Guo, A. Harbuzaru, M. A. Uddin, I. Arrechea-Marcos, S. Ling, J. Yu, Y. Tang, H. Sun, J. T. López Navarrete, R. P. Ortiz, H. Y. Woo, X. Guo, *J. Am. Chem. Soc.* **2018**, *140*, 6095–6108.
- [5] For other bichalcogenophene analogues of BTI, see: a) S. Shi, L. Tang, H. Guo, M. A. Uddin, H. Wang, K. Yang, B. Liu, Y. Wang, H. Sun, H. Y. Woo, X. Guo, *Macromolecules* **2019**, *52*, 7301–7312; b) S. V. Mulay, B. Bogoslavky, I. Galanti, E. Galun, O. Gidron, *J. Mater. Chem. C* **2018**, *6*, 11951–11955; c) S. V. Mulay, O.

Dishi, Y. Fang, M. R. Niazi, L. J. W. Shimon, D. F. Perepichka, O. Gidron, *Chem. Sci.* **2019**, *10*, 8527–8532.

- [6] For P analogues of BTI, see: X. He, J. Borau-Garcia, A. Y. Y. Woo, S. Trudel, T. Baumgartner, *J. Am. Chem. Soc.* **2013**, *135*, 1137–1147.
- [7] A. Nowak-Król, F. Würthner, *Org. Chem. Front.* **2019**, *6*, 1272–1318.
- [8] a) K. Krogh-Jespersen, D. Cremer, J. D. Dill, J. A. Pople, Schleyer, P. v. R., *J. Am. Chem. Soc.* **1981**, *103*, 2589–2594; b) C. A. Jaska, D. J. H. Emslie, M. J. D. Bosdet, W. E. Piers, T. S. Sorensen, M. Parvez, *J. Am. Chem. Soc.* **2006**, *128*, 10885–10896; c) H. Braunschweig, I. Fernández, G. Frenking, T. Kupfer, *Angew. Chem. Int. Ed.* **2008**, *47*, 1951–1954; *Angew. Chem.* **2008**, *120*, 1977–1980; d) A. Wakamiya, K. Mori, T. Araki, S. Yamaguchi, *J. Am. Chem. Soc.* **2009**, *131*, 10850–10851; e) A. J. V. Marwitz, M. H. Matus, L. N. Zakharov, D. A. Dixon, S.-Y. Liu, *Angew. Chem. Int. Ed.* **2009**, *48*, 973–977; *Angew. Chem.* **2009**, *121*, 991–995; f) C. Tanjaroon, A. Daly, A. J. V. Marwitz, S.-Y. Liu, S. Kukolich, *J. Chem. Phys.* **2009**, *131*, 224312; g) P. G. Campbell, E. R. Abbey, D. Neiner, D. J. Grant, D. A. Dixon, S.-Y. Liu, *J. Am. Chem. Soc.* **2010**, *132*, 18048–18050; h) C. Fan, L. G. Mercier, W. E. Piers, H. M. Tuononen, M. Parvez, *J. Am. Chem. Soc.* **2010**, *132*, 9604–9606; i) D. E. Bean, P. W. Fowler, *J. Phys. Chem. A* **2011**, *115*, 13649–13656; j) A. Iida, S. Yamaguchi, *J. Am. Chem. Soc.* **2011**, *133*, 6952–6955; k) H. Braunschweig, A. Damme, R. D. Dewhurst, S. Ghosh, T. Kramer, B. Pfaffinger, K. Radacki, A. Vargas, *J. Am. Chem. Soc.* **2013**, *135*, 1903–1911; l) S. Xu, T. C. Mikulas, L. N. Zakharov, D. A. Dixon, S.-Y. Liu, *Angew. Chem. Int. Ed.* **2013**, *52*, 7527–7531; *Angew. Chem.* **2013**, *125*, 7675–7679; m) H. Braunschweig, C. Hörl, L. Mailänder, K. Radacki, J. Wahler, *Chem. Eur. J.* **2014**, *20*, 9858–9861; n) M. Baranac-Stojanović, *Chem. Eur. J.* **2014**, *20*, 16558–16565; o) J. O. C. Jimenez-Halla, E. Matito, M. Solà, H. Braunschweig, C. Hörl, I. Krummenacher, J. Wahler, *Dalton Trans.* **2015**, *44*, 6740–6747; p) W. Wu, X. Li, L. Meng, S. Zheng, Y. Zeng, *J. Phys. Chem. A* **2015**, *119*, 2091–2097; q) T. Kupfer, H. Braunschweig, K. Radacki, *Angew. Chem. Int. Ed.* **2015**, *54*, 15084–15088; *Angew. Chem.* **2015**, *127*, 15299–15303; r) E. von Grotthuss, M. Diefenbach, M. Bolte, H.-W. Lerner, M. C. Holthausen, M. Wagner, *Angew. Chem. Int. Ed.* **2016**, *55*, 14067–14071; *Angew. Chem.* **2016**, *128*, 14273–14277; s) T. Araki, M. Hirai, A. Wakamiya, W. E. Piers, S. Yamaguchi, *Chem. Lett.* **2017**, *46*, 1714–1717; t) B. Su, R. Kinjo, *Synthesis* **2017**, *49*, 2985–3034; u) W. Zhang, D. Yu, Z. Wang, B. Zhang, L. Xu, G. Li, N. Yan, E. Rivard, G. He, *Org. Lett.* **2019**, *21*, 109–113.
- [9] a) L. G. Mercier, W. E. Piers, M. Parvez, *Angew. Chem. Int. Ed.* **2009**, *48*, 6108–6111; *Angew. Chem.* **2009**, *121*, 6224–6227; b) A. Caruso, J. D. Tovar, *Org. Lett.* **2011**, *13*, 3106–3109; c) D. R. Levine, A. Caruso, M. A. Siegler, J. D. Tovar, *Chem. Commun.* **2012**, *48*, 6256–6258; d) A. Iida, S. Saito, T. Sasamori, S. Yamaguchi, *Angew. Chem. Int. Ed.* **2013**, *52*, 3760–3764; *Angew. Chem.* **2013**, *125*, 3848–3852; e) D. R. Levine, M. A. Siegler, J. D. Tovar, *J. Am. Chem. Soc.* **2014**, *136*, 7132–7139; f) R. E. Messersmith, S. Yadav, M. A. Siegler, H. Ottosson, J. D. Tovar, *J. Org. Chem.* **2017**, *82*, 13440–13448; g) D. R. Levine, R. E. Messersmith, M. A. Siegler, J. D. Tovar, *Can. J. Chem.* **2017**, *95*, 381–389; h) K. Schickedanz, J. Radtke, M. Bolte, H.-W. Lerner, M. Wagner, *J. Am. Chem. Soc.* **2017**, *139*, 2842–2851; i) V.

- A. K. Adiraju, C. D. Martin, *Chem. Eur. J.* **2017**, *23*, 11437–11444; j) Y. Adachi, J. Ohshita, *Organometallics* **2018**, *37*, 869–881; k) R. E. Messersmith, J. D. Tovar, *J. Phys. Chem. A* **2019**, *123*, 881–888; l) W. Yang, K. E. Krantz, L. A. Freeman, D. A. Dickie, A. Molino, A. Kaur, D. J. D. Wilson, R. J. Gilliard, Jr., *Chem. Eur. J.* **2019**, *25*, 12512–12516; m) Y. Adachi, F. Arai, F. Jäkle, *Chem. Commun.* **2020**, *56*, 5119–5122.
- [10] a) Z. Liu, T. B. Marder, *Angew. Chem. Int. Ed.* **2008**, *47*, 242–244; *Angew. Chem.* **2008**, *120*, 248–250; b) M. J. D. Bosdet, W. E. Piers, *Can. J. Chem.* **2009**, *87*, 8–29; c) P. G. Campbell, A. J. V. Marwitz, S.-Y. Liu, *Angew. Chem. Int. Ed.* **2012**, *51*, 6074–6092; *Angew. Chem.* **2012**, *124*, 6178–6197; d) X.-Y. Wang, J.-Y. Wang, J. Pei, *Chem. Eur. J.* **2015**, *21*, 3528–3539; e) D. Bonifazi, F. Fasano, M. M. Lorenzo-Garcia, D. Marinelli, H. Oubaha, J. Tasseroul, *Chem. Commun.* **2015**, *51*, 15222–15236; f) M. M. Morgan, W. E. Piers, *Dalton Trans.* **2016**, *45*, 5920–5924; g) H. Helten, *Chem. Eur. J.* **2016**, *22*, 12972–12982; i) G. Bélanger-Chabot, H. Braunschweig, D. K. Roy, *Eur. J. Inorg. Chem.* **2017**, 4353–4368; h) Z. X. Giustra, S.-Y. Liu, *J. Am. Chem. Soc.* **2018**, *140*, 1184–1194; i) C. R. McConnell, S.-Y. Liu, *Chem. Soc. Rev.* **2019**, *48*, 3436–3453; non-aromatic BN isosteres: j) A. Staubitz, A. P. M. Robertson, M. E. Sloan, I. Manners, *Chem. Rev.* **2010**, *110*, 4023–4078.
- [11] For the application of this concept to polymer chemistry, see: a) A. W. Baggett, F. Guo, B. Li, S.-Y. Liu, F. Jäkle, *Angew. Chem. Int. Ed.* **2015**, *54*, 11191–11195; *Angew. Chem.* **2015**, *127*, 11343–11347; b) X.-Y. Wang, F.-D. Zhuang, J.-Y. Wang, J. Pei, *Chem. Commun.* **2015**, *51*, 17532–17535; c) T. Lorenz, A. Lik, F. A. Plamper, H. Helten, *Angew. Chem. Int. Ed.*, **2016**, *55*, 7236–7241; *Angew. Chem.* **2016**, *128*, 7352–7357; d) O. Ayhan, T. Eckert F. A. Plamper, H. Helten, *Angew. Chem. Int. Ed.* **2016**, *55*, 13321–13325; *Angew. Chem.* **2016**, *128*, 13515–13519; e) T. Lorenz, M. Crumbach, T. Eckert, A. Lik, H. Helten, *Angew. Chem. Int. Ed.* **2017**, *56*, 2780–2784; *Angew. Chem.* **2017**, *129*, 2824–2828; f) N. A. Riensch, A. Deniz, S. Kühl, L. Müller, A. Adams, A. Pich, H. Helten, *Polym. Chem.* **2017**, *8*, 5264–5268; g) O. Ayhan, N. A. Riensch, C. Glasmacher, H. Helten, *Chem. Eur. J.* **2018**, *24*, 5883–5894; h) W. Zhang, G. Li, L. Xu, Y. Zhuo, W. Wan, N. Yan, G. He, *Chem. Sci.* **2018**, *9*, 4444–4450; i) F. Brosge, T. Lorenz, H. Helten, C. Bolm, *Chem. Eur. J.* **2019**, *25*, 12708–12711.
- [12] H. Wei, Y. Liu, T. Y. Gopalakrishna, H. Phan, X. Huang, L. Bao, J. Guo, J. Zhou, S. Luo, J. Wu, Z. Zeng, *J. Am. Chem. Soc.* **2017**, *139*, 15760–15767.
- [13] M. Fingerle, C. Maichle-Mössmer, S. Schundelmeier, B. Speiser, H. F. Bettinger, *Org. Lett.* **2017**, *19*, 4428–4431.
- [14] A. S. Scholz, J. G. Massoth, M. Bursch, J.-M. Mewes, T. Hetzke, B. Wolf, M. Bolte, H.-W. Lerner, S. Grimme, M. Wagner, *J. Am. Chem. Soc.* **2020**, *142*, 11072–11083.
- [15] M. Crumbach, O. Ayhan, L. Fritze, J. A. P. Sprenger, L. Zapf, M. Finze, H. Helten, *Chem. Commun.* **2021**, *57*, 2408–2411.
- [16] Q. Yan, M. Yin, C. Chen, Y. Zhang, *J. Org. Chem.* **2018**, *83*, 9096–9102.
- [17] A. Das, A. Hübner, M. Weber, M. Bolte, H.-W. Lerner, M. Wagner, *Chem. Commun.* **2011**, *47*, 11339–11341.

- [18] J. Radtke, K. Schickedanz, M. Bamberg, L. Menduti, D. Schollmeyer, M. Bolte, H.-W. Lerner, M. Wagner, *Chem. Sci.* **2019**, *10*, 9017–9027.
- [19] a) N. Shimada, M. Hirata, M. Koshizuka, N. Ohse, R. Kaito, K. Makino, *Org. Lett.* **2019**, *21*, 4303–4308; b) M. Koshizuka, K. Makino, N. Shimada, *Org. Lett.* **2020**, *22*, 8658–8664; c) N. Shimada, N. Takahashi, N. Ohse, M. Koshizuka, K. Makino, *Chem. Commun.* **2020**, *56*, 13145–13148.
- [20] D. Tian, Q. Li, Y. Zhao, Z. Wang, W. Li, S. Xia, S. Xing, B. Zhu, J. Zhang, C. Cui, *J. Org. Chem.* **2020**, *85*, 526–536.
- [21] a) A. Stanger, *J. Org. Chem.* **2006**, *71*, 883–893; b) R. Gershoni-Poranne, A. Stanger, *Chem. Eur. J.* **2014**, *20*, 5673–5688; c) R. Herges, D. Geuenich, *J. Phys. Chem. A* **2001**, *105*, 3214–3220; d) D. Geuenich, K. Hess, F. Köhler, R. Herges, *Chem. Rev.* **2005**, *105*, 3758–3772.
- [22] The local maximum at the center of the NICS-X-scan for the azadiborepin ring of 6^{Mes} results from σ effects,^[15,21b] which are eliminated at scan heights above ca. 2.0 Å (see SI, Figure S48).
- [23] K. Ruhlandt-Senge, J. J. Ellison, R. J. Wehmschulte, F. Pauer, P. P. Power, *J. Am. Chem. Soc.* **1993**, *115*, 11353–11357.
- [24] G. E. Carr, R. D. Chambers, T. F. Holmes, D. G. Parker, *J. Organomet. Chem.* **1987**, *325*, 13–23.
- [25] S. Liou, C. Ke, J. Chen, Y. Luo, S. Kuo, Y. Chen, C. Fang, C. Wu, C. Chiang, Y. Chan, *ACS Macro Lett.* **2016**, *5*, 154–157.
- [26] P. M. Beaujuge, H. N. Tsao, M. R. Hansen, C. M. Amb, C. Risko, J. Subbiah, K. R. Choudhury, A. Mavrinckiy, W. Pisula, J.-L. Brédas, F. So, K. Müllen, J. R. Reynolds, *J. Am. Chem. Soc.* **2012**, *134*, 8944–8957.
- [27] G. M. Sheldrick, *Acta Crystallogr. A* **2015**, *71*, 3–8.
- [28] Sheldrick, *Acta Crystallogr. A* **2008**, *64*, 112–122.
- [29] C. B. Hubschle, G. M. Sheldrick, B. Dittrich, *J. Appl. Crystallogr.* **2011**, *44*, 1281–1284.
- [30] O. V. Dolomanov, L. J. Bourhis, R. J. Gildea, J. A. K. Howard, H. Puschmann, *J. Appl. Crystallogr.* **2009**, *42*, 339–341.
- [31] R. Ahlrichs, M. Bär, M. Häser, H. Horn, C. Kölmel, *Chem. Phys. Lett.* **1989**, *162*, 165–169.
- [32] A. Stanger, *J. Org. Chem.* **2006**, *71*, 883–893.
- [33] R. Gershoni-Poranne, A. Stanger, *Chem. Eur. J.* **2014**, *20*, 5673–5688.
- [34] a) D. Geuenich, R. Herges, *J. Phys. Chem. A* **2001**, *105*, 3214–3220; b) D. Geuenich, K. Hess, F. Köhler, R. Herges, *Chem. Rev.* **2005**, *105*, 3758–3772.
- [35] Gaussian 09, Revision D.01, M. J. Frisch, G. W. Trucks, H. B. Schlegel, G. E. Scuseria, M. A. Robb, J. R. Cheeseman, G. Scalmani, V. Barone, G. A. Petersson, H. Nakatsuji, X. Li, M. Caricato, A. Marenich, J. Bloino, B. G. Janesko, R. Gomperts, B. Mennucci, H. P. Hratchian, J. V. Ortiz, A. F. Izmaylov, J. L. Sonnenberg, D. Williams-Young, F. Ding, F. Lipparini, F. Egidi, J. Goings, B. Peng, A. Petrone, T. Henderson, D. Ranasinghe, V. G. Zakrzewski, J. Gao, N. Rega, G. Zheng, W. Liang, M. Hada, M. Ehara, K. Toyota, R. Fukuda, J. Hasegawa, M. Ishida, T. Nakajima, Y. Honda, O. Kitao, H. Nakai, T. Vreven, K. Throssell, J. A. Montgomery, Jr., J. E.

Peralta, F. Ogliaro, M. Bearpark, J. J. Heyd, E. Brothers, K. N. Kudin, V. N. Staroverov, T. Keith, R. Kobayashi, J. Normand, K. Raghavachari, A. Rendell, J. C. Burant, S. S. Iyengar, J. Tomasi, M. Cossi, J. M. Millam, M. Klene, C. Adamo, R. Cammi, J. W. Ochterski, R. L. Martin, K. Morokuma, O. Farkas, J. B. Foresman, D. J. Fox, Gaussian Inc., Wallingford CT, 2016.

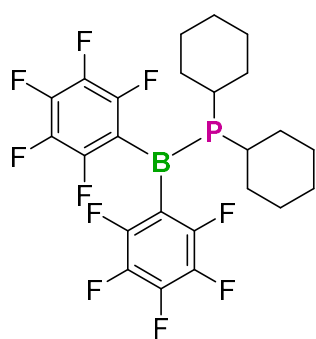
- [36] a) P. A. M. Dirac, *Proc. R. Soc. London, Ser. A* **1929**, *123*, 714–733; b) J. C. Slater, *Phys. Rev.* **1951**, *81*, 385–390; c) A. D. Becke, *Phys. Rev. A* **1988**, *38*, 3098–3100; d) C. Lee, W. Yang, R. G. Parr, *Phys. Rev. B* **1988**, *37*, 785–89; e) A. D. Becke, *J. Chem. Phys.* **1993**, *98*, 5648–5652.
- [37] a) S. Grimme, J. Antony, S. Ehrlich, H. Krieg, *J. Chem. Phys.* **2010**, *132*, 154104; b) S. Grimme, S. Ehrlich, L. J. Goerigk, *J. Comput. Chem.* **2011**, *32*, 1456–1465.
- [38] a) P. Deglmann, F. Furche, R. Ahlrichs, *Chem. Phys. Lett.* **2002**, *362*, 511–518; b) P. Deglmann, F. Furche, *J. Chem. Phys.* **2002**, *117*, 9535–9538.
- [39] a) R. Bauernschmitt, R. Ahlrichs, *Chem. Phys. Lett.* **1996**, *256*, 454–464; b) R. Bauernschmitt, R. Ahlrichs, *J. Chem. Phys.* **1996**, *104*, 9047–9052; c) F. Furche, D. Rappoport, *Density functional methods for excited states: equilibrium structure and electronic spectra*. In M. Olivucci, Ed., *Computational Photochemistry*, Vol. 16 of *Computational and Theoretical Chemistry*, ch. III., Elsevier, Amsterdam, **2005**.
- [40] A. Schäfer, H. Horn, R. Ahlrichs, *J. Chem. Phys.* **1992**, *97*, 2571–2577.

4.3 First Molecular Model Compounds for a Boron-Phosphorus Analogue of Poly(*p*-phenylene vinylene)

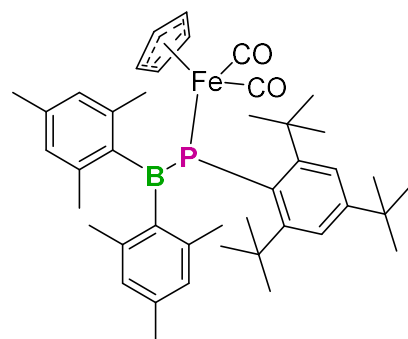
First model compounds for a BP analogue of the conjugated polymer PPV have been synthesized. Incorporation of Mes* substituents at phosphorus led to a fully planarized P center, enabling effective π -conjugation over the BP unit. Theoretical and photophysical investigations indicate a clear B=P double bond character and conjugation throughout the system.

4.3.1 Introduction

Replacing C=C units with isoelectronic and isosteric BN units has emerged as a viable strategy to tune the electronic properties of a material while maintaining its structural properties.^[1] Although the inclusion of phosphorus into π -conjugated systems has attracted some interest in recent years,^[2] the incorporation of BP units, which are valence isoelectronic to C=C units, has scarcely been investigated.^[3] In order to access the π -donor ability of phosphorus, the phosphorus center in the BP unit has to be planarized.^[4] This can be achieved by incorporating electron withdrawing groups at the boron center and electron pushing groups at phosphorus, as reported by Stephan *et al.* in 2011 (Figure 4.3.1).^[5] Another possibility to planarize the phosphorus center is to introduce sterically highly demanding substituents at phosphorus,^[3b] as reported by Mizuta and co-workers in 2012.^[6]



Stephan 2011



Mizuta 2012

Figure 4.3.1. Examples of planarized phosphorus centers in BP units.

4.3.2 Results and Discussion

Herein, we investigate conjugated BP compounds and the effect of different bulky substituents at phosphorus on the BP bond characteristics. This study gives insight into conjugated BP systems as model compounds for conjugated BP-linked polymers. Theoretical investigations have been carried out, in order to assess the influence of different bulky substituents on the planarity of the phosphorus center. The first investigated model compounds feature one BP unit linking two phenyl groups, mesityl substituents at boron and different sterically demanding substituents at phosphorus (Figure 4.3.2).

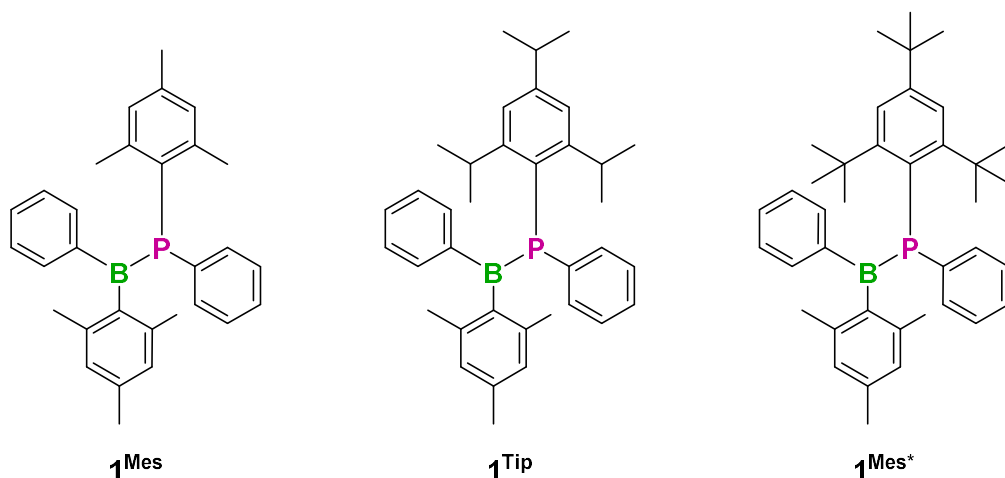


Figure 4.3.2. Structures of investigated model compounds featuring one BP unit.

Optimization of the structure of compound $\mathbf{1}^{\text{Mes}}$ by density-functional theory (DFT) calculations revealed a B-P bond length of 1.871 Å and a sum of the angles around phosphorus of 335.5° (Table 4.3.1). Therefore, $\mathbf{1}^{\text{Mes}}$ already falls into the phosphinoborane categorization proposed by Pringle, which requires a B-P bond length shorter than 1.88 Å with a sum of angles around P of at least 330°.^[3d] Surprisingly the incorporation of a Tip substituent instead of mesityl seems not to lead to an increased planarity of P or a shorter B-P bond, the B-P moiety in $\mathbf{1}^{\text{Tip}}$ exhibits nearly the same structural parameters as that in $\mathbf{1}^{\text{Mes}}$.

Table 4.3.1. Structural parameters according to theoretical investigations (B3LYP-D3(BJ)/def2-SV(P)).

compound	B-P bond length / Å	sum of angles around B / °	sum of angles around P / °
$\mathbf{1}^{\text{Mes}}$	1.871	359.1	335.5
$\mathbf{1}^{\text{Tip}}$	1.868	359.3	335.1
$\mathbf{1}^{\text{Mes}^*}$	1.816	360.0	360.0

According to our calculations the incorporation of a sterically very demanding supermesityl group might lead to the desired properties. For compound $\mathbf{1}^{\text{Mes}^*}$ they predict a very short B-P bond length of 1.816 Å and a sum of the angles around P and B of 360.0° each. This indicates a strong B=P double bond character for compound $\mathbf{1}^{\text{Mes}^*}$, enabling possible π -conjugation over the BP unit.

This indication of π -conjugation is also supported by TD-DFT calculations, conducted for the compounds $\mathbf{1}^{\text{Mes}}$, $\mathbf{1}^{\text{Tip}}$ and $\mathbf{1}^{\text{Mes}^*}$ featuring one BP unit, as well as dimer-like compounds $\mathbf{2}$ and $\mathbf{3}$, which both feature two BP units (Figure 4.3.3). The TD-DFT calculations revealed that all these compounds should show a HOMO-LUMO transition upon low-energy absorption (Table 4.3.2).

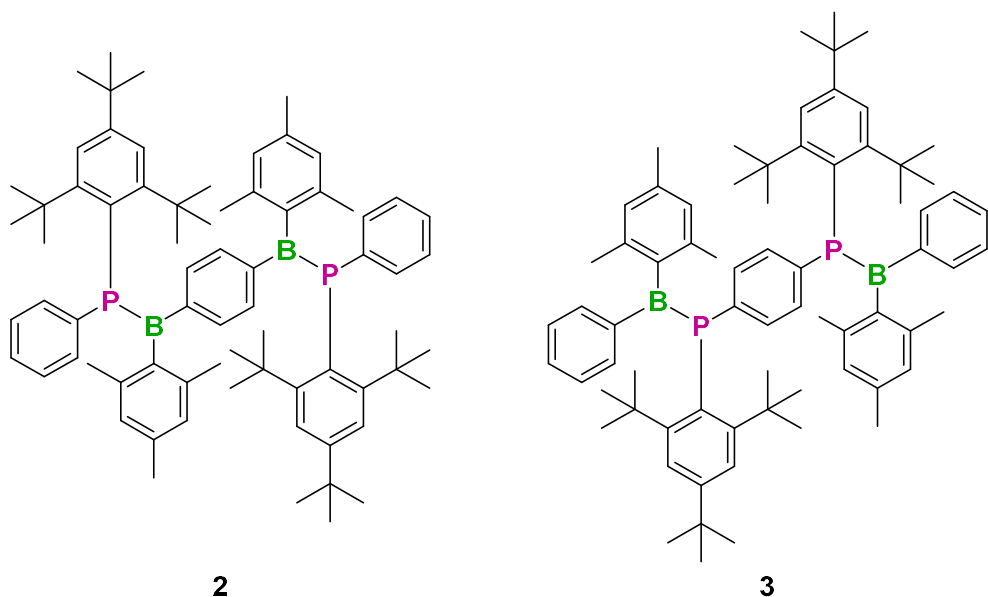


Figure 4.3.3. Structures of investigated model compounds featuring two BP units.

Table 4.3.2. Results from TD-DFT calculations for compounds $\mathbf{1}^{\text{Mes}}$, $\mathbf{1}^{\text{Tip}}$, $\mathbf{1}^{\text{Mes}^*}$, $\mathbf{2}$ and $\mathbf{3}$.

compound	λ / nm	oscillator strength <i>f</i>	orbital contributions	$ c ^2 / \%$
$\mathbf{1}^{\text{Mes}}$	368	0.189918	HOMO \rightarrow LUMO	94.0
$\mathbf{1}^{\text{Tip}}$	375	0.193297	HOMO \rightarrow LUMO	96.8
$\mathbf{1}^{\text{Mes}^*}$	361	0.424503	HOMO \rightarrow LUMO	98.5
$\mathbf{2}$	430	0.825734	HOMO \rightarrow LUMO	98.8
$\mathbf{3}$	432	0.896669	HOMO \rightarrow LUMO	98.7

Figure 4.3.4 depicts the calculated frontier orbitals of compounds $\mathbf{1}^{\text{Mes}}$, $\mathbf{1}^{\text{Tip}}$ and $\mathbf{1}^{\text{Mes}^*}$. The HOMO orbitals of $\mathbf{1}^{\text{Mes}}$ and $\mathbf{1}^{\text{Tip}}$ show strong contributions from the phosphorus center and a π -type contribution from the phenyl group attached to it. The boron center and the phenyl group on boron show very small contributions to the HOMOs. The LUMO orbitals of $\mathbf{1}^{\text{Mes}}$ and $\mathbf{1}^{\text{Tip}}$ show strong contributions of the boron center and the attached phenyl group, whereas the phosphorus center only has a small contribution and the P-attached phenyl group has almost no contribution. These different contributions are due to the not fully planarized phosphorus center and indicate some charge transfer character upon excitation. The frontier orbitals of compound $\mathbf{1}^{\text{Mes}^*}$ look significantly different, the HOMO orbital has equal contributions from both phenyl groups and has the strongest contribution from the BP unit, which has π character. The corresponding LUMO also has contributions from both phenyl groups and the B and P unit. This shows that excitation of $\mathbf{1}^{\text{Mes}^*}$ leads to a $\pi-\pi^*$ transition.

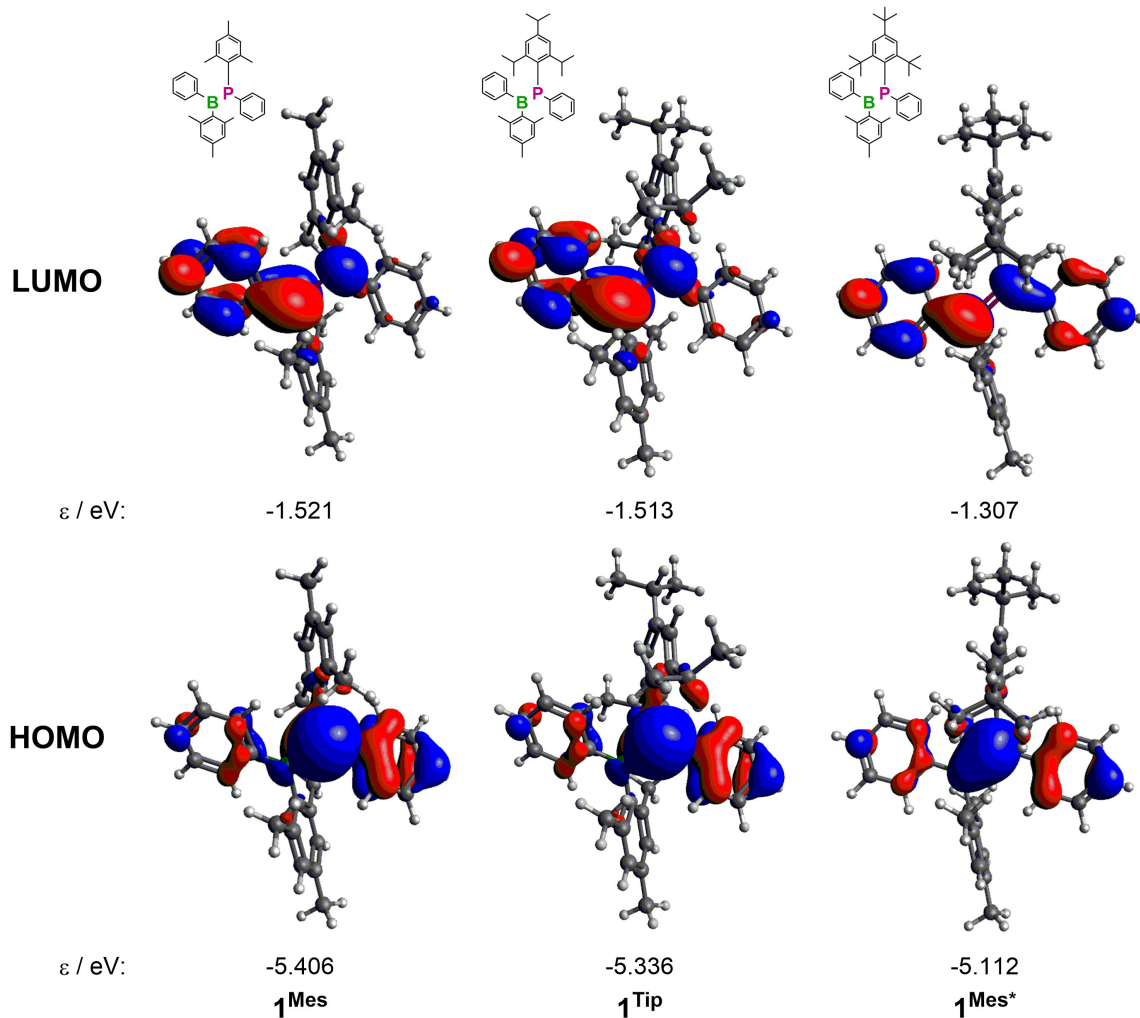


Figure 4.3.4. B3LYP-D3(BJ)/def2-SV(P) calculated frontier orbitals of $\mathbf{1}^{\text{Mes}}$, $\mathbf{1}^{\text{Tip}}$ and $\mathbf{1}^{\text{Mes}^*}$ (isovalue 0.030).

The calculated frontier orbitals of compounds **2** and **3** indicate a $\pi-\pi^*$ transition upon excitation as well (Figure 4.3.5). The HOMOs are mostly localized on the inner phenyl ring and the BP units, whereas the LUMOs are distributed throughout the whole system. Compound **3** shows a more coplanar arrangement of the phenyl rings and therefore exhibits stronger conjugation in comparison with **2**. Compound **3** exhibits phenyl-phenyl twist angles of 9.65° and 6.01° (central phenyl to terminal phenyl rings, respectively), whereas compound **2** exhibits phenyl-phenyl twist angles of 10.71° and 37.92° .

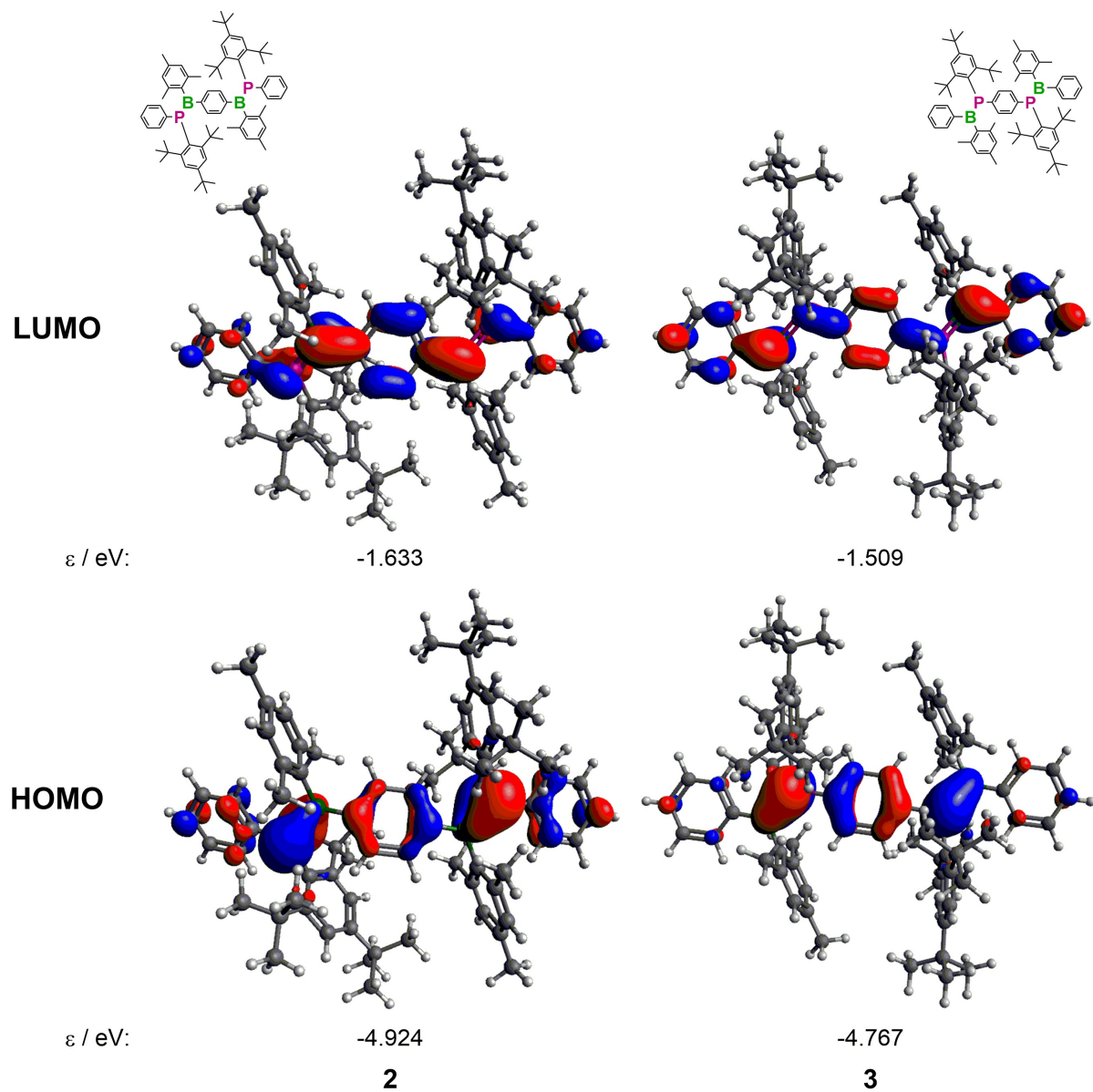
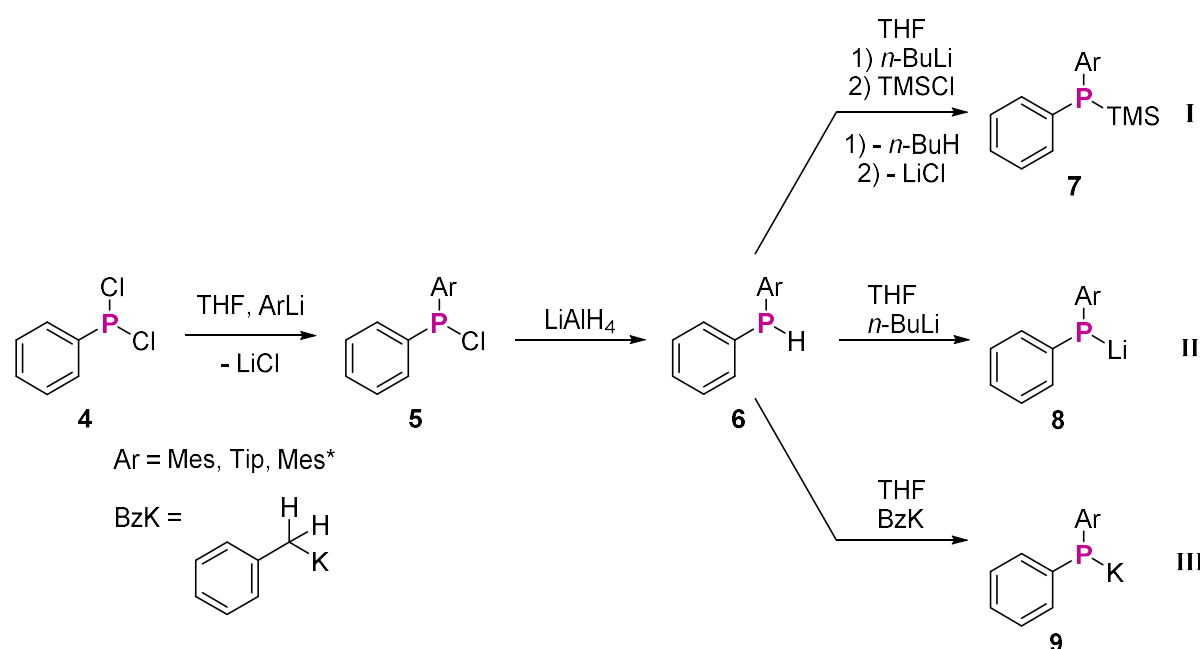


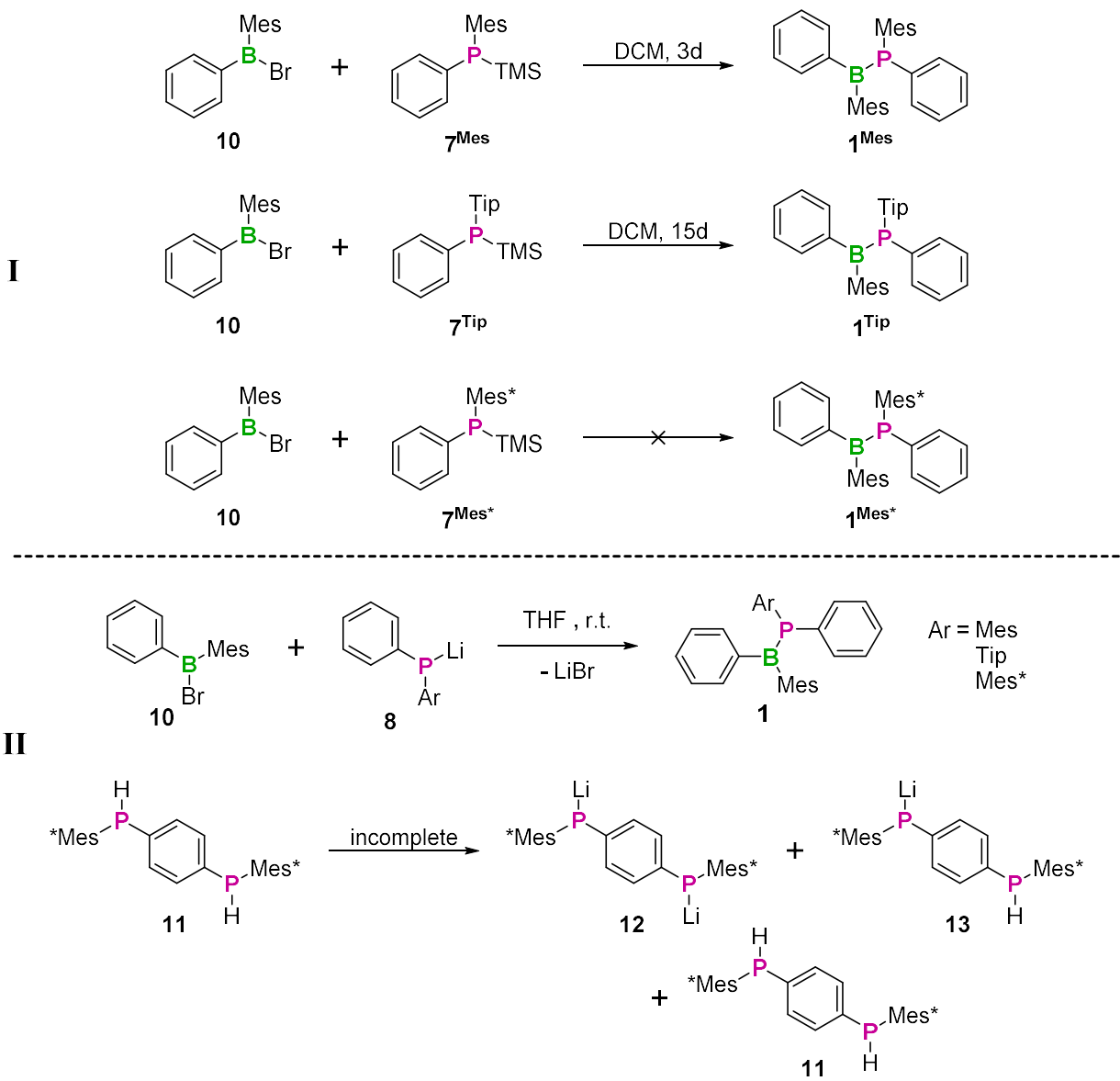
Figure 4.3.5. B3LYP-D3(BJ)/def2-SV(P) calculated frontier orbitals of **2** and **3** (isovalue 0.030).

For the synthesis of compounds **1–3**, three synthetic routes were investigated, featuring different reactive species of silylated or metalated diarylphosphanes, respectively (Scheme 4.3.1, **I–III**). Starting from *P,P*-dichlorophenylphosphine (**4**), reaction with the corresponding aryllithium compound leads to **5** and reduction with lithium aluminium hydride gives the corresponding aryl(phenyl)phosphane **6**. Compounds **6** can be lithiated and subsequently silylated with trimethylsilyl chloride to obtain **7** as the reactive phosphorus species for synthesis route **I**. For synthesis route **II**, compounds **6** are also lithiated and used as such. The last approach is accessible by reacting **6** with benzyl potassium to obtain potassium aryl(phenyl)phosphanide (**9**) as the reactive species for the synthesis route **III**.



Scheme 4.3.1. General synthetic pathway to phosphorus compounds in three different reactive species.

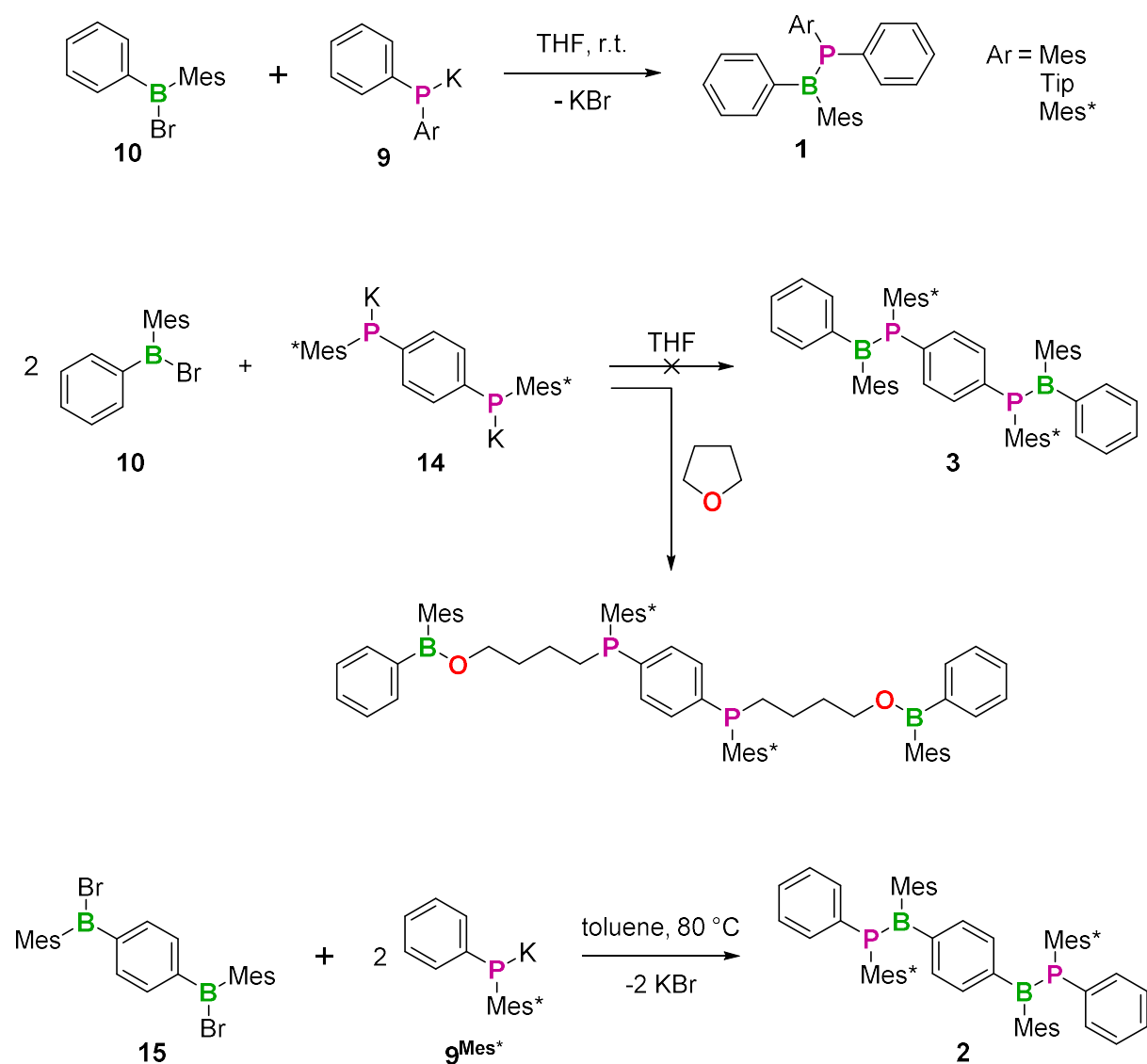
The first approach makes use of the Si/B exchange reaction, which was reported as a means for B-P bond formation by Pringle *et al.* in 2014^[7] and applied for the synthesis of the BN-PPV analogue by Helten *et al.* in 2017.^[8] Compound **1^{Mes}** was accessible via Si/B exchange reaction in 3 days, but **1^{Tip}** already had a reaction time of 15 days and showed large amounts of side products, due to occurring hydrolysis on that time scale (Scheme 4.3.2, **I**). Compound **1^{Mes*}** was not accessible via Si/B exchange reaction, which demonstrates that this procedure is strongly dependent on the steric demand of the substituents. Since our theoretical considerations predicted that the Mes* substituent is needed to planarize the phosphorus center, the Si/B exchange route is not applicable to access a BP-PPV analogue.



Scheme 4.3.2. Attempted syntheses with routes I and II.

The second synthesis route investigated was the lithium-salt elimination, which proved to be a viable strategy in the synthesis of BP compounds.^[5, 9] Compounds 1^{Mes} , 1^{Tip} and 1^{Mes^*} were accessible *via* this route in short times and with a significantly lesser extent of hydrolysis compared to the Si/B exchange reaction. The preparation of compound **3** *via* this route proved problematic. Attempted twofold lithiation of *p*-phenylene diphosphine remained incomplete (Scheme 4.3.2, **II**). This gave a mixture of one- and two-times lithiated alongside unlithiated species, which could not be separated. With a view to accessing a BP-PPV analogue, this compound would be an appropriate co-monomer. This, however, should only be feasible if the functionalized diphosphide is highly pure. Therefore, we conclude that the Li-salt elimination route is not suitable for this purpose.

The last investigated synthetic strategy uses potassium salt-elimination instead of lithium. The potassium phosphide compounds are accessible *via* adapted syntheses reported by Izod and co-workers in 2017.^[10] Compounds $\mathbf{1}^{\text{Mes}}$, $\mathbf{1}^{\text{Tip}}$ and $\mathbf{1}^{\text{Mes}^*}$ were obtained *via* K-salt elimination in THF (Scheme 4.3.3). Compound $\mathbf{3}$ was tried to be synthesized in THF as well, but cleavage of the THF occurred and butoxy groups were incorporated between the B and P centers of the product (Scheme 4.3.3 and Figure 4.3.6).



Scheme 4.3.3. Syntheses of compounds $\mathbf{1}^{\text{Mes}}$, $\mathbf{1}^{\text{Tip}}$, $\mathbf{1}^{\text{Mes}^*}$ in THF, attempted synthesis of $\mathbf{3}$ in THF and synthesis of $\mathbf{2}$ in toluene.

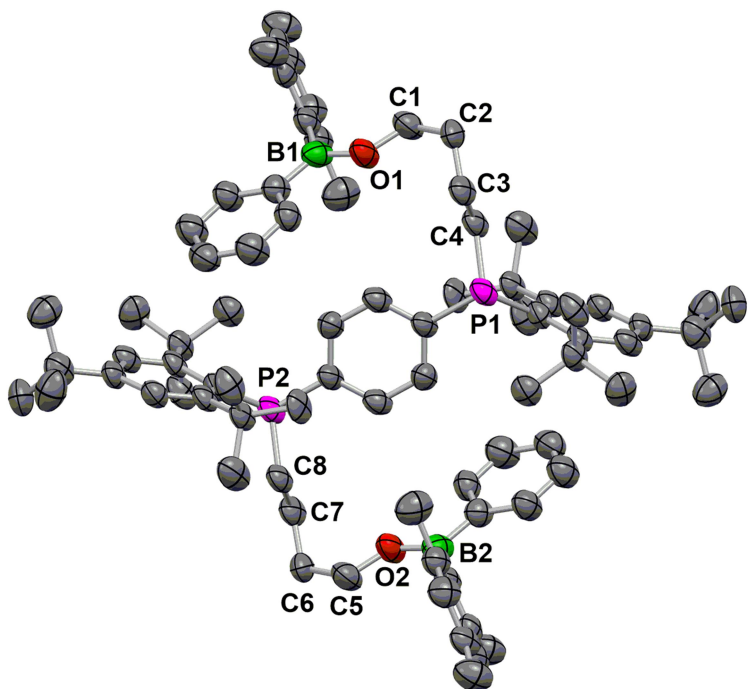


Figure 4.3.6. Molecular structure of the THF-cleavage product of **3** in the solid state by single-crystal X-ray diffraction (H-atoms omitted for clarity).^[†]

Concluding that THF is not suitable as the solvent for this kind of reaction, the synthesis of compound **2** was carried out in toluene, resulting in the desired compound as evidenced by its HRMS peak at $m/z = 1042.6995$ (figure 4.3.7). However, the HRMS still shows an additional signal at $m/z = 1114.7577$, which corresponds to the product of the cleavage of one THF molecule, that is, compound **2** with one butoxy group between one B and P. This THF molecule probably originates from the synthesis of the potassium phosphide, which is carried out in THF and might coordinate to the potassium (scheme 4.3.1). Therefore, we conclude that the potassium-salt elimination is a suitable synthesis route, but all reactions need to be carried out in absence of any ether solvent.

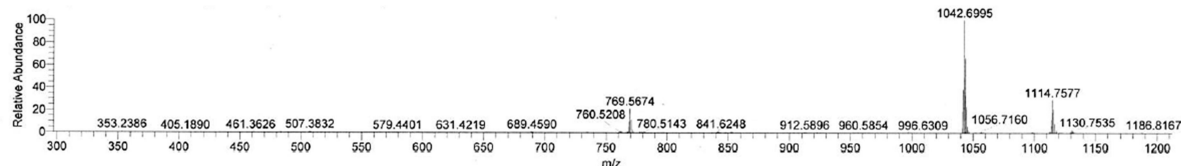


Figure 4.3.7. HRMS spectrum of compound **2**.

The structures of **1^{TiP}** and **1^{Mes*}** in the solid state were determined by single-crystal X-ray diffractometry. Figures 4.3.8 and 4.3.9 show the molecular structures with views perpendicular and parallel to the phenyl-BP-phenyl plane, respectively; selected structural parameters are listed in Table 4.3.3. The single-crystal X-ray diffraction analysis of

compound **1^{Tip}** revealed a B-P bond length of 1.839(2) Å, which is significantly shorter than the B-P bond length of 1.868 Å, predicted by our theoretical investigations. The experimental value for the sum of the angles around boron, 359.3°, matches the value we predicted by theory, revealing a planar boron center. The phosphorus center is stronger planarized by the Tip substituent than anticipated. It shows a sum of the angles of 347.4° in the solid state, whereas the theoretical investigation predicted a value of only 335.1°. Therefore, it can be concluded that the theoretical calculations underestimate the influence of the steric demand of the Tip substituent, but the Tip substituent is still not bulky enough to fully planarize the phosphorus center.

Table 4.3.3. Structural parameters according to single-crystal X-ray diffraction.

compound	B-P bond length / Å	sum of angles around B / °	sum of angles around P / °
1^{Tip}	1.839(2)	359.3	347.4
1^{Mes*}	1.812(3)	359.9	359.7

Compound **1^{Mes*}** shows a B-P bond length of 1.812(3) Å, according to the single-crystal X-ray diffraction study, which is in good agreement with the computationally predicted value of 1.816 Å. The boron center exhibits a sum of the angles of 359.9°, which also is in accordance with the predicted value of 360.0°. The geometry at the phosphorus center also matches the theoretical prediction by showing a sum of the angles of 359.7° in the solid state. This proves that a Mes* substituent effectively planarizes a phosphorus center in a BP unit, providing the prerequisite for effective conjugation over the BP unit.

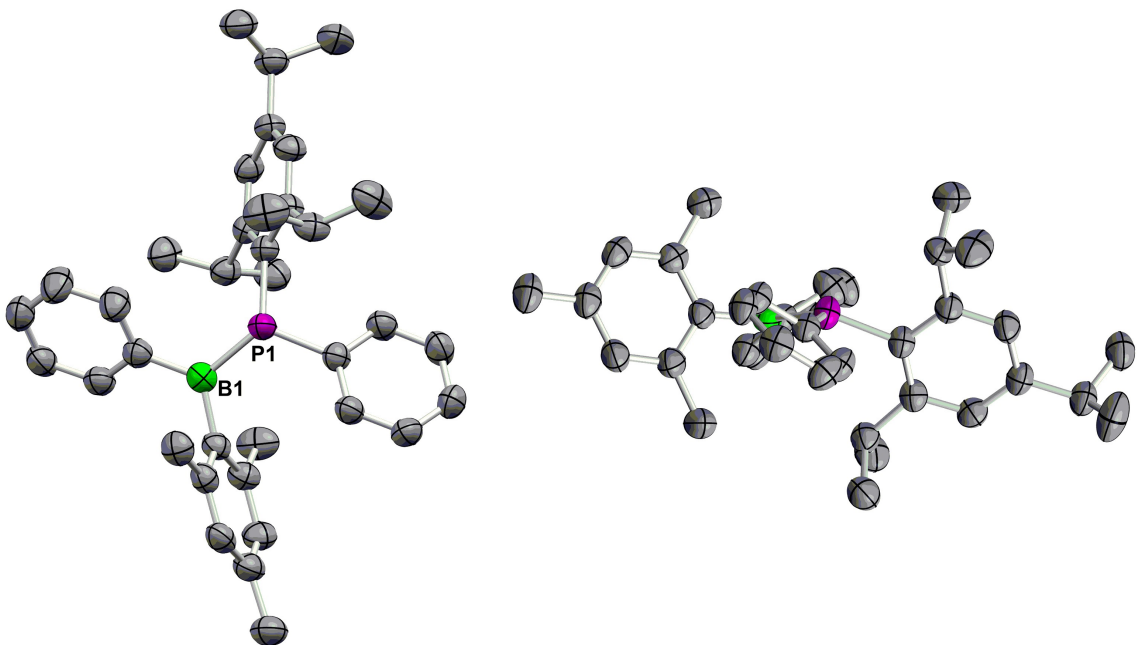


Figure 4.3.8. Molecular structure of $\mathbf{1}^{\text{Tip}}$ (with views perpendicular and parallel to the Ph-BP-Ph plane) in the solid state by single-crystal X-ray diffraction (H-atoms omitted for clarity).

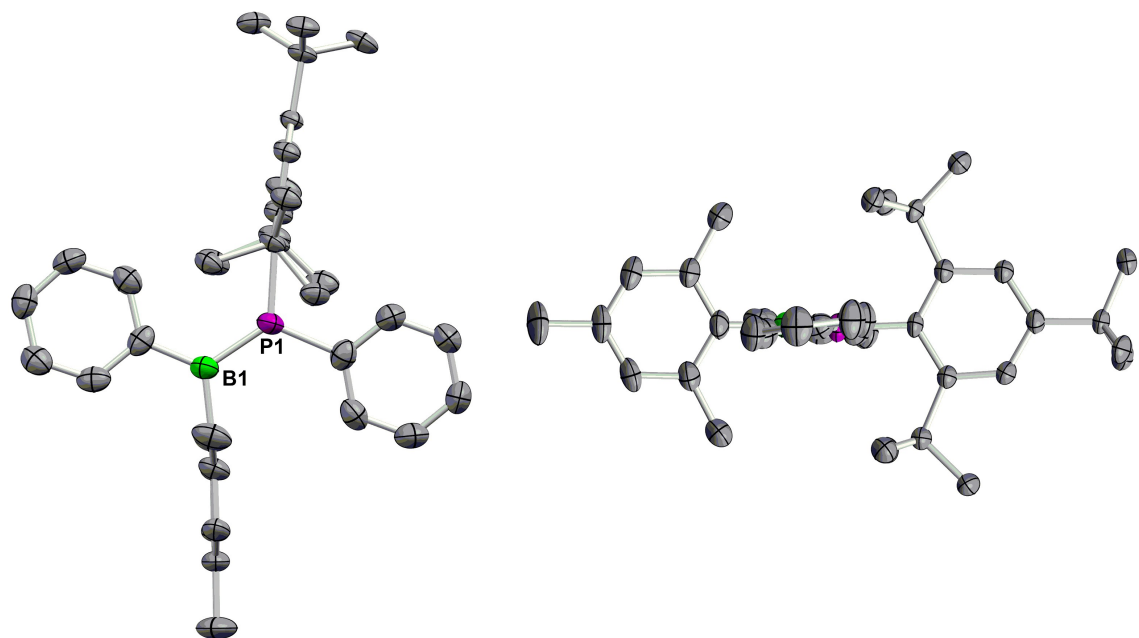


Figure 4.3.9. Molecular structure of $\mathbf{1}^{\text{Mes}*}$ (with views perpendicular and parallel to the Ph-BP-Ph plane) in the solid state by single-crystal X-ray diffraction (H-atoms omitted for clarity).

The UV-vis absorption spectra for **1^{Mes}**, **1^{Tip}** and **1^{Mes*}** in THF display one absorption band each, which we assign on the basis of the above mentioned calculations to a charge transfer or a π - π^* transition, respectively (Figures 4.3.4, 4.3.10 and Table 4.3.2). Compounds **1^{Tip}** and **1^{Mes*}** show weak fluorescence with large Stokes shifts ($8500 - 10154 \text{ cm}^{-1}$), whereas **1^{Mes}** shows extremely weak emission. With increasing steric demand of the phosphorus substituent, a slight red shift of the absorption maxima occurs, which, however, is hardly significant. The molar attenuation coefficients for compounds **1^{Mes}** and **1^{Tip}** are almost the same, both at around $20000 \text{ L}\cdot\text{mol}^{-1}\cdot\text{cm}^{-1}$, indicating that the orbital overlap is hardly influenced by the introduction of the Tip substituent (Table 4.3.4). Compound **1^{Mes*}**, on the other hand, exhibits a molar attenuation coefficient of approximately $35000 \text{ L}\cdot\text{mol}^{-1}\cdot\text{cm}^{-1}$, which indicates that the orbital overlap is greatly improved upon planarization of the phosphorus center.

Table 4.3.4. Photophysical data for **1^{Mes}**, **1^{Tip}** and **1^{Mes*}**.^[a]

compound	$\lambda_{\text{abs}} / \text{nm}$	$\lambda_{\text{em}} / \text{nm}$	$\Phi_{\text{fl}}^{[b]}$	FWHM / cm^{-1} (eV)	$\epsilon / \text{L}\cdot\text{mol}^{-1}\cdot\text{cm}^{-1}$ ^[c]
1^{Mes}	368	-	-	-	20698
1^{Tip}	372	544	0.02	-	19594
1^{Mes*}	374	603	0.06	4259 (0.53)	35324

^[a] In THF. ^[b] Fluorescence quantum yield determined absolutely with an integrating sphere. ^[c] Determined at the respective absorption maximum.

Compound **1^{Tip}** exhibits an emission maximum at 544 nm with a fluorescence quantum yield of 2%. Compared to **1^{Tip}**, although the absorption maximum is almost at the same wavelength, the absorption band of compound **1^{Mes*}** has a larger Stokes shift with a maximum at 603 nm, showing a fluorescence quantum yield of 6% and a quite large full-width at half-maximum of 4259 cm^{-1} .

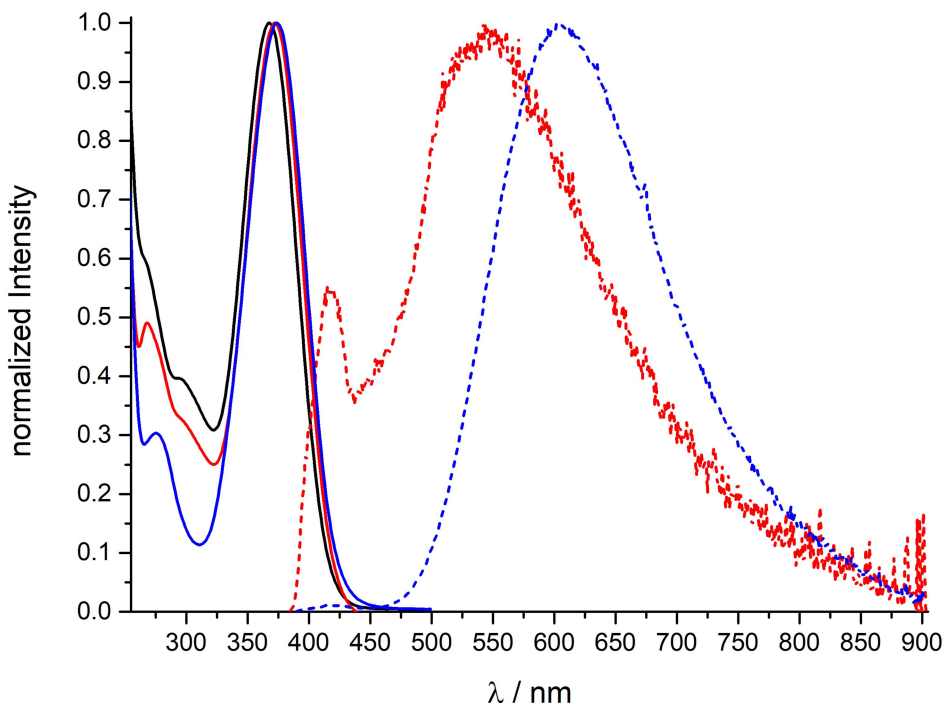


Figure 4.3.10. UV-vis absorption spectra (solid lines, in THF) of $\mathbf{1}^{\text{Mes}}$ (black), $\mathbf{1}^{\text{Tip}}$ (red) and $\mathbf{1}^{\text{Mes}^*}$ (blue) and fluorescence spectra (dashed lines, in THF) of $\mathbf{1}^{\text{Tip}}$ (red) and $\mathbf{1}^{\text{Mes}^*}$ (blue).

4.3.3 Conclusion

In conclusion, we have investigated the theoretical and synthetic approach to the first molecular model compounds of a boron-phosphorus analogue of the conjugated polymer PPV. Theoretical studies regarding the influence of sterically demanding substituents on the planarity of phosphorus revealed that the supermesityl substituent is effective to fully planarize the phosphorus center, therefore enabling conjugation over the BP unit. A synthetic route to access such compounds has been found and first model compounds have been synthesized and characterized, supporting the theoretical findings by indicating strong double bond character in the B-P bond. Our studies provide a theoretical insight into BP unit-containing systems and a synthetic pathway to a conjugated polymer linked by BP units.

4.3.4 Experimental Section

General procedures. All manipulations before the aqueous workup were performed under an atmosphere of dry argon using standard Schlenk techniques or in an MBraun glovebox. Solvents (dichloromethane, *n*-hexane, toluene, THF, and diethyl ether) were dried and degassed by means of an MBraun SPS-800 solvent purification system. CDCl₃, C₆D₆ and THF-d₈ for NMR spectroscopy were dried and degassed at reflux over CaH₂ or Na, respectively, and freshly distilled prior to use. *n*-Butyllithium solutions (1.6 M and 2.5 M in hexanes), Hydrogen chloride solution (2.0 M in diethyl ether), Lithiumaluminiumhydrid, Boron tribromide, 1,3,5-trimethylphenyl bromide, 1-Bromo-2,4,6-triisopropylbenzene, 1,3,5-tri-*tert*-butylbenzene, dimethylamine, 1,4-Diodobenzene, Phosphorus trichloride and *P,P*-Dichlorophenylphosphine were commercially purchased and used as received. Trimethylsilyl chloride was purified by inert-gas distillation. 2,4,6-trimethylphenyllithium,^[11] 2,4,6-triisopropylphenyllithium,^[12] 2-bromo-1,3,5-tri-*tert*-butylbenzene,^[13] 2,4,6-tri-*tert*-butylphenyl-lithium,^[14] Dibromoborylbenzene,^[15] 1,4-bis(dibromoboryl)benzene,^[16] Benzyl potassium,^[17] Bis(*N,N*-dimethylamino)chlorophosphine^[18] and 1,4-dilithiobenzene^[19] were prepared according to literature procedures. (2,4,6-trimethylphenyl)bromoborylbenzene^[20] and 1,4-bis[(2,4,6-trimethylphenyl)bromoboryl]benzene^[8] were prepared *via* adapted literature procedures. NMR spectra were recorded at 25 °C on a Bruker Avance III HD spectrometer operating at 300 MHz or on a Bruker Avance 500 spectrometer operating at 500 MHz. Chemical shifts were referenced to residual protic impurities in the solvent (¹H) or the deuterio solvent itself (¹³C) and reported relative to external SiMe₄ (¹H, ¹³C, ²⁹Si), BF₃·OEt₂ (¹¹B) or CFCl₃ (¹⁹F) standards. Mass spectra were obtained with the use of a Thermo Scientific Exactive Plus Orbitrap MS system employing Liquid Injection Field Desorption Ionisation (LIFDI). UV-vis spectra were obtained using a Jasco V-630 spectrophotometer. Emission spectra were recorded using an Edinburgh Instruments FLSP920 spectrometer equipped with a double monochromator for both excitation and emission, operating in right-angle geometry mode, and all spectra were fully corrected for the spectral response of the instrument. Fluorescence quantum yields were measured using a calibrated integrating sphere from Edinburgh Instruments combined with the FLSP920 spectrometer described above.

Crystals suitable for single-crystal X-ray diffraction were selected, coated in perfluoropolyether oil, and mounted on MiTeGen sample holders. Diffraction data were collected on Bruker X8 Apex II 4-circle diffractometers with CCD area detectors using Mo K α radiation (2Sn) or on XtaLAB Synergy, Dualflex, HyPix diffractometer equipped using

Cu K α radiation (micro-focus sealed X-ray tube, $\lambda = 1.54184 \text{ \AA}$). The crystals were cooled using an Oxford Cryostreams low-temperature device. Data were collected at 100 K. The images were processed and corrected for Lorentz-polarization effects and absorption as implemented in the Bruker software packages (2Sn) or as implemented in CrysAlisPro (Version 40_64.45a). The structures were solved using the intrinsic phasing method (SHELXT)^[21] and Fourier expansion technique. All non-hydrogen atoms were refined in anisotropic approximation, with hydrogen atoms ‘riding’ in idealized positions, by full-matrix least squares against F2 of all data, using SHELXL^[22] software and the SHELXLE graphical user interface.^[23] Other structural information was extracted using OLEX2 software.^[24]

Spectra. All spectra and other result figures are shown in Appendix 7.3

Synthesis of (2,4,6-trimethylphenyl)bromoborylbenzene (10) [PhMesBBr]. To a stirred suspension of MesLi (1.2547 g, 9.95 mmol) in toluene (10 mL) was added dropwise a solution of dibromoboryl-benzene (2.6065 g, 10.52 mmol) in toluene (10 mL) at -78°C . Subsequently, the mixture was warmed to room temperature and stirred overnight. The solid was filtered off and all volatiles were removed *in vacuo*. The slight yellowish oil was purified via distillation ($105^\circ\text{C}, 4 \cdot 10^{-2} \text{ mbar}$) to obtain the product as a colourless oil. Yield: 2.473 g (8.62 mmol, 87 %). ^1H NMR (400 MHz, CDCl₃): $\delta = 8.06$ (d, $J = 7.53 \text{ Hz}$, 2H, *o*-Ph-H), 7.67 (t, $J = 7.53 \text{ Hz}$, 1H, *p*-Ph-H), 7.49 (dd, $J = 7.53 \text{ Hz}$, 2H, *m*-Ph-H), 6.92 (s, 2H, Mes-CH arom.), 2.39 (s, 3H, *p*-Mes-CH₃), 2.19 ppm (s, 6H, *o*-Mes-CH₃); $^{11}\text{B}\{\text{H}\}$ NMR (128 MHz, CDCl₃): $\delta = 70.8 \text{ ppm}$ (s).

Synthesis of 1,4-bis[(2,4,6-trimethylphenyl)bromoboryl]benzene (15) [Ph(MesBBr)₂]. To a suspension of 1,4-bis(dibromoboryl)benzene (1.6531 g, 3.96 mmol) in toluene (20 mL) was slowly added a suspension of MesLi (1.00 g; 7.93 mmol) in toluene (20 mL) at -78°C . Subsequently, the mixture was warmed to room temperature and stirred overnight. The solid was filtered off and all volatiles were removed *in vacuo*. The residue was recrystallized from DCM to obtain the product as an off-white solid. Yield: 1.659 g (3.28 mmol, 83 %). ^1H NMR

(500 MHz, C₆D₆): δ = 7.99 (s, 4H, Ph-H), 6.71 (s, 4H, Mes-CH arom.), 2.17 (s, 6H, *p*-Mes-CH₃), 2.05 ppm (s, 12H, *o*-Mes-CH₃); ¹¹B{¹H} NMR (160 MHz, C₆D₆): 73.3 ppm (s).

General synthesis of aryl(phenyl)chlorophosphine (5**) [ArPhPCl].** To a stirred suspension of the corresponding aryllithium compound (10.00 mmol) in toluene (30 mL) was added dropwise neat *P,P*-dichlorophenylphosphine (11.00 mmol) at -78 °C. Subsequently, the mixture was warmed to room temperature and stirred overnight. All volatiles were removed *in vacuo* and the residue was dissolved in *n*-hexane (30 mL) and filtered. After removing all volatiles *in vacuo* the products were obtained as yellowish oils. Yields: 95 % (Mes); 95 % (Tip); 96 % (Mes*).

Mes: ¹H NMR (400 MHz, CDCl₃): δ = 7.36 (m, 5H, Ph-H), 6.93 (d, *J* = 3.07 Hz, 2H, Mes-CH arom.), 2.43 (d, *J* = 1.97 Hz, 6H, *o*-Mes-CH₃), 2.32 ppm (s, 3H, *p*-Mes-CH₃). ³¹P{¹H} NMR (202 MHz, CDCl₃): δ = 82.1 ppm (s);

Tip: ¹H NMR (400 MHz, CDCl₃): δ = 7.36 (m, 5H, Ph-H), 7.11 (d, *J* = 2.89 Hz, 2H, Tip-CH arom.), 3.76 (oct, *J* = 6.51 Hz, 2H, *o*-Tip-CH), 2.93 (sept, *J* = 6.97 Hz, 1H, *p*-Tip-CH), 1.30 (d, *J* = 6.92 Hz, 6H, *o*-Tip-CH₃), 1.24 (d, *J* = 6.79 Hz, 6H, *o*-Tip-CH₃), 1.01 ppm (d, *J* = 6.74 Hz, 6H, *p*-Tip-CH₃); ³¹P{¹H} NMR (202 MHz, CDCl₃): δ = 78.6 ppm (s);

Mes*: ¹H NMR (400 MHz, CDCl₃): δ = 7.47 (d, *J* = 2.52 Hz, 2H, Mes*-CH arom.), 7.14 (m, 3H, Ph-H), 6.75 (m, 2H, Ph-H), 1.41 (s, 18H, *o*-Mes*-CH₃), 1.36 ppm (s, 9H, *p*-Mes*-CH₃). ³¹P{¹H} NMR (202 MHz, CDCl₃): δ = 75.3 ppm (s).

General synthesis of aryl(phenyl)phosphane (6**) [ArPhPH].** To a stirred suspension of lithium aluminium hydride (11.00 mmol) in diethyl ether (20 mL) was added dropwise a solution of the corresponding aryl(phenyl)chlorophosphine (10.00 mmol) in diethyl ether (20 mL) at 0 °C. The cooling bath was removed and the mixture was stirred for 1 h. Subsequently, degassed water was added at 0 °C to quench the remaining lithium aluminium hydride until the solid clumped together. The supernatant solution was separated and dried in *vacuo*. The products were obtained as colourless oils (Mes and Tip) or a white solid (Mes*), respectively. Yields: 85 % (Mes); 80 % (Tip); 80 % (Mes*).

Mes: ^1H NMR (400 MHz, CDCl_3): $\delta = 7.24$ (m, 5H, Ph-H), 6.96 (s, 2H, Mes-CH arom.), 5.37 (d, $J = 223.56$ Hz, 1H, PH), 2.42 (s, 6H, *o*-Mes- CH_3), 2.31 ppm (s, 3H, *p*-Mes- CH_3). $^{31}\text{P}\{\text{H}\}$ NMR (202 MHz, CDCl_3): $\delta = -76.6$ ppm (s);

Tip: ^1H NMR (400 MHz, CDCl_3): $\delta = 7.24$ (m, 5H, Ph-H), 7.10 (d, $J = 2.32$ Hz, 2H, Tip-CH arom.), 5.39 (d, $J = 221.85$ Hz, 1H, PH), 3.60 (oct, $J = 6.79$ Hz, 2H, *o*-Tip-CH), 2.93 (sept, $J = 6.91$ Hz, 1H, *p*-Tip-CH), 1.30 (d, $J = 6.91$ Hz, 6H, *p*-Tip- CH_3), 1.19 (d, $J = 6.79$ Hz, 6H, *o*-Tip- CH_3), 1.15 ppm (d, $J = 6.85$ Hz, 6H, *o*-Tip-CH); $^{31}\text{P}\{\text{H}\}$ NMR (202 MHz, CDCl_3): $\delta = -82.8$ ppm (s);

Mes*: ^1H NMR (400 MHz, CDCl_3): $\delta = 7.53$ (d, $J = 2.26$ Hz, 2H, Mes*-CH arom.), 7.12 (m, 3H, Ph-H), 6.70 (m, 2H, Ph-H), 6.10 (br d, $J = 200.03$ Hz, 1H, PH), 1.49 (s, 18H, *o*-Mes*- CH_3), 1.38 ppm (s, 9H, *p*-Mes*- CH_3); $^{31}\text{P}\{\text{H}\}$ NMR (202 MHz, CDCl_3): $\delta = -65.1$ ppm (s).

General synthesis of aryl(phenyl)(trimethylsilyl)phosphane (7) [ArPhPTMS]. To a stirred solution of the corresponding aryl(phenyl)phosphane (22.00 mmol) in THF (35 mL) was added *n*-BuLi (2.5 M in hexanes, 33.00 mmol) at -60°C . After stirring for 2 h, the mixture was cooled to -78°C and trimethylsilyl chloride (36.00 mmol) was added. The mixture was warmed to room temperature and stirred overnight. All volatiles were removed *in vacuo* and the residue was taken up in *n*-hexane (40 mL). After filtration, all volatiles were removed *in vacuo* and the products were obtained as brownish-black oil (Mes), orange solid (Tip) or yellowish-white solid (Mes*), respectively.

Mes: ^1H NMR (400 MHz, C_6D_6): $\delta = 7.27$ (m, 2H, Ph-H), 7.04 (m, 2H, Ph-H), 6.94 (m, 1H, *p*-Ph-H), 6.84 (d, $J = 2.20$ Hz, 2H, Mes-CH arom.), 2.44 (s, 6H, *o*-Mes- CH_3), 2.11 (s, 3H, *p*-Mes- CH_3), 0.26 ppm (d, $J = 5.38$ Hz, 9H, Si-(CH_3)₃); $^{31}\text{P}\{\text{H}\}$ NMR (162 MHz, C_6D_6): $\delta = -72.4$ ppm (s);

Tip: ^1H NMR (400 MHz, C_6D_6): $\delta = 7.29$ (m, 2H, Ph-H), 7.22 (d, $J = 2.51$ Hz, 2H, Tip-CH arom.), 6.97 (m, 2H, Ph-H), 6.91 (m, 1H, *p*-Ph-H), 4.07 (oct, $J = 6.78$ Hz, 2H, *o*-Tip-CH), 2.78 (sept, $J = 7.03$ Hz, 1H, *p*-Tip-CH), 1.23 (d, $J = 6.78$ Hz, 12H, *o*-Tip- CH_3), 1.20 (d, $J = 7.03$ Hz, 6H, *p*-Tip- CH_3); 0.35 (d, $J = 6.02$ Hz, 9H, Si-(CH_3)₃); $^{31}\text{P}\{\text{H}\}$ NMR (162 MHz, C_6D_6): $\delta = -63.1$ ppm (s);

Mes*: ^1H NMR (400 MHz, C_6D_6): $\delta = 7.72$ (d, $J = 2.66$ Hz, 2H, Mes*-CH arom.), 7.00 (m, 4H, Ph-CH), 6.86 (m, 1H, *p*-Ph-CH), 1.65 (s, 18H, *o*-Mes*- CH_3), 1.32 (s, 9H, *p*-Mes*- CH_3),

0.46 ppm (d, $J = 6.42$ Hz, 9H, Si-(CH_3)₃); $^{31}P\{^1H\}$ NMR (162 MHz, C₆D₆): $\delta = -56.6$ ppm (s).

General synthesis of potassium aryl(phenyl)phosphanide (9) [ArPhPK]. Benzyl potassium (2.00 mmol) and the corresponding aryl(phenyl)phosphane (2.05 mmol) were placed in a Schlenk flask and THF (10 mL) was added. After stirring for 2 h, all volatiles were removed *in vacuo*. *n*-Hexane (40 mL) was added and the precipitate was filtered. Drying the precipitate *in vacuo* gave the products as yellow (Mes and Tip) and orange (Mes*) solids.

Mes: 1H NMR (400 MHz, THF-d₈): $\delta = 6.71$ (d, 2H, Mes-CH arom.), 6.69 (t, 2H, *o*-Ph-H), 6.48 (t, 2H, *m*-Ph-H), 6.06 (t, 1H, *p*-Ph-H), 2.48 (s, 6H, *o*-Mes-CH₃), 2.16 ppm (s, 3H, *p*-Mes-CH₃); $^{31}P\{^1H\}$ NMR (202 MHz, THF-d₈): $\delta = -34.5$ ppm (s);

Tip: 1H NMR (400 MHz, THF-d₈): $\delta = 6.86$ (d, $J = 1.04$ Hz, 2H, Tip-CH arom.), 6.59 (t, 2H, *o*-Ph-H), 6.40 (t, 2H, *m*-Ph-H), 5.95 (t, 1H, *p*-Ph-H), 4.48 (oct, $J = 6.91$ Hz, 2H, *o*-Tip-CH), 2.79 (sept, $J = 6.91$ Hz, 1H, *p*-Tip-CH), 1.23 (d, $J = 6.91$ Hz, 6H, *p*-Tip-CH₃), 1.10 ppm (d, $J = 6.91$ Hz, 12H, *o*-Tip-CH₃); $^{31}P\{^1H\}$ NMR (202 MHz, THF-d₈): $\delta = -56.1$ ppm (s);

Mes*: 1H NMR (400 MHz, THF-d₈): $\delta = 7.33$ (d, $J = 1.04$ Hz, 2H, Mes*-CH arom.), 6.75 (br, 1H, Ph-H), 6.24 (br, 2H, Ph-H), 5.69 (t, 1H, *p*-Ph-H), 5.08 (br, 1H, Ph-H), 1.70 (d, $J = 1.28$ Hz, 18H, *o*-Mes*-CH₃), 1.30 ppm (s, 9H, *p*-Mes*-CH₃); $^{31}P\{^1H\}$ NMR (202 MHz, THF-d₈): $\delta = -14.5$ ppm (s).

Synthesis of *p*-phenylene-bis(*N,N,N',N'*-tetramethyl-phosphanediamine) [Ph(P(NMe₂)₂)₂]. To a suspension of 1,4-dilithiobenzene (60 mmol) in diethyl ether (120 mL) was added neat bis(*N,N*-dimethylamino)chlorophosphine (18.25 g, 118.06 mmol) at -40 °C. After stirring for 30 min at -40 °C the mixture was warmed to room temperature and stirred overnight. The solid was filtered off and all volatiles were removed *in vacuo*. Recrystallization from DCM gave the product as an off-white solid. Yield: 15.2 g (48.3 mmol, 81 %). 1H NMR (400 MHz, CDCl₃): $\delta = 7.38$ (t, $J = 3.92$ Hz, 4H, Ph-H), 2.78 ppm (d, $J = 9.17$ Hz, 24H, N-CH₃); $^{31}P\{^1H\}$ NMR (122 MHz, CDCl₃): $\delta = 100.1$ ppm (s).

Synthesis of *p*-phenylene-bis(dichlorophosphine) [Ph(PCl₂)₂]. To a solution of *p*-phenylene-bis(*N,N,N',N'*-tetramethyl-phosphanediamine) (6.8 g, 21.63 mmol) in diethyl

ether (200 mL) was added hydrogen chloride (2.0 M in diethyl ether, 88 mL, 176.00 mmol) at 0 °C. Subsequently, the mixture was warmed to room temperature and stirred overnight. The solid was filtered off and all volatiles were removed *in vacuo*. Subsequently the residue was taken up in DCM, precipitated by adding *n*-pentane and cooled to –20 °C. The precipitate was filtered and dried *in vacuo* to obtain the product as a yellow solid. Yield: 4.68 g (16.7 mmol; 76 %). ^1H NMR (300 MHz, C_6D_6): δ = 7.31 ppm (q, 4H, Ph-*H*); $^{31}\text{P}\{\text{H}\}$ NMR (122 MHz, C_6D_6): δ = 157.1 ppm (s).

Synthesis of *p*-phenylene-bis[(2,4,6-tris-*tert*-butylphenyl)chlorophosphine] [Ph(Mes*PCl)₂]. To a suspension of Mes*Li (4.86 g, 19.26 mmol) in toluene (70 mL) was added a suspension of *p*-phenylene-bis(dichlorophosphine) (2.625 g, 9.38 mmol) in toluene (30 mL) at –78 °C. Subsequently, the mixture was warmed to room temperature and stirred overnight. The solid was filtered off and all volatiles were removed *in vacuo*. The product was obtained as a white solid. Yield: 5.45 g (7.79 mmol, 83 %). ^1H NMR (300 MHz, C_6D_6): δ = 7.54 (d, J = 6.05 Hz, 4H, Mes*-CH arom.), 6.76 (d, J = 16.32 Hz, 4H, Ph-*H*), 1.50 (d, J = 2.57 Hz, 36H *o*-Mes*-CH₃), 1.24 ppm (d, J = 3.85 Hz, 18H, *p*-Mes*-CH₃); $^{31}\text{P}\{\text{H}\}$ NMR (122 MHz, C_6D_6): δ = 74.9 (d, J = 1.94 Hz), 74.0 ppm (d, J = 1.94 Hz).

Synthesis of *p*-phenylene-bis[(2,4,6-tris-*tert*-butylphenyl)phosphane] (11) [Ph(Mes*PH)₂]. To a stirred suspension of lithium aluminium hydride (1.2 g, 31.62 mmol) in THF (60 mL) was added a suspension of *p*-phenylene-bis((2,4,6-tris-*tert*-butylphenyl)chlorophosphine) (4.901 g, 7.00 mmol) in THF (55 mL) at –78 °C. After stirring for 2 h at –78 °C the mixture was warmed to room temperature and stirred overnight. Degassed water was added at 0 °C until the remaining lithium aluminium hydride clumped together. The solid was washed with *n*-hexane (2 x 50 mL), the solution dried over MgSO₄, filtered and dried *in vacuo*. Recrystallization from THF gave the product as a white solid. Yield: 3.14 g (4.97 mmol, 71 %). ^1H NMR (500 MHz, C_6D_6): 7.62 (d, J = 2.09 Hz, 4H, Mes*-CH arom.), 6.64 (m, 4H, Ph-*H*), 6.12 (dd, J = 227.70 Hz, 2H, PH), 1.49 (br, 36H, *o*-Mes*-CH₃), 1.30 ppm (s, 18H, *p*-Mes*-CH₃); $^{31}\text{P}\{\text{H}\}$ NMR (202 MHz, C_6D_6): δ = –64.9 ppm (d, J = 11.56 Hz).

Synthesis of potassium *p*-phenylene-bis[(2,4,6-tris-*tert*-butylphenyl)phosphanide] (14) [Ph(Mes*PK)₂]. Benzyl potassium (0.0801 g, 0.62 mmol) and *p*-phenylene-bis((2,4,6-tris-

tert-butylphenyl)-phosphane) (0.1892 g, 0.30 mmol) were placed in a schlenk flask and THF (12 mL) was added. The mixture was stirred for 42 h at 50 °C. All volatiles were removed *in vacuo* and the residue was taken up in toluene (10 mL). After filtration and removing all volatiles *in vacuo* the product was obtained as a dark red solid. Yield: 0.1360 g (0.19 mmol, 63 %). ^1H NMR (400 MHz, THF-d₈): δ = 7.24 (s, 4H, Mes*-CH arom.), 7.19 (br, 4H, Ph-H), 1.31 (s, 36H, *o*-Mes*-CH₃), 1.25 ppm (s, 18H, *p*-Mes*-CH₃); $^{31}\text{P}\{\text{H}\}$ NMR (162 MHz, THF-d₈): δ = -22.7 ppm (s).

General synthesis of 1. Compound **10** (0.50 mmol) and the corresponding **9** (0.50 mmol) were placed in a Schlenk flask, THF (10 mL) was added and the mixture was stirred for 3 h. All volatiles were removed *in vacuo*, the residue dissolved in *n*-hexane and crystallized. The products were obtained as yellow solids.

Mes: ^1H NMR (500 MHz, THF-d₈): δ = 7.24 (m, 2H, B-*o*-Ph-H), 7.20 (m, 1H, B-*p*-Ph-H), 7.09 (d, J = 2.52 Hz, 2H, P-Mes-CH arom.), 7.06 (t, J = 7.57 Hz, 2H, B-*m*-Ph-H), 6.98 (m, 1H, P-*p*-Ph-H), 6.93 (m, 2H, P-*o*-Ph-H), 6.84 (s, B-Mes-CH arom.), 6.62 (m, 2H, P-*m*-Ph-H), 2.46 (s, 6H, P-*o*-Mes-CH₃), 2.35 (s, 3H, P-*p*-Mes-CH₃), 2.31 (s, 3H, B-*p*-Mes-CH₃), 2.14 (d, J = 1.58 Hz, 3H, B-*o*-Mes-CH₃); $^{11}\text{B}\{\text{H}\}$ NMR (160 MHz, THF-d₈): δ = 65.1 ppm; $^{13}\text{C}\{\text{H}\}$ NMR (126 MHz, THF-d₈): δ = 144.9 (d, J = 9.54 Hz, quart. P-*o*-Mes-C), 140.9 (br, quart. Ph-C-B), 140.7 (d, J = 2.15 Hz, quart. P-*p*-Mes-C), 139.6 (br, quart. Mes-C-B), 138.1 (d, J = 8.73 Hz, quart. B-*o*-Mes-C), 136.8 (d, J = 2.28 Hz, quart. B-*p*-Mes-C), 133.6 (d, J = 12.90 Hz, B-*o*-Ph-C), 132.8 (d, J = 36.94 Hz, quart. Ph-C-P), 130.3 (d, J = 2.69 Hz, B-*p*-Ph-C), 129.1 (d, J = 7.79 Hz, P-Mes-CH arom.), 128.7 (d, J = 10.61 Hz, P-*m*-Ph-CH), 127.8 (d, J = 10.34 Hz, P-*o*-Ph-CH), 127.5 (s, B-*m*-Ph-CH), 127.4 (d, J = 1.34 Hz, B-Mes-CH arom.), 126.1 (s, P-*o*-Ph-CH), 126.0 (d, J = 41.51 Hz, quart. Mes-C-P), 23.5 (d, J = 10.17 Hz, P-*o*-Mes-CH₃), 22.3 (d, J = 2.42 Hz, B-*o*-Mes-CH₃), 20.4 ppm (dd, B-*p*-Mes-CH₃ and P-*p*-Mes-CH₃); $^{31}\text{P}\{\text{H}\}$ NMR (202 MHz, THF-d₈): δ = -8.9 ppm (s); HRMS (LIFDI): m/z (%) = 434.2328, calcd. for C₃₀H₃₂BP: 434.2335; UV-vis (THF): $\lambda_{\text{abs,max}}$ 368 nm (ε = 20698 L mol⁻¹ cm⁻¹); fluorescence (THF): quantum yield not quantifiable;

Tip: ^1H NMR (500 MHz, THF-d₈): δ = 7.25 (d, J = 3.31 Hz, 2H, Tip-CH arom.), 7.16 (m, 1H, B-*p*-Ph-H), 7.13 (m, 2H, B-*o*-Ph-H), 7.00 (t, J = 7.57 Hz, 2H, B-*m*-Ph-H), 6.95 (m, 3H, P-Ph-H), 6.88 (s, 2H, Mes-CH arom.), 6.65 (m, 2H, P-Ph-H), 3.92 (oct, J = 6.78 Hz, 2H, *o*-Tip-CH), 3.00 (sept, J = 6.78 Hz, 1H, *p*-Tip-CH), 2.33 (s, 3H, *p*-Mes-CH₃), 2.19 (d,

$J = 1.73$ Hz, 6H, *o*-Mes-CH₃), 1.34 (d, $J = 6.94$ Hz, 6H, *p*-Tip-CH₃), 1.10 (d, $J = 6.94$ Hz, 6H, *o*-Tip-CH₃), 1.01 ppm (d, $J = 6.94$ Hz, 6H, *o*-Tip-CH₃); ¹¹B{¹H} NMR (160 MHz, THF-d₈): $\delta = 62.3$ ppm; ¹³C{¹H} NMR (126 MHz, THF-d₈): $\delta = 155.0$ (d, $J = 9.40$ Hz, quart. *o*-Tip-C), 152.4 (d, $J = 2.28$ Hz, quart. *p*-Tip-C), 140.7 (br, quart. Ph-C-B), 139.8 (br, quart. Mes-C-B), 138.2 (d, $J = 8.87$ Hz, quart. *o*-Mes-C), 136.9 (s, quart. *p*-Mes-C), 134.3 (d, $J = 40.97$ Hz, quart. Ph-C-P), 134.2 (d, $J = 13.16$ Hz, P-*o*-Ph-CH), 129.9 (d, $J = 2.96$ Hz, P-*p*-Ph-CH), 128.8 (d, $J = 10.07$ Hz, B-*o*-Ph-CH), 127.7 (d, $J = 10.61$ Hz, B-*m*-Ph-CH), 127.5 (d, $J = 1.34$ Hz, Mes-CH), 127.2 (s, P-*m*-Ph-CH), 126.0 (d, $J = 2.82$ Hz, B-*p*-Ph-CH), 124.6 (d, $J = 45.40$ Hz, Tip-C-P), 122.4 (d, $J = 8.19$ Hz, Tip-CH), 35.1 (d, $J = 10.21$ Hz, *o*-Tip-CH), 34.4 (s, *p*-Tip-CH), 24.2 (s, *o*-Tip-CH₃), 23.6 (s, *o*-Tip-CH₃), 23.2 (s, *p*-Tip-CH₃), 22.1 (d, $J = 2.42$ Hz, *o*-Mes-CH₃), 20.4 ppm (d, $J = 0.81$ Hz, *p*-Mes-CH₃); ³¹P{¹H} NMR (202 MHz, THF-d₈): $\delta = -12.3$ ppm (s); HRMS (LIFDI): m/z (%) = 518.3268, calcd. for C₃₆H₄₄BP: 518.3274; UV/vis (THF): $\lambda_{\text{abs,max}}$ 372 nm ($\varepsilon = 19594$ L mol⁻¹ cm⁻¹); fluorescence (THF): $\lambda_{\text{em}} = 544$ nm (for $\lambda_{\text{ex}} = 372$ nm; $\Phi_f = 0.02$);

Mes*: ¹H NMR (500 MHz, THF-d₈): $\delta = 7.83$ (m, 2H, Mes*-CH arom.), 7.12 (m, 3H, B-Ph-H), 7.00 (m, 2H, B-*m*-Ph-H), 6.95 (s, Mes-CH arom.), 6.90 (m, 3H, P-Ph-H), 6.50 (m, 2H, P-*m*-Ph-H), 2.37 (s, 3H, *p*-Mes-CH₃), 2.27 (s, 6H, *o*-Mes-CH₃), 1.54 (d, $J = 2.52$ Hz, 18H, *o*-Mes*-CH₃), 1.45 ppm (d, $J = 1.42$ Hz, 9H, *p*-Mes*-CH₃); ¹¹B{¹H} NMR (160 MHz, THF-d₈): $\delta = 49.7$ ppm; ¹³C{¹H} NMR (126 MHz, THF-d₈): $\delta = 157.7$ (d, $J = 5.64$ Hz, quart. *o*-Mes*-C), 153.5 (d, $J = 2.96$ Hz, quart. *p*-Mes*-C), 140.0 (br, quart. Mes-C-B), 139.6 (br, quart. Ph-C-B), 139.4 (d, $J = 9.80$ Hz, quart. *o*-Mes-C), 137.7 (d, $J = 66.22$ Hz, quart. Ph-C-P), 136.8 (d, $J = 2.28$ Hz, quart. *p*-Mes-C), 135.8 (d, $J = 12.90$ Hz, B-*o*-Ph-CH), 129.2 (d, $J = 2.69$ Hz, B-*p*-Ph-CH), 128.8 (d, $J = 7.25$ Hz, P-*m*-Ph-CH), 127.8 (s, Mes-CH arom.), 127.6 (d, $J = 12.49$ Hz, P-*o*-Ph-CH), 126.8 (s, B-*m*-Ph-CH), 125.7 (d, $J = 3.90$ Hz, P-*p*-Ph-CH), 124.4 (d, $J = 10.48$ Hz, Mes*-CH arom.), 121.3 (d, $J = 52.79$ Hz, quart. Mes*-C-P), 39.6 (s, quart. *o*-Mes*-*t*Bu-C), 35.2 (s, quart. *p*-Mes*-*t*Bu-C), 32.7 (s, *o*-Mes*-CH₃), 30.6 (s, *p*-Mes*-CH₃), 22.7 (s, *o*-Mes-CH₃), 20.5 ppm (s, *p*-Mes-CH₃); ³¹P{¹H} NMR (202 MHz, THF-d₈): $\delta = 16.4$ ppm (s); HRMS (LIFDI): m/z (%) = 560.3735, calcd. for C₃₉H₅₀BP: 560.3743; UV/vis (THF): $\lambda_{\text{abs,max}}$ 374 nm ($\varepsilon = 35324$ L mol⁻¹ cm⁻¹); fluorescence (THF): $\lambda_{\text{em}} = 603$ nm (for $\lambda_{\text{ex}} = 374$ nm; $\Phi_f = 0.06$).

Synthesis of 2. Compound **15** (0.1484 g, 0.30 mmol) and **9^{Mes*}** (0.2353 g, 0.60 mmol) were placed in a Schlenk flask, toluene (10 mL) was added and the mixture was stirred for 43 h at 80 °C. The solid was filtered off and all volatiles were removed *in vacuo*. The residue was dissolved in *n*-hexane and crystallized. **5** was obtained as a yellow solid. $^{11}\text{B}\{\text{H}\}$ NMR (128 MHz, THF-d₈): δ = 49.3 ppm; HRMS (LIFDI): m/z (%) = 1042.7017, calcd. for C₇₂H₉₄B₂P₂: 1042.6995.

Synthesis of 3. Compound **14** (0.0707 g, 0.10 mmol) and **10** (0.0577 g, 0.20 mmol) were placed in a schlenk flask, toluene (5 mL) was added and the mixture was stirred for 39 h at 80 °C. The solid was filtered off and all volatiles were removed *in vacuo*. The residue was dissolved in *n*-hexane and crystallized. **7** was obtained as a yellow solid. ^1H NMR (400 MHz, THF-d₈): δ = 7.26 (m, 4H), 7.46 (d, 4H, J = 12.47 Hz, Mes*-CH arom.), 7.36 (m, 2H), 7.25 (m, 4H), 6.81 (d, 4H, J = 4.40 Hz, Mes-CH arom.), 6.72 ppm (dt, 4H, J = 23.35 Hz, P-C₆H₄-P); $^{11}\text{B}\{\text{H}\}$ NMR (128 MHz, THF-d₈): δ = 48.4 ppm; $^{31}\text{P}\{\text{H}\}$ NMR (162 MHz, THF-d₈): δ = -19.5 ppm (s).

Crystal structures

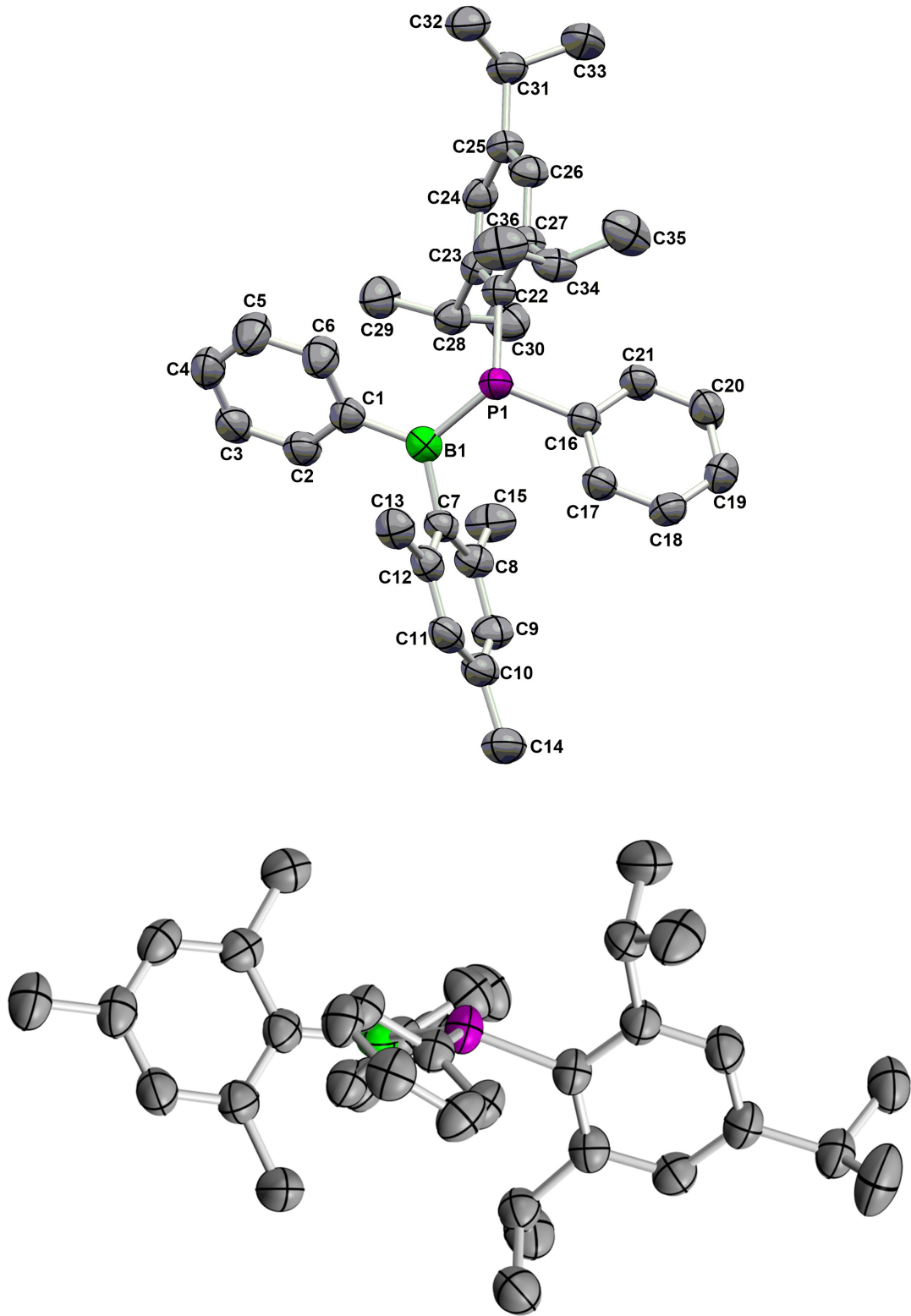


Figure 4.3.11. Molecular structure of $\mathbf{1}^{\text{Tip}}$ in the solid state by single-crystal X-ray diffraction (H-atoms omitted for clarity).

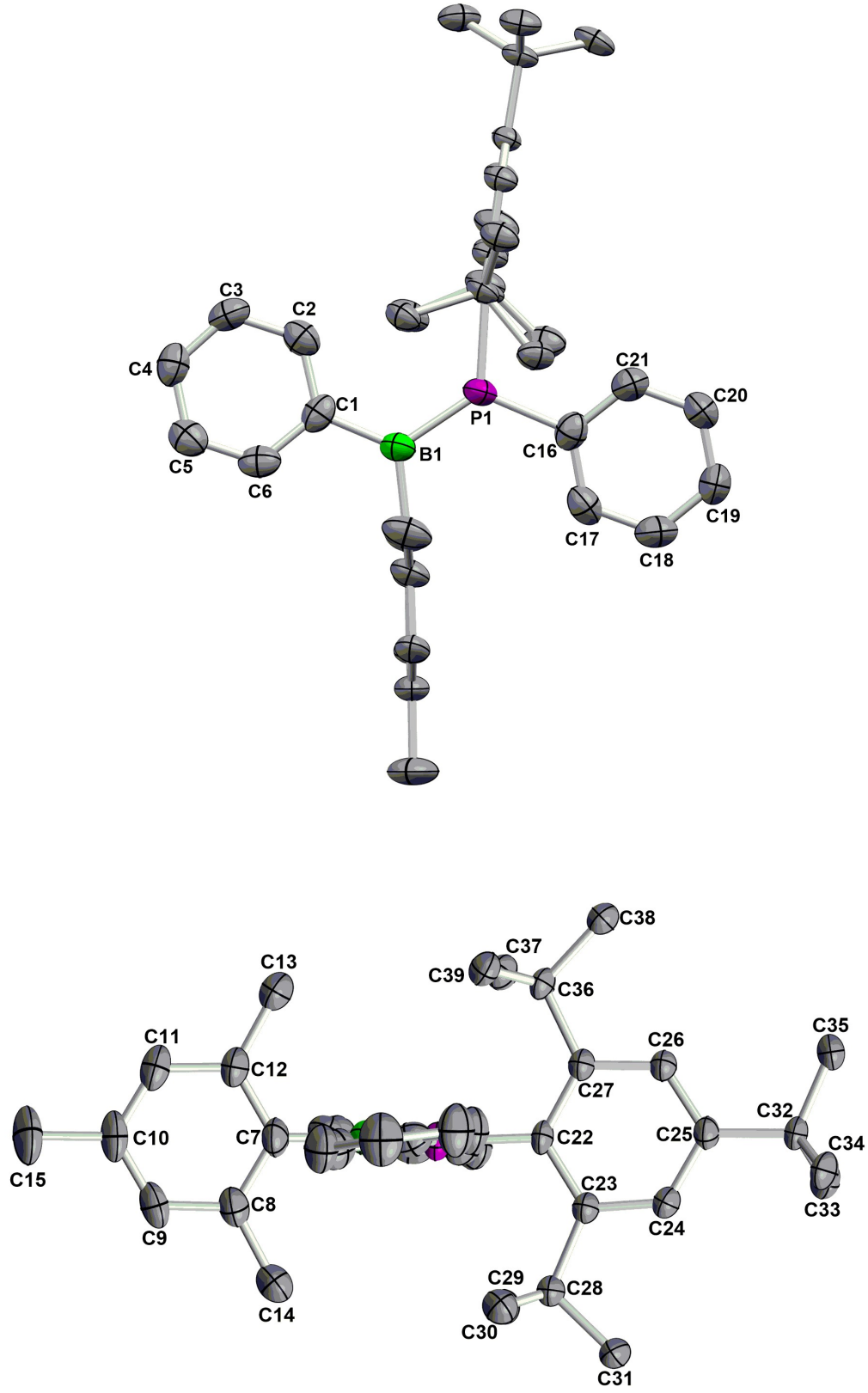


Figure 4.3.12. Molecular structure of $\mathbf{1}^{\text{Mes}*}$ (with views perpendicular and parallel to the Ph-BP-Ph plane) in the solid state by single-crystal X-ray diffraction (H-atoms omitted for clarity).

Table 4.3.5. Crystallographic data of $\mathbf{1}^{\text{Tip}}$ and $\mathbf{1}^{\text{Mes}^*}$.

No.	$\mathbf{1}^{\text{Tip}}$	$\mathbf{1}^{\text{Mes}^*}$
Size / mm	0.232 x 0.114 x 0.041	0.159 x 0.120 x 0.053
Empiric Formula	C ₃₆ H ₄₄ BP	C ₄₅ H ₆₄ BP
M	518.49	646.74
Crystal system	monoclinic	triclinic
Space group	C 2/c	P -1
a/Å	15.12310(10)	10.39980(10)
b/Å	12.70490(10)	10.43580(10)
c/Å	32.6233(2)	18.8046(2)
$\alpha/^\circ$	90	90.8600(10)
$\beta/^\circ$	92.2170(10)	90.6730(10)
$\gamma/^\circ$	90	101.8830(10)
V/Å³	6263.47(8)	1996.68(4)
Z	8	2
μ/mm^{-1}	0.918	0.802
T/K	100	100
$\theta_{\min,\max}$	2.711, 72.123	2.350, 72.121
Completeness	1.000	1.000
Reflections: total/independent	6180, 5976	7852, 7375
R_{int}	0.0347	0.0314
Final R1 and wR2	0.0521, 0.1356	0.0829, 0.2216
Largest peak, hole/eÅ⁻³	0.538, -0.361	3.654, -0.694
$\rho_{\text{calc}}/\text{g cm}^{-3}$	1.100	1.076

Computational methods. Optimization and TD-DFT calculations were carried out with the TURBOMOLE V7.0.1 program package.^[25] Becke's three parameter exchange-correlation hybrid functional B3LYP^[26] was used in combination with the valence-double- ζ basis set def2-SV(P).^[27] The empirical dispersion correction DFT-D3 by Grimme was used including the three-body term and with Becke-Johnson (BJ) damping.^[28] The stationary points were characterized as minima by an analytical vibrational frequency calculation,^[29] which revealed

the absence of imaginary frequencies. Vertical singlet excitations were calculated by means of time-dependent DFT^[30] using the same density functional and basis set.

Computational results:

Table 4.3.6. Results from TD-DFT calculations for compounds $\mathbf{1}^{\text{Mes}}$, $\mathbf{1}^{\text{Tip}}$, $\mathbf{1}^{\text{Mes}^*}$, $\mathbf{2}$ and $\mathbf{3}$.

compound	λ / nm	oscillator strength f	orbital contributions	$ c ^2 / \%$
$\mathbf{1}^{\text{Mes}}$	368	0.189918	HOMO \rightarrow LUMO	94.0
$\mathbf{1}^{\text{Tip}}$	375	0.193297	HOMO \rightarrow LUMO	96.8
$\mathbf{1}^{\text{Mes}^*}$	361	0.424503	HOMO \rightarrow LUMO	98.5
$\mathbf{2}$	430	0.825734	HOMO \rightarrow LUMO	98.8
$\mathbf{3}$	432	0.896669	HOMO \rightarrow LUMO	98.7

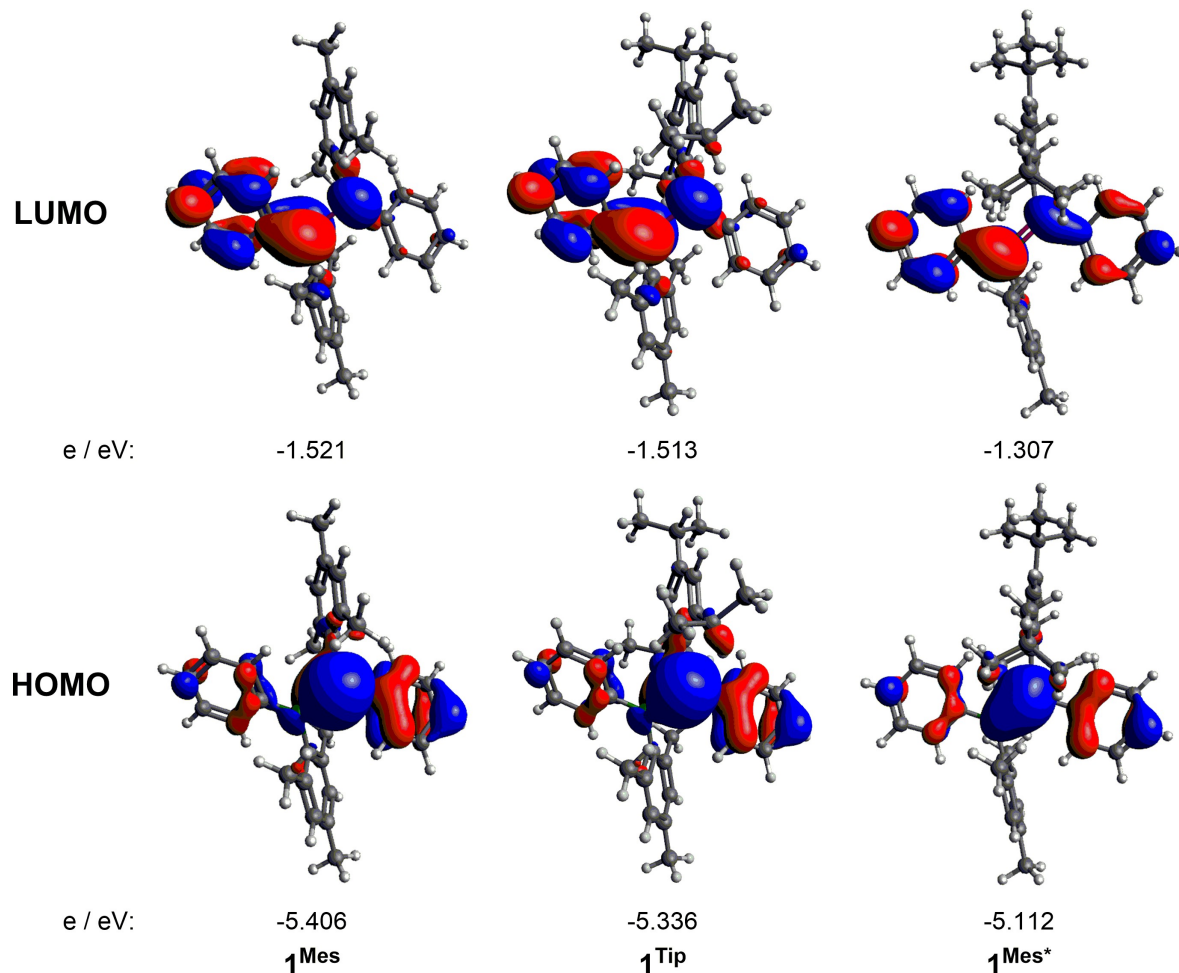


Figure 4.3.13. B3LYP-D3(BJ)/def2-SV(P) calculated frontier orbitals of $\mathbf{1}^{\text{Mes}}$, $\mathbf{1}^{\text{Tip}}$ and $\mathbf{1}^{\text{Mes}^*}$ (isovalue 0.030).

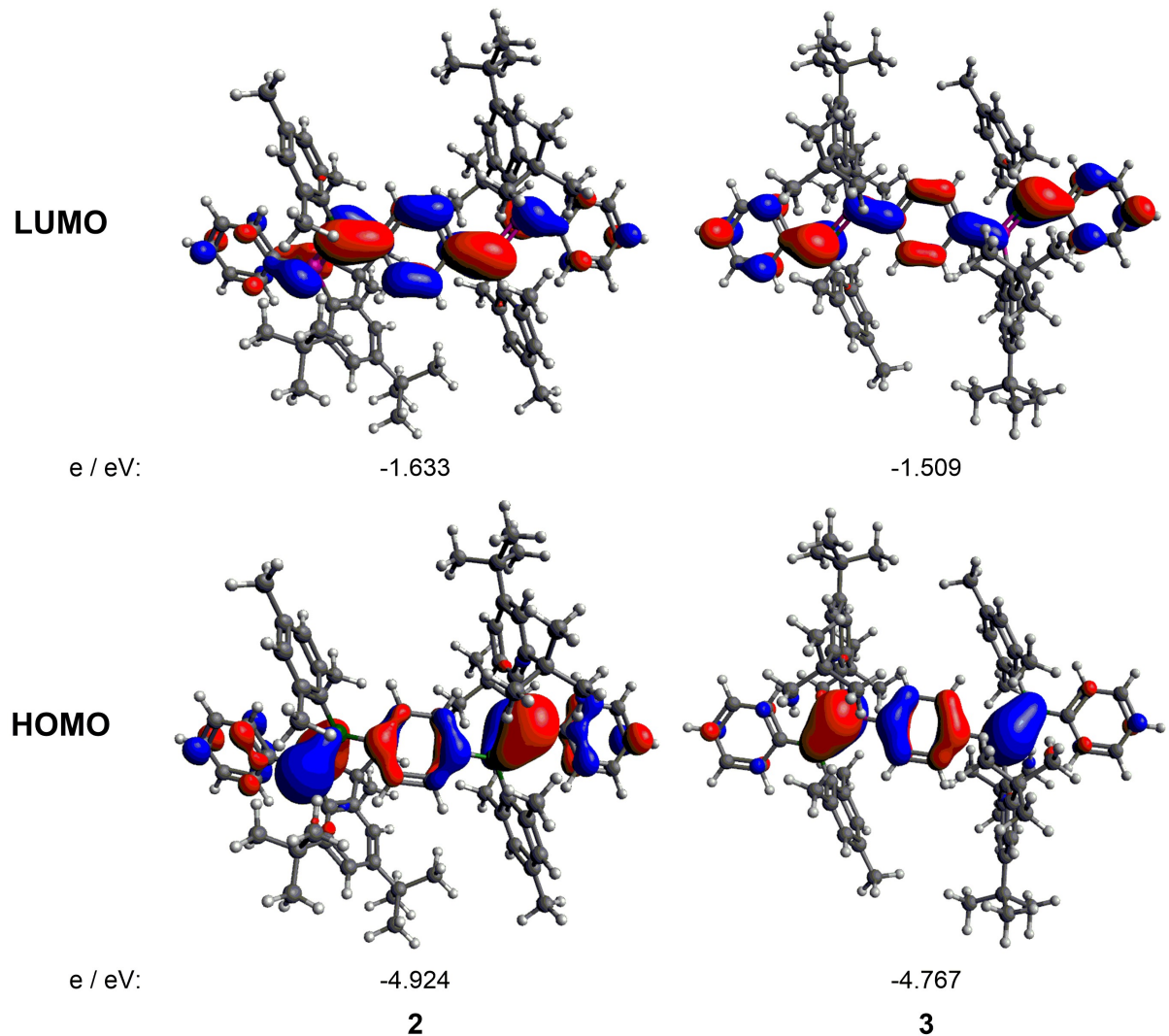


Figure 4.3.14. B3LYP-D3(BJ)/def2-SV(P) calculated frontier orbitals of **2** and **3** (isovalue 0.030).

4.3.5 References

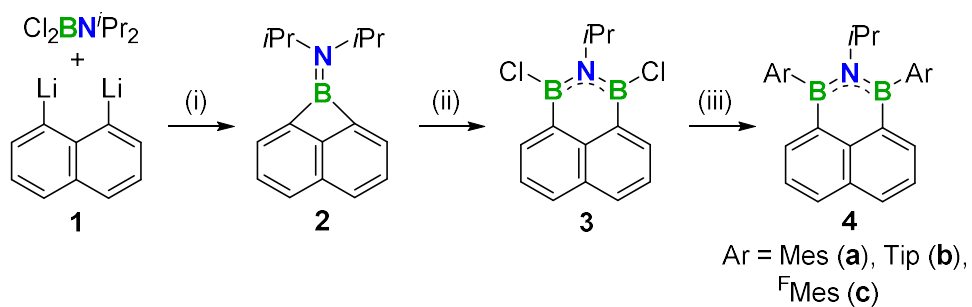
- [1] a) Z. Liu, T. B. Marder, *Angew. Chem. Int. Ed.* **2008**, *47*, 242-244; b) M. J. D. Bosdet, W. E. Piers, *Can. J. Chem.* **2009**, *87*, 8-29; c) P. G. Campbell, A. J. V. Marwitz, S.-Y. Liu, *Angew. Chem. Int. Ed.* **2012**, *51*, 6074-6092; d) D. Bonifazi, F. Fasano, M. M. Lorenzo-Garcia, D. Marinelli, H. Oubaha, J. Tasseroul, *Chem. Commun.* **2015**, *51*, 15222-15236; e) M. M. Morgan, W. E. Piers, *Dalton Transactions* **2016**, *45*, 5920-5924.
- [2] a) T. Hatakeyama, S. Hashimoto, M. Nakamura, *Org. Lett.* **2011**, *13*, 2130-2133; b) T. Baumgartner, *Acc. Chem. Res.* **2014**, *47*, 1613-1622; c) D. Joly, P. A. Bouit, M. Hissler, *J. Mater. Chem. C* **2016**, *4*, 3686-3698; d) A. Lik, D. Kargin, S. Isenberg, Z. Kelemen, R. Pietschnig, H. Helten, *Chem. Commun.* **2018**, *54*, 2471-2474.
- [3] a) P. P. Power, *Angew. Chem. Int. Ed.* **1990**, *29*, 449-460; b) D. C. Pestana, P. P. Power, *J. Am. Chem. Soc.* **1991**, *113*, 8426-8437; c) R. T. Paine, H. Noeth, *Chem. Rev.* **1995**, *95*, 343-379; d) J. A. Bailey, P. G. Pringle, *Coord. Chem. Rev.* **2015**, *297-298*, 77-90.
- [4] a) L. Nyulászi, A. Belghazi, S. K. Szétsi, T. Veszprémi, J. Heinicke, *Journal of Molecular Structure: THEOCHEM* **1994**, *313*, 73-81; b) J. Kapp, C. Schade, A. M. El-Nahasa, P. von Ragué Schleyer, *Angew. Chem. Int. Ed.* **1996**, *35*, 2236-2238.
- [5] S. J. Geier, T. M. Gilbert, D. W. Stephan, *Inorg. Chem.* **2011**, *50*, 336-344.
- [6] K. Kubo, T. Kawanaka, M. Tomioka, T. Mizuta, *Organometallics* **2012**, *31*, 2026-2034.
- [7] J. A. Bailey, M. F. Haddow, P. G. Pringle, *Chem. Commun.* **2014**, *50*, 1432-1434.
- [8] T. Lorenz, M. Crumbach, T. Eckert, A. Lik, H. Helten, *Angew. Chem. Int. Ed.* **2017**, *56*, 2780-2784.
- [9] S. J. Geier, T. M. Gilbert, D. W. Stephan, *J. Am. Chem. Soc.* **2008**, *130*, 12632-12633.
- [10] K. Izod, P. Evans, P. G. Waddell, *Dalton Trans.* **2017**, *46*, 13824-13834.
- [11] B. M. Lindkey, B. P. Jacobs, S. N. MacMillan, P. T. Wolczanski, *Chem. Commun.* **2016**, *52*, 3891-3894.
- [12] K. Ruhlandt-Senge, J. J. Ellison, R. J. Wehmschulte, F. Pauer, P. P. Power, *J. Am. Chem. Soc.* **1993**, *115*, 11353-11357.
- [13] D. E. Pearson, M. G. Frazer, V. S. Frazer, L. C. Washburn, *Synthesis* **1976**, *9*, 621-623.
- [14] X. Yin, J. Chen, R. A. Lalancette, T. B. Marder, F. Jäkle, *Angew. Chem. Int. Ed.* **2014**, *53*, 9761-9765.
- [15] D. Kaufmann, *Chem. Ber.* **1987**, *120*, 853-854.
- [16] M. C. Haberecht, J. B. Heilmann, A. Haghiri, M. Bolte, J. W. Bats, H.-W. Lerner, M. C. Holthausen, M. Wagner, *Z. Anorg. Allg. Chem.* **2004**, *630*, 904-913.
- [17] S. Kundu, S. Sinhababu, M. M. Siddiqui, A. V. Luebben, B. Dittrich, T. Yang, G. Frenking, H. W. Roesky, *J. Am. Chem. Soc.* **2018**, *140*, 9409-9412.
- [18] D. J. Dellinger, D. M. Sheehan, N. K. Christensen, J. G. Lindberg, M. H. Caruthers, *J. Am. Chem. Soc.* **2003**, *125*, 940-950.

- [19] K. R. Flower, A. T. McGown, P. J. Miles, R. G. Pritchard, J. E. Warren, *Dalton Trans.* **2010**, *39*, 3509-3520.
- [20] A. Sundararaman, F. Jäkle, *J. Organomet. Chem.* **2003**, *681*, 134-142.
- [21] G. M. Sheldrick, *Acta Crystallogr. A* **2015**, *71*, 3-8.
- [22] Sheldrick, *Acta Crystallogr. A* **2008**, *64*, 112-122.
- [23] C. B. Hubschle, G. M. Sheldrick, B. Dittrich, *J. Appl. Crystallogr.* **2011**, *44*, 1281-1284.
- [24] O. V. Dolomanov, L. J. Bourhis, R. J. Gildea, J. A. K. Howard, H. Puschmann, *J. Appl. Crystallogr.* **2009**, *42*, 339-341.
- [25] R. Ahlrichs, M. Bär, M. Häser, H. Horn, C. Kölmel, *Chem. Phys. Lett.* **1989**, *162*, 165-169.
- [26] a) P. A. M. Dirac, *Proc. R. Soc. London, Ser. A* **1929**, *123*, 714-733; b) J. C. Slater, *Phys. Rev.* **1951**, *81*, 385-390; c) A. D. Becke, *Phys. Rev. A* **1988**, *38*, 3098-3100; d) C. Lee, W. Yang, R. G. Parr, *Phys. Rev. B* **1988**, *37*, 785-789; e) A. D. Becke, *J. Chem. Phys.* **1993**, *98*, 5648-5652.
- [27] A. Schäfer, H. Horn, R. Ahlrichs, *J. Chem. Phys.* **1992**, *97*, 2571-2577.
- [28] a) S. Grimme, J. Antony, S. Ehrlich, H. Krieg, *J. Chem. Phys.* **2010**, *132*, 154104; b) S. Grimme, S. Ehrlich, L. J. Goerigk, *J. Comput. Chem.* **2011**, *32*, 1456-1465.
- [29] P. Deglmann, F. Furche, R. Ahlrichs, *Chem. Phys. Lett.* **2002**, *362*, 511-518; b) P. Deglmann, F. Furche, *J. Chem. Phys.* **2002**, *117*, 9535-9538.
- [30] a) R. Bauernschmitt, R. Ahlrichs, *Chem. Phys. Lett.* **1996**, *256*, 454-464; b) R. Bauernschmitt, R. Ahlrichs, *J. Chem. Phys.* **1996**, *104*, 9047-9052; c) F. Furche, D. Rappoport, *Density functional methods for excited states: equilibrium structure and electronic spectra*. In M. Olivucci, Ed., *Computational Photochemistry*, Vol. 16 of *Computational and Theoretical Chemistry*, ch. III., Elsevier, Amsterdam, **2005**.
- [†] Crystal structure was obtained in a “what is this”-measurement, a short time experiment to reveal the structure of a sample without recording the full data set.

5 Conclusion

This work has provided access to novel BNB-doped polycyclic aromatic systems with intriguing optoelectronic properties. Detailed theoretical investigations towards their aromaticity have been performed. Furthermore, first molecular model compounds for a BP analogue of the conjugated organic polymer poly(*p*-phenylene vinylene) (PPV) have been investigated.

In the first chapter, novel BNB-doped phenalenyl derivatives are presented. *Via* a highly efficient ring expansion-substitution procedure, convenient synthesis with facile scalability was achieved, which also allows for the introduction of different *B*-substituents at a late stage (Scheme 5.1).



Scheme 5.1. Synthesis of **4a-c**. Reagents and conditions: (i) *n*-hexane/ Et_2O , -30°C . (ii) BCl_3 , CH_2Cl_2 , -78°C to *r.t.* (iii) ArLi , toluene, -78°C to *r.t.*

The synthesized compounds **4a-c** feature sterically demanding *B*-substituents, such as mesityl, Tip (Tip = 2,4,6-triisopropylphenyl) or $^{\text{F}}\text{Mes}$ ($^{\text{F}}\text{Mes}$ = 2,4,6-tris(trifluoromethyl)-phenyl), which lead to perfect air and moisture stability.

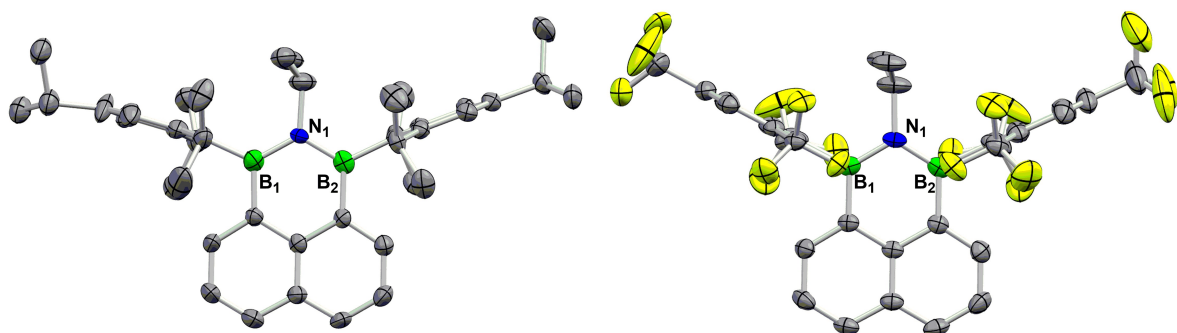


Figure 5.1. Molecular structures of **4b** (left) and **4c** (right) in the solid-state by single-crystal X-ray diffraction (H atoms omitted for clarity).

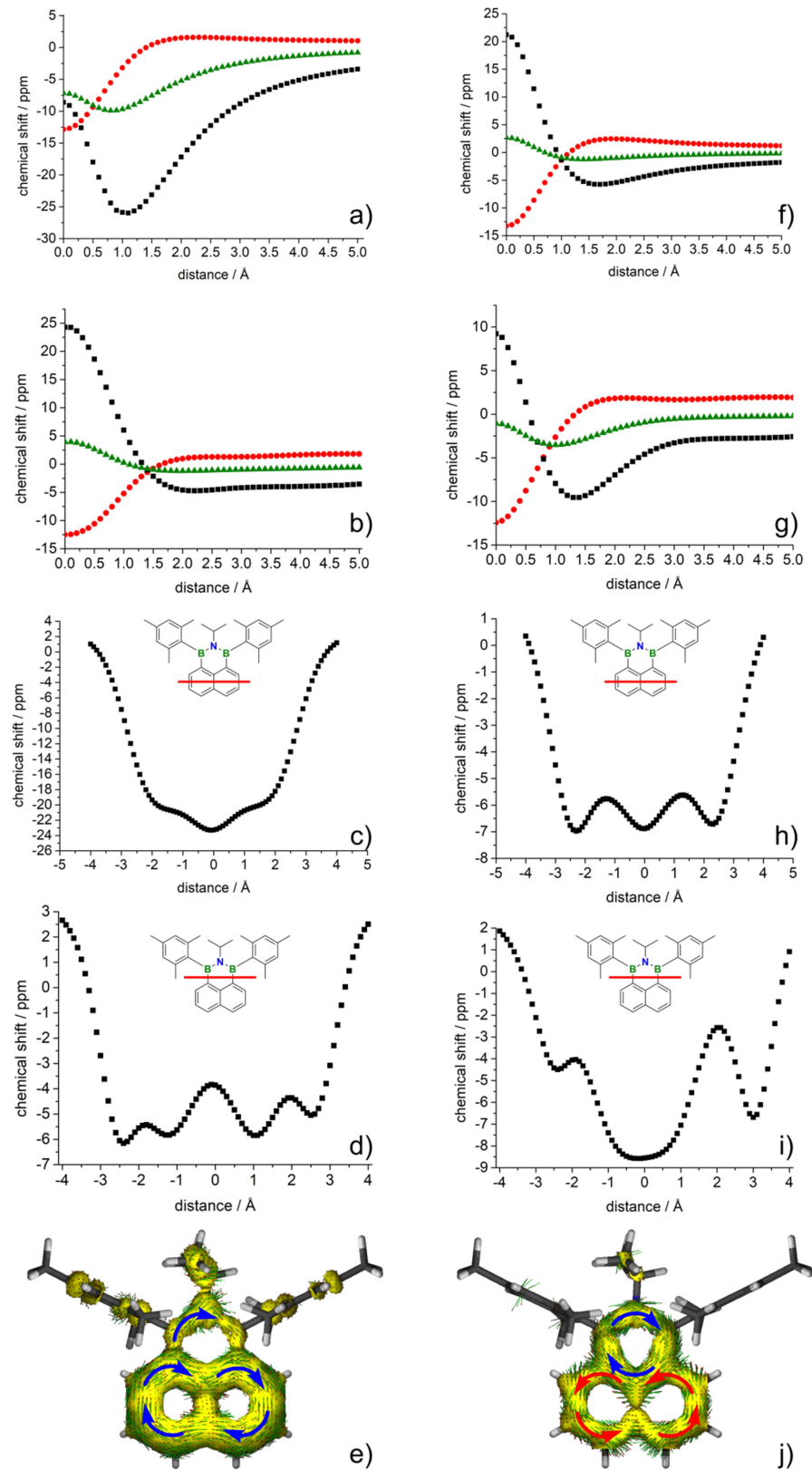
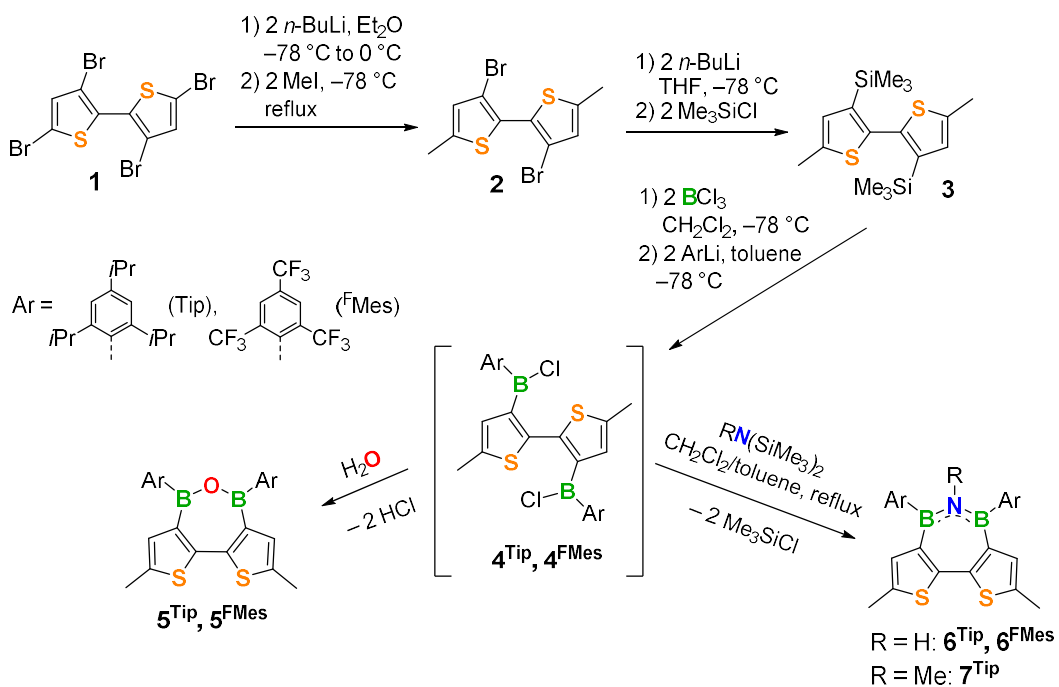


Figure 5.2. NICS-scans (for **4a**: naphthalenic part (a), hetero ring (b); **4a⁻**: naphthalenic part (f), hetero ring (g); out-of-plane (black), in-plane (red) and isotropic (green)), NICS-X-scans (for **4a**: naphthalenic part (c), hetero ring (d); **4a⁻**: naphthalenic part (h); hetero ring (i)) and ACID plots (for **4a** (e), for **4a⁻** (j); isovalue 0.015); B3LYP-D3(BJ)/6-31+G*.

These compounds exhibit favorable optoelectronic properties with fluorescence quantum yields of up to 47 % and narrow full-width at half-maximum values of down to 2689 cm⁻¹, which is of great interest for the generation of pure luminescence colours. The molecular structures of **4b** and **4c** were determined by single-crystal X-ray diffraction. They exhibit fully planar tricyclic systems, which are essentially unstrained, having B-N-B bond angles close to 120° (Figure 5.1). The B-N bond lengths are in the range of typical BN aromatics and the aryl planes of the bulky *B*-substituents are oriented almost perpendicularly to the phenalenyl plane. Cyclic voltammetry (CV) revealed electrochemically reversible reduction processes, in which the electron injection is facilitated by the incorporation of ^FMes at boron. Detailed theoretical investigations with NICS-scans (Nucleus Independent Chemical Shift) and the ACID (Anisotropy of the Induced Current Density) method showed that compounds **4a-c** are fully aromatic (Figure 5.2). They furthermore revealed an intramolecular aromaticity switch upon one-electron reduction.

In the second chapter, the novel class of azadiborepins and oxadiborepins is presented. These compounds are accessible via a modular synthesis route from a common precursor (Scheme 5.2).



Scheme 5.2. Synthesis of dithienooxa- and azadiborepins **5**, **6** and **7**.

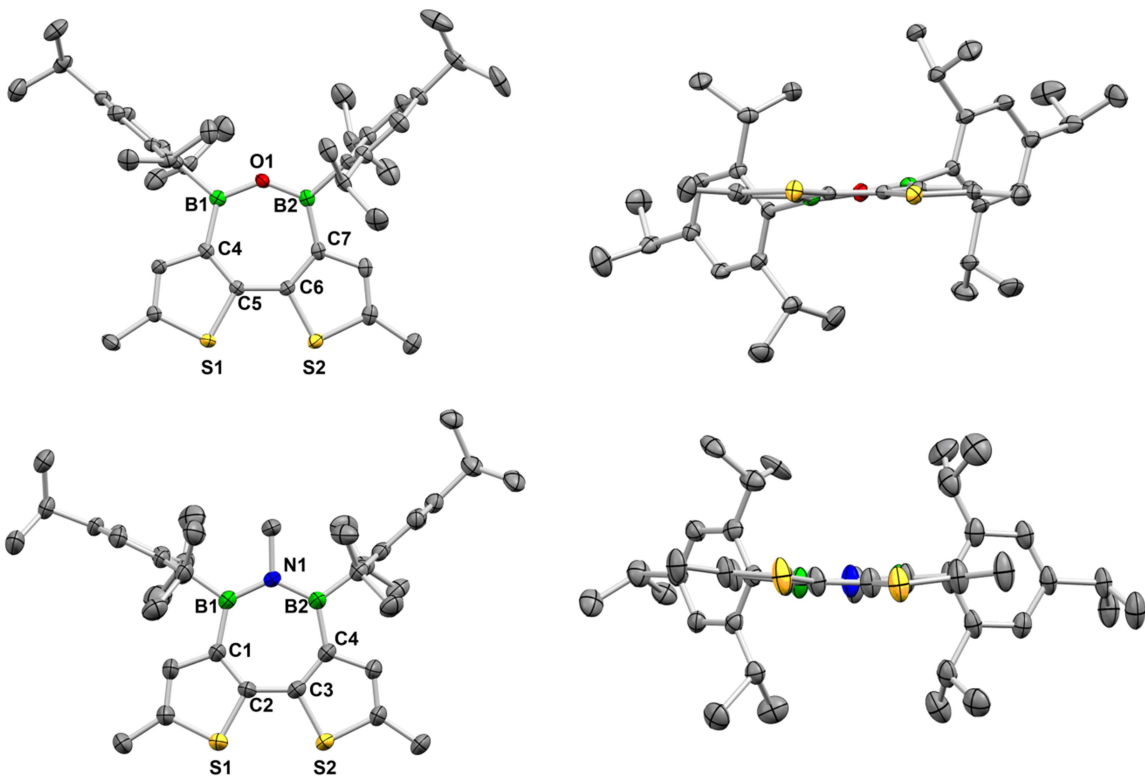


Figure 5.3. Molecular structures of 5^{Tip} and 7^{Tip} (with views perpendicular and parallel to the polycyclic plane) in the solid state by single-crystal X-ray diffraction (H-atoms and disorder of a Tip group in 7^{Tip} omitted for clarity).

All synthesized aza- and oxadiborepins are fully stable towards water and air and emit intense blue light, some of which with fluorescence quantum yields close to unity. Cyclic voltammetry (CV) revealed electrochemically reversible one-electron reduction processes. Compounds 5^{Tip} and 7^{Tip} were additionally characterized by single-crystal X-ray diffractometry (Figure 5.3). In their solid-state structures, both species feature a quasi-planar tricycle, with the Tip groups being almost perpendicularly oriented to that plane and B-N bond lengths in the range of typical BN aromatics. The seven-membered rings are close to planar, as suggested by the sums of their interior angles being close to 900° . The conducted theoretical investigations revealed that the bithiophene subunit is clearly aromatic, whereas the novel azadiborepin ring system exhibits a weak aromatic character (Figure 5.4).

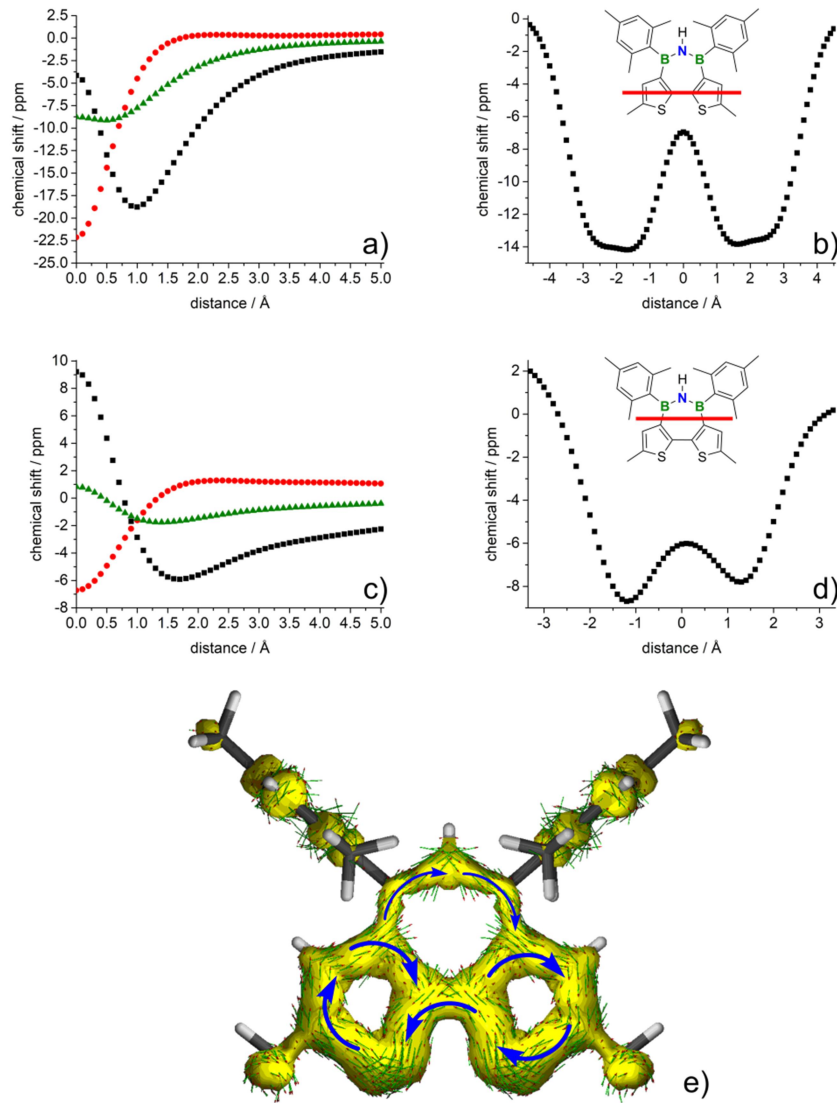
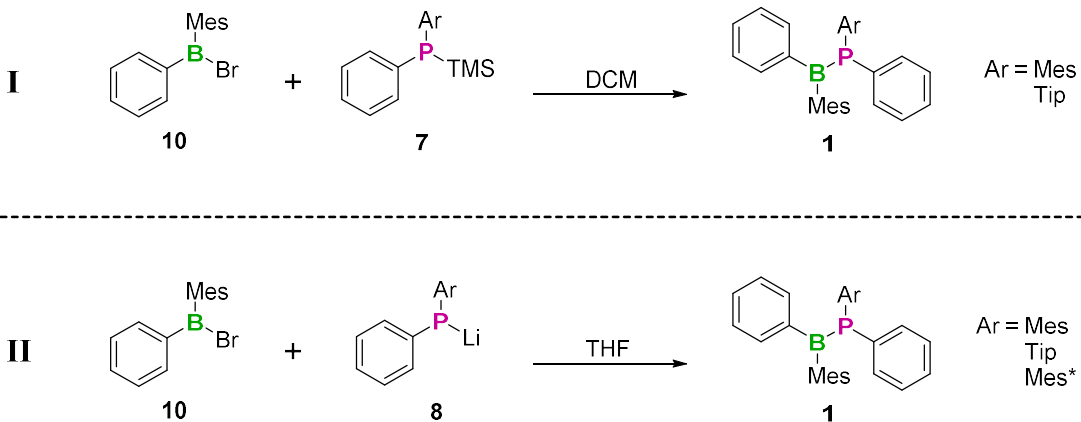


Figure 5.4. NICS-scan (thiophene ring (a); hetero ring (c); out-of-plane (black), in-plane (red) component, and isotropic chemical shift (green)), NICS-X-scan (bithiophene (b); hetero ring (d)) and ACID plot (e) (isovalue 0.02) of **6^{Mes}**.

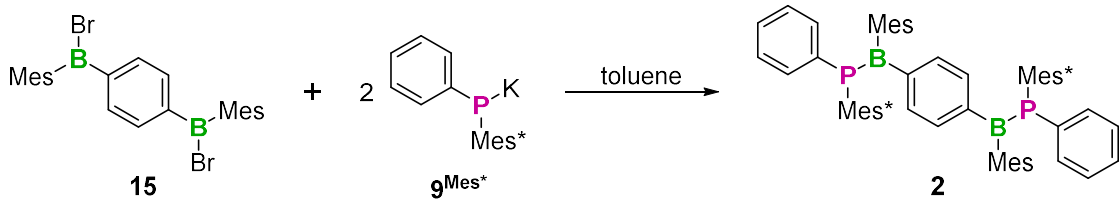
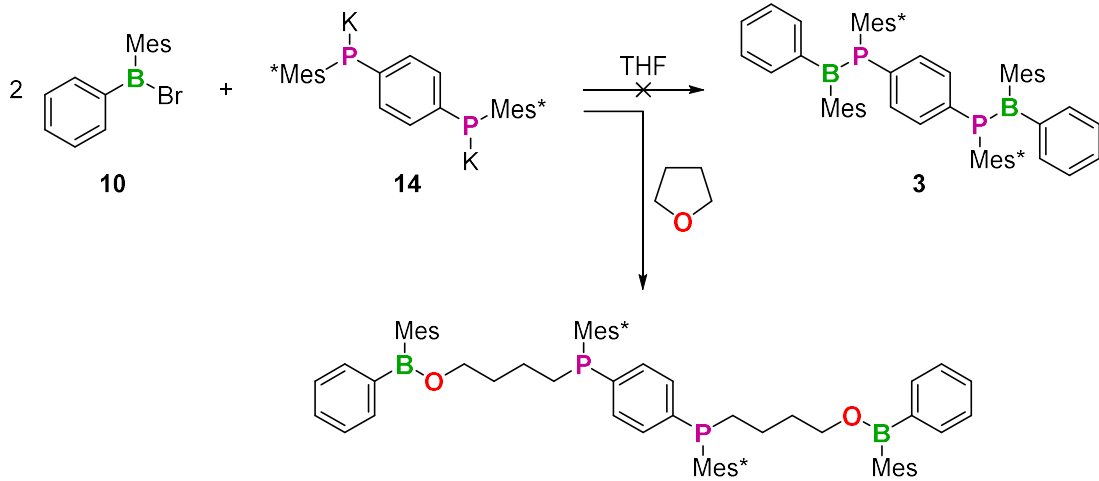
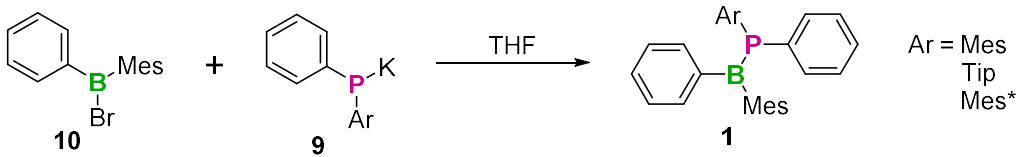
First molecular model compounds for a BP analogue of PPV are presented in the third chapter. Theoretical investigations revealed that a supermesityl (Mes^*) substituent is needed at phosphorus in order to fully planarize the P center to increase the B=P double bond character and enhance the possibility of conjugation over the BP unit. In view of accessing a BP analogue of PPV, molecular model compounds were targeted first. The synthesis thereof was attempted via three different synthetic approaches. At first the Si/B exchange reaction was applied to access compound **1^{Mes}**, which was obtained after 3 days (Scheme 5.3, **I**). The reaction to give compound **1^{Tip}** took already 15 days and showed large amounts of side products, due to occurring hydrolysis on that time scale, whereas **1^{Mes*}** was not obtained via

Si/B exchange reaction. To access the desired compound with the Mes* substituent at boron, a lithium salt-elimination route was applied (Scheme 5.3, **II**). Compounds **1^{Mes}**, **1^{Tip}** and **1^{Mes*}** were synthesized with reduced reaction times and less amounts of side products, but molecular model compounds featuring two BP units were not obtained *via* this route.



Scheme 5.3. Synthesis of **1^{Mes}** and **1^{Tip}** via route **I** and **1^{Mes}**, **1^{Tip}** and **1^{Mes*}** via route **II**.

The third synthetic approach uses potassium salt-elimination and proved to be a viable strategy to access the desired molecular model compounds (Scheme 5.4). Compounds **1^{Mes}**, **1^{Tip}** and **1^{Mes*}** were synthesized in THF, whereas compound **3** underwent THF cleavage and was not obtained. Therefore, the synthesis of compound **2** was carried out in toluene and the desired product could be obtained, as evidenced by HRMS.



Scheme 5.4. Synthesis of compounds $\mathbf{1}^{\text{Mes}}$, $\mathbf{1}^{\text{Tip}}$, $\mathbf{1}^{\text{Mes}^*}$ in THF, attempted synthesis of $\mathbf{3}$ in THF and synthesis of $\mathbf{2}$ in toluene.

The molecular structures of compounds $\mathbf{1}^{\text{Tip}}$ and $\mathbf{1}^{\text{Mes}^*}$ were determined by single-crystal X-ray diffraction (Figure 5.5). The Tip substituent planarizes the P center more than theoretically predicted, but still is not bulky enough to fully planarize the phosphorus center. The compound $\mathbf{1}^{\text{Mes}^*}$ exhibits a sum of the angles around the phosphorus of 359.7° with a B-P bond length of $1.812(3)$ Å. Therefore, compound $\mathbf{1}^{\text{Mes}^*}$ features a fully planarized P center, as predicted by our theoretical investigations, and one of the shortest B-P bond lengths reported so far, indicating a strong B=P double bond character. Photophysical investigations revealed that compounds $\mathbf{1}^{\text{Tip}}$ and $\mathbf{1}^{\text{Mes}^*}$ exhibit weak fluorescence ($\Phi_{\text{fl}} = 0.02$ and 0.06 , respectively) with large Stokes shifts (8500 and 10157 cm $^{-1}$, respectively).

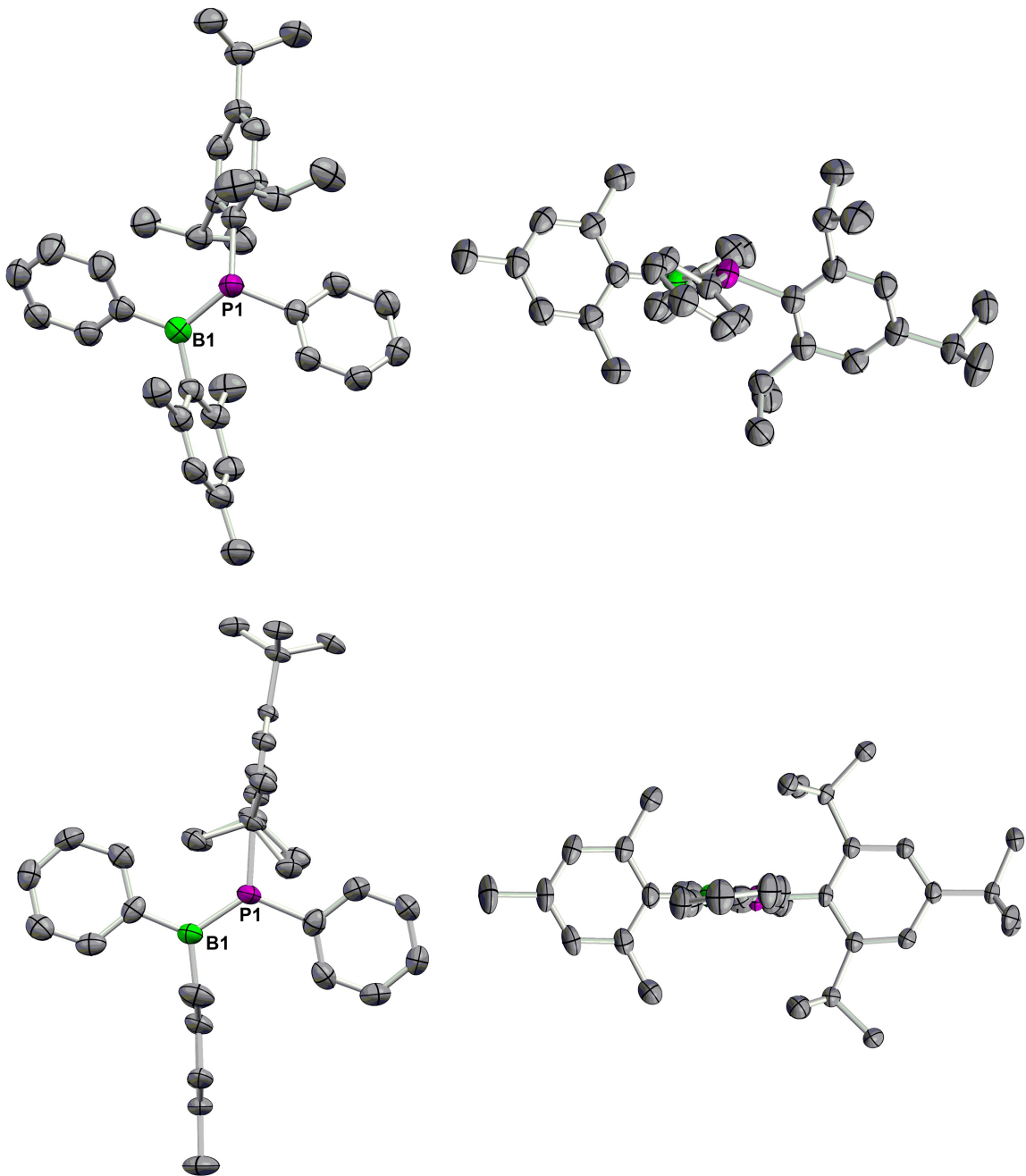
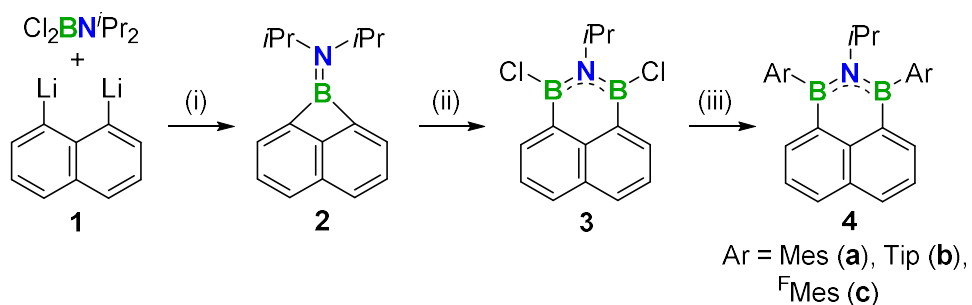


Figure 5.5. Molecular structures of $\mathbf{1}^{\text{Tip}}$ (top) and $\mathbf{1}^{\text{Mes}^*}$ (bottom) (with views perpendicular and parallel to the Ph-BP-Ph plane) in the solid state by single-crystal X-ray diffraction (H-atoms omitted for clarity).

6 Zusammenfassung

Diese Arbeit hat den Zugang zu neuartigen BNB-dotierten polyzyklischen aromatischen Systemen mit faszinierenden optoelektronischen Eigenschaften ermöglicht. Es wurden detaillierte theoretische Untersuchungen zu deren Aromatizität durchgeführt. Außerdem wurden erste molekulare Modellverbindungen für ein BP-Analogon des konjugierten organischen Polymers Poly(*p*-phenylen-vinylen) (PPV) untersucht.

Im ersten Kapitel werden neuartige BNB-dotierte Phenalenylderivate vorgestellt. Über ein hocheffizientes Ringerweiterungs-Substitutionsverfahren wurde eine geeignete Synthese mit leichter Skalierbarkeit erreicht, die auch die Einführung verschiedener *B*-Substituenten in einem späten Stadium erlaubt (Schema 6.1).



Schema 6.1. Synthese von **4a-c**. Reagenzien und Bedingungen: (i) *n*-Hexan/Et₂O, −30 °C. (ii) BCl₃, CH₂Cl₂, −78 °C bis RT (iii) ArLi, Toluol, −78 °C bis RT.

Die synthetisierten Verbindungen **4a-c** weisen sterisch anspruchsvolle *B*-Substituenten, wie Mesityl, Tip (Tip = 2,4,6-Triisopropylphenyl) oder F^{FMes} (F^{FMes} = 2,4,6-Tris(trifluormethyl)-phenyl) auf, die zu einer ausgezeichneten Luft- und Wasserstabilität führen.

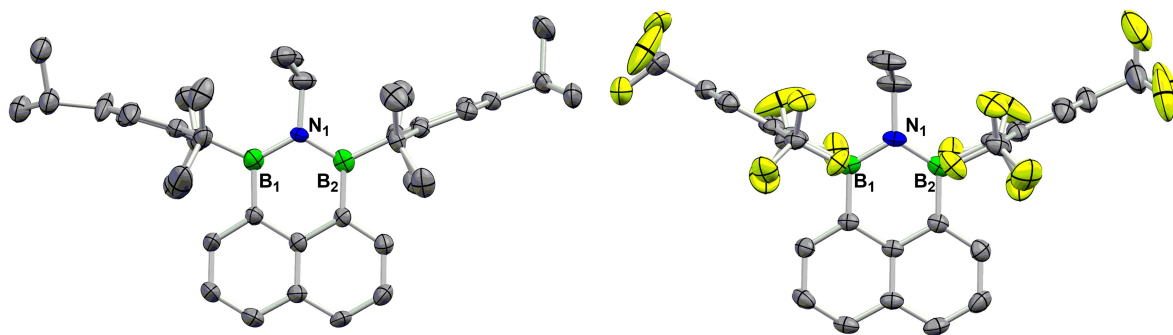


Abbildung 6.1. Molekülstrukturen von **4b** (links) und **4c** (rechts) im Festkörper, bestimmt mittels Einkristall-Röntgendiffraktometrie (H-Atome sind zur besseren Übersichtlichkeit weggelassen).

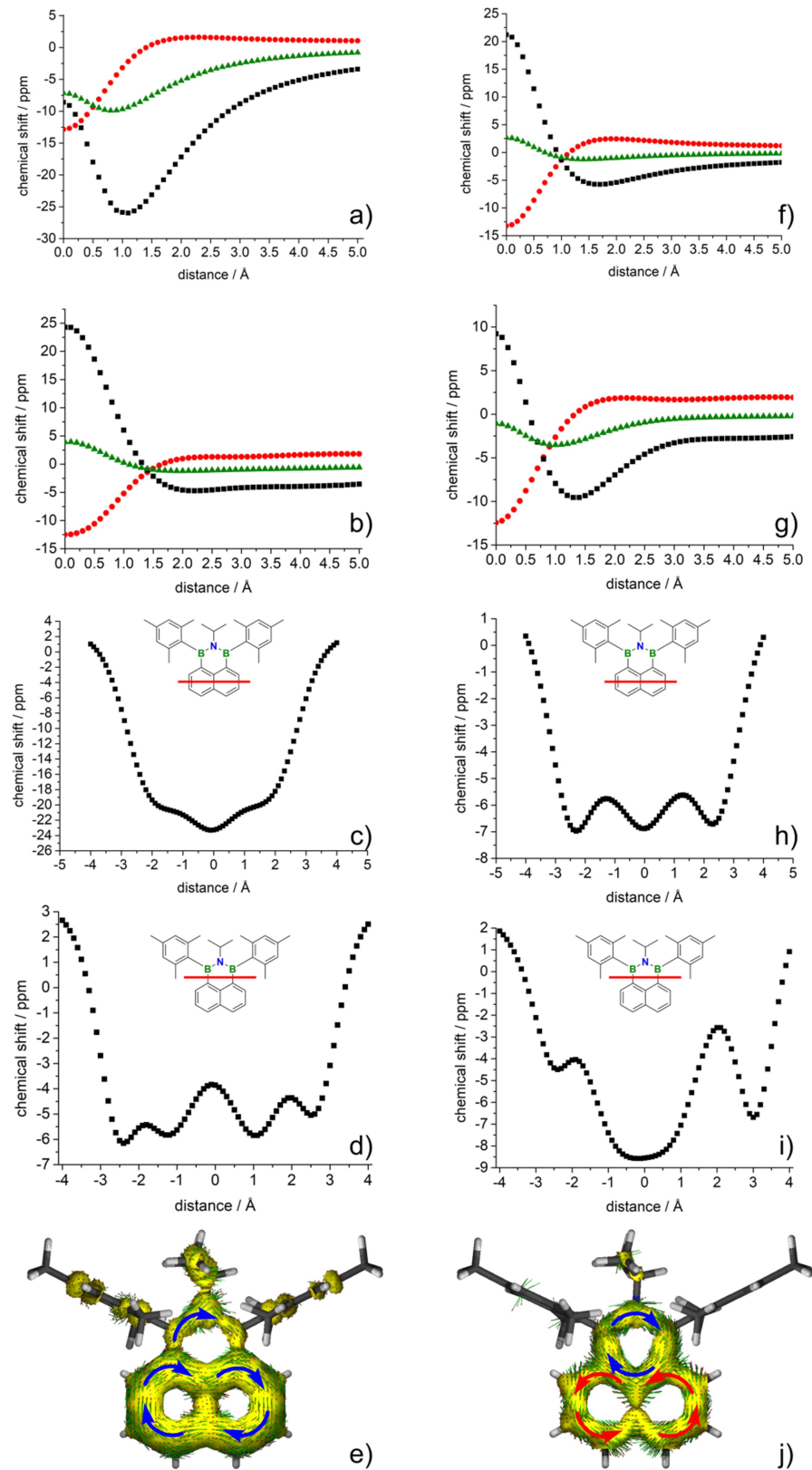
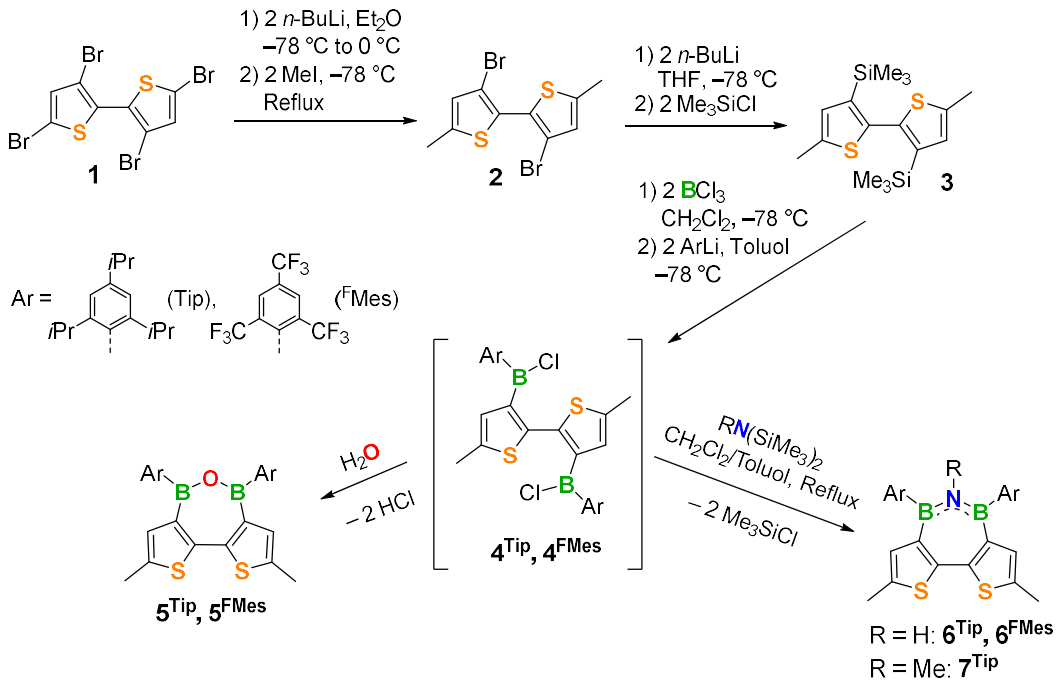


Abbildung 6.2. NICS-Scans (für **4a**: Naphthalin-Teil (a), Hetero-Ring (b); **4a⁻**: Naphthalin-Teil (f), Hetero-Ring (g); “out-of-plane” (schwarz), “in-plane” (rot) und “isotropic” (grün)), NICS-X-Scans (für **4a**: Naphthalin-Teil (c), Hetero-Ring (d); **4a⁻**: Naphthalin-Teil (h); Hetero-Ring (i)) und ACID Auftragungen (für **4a** (e), für **4a⁻** (j); Iso-Wert 0.015); B3LYP-D3(BJ)/6-31+G*.

Diese Verbindungen zeigen günstige optoelektronische Eigenschaften mit Fluoreszenzquantenausbeuten von bis zu 47 % und schmalen „Full-Width at Half-Maximum“-Werten (FWHM) von bis zu 2689 cm^{-1} , was für die Erzeugung von reinen Lumineszenzfarben von großem Interesse ist. Die Molekülstrukturen von **4b** und **4c** wurden durch Einkristall-Röntgendiffraktometrie bestimmt. Sie zeigen vollplanare trizyklische Systeme, die im Wesentlichen ungespannt sind und B-N-B-Bindungswinkel nahe 120° aufweisen (Abbildung 6.1). Die B-N-Bindungslängen liegen im Bereich typischer BN-Aromaten und die Arylebenen der sperrigen *B*-Substituenten sind fast orthogonal zur Phenalenylebene angeordnet. Cyclovoltammetrische Untersuchungen (CV) zeigten elektrochemisch reversible Reduktionsprozesse, bei denen die Elektronenaufnahme durch den Einbau von $^{\text{F}}\text{Mes}$ am Bor erleichtert wird. Detaillierte theoretische Untersuchungen mit NICS-Scans (Nucleus Independent Chemical Shift) und der ACID-Methode (Anisotropy of the Induced Current Density) zeigten, dass die Verbindungen **4a-c** vollständig aromatisch sind (Abbildung 6.2). Darüber hinaus zeigten sie, dass ein intramolekularer Aromatizitätswechsel bei Ein-Elektronen-Reduktion auftritt.

Im zweiten Kapitel wird die neue Klasse der Azadiborepine und Oxadiborepine vorgestellt. Diese Verbindungen sind über einen modularen Syntheseweg aus einer gemeinsamen Vorstufe zugänglich (Schema 6.2).



Schema 6.2. Synthese von Dithienooxa- und azadiborepinen **5**, **6** und **7**.

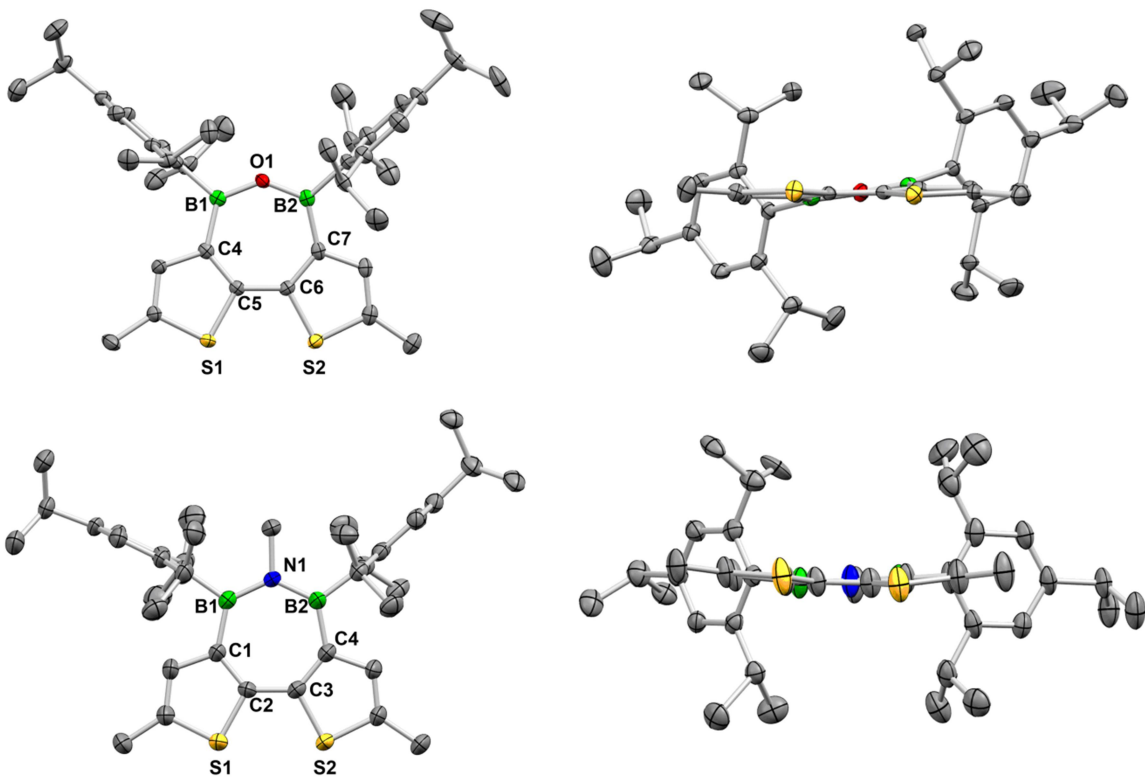


Abbildung 6.3. Molekülstrukturen von 5^{Tip} und 7^{Tip} (mit Ansichten senkrecht und parallel zur polyzyklischen Ebene) im Festkörper, bestimmt mittels Einkristall-Röntgendiffraktometrie (H-Atome und Fehlordnung in einer Tip-Gruppe von 7^{Tip} sind zur besseren Übersichtlichkeit weggelassen).

Alle synthetisierten Aza- und Oxadiborepine sind vollständig stabil gegenüber Wasser und Luft und emittieren intensives blaues Licht, einige davon mit einer Fluoreszenzquantenausbeute von annähernd 1. Cyclovoltammetrische Untersuchungen (CV) zeigten elektrochemisch reversible Ein-Elektronen-Reduktionsprozesse. Verbindungen 5^{Tip} und 7^{Tip} wurden zusätzlich mittels Einkristall-Röntgendiffraktometrie charakterisiert (Abbildung 6.3). In ihren Festkörperstrukturen weisen beide Spezies ein quasi-planares trizyklisches System auf, wobei die Tip-Gruppen fast senkrecht zu dieser Ebene orientiert sind und die B-N-Bindungslängen im Bereich typischer BN-Aromaten liegen. Die siebengliedrigen Ringe sind annähernd planar, wie die Summen ihrer Innenwinkel mit annähernd 900° nahelegen. Die durchgeführten theoretischen Untersuchungen ergaben, dass die Bithiophen-Untereinheit eindeutig aromatisch ist, während das neuartige Azadiborepin-Ringsystem einen schwach aromatischen Charakter aufweist (Abbildung 6.4).

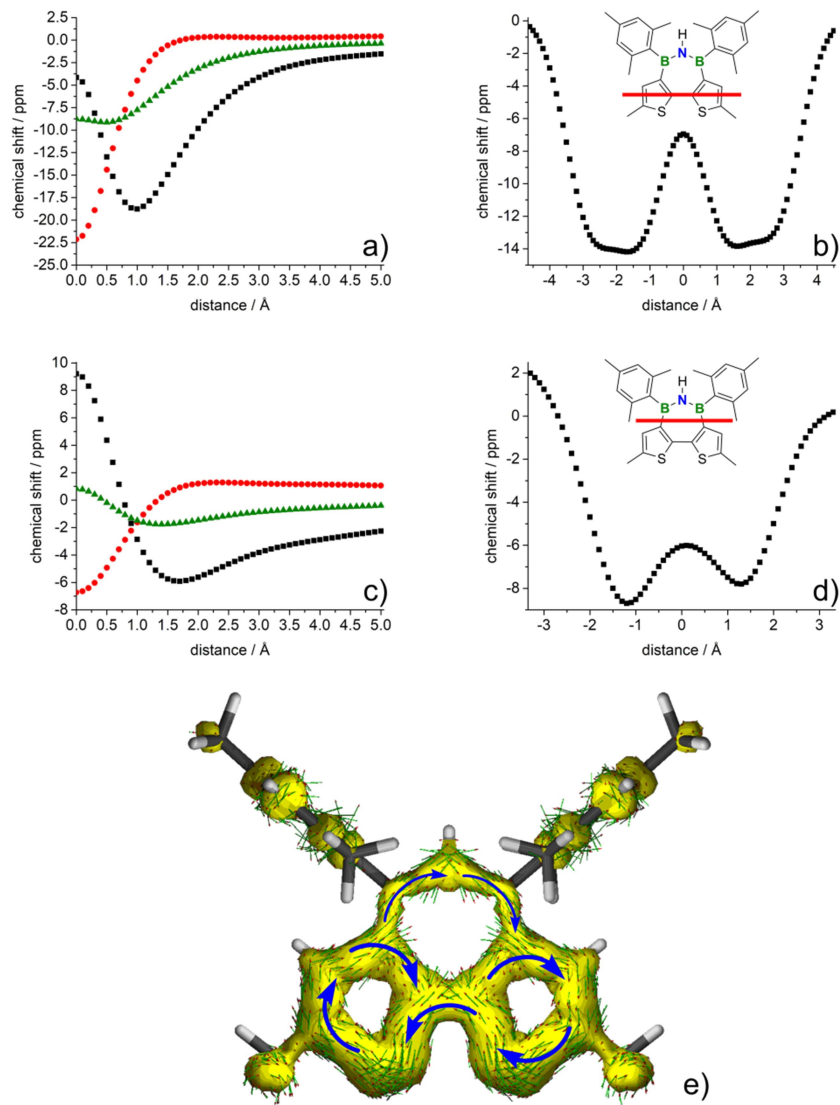
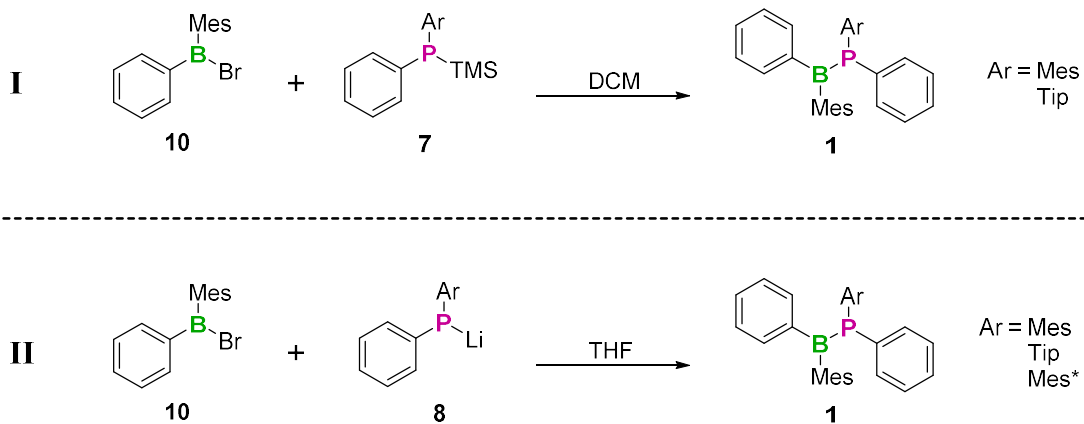


Abbildung 6.4. NICS-Scan (Thiophene-Ring (a); Hetero-Ring (c); “out-of-plane” (schwarz), “in-plane” (rot) “isotropic chemical shift” (grün)), NICS-X-Scan (Bithiophen (b); Hetero-Ring (d)) und ACID Auftragung (e) (Iso-Wert 0.02) für **6**^{Mes}.

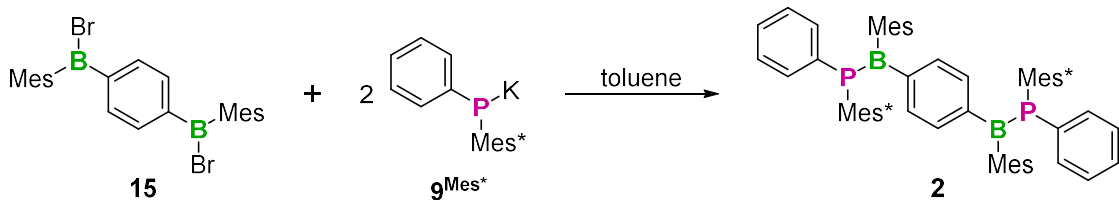
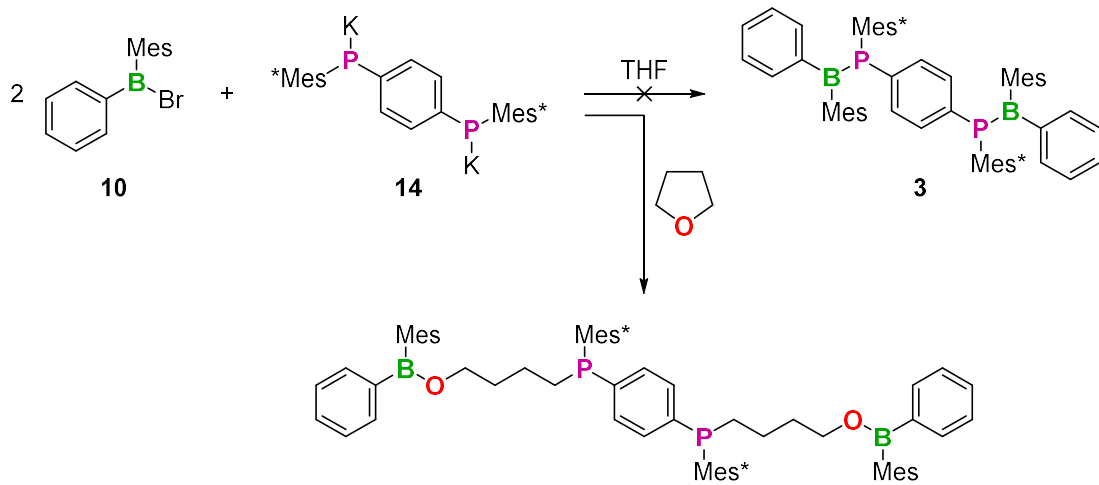
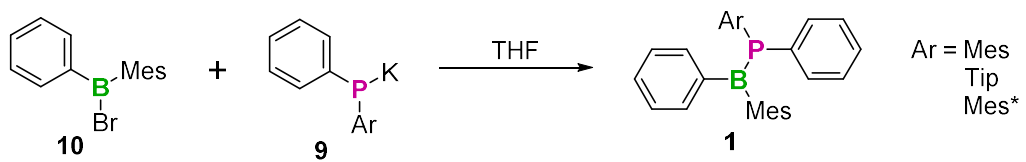
Erste molekulare Modellverbindungen für ein BP-Analogon von PPV werden im dritten Kapitel vorgestellt. Theoretische Untersuchungen ergaben, dass ein Supermesityl-Substituent (Mes^*) am Phosphor erforderlich ist, um das P-Zentrum vollständig zu planarisieren, somit den B=P-Doppelbindungscharakter zu erhöhen und die Möglichkeit der Konjugation über die BP-Einheit zu verbessern. Im Hinblick auf den Zugang zu einem BP-Analogon von PPV wurden zunächst molekulare Modellverbindungen anvisiert. Deren Synthese wurde über drei verschiedene Syntheseansätze versucht. Zunächst wurde die Si/B-Austauschreaktion angewandt, um zu Verbindung **1**^{Mes} zu gelangen, welche nach 3 Tagen erhalten wurde (Schema 6.3, I). Die Reaktion zur Verbindung **1**^{Tip} dauerte bereits 15 Tage und wies große

Mengen an Nebenprodukten auf, da in dieser Zeitspanne Hydrolyse stattfand, während $\mathbf{1}^{\text{Mes}^*}$ nicht über die Si/B-Austauschreaktion erhalten wurde. Um die gewünschte Verbindung mit dem Mes*-Substituenten am Bor zu erhalten, wurde eine Syntheseroute angewendet, bei der ein Lithiumsalz eliminiert wird (Schema 6.3, **II**). Die Verbindungen $\mathbf{1}^{\text{Mes}}$, $\mathbf{1}^{\text{Tip}}$ und $\mathbf{1}^{\text{Mes}^*}$ wurden mit reduzierten Reaktionszeiten und geringeren Mengen an Nebenprodukten synthetisiert, jedoch konnten molekulare Modellverbindungen mit zwei BP-Einheiten über diese Route nicht erhalten werden.



Schema 6.3. Synthesen von $\mathbf{1}^{\text{Mes}}$ und $\mathbf{1}^{\text{Tip}}$ über Route **I** und $\mathbf{1}^{\text{Mes}}$, $\mathbf{1}^{\text{Tip}}$ und $\mathbf{1}^{\text{Mes}^*}$ über Route **II**.

Der dritte Syntheseansatz nutzt die Eliminierung vom Kaliumsalzen und erwies sich als praktikable Strategie, um zu den gewünschten molekularen Modellverbindungen zu gelangen (Schema 6.4). Die Verbindungen $\mathbf{1}^{\text{Mes}}$, $\mathbf{1}^{\text{Tip}}$ und $\mathbf{1}^{\text{Mes}^*}$ wurden in THF synthetisiert, während es bei Verbindung **3** zu einer THF-Spaltung kam und das Zielprodukt nicht erhalten wurde. Daher wurde die Synthese von Verbindung **2** in Toluol durchgeführt und das gewünschte Produkt erhalten, wie durch HRMS bewiesen werden konnte.



Schema 6.4. Synthesen von Verbindungen $\mathbf{1}^{\text{Mes}}$, $\mathbf{1}^{\text{Tip}}$, $\mathbf{1}^{\text{Mes}^*}$ in THF, versuchte Synthese von $\mathbf{3}$ in THF und Synthese von $\mathbf{2}$ in Toluol.

Die Molekülstrukturen der Verbindungen $\mathbf{1}^{\text{Tip}}$ und $\mathbf{1}^{\text{Mes}^*}$ wurden durch Einkristall-Röntgendiffraktometrie bestimmt (Abbildung 6.5). Der Tip-Substituent planarisiert das P-Zentrum stärker als theoretisch vorhergesagt, ist jedoch nicht sterisch anspruchsvoll genug, um das Phosphor-Zentrum vollständig zu planarisieren. Die Verbindung $\mathbf{1}^{\text{Mes}^*}$ zeigt eine Winkelsumme um den Phosphor von $359,7^\circ$ mit einer B-P-Bindungslänge von $1,812(3)$ Å. Daher besitzt die Verbindung $\mathbf{1}^{\text{Mes}^*}$ ein vollständig planarisieretes P-Zentrum, wie von unseren theoretischen Untersuchungen vorhergesagt, und eine der kürzesten bisher berichteten B-P-Bindungslängen, was auf einen starken B=P-Doppelbindungscharakter hinweist. Photophysikalische Untersuchungen zeigten, dass die Verbindungen $\mathbf{1}^{\text{Tip}}$ und $\mathbf{1}^{\text{Mes}^*}$ eine schwache Fluoreszenz ($\Phi_{\text{fl}} = 0,02$ bzw. $0,06$) mit großen Stokes-Verschiebungen (8500 bzw. 10157 cm $^{-1}$) aufweisen.

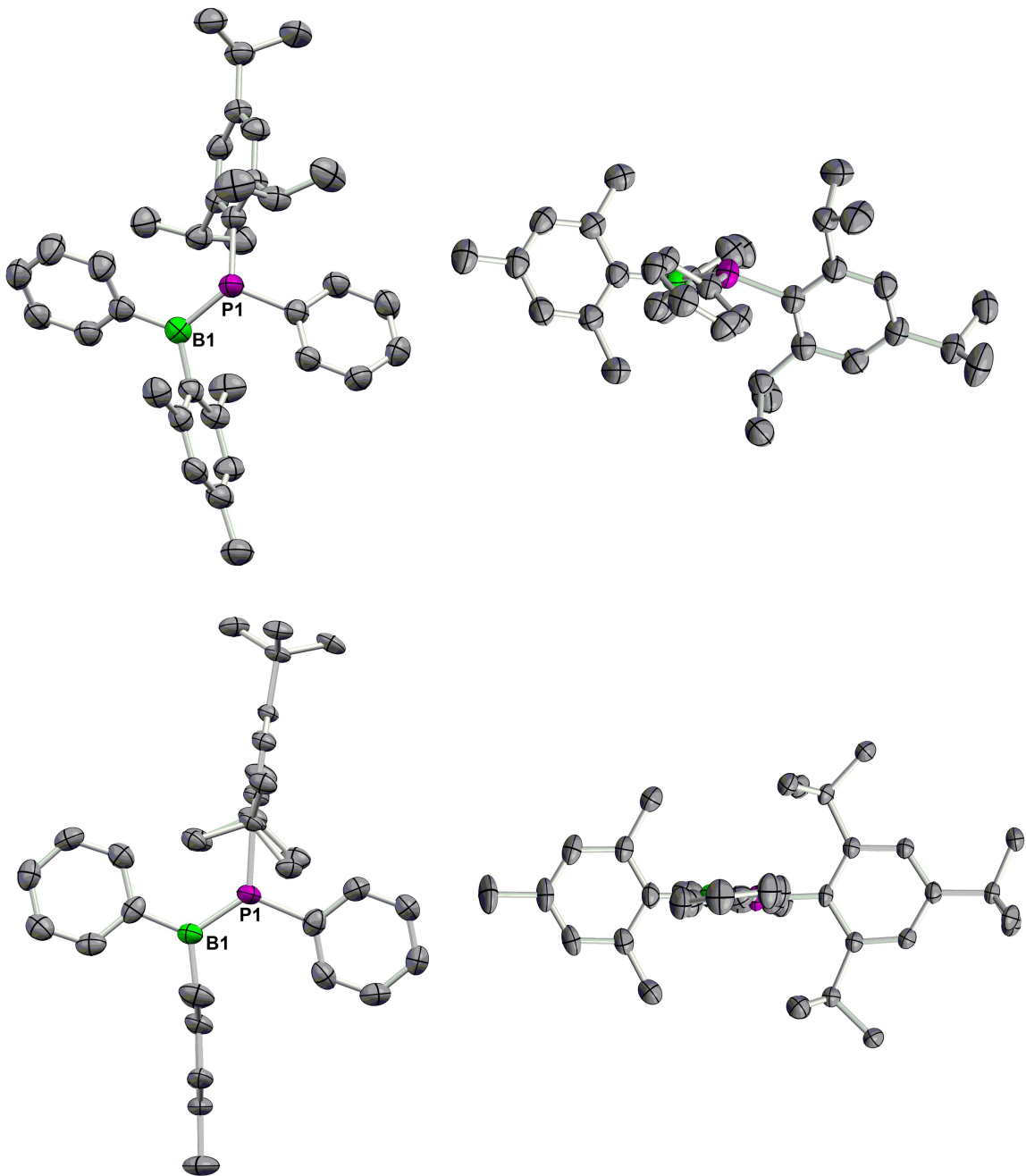


Abbildung 6.5. Molekülstrukturen von $\mathbf{1}^{\text{Tip}}$ (oben) und $\mathbf{1}^{\text{Mes}^*}$ (unten) (mit Ansichten senkrecht und parallel zur Ph-BP-Ph Ebene) im Festkörper, bestimmt mittels Einkristall-Röntgendiffraktometrie (H-Atome sind zur besseren Übersichtlichkeit weggelassen).

7 Appendix

7.1 BNB-Doped phenalenyls – aromaticity switch upon one-electron reduction

NMR spectra

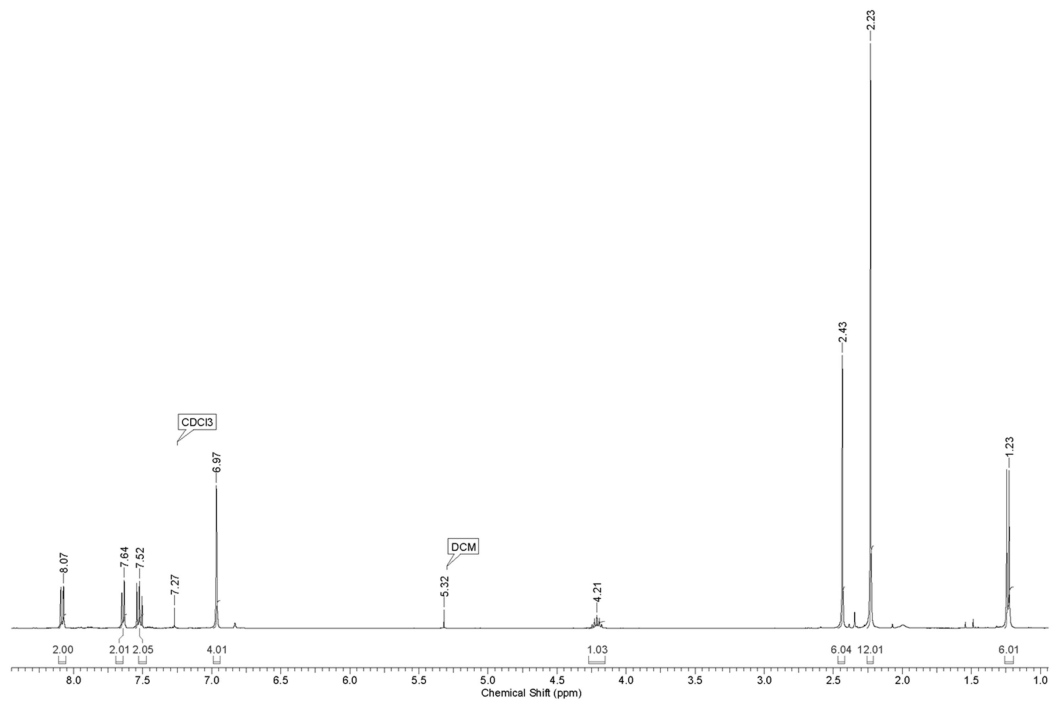


Figure 7.1.1. ^1H NMR spectrum of **4a** in CDCl_3 .

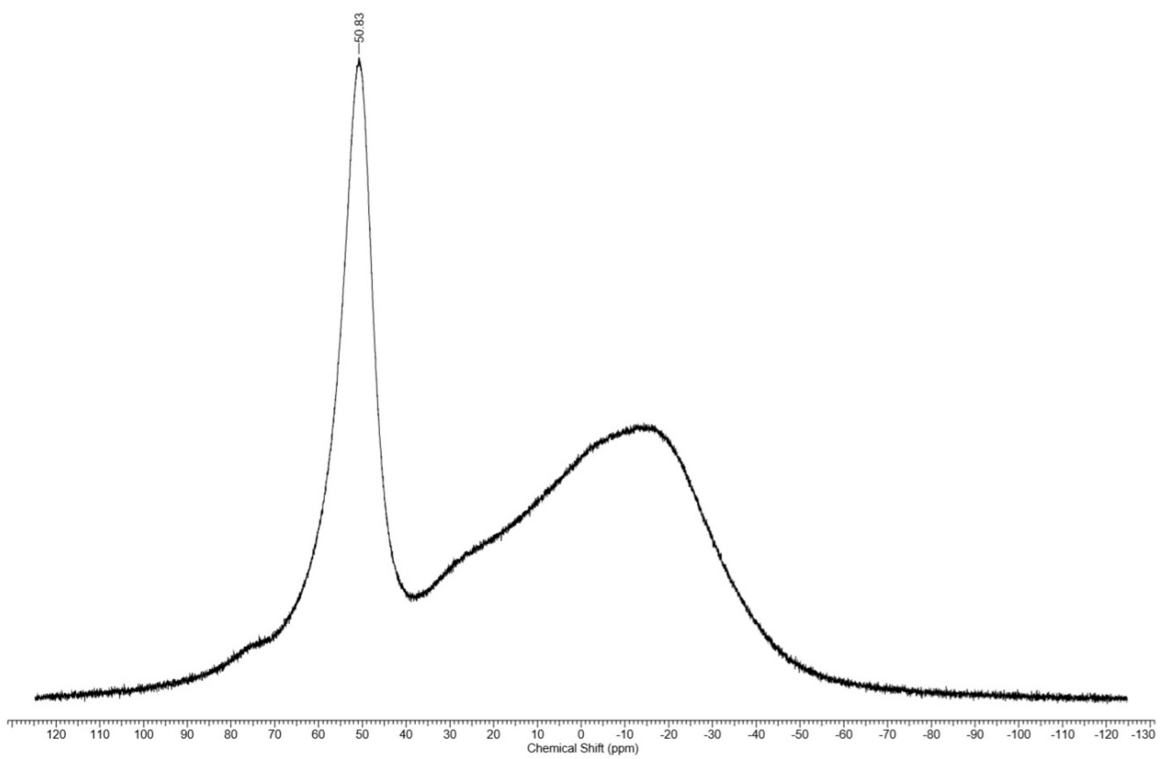


Figure 7.1.2. $^{11}\text{B}\{^1\text{H}\}$ NMR spectrum of **4a** in CDCl_3 .

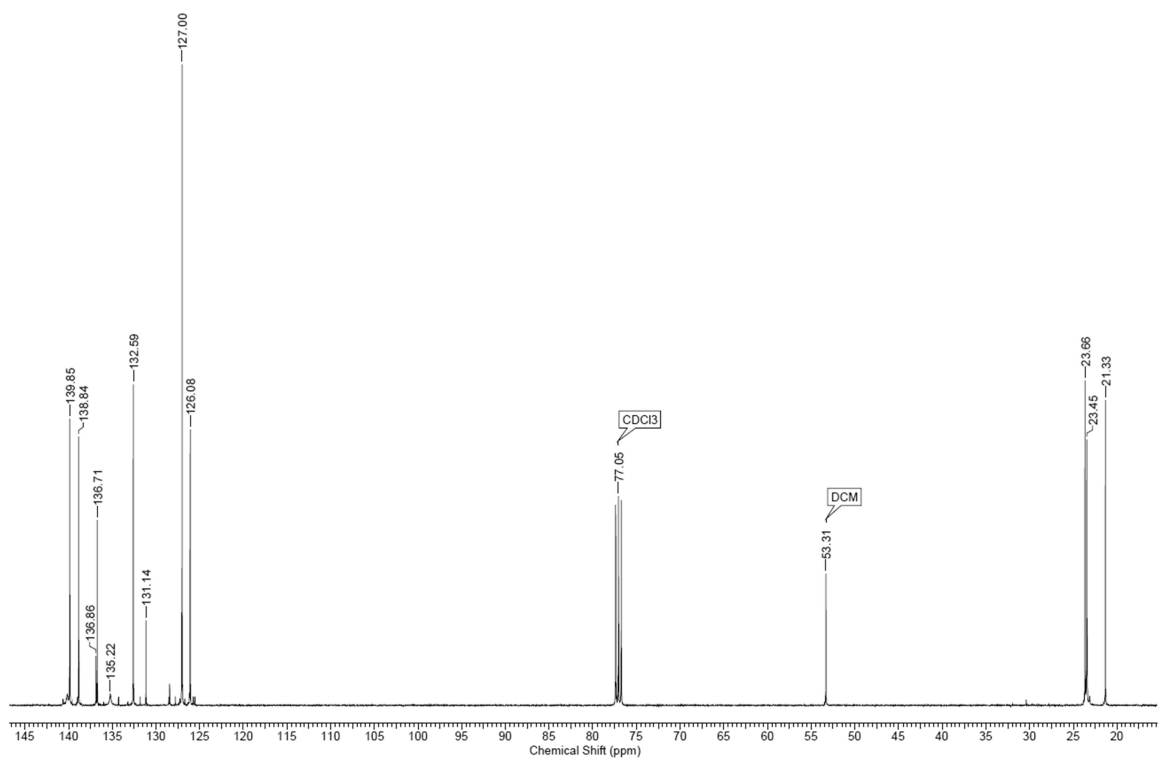


Figure 7.1.3. $^{13}\text{C}\{^1\text{H}\}$ NMR spectrum of **4a** in CDCl_3 .

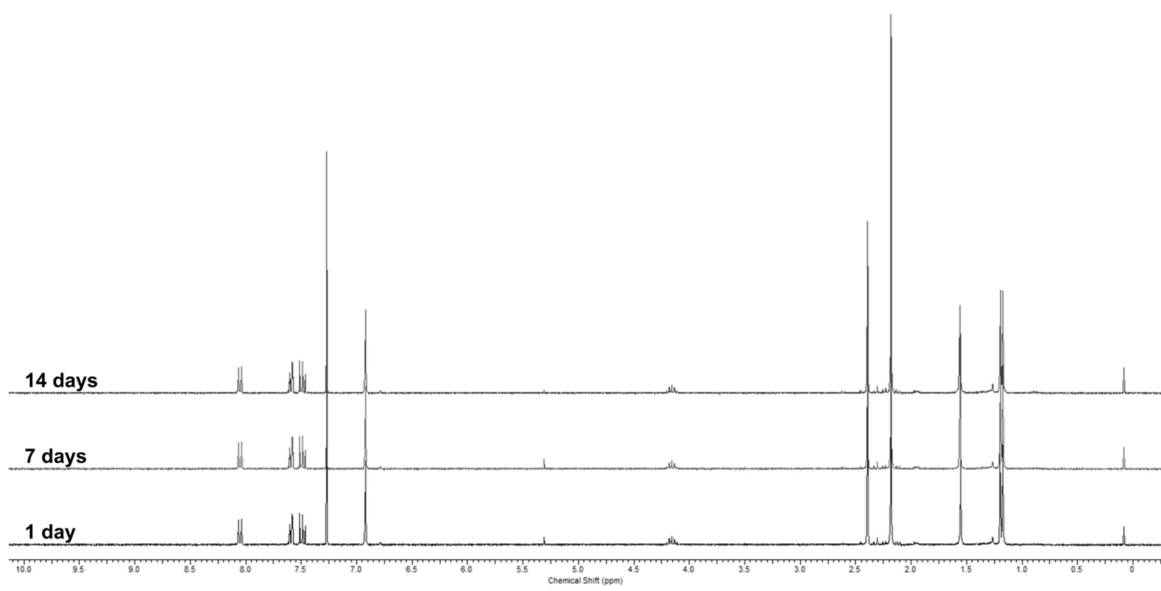


Figure 7.1.4. ¹H NMR spectrum of **4a** in moist solution over time in CDCl_3 .

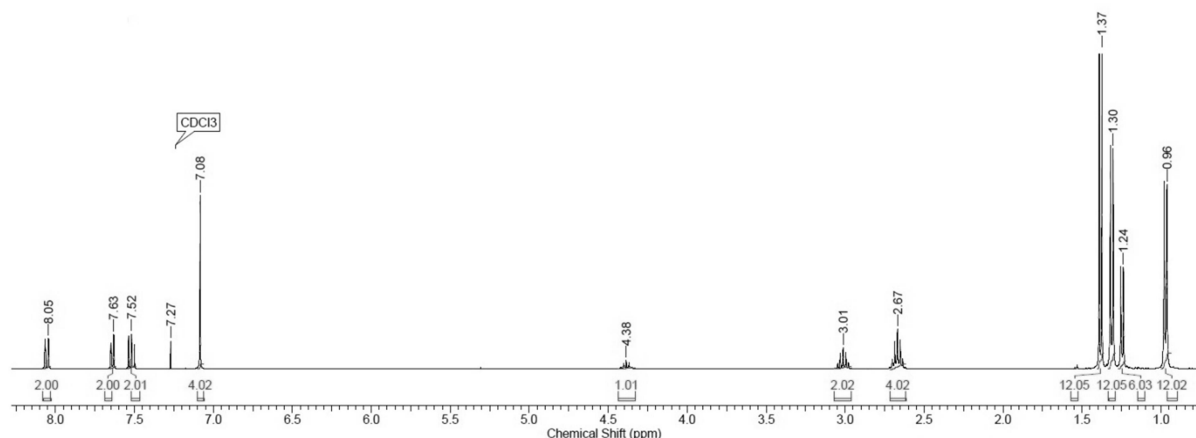


Figure 7.1.5. ¹H NMR spectrum of **4b** in CDCl_3 .

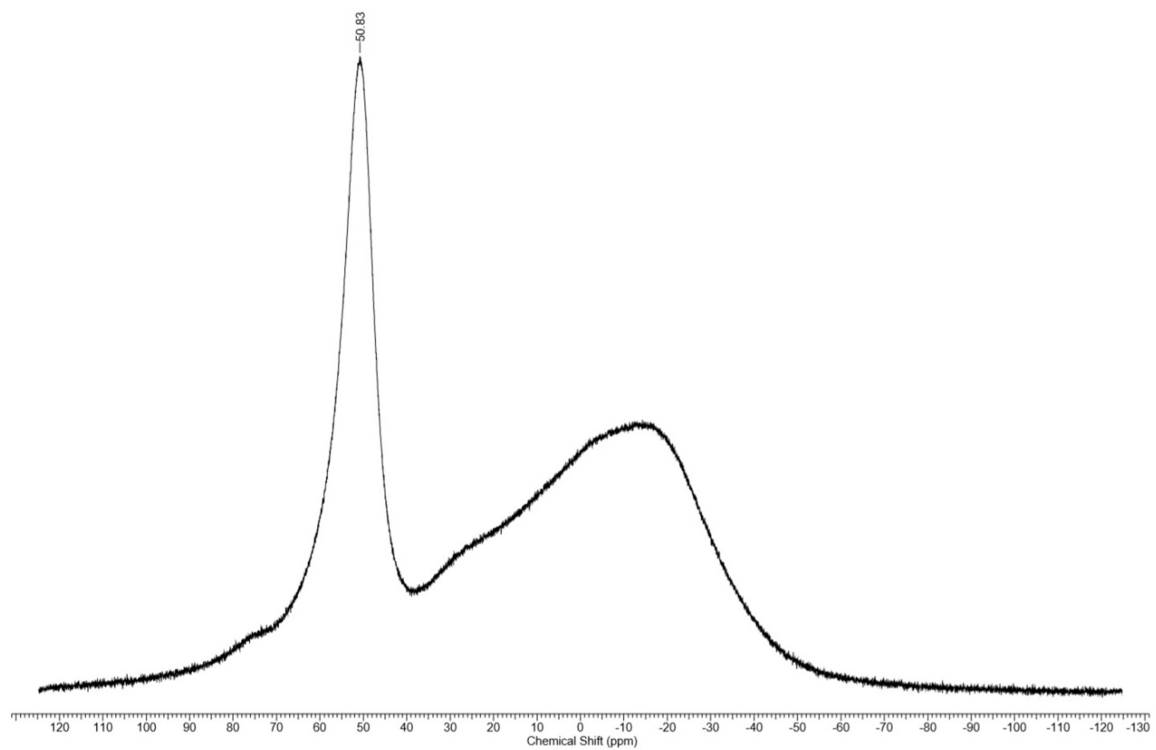


Figure 7.1.6. $^{11}\text{B}\{^1\text{H}\}$ NMR spectrum of **4b** in CDCl_3 .

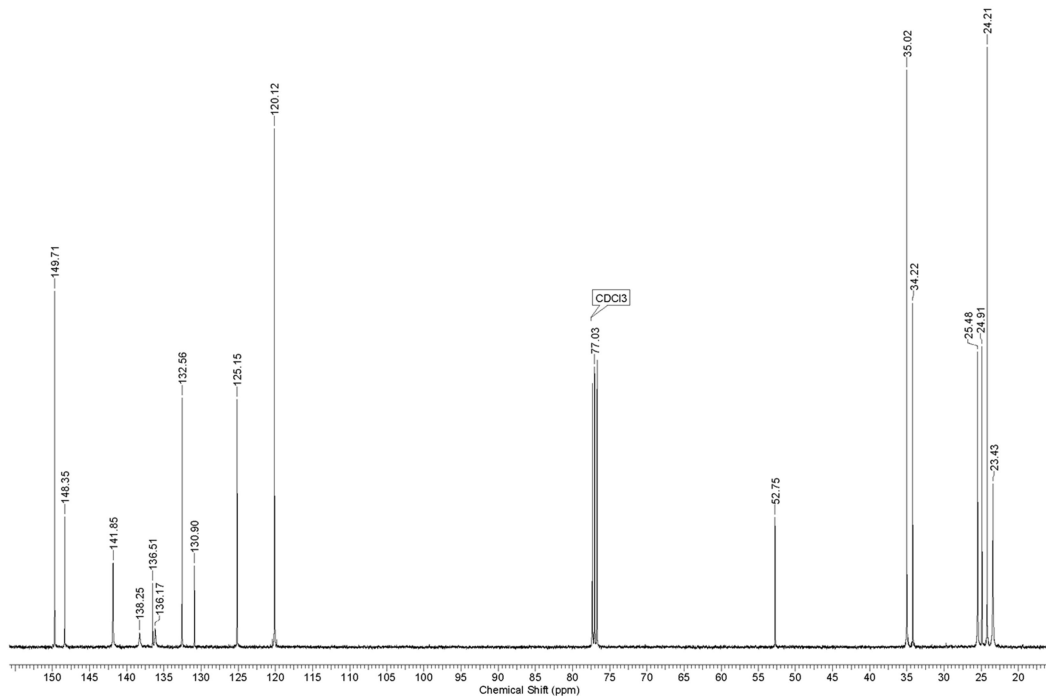


Figure 7.1.7. $^{13}\text{C}\{^1\text{H}\}$ NMR spectrum of **4b** in CDCl_3 .

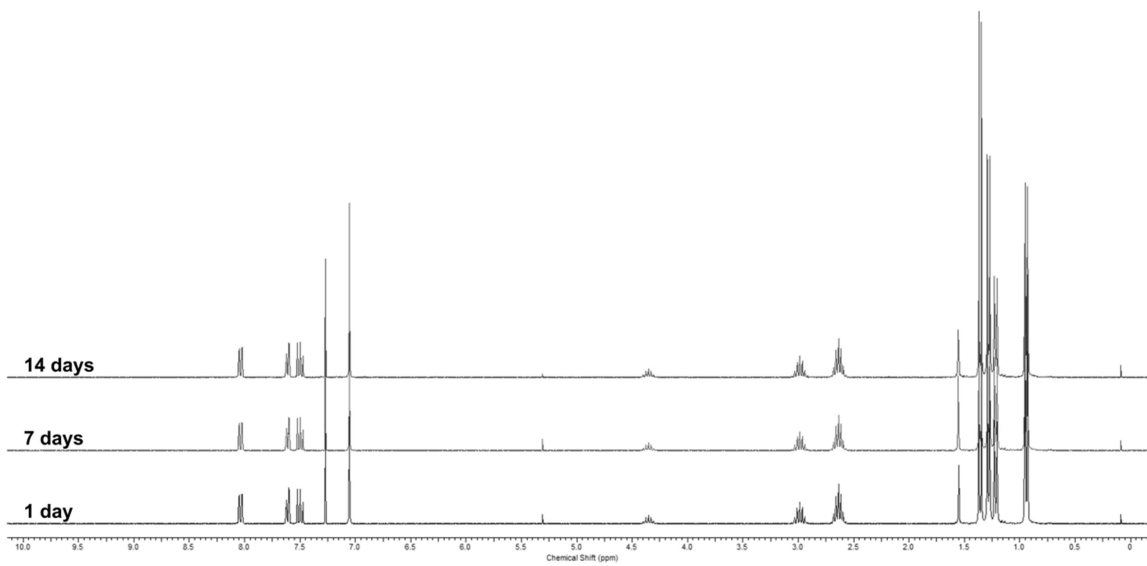


Figure 7.1.8. ¹H NMR spectrum of **4b** in moist solution over time in CDCl_3 .

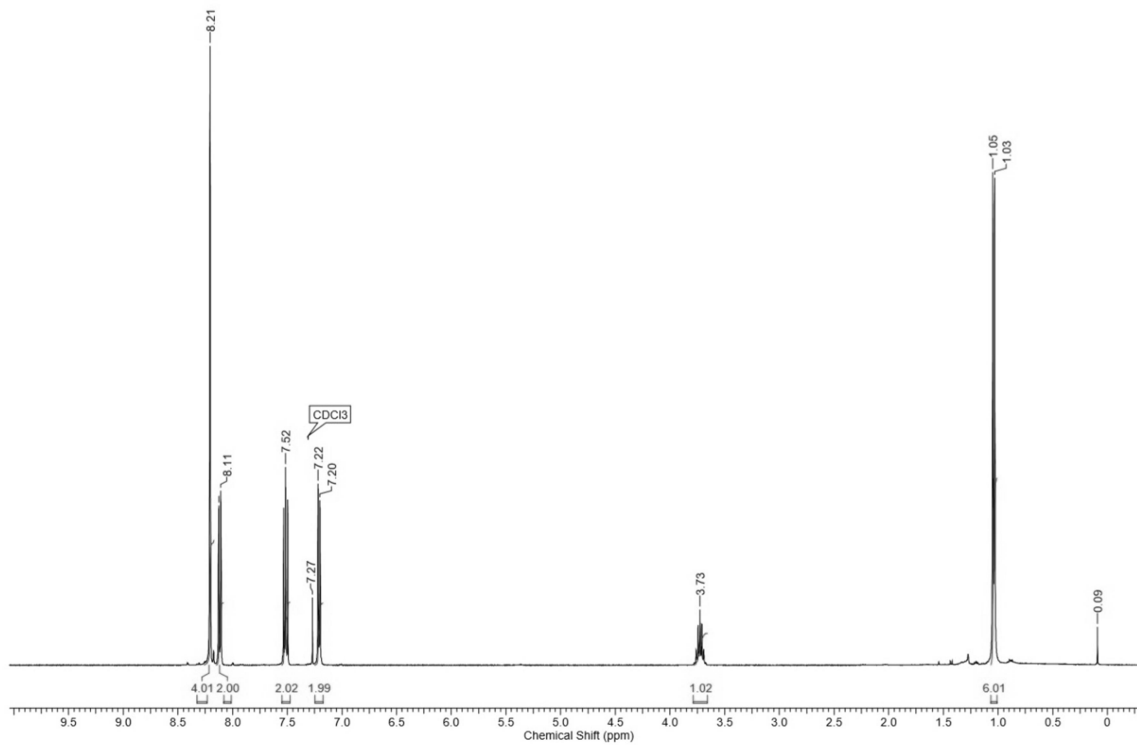


Figure 7.1.9. ¹H NMR spectrum of **4c** in CDCl_3 .

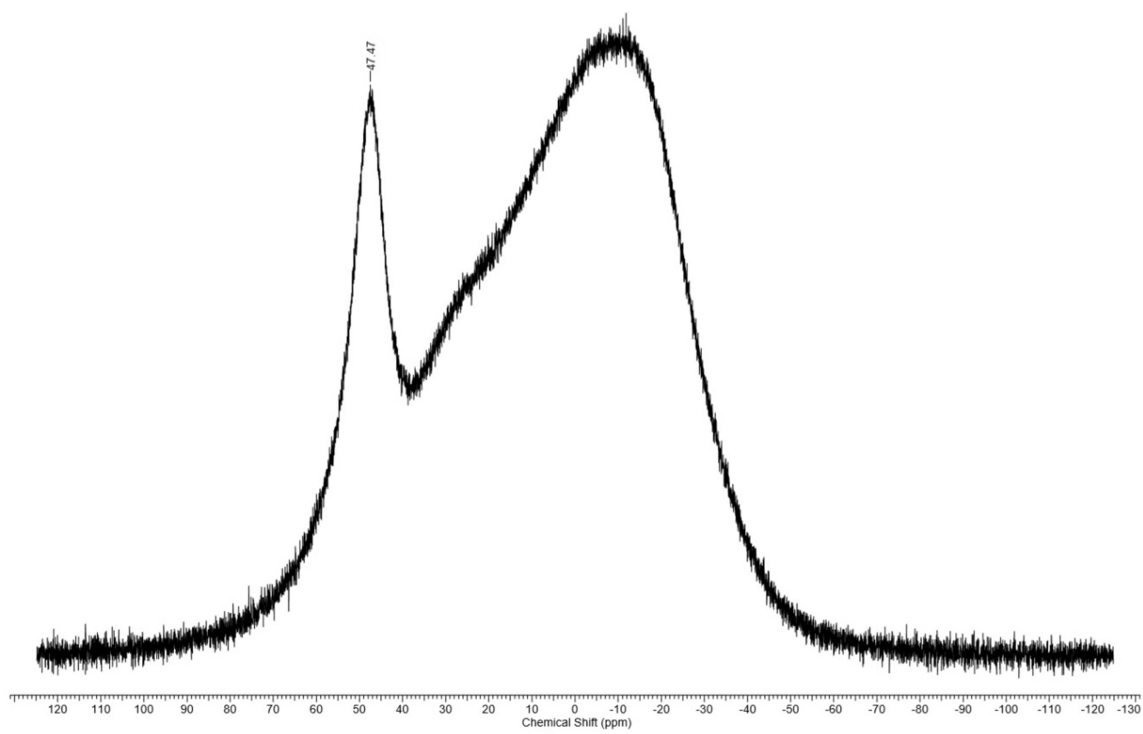


Figure 7.1.10. $^{11}\text{B}\{\text{H}\}$ NMR spectrum of **4c** in CDCl_3 .

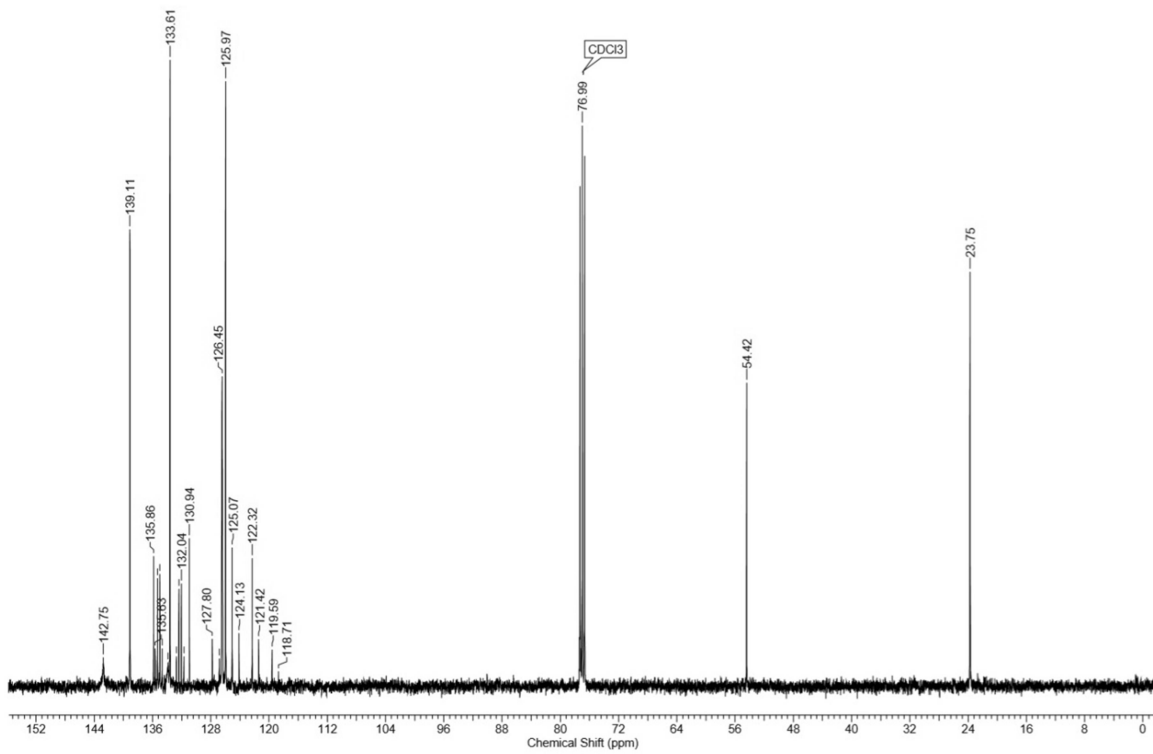


Figure 7.1.11. $^{13}\text{C}\{\text{H}\}$ NMR spectrum of **4c** in CDCl_3 .

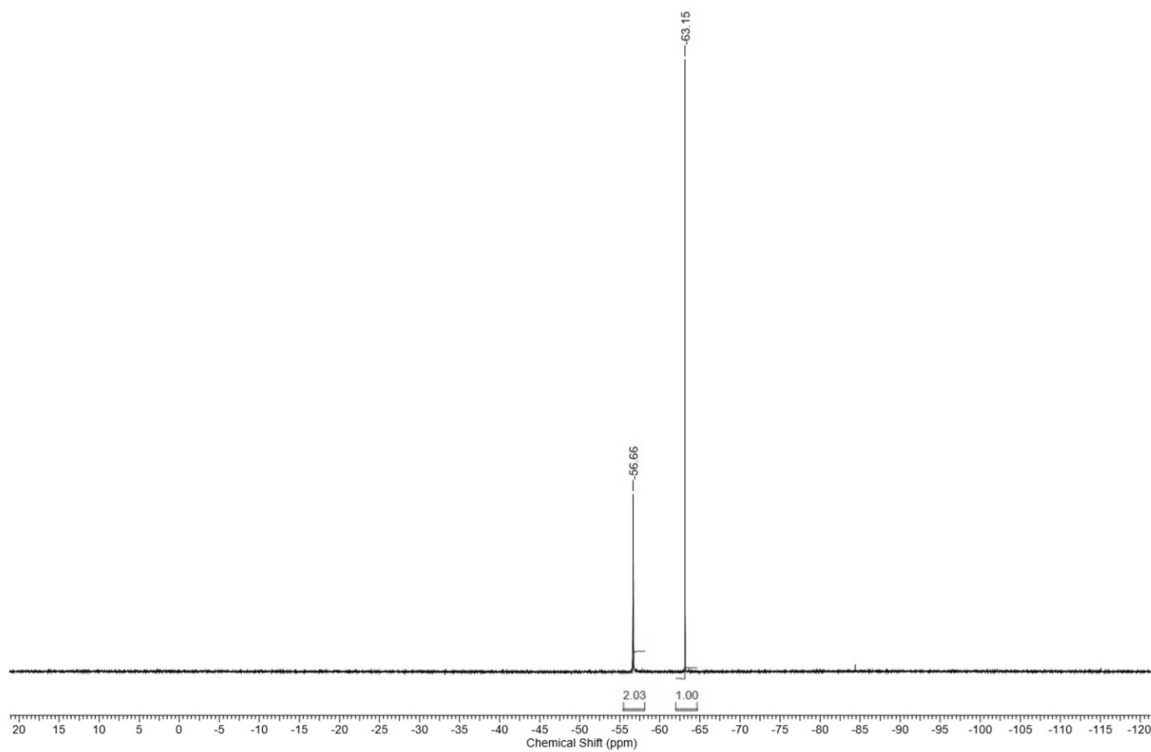


Figure 7.1.12. $^{19}\text{F}\{\text{H}\}$ NMR spectrum of **4c** in CDCl_3 .

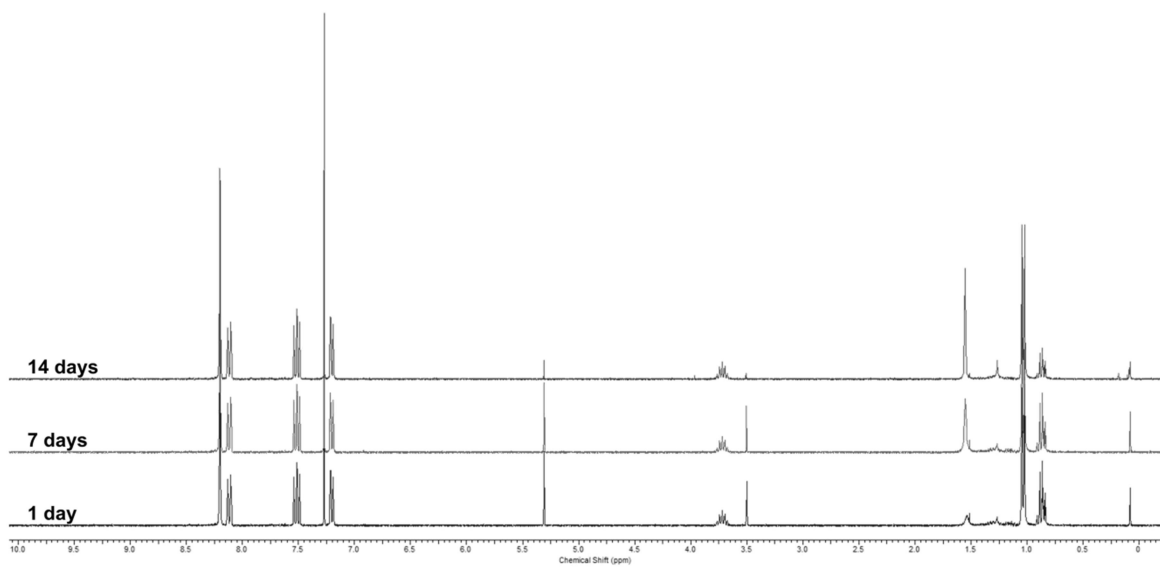


Figure 7.1.13. ^1H NMR spectrum of **4c** in moist solution over time in CDCl_3 .

Mass spectra

MC-MesD-2021-01-12-2

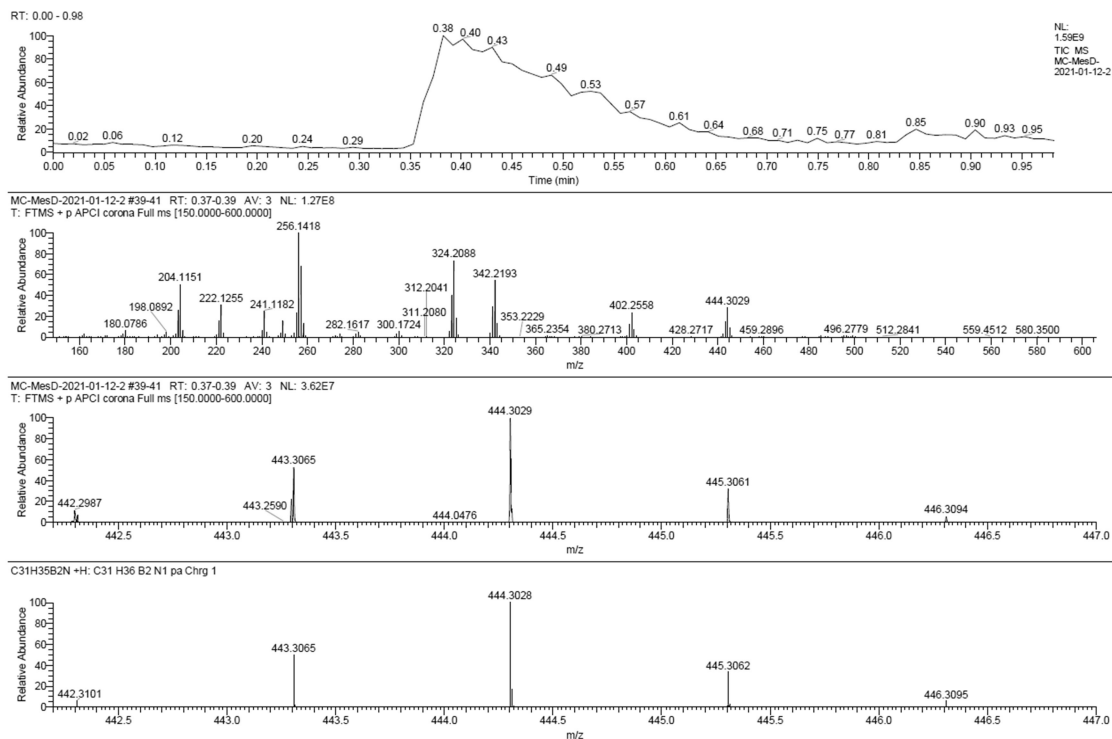


Figure 7.1.14. APCI HRMS spectrum of **4a**.

MC-TipD-2021-01-12-1

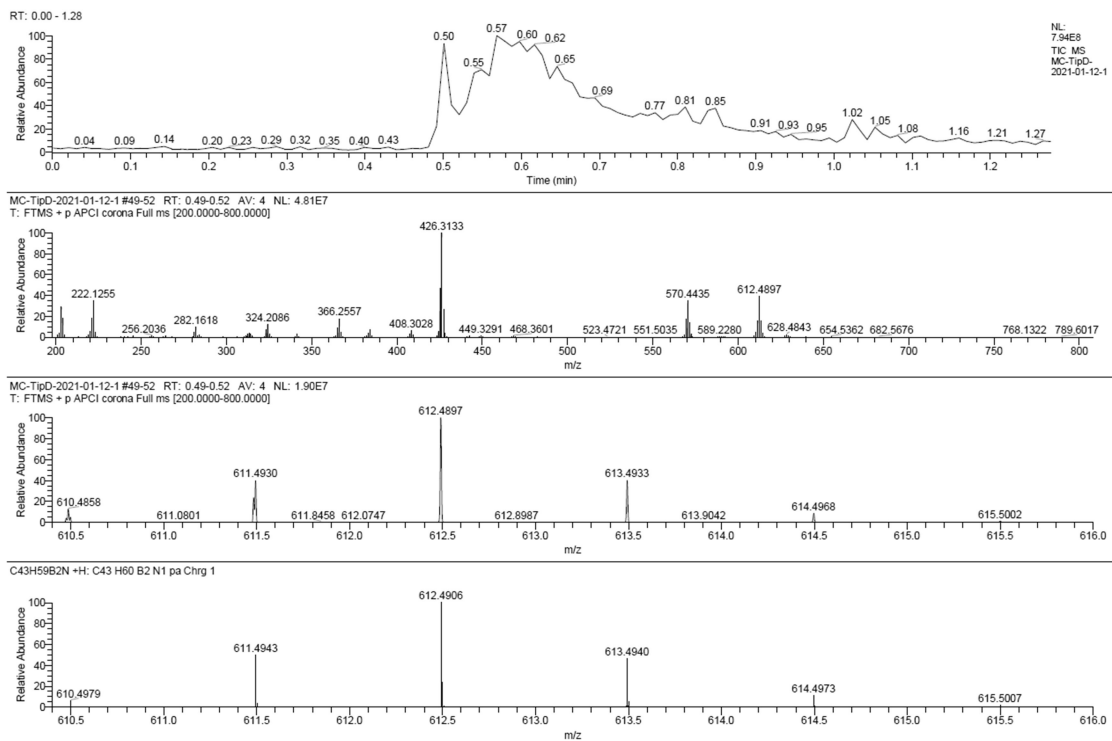


Figure 7.1.15. APCI HRMS spectrum of **4b**.

MC-FMesD-2021-01-12-1

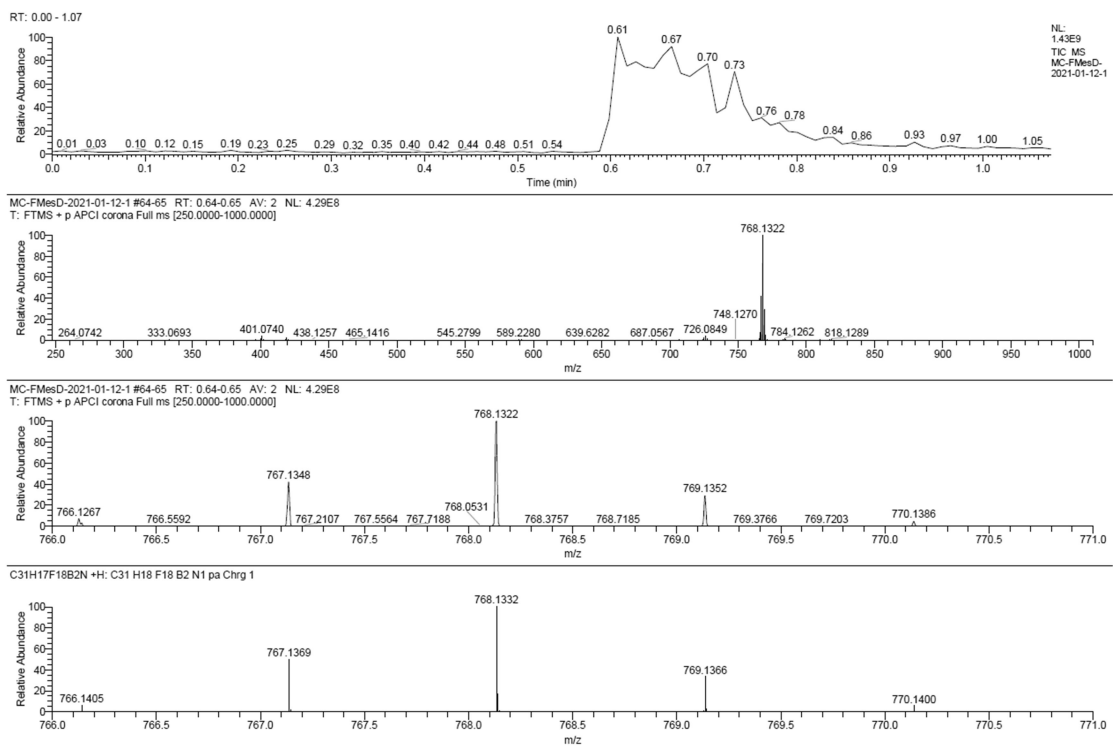


Figure 7.1.16. APCI HRMS spectrum of **4c**.

UV/vis and fluorescence spectra

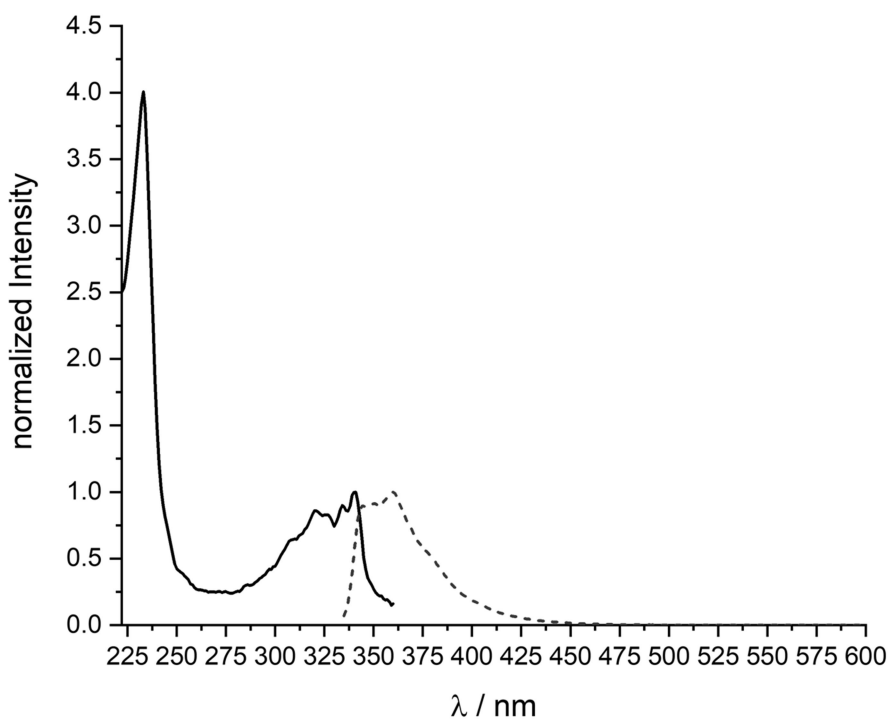


Figure 7.1.17. UV/vis and fluorescence spectrum of **4a** in hexane.

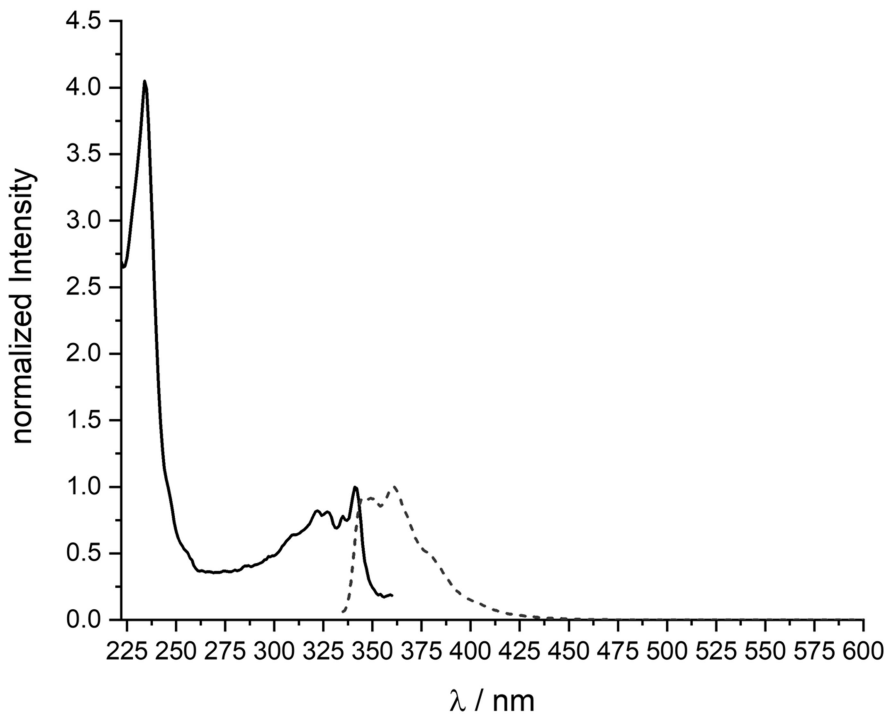


Figure 7.1.18. UV/vis and fluorescence spectrum of **4b** in hexane.

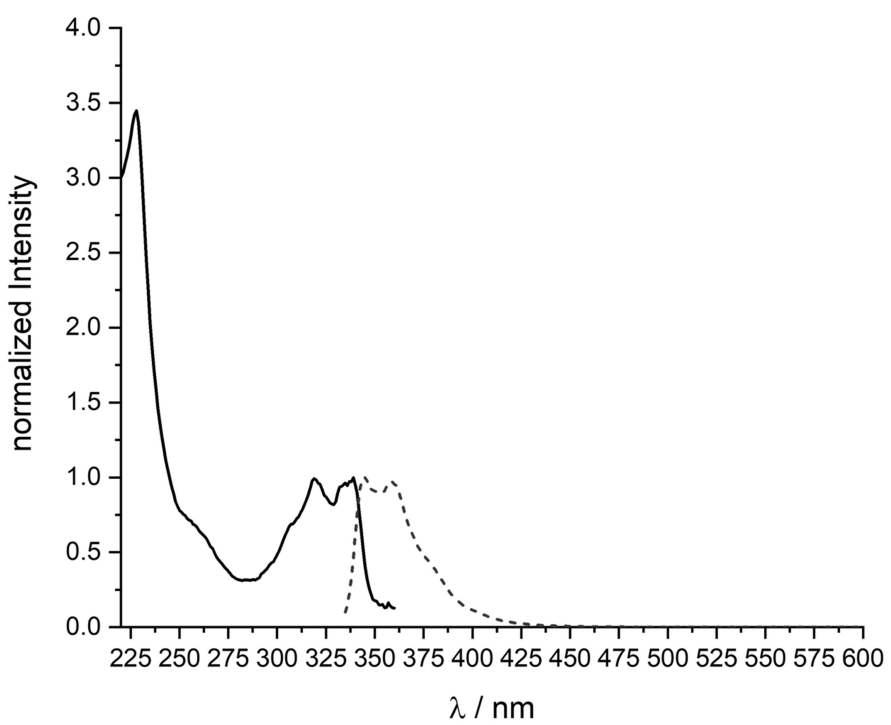


Figure 7.1.19. UV/vis and fluorescence spectrum of **4c** in hexane.

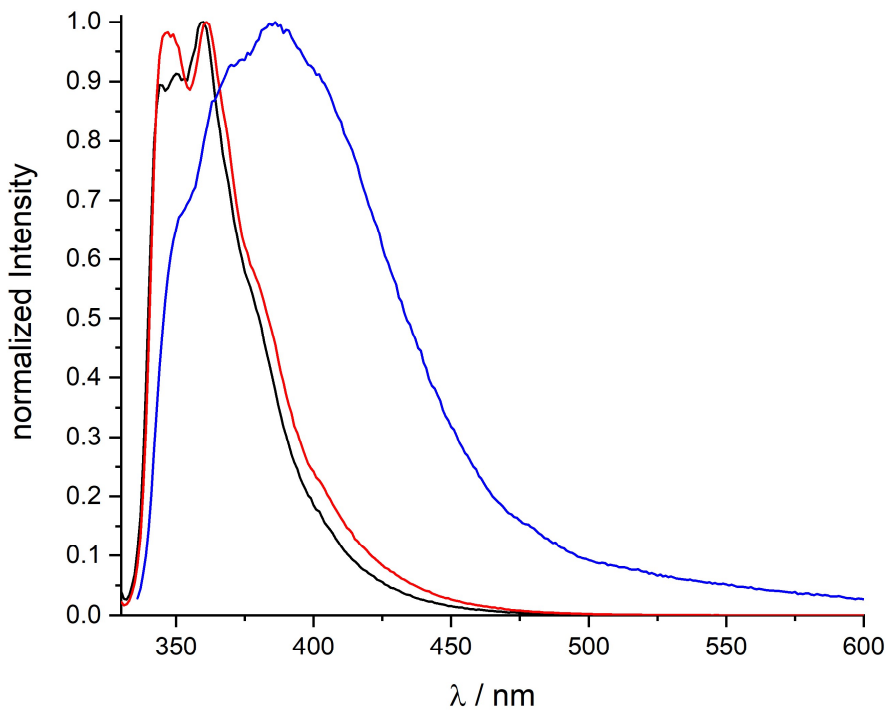


Figure 7.1.20. Solvatochromic effect on the emission of **4a** in hexane (black), Et₂O (red) and DCM (blue).

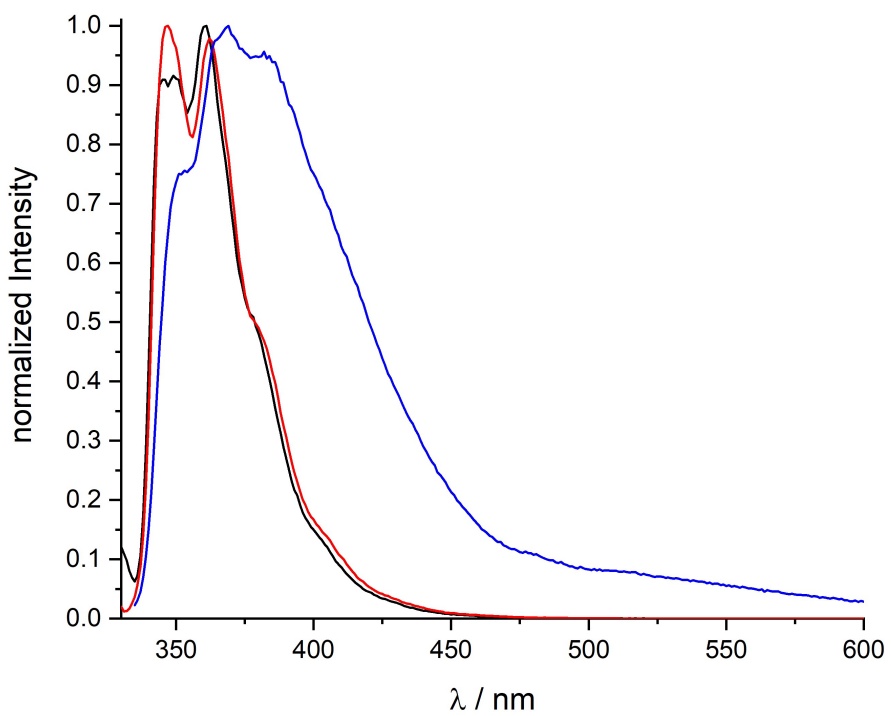


Figure 7.1.21. Solvatochromic effect on the emission of **4b** in hexane (black), Et_2O (red) and DCM (blue).

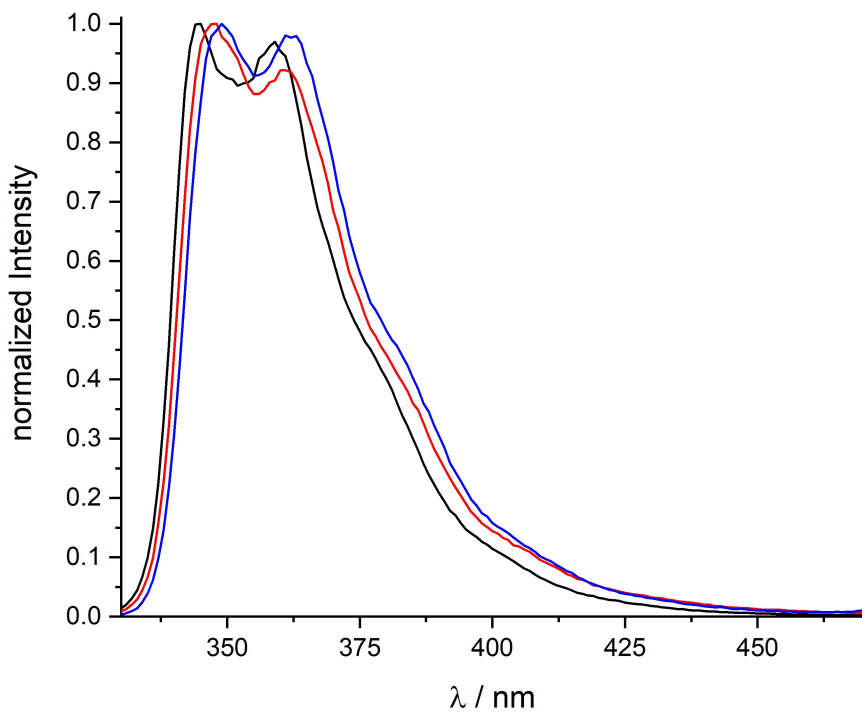


Figure 7.1.22. Solvatochromic effect on the emission of **4c** in hexane (black), Et_2O (red) and DCM (blue).

Table 7.1.1. Solvatochromic effect on the absorption and emission maxima of **4a**, **4b** and **4c**.

compound	λ_{abs} [nm]	λ_{abs} [nm]	λ_{abs} [nm]	λ_{em} [nm]	λ_{em} [nm]	λ_{em} [nm]
	hexane	Et ₂ O	DCM	Hexane	Et ₂ O	DCM
4a	321	<u>321</u>	321	344	347	351
	<u>341</u>	341	<u>341</u>	<u>360</u>	<u>361</u>	<u>386</u>
4b	322	323	326	345	<u>347</u>	353
	<u>341</u>	<u>342</u>	<u>342</u>	<u>361</u>	362	<u>369</u>
4c	319	<u>320</u>	<u>320</u>	<u>345</u>	348	349
	<u>339</u>	339	339	359	360	361

Table 7.1.2. Fluorescence lifetime data of compounds **4a**, **4b** and **4c** in hexane, Et₂O and DCM.

Compound	hexane	Et ₂ O	DCM
4a	1.11 ns (12 %)	3.33 ns (100 %)	2.81 ns (69%)
	3.74 ns (88%)		4.72 ns (31%)
4b	1.17 ns (11 %)	3.02 ns (100 %)	2.08 ns (10%)
	3.20 ns (89 %)		4.36 ns (88%)
4c	1.40 ns (5 %)	4.40 ns (100 %)	2.44 ns (100%)
	5.26 ns (95 %)		

Table 7.1.3. Fluorescence quantum yield of compounds **4a**, **4b** and **4c** in hexane, Et₂O and DCM.

Compound	hexane	Et ₂ O	DCM
4a	34 %	20 %	17 %
4b	36 %	26 %	26 %
4c	47 %	36 %	30 %

CV traces

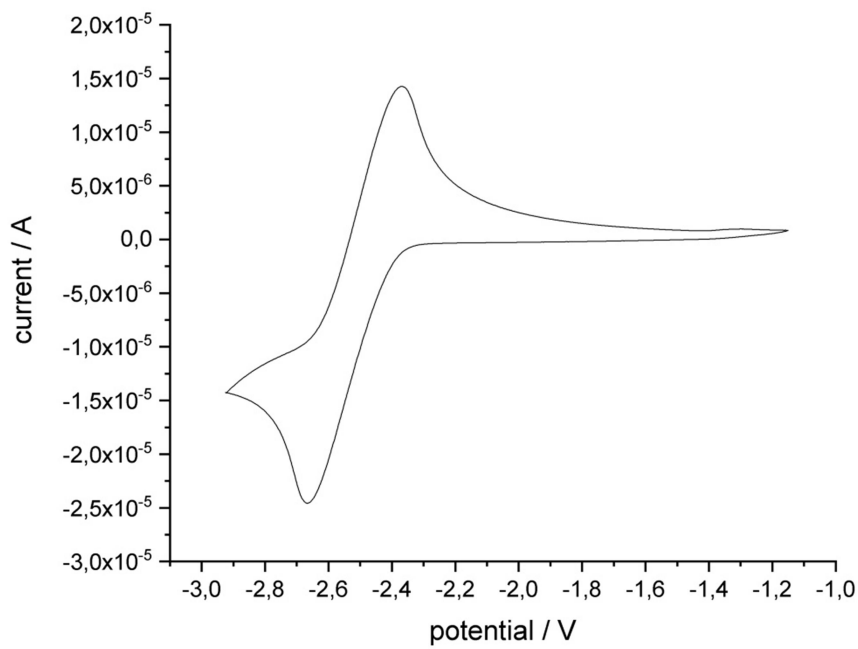


Figure 7.1.23. Cyclic voltammogram of **4a**.

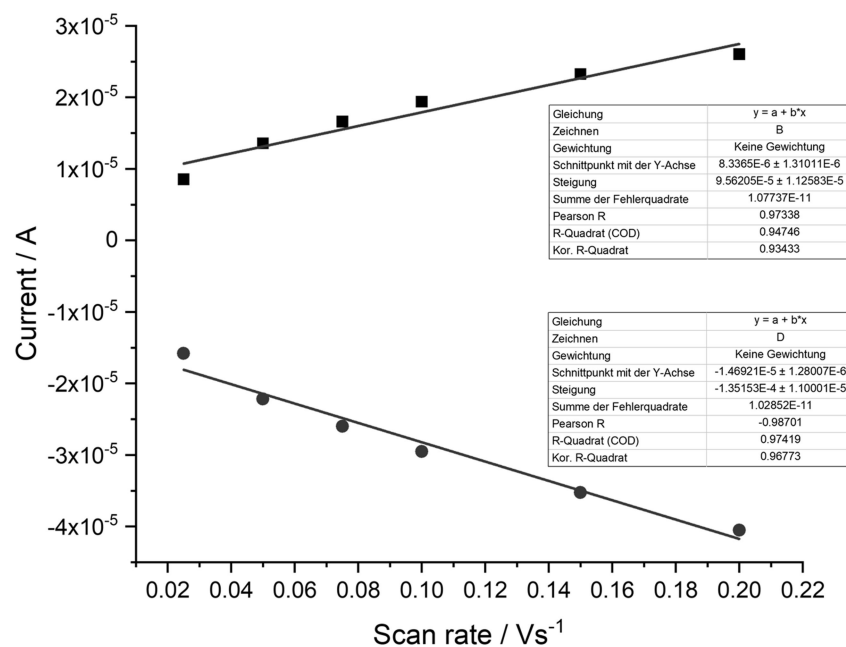


Figure 7.1.24. Plot for the linear dependence of oxidation and reduction peak current vs. scan rate of **4a**.

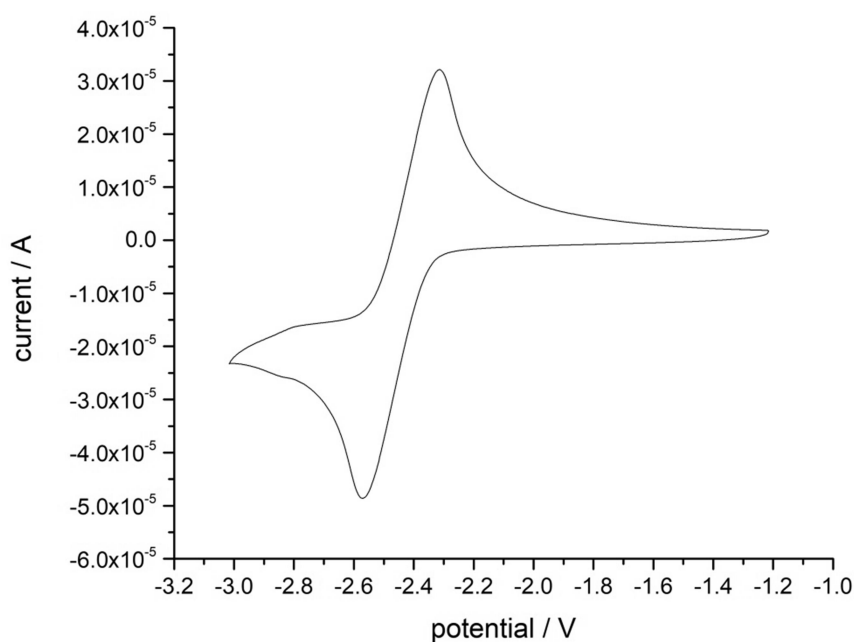


Figure 7.1.25. Cyclic voltammogram of **4b**.

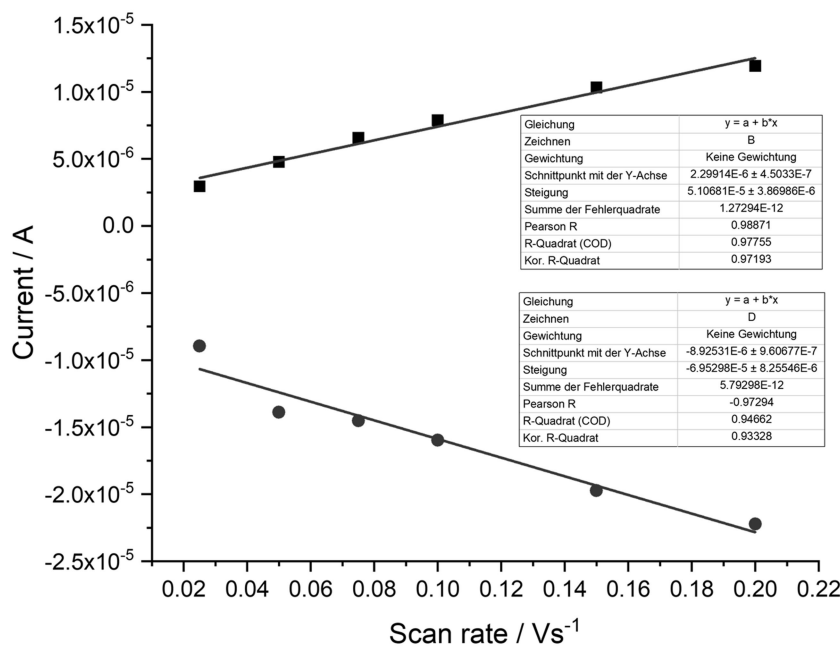


Figure 7.1.26. Plot for the linear dependence of oxidation and reduction peak current vs. scan rate of **4b**.

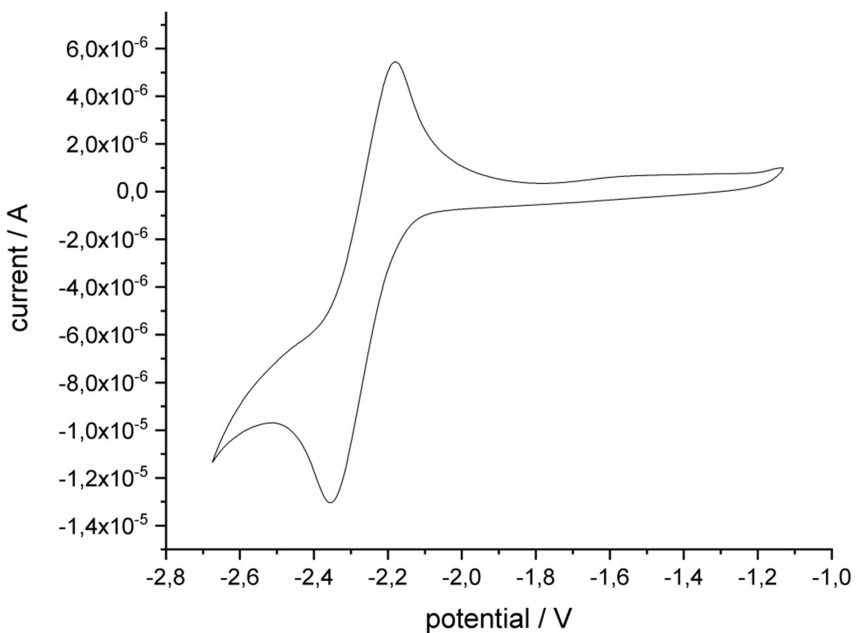


Figure 7.1.27. Cyclic voltammogram of **4c**.

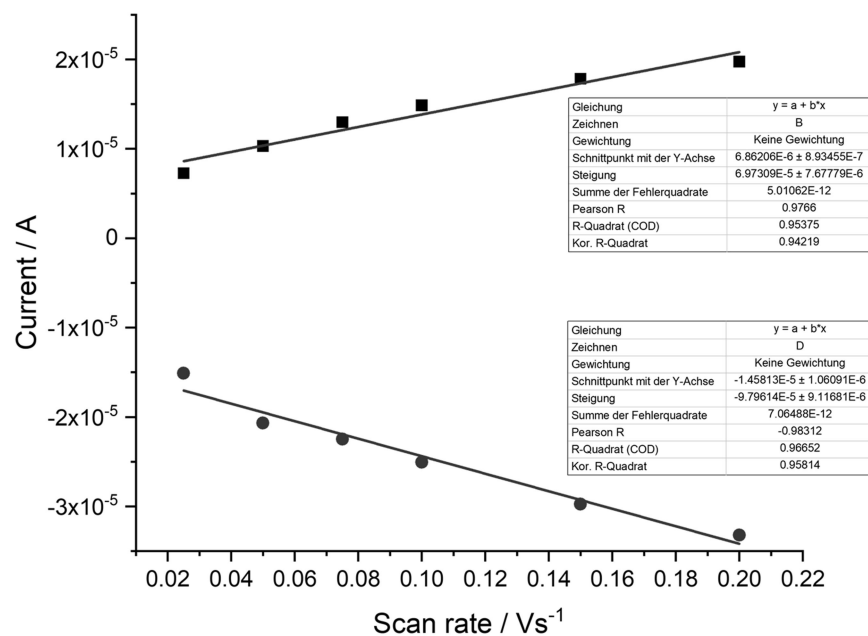


Figure 7.1.28. Plot for the linear dependence of oxidation and reduction peak current vs. scan rate of **4c**.

Table 7.1.4. Differences in potential between the anodic and cathodic peak in V.

Scan rate / Vs ⁻¹	4a	4b	4c
0.025	0.1868	0.1248	0.2374
0.050	0.2328	0.1575	0.2979
0.075	0.2631	0.1520	0.3235
0.100	0.2884	0.1666	0.3696
0.150	0.3284	0.1926	0.4086
0.200	0.3436	0.2264	0.4398

Differential scanning calorimetry

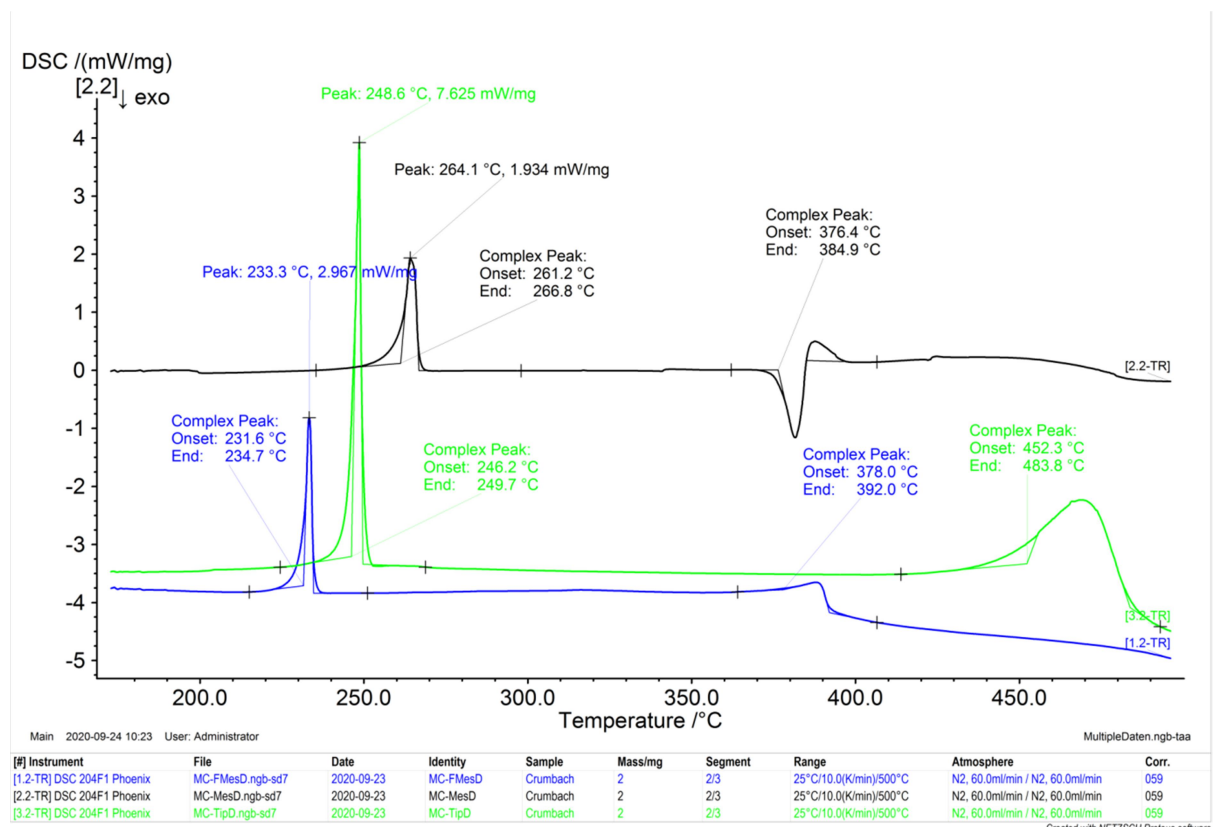


Figure 7.1.29. Differential scanning calorimetry graphs for **4a** (black), **4b** (green), and **4c** (blue).

NICS and ACID plots

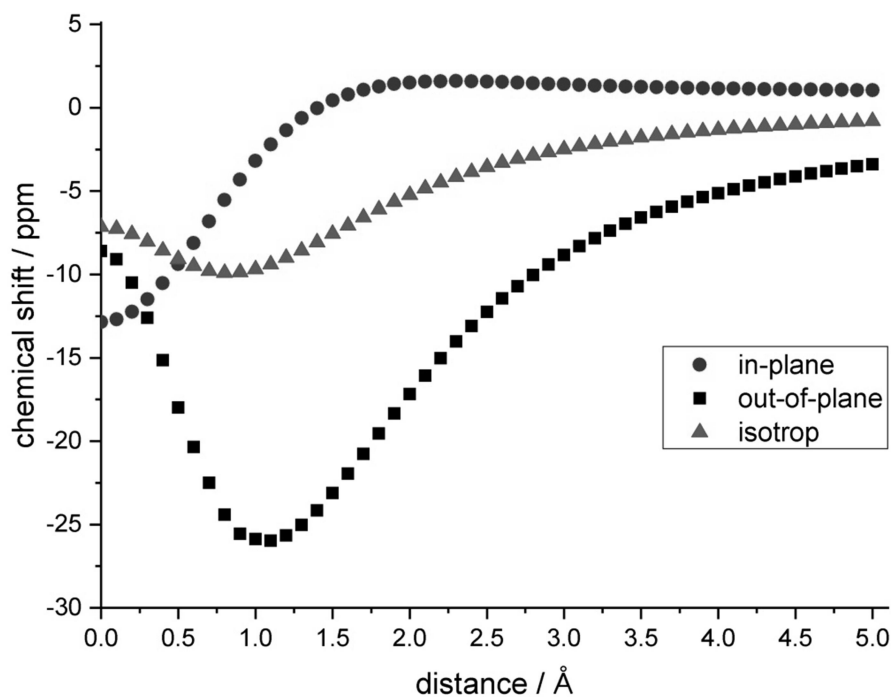


Figure 7.1.30. NICS Scan of naphthalenic rings of neutral **4a**.

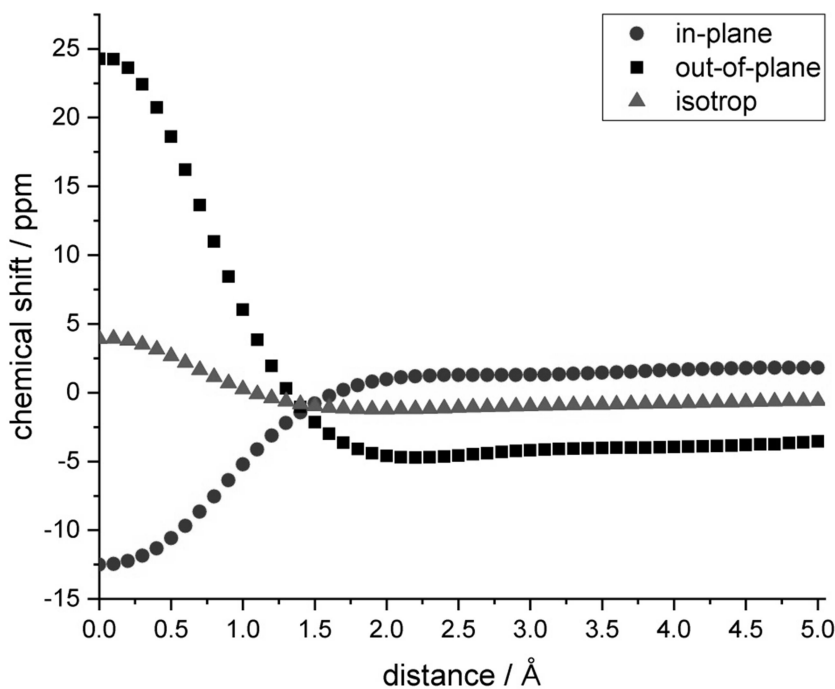


Figure 7.1.31. NICS Scan of hetero ring of neutral **4a**.

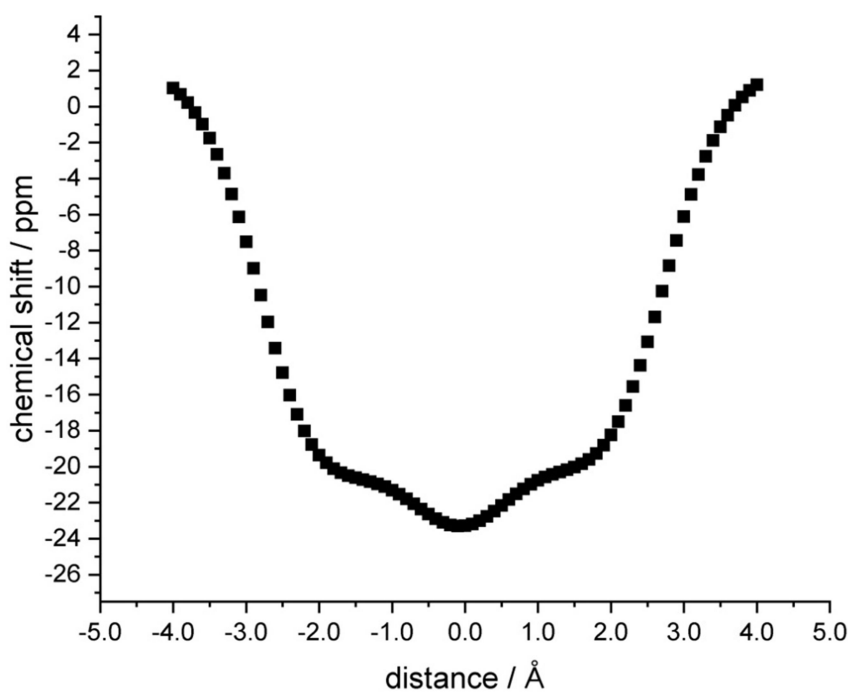


Figure 7.1.32. NICS XY-Scan of naphthalenic rings of neutral **4a**.

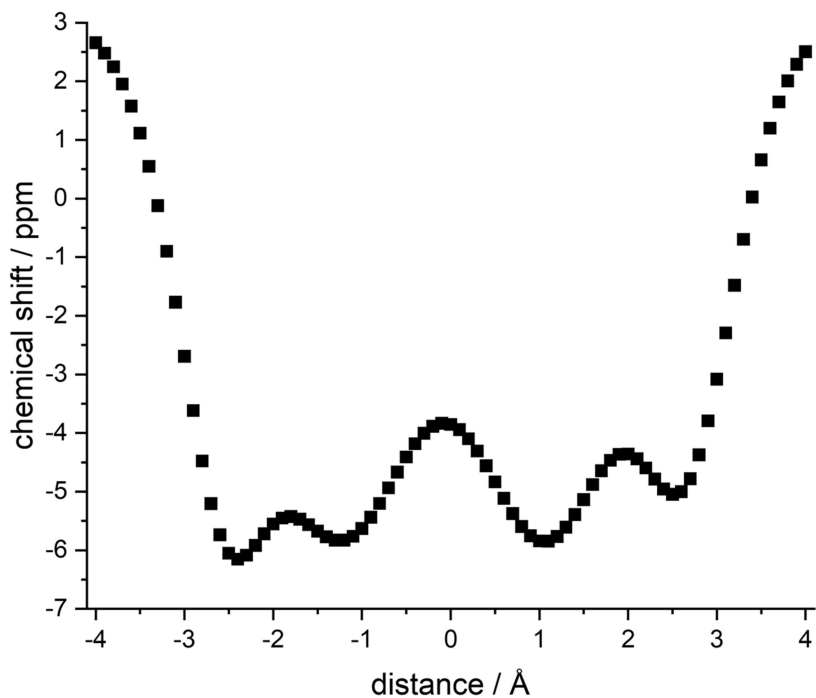


Figure 7.1.33. NICS XY-Scan of hetero ring of neutral **4a**.

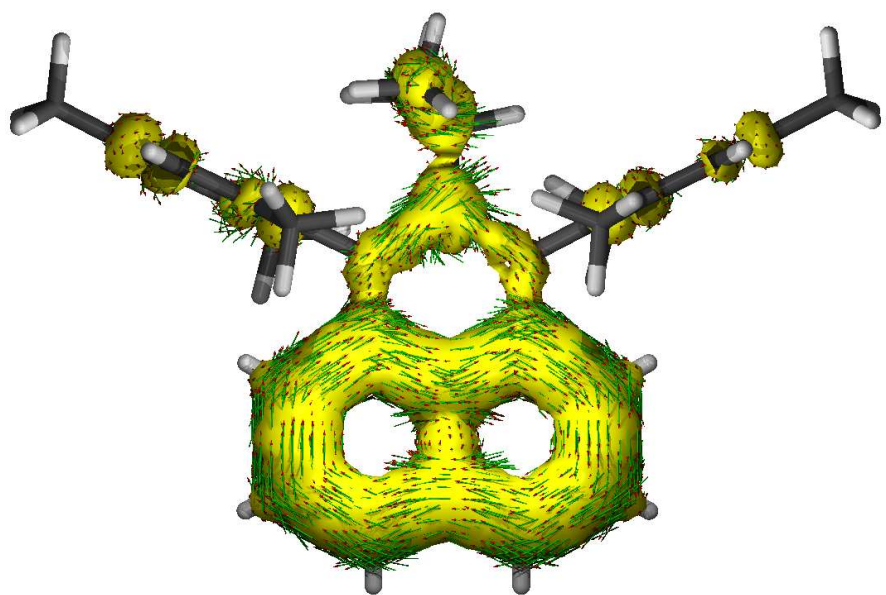


Figure 7.1.34. ACID map of neutral **4a** (isovalue 0.015).

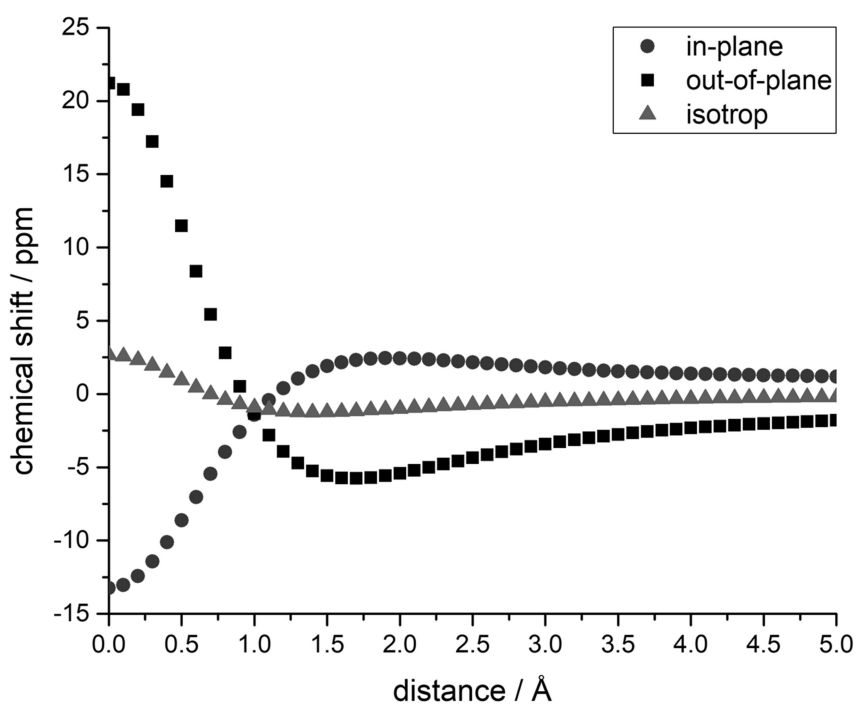


Figure 7.1.35. NICS Scan of naphthalenic rings of mono anionic **4a**.

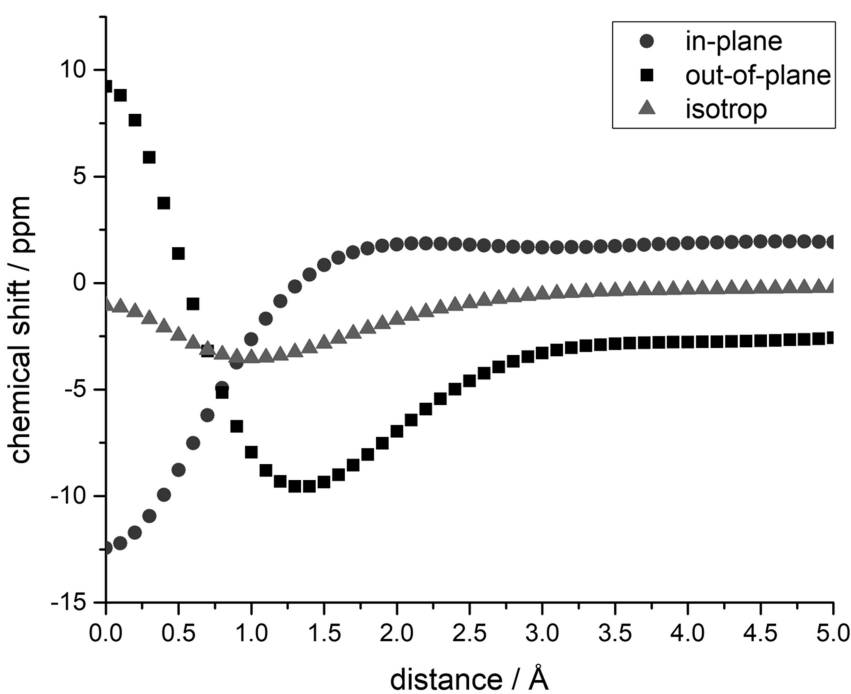


Figure 7.1.36. NICS Scan of hetero ring of mono anionic **4a**.

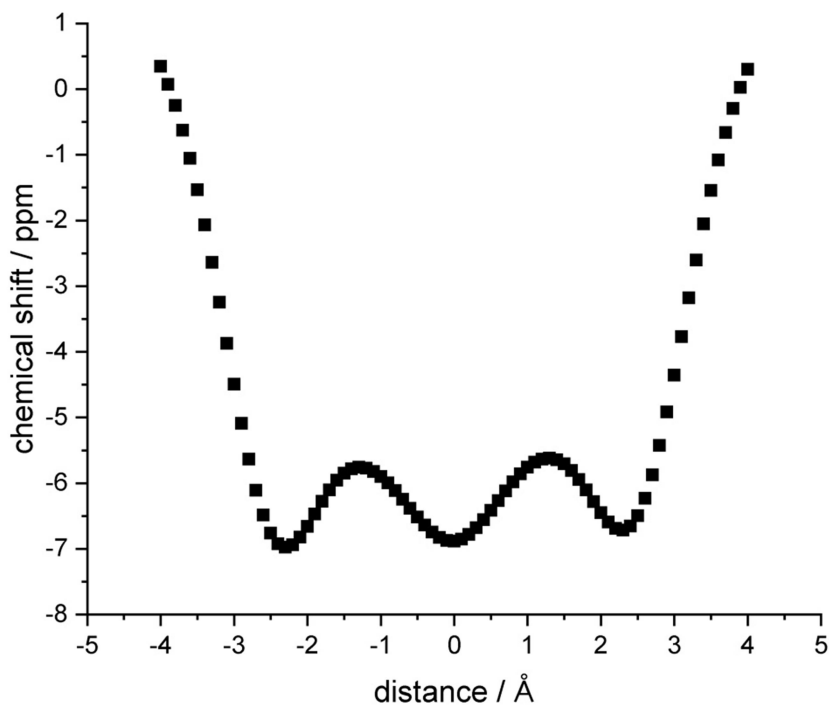


Figure 7.1.37. NICS XY-Scan of naphthalenic rings of mono anionic **4a**.

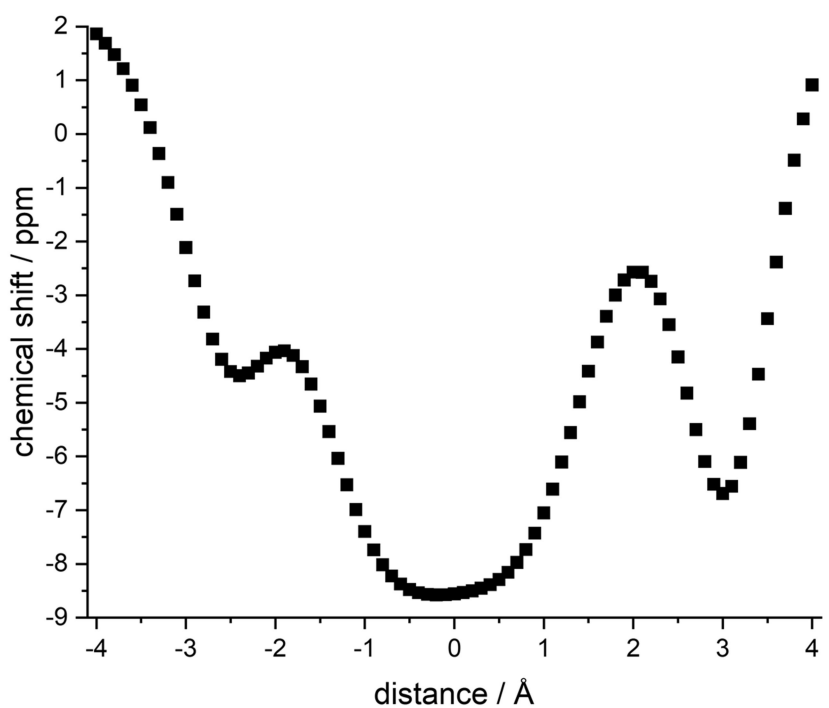


Figure 7.1.38. NICS XY-Scan of hetero ring of mono anionic **4a**.

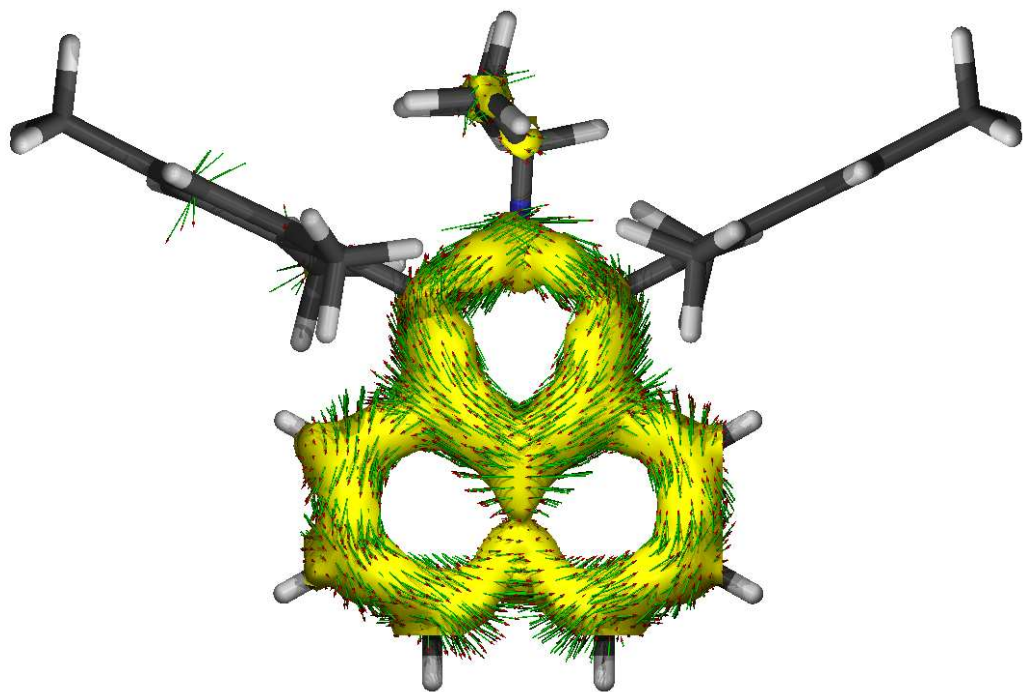


Figure 7.1.39. ACID map of mono anionic **4a** (isovalue 0.015).

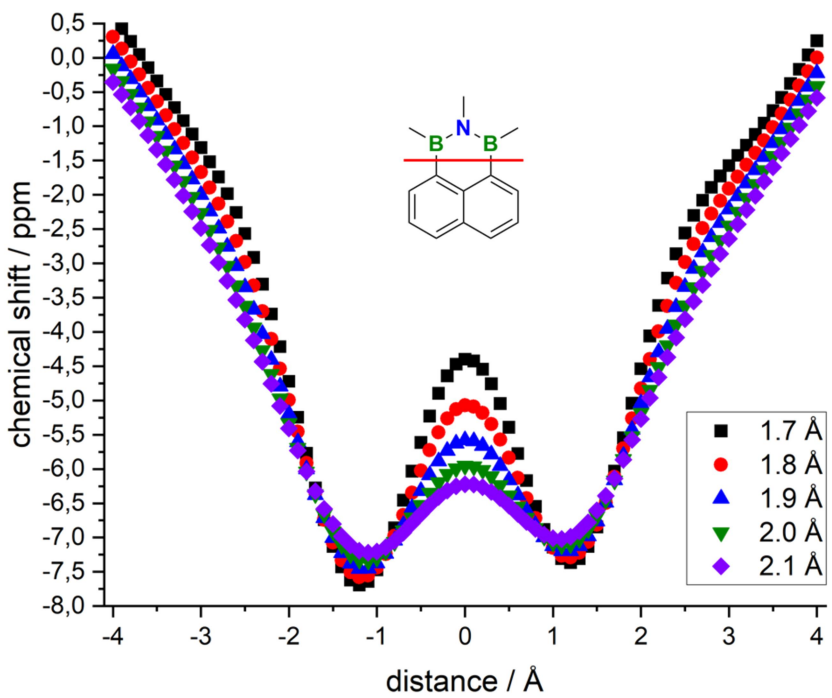


Figure 7.1.40. NICS-X-height-scan for the hetero ring of a model compound with only methyl groups on boron and nitrogen (see structure as inset). This indicates that a scan-height of 2.1 Å or higher is more appropriate in this case. With increasing scan-height, the maximum at 0.0 Å decreases, whereas the minima almost stay at the same level. A scan-height of 1.7 Å corresponds to the NICS-X-height scans reported for all-carbon systems by Stanger *et al.*^[17b] As the naphthalenic rings lose a major part of the π -effects at the height of 2.1 Å (cf. Figure 7.1.41), all NICS-X-scans were performed at 1.7 Å above the ring plane.

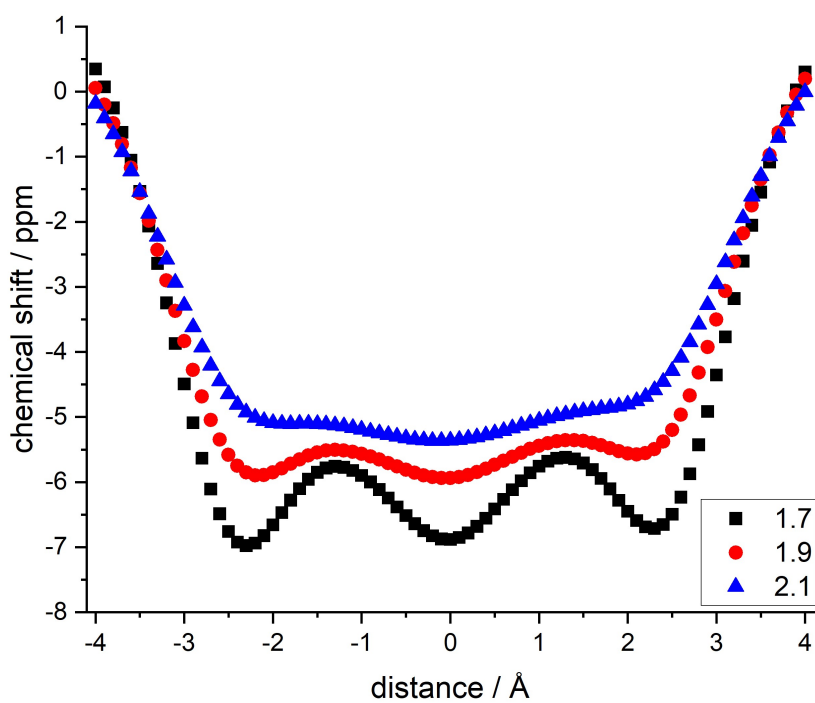


Figure 7.1.41. NICS-X-height-scan of naphthalenic rings of mono anionic **4a**, indicating a scan-height of 1.7 Å for all-carbon systems to be the most appropriate, as shown by Stanger *et al.*^[17b] Upon increasing the scan-height, the minima as well as the maxima decrease, which shows that the system loses major parts of its π -effects at this height. Therefore, all NICS-X-Scans were performed at a height of 1.7 Å.

Cartesian coordinates (Å) and total energies (a.u.) of optimized stationary points

neutral 4a:

Total energy (B3LYP-D3(BJ)/def2-SV(P)): -1305.281722585

C	-0.171518	0.016715	-0.070161
C	-0.156848	0.013049	1.357787
C	1.088602	0.008046	2.064898
C	2.301405	0.008209	1.323582
C	2.281511	0.012063	-0.057595
C	1.046801	0.015586	-0.746707
C	-1.392950	0.012523	2.073926
C	-1.347465	0.005357	3.466912
C	-0.123493	0.000026	4.175060
C	1.073465	0.001814	3.486160
B	-2.763551	0.022864	1.317168
N	-2.777589	0.040308	-0.128477
B	-1.524996	0.023677	-0.847508
C	-1.466223	0.005250	-2.428935
C	-1.405563	-1.223233	-3.126128
C	-1.316632	-1.228081	-4.522716
C	-1.275329	-0.037541	-5.261907
C	-1.313337	1.172131	-4.560194
C	-1.403092	1.209327	-3.161154
C	-1.415900	-2.528228	-2.361515
C	-1.419910	2.537648	-2.438235
C	-4.063353	0.006739	2.219891
C	-4.620747	1.209532	2.699453
C	-5.762488	1.175946	3.513803
C	-6.355150	-0.031558	3.897202
C	-5.751931	-1.223318	3.470867
C	-4.613251	-1.219742	2.657456

C	-3.957493	2.536482	2.403487
C	-3.936300	-2.527608	2.311854
H	-2.285210	0.004176	4.030700
H	-0.128759	-0.005525	5.269370
H	1.048012	0.017979	-1.841126
H	3.219407	0.011966	-0.621454
H	-1.273155	-2.187696	-5.050847
C	-1.187720	-0.071431	-6.769087
H	-1.267869	2.114973	-5.116659
C	-4.035462	0.065987	-0.935098
H	-6.179732	-2.182338	3.785822
C	-7.601800	-0.062162	4.748455
H	-6.198109	2.119856	3.860783
H	-3.197578	2.767728	3.174289
H	-3.433063	2.533616	1.433995
H	-4.686021	3.366062	2.395422
H	-4.642842	-3.375150	2.344239
H	-3.474343	-2.506159	1.311142
H	-3.122852	-2.742272	3.030964
H	-1.366973	-3.396900	-3.039760
H	-0.557221	-2.589975	-1.667467
H	-2.327667	-2.632274	-1.745994
H	-0.591511	2.606408	-1.709069
H	-1.325279	3.383503	-3.140106
H	-2.356417	2.677698	-1.868325
H	2.026575	-0.002159	4.025672
H	3.252704	0.004567	1.866256
H	-7.876182	0.946854	5.100705
H	-8.463660	-0.465399	4.183323
H	-7.468845	-0.707814	5.636131
H	-1.110217	0.944447	-7.192656

H	-0.307338	-0.648056	-7.109266
H	-2.079038	-0.553675	-7.213130
H	-3.701898	0.083062	-1.981142
C	-4.892666	-1.193230	-0.774195
C	-4.870071	1.333267	-0.724425
H	-5.656135	1.383907	-1.499259
H	-5.364286	1.344938	0.259476
H	-4.248234	2.239877	-0.816790
H	-5.688616	-1.191613	-1.540541
H	-4.290592	-2.106247	-0.918560
H	-5.375477	-1.242001	0.214338

mono anionic 4a:

Total energy (B3LYP-D3(BJ)/def2-SV(P)): -1305.308885

C	-3.372033	-0.912921	1.233217
C	-2.708668	-0.596325	0.026698
C	-3.36053	-0.898362	-1.190873
C	-4.608874	-1.53597	-1.187628
C	-5.253714	-1.881374	0.006642
C	-4.621371	-1.549608	1.210593
B	-1.299073	0.157773	0.030551
C	-1.289109	1.684803	-0.001348
C	-0.040666	2.392337	-0.014812
C	-0.033748	3.839444	-0.043238
C	-1.274748	4.531981	-0.057102
C	-2.486952	3.832908	-0.04483
C	-2.496555	2.439585	-0.017645
C	1.21311	4.520749	-0.058335
C	2.417505	3.808056	-0.049054
C	2.412968	2.414882	-0.023818
C	1.199579	1.668108	-0.00445

B	1.205771	0.137178	0.024091
N	-0.053806	-0.590459	0.05343
C	-0.144217	-2.069023	0.098385
C	0.390739	-2.762954	-1.161152
C	-2.722907	-0.495199	-2.50131
C	-6.579022	-2.607444	-0.006538
C	-2.737354	-0.542252	2.554392
C	2.633567	-0.581099	0.00134
C	3.277994	-0.862383	-1.226182
C	4.541399	-1.468983	-1.242419
C	5.219168	-1.785272	-0.058042
C	4.613207	-1.434187	1.153175
C	3.349277	-0.825997	1.194183
C	2.642147	-0.431323	-2.528635
C	2.795001	-0.35731	2.520691
C	6.554972	-2.490688	-0.091317
C	0.467202	-2.692165	1.360403
H	3.36642	1.875783	-0.01842
H	3.370684	4.351675	-0.062241
H	-3.453405	1.90626	-0.006783
H	-3.433928	4.387268	-0.056706
H	-5.095743	-1.763664	-2.14427
H	-5.118188	-1.787363	2.159544
H	5.014833	-1.692998	-2.206694
H	5.14266	-1.631549	2.093771
H	3.029771	0.713739	2.670389
H	1.697397	-0.437613	2.55773
H	3.22235	-0.924107	3.368367
H	3.079834	-0.962151	-3.393937
H	1.552759	-0.593869	-2.528345
H	2.789635	0.654888	-2.678548

H	-3.312777	-0.846704	-3.367169
H	-2.629121	0.604434	-2.563186
H	-1.698076	-0.895795	-2.593752
H	-2.504165	0.537316	2.584121
H	-3.39829	-0.784402	3.406272
H	-1.778632	-1.070956	2.704131
H	1.214872	5.617284	-0.079096
H	-1.265415	5.628496	-0.078886
H	7.128999	-2.314513	0.83626
H	6.434131	-3.587662	-0.197328
H	7.172631	-2.151313	-0.943271
H	-7.14796	-2.428533	0.923738
H	-7.208939	-2.288126	-0.857077
H	-6.442681	-3.703905	-0.099305
H	-1.218255	-2.29973	0.136742
H	0.176889	-3.758047	1.426701
H	1.567414	-2.639334	1.356385
H	0.097021	-2.182742	2.266488
H	0.120007	-3.835814	-1.139227
H	-0.053193	-2.32078	-2.069391
H	1.487418	-2.690772	-1.236564

7.2 Dithiophene-Fused Oxadiborepins and Azadiborepins: A New Class of Highly Fluorescent Heteroaromatics

NMR spectra

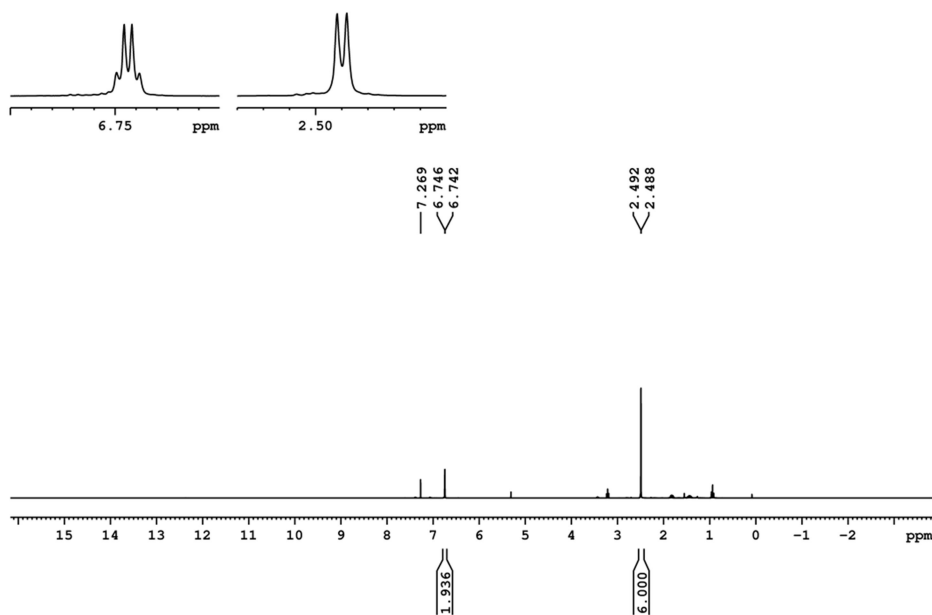


Figure 7.2.1. ¹H NMR spectrum of **2** in CDCl₃.

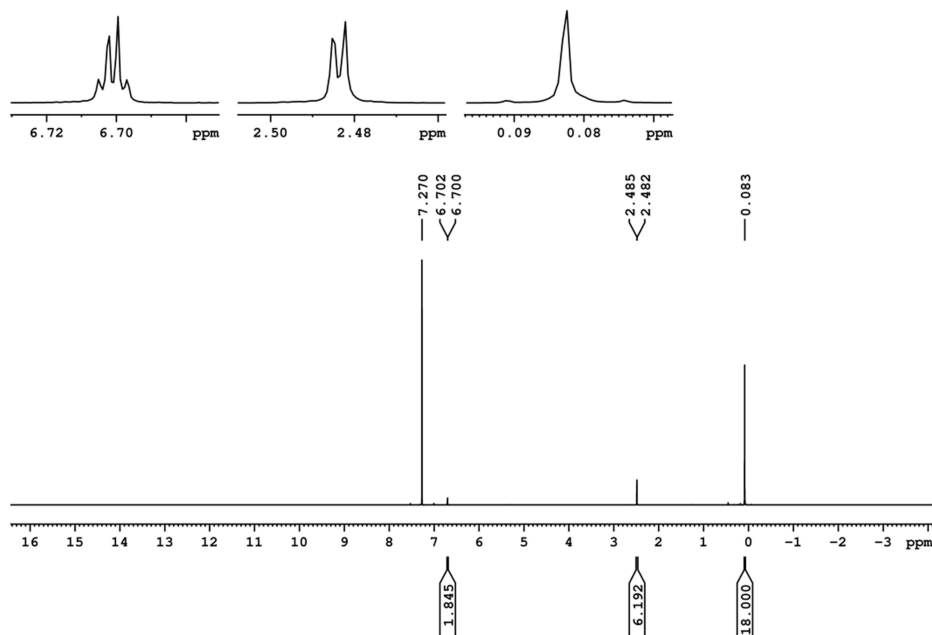


Figure 7.2.2. ¹H NMR spectrum of **3** in CDCl₃.

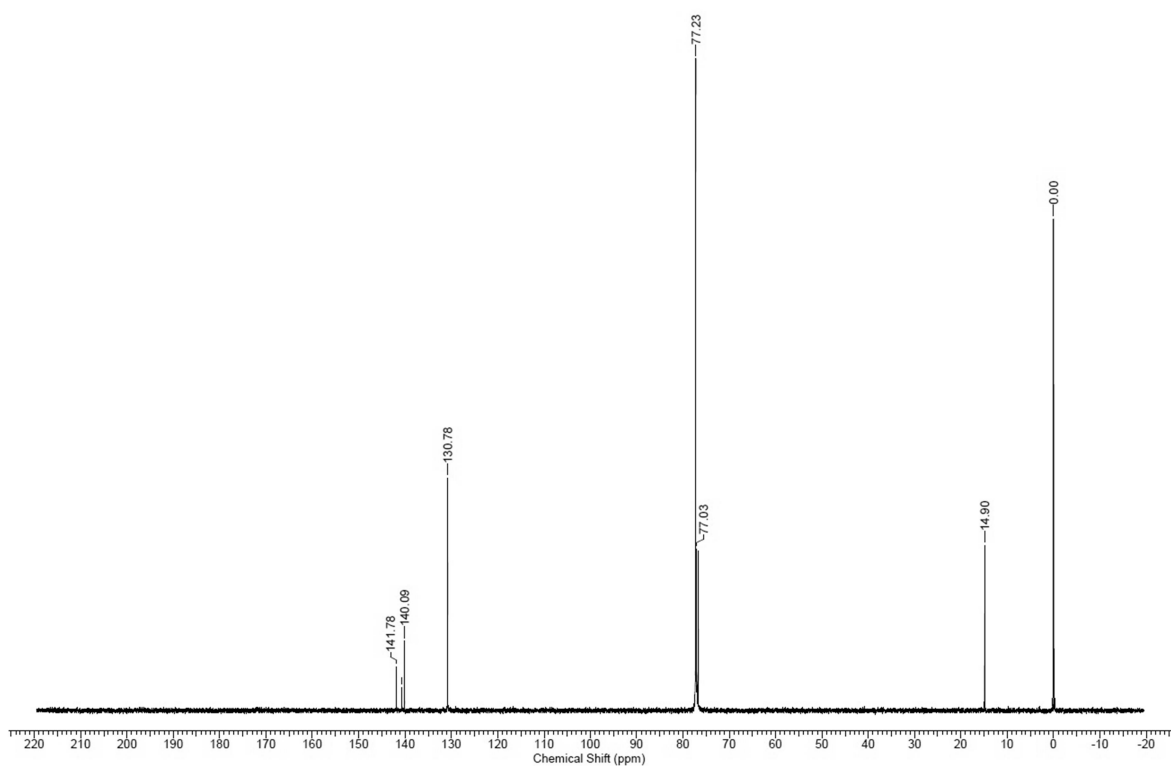


Figure 7.2.3. $^{13}\text{C}\{\text{H}\}$ NMR spectrum of **3** in CDCl_3 .

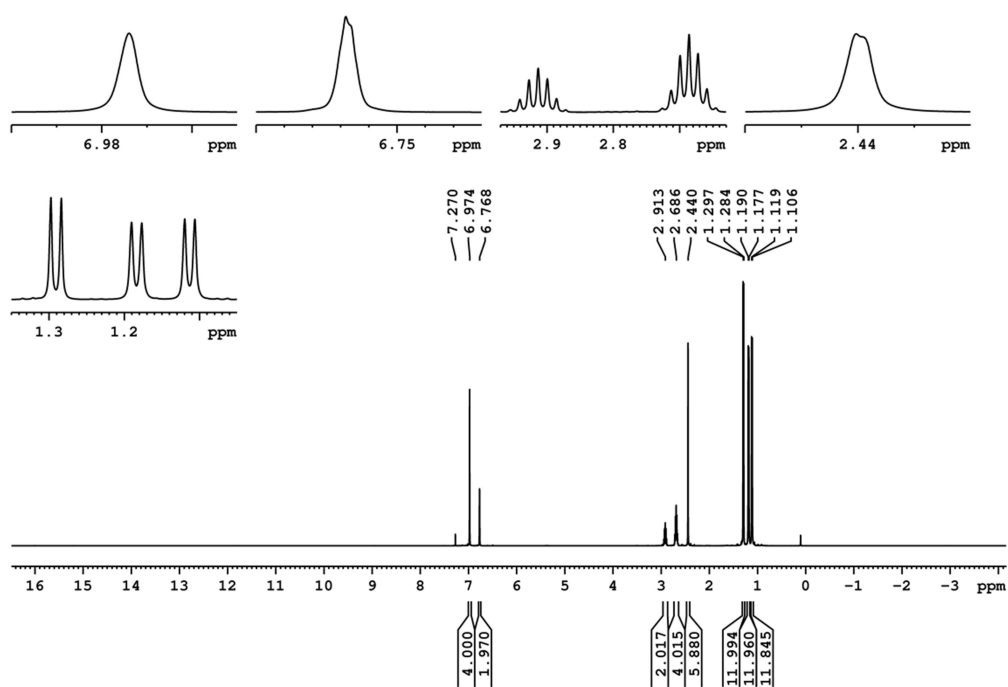


Figure 7.2.4. ^1H NMR spectrum of **5**^{Tip} in CDCl_3 .

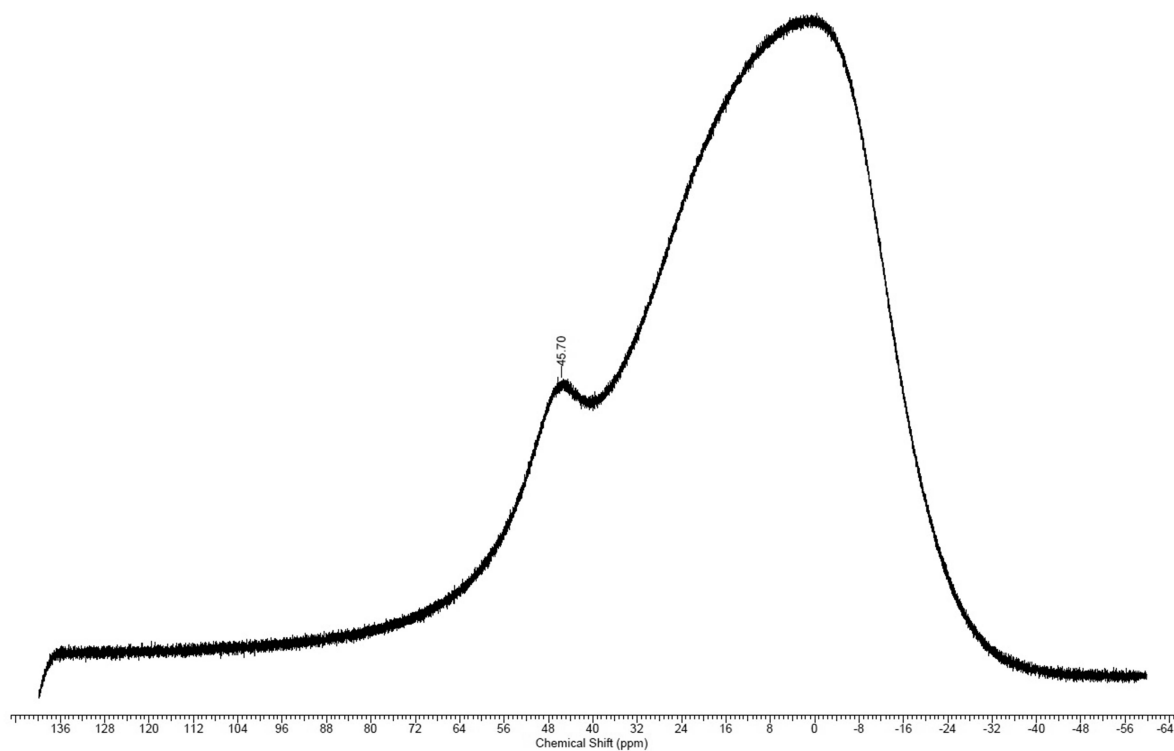


Figure 7.2.5. $^{11}\text{B}\{\text{H}\}$ NMR spectrum of **5^{Tip}** in CDCl_3 .

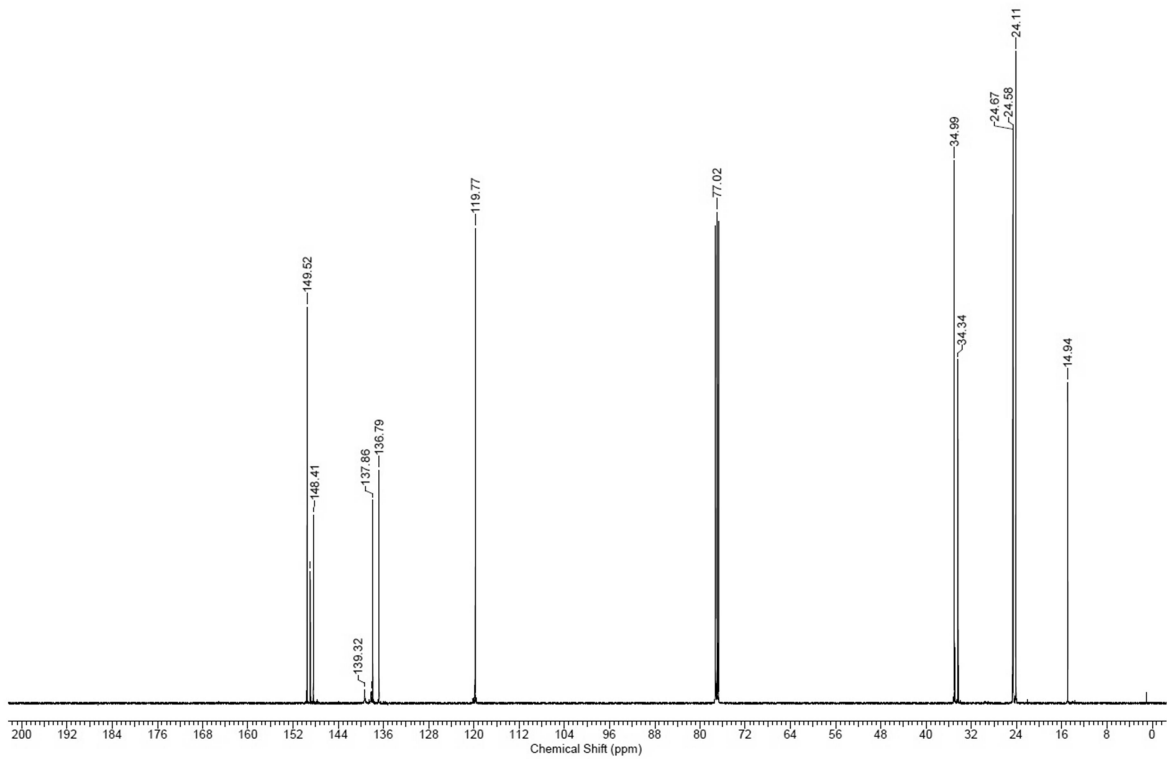


Figure 7.2.6. $^{13}\text{C}\{\text{H}\}$ NMR spectrum of **5^{Tip}** in CDCl_3 .

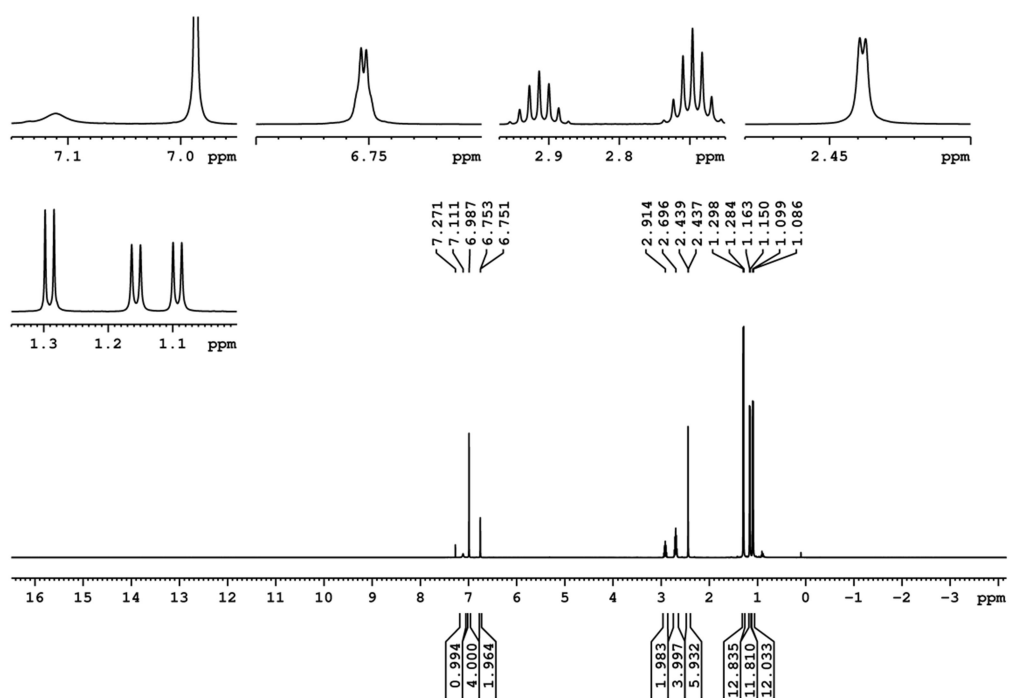


Figure 7.2.7. ^1H NMR spectrum of $\mathbf{6}^{\text{Tip}}$ in CDCl_3 .

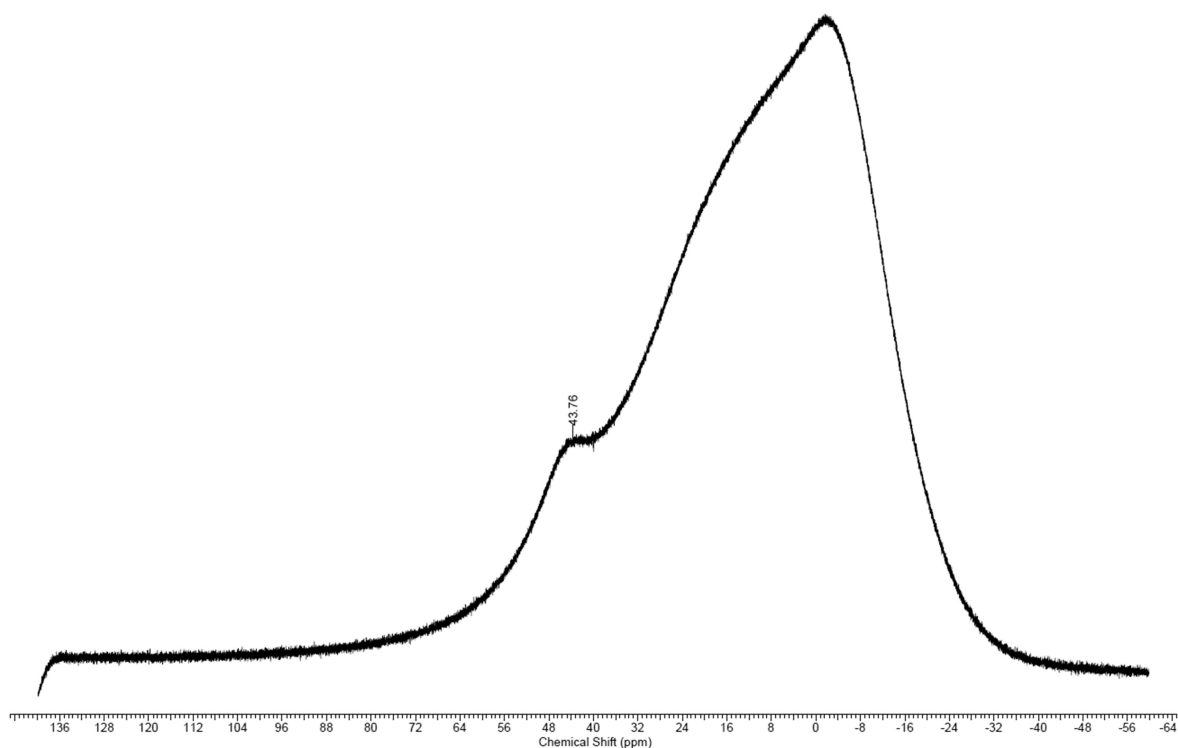


Figure 7.2.8. $^{11}\text{B}\{^1\text{H}\}$ NMR spectrum of $\mathbf{6}^{\text{Tip}}$ in CDCl_3 .

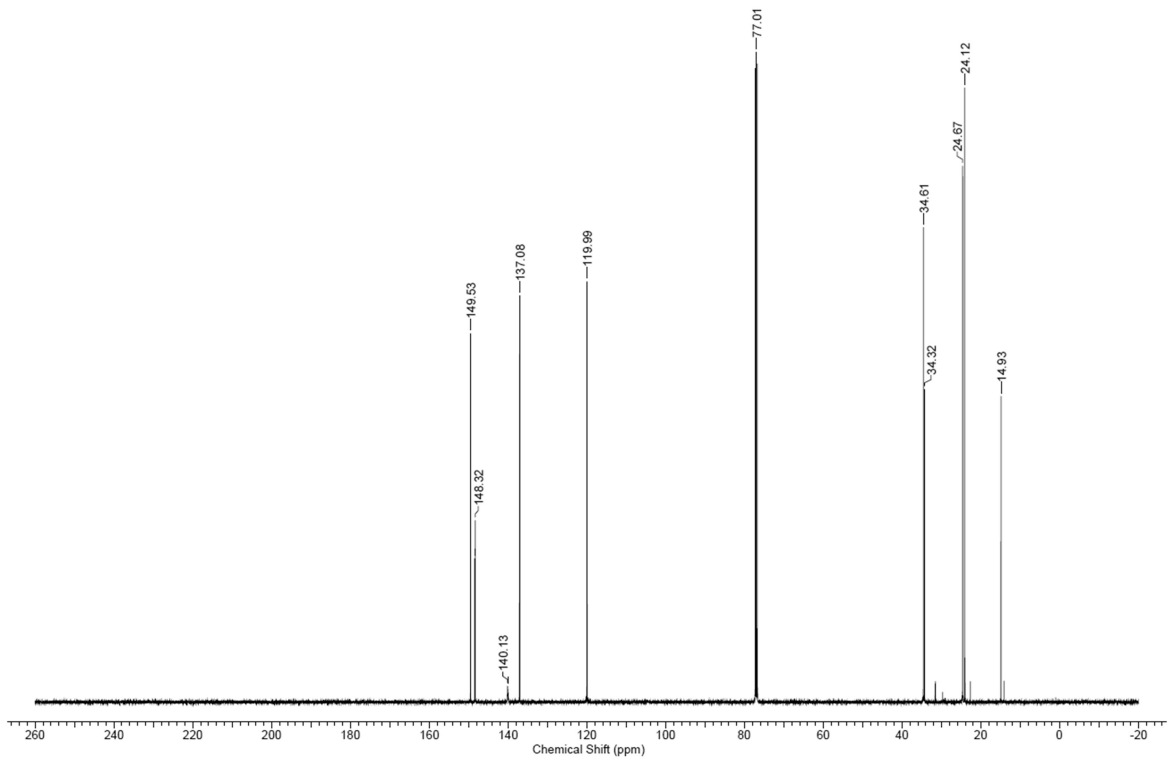


Figure 7.2.9. $^{13}\text{C}\{^1\text{H}\}$ NMR spectrum of **6^{Tip}** in CDCl_3 .

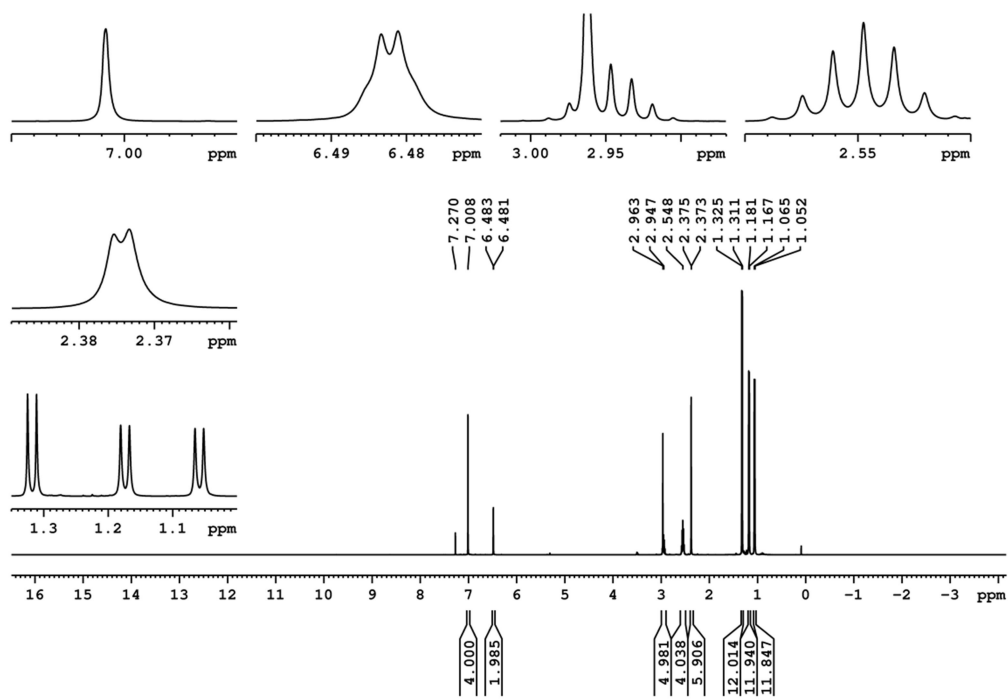


Figure 7.2.10. ^1H NMR spectrum of **7^{Tip}** in CDCl_3 .

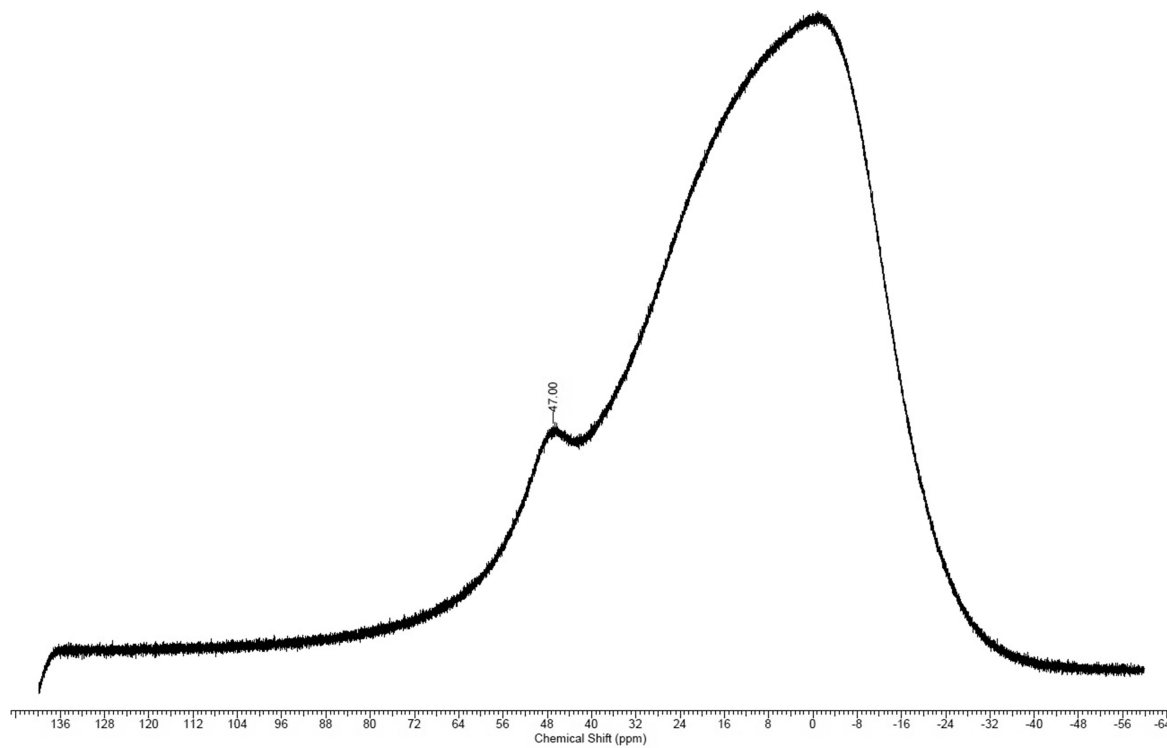


Figure 7.2.11. $^{11}\text{B}\{^1\text{H}\}$ NMR spectrum of 7^{Tip} in CDCl_3 .

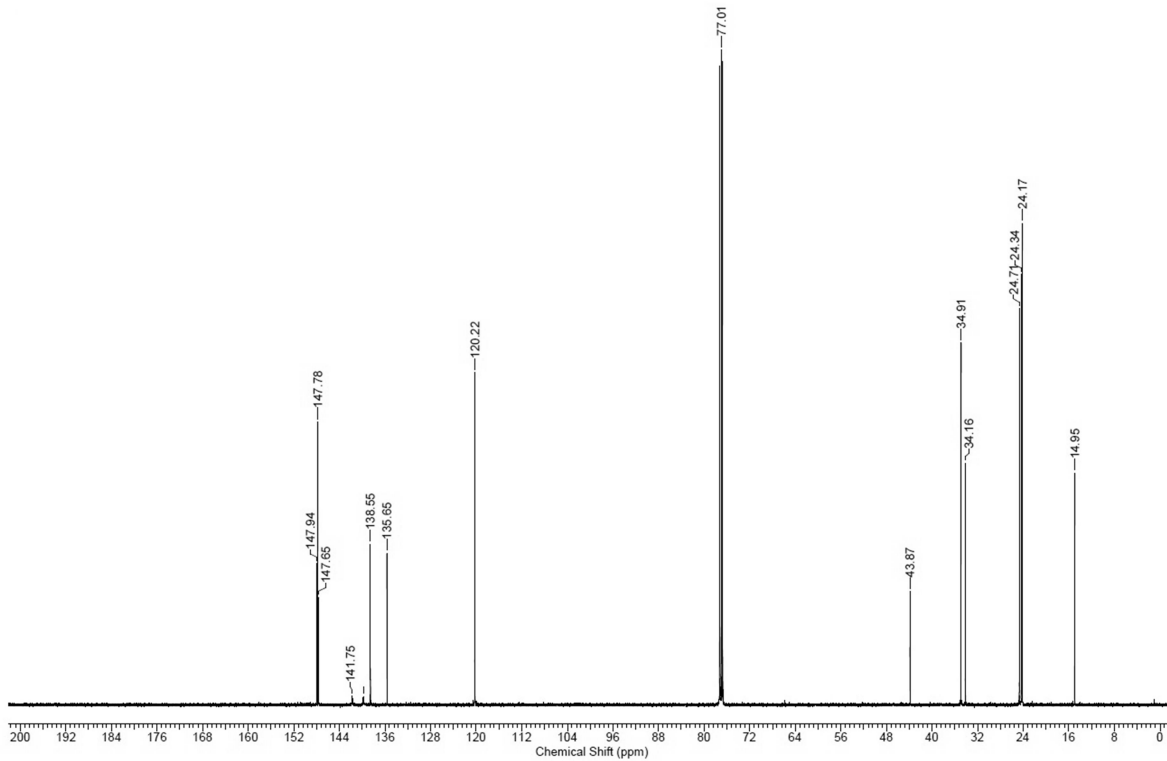


Figure 7.2.12. $^{13}\text{C}\{^1\text{H}\}$ NMR spectrum of 7^{Tip} in CDCl_3 .

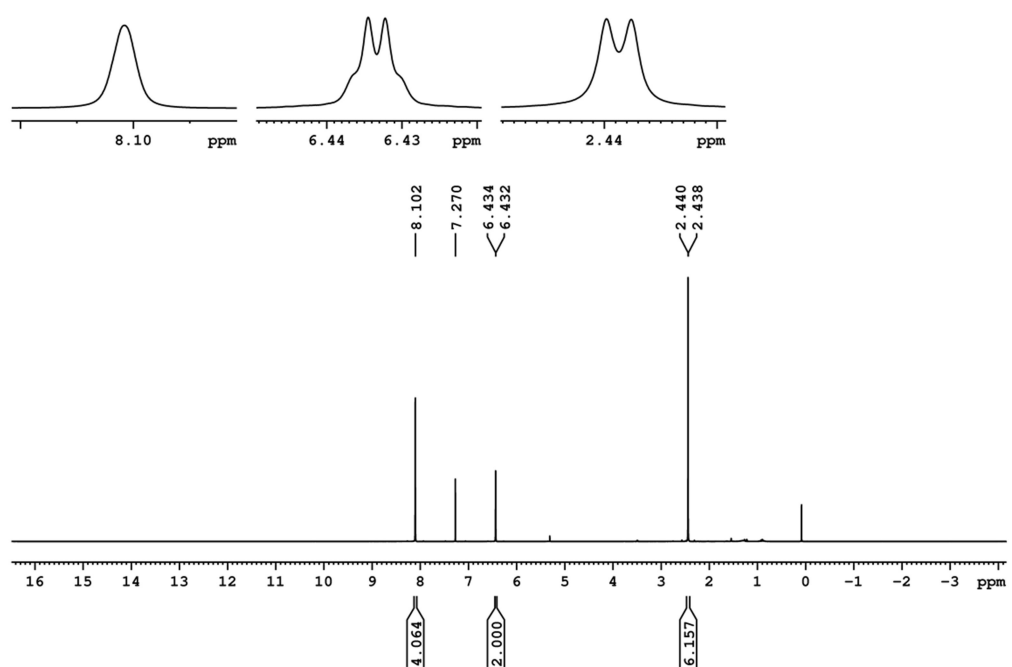


Figure 7.2.13. ${}^1\text{H}$ NMR spectrum of $\mathbf{5}^{\text{FMe}}$ in CDCl_3 .

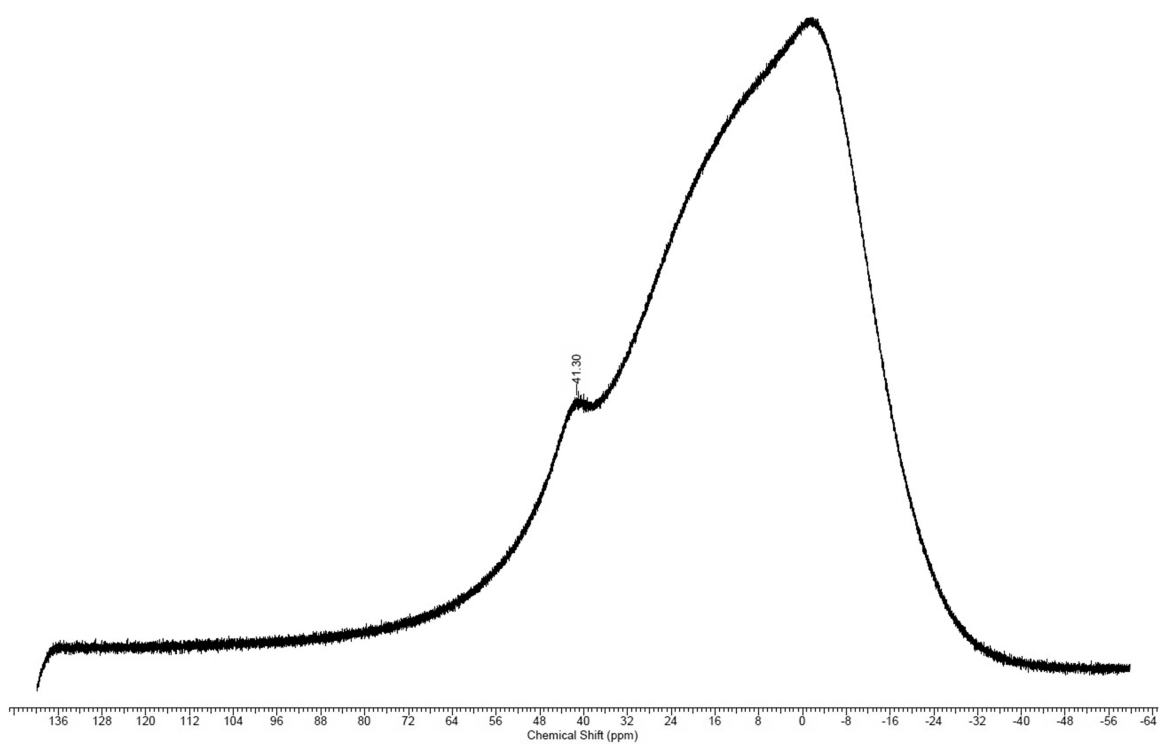


Figure 7.2.14. ${}^{11}\text{B}\{{}^1\text{H}\}$ NMR spectrum of $\mathbf{5}^{\text{FMe}}$ in CDCl_3 .

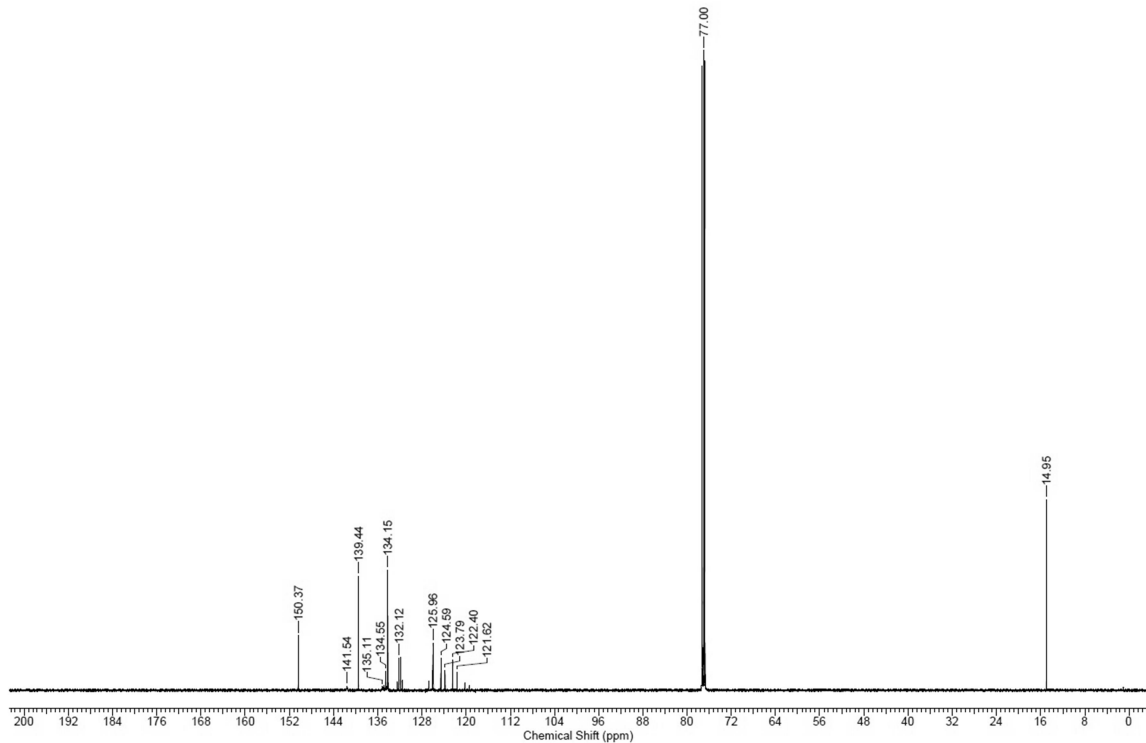


Figure 7.2.15. $^{13}\text{C}\{^1\text{H}\}$ NMR spectrum of $\mathbf{5}^{\text{FMes}}$ in CDCl_3 .

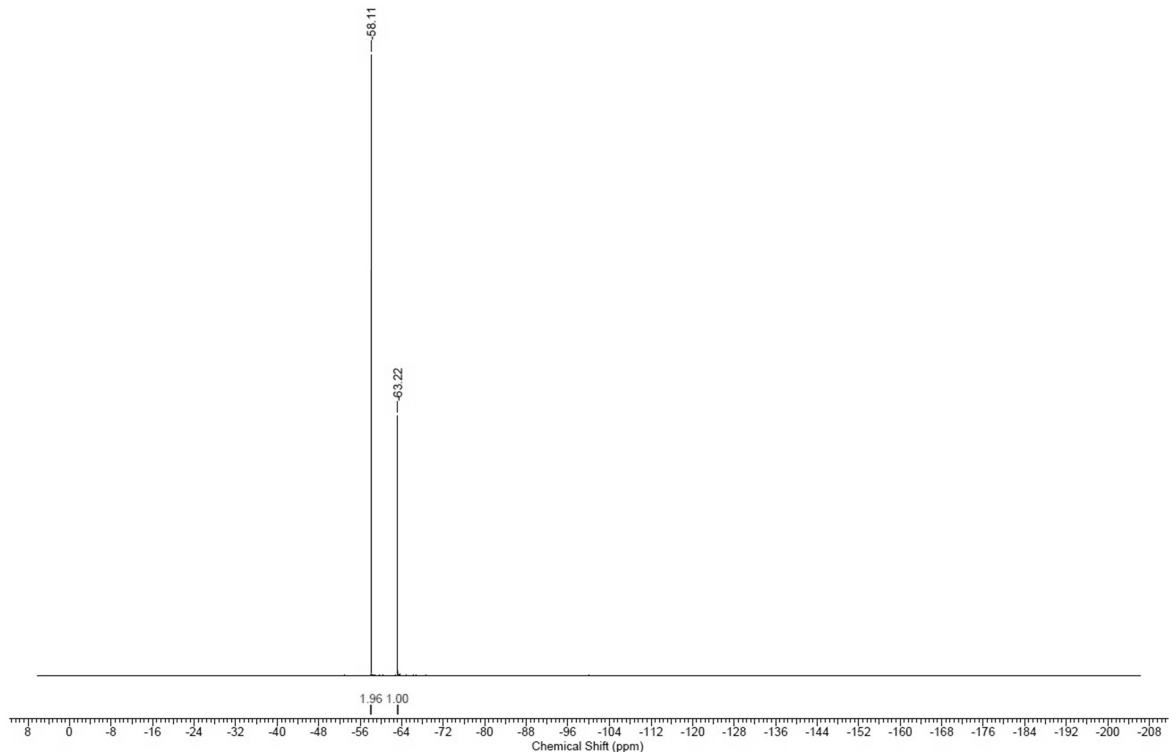


Figure 7.2.16. $^{19}\text{F}\{^1\text{H}\}$ NMR spectrum of $\mathbf{5}^{\text{FMes}}$ in CDCl_3 .

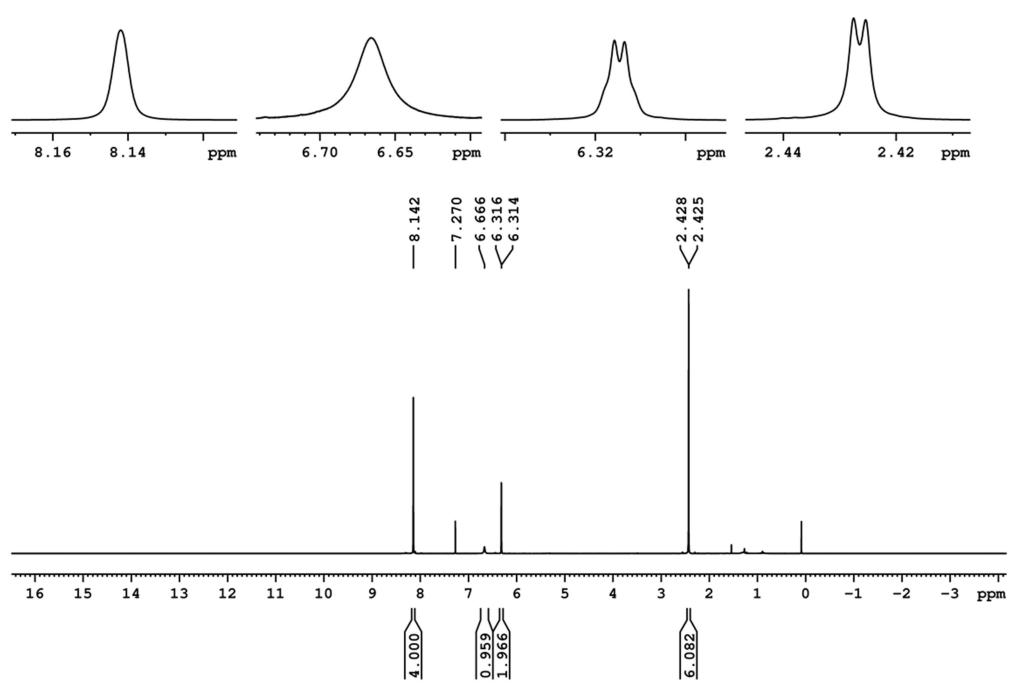


Figure 7.2.17. ^1H NMR spectrum of $\mathbf{6}^{\text{FMe}s}$ in CDCl_3 .

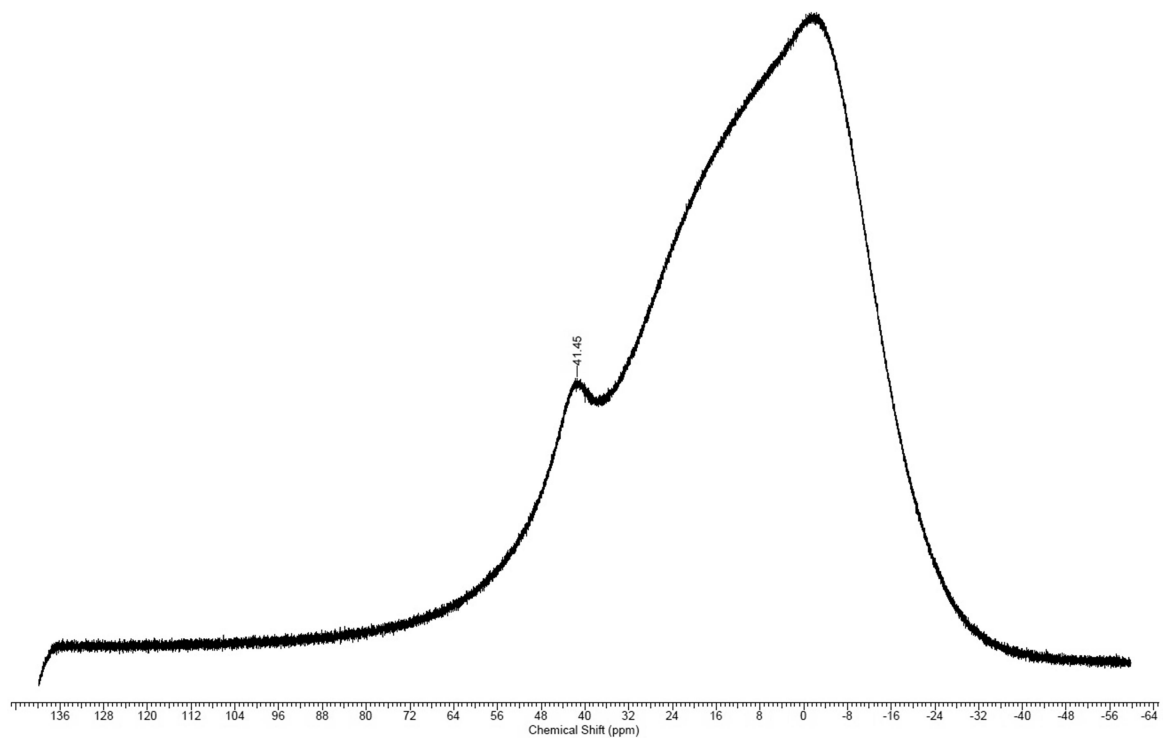


Figure 7.2.18. $^{11}\text{B}\{^1\text{H}\}$ NMR spectrum of $\mathbf{6}^{\text{FMe}s}$ in CDCl_3 .

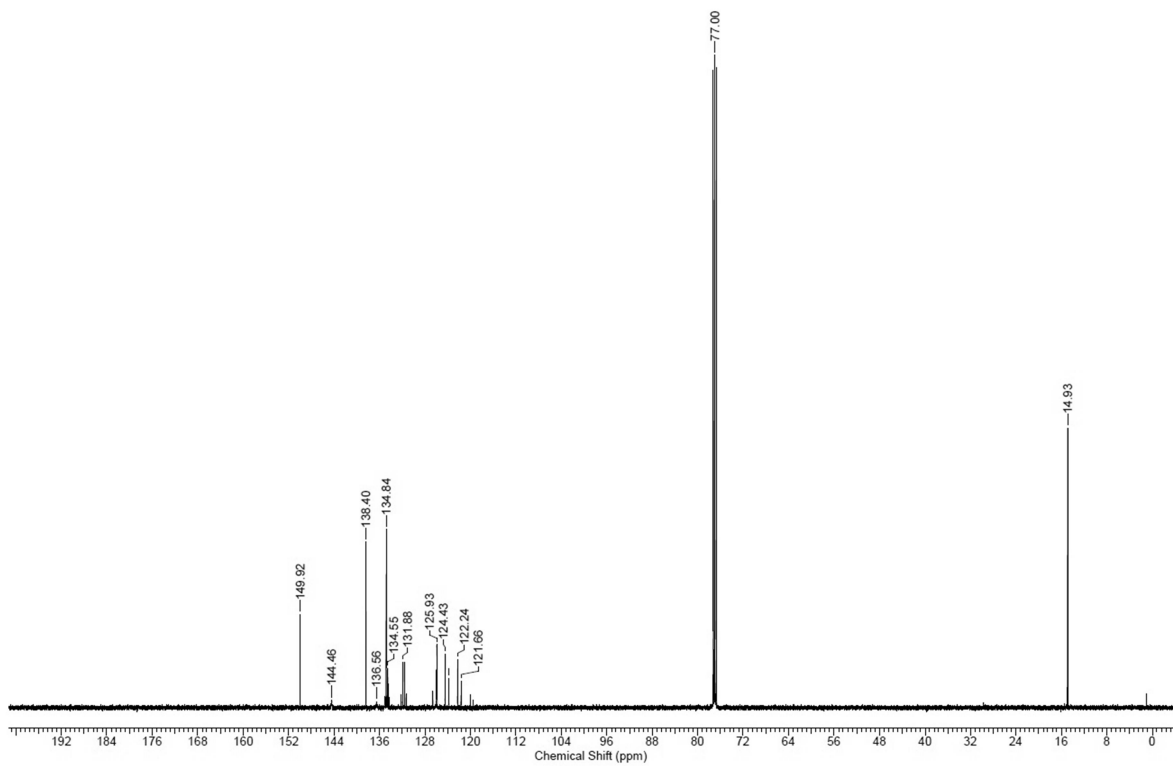


Figure 7.2.19. $^{13}\text{C}\{^1\text{H}\}$ NMR spectrum of $\mathbf{6}^{\text{FMes}}$ in CDCl_3 .

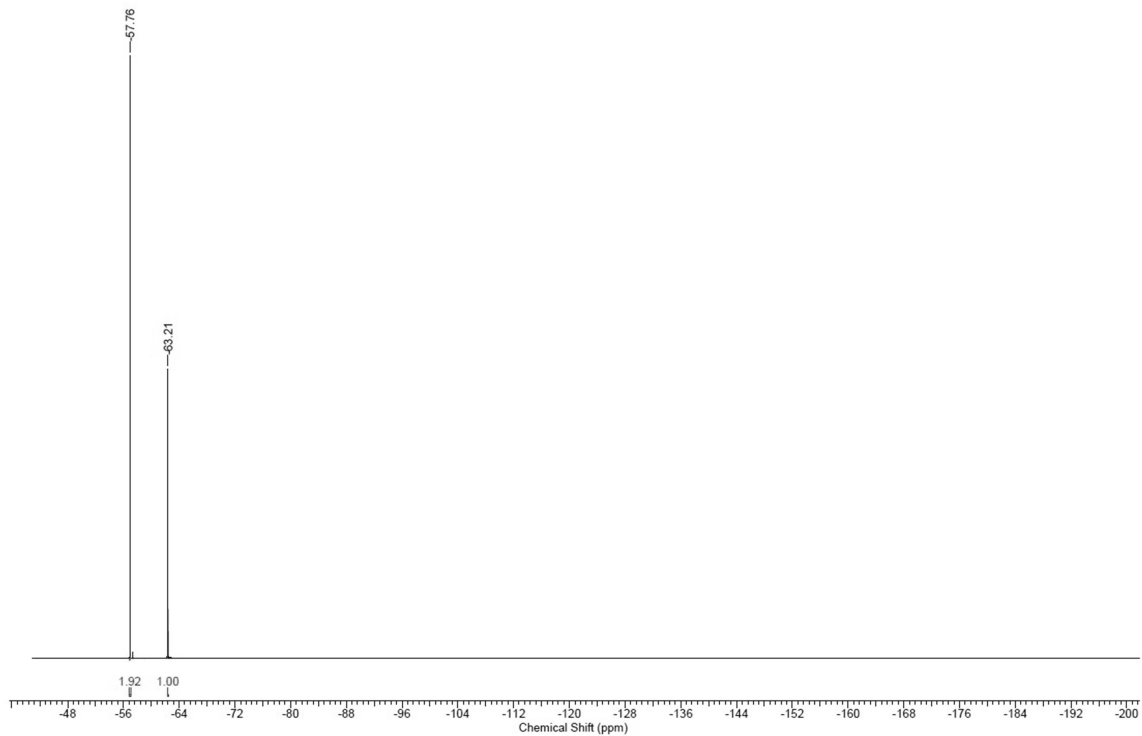


Figure 7.2.20. $^{19}\text{F}\{^1\text{H}\}$ NMR spectrum of $\mathbf{6}^{\text{FMes}}$ in CDCl_3 .

Mass spectra

MC-TipBOB-2020-06-17-1

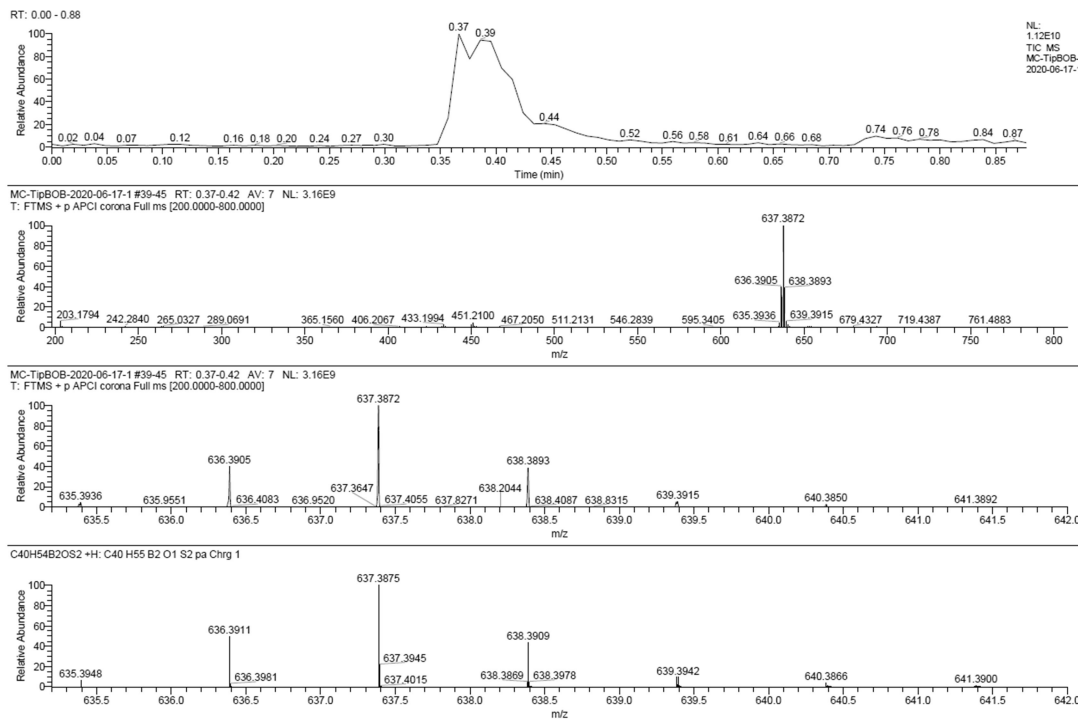


Figure 7.2.21. APCI MS spectrum of **5^{Tip}**.

MC-TipBNH-2020-06-17-1

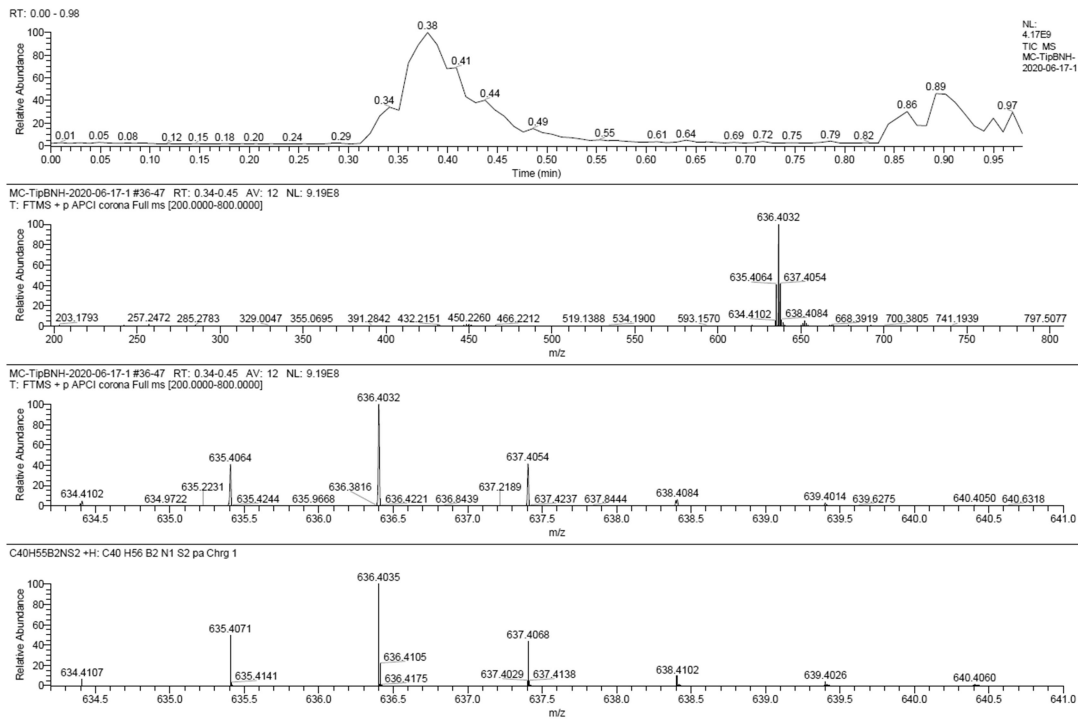


Figure 7.2.22. APCI MS spectrum of **6^{Tip}**.

MC-TipBNME-2020-06-17-1

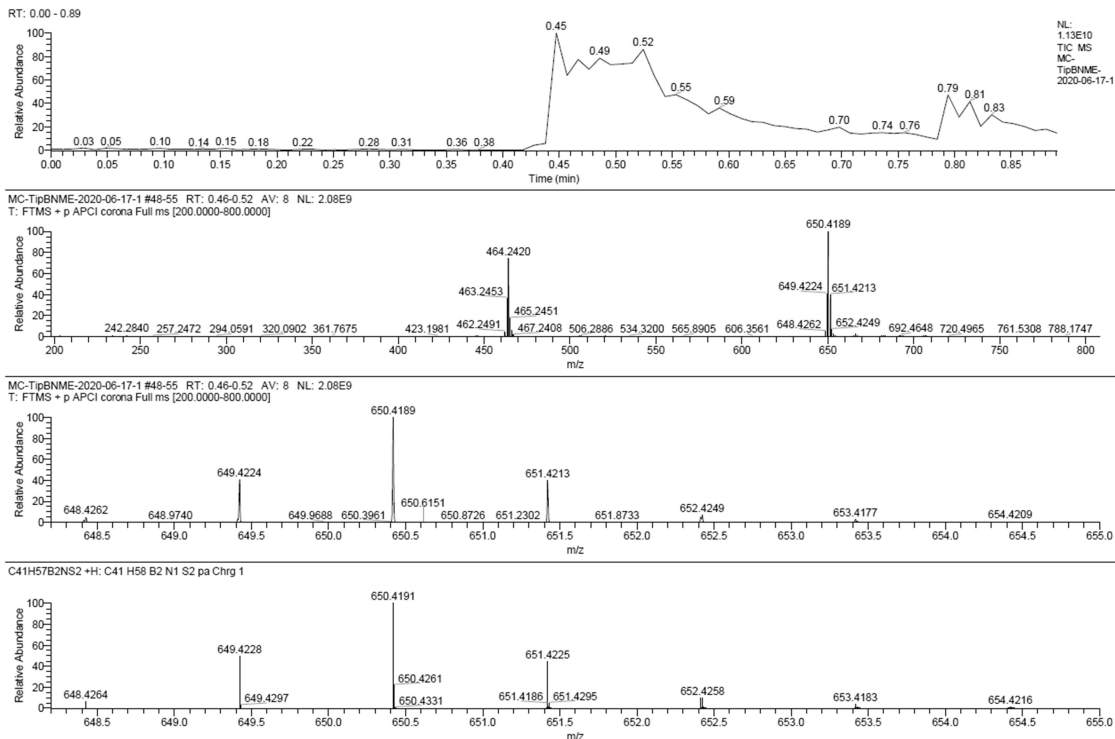


Figure 7.2.23. APCI MS spectrum of 7^{Tip} .

MC-FMeSBOB-2020-06-17-1

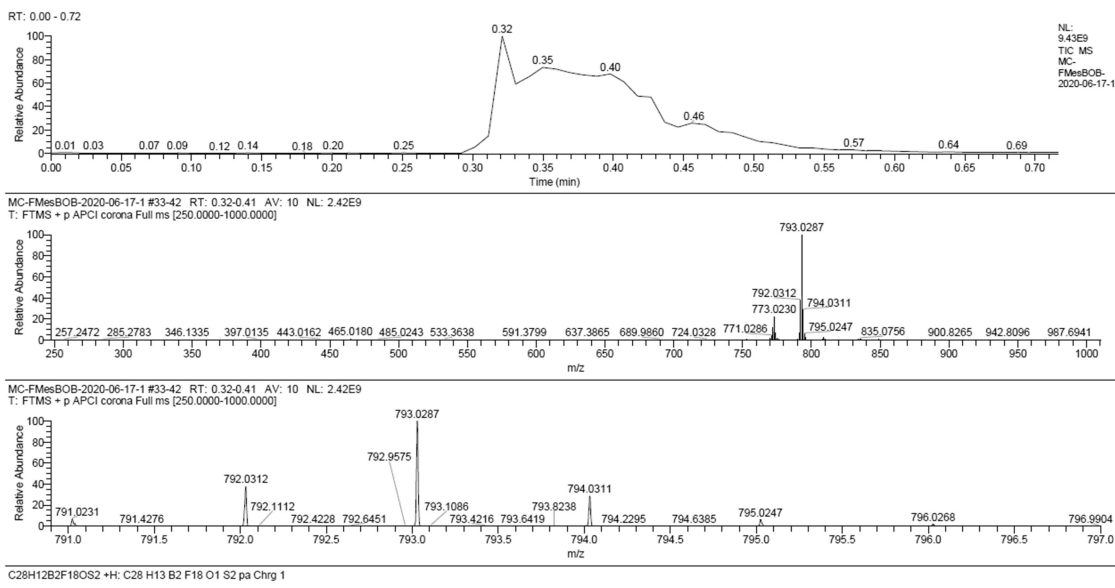


Figure 7.2.24. APCI MS spectrum of 5^{FMeS} .

MC-FMesBNH-2020-06-17-1

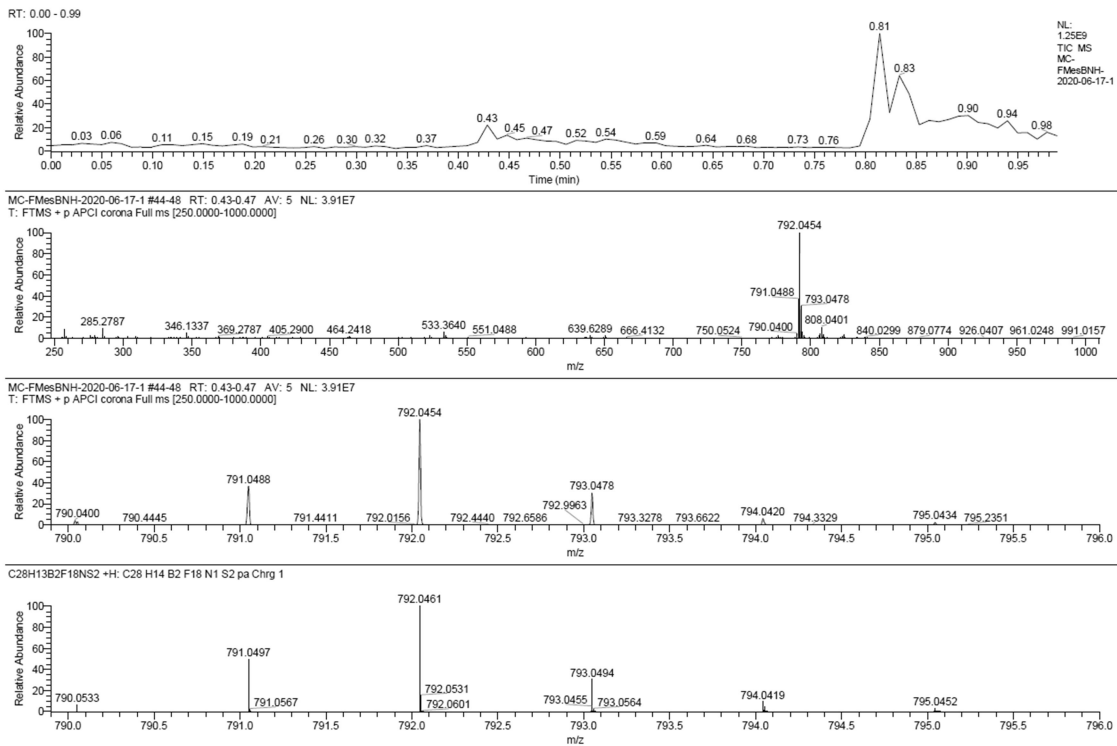


Figure 7.2.25. APCI MS spectrum of **6^{FMes}**.

UV/vis and Fluorescence spectra

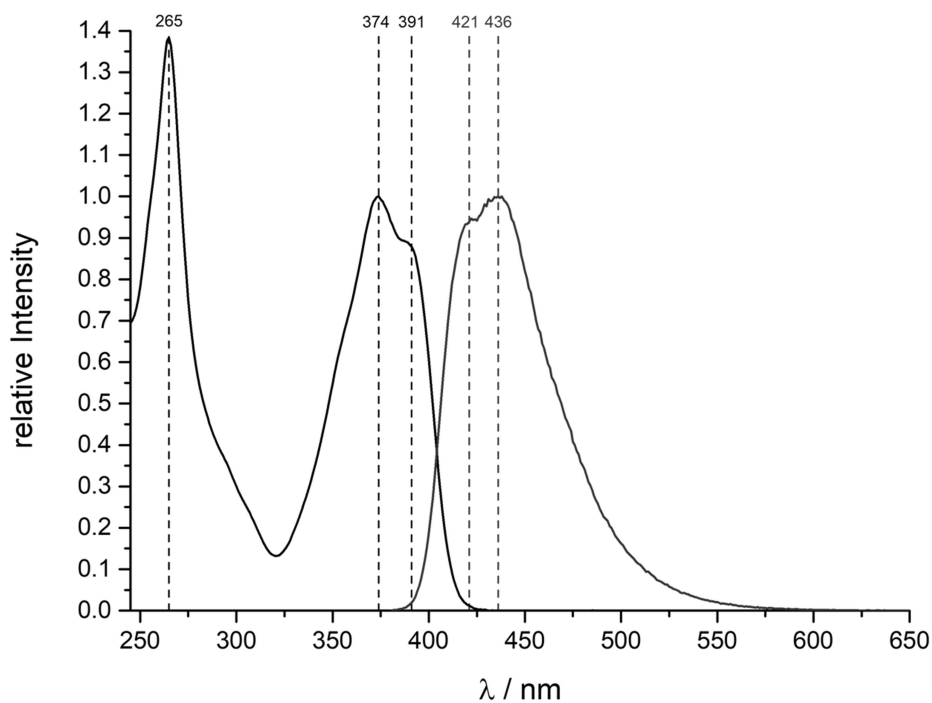


Figure 7.2.26. UV/vis and Fluorescence spectrum of 5^{Tip} .

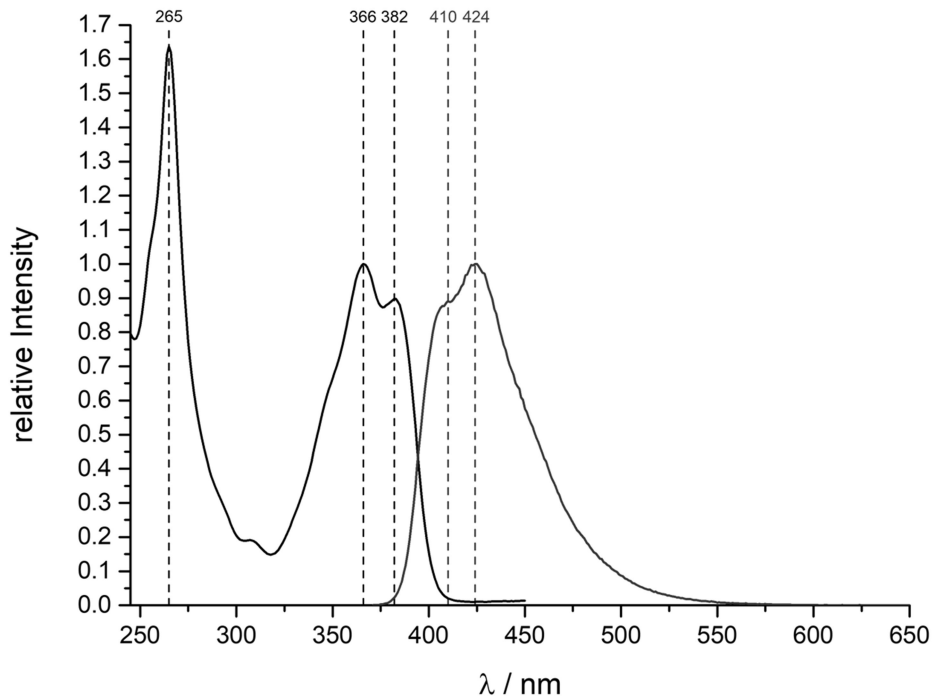


Figure 7.2.27. UV/vis and Fluorescence spectrum of 6^{Tip} .

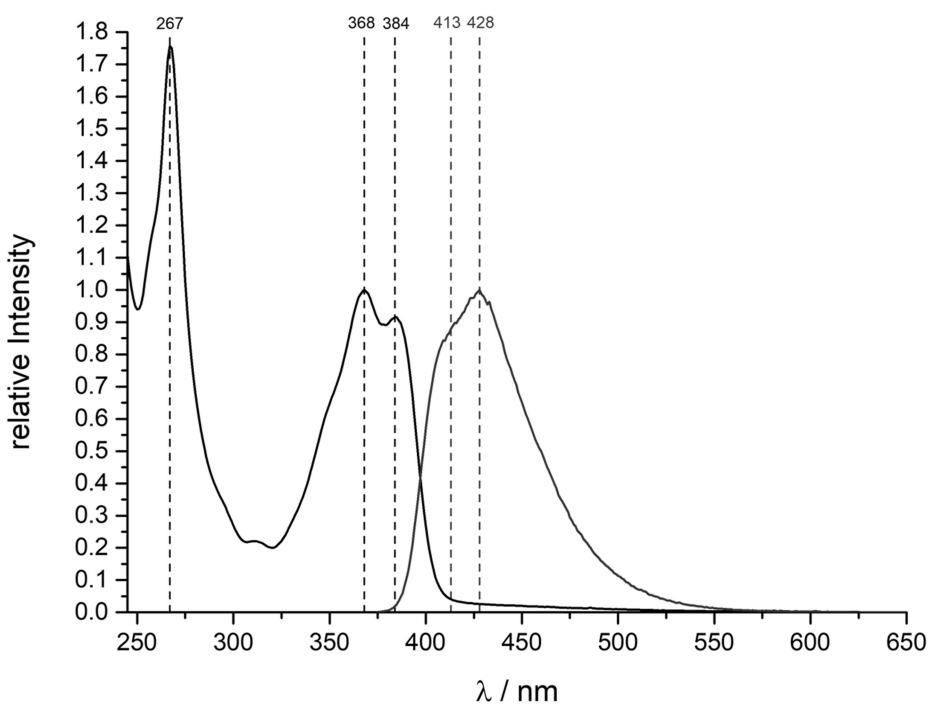


Figure 7.2.28. UV/vis and Fluorescence spectrum of 7^{Tip} .

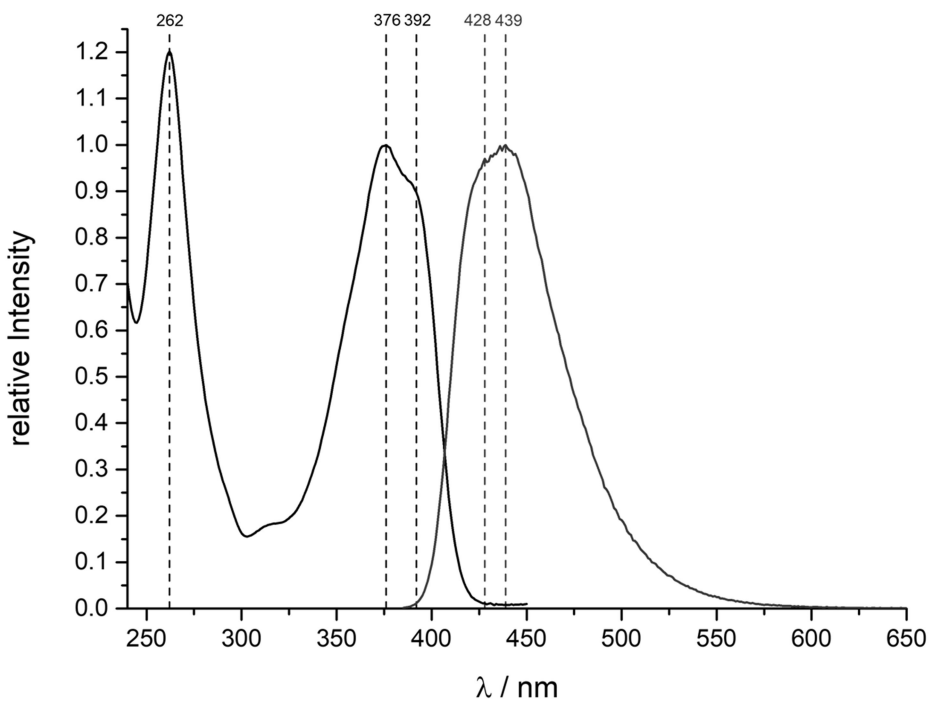


Figure 7.2.29. UV/vis and Fluorescence spectrum of 5^{FMes} .

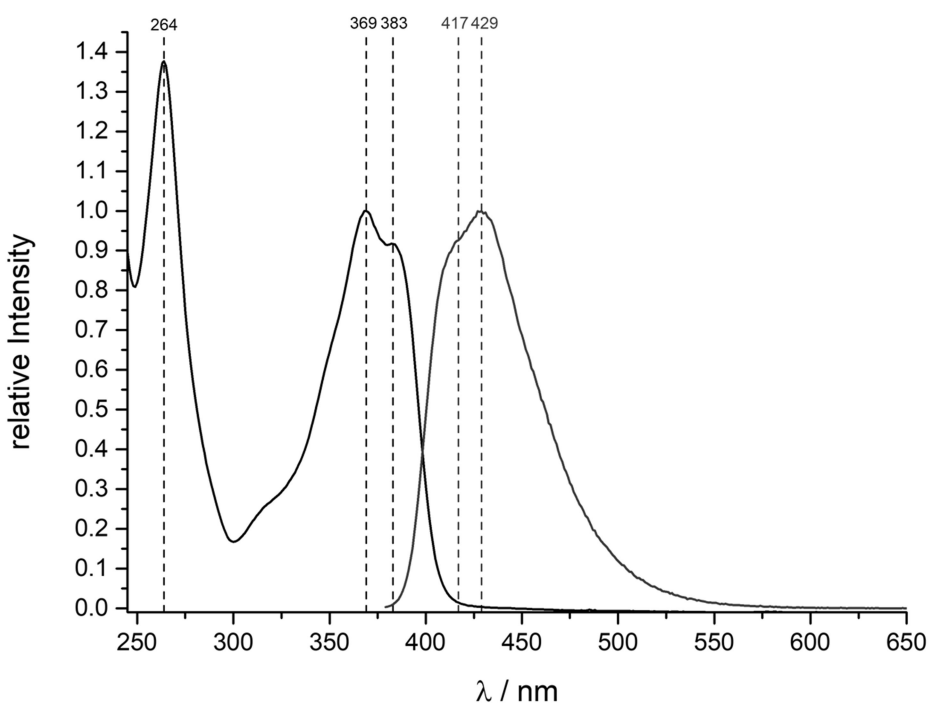


Figure 7.2.30. UV-vis and Fluorescence spectrum of $\mathbf{6}^{\text{FMes}}$.

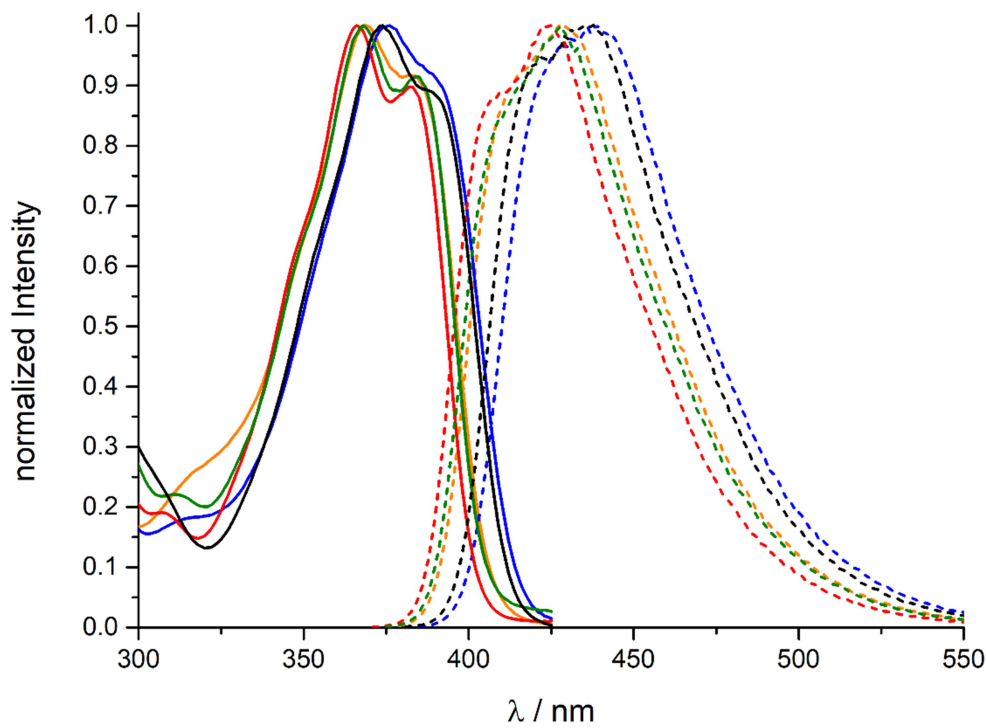


Figure 7.2.31. UV-vis absorption (solid lines) and fluorescence (dashed lines) spectra of $\mathbf{5}^{\text{Tip}}$ (black), $\mathbf{6}^{\text{Tip}}$ (red), $\mathbf{7}^{\text{Tip}}$ (green), $\mathbf{5}^{\text{FMes}}$ (blue) and $\mathbf{6}^{\text{FMes}}$ (orange) in CH_2Cl_2 .

CV traces

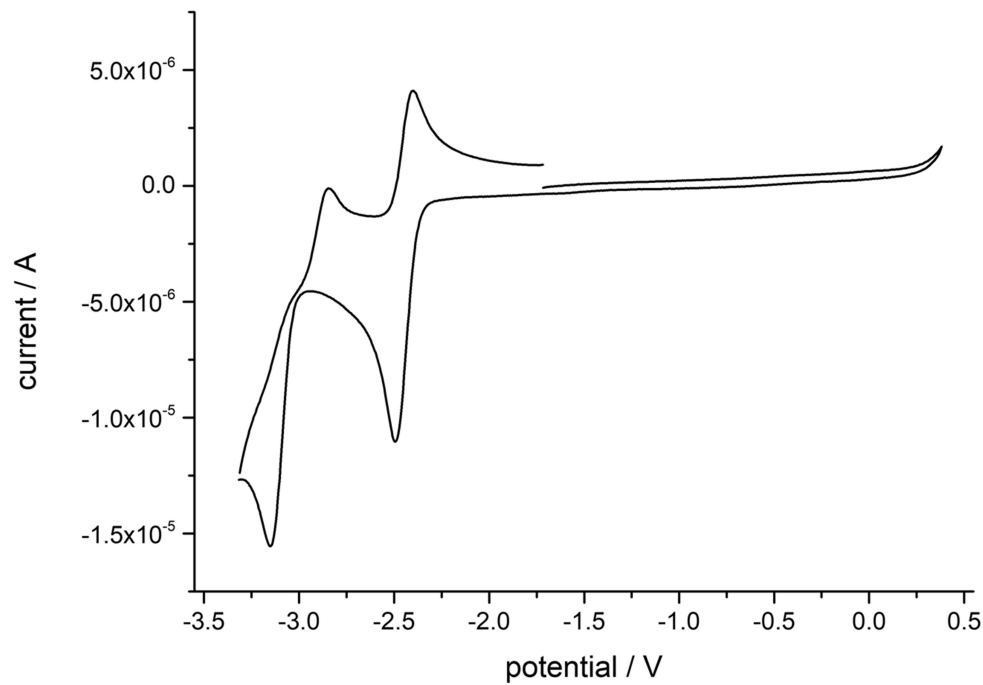


Figure 7.2.32. Complete cyclic voltammogram of **5^{Tip}** (vs. Fc/Fc⁺ at 250 mV/s).

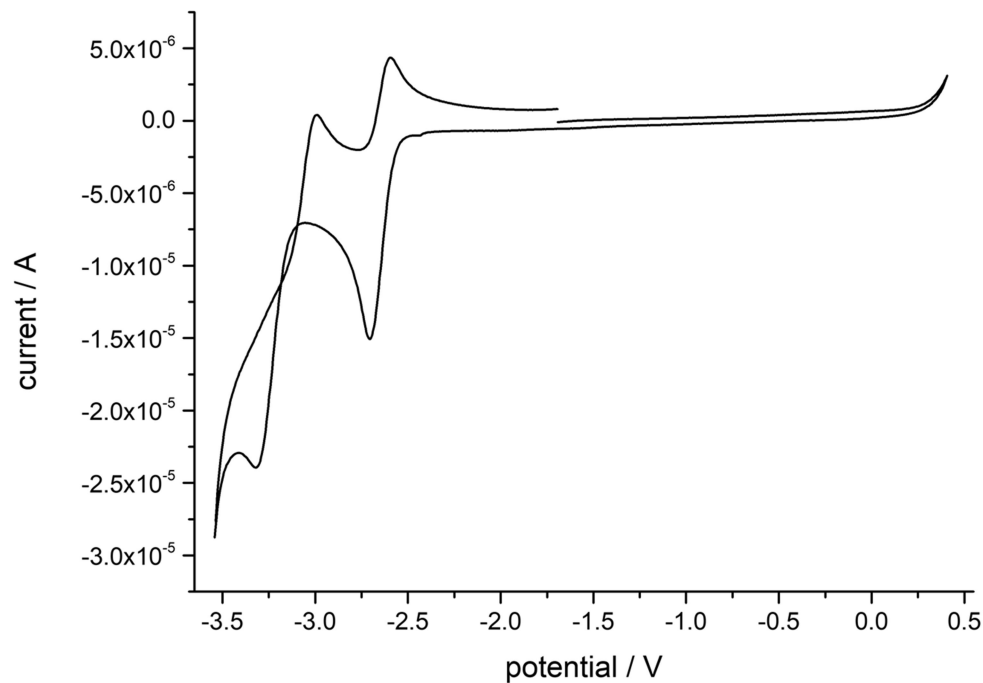


Figure 7.2.33. Complete cyclic voltammogram of **6^{Tip}** (vs. Fc/Fc⁺ at 250 mV/s).

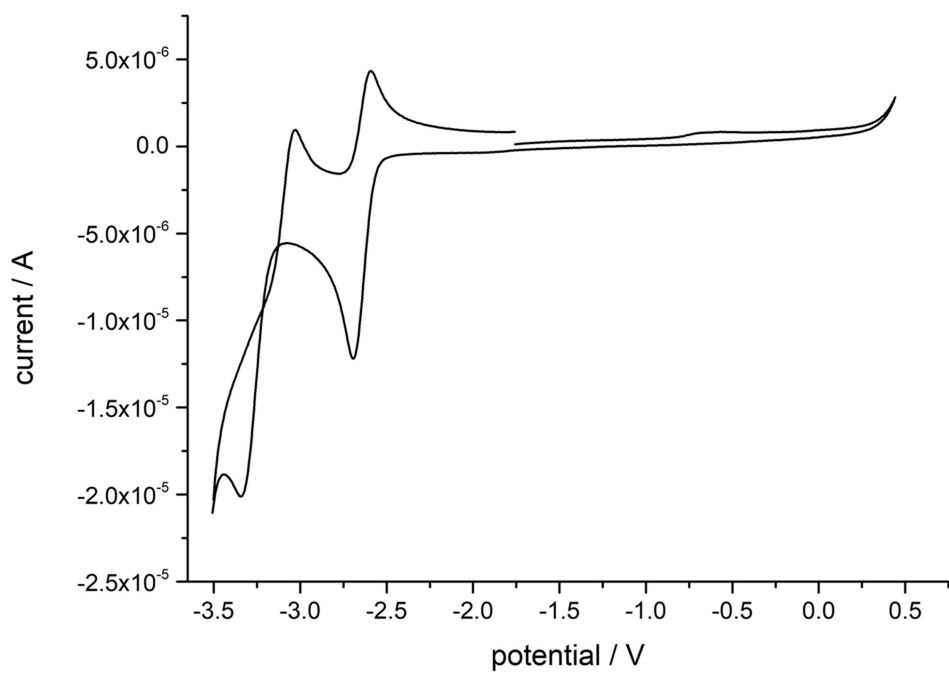


Figure 7.2.34. Complete cyclic voltammogram of 7^{Tip} (vs. Fc/Fc⁺ at 250 mV/s).

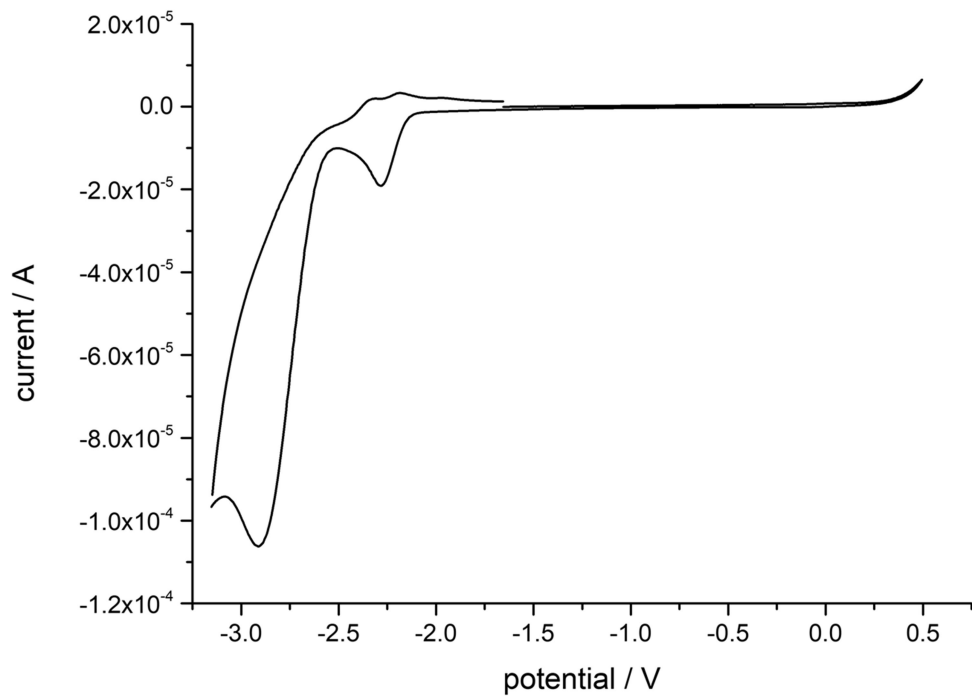


Figure 7.2.35. Complete cyclic voltammogram of 5^{FMeS} (vs. Fc/Fc⁺ at 250 mV/s).

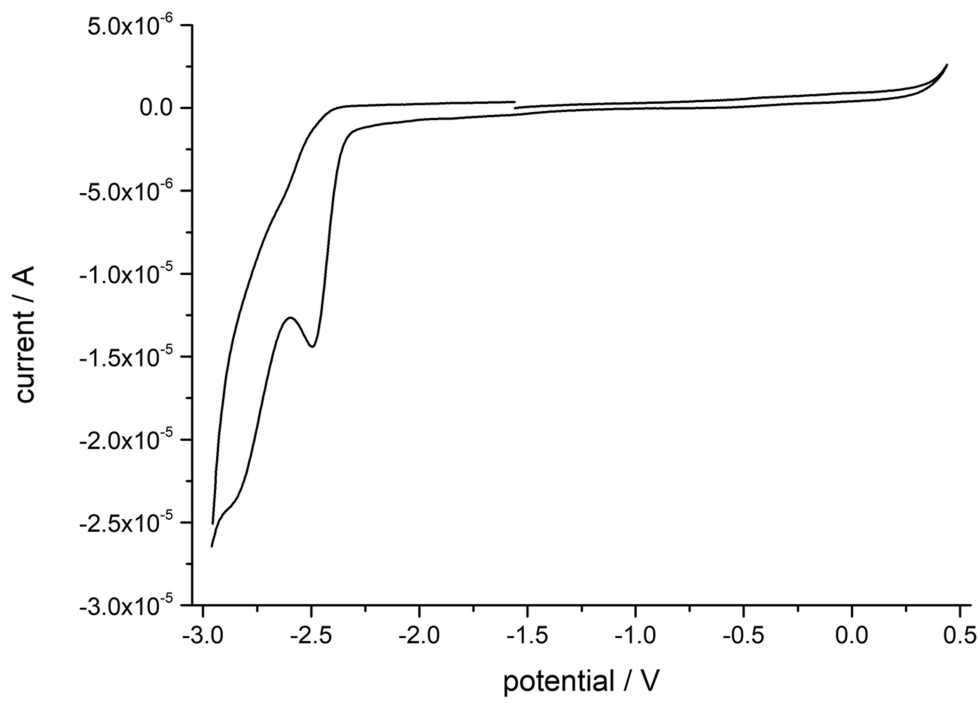


Figure 7.2.36. Complete cyclic voltammogram of $\mathbf{6}^{\text{FMes}}$ (vs. Fc/Fc^+ at 250 mV/s).

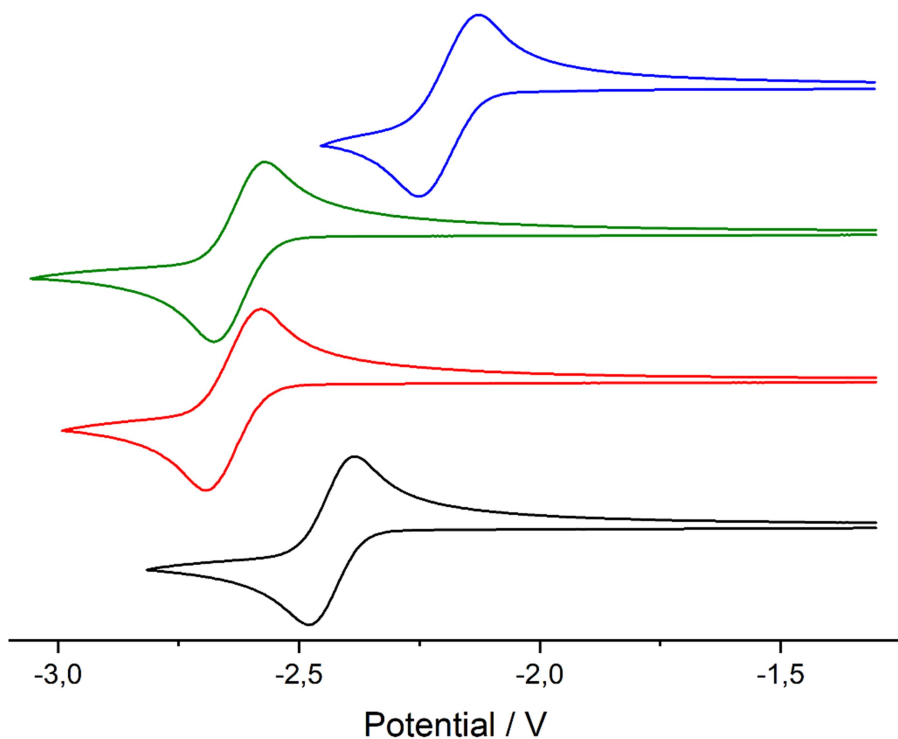


Figure 7.2.37. Cyclic voltammograms of $\mathbf{5}^{\text{Tip}}$ (black), $\mathbf{6}^{\text{Tip}}$ (red), $\mathbf{7}^{\text{Tip}}$ (green), and $\mathbf{5}^{\text{FMes}}$ (blue) in THF (vs. $[\text{Cp}_2\text{Fe}]^{0+/+}$, scan rate: 250 mVs⁻¹).

NICS and AICD plots

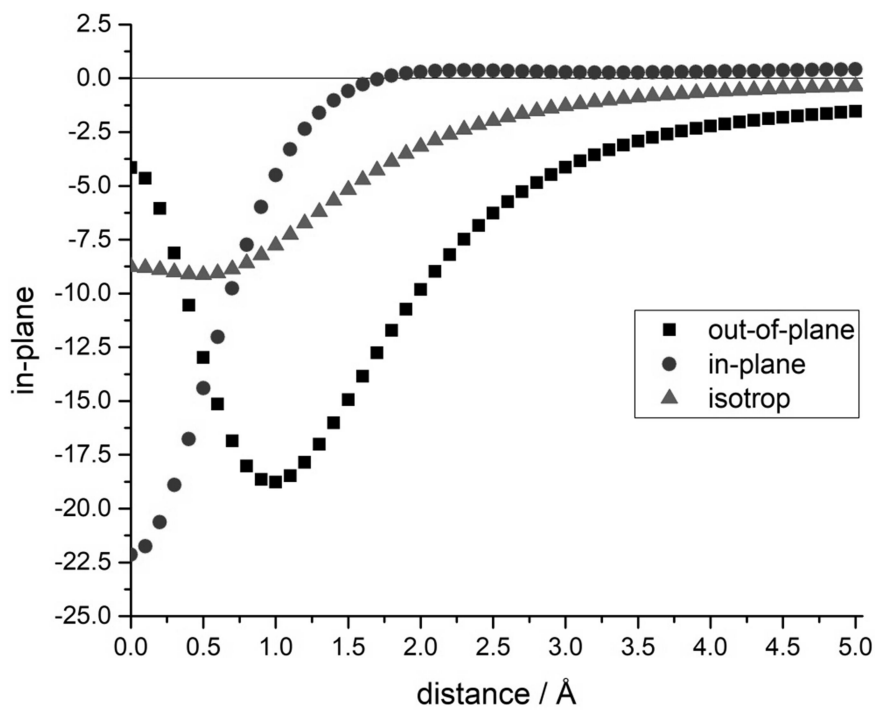


Figure 7.2.38. NICS Scan through a thiophene ring of $\mathbf{6}^{\text{Mes}}$.

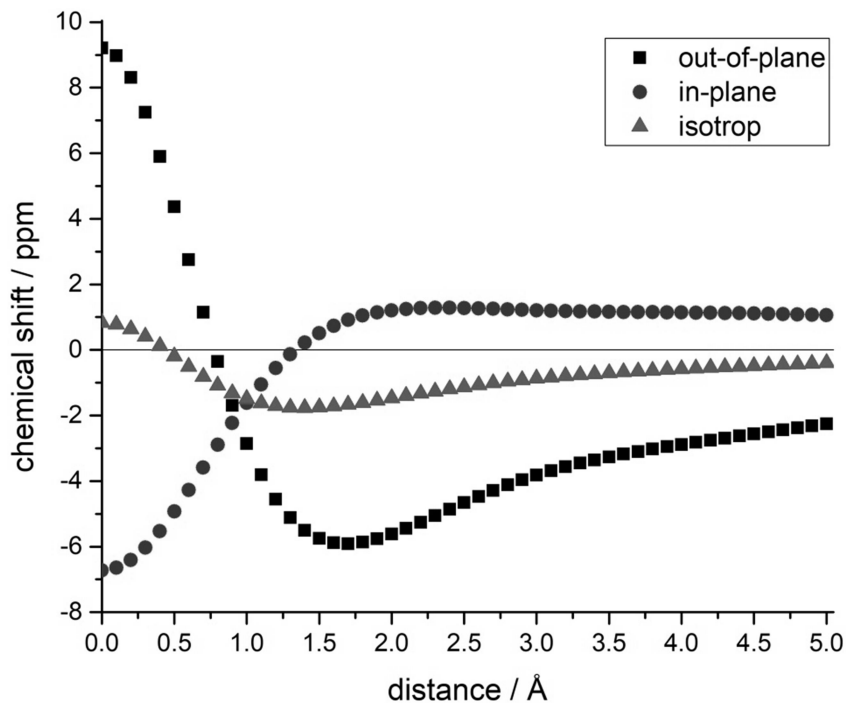


Figure 7.2.39. NICS Scan through the azadiborepin ring of $\mathbf{6}^{\text{Mes}}$.

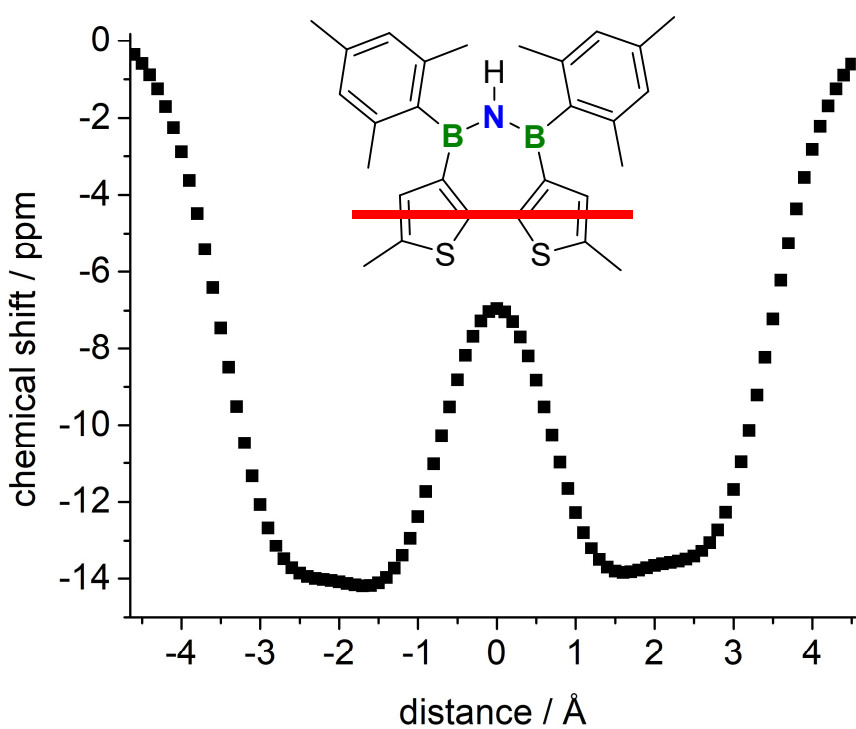


Figure 7.2.40. NICS XY-Scan through the bithiophene unit of $\mathbf{6}^{\text{Mes}}$.

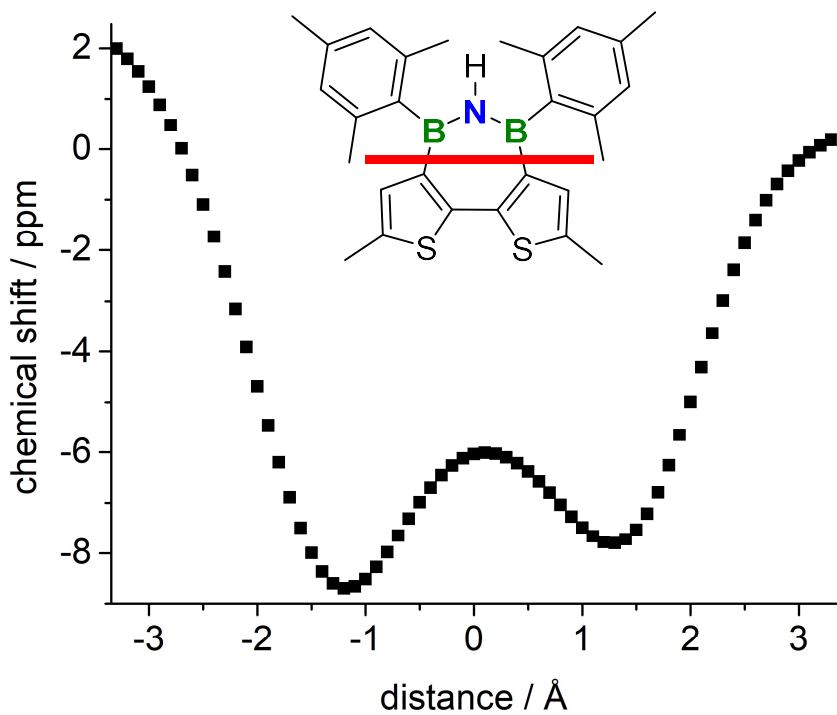


Figure 7.2.41. NICS XY-Scan through the azadiborepin ring of $\mathbf{6}^{\text{Mes}}$.

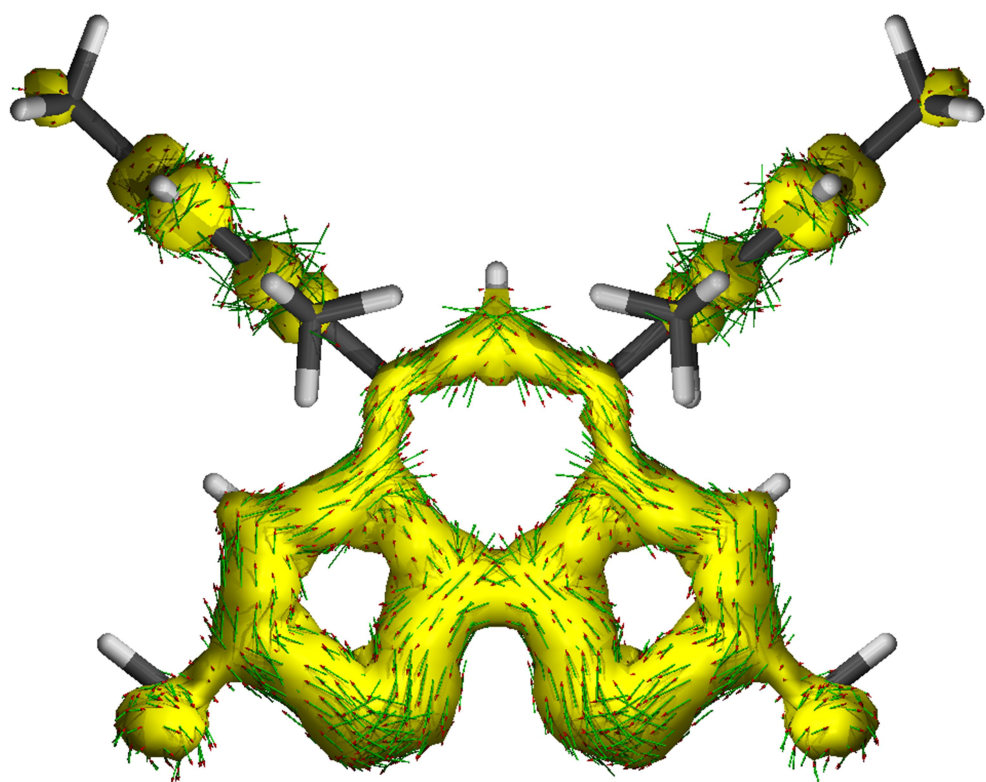


Figure 7.2.42. ACID map for 6^{Mes} (isovalue 0.020).

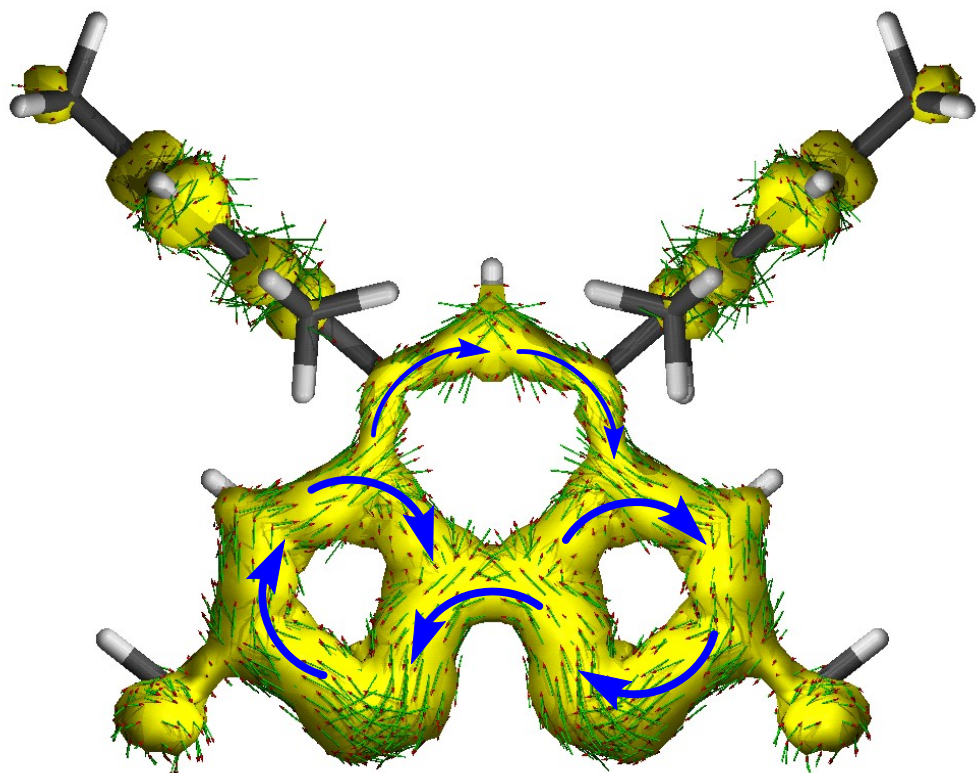


Figure 7.2.43. ACID map with indicative arrows for 6^{Mes} (isovalue 0.020).

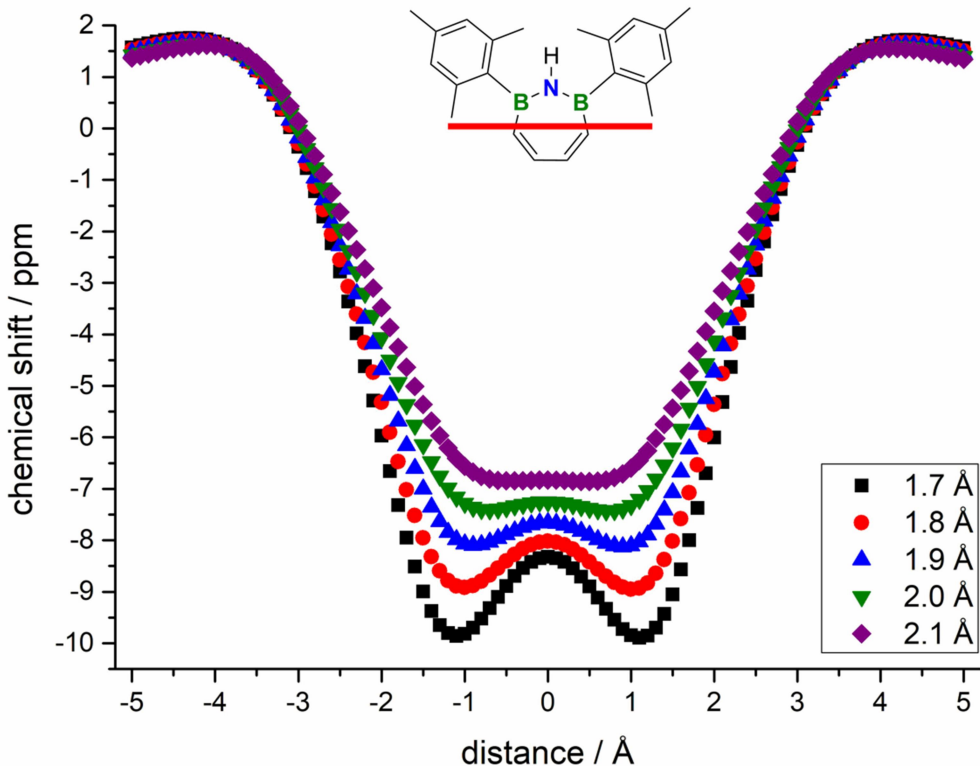


Figure 7.2.44. NICS-*X*-height-scan for the parent *B*-mesityl-azadiborepin without fused thiophene rings (see structure as inset; optimized with the Gaussian 09 program package, revision D.01, at b3lyp/6-311+G* level of theory). With increasing height, the maximum at 0.0 Å decreases. This indicates that a scan-height of ca. 2.0 Å should provide the most meaningful description in this case. Still all other scans were performed consistently at 1.7 Å height, in order to maintain comparability with the all-carbon subunits and other systems. A scan-height of 1.7 Å corresponds to the standard NICS-*X*-scan height reported for organic hydrocarbon systems.

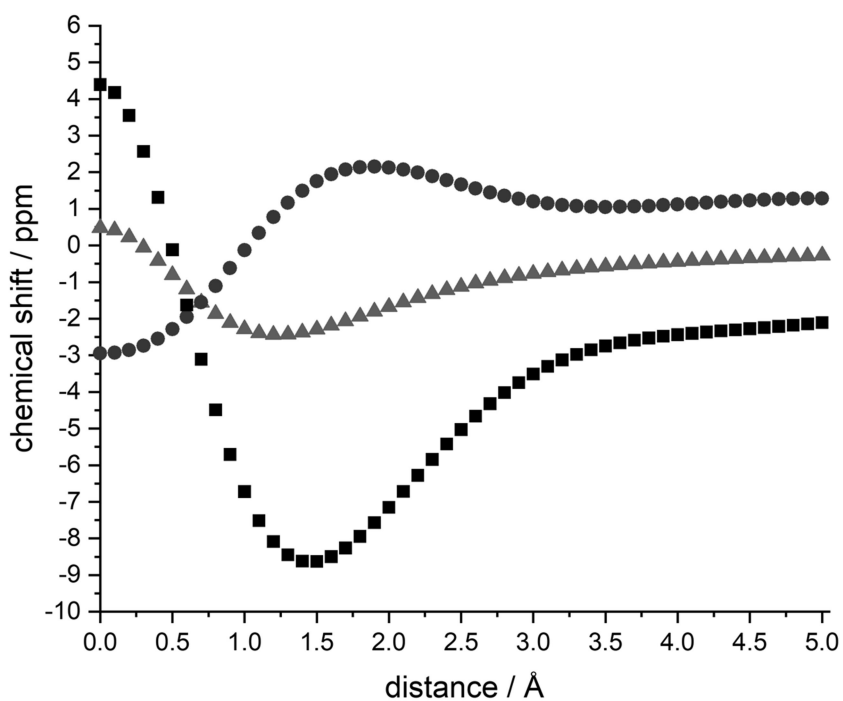


Figure 7.2.45. NICS-Z-scan for the parent *B*-mesityl-azadiborepin without fused thiophene rings (see inset in Figure 7.2.44 for the structure).

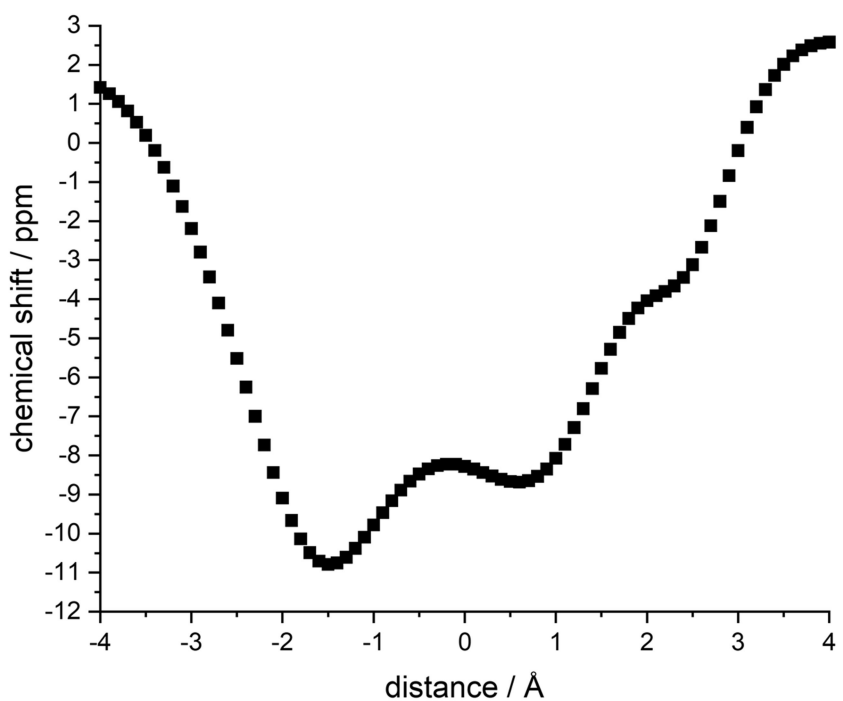


Figure 7.2.46. NICS-X-scan for the parent *B*-mesityl-azadiborepin without fused thiophene rings (see inset in Figure 7.2.44 for the structure).

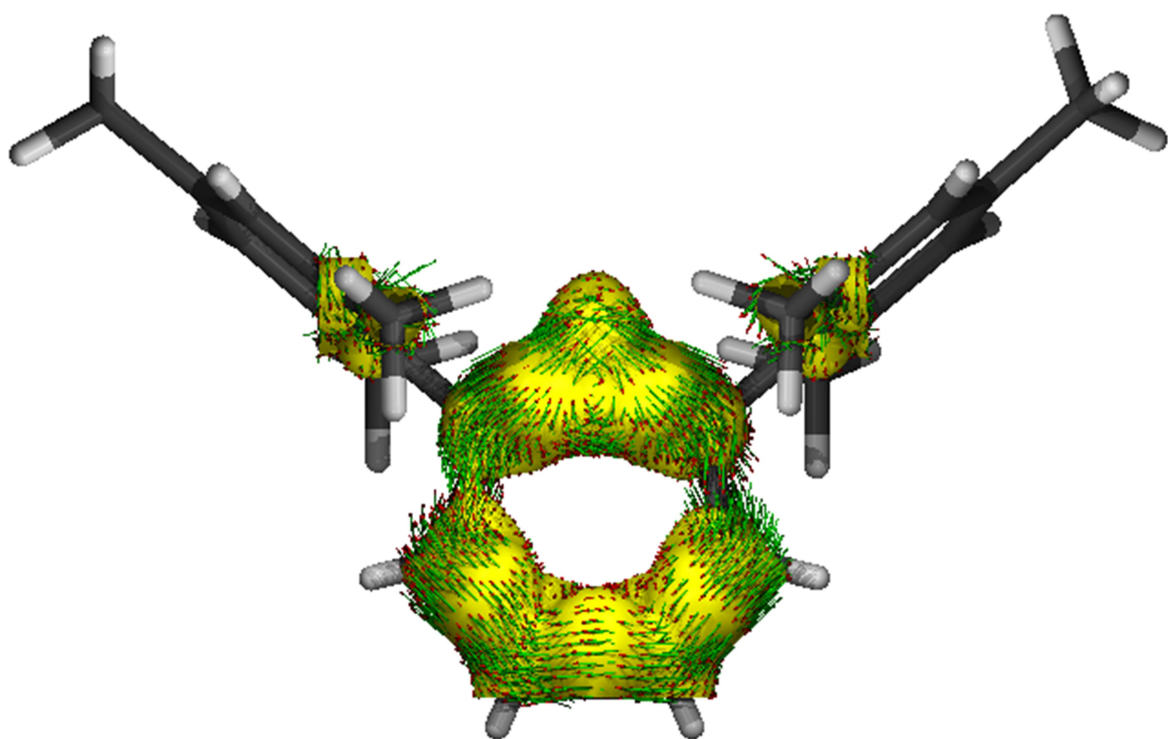


Figure 7.2.47. ACID map (isovalue: 0.008) for the parent *B*-mesityl-azadiborepin without fused thiophene rings (see inset in Figure 7.2.44 for the structure).

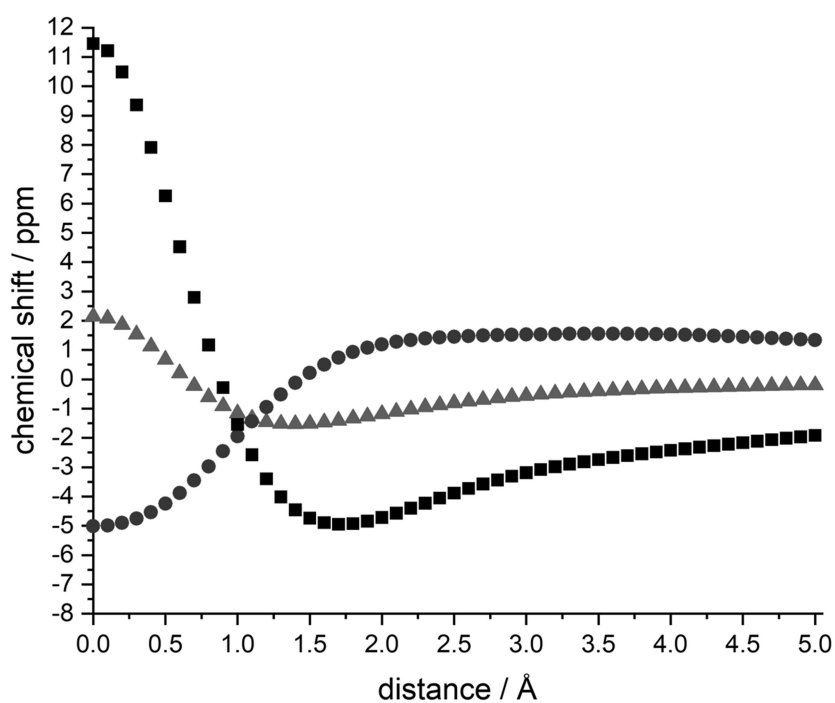


Figure 7.2.48. NICS-Z-scan for the parent *B*-mesityl-oxadiborepin without fused thiophene rings.

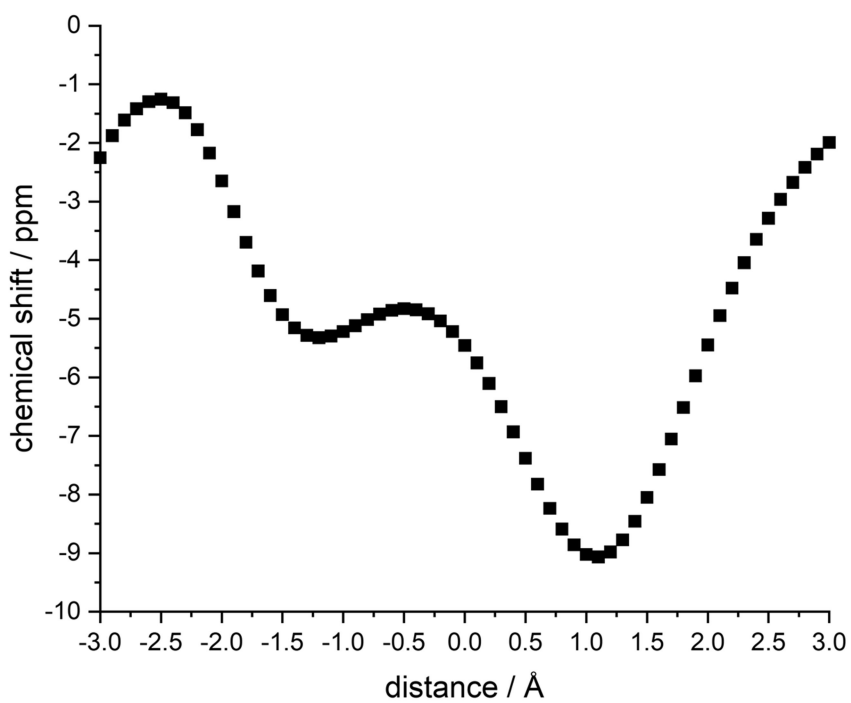


Figure 7.2.49. NICS-X-scan for the parent *B*-mesityl-oxadiborepin without fused thiophene rings.

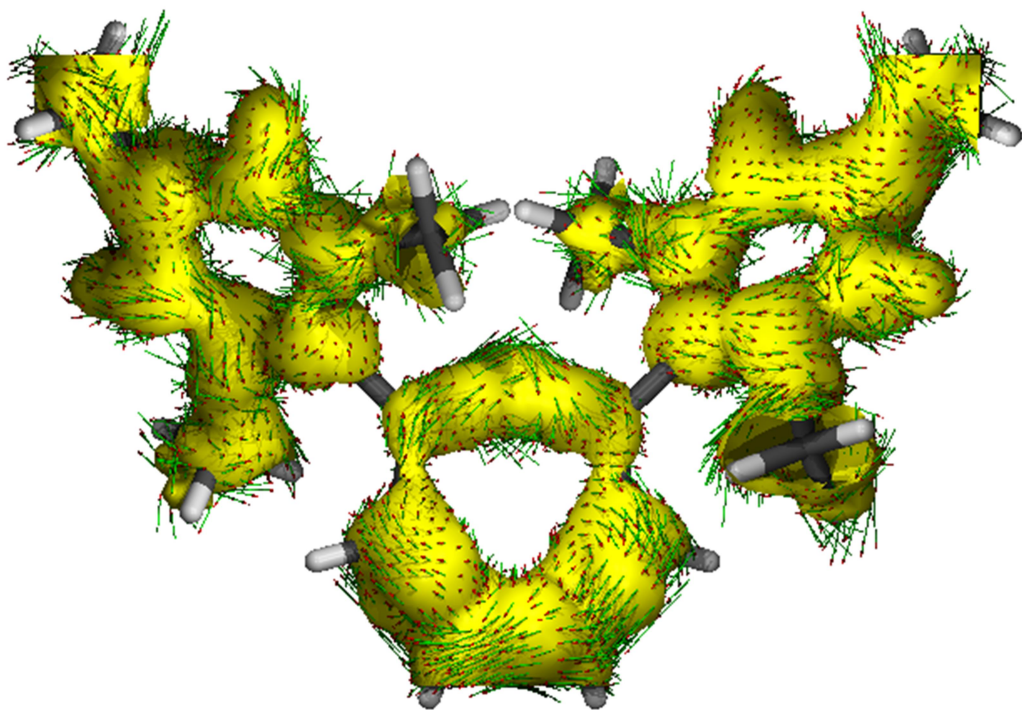


Figure 7.2.50. ACID map for the parent *B*-mesityl-oxadiborepin without fused thiophene rings (isovalue: 0.009).

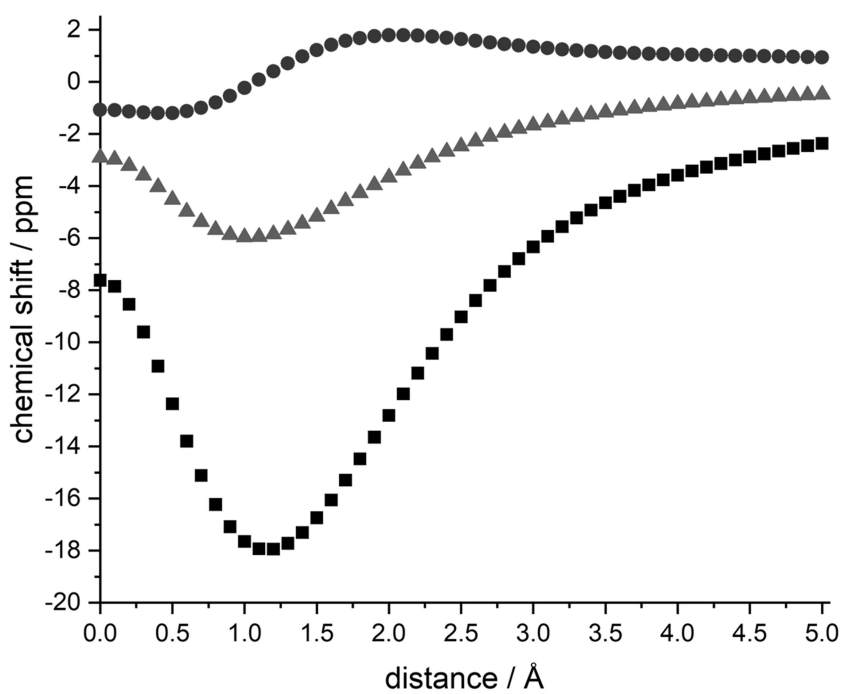


Figure 7.2.51. NICS-Z-scan for *B*-mesityl-borepin.

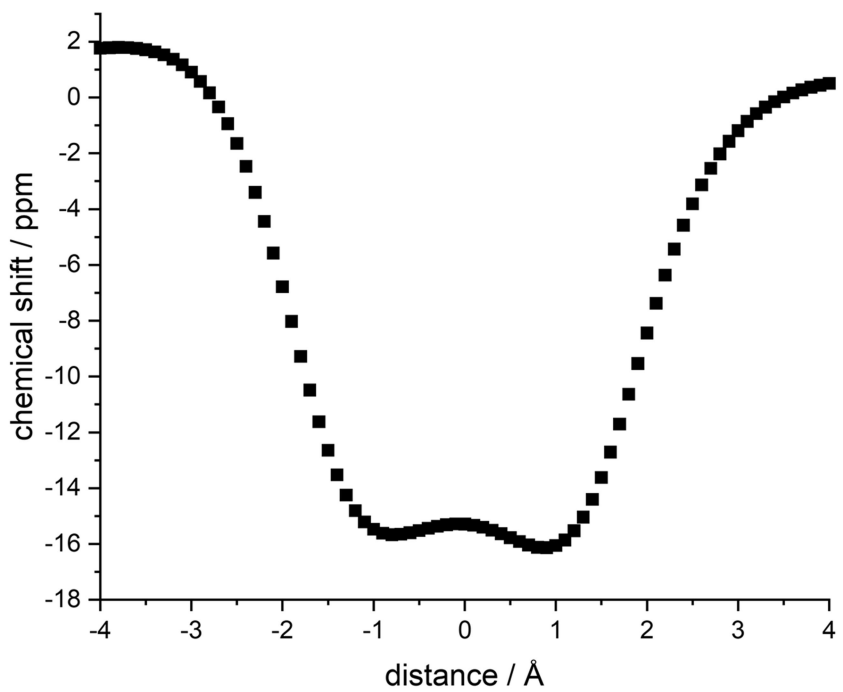


Figure 7.2.52. NICS-X- scan for *B*-mesityl-borepin.

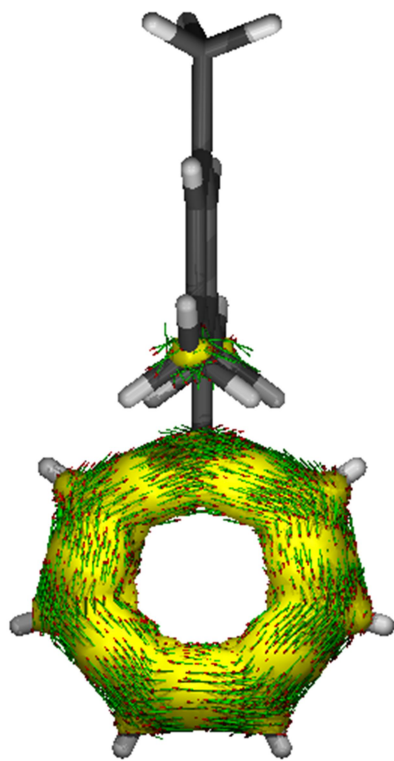


Figure 7.2.53. ACID map for *B*-mesityl-borepin (isovalue: 0.0205).

Cartesian coordinates (\AA) and total energies (a.u.) of optimized stationary points

5^{FMes}:

Total energy (B3LYP-D3(BJ)/def2-SV(P)): -3789.1020495580

S	-3.942337	-0.260710	-1.562263
C	-3.157743	-0.381331	-3.116212
C	-1.799620	-0.287105	-2.968642
C	-1.343707	-0.115283	-1.617634
C	-2.418904	-0.080885	-0.716550
C	-2.419413	0.080083	0.717503
S	-3.943965	0.248374	1.563621
C	-3.160036	0.370789	3.117801
C	-1.801351	0.285173	2.970027
C	-1.344486	0.119587	1.618604
B	0.146243	0.020848	1.264430
O	0.649421	0.012711	0.000288

H	-1.119209	-0.336617	-3.821444
H	-1.121068	0.336906	3.822818
C	1.272915	-0.023644	2.396360
B	0.146490	-0.006453	-1.263804
C	1.538050	-1.183799	3.146138
C	2.549178	-1.222817	4.110531
C	3.322595	-0.087740	4.350279
C	3.092993	1.076150	3.614295
C	2.088780	1.098186	2.644547
C	0.708784	-2.432713	2.936774
H	2.734189	-2.139081	4.673004
C	4.444260	-0.128829	5.359535
H	3.694688	1.967484	3.798992
C	1.924773	2.356038	1.815918
C	1.273320	0.033669	-2.395820
C	1.532935	1.187148	-3.157486
C	2.543225	1.220894	-4.123105
C	3.321503	0.087002	-4.351750
C	3.097886	-1.070236	-3.603342
C	2.094401	-1.087040	-2.632845
C	0.698860	2.434735	-2.959929
H	2.724205	2.132372	-4.694560
C	4.441644	0.121096	-5.362965
H	3.703635	-1.960639	-3.779174
C	1.937640	-2.336928	-1.790708
F	2.604448	-2.236516	-0.628263
F	0.645498	-2.573152	-1.486134
F	2.404020	-3.426058	-2.422268
F	1.375066	3.544270	-3.292746
F	-0.417045	2.413121	-3.713107
F	0.307342	2.570230	-1.677269
F	4.590848	-1.067838	-5.970826

F	4.223967	1.043794	-6.314138
F	5.617389	0.417872	-4.781317
F	1.388132	-3.542588	3.261842
F	-0.408660	-2.420892	3.687886
F	0.320092	-2.559172	1.652336
F	2.593107	2.272802	0.653105
F	0.631295	2.586967	1.512620
F	2.383238	3.441211	2.459966
F	4.601491	1.058480	5.968387
F	4.222813	-1.051351	6.310110
F	5.617219	-0.432190	4.775630
C	-3.957475	-0.560311	-4.369007
H	-4.557117	-1.489163	-4.345539
H	-4.656490	0.280700	-4.532962
H	-3.280370	-0.613612	-5.237862
C	-3.960905	0.542118	4.370943
H	-4.566293	1.467285	4.349446
H	-4.654701	-0.303562	4.533042
H	-3.284189	0.597736	5.239957

6^FMes:

Total energy (B3LYP-D3(BJ)/def2-SV(P)): -3769.2361542090

C	-1.338150	1.463225	3.220483
C	-0.143099	1.238498	2.508383
C	0.977661	2.004806	2.894223
C	0.918554	2.922165	3.945771
C	-0.279421	3.113432	4.634837
C	-1.411006	2.386634	4.267615
B	-0.058797	0.187281	1.302554
N	-0.018938	0.758575	0.000909
B	0.034746	0.190837	-1.301668

C	0.133169	1.243749	-2.504805
C	-0.982703	2.008216	-2.907691
C	-0.909344	2.925329	-3.958424
C	0.298706	3.118238	-4.629383
C	1.425745	2.393443	-4.244855
C	1.338582	1.470008	-3.198750
C	-2.296100	1.883257	-2.162485
C	0.394921	4.150444	-5.726484
C	2.588034	0.683542	-2.855125
C	2.280772	1.882204	2.130321
C	-0.362342	4.146040	5.732655
C	-2.591699	0.675522	2.895571
C	-0.048812	-1.308646	-1.626164
C	-0.056964	-2.380915	-0.721598
S	-0.204949	-3.910745	-1.567113
C	-0.256393	-3.133253	-3.127432
C	-0.163753	-1.775669	-2.981559
C	0.043226	-2.382535	0.715105
S	0.200842	-3.914029	1.555767
C	0.253736	-3.140772	3.118051
C	0.154859	-1.783186	2.976354
C	0.032922	-1.312714	1.622714
C	0.390211	-3.947644	4.371638
C	-0.385779	-3.936970	-4.383798
H	0.168255	-1.111764	3.837350
H	-0.176713	-1.101700	-3.840624
H	-1.795514	3.487343	-4.255989
H	2.375009	2.546517	-4.760090
H	1.808148	3.485663	4.229887
H	-2.352665	2.538204	4.797144
F	-2.686167	0.402565	1.582050
F	-2.621150	-0.499823	3.549998

F	-3.701264	1.346568	3.245905
F	3.313654	2.403543	2.808744
F	2.585391	0.603744	1.852900
F	2.213631	2.537833	0.950459
F	-1.298931	3.828430	6.641125
F	0.808863	4.275159	6.377439
F	-0.680077	5.357326	5.241141
F	-3.320146	2.404031	-2.854516
F	-2.602752	0.603885	-1.890812
F	-2.245974	2.537212	-0.980940
F	2.666236	0.415542	-1.539426
F	2.625088	-0.494225	-3.504655
F	3.702035	1.352972	-3.194166
F	1.360636	3.847140	-6.608868
F	-0.760538	4.259314	-6.402838
F	0.678809	5.367561	-5.228715
H	-0.452950	-4.651588	4.500300
H	1.321884	-4.543429	4.378347
H	0.408716	-3.276314	5.246489
H	0.459770	-4.638287	-4.511076
H	-1.315837	-4.535194	-4.395977
H	-0.402585	-3.263191	-5.256812
H	-0.021505	1.776033	0.002087

5^{Mes}:

Total energy (B3LYP-D3(BJ)/def2-SV(P)): -2004.6093910730

S	-3.818870	-0.584491	-1.489071
C	-3.027135	-0.889170	-3.015901
C	-1.675615	-0.697686	-2.895405
C	-1.228137	-0.306223	-1.587020
C	-2.303073	-0.199685	-0.695121
C	-2.304195	0.192161	0.694720

S	-3.821763	0.572109	1.487616
C	-3.032069	0.879354	3.014993
C	-1.679879	0.691976	2.895502
C	-1.230246	0.302048	1.587401
B	0.261550	0.014535	1.281186
O	0.745425	0.002006	0.000728
H	-0.984904	-0.833373	-3.731538
H	-0.990183	0.829841	3.732118
C	1.308376	-0.219804	2.435031
B	0.262450	-0.013176	-1.280027
C	1.183492	-1.312618	3.323556
C	2.132347	-1.496072	4.338433
C	3.206099	-0.615045	4.509923
C	3.319037	0.465579	3.625805
C	2.400090	0.668486	2.589458
C	0.043758	-2.301782	3.192870
H	2.031569	-2.353073	5.014130
C	4.234181	-0.840640	5.592122
H	4.150731	1.169239	3.745797
C	2.587098	1.840964	1.649978
C	1.308972	0.223454	-2.433669
C	1.179819	1.313548	-3.324791
C	2.127767	1.498064	-4.340428
C	3.204863	0.620858	-4.509850
C	3.322251	-0.457032	-3.622852
C	2.404342	-0.660883	-2.585873
C	0.036388	2.298754	-3.196498
H	2.023258	2.352653	-5.018592
C	4.231900	0.846979	-5.592940
H	4.156604	-1.157820	-3.741287
C	2.596384	-1.829955	-1.643163
H	2.877058	-1.485868	-0.631799

H	1.669451	-2.421777	-1.528998
H	3.386102	-2.509237	-2.006382
H	0.230998	3.211448	-3.785201
H	-0.915944	1.865189	-3.553071
H	-0.129233	2.604116	-2.147951
H	4.607813	-0.108383	-6.000075
H	3.817166	1.437394	-6.428422
H	5.107897	1.400764	-5.202236
H	0.240506	-3.214026	3.781549
H	-0.910746	-1.871694	3.547800
H	-0.118830	-2.607317	2.143874
H	2.869462	1.500876	0.637729
H	1.657556	2.428975	1.537316
H	3.373747	2.522757	2.015154
H	4.619212	0.114813	5.990271
H	3.816907	-1.420746	6.433596
H	5.104268	-1.405249	5.203663
C	-3.814632	-1.301727	-4.221028
H	-4.355188	-2.252247	-4.054779
H	-4.566079	-0.540586	-4.502381
H	-3.135420	-1.442499	-5.078596
C	-3.821689	1.289961	4.219399
H	-4.364744	2.238940	4.052492
H	-4.571251	0.526799	4.500302
H	-3.143578	1.432817	5.077493

6^{Mes.}:

Total energy (B3LYP-D3(BJ)/def2-SV(P)): -1984.7469265140

C	-0.163321	-0.184514	-2.892668
C	0.607696	-0.139433	-4.074086
C	2.012828	-0.047868	-3.975479
C	2.619955	-0.001080	-2.713776

C	1.865456	-0.040303	-1.534036
C	0.472364	-0.135913	-1.645008
B	-0.094082	-0.191775	-5.491508
N	-0.454239	1.060898	-6.077023
B	-1.083951	1.451177	-7.298851
C	-1.290139	3.002985	-7.529868
C	-2.466812	3.641190	-7.081539
C	-2.636741	5.015342	-7.293806
C	-1.661505	5.784182	-7.942423
C	-0.500156	5.138793	-8.385830
C	-0.302148	3.765722	-8.188513
C	-3.542711	2.836845	-6.385133
C	-1.845408	7.271136	-8.130995
C	0.958516	3.095946	-8.690111
C	2.856594	-0.013733	-5.231001
C	2.533028	0.047896	-0.182346
C	-1.669819	-0.296880	-2.978525
C	-1.564789	0.457241	-8.380880
C	-1.489667	-0.943326	-8.382309
S	-2.182732	-1.608209	-9.853429
C	-2.575123	-0.025415	-10.474737
C	-2.187215	0.940801	-9.585363
C	-0.950782	-1.841401	-7.393300
S	-1.006880	-3.572209	-7.689731
C	-0.230788	-3.934966	-6.169399
C	0.045212	-2.777477	-5.491803
C	-0.350276	-1.563503	-6.156618
C	0.045810	-5.350004	-5.764963
C	-3.241756	0.135041	-11.805981
H	0.531960	-2.772038	-4.513574
H	-2.338269	2.006366	-9.773848
H	-3.556382	5.499737	-6.946000

H	0.271941	5.721021	-8.901679
H	3.712048	0.065371	-2.648699
H	-0.135560	-0.175988	-0.733908
H	-2.109826	0.559829	-3.522800
H	-1.972994	-1.207864	-3.527613
H	-2.132577	-0.333869	-1.977807
H	3.933030	0.043512	-4.996362
H	2.690652	-0.915371	-5.849744
H	2.602794	0.855411	-5.866617
H	1.944400	-0.470318	0.594928
H	3.544060	-0.395706	-0.200052
H	2.644624	1.101510	0.140513
H	-4.409908	3.463767	-6.116924
H	-3.904636	2.011759	-7.026607
H	-3.163164	2.370500	-5.456512
H	1.520602	2.619700	-7.864876
H	0.724709	2.294289	-9.415448
H	1.632139	3.815699	-9.185289
H	-1.287147	7.640288	-9.009092
H	-2.909551	7.533841	-8.265534
H	-1.479681	7.834348	-7.250192
H	-0.882500	-5.947049	-5.692657
H	0.710835	-5.862164	-6.485334
H	0.537695	-5.364957	-4.777818
H	-2.630052	-0.284734	-12.626404
H	-4.225505	-0.369582	-11.838025
H	-3.401804	1.206238	-12.014718
H	-0.206538	1.856457	-5.489421

γ^{Mes} :

Total energy (B3LYP-D3(BJ)/def2-SV(P)): -2023.9904488200

S -3.87310069 0.02799102 -1.56406693

C	-3.08472594	0.01595778	-3.12120609
C	-1.72540708	-0.00856250	-2.96305427
C	-1.25806711	-0.02207819	-1.59799512
C	-2.34005562	-0.00156659	-0.67295565
C	-2.32804162	0.00891682	0.72399859
S	-3.84872768	0.06123598	1.59836257
C	-3.03900091	0.06467186	3.14347239
C	-1.68212519	0.02807749	2.96669765
C	-1.23220586	-0.00660599	1.59585458
B	0.29039038	-0.06031894	1.29002191
N	0.90086373	-0.11462749	-0.01429021
H	-1.04190221	-0.01754174	-3.81439588
H	-0.98869751	0.02539906	3.80974348
C	1.22425603	-0.04015040	2.57499338
B	0.26370867	-0.06137059	-1.30857967
C	1.56875776	-1.23862560	3.23647560
C	2.35245110	-1.19376344	4.39586800
C	2.81125545	0.02011498	4.92589428
C	2.46014575	1.20210164	4.26258335
C	1.67706291	1.18763149	3.10014689
C	1.08842265	-2.56266149	2.68642484
H	2.61152973	-2.13102773	4.90183579
C	3.68041148	0.04433438	6.16056330
H	2.80353584	2.16273978	4.66292496
C	1.31167259	2.48205736	2.40843936
C	1.19798343	-0.03129299	-2.59176932
C	1.64103479	1.20313909	-3.11222225
C	2.44783527	1.22700642	-4.25689788
C	2.83064770	0.04806737	-4.91022701
C	2.37177970	-1.16978749	-4.39263998
C	1.56330484	-1.22397886	-3.24923802
C	1.22470172	2.49485483	-2.44397290

H	2.78493776	2.19203015	-4.65241311
C	3.73318485	0.09023355	-6.12019138
H	2.64919969	-2.10343216	-4.89518824
C	1.06136995	-2.55350955	-2.73119737
H	1.31365680	-2.69864382	-1.66382871
H	-0.04040785	-2.61891162	-2.80492970
H	1.48952082	-3.39907963	-3.29585939
H	1.68181731	3.37201894	-2.93243301
H	0.12651409	2.62301471	-2.47416276
H	1.51405004	2.51532082	-1.37616191
H	3.59152173	-0.79641768	-6.76253591
H	3.54806185	0.99049032	-6.73257491
H	4.80005247	0.11262317	-5.82337417
H	1.42912022	-3.40981188	3.30564850
H	-0.01581920	-2.59907882	2.63669473
H	1.45716351	-2.72822361	1.65633930
H	1.68656261	2.50388108	1.36765720
H	0.21462785	2.61068705	2.35212722
H	1.72945136	3.35731370	2.93422271
H	3.68558267	1.04208931	6.63237422
H	3.33632203	-0.68830486	6.91254743
H	4.73014062	-0.21080820	5.91688970
C	-3.88243936	0.03232290	-4.38833694
H	-4.54958715	-0.84648013	-4.46694951
H	-4.51756075	0.93479943	-4.46422197
H	-3.20175188	0.02138699	-5.25620785
C	-3.81795693	0.10405904	4.42171202
H	-4.44916854	1.00965573	4.49215509
H	-4.48655880	-0.77119260	4.52420412
H	-3.12467401	0.10487374	5.27958175
C	2.37775355	-0.19161153	-0.06371431
H	2.70372282	-1.05339317	-0.66671490

H	2.80380170	0.71172146	-0.53056862
H	2.79391152	-0.29060400	0.94662988

Non-fused *B*-mesityl-azadiborepin:

Total energy (B3LYP-D3(BJ)/def2-SV(P)): -957.889847

C	-3.027630	-1.202230	-0.885291
C	-2.553311	-0.573833	0.284976
C	-3.065340	-0.977583	1.538216
C	-4.032336	-1.987262	1.601912
C	-4.512283	-2.618521	0.445710
C	-3.998349	-2.209555	-0.790002
B	-1.455114	0.559987	0.196964
N	-0.088505	0.142163	0.152796
B	1.159693	0.833503	0.063503
C	1.273957	2.376561	0.002696
C	0.300442	3.331641	0.010185
C	-1.139383	3.181008	0.080076
C	-1.890742	2.045662	0.159225
C	-2.559239	-0.322874	2.805189
C	-5.541666	-3.719232	0.541526
C	-2.489253	-0.790829	-2.238955
C	2.471366	-0.048345	0.024171
C	2.960423	-0.546195	-1.202528
C	4.116746	-1.336970	-1.220973
C	4.808913	-1.652492	-0.045168
C	4.310455	-1.157620	1.166940
C	3.157956	-0.363521	1.216687
C	2.231586	-0.232082	-2.491250
C	2.638552	0.146387	2.543524
C	6.073544	-2.476766	-0.084300
H	-1.480184	-0.516479	2.956813
H	-2.679010	0.776006	2.768140

H	-3.094443	-0.692474	3.696312
H	-4.424677	-2.290714	2.579520
H	-2.578981	0.300266	-2.395808
H	-1.414693	-1.035500	-2.340338
H	-3.025632	-1.296173	-3.059900
H	-4.364844	-2.686611	-1.705907
H	2.091281	0.857339	-2.620950
H	1.221185	-0.683272	-2.506849
H	2.779999	-0.609645	-3.370826
H	4.487899	-1.718858	-2.178935
H	3.312265	-0.122367	3.374697
H	2.528415	1.246946	2.537961
H	1.638630	-0.268400	2.773615
H	4.833797	-1.399094	2.099223
H	-5.100728	-4.645670	0.957079
H	-5.962493	-3.967075	-0.448064
H	-6.377488	-3.434049	1.206090
H	6.183491	-3.094017	0.824828
H	6.091826	-3.149548	-0.959566
H	6.970554	-1.830328	-0.149737
H	2.298677	2.769157	-0.059154
H	0.625779	4.380478	-0.044614
H	-1.678029	4.139503	0.065308
H	-2.975454	2.217102	0.199440
H	0.019593	-0.871802	0.188897

Non-fused *B*-mesityl-oxadiborepin:

Total energy (B3LYP-D3(BJ)/def2-SV(P)): -977.752224

B	-1.279076	1.252009	0.131077
B	1.278532	1.250196	-0.137687
C	-1.559951	2.766259	0.347599
C	-2.423764	0.172375	0.102769

C	1.562692	2.763825	-0.353794
C	2.422293	0.169532	-0.105115
C	-0.697675	3.810548	0.197050
C	-2.314341	-1.002197	0.895274
C	-3.567558	0.332685	-0.715792
C	0.702224	3.809554	-0.203077
C	2.318614	-1.001450	-0.900950
C	3.556539	0.323623	0.729646
C	-1.120672	-1.253133	1.794364
C	-3.336311	-1.957099	0.865926
C	-3.758772	1.551522	-1.595986
C	-4.559345	-0.657524	-0.736290
C	1.131175	-1.250267	-1.808773
C	3.338075	-1.960560	-0.861909
C	3.733317	1.536318	1.621305
C	4.544049	-0.668820	0.759560
H	-0.221751	-1.519365	1.210903
H	-0.853099	-0.361995	2.389301
H	-1.328085	-2.077478	2.497343
C	-4.466005	-1.808756	0.050836
H	-3.249000	-2.848998	1.497065
H	-4.175784	2.403433	-1.026160
H	-2.814081	1.899456	-2.046984
H	-4.463669	1.335556	-2.417148
H	-5.430911	-0.525606	-1.387555
H	0.865327	-0.356364	-2.400299
H	0.229270	-1.521881	-1.232271
H	1.344561	-2.070190	-2.515135
C	4.459606	-1.815854	-0.037058
H	3.252158	-2.853717	-1.491168
H	4.443176	1.322268	2.438628
H	4.136145	2.399742	1.058893

H	2.784760	1.866511	2.078017
H	5.404130	-0.544875	1.427705
C	-5.531535	-2.876443	0.008221
C	5.556652	-2.851957	-0.025610
H	-5.204338	-3.741657	-0.600508
H	-6.468811	-2.496713	-0.433417
H	-5.758714	-3.260524	1.018937
H	6.025509	-2.934150	0.970805
H	5.176196	-3.848298	-0.310612
H	6.358733	-2.589976	-0.743091
H	2.583041	3.042710	-0.649549
H	1.101136	4.819488	-0.376495
H	-1.094824	4.821040	0.371257
H	-2.579452	3.047148	0.644174
O	-0.000670	0.783512	-0.004662

B-mesityl-borepin:

Total energy (B3LYP-D3(BJ)/def2-SV(P)): -605.867649

C	6.238768	1.221522	-3.720457
C	5.822176	0.486092	-2.602842
C	4.485565	0.476612	-2.186126
C	3.518179	1.217298	-2.901533
C	3.926918	1.957838	-4.030853
C	5.273041	1.951258	-4.422682
C	4.072839	-0.332628	-0.976154
B	2.001585	1.210995	-2.448335
C	1.548047	2.216356	-1.381029
C	0.299195	2.405290	-0.833184
C	-0.919403	1.715644	-1.104936
C	-1.175577	0.683357	-1.980282
C	-0.297958	0.000723	-2.873546
C	1.046032	0.199394	-3.095826

C	2.912393	2.758780	-4.817496
C	7.691088	1.241047	-4.134767
H	2.410955	3.513037	-4.182088
H	2.112920	2.111389	-5.224698
H	3.381308	3.288456	-5.664259
H	7.811998	1.608428	-5.168609
H	8.143007	0.234327	-4.075613
H	8.288187	1.902338	-3.477043
H	4.933530	-0.852410	-0.521583
H	3.614733	0.307138	-0.198475
H	3.316102	-1.095809	-1.238484
H	5.575698	2.531624	-5.301960
H	6.560501	-0.098044	-2.040797
H	1.479708	-0.475388	-3.848644
H	-0.791755	-0.791217	-3.454611
H	-2.213394	0.328387	-1.996509
H	-1.782628	2.064229	-0.524943
H	0.197235	3.194523	-0.074506
H	2.317988	2.895209	-0.985664

2,2‘-bithiophene-3,3‘-dicarboximide:

Total energy (B3LYP-D3(BJ)/def2-SV(P)): -1384.617900

C	-0.068064	-2.393212	-4.699694
C	-1.233840	-1.886481	-3.943903
C	-1.315377	-0.810273	-3.062408
C	-0.285197	0.104499	-2.643432
C	1.057920	0.148717	-3.012428
C	1.805399	-0.729204	-3.938428
N	1.188363	-1.792064	-4.601352
C	-2.486669	-2.562690	-4.103763
C	-3.491831	-2.010769	-3.360912
S	-2.942256	-0.649619	-2.443424

S	-0.650007	1.385420	-1.511221
C	0.982046	1.961962	-1.542498
C	1.768840	1.216355	-2.374200
H	1.263132	2.824978	-0.938098
H	2.829751	1.388797	-2.555570
H	-2.593219	-3.426948	-4.759401
H	-4.534387	-2.323277	-3.294256
O	-0.177593	-3.359244	-5.435334
O	2.991948	-0.543534	-4.147740
H	1.861743	-2.279622	-5.193255

2,2‘-bithiophene-3,3‘-dicarboxylic anhydride:

Total energy (B3LYP-D3(BJ)/def2-SV(P)): -1404.447780

C	-0.098135	-2.385286	-4.713359
C	-1.191691	-1.922092	-3.912332
C	-0.884739	-0.762589	-3.207117
S	0.739034	-0.236588	-3.564244
C	1.000167	-1.575072	-4.632415
C	-1.715568	-0.045529	-2.276197
C	-3.088266	-0.166754	-2.082903
C	-3.588966	0.747871	-1.100735
C	-2.607965	1.523024	-0.547566
S	-1.050735	1.172958	-1.220729
C	-4.042004	-1.020980	-2.819733
O	-5.220418	-0.793506	-2.835943
C	-2.424128	-2.733804	-3.841750
O	-2.452199	-3.881756	-4.190902
O	-3.618358	-2.170056	-3.450072
H	1.957931	-1.681684	-5.142681
H	-0.161412	-3.292114	-5.315694
H	-4.646653	0.800184	-0.840310
H	-2.704584	2.286112	0.225262

7.3 First Molecular Model Compounds for a Boron-Phosphorus Analogue of Poly(*p*-phenylene vinylene)

NMR Spectra

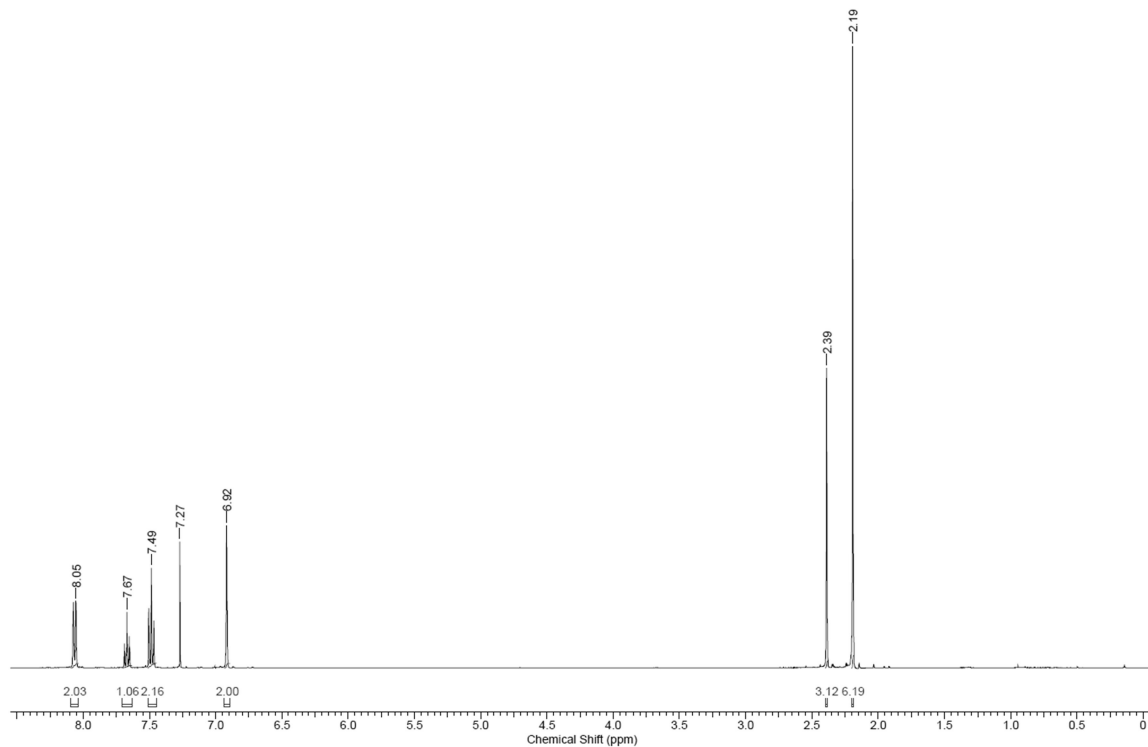


Figure 7.3.1. ¹H NMR spectrum of **10** in CDCl_3 .

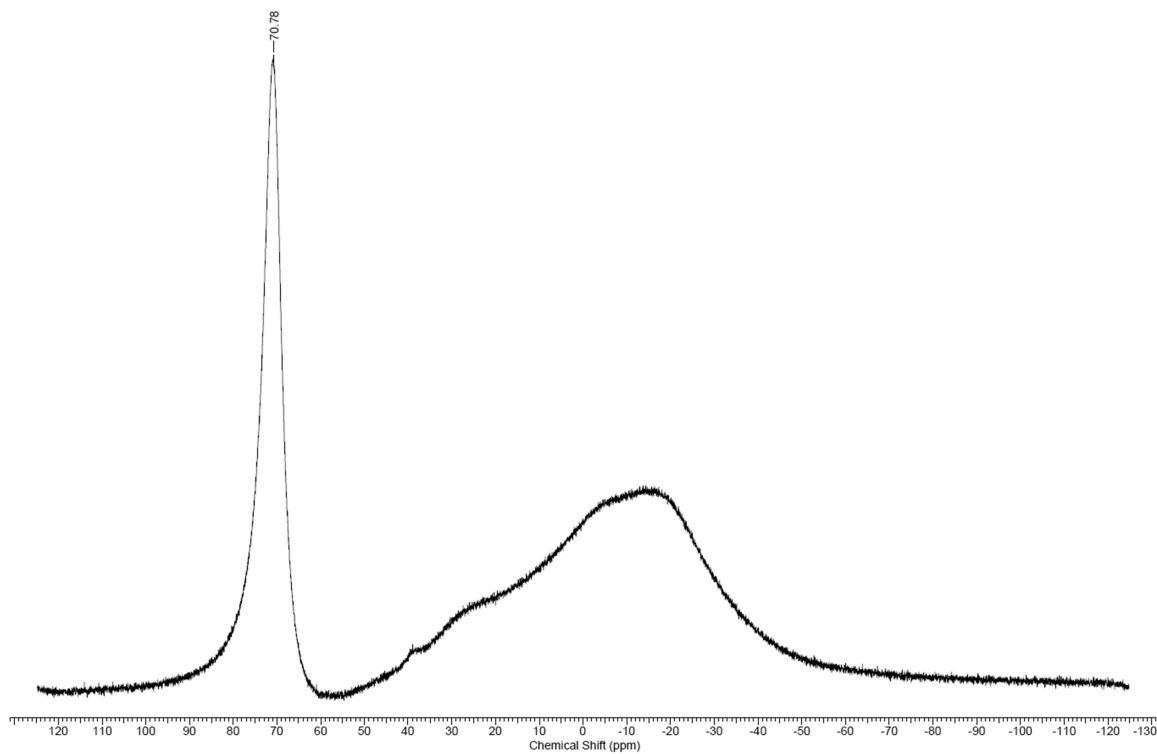


Figure 7.3.2. $^{11}\text{B}\{^1\text{H}\}$ NMR spectrum of **10** in CDCl_3 .

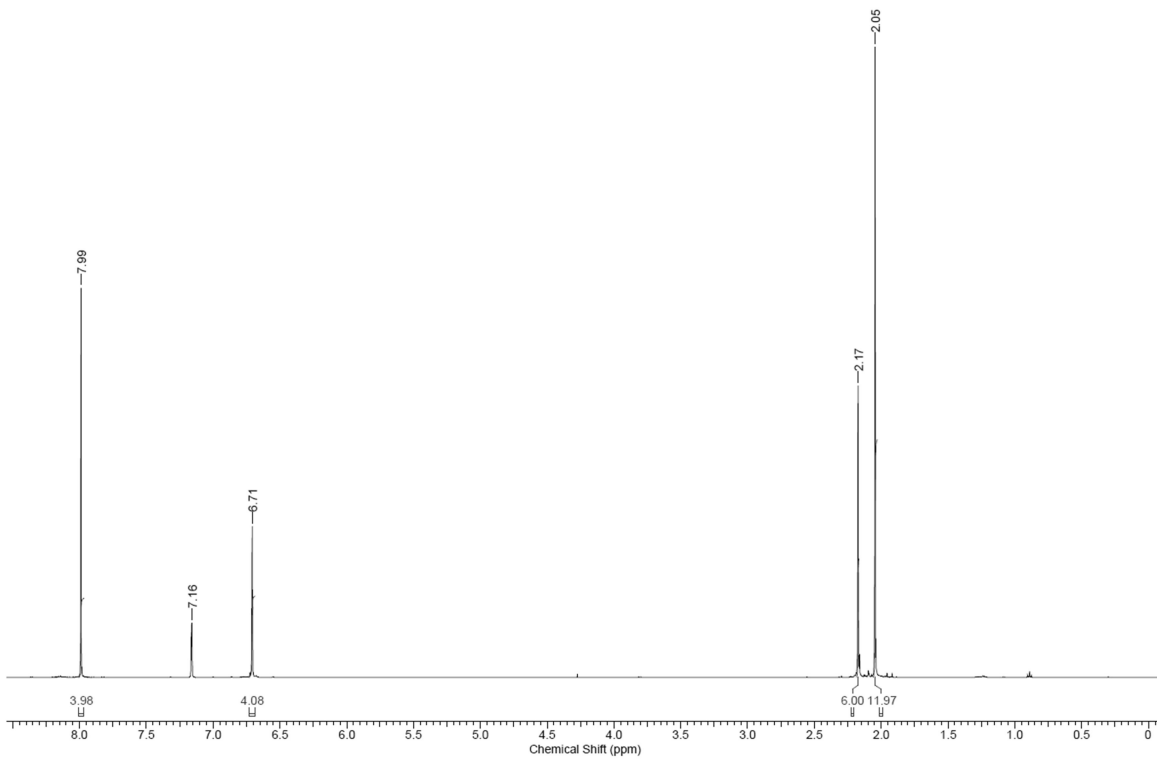


Figure 7.3.3. ^1H NMR spectrum of **15** in C_6D_6 .

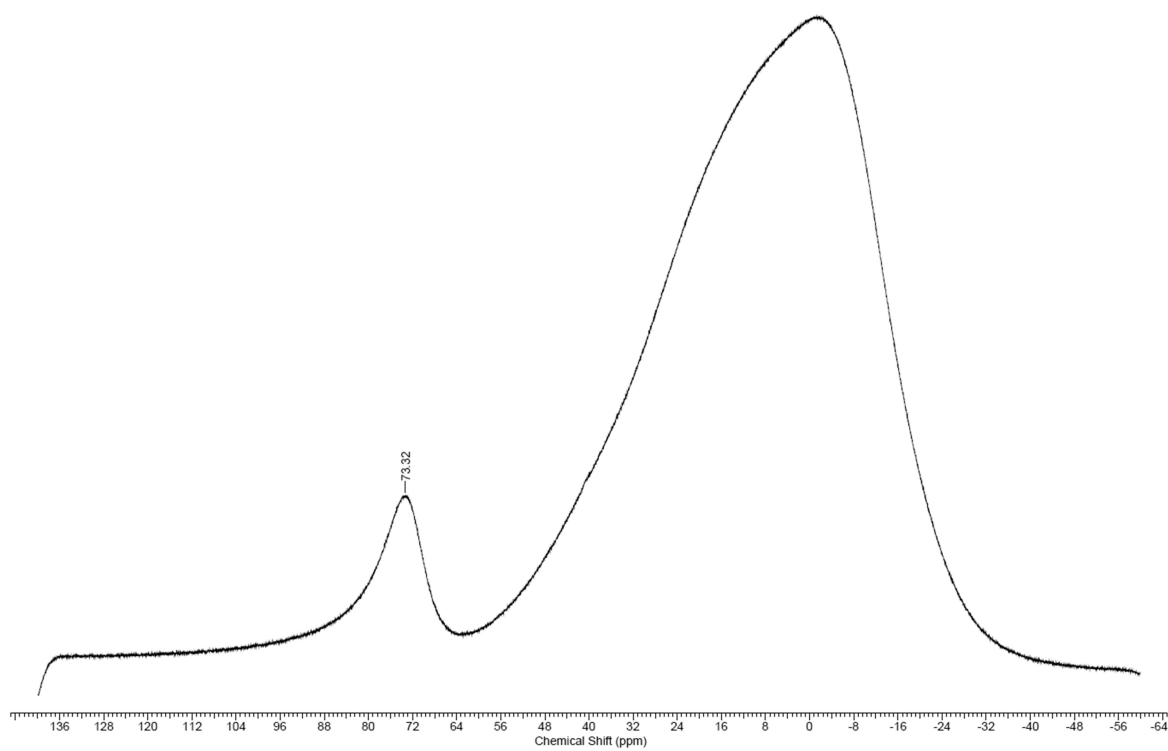


Figure 7.3.4. $^{11}\text{B}\{^1\text{H}\}$ NMR spectrum of **15** in C_6D_6 .

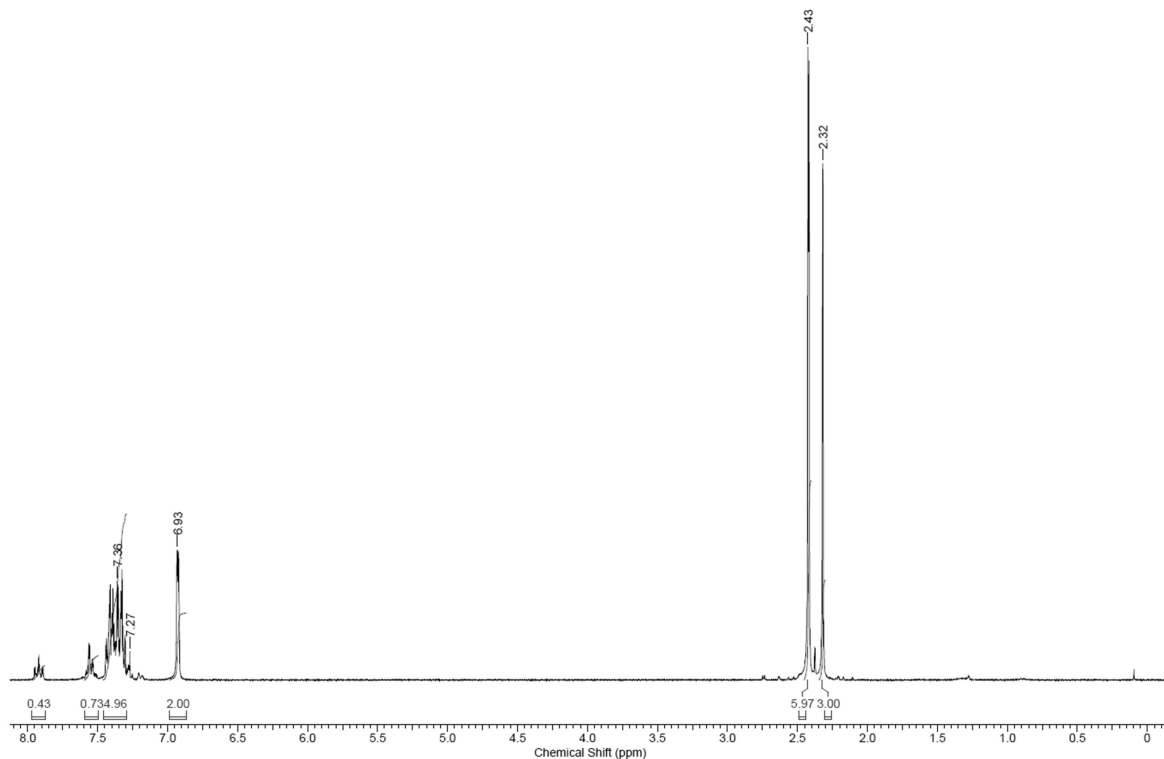


Figure 7.3.5. ^1H NMR spectrum of **5^{Mes}** in CDCl_3 .

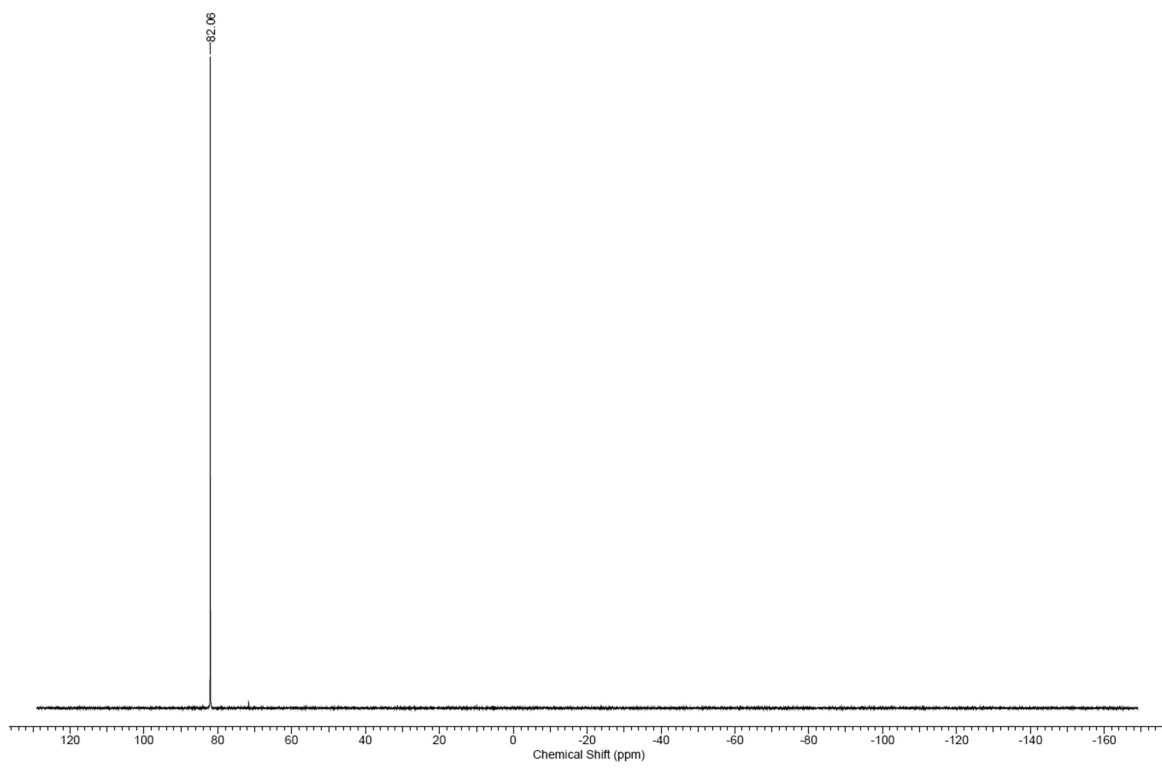


Figure 7.3.6. $^{31}\text{P}\{\text{H}\}$ NMR spectrum of $\mathbf{5}^{\text{Mes}}$ in CDCl_3 .

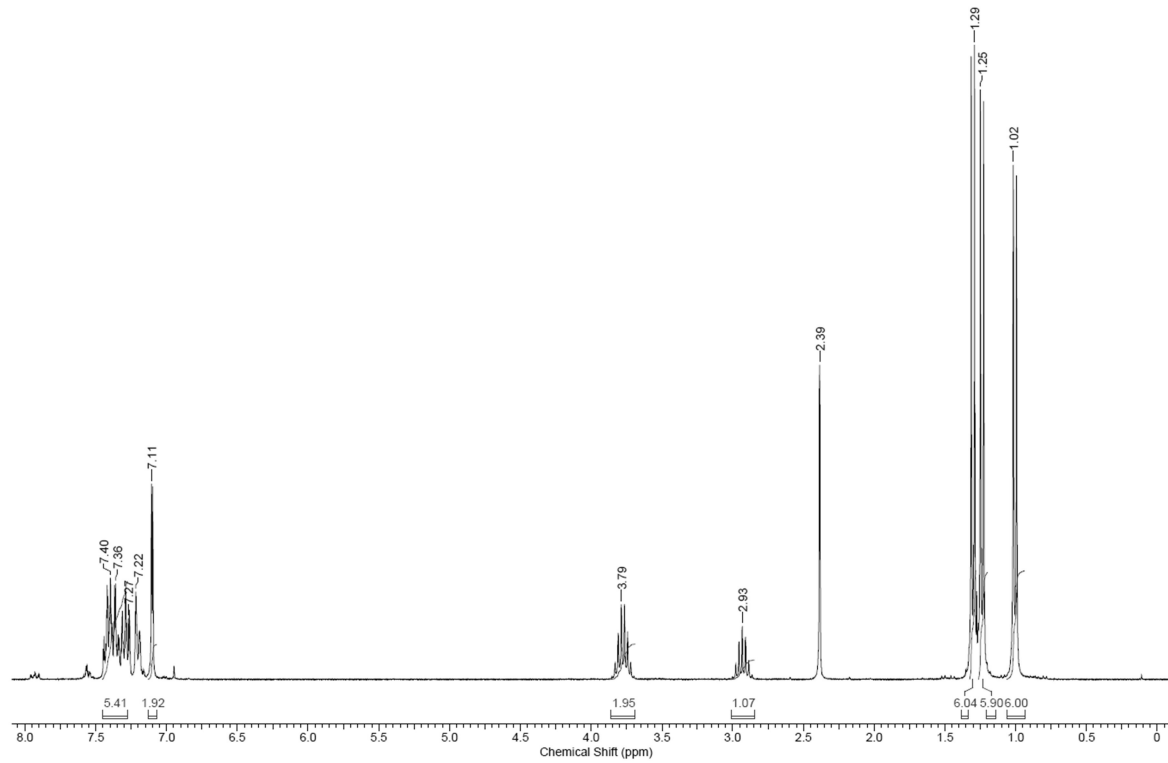


Figure 7.3.7. ^1H NMR spectrum of $\mathbf{5}^{\text{Tip}}$ in CDCl_3 .

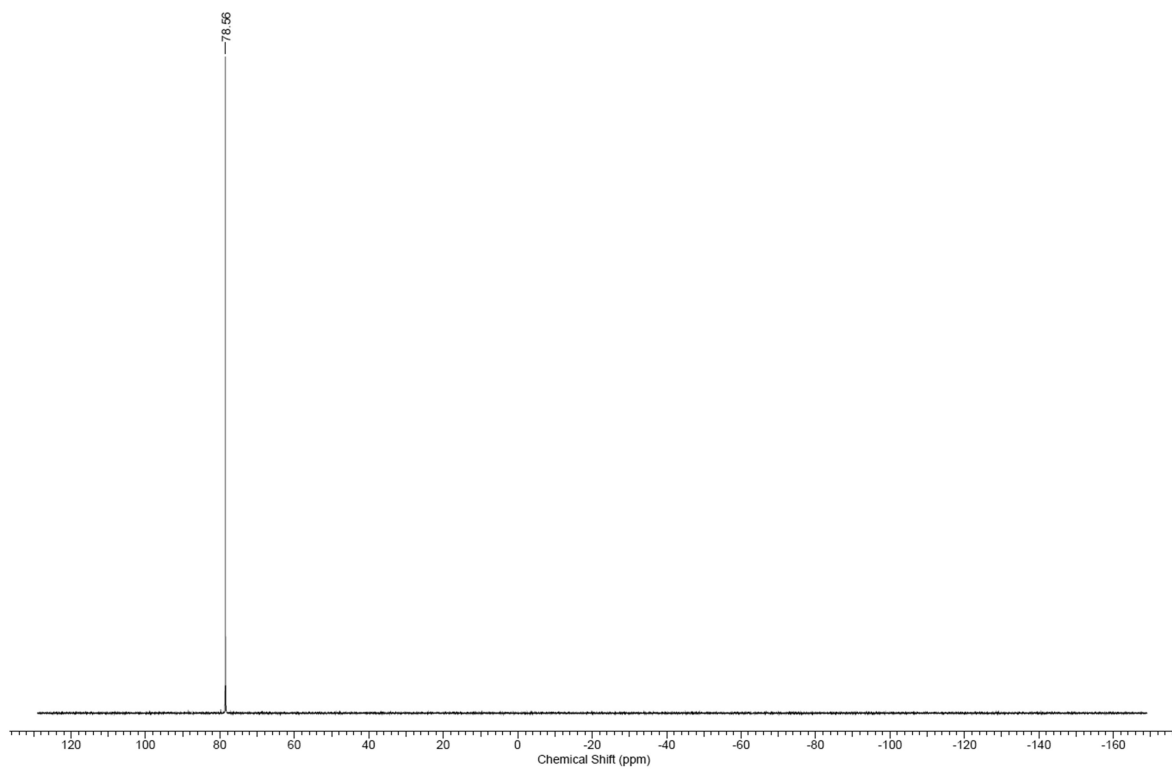


Figure 7.3.8. $^{31}\text{P}\{\text{H}\}$ NMR spectrum of $\mathbf{5}^{\text{Tip}}$ in CDCl_3 .

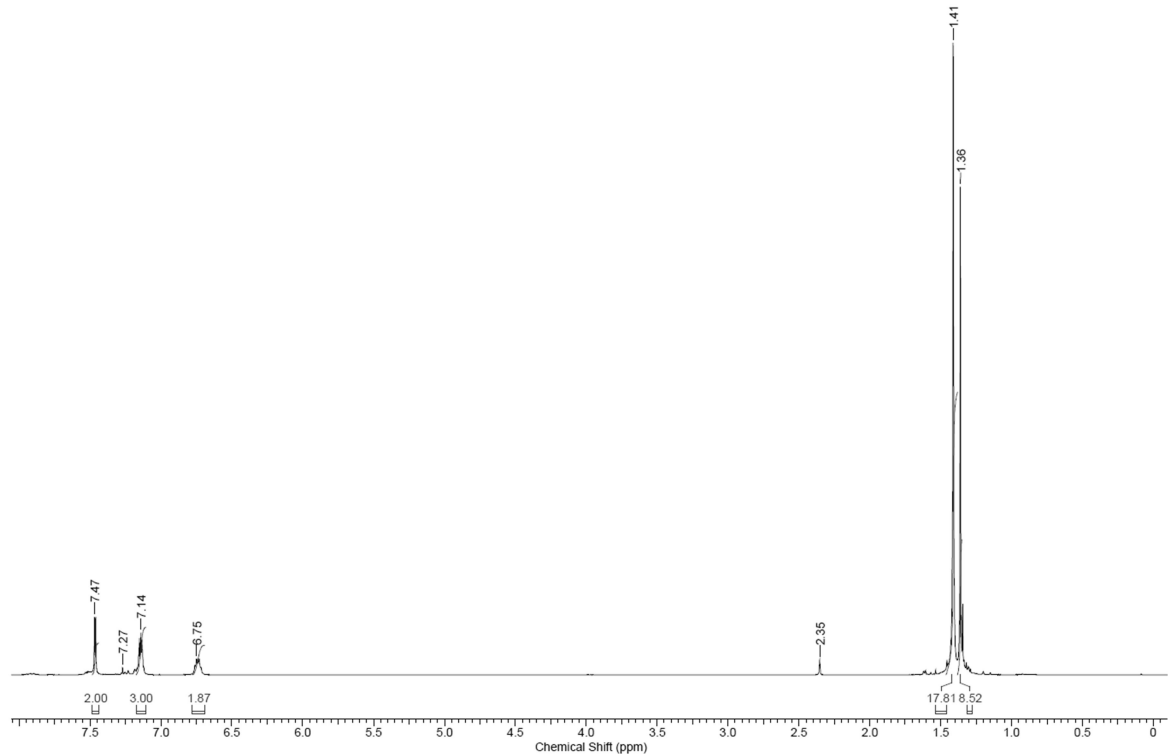


Figure 7.3.9. ^1H NMR spectrum of $\mathbf{5}^{\text{Mes}^*}$ in CDCl_3 .

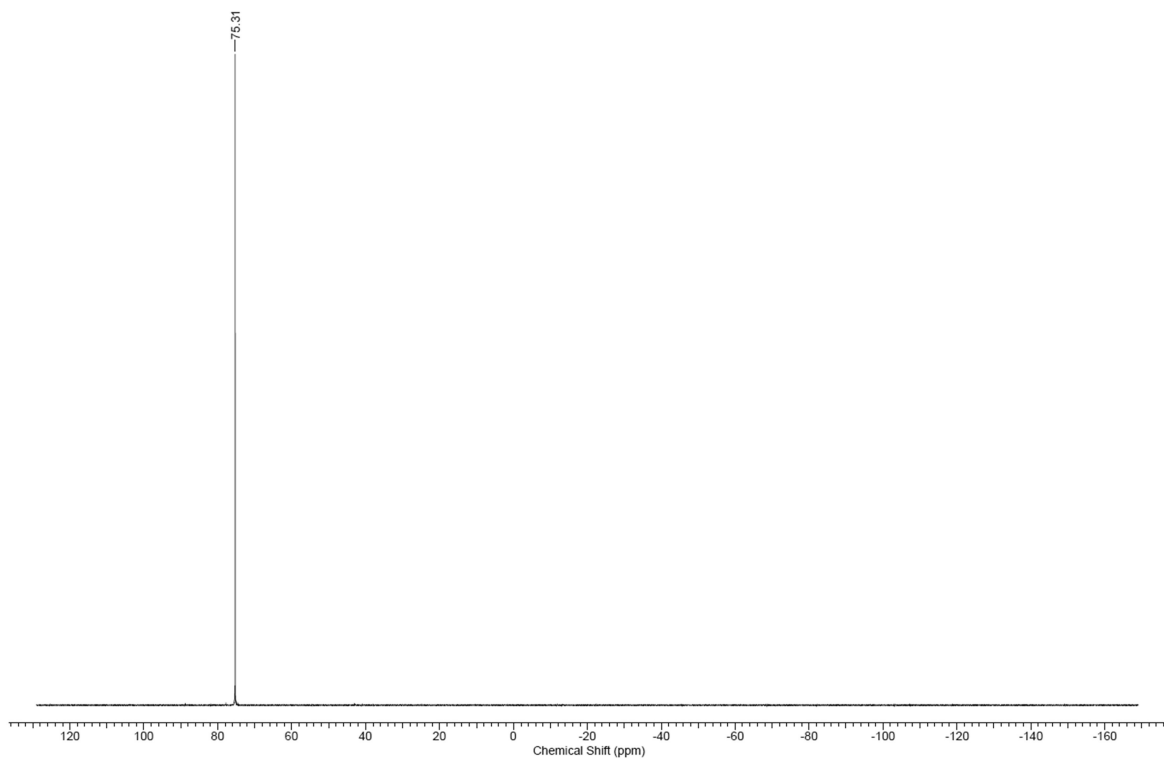


Figure 7.3.10. $^{31}\text{P}\{\text{H}\}$ NMR spectrum of $\mathbf{5}^{\text{Mes}*}$ in CDCl_3 .

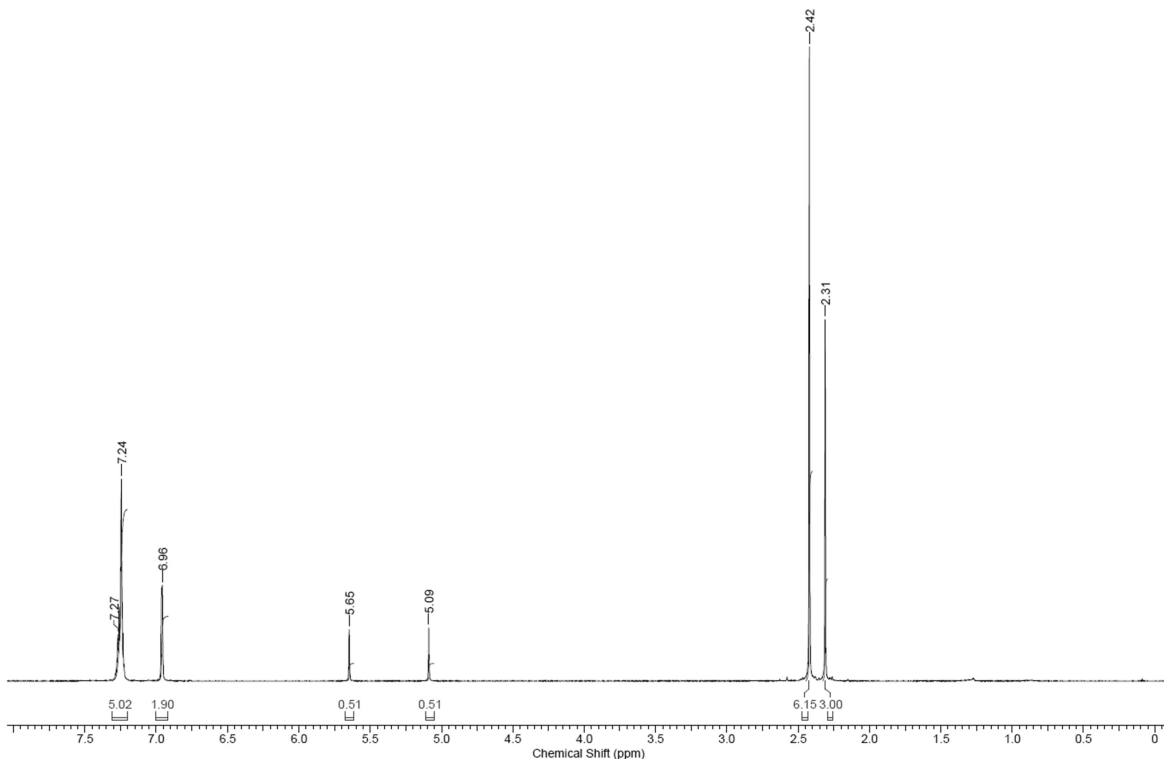


Figure 7.3.11. ^1H NMR spectrum of $\mathbf{6}^{\text{Mes}}$ in CDCl_3 .

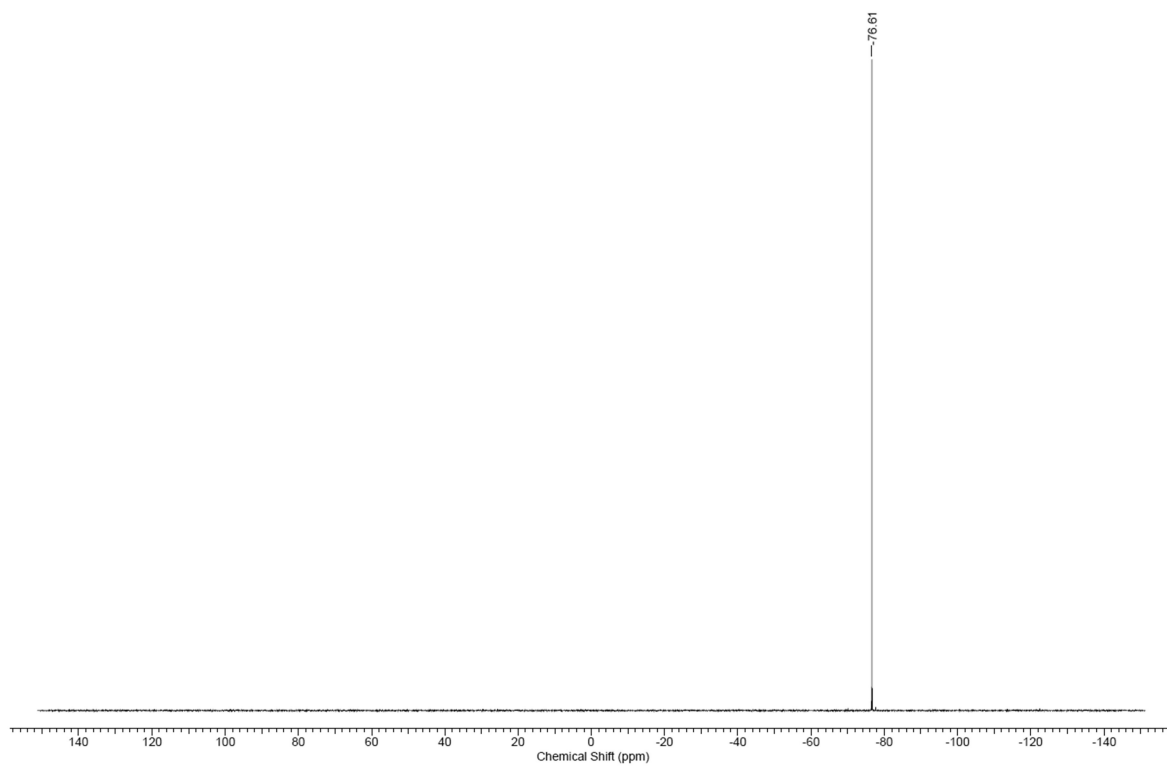


Figure 7.3.12. $^{31}\text{P}\{\text{H}\}$ NMR spectrum of $\mathbf{6}^{\text{Mes}}$ in CDCl_3 .

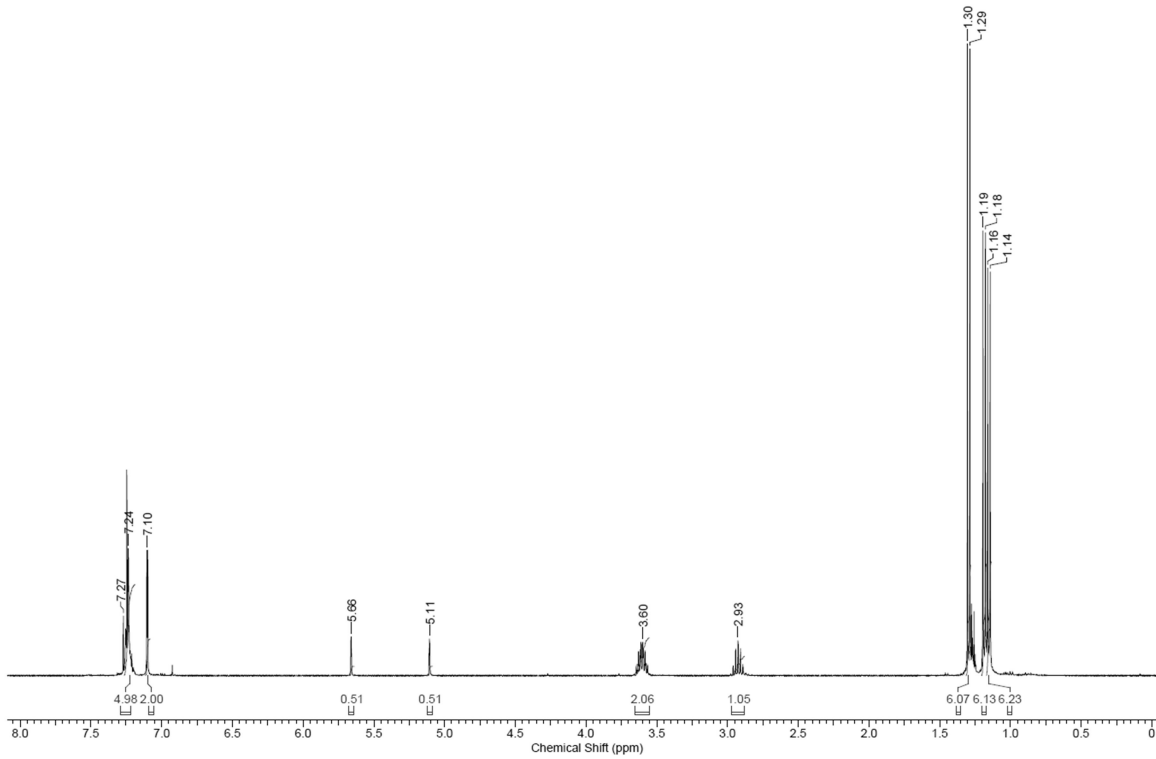


Figure 7.3.13. ^1H NMR spectrum of $\mathbf{6}^{\text{Tip}}$ in CDCl_3 .

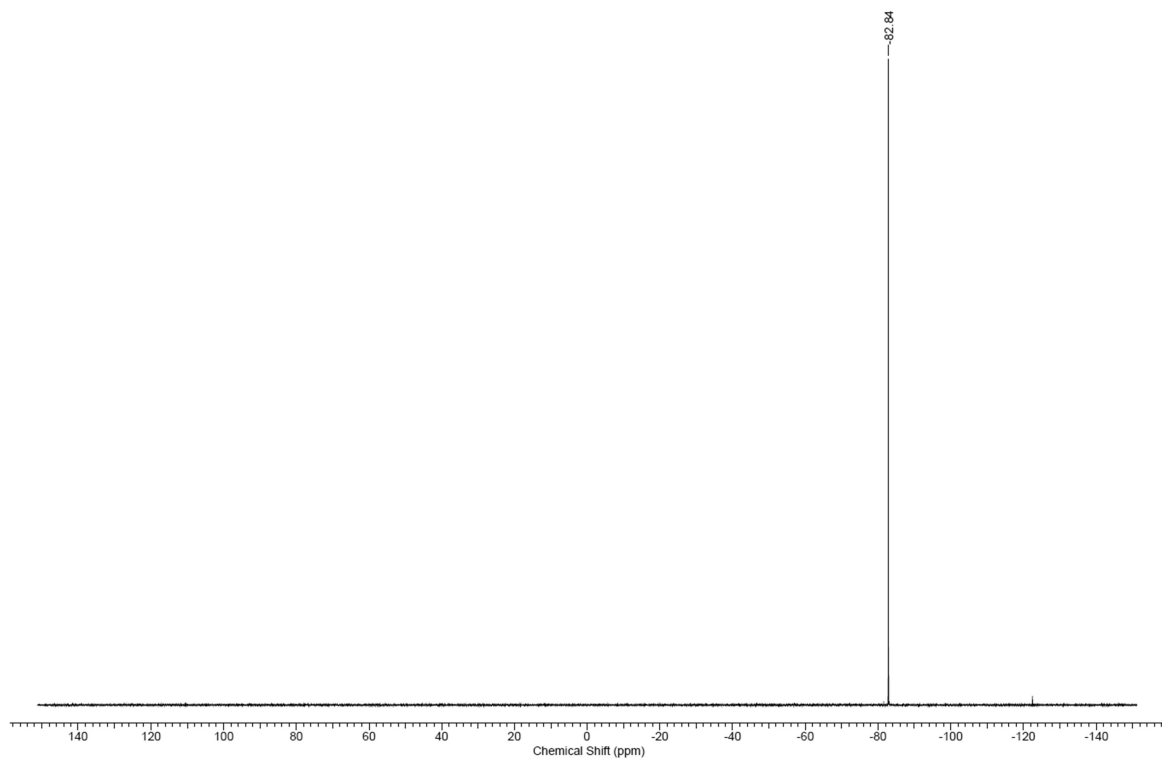


Figure 7.3.14. $^{31}\text{P}\{\text{H}\}$ NMR spectrum of $\mathbf{6}^{\text{Tip}}$ in CDCl_3 .

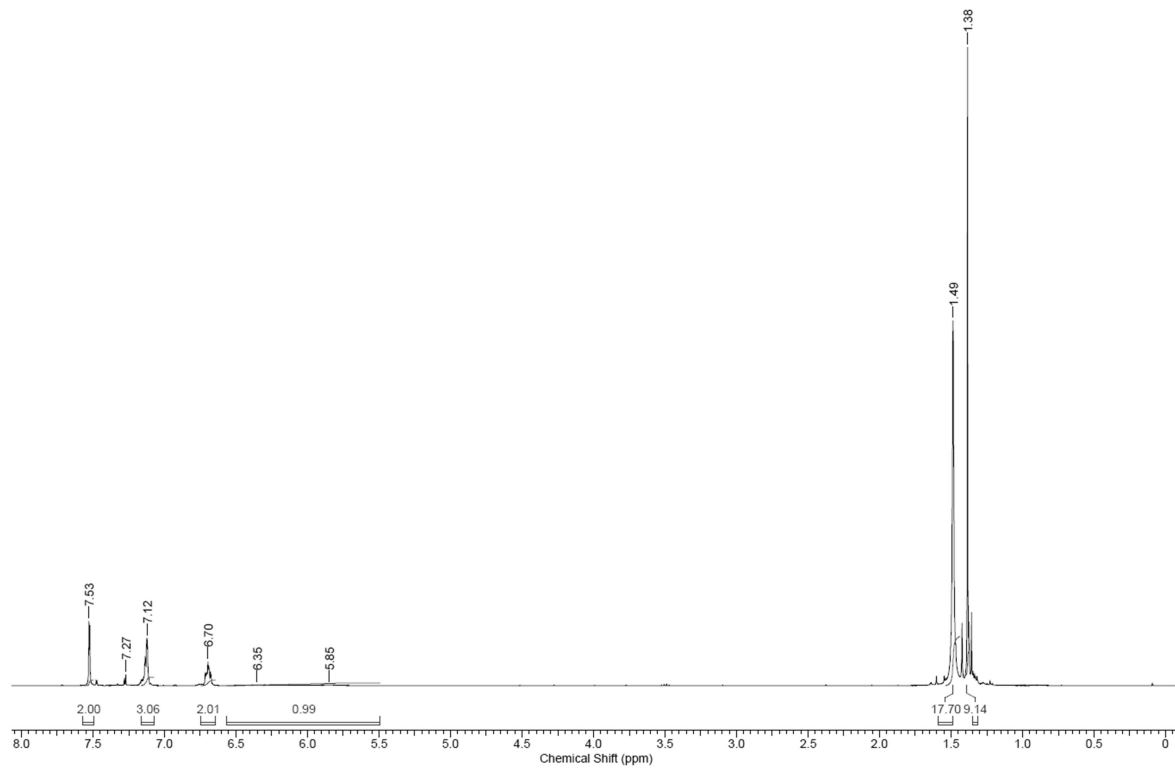


Figure 7.3.15. ^1H NMR spectrum of $\mathbf{6}^{\text{Mes}^*}$ in CDCl_3 .

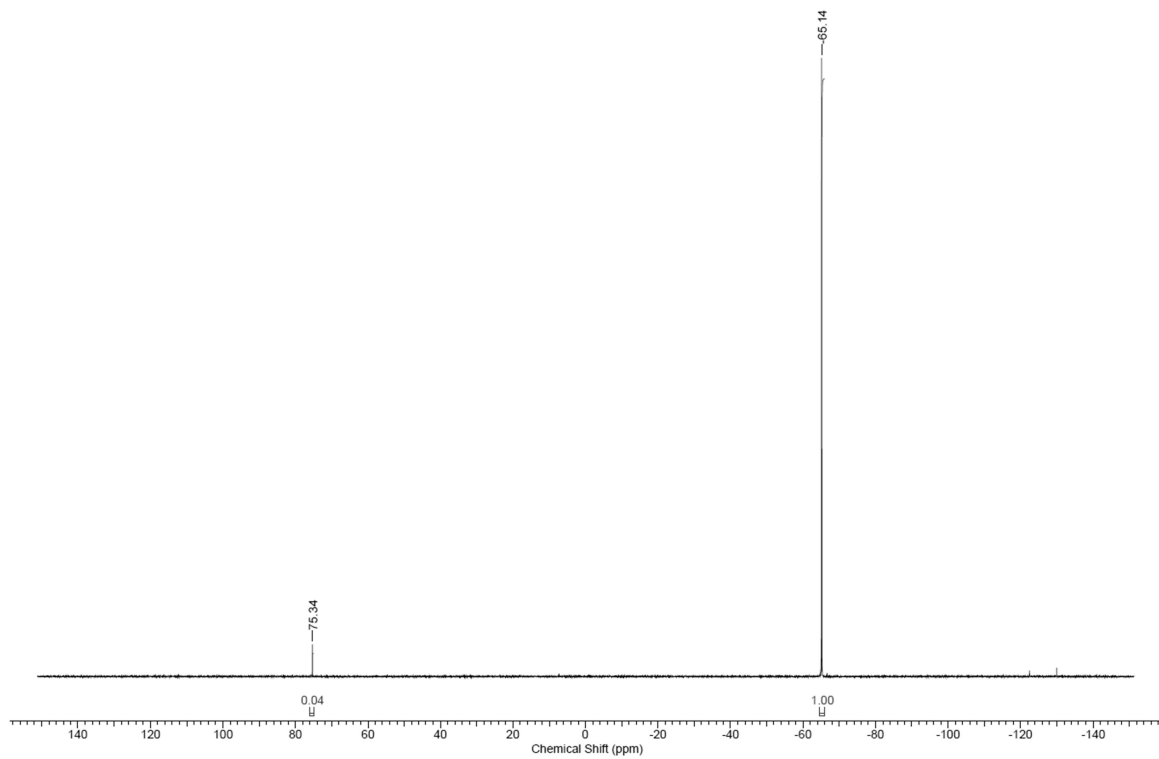


Figure 7.3.16. $^{31}\text{P}\{\text{H}\}$ NMR spectrum of $\mathbf{6}^{\text{Mes}*}$ in CDCl_3 .

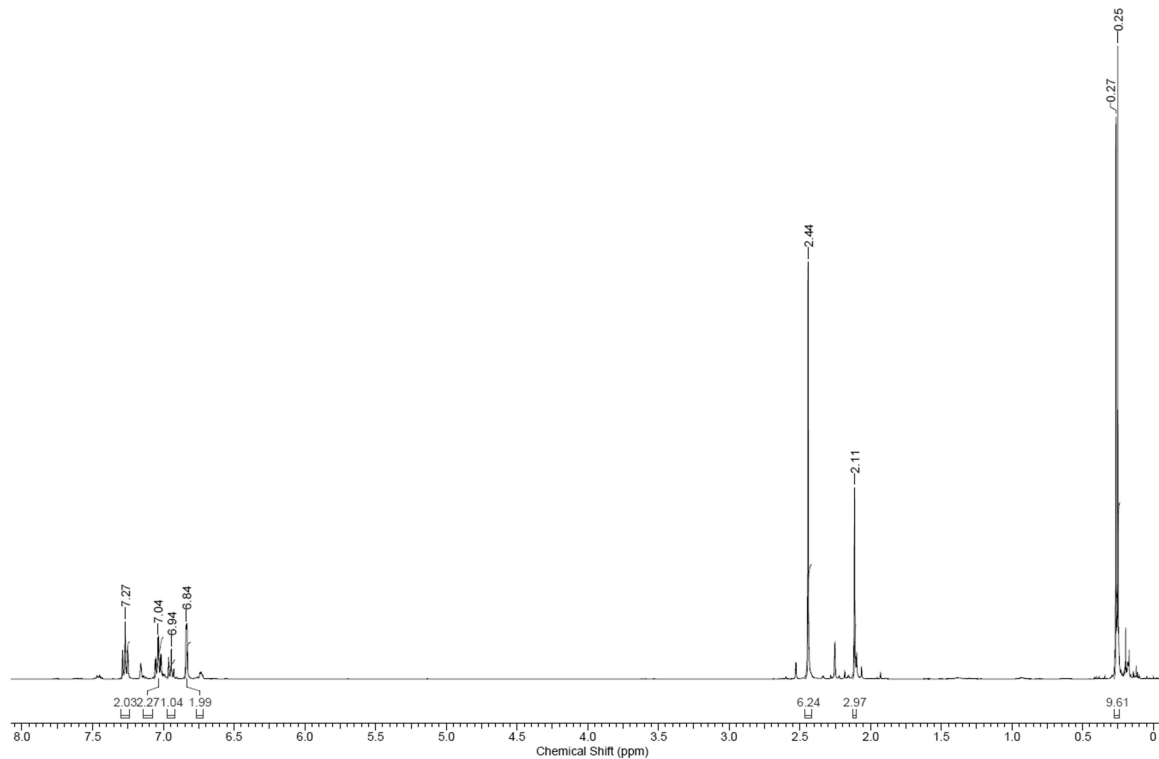


Figure 7.3.17. ^1H NMR spectrum of $\mathbf{7}^{\text{Mes}}$ in C_6D_6 .

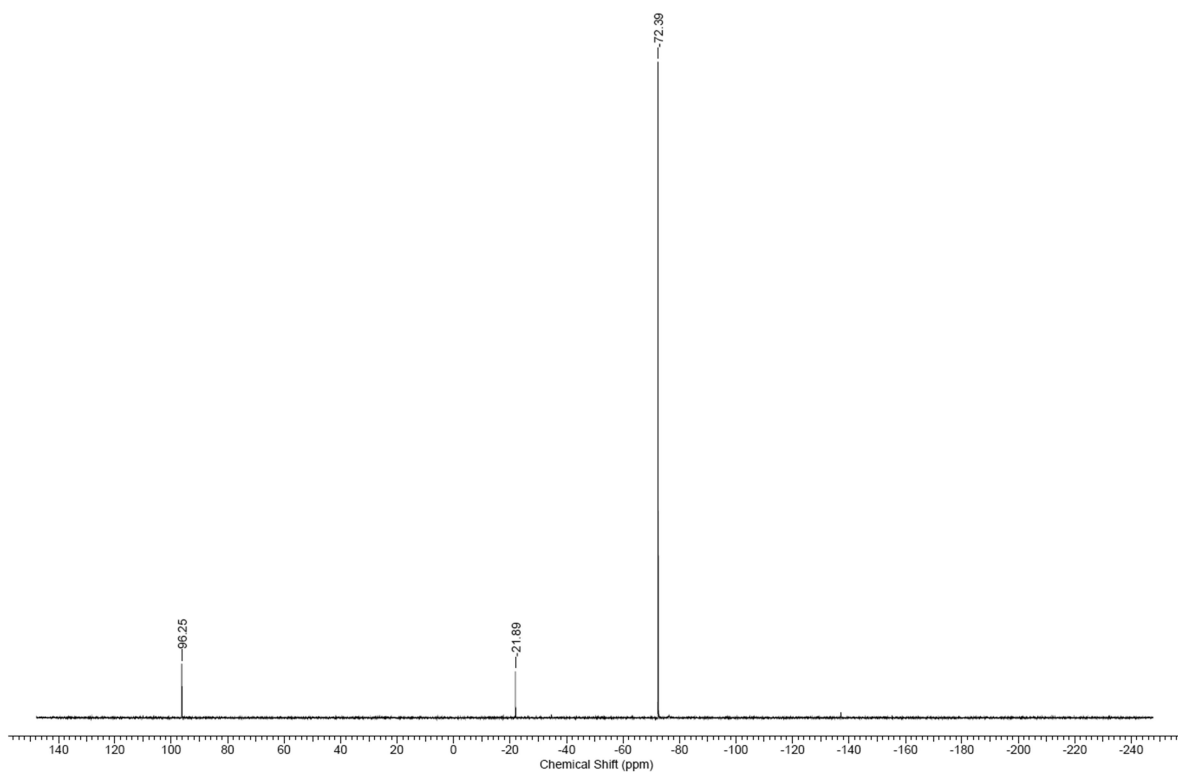


Figure 7.3.18. $^{31}\text{P}\{\text{H}\}$ NMR spectrum of 7^{Mes} in C_6D_6 .

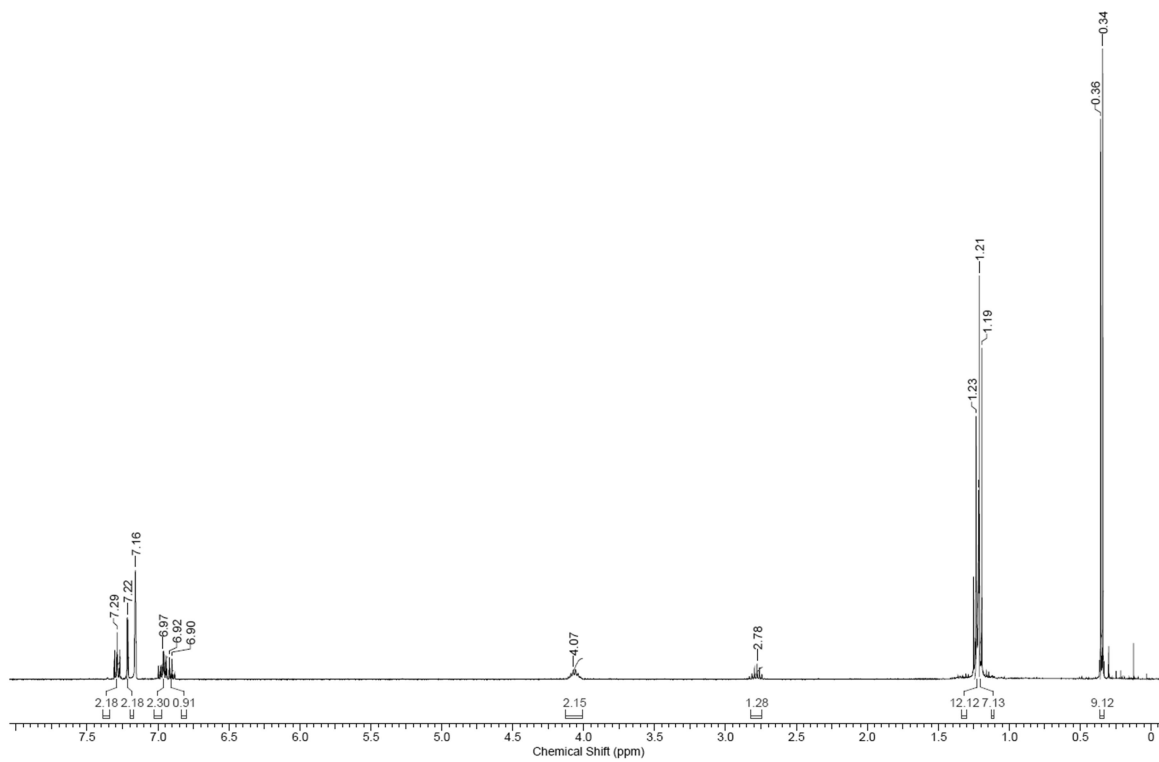


Figure 7.3.19. ^1H NMR spectrum of 7^{Tip} in C_6D_6 .

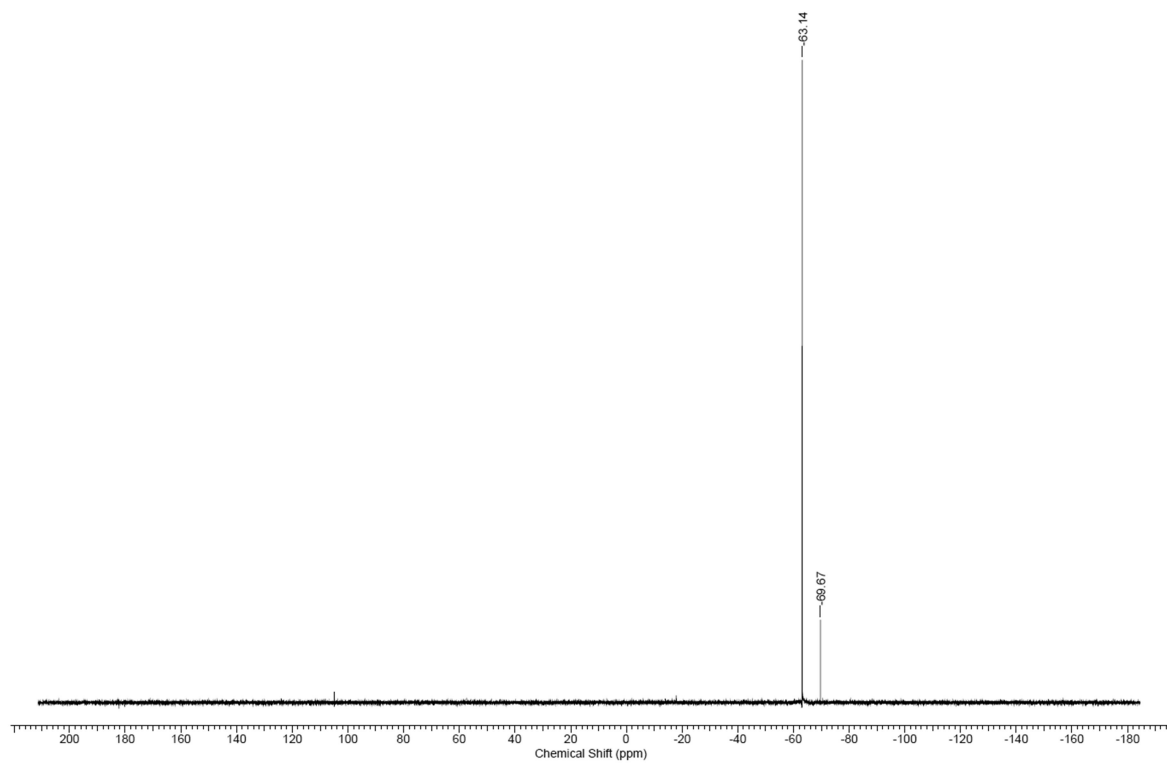


Figure 7.3.20. $^{31}\text{P}\{\text{H}\}$ NMR spectrum of 7^{Tip} in C_6D_6 .

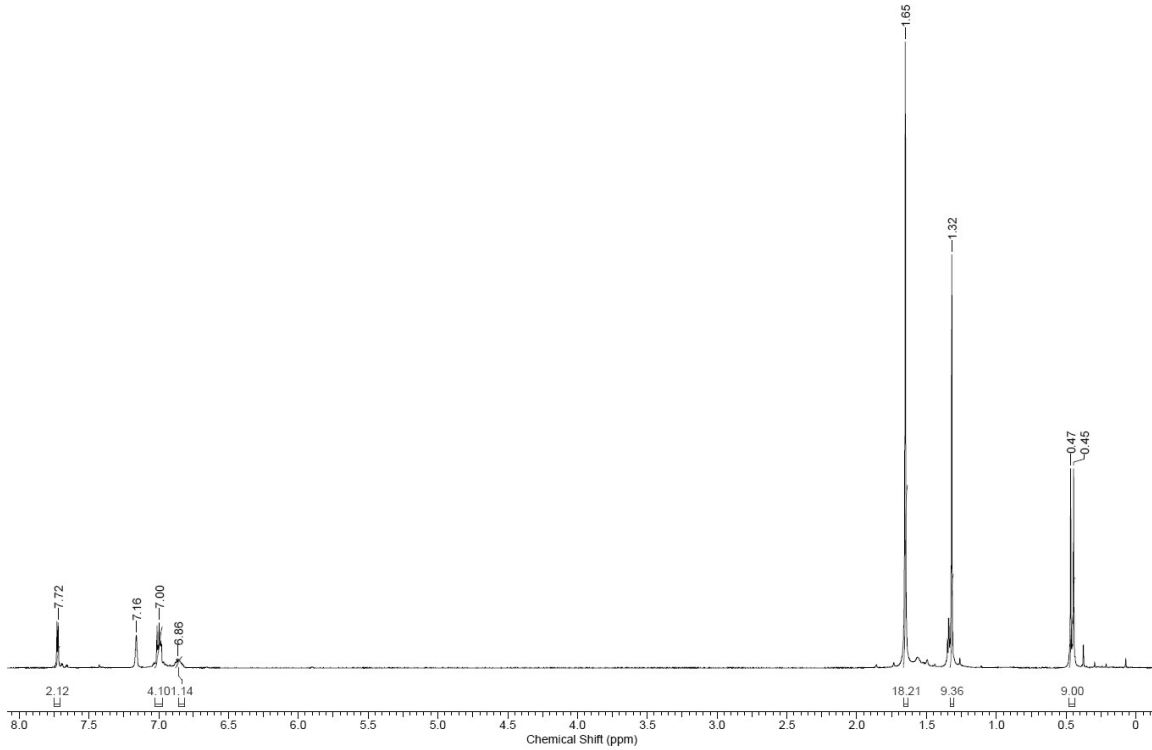


Figure 7.3.21. ^1H NMR spectrum of 7^{Mes^*} in C_6D_6 .

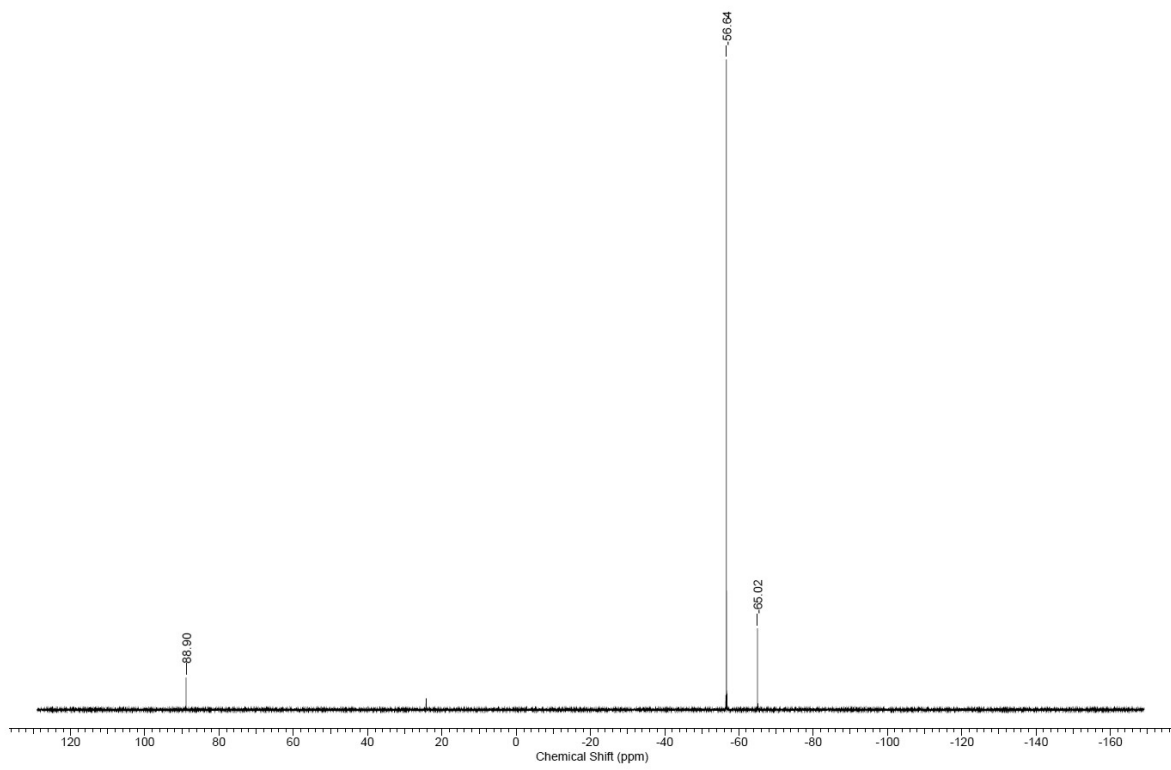


Figure 7.3.22. $^{31}\text{P}\{\text{H}\}$ NMR spectrum of $7^{\text{Mes}*}$ in C_6D_6 .

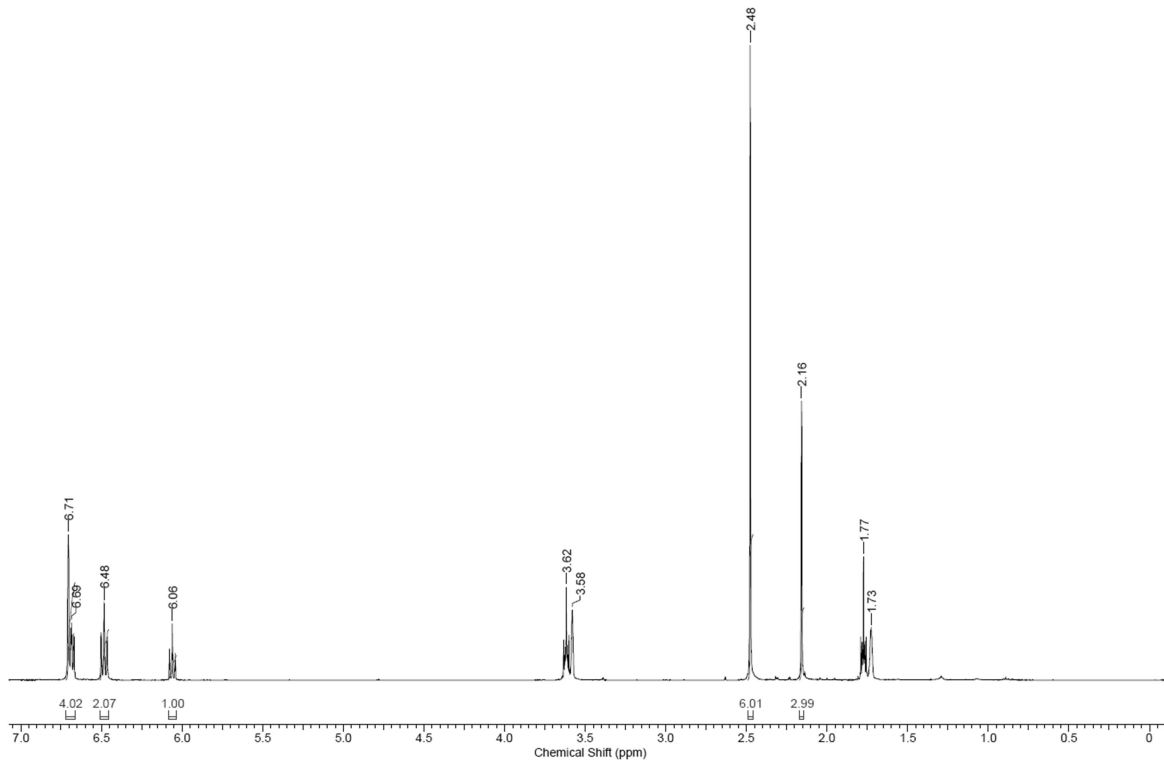


Figure 7.3.23. ^1H NMR spectrum of 9^{Mes} in THF-d_8 .

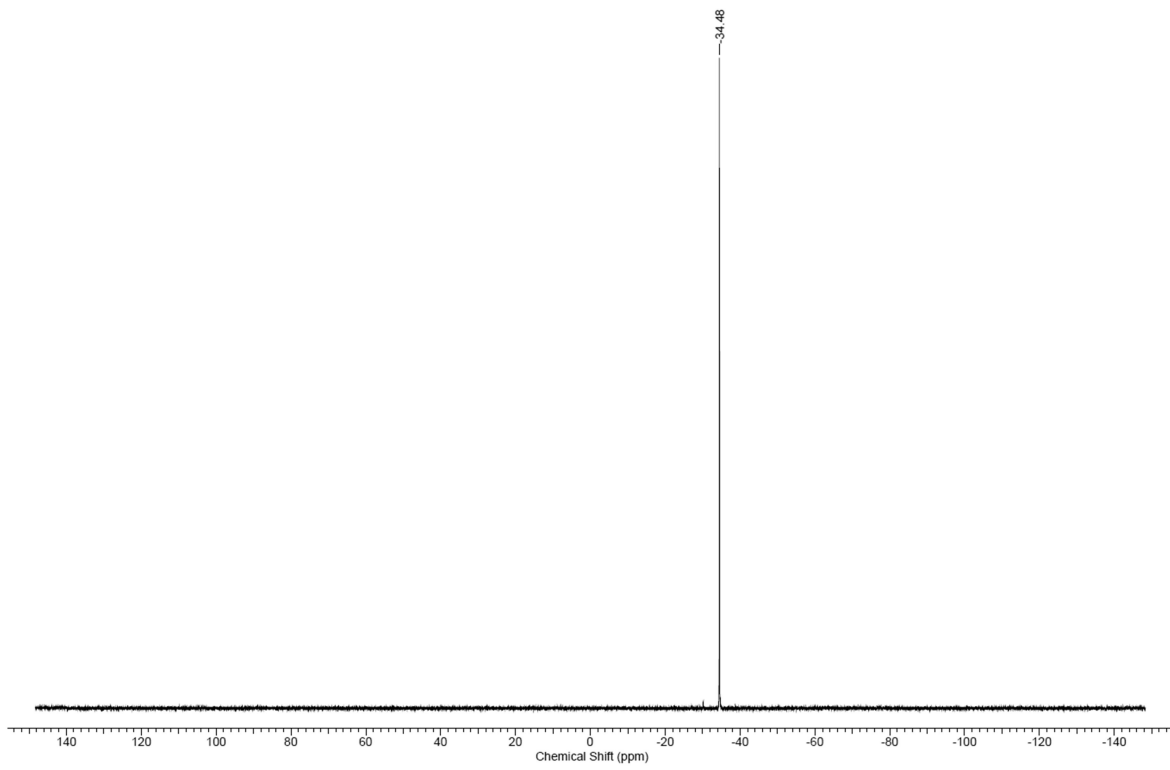


Figure 7.3.24. $^{31}\text{P}\{\text{H}\}$ NMR spectrum of $\mathbf{9}^{\text{Mes}}$ in THF-d_8 .

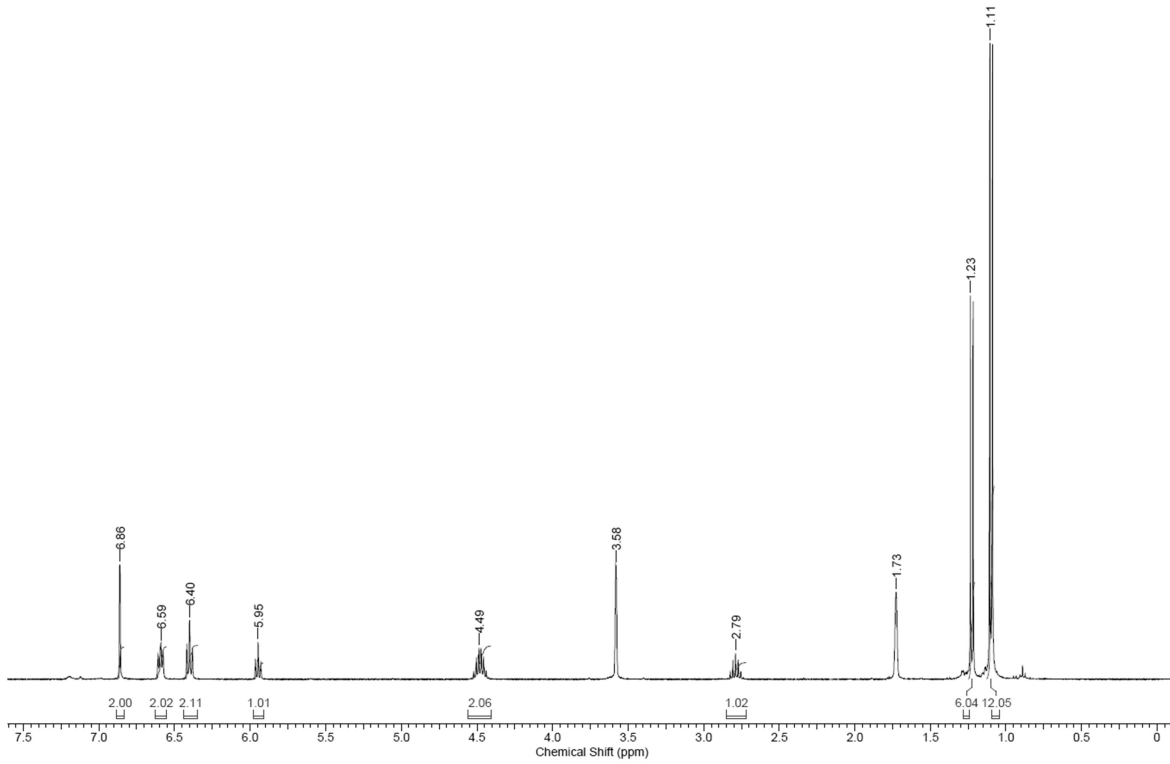


Figure 7.3.25. ^1H NMR spectrum of $\mathbf{9}^{\text{Tip}}$ in THF-d_8 .

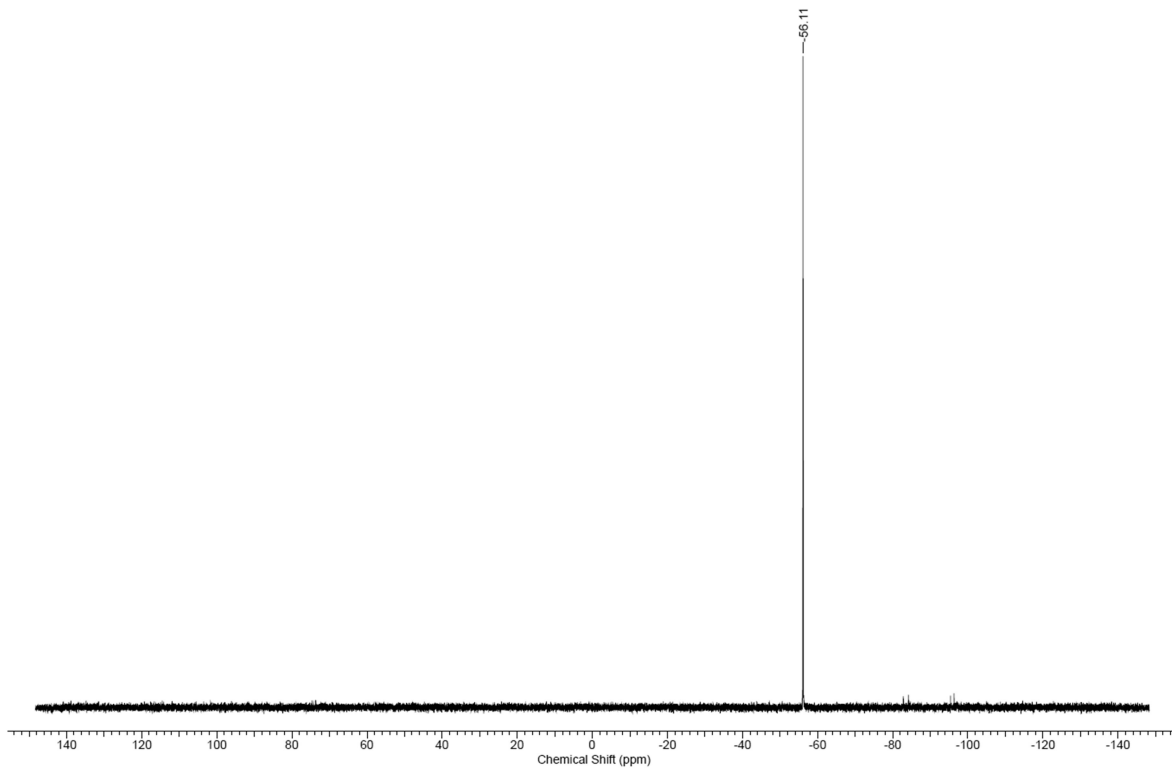


Figure 7.3.26. $^{31}\text{P}\{\text{H}\}$ NMR spectrum of $\mathbf{9}^{\text{Tip}}$ in THF-d_8 .

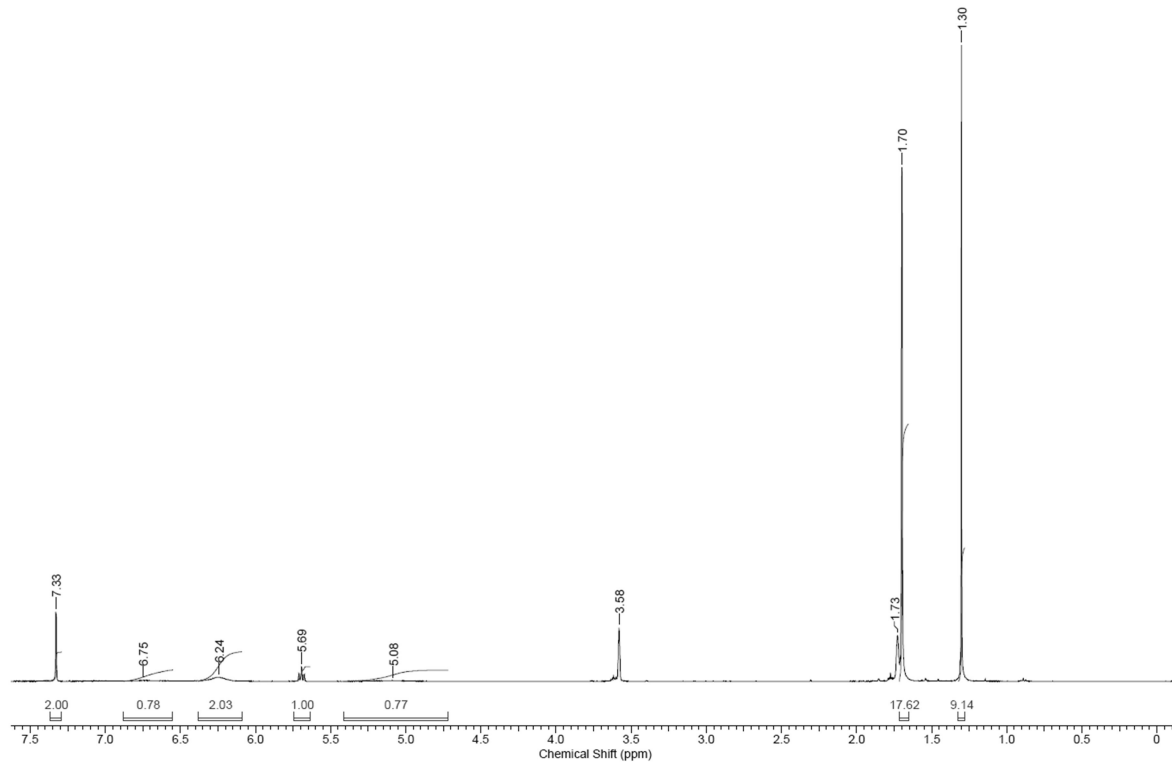


Figure 7.3.27. ^1H NMR spectrum of $\mathbf{9}^{\text{Mes}^*}$ in THF-d_8 .

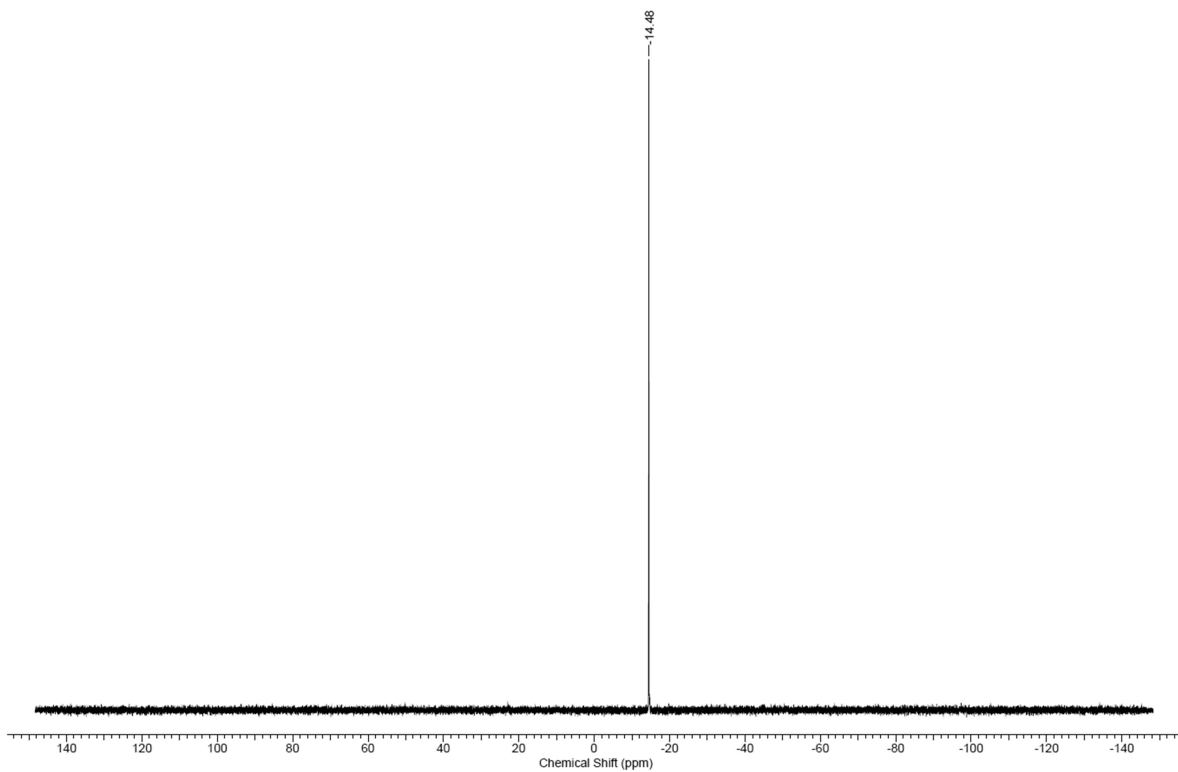


Figure 7.3.28. $^{31}\text{P}\{\text{H}\}$ NMR spectrum of $\mathbf{9}^{\text{Mes}*}$ in THF-d_8 .

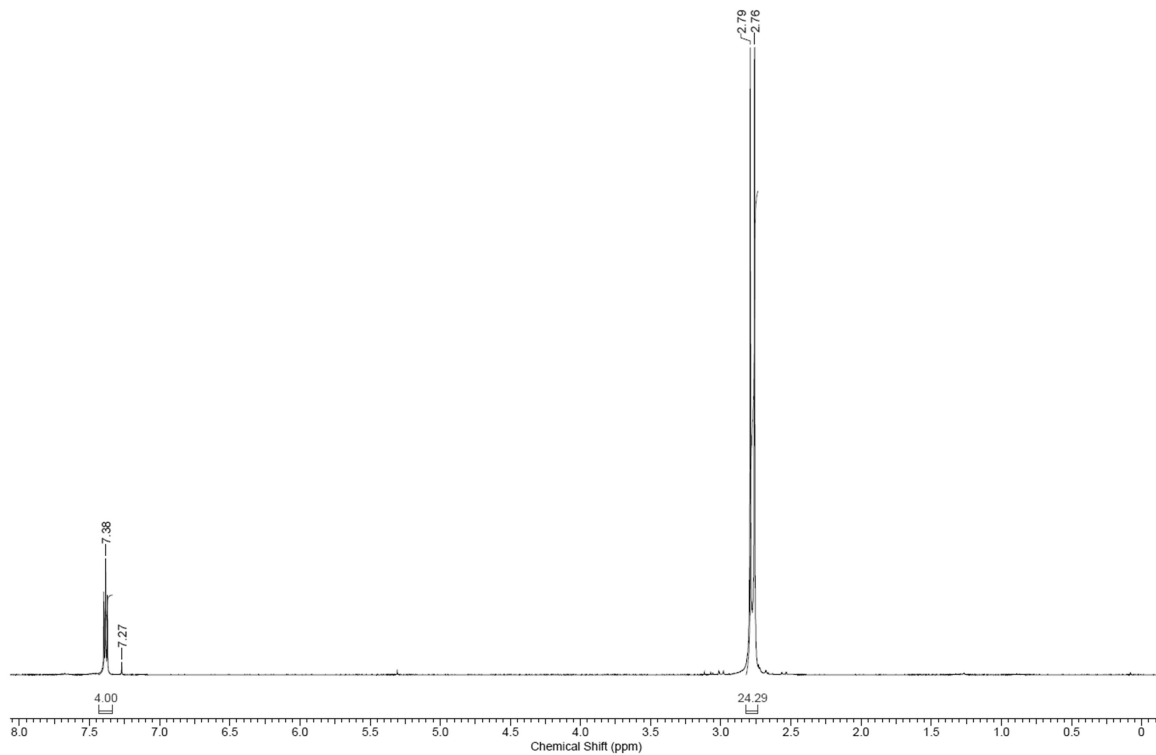


Figure 7.3.29. ^1H NMR spectrum of *p*-phenylene-bis(*N,N,N',N'*-tetramethyl-phosphanediamine) in CDCl_3 .

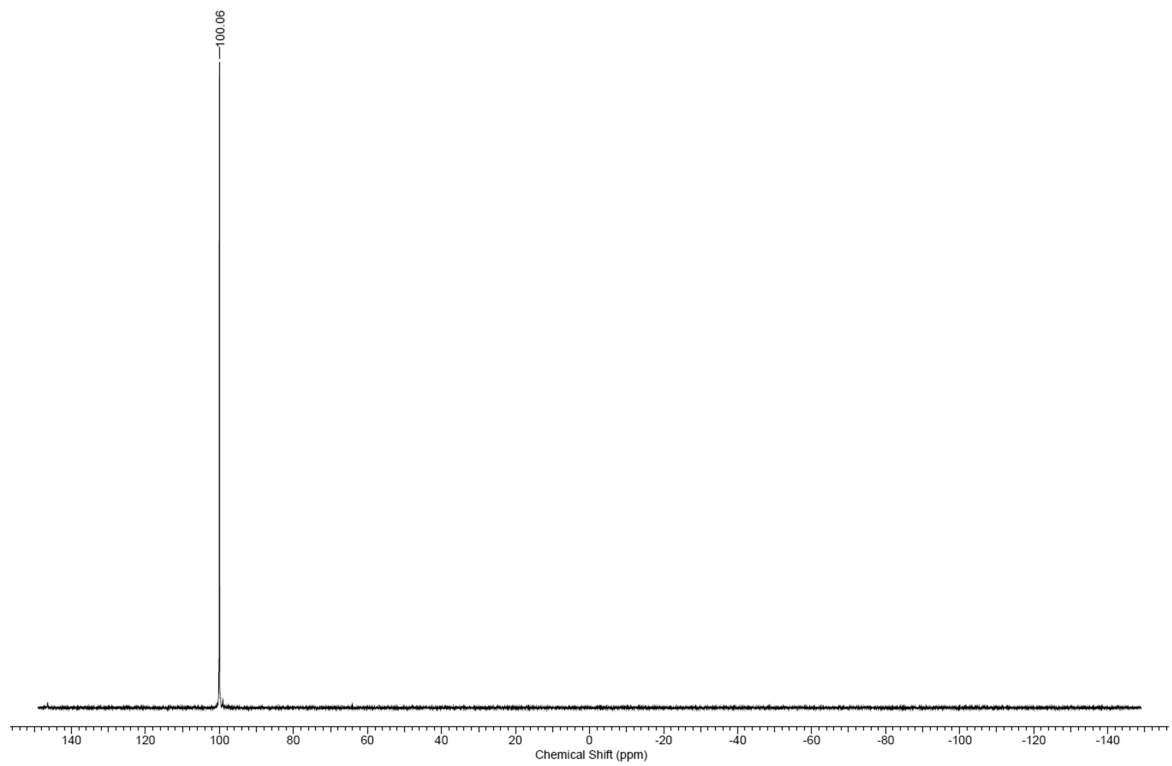


Figure 7.3.30. $^{31}\text{P}\{\text{H}\}$ NMR spectrum of *p*-phenylene-bis(*N,N,N',N'*-tetramethyl-phosphanediamine) in CDCl_3 .

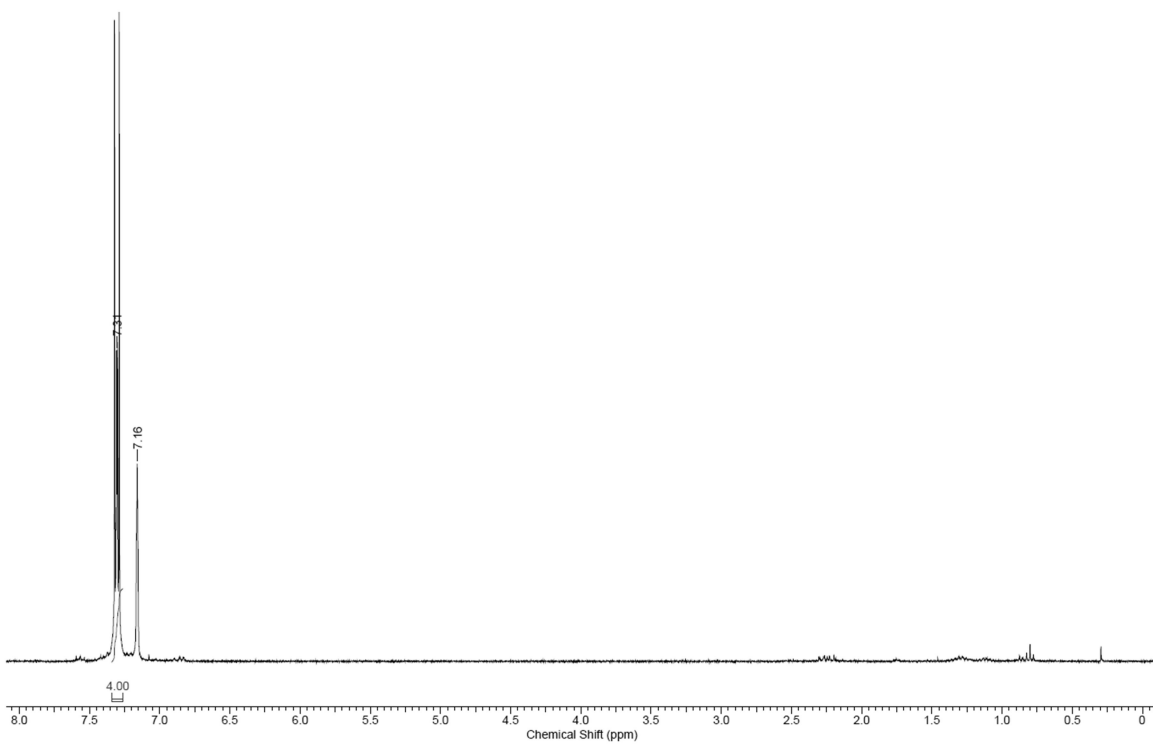


Figure 7.3.31. ^1H NMR spectrum of *p*-phenylene-bis(dichlorophosphine) in C_6D_6 .

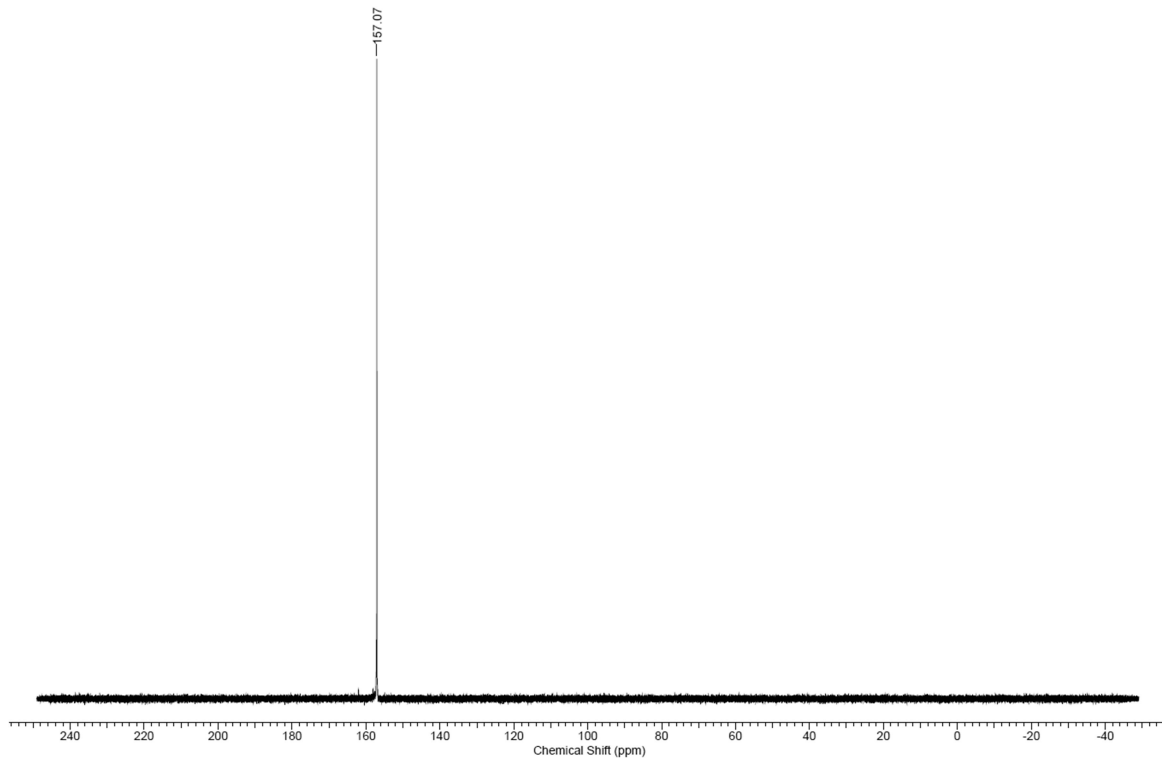


Figure 7.3.32. $^{31}\text{P}\{\text{H}\}$ NMR spectrum of *p*-phenylene-bis(dichlorophosphine) in C_6D_6 .

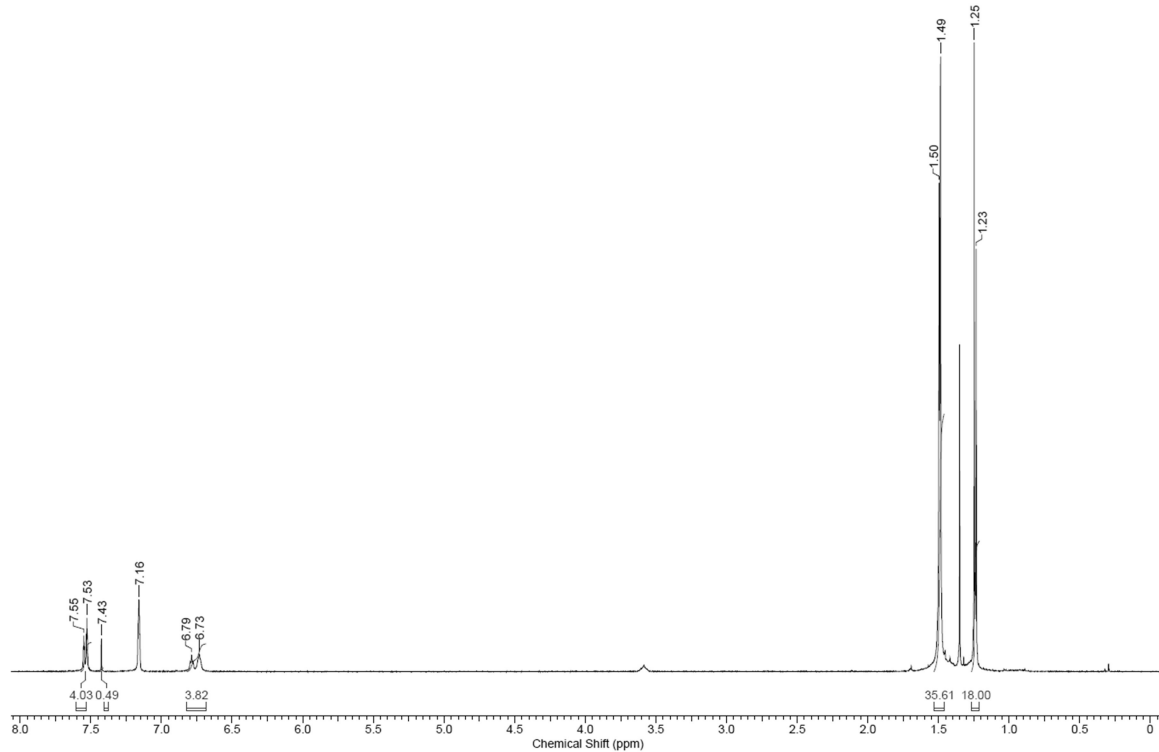


Figure 7.3.33. ^1H NMR spectrum of *p*-phenylene-bis[(2,4,6-tris-*tert*-butylphenyl)chlorophosphine] in C_6D_6 .

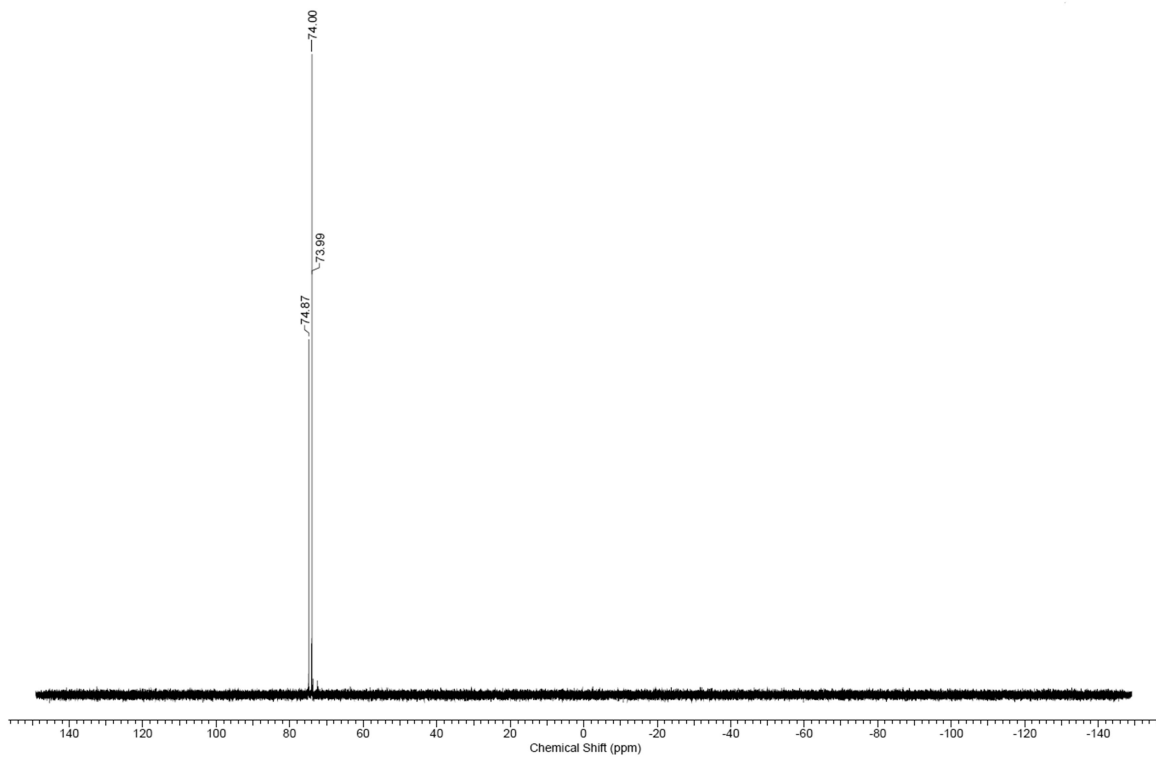


Figure 7.3.34. $^{31}\text{P}\{\text{H}\}$ NMR spectrum of *p*-phenylene-bis[(2,4,6-tris-*tert*-butylphenyl)chlorophosphine] in C_6D_6 .

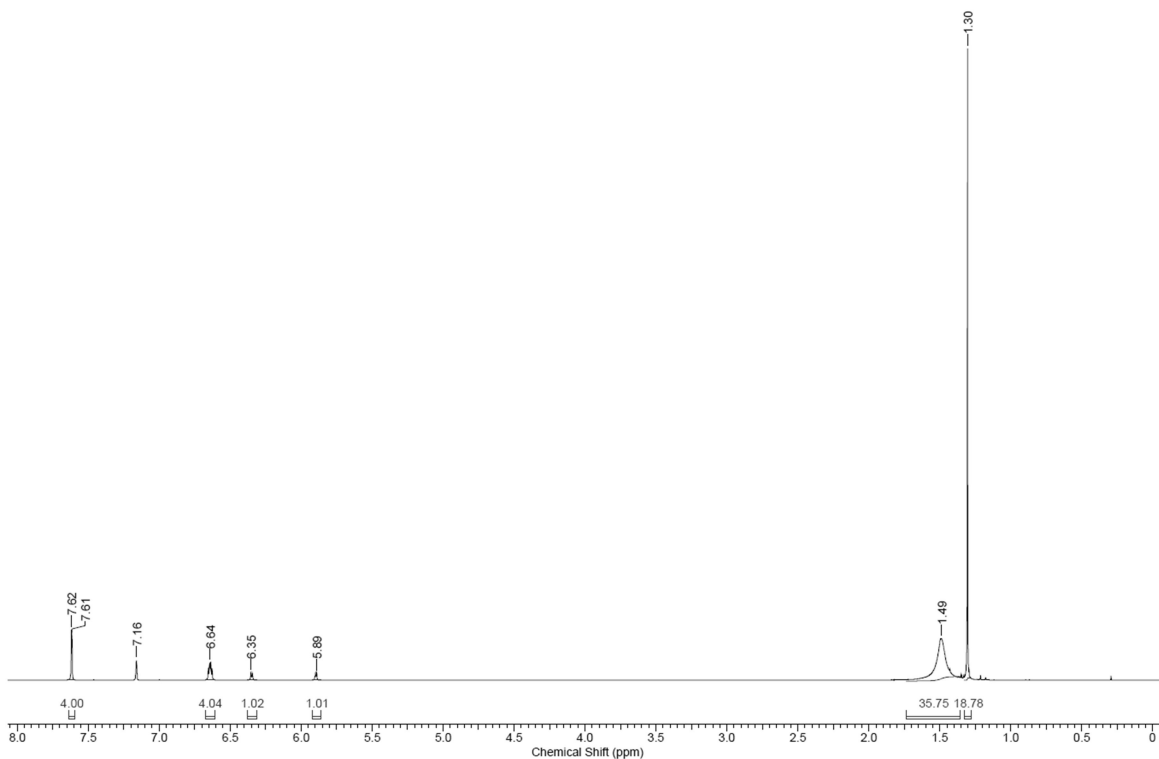


Figure 7.3.35. ^1H NMR spectrum of **11** in C_6D_6 .

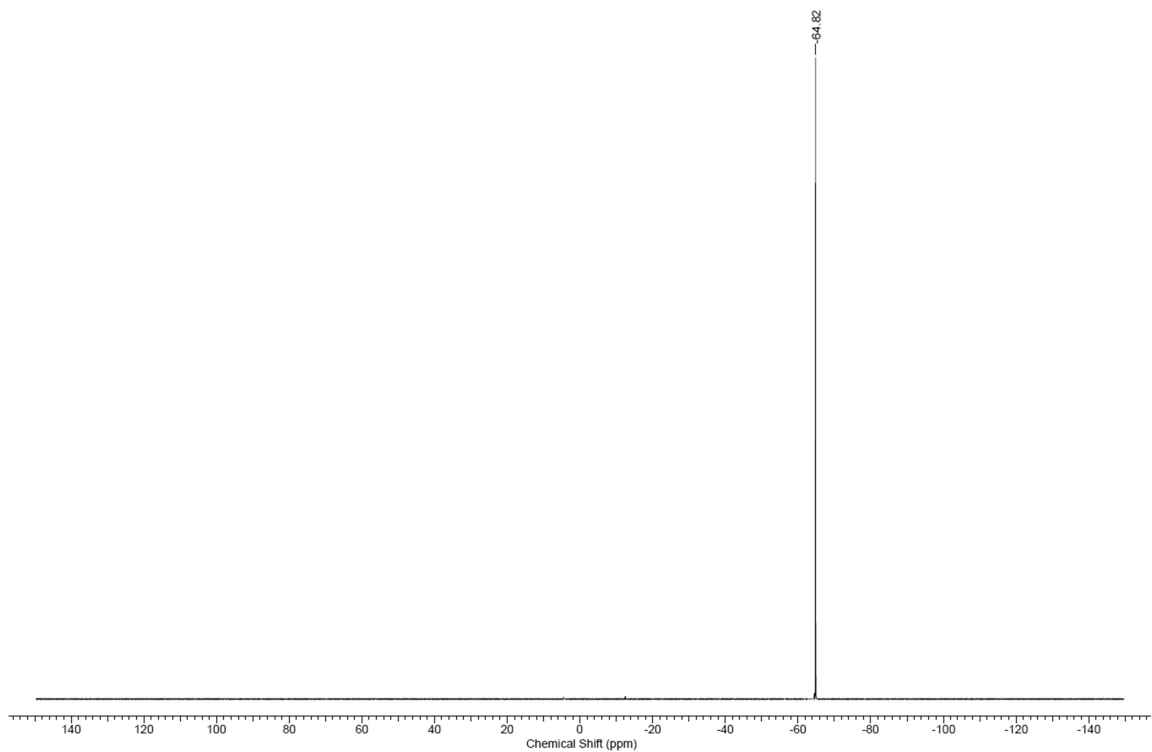


Figure 7.3.36. ${}^{31}\text{P}\{{}^1\text{H}\}$ NMR spectrum of **11** in C_6D_6 .

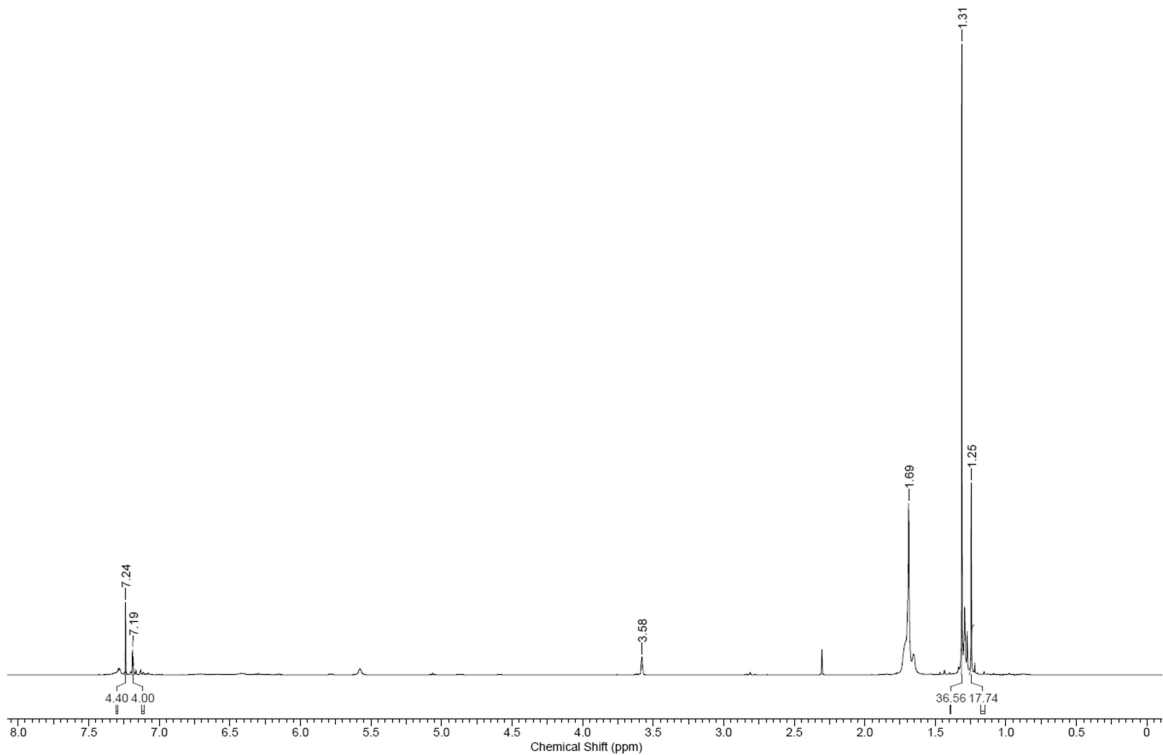


Figure 7.3.37. ${}^1\text{H}$ NMR spectrum of **14** in $\text{THF}-\text{d}_8$.

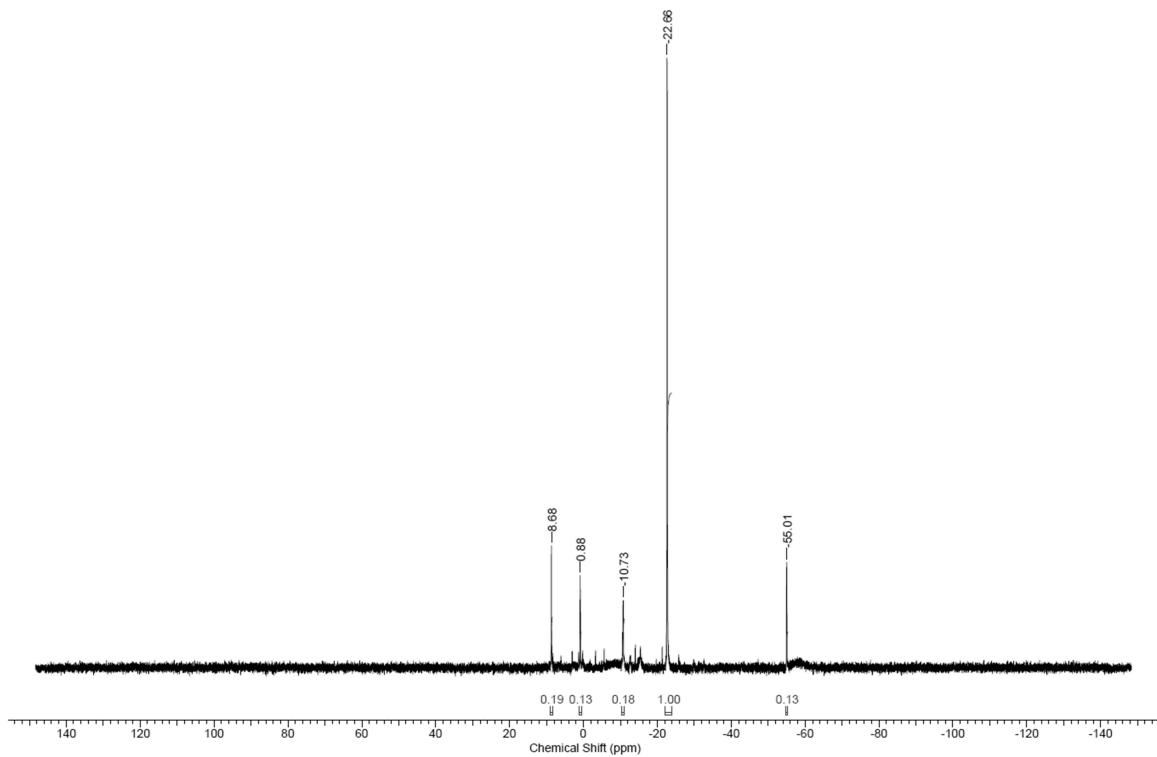


Figure 7.3.38. $^{31}\text{P}\{\text{H}\}$ NMR spectrum of **14** in THF-d_8 .

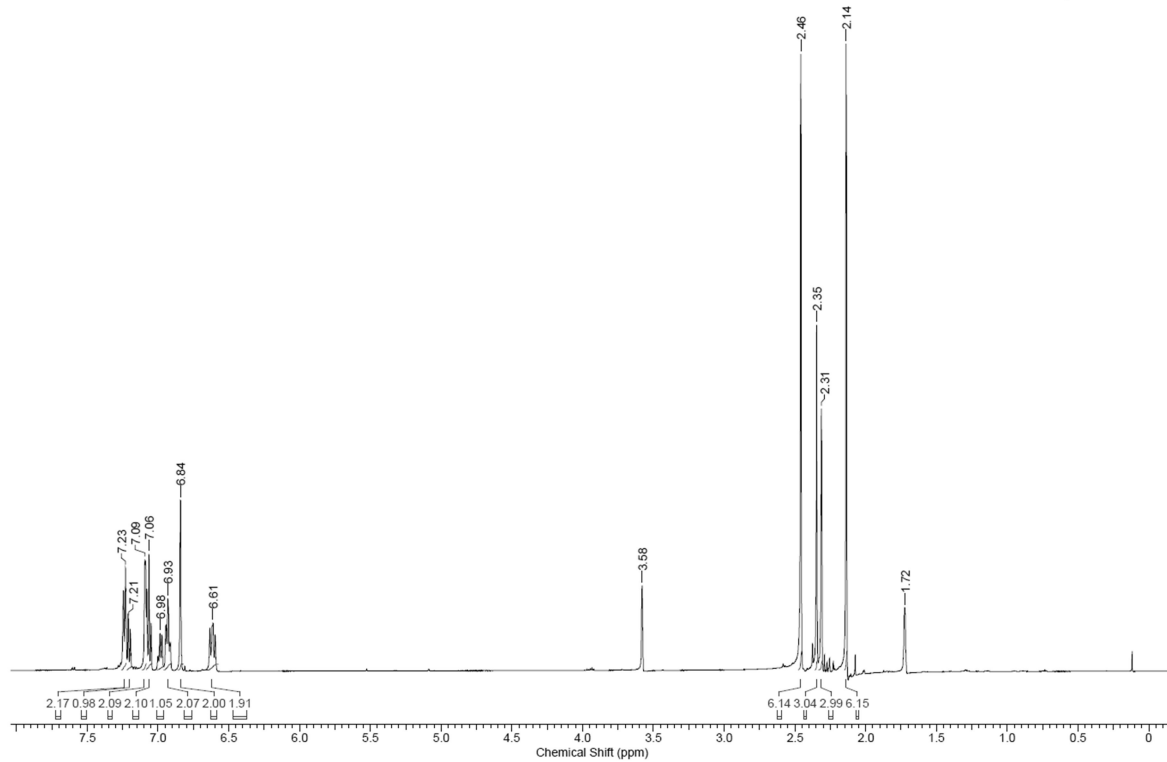


Figure 7.3.39. ^1H NMR spectrum of $\mathbf{1}^{\text{Mes}}$ in THF-d_8 .

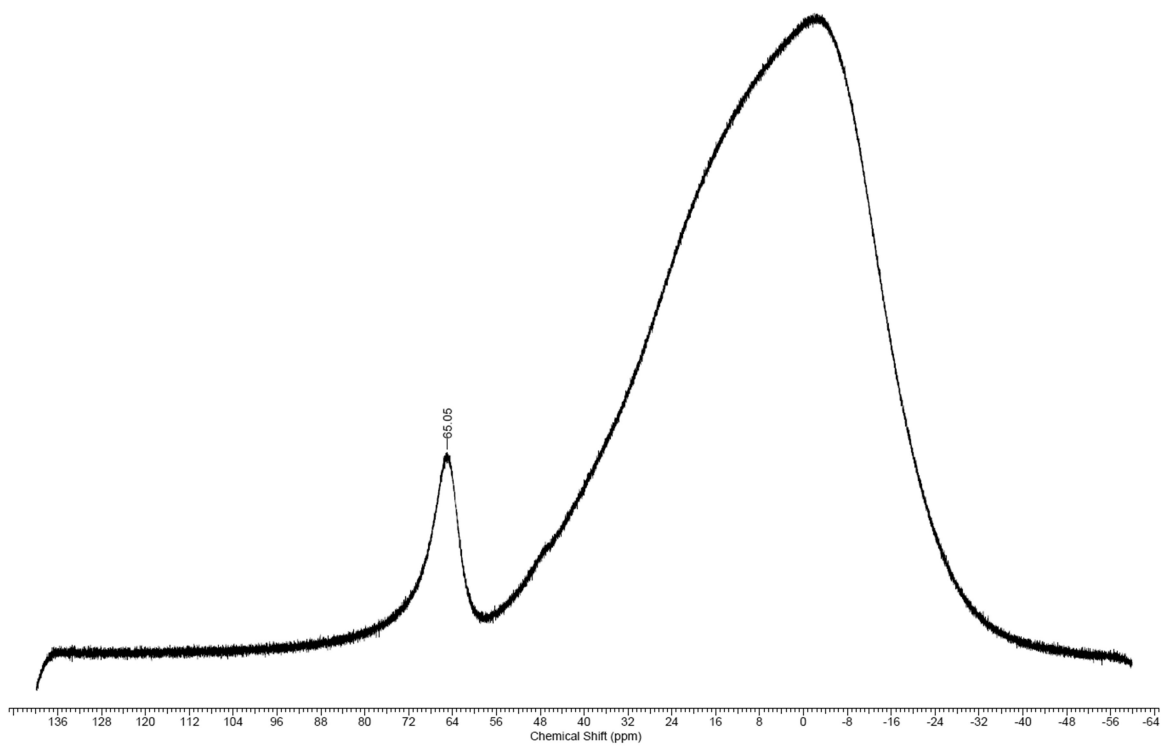


Figure 7.3.40. $^{11}\text{B}\{^1\text{H}\}$ NMR spectrum of $\mathbf{1}^{\text{Mes}}$ in THF-d_8 .

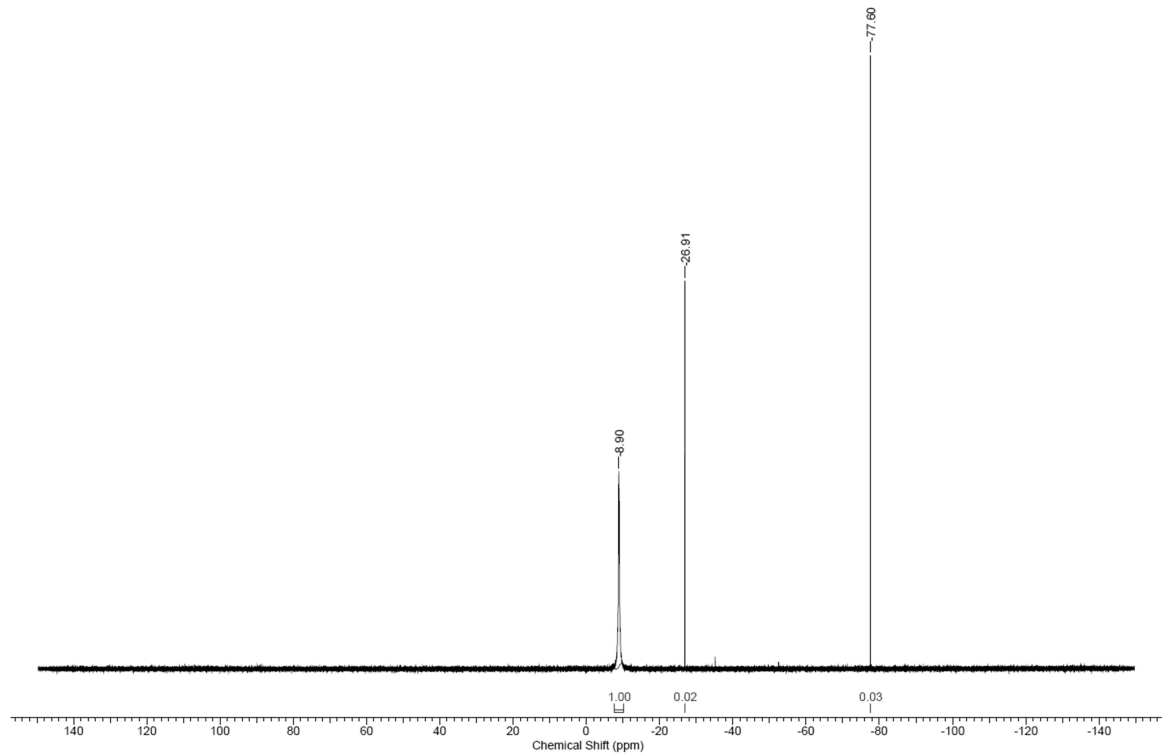


Figure 7.3.41. $^{31}\text{P}\{^1\text{H}\}$ NMR spectrum of $\mathbf{1}^{\text{Mes}}$ in THF-d_8 .

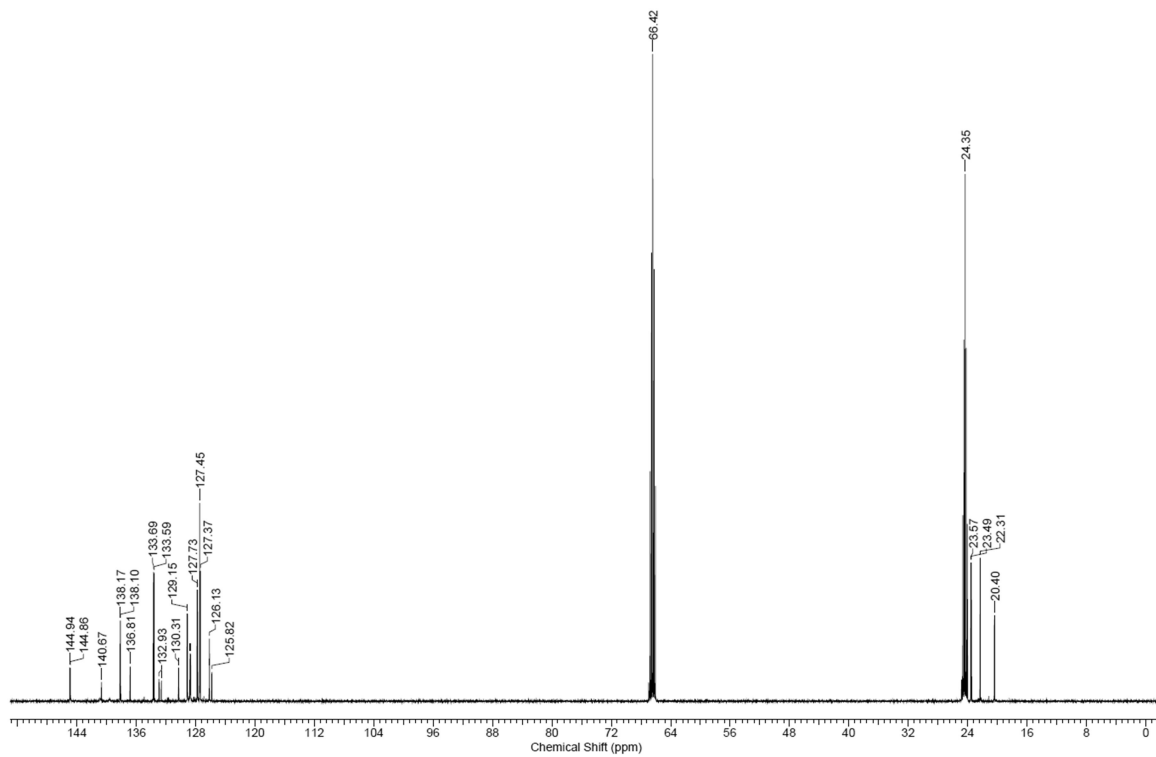


Figure 7.3.42. $^{13}\text{C}\{^1\text{H}\}$ NMR spectrum of $\mathbf{1}^{\text{Mes}}$ in THF-d_8 .

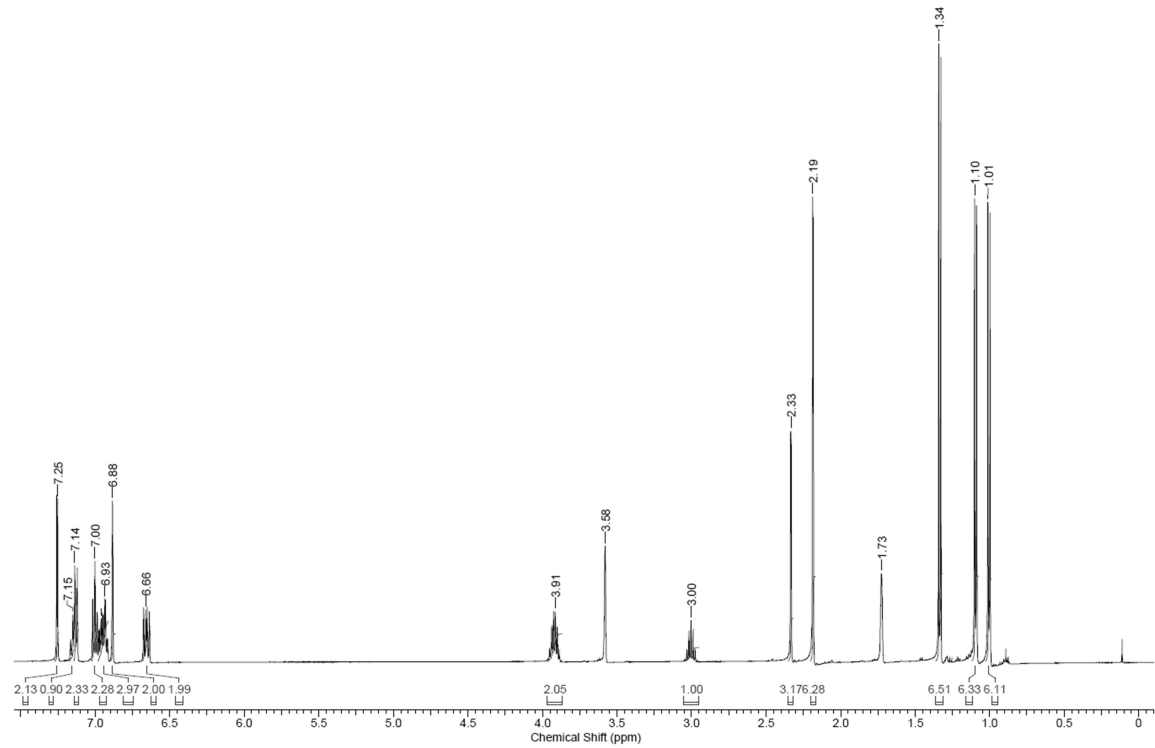


Figure 7.3.43. ^1H NMR spectrum of $\mathbf{1}^{\text{Tip}}$ in THF-d_8 .

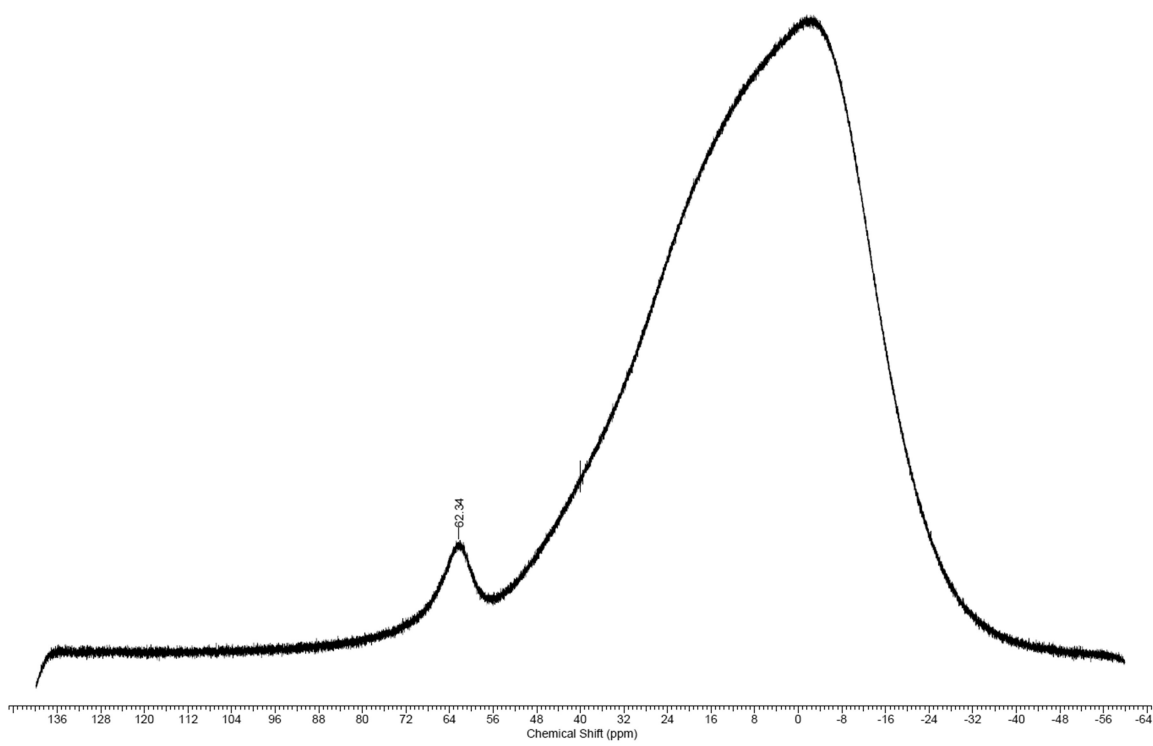


Figure 7.3.44. $^{11}\text{B}\{\text{H}\}$ NMR spectrum of $\mathbf{1}^{\text{Tip}}$ in THF-d_8 .

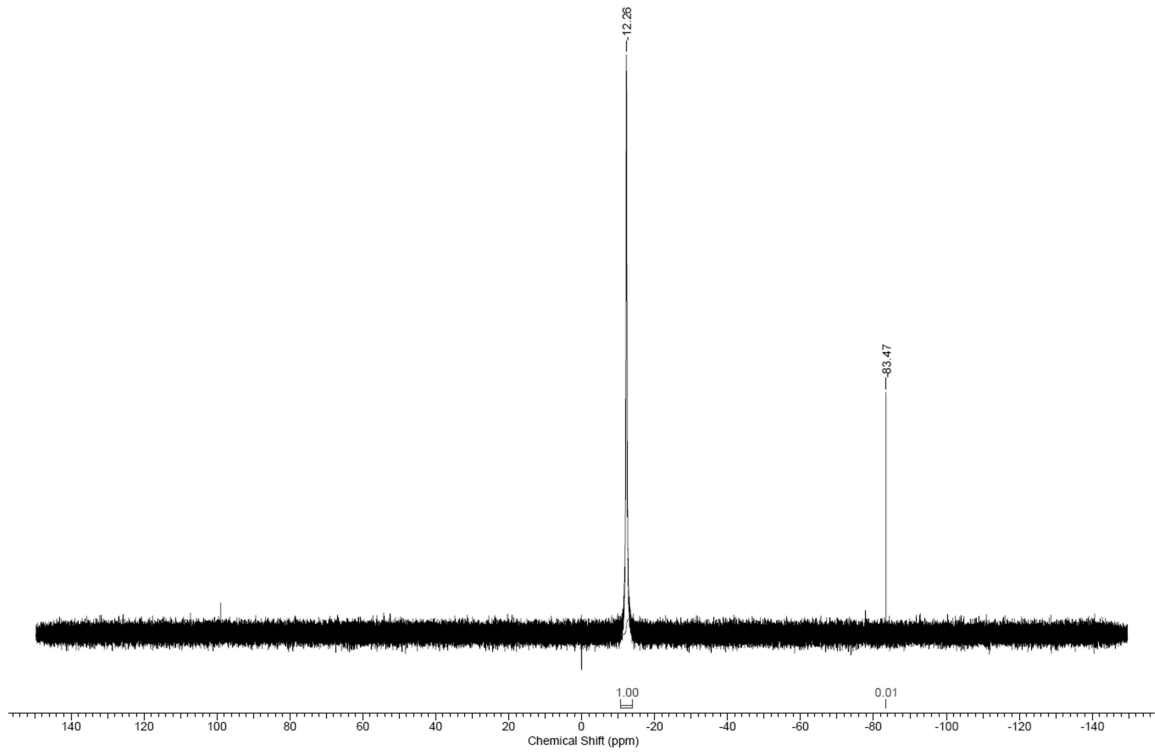


Figure 7.3.45. $^{31}\text{P}\{\text{H}\}$ NMR spectrum of $\mathbf{1}^{\text{Tip}}$ in THF-d_8 .

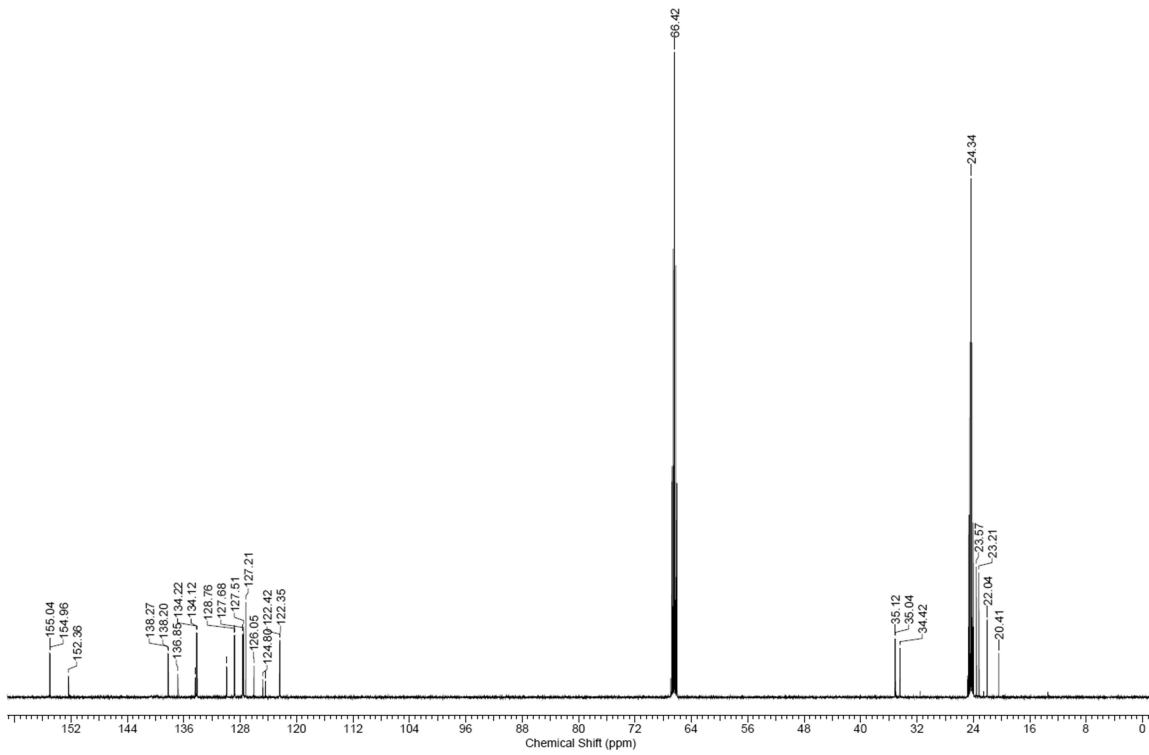


Figure 7.3.46. $^{13}\text{C}\{^1\text{H}\}$ NMR spectrum of $\mathbf{1}^{\text{Tip}}$ in THF-d_8 .

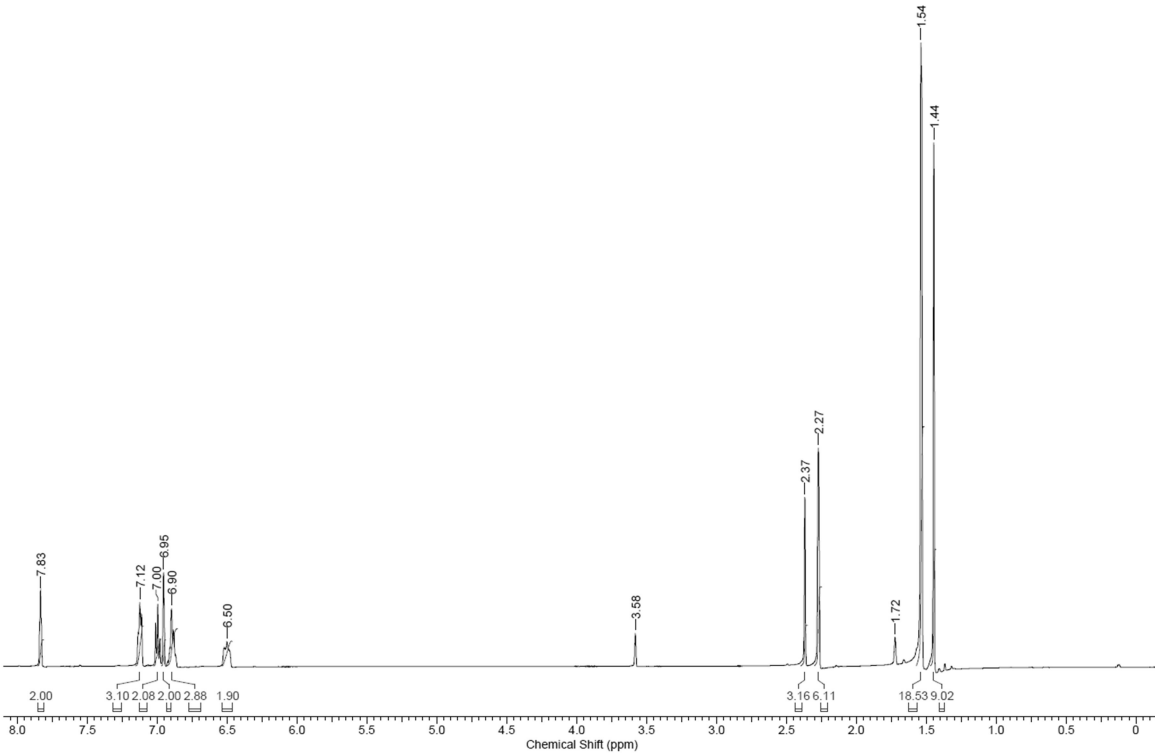


Figure 7.3.47. ^1H NMR spectrum of $\mathbf{1}^{\text{Mes}^*}$ in THF-d_8 .

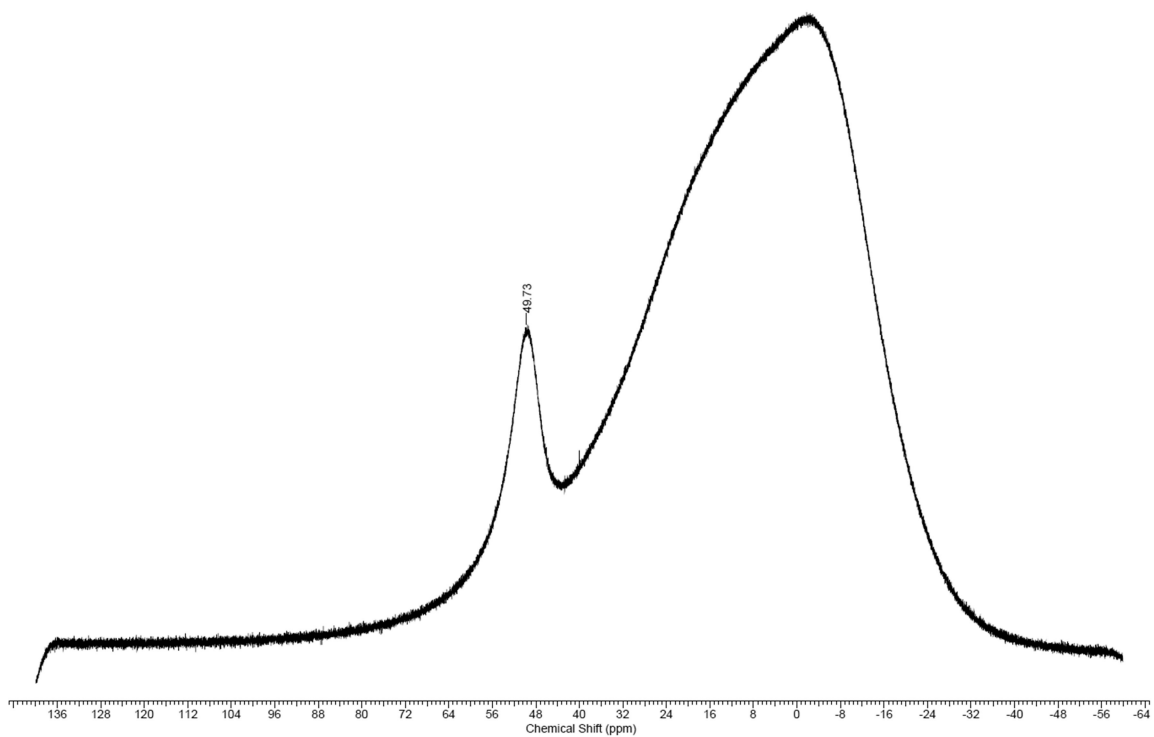


Figure 7.3.48. $^{11}\text{B}\{\text{H}\}$ NMR spectrum of $\mathbf{1}^{\text{Mes}^*}$ in THF-d_8 .

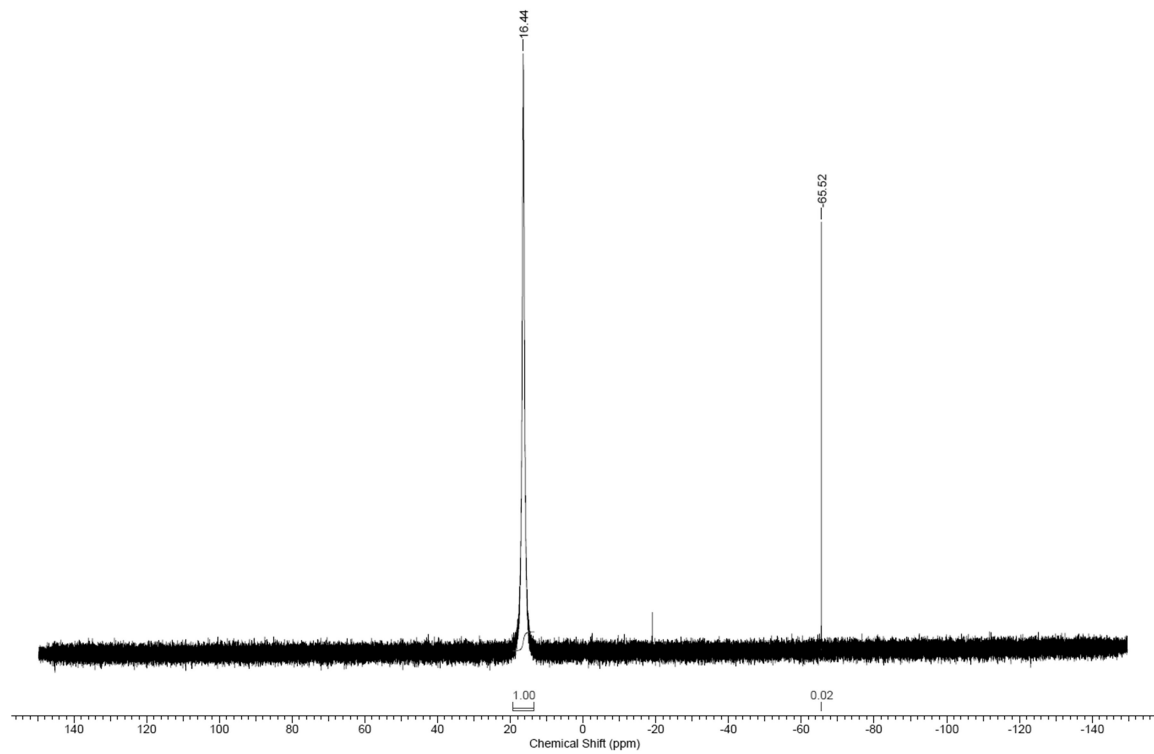


Figure 7.3.49. $^{31}\text{P}\{\text{H}\}$ NMR spectrum of $\mathbf{1}^{\text{Mes}^*}$ in THF-d_8 .

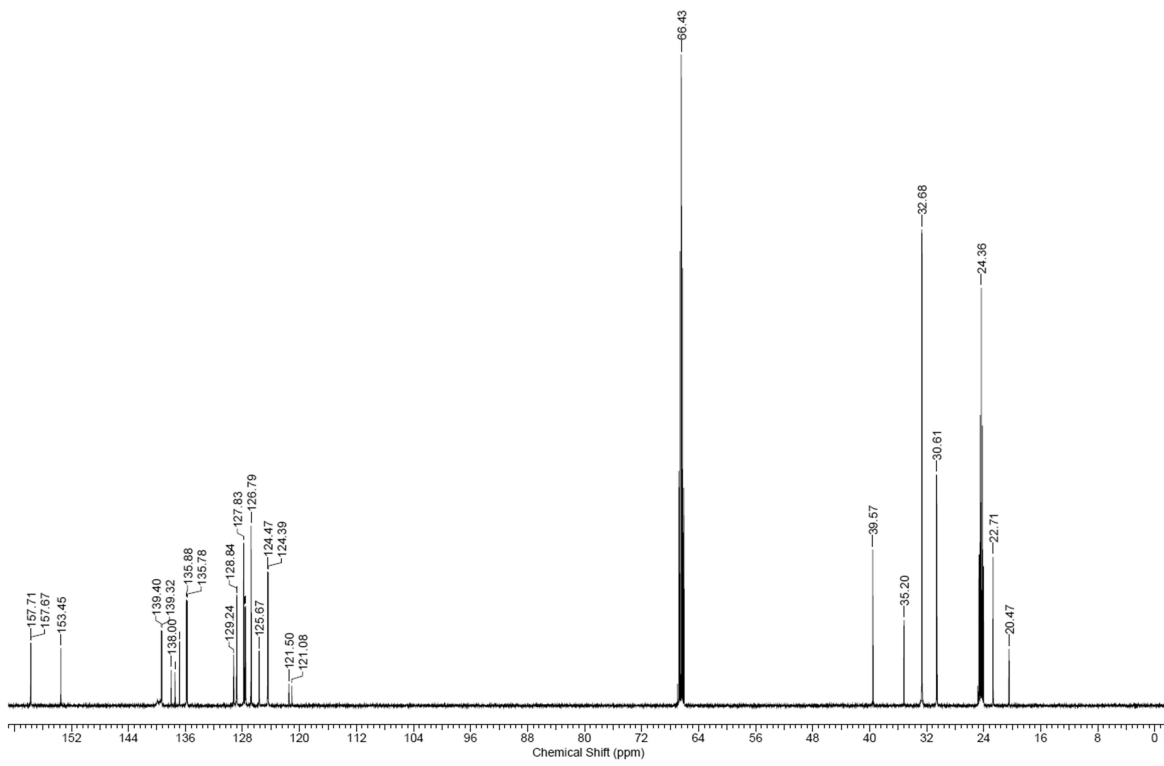


Figure 7.3.50. $^{13}\text{C}\{^1\text{H}\}$ NMR spectrum of $\mathbf{1}^{\text{Mes}^*}$ in THF-d_8 .

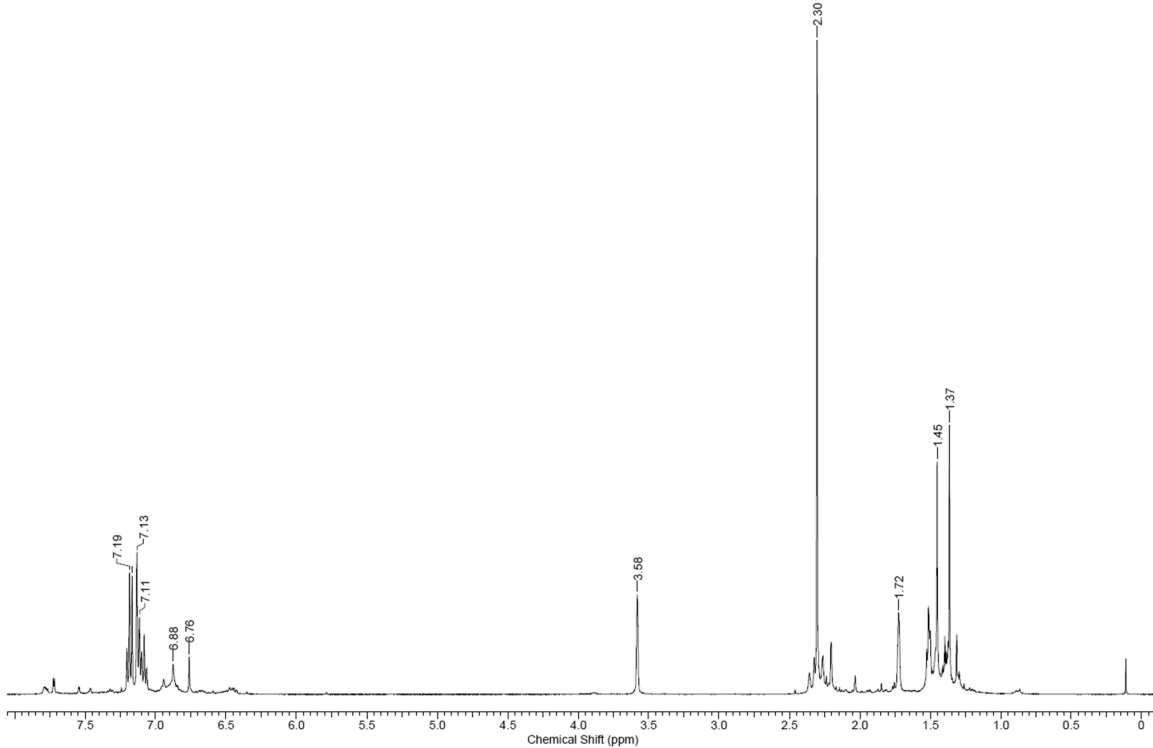


Figure 7.3.51. ^1H NMR spectrum of $\mathbf{2}$ in THF-d_8 .

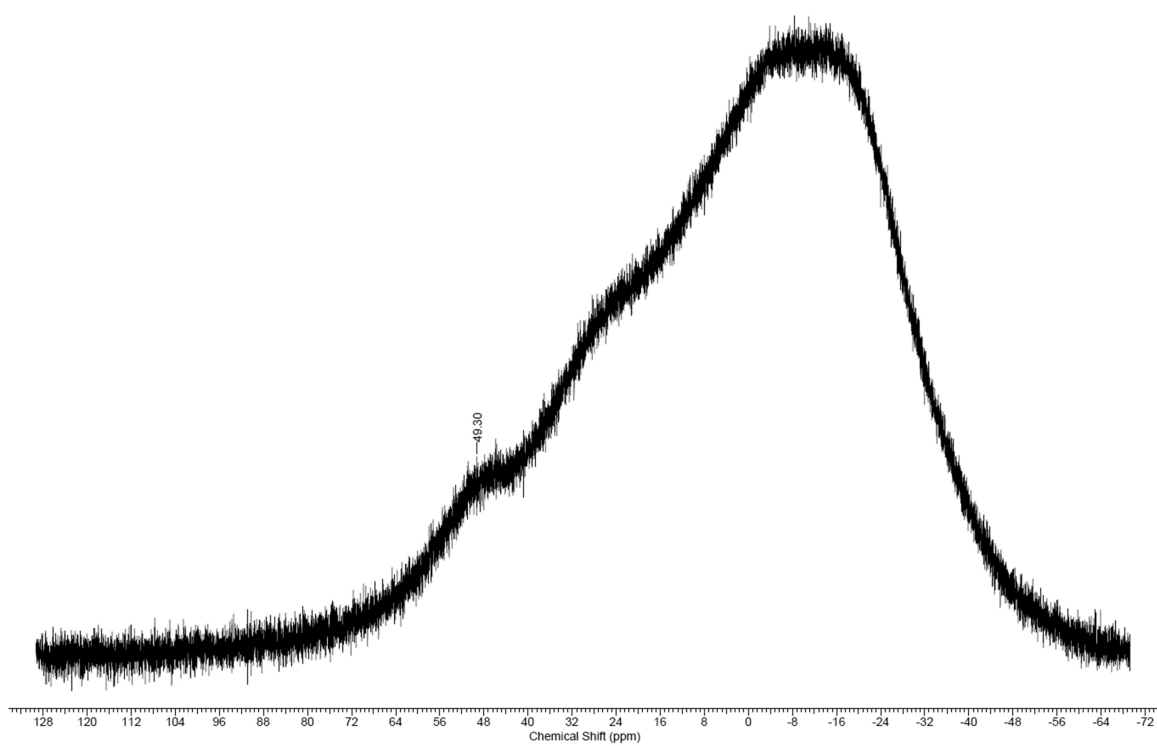


Figure 7.3.52. $^{11}\text{B}\{^1\text{H}\}$ NMR spectrum of **2** in THF-d_8 .

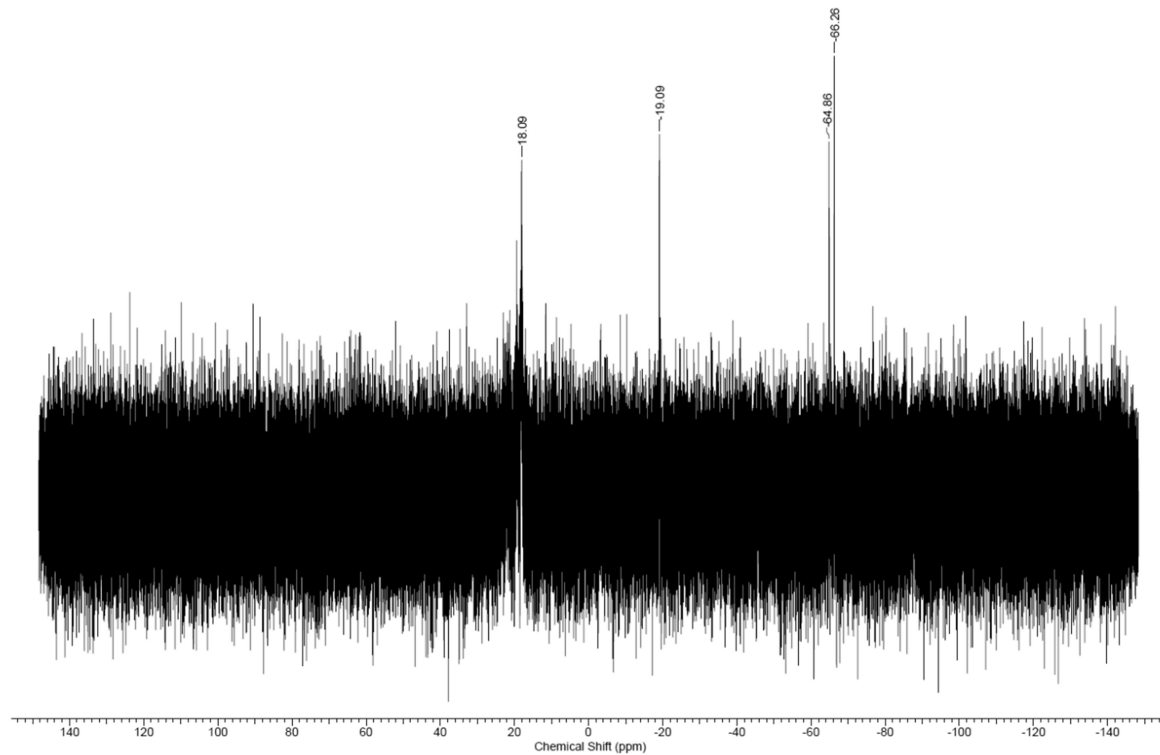


Figure 7.3.53. $^{31}\text{P}\{^1\text{H}\}$ NMR spectrum of **2** in THF-d_8 .

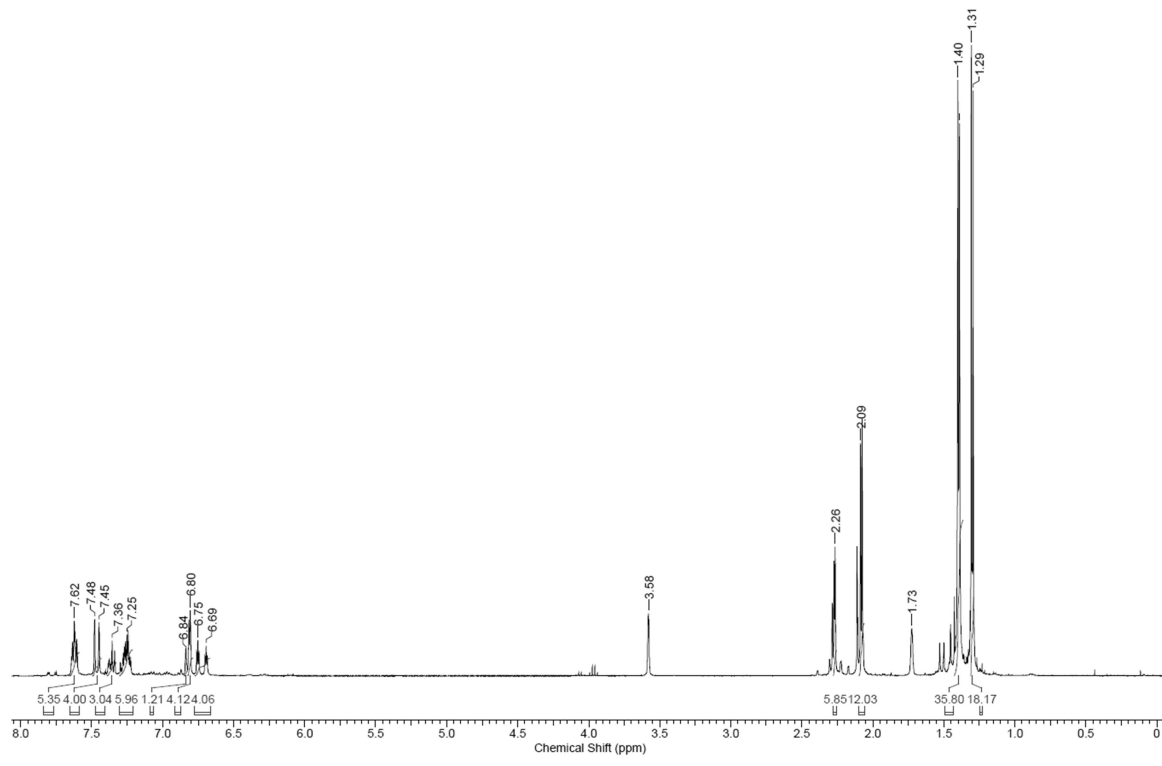


Figure 7.3.54. ^1H NMR spectrum of **3** in THF-d_8 .

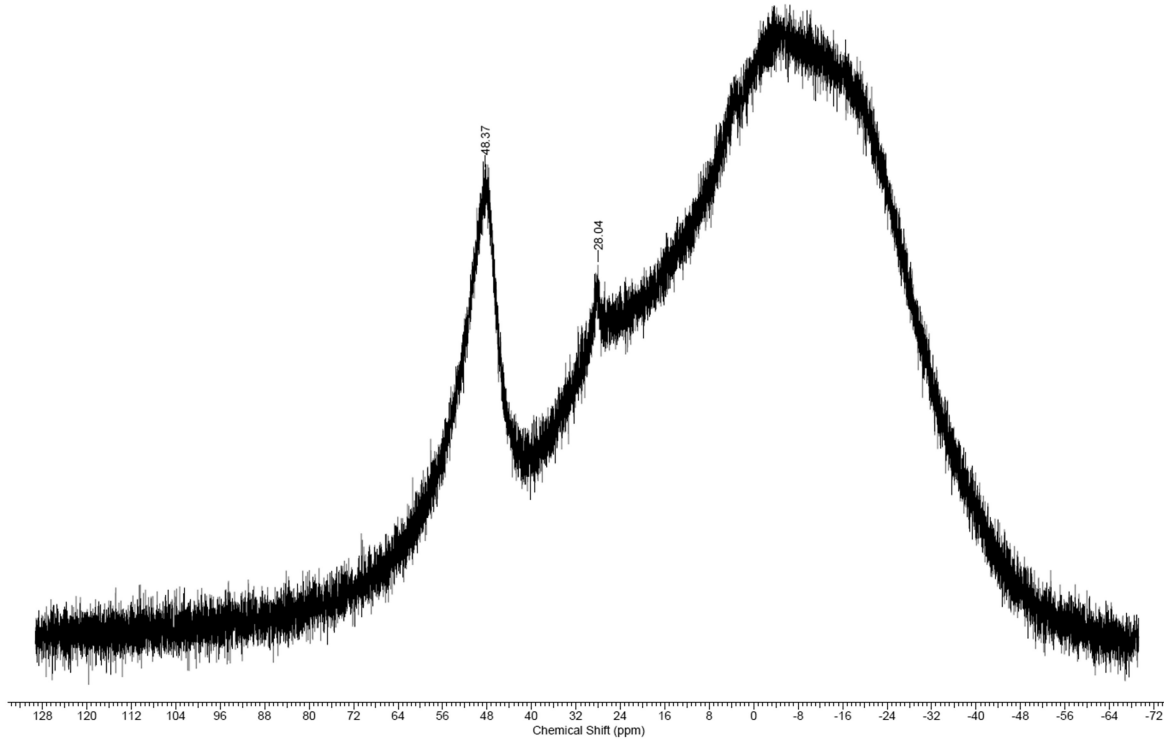


Figure 7.3.55. $^{11}\text{B}\{^1\text{H}\}$ NMR spectrum of **3** in THF-d_8 .

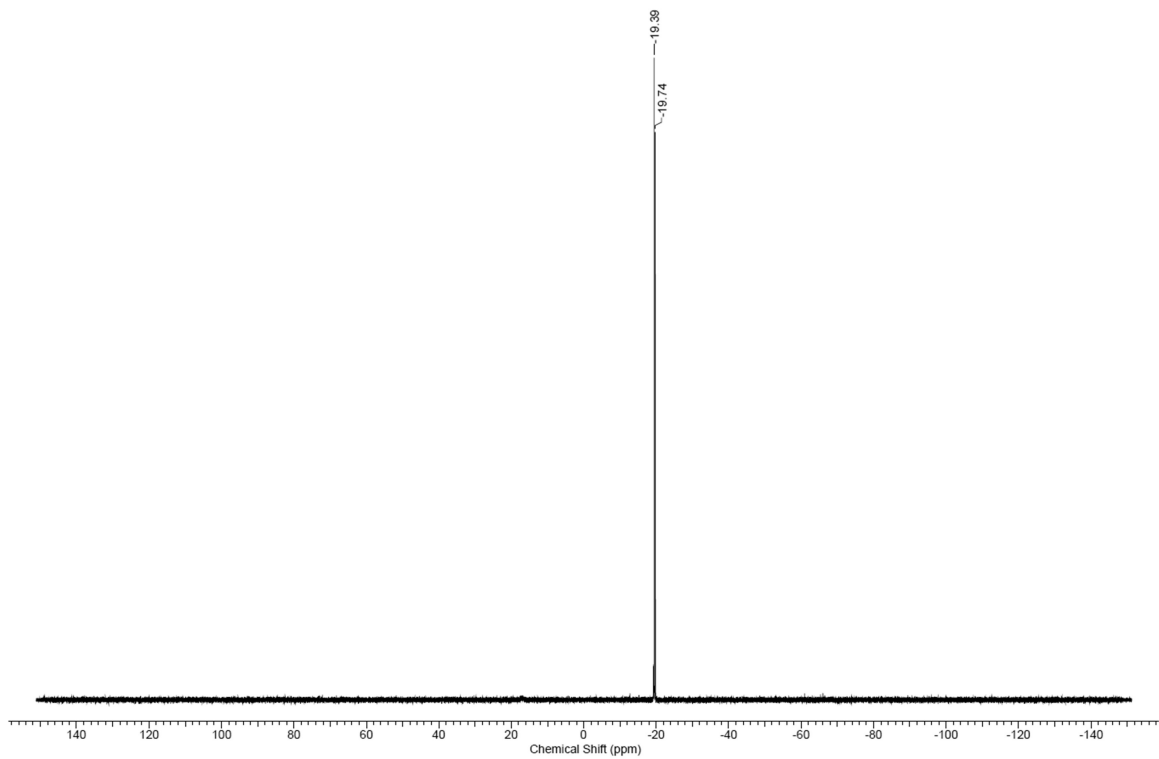


Figure 7.3.56. $^{31}\text{P}\{\text{H}\}$ NMR spectrum of **3** in THF-d_8 .

Mass Spectra

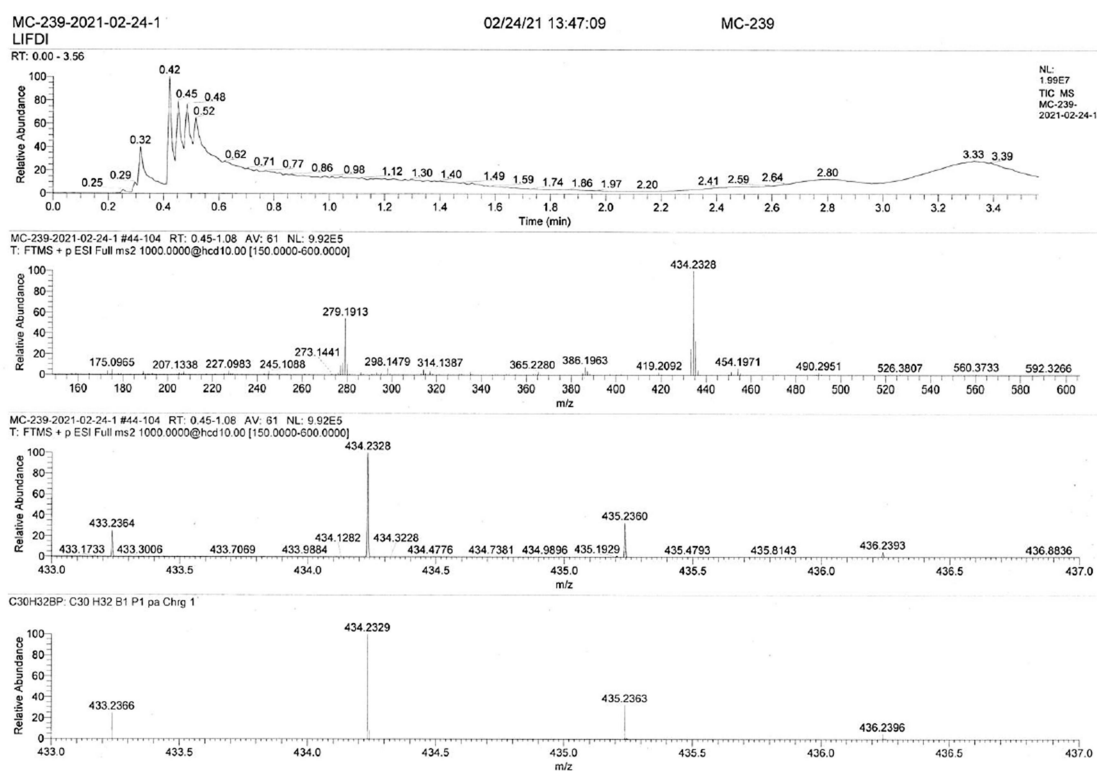


Figure 7.3.57. LIFDI MS spectrum of $\mathbf{1}^{\text{Mes}}$.

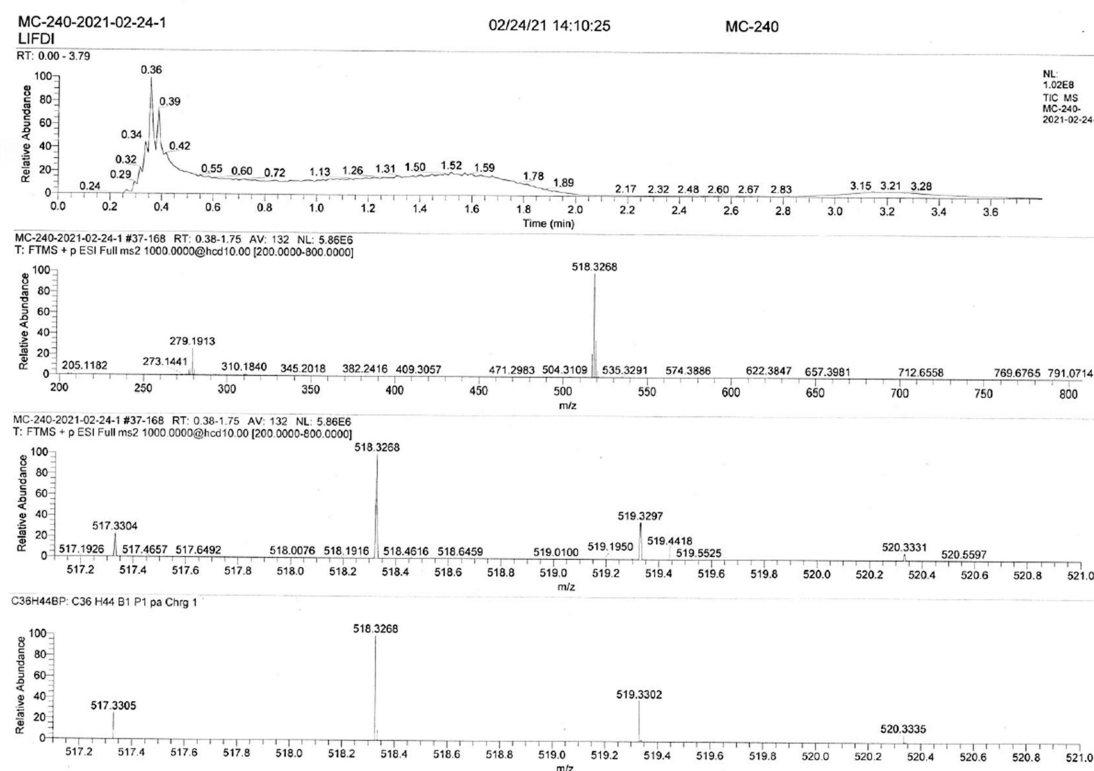


Figure 7.3.58. LIFDI MS spectrum of $\mathbf{1}^{\text{Tip}}$.

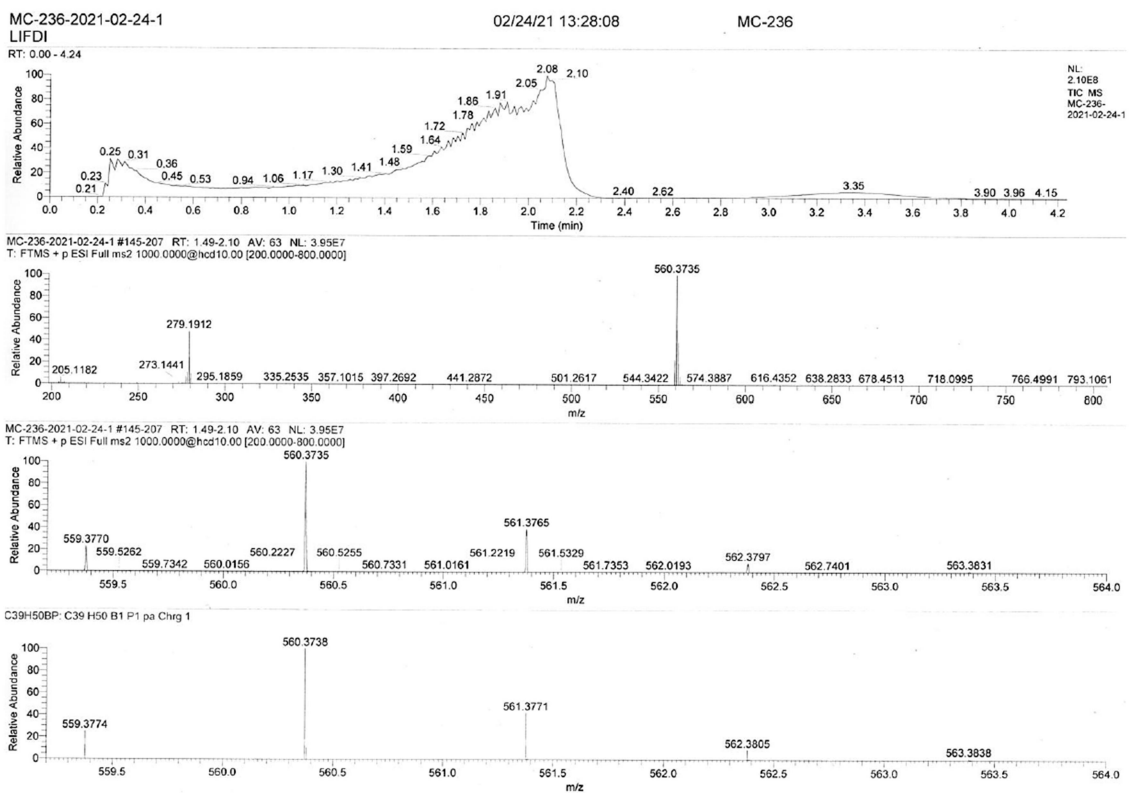


Figure 7.3.59. LIFDI MS spectrum of 1^{Mes^*} .

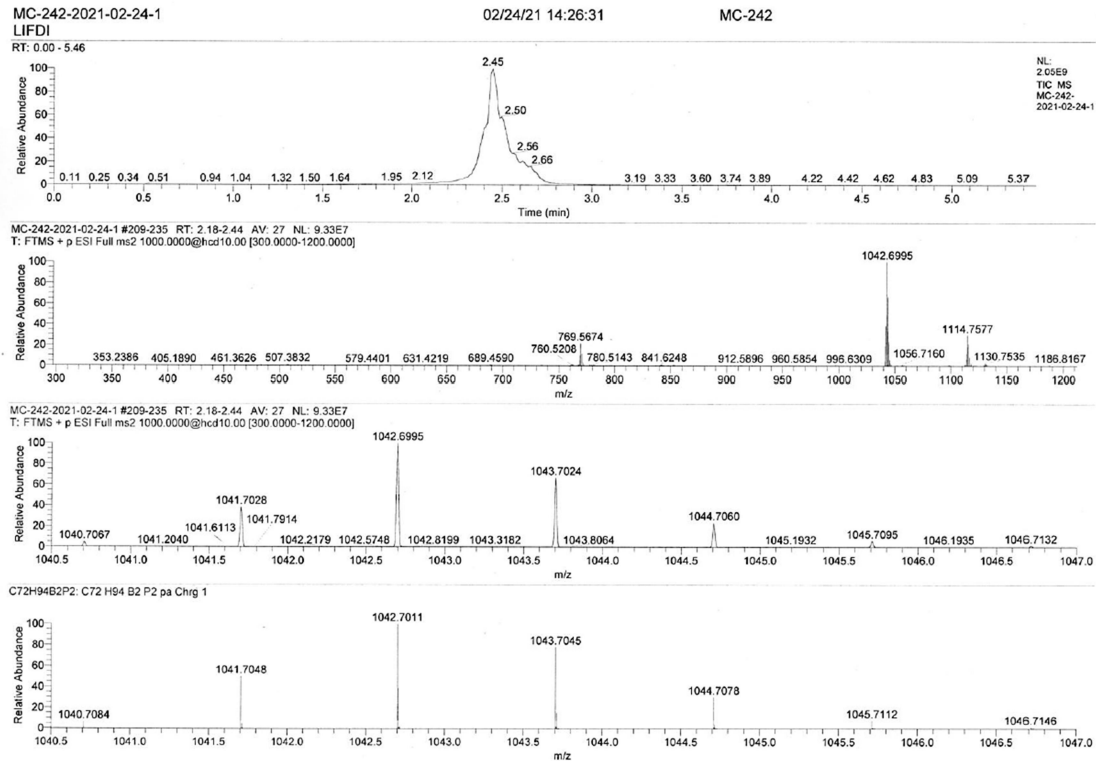


Figure 7.3.60. LIFDI MS spectrum of 2 .

UV/vis and Fluorescence spectra

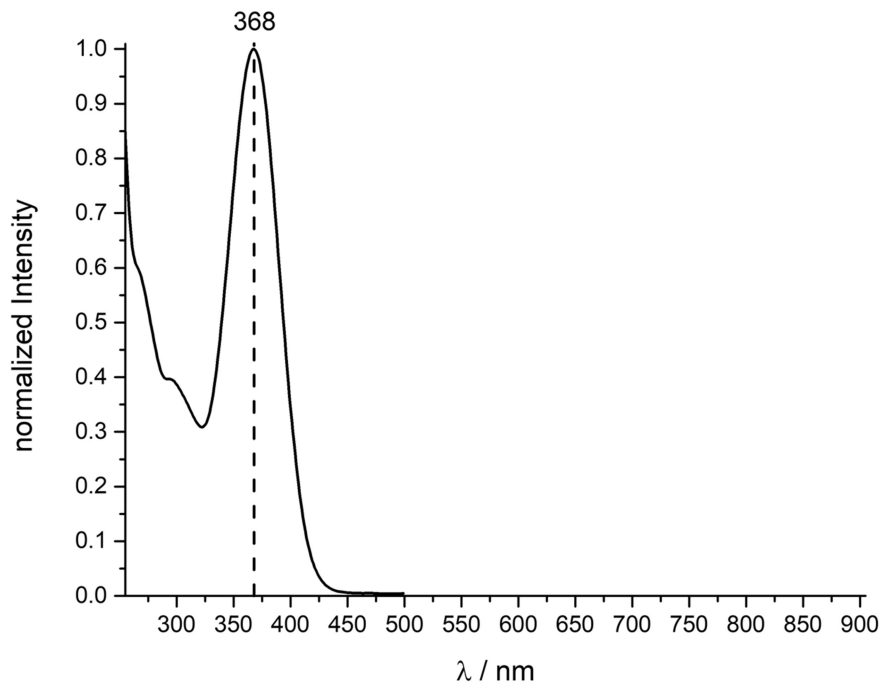


Figure 7.3.61. UV/vis and fluorescence spectrum of $\mathbf{1}^{\text{Mes}}$.

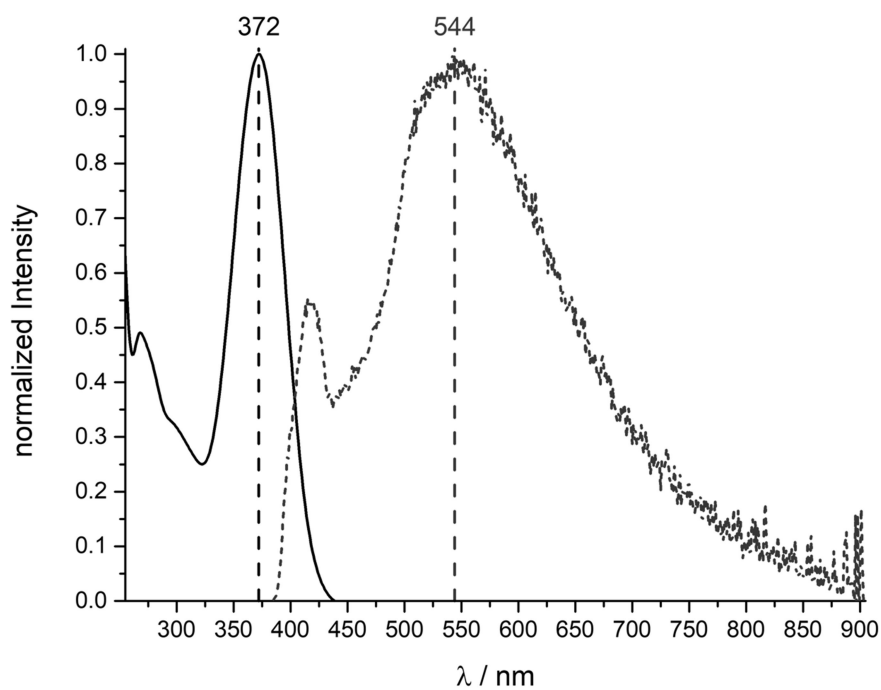


Figure 7.3.62. UV/vis and fluorescence spectrum of $\mathbf{1}^{\text{Tip}}$.

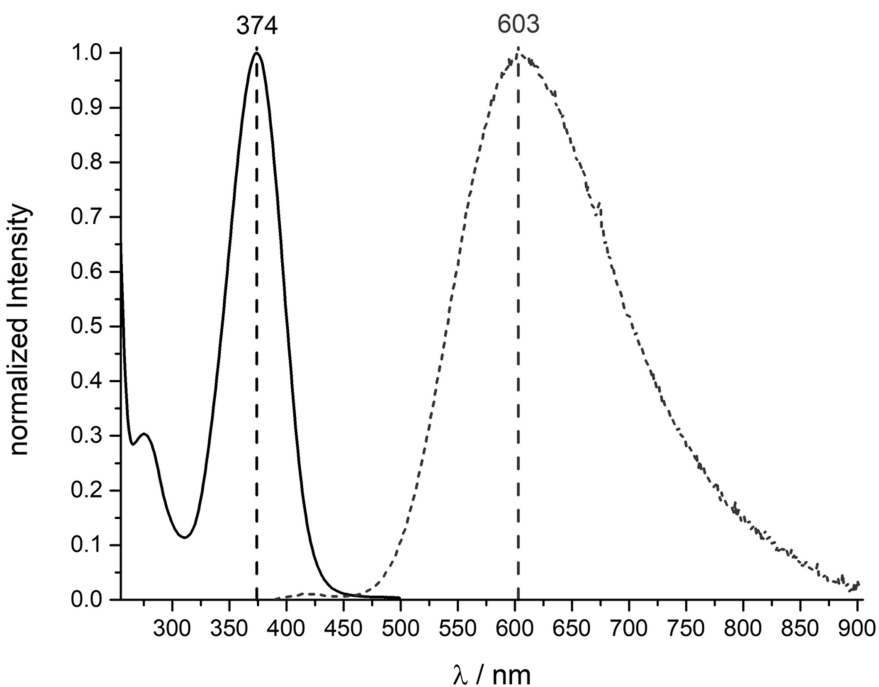


Figure 7.3.63. UV/vis and fluorescence spectrum of $\mathbf{1}^{\text{Mes}^*}$.

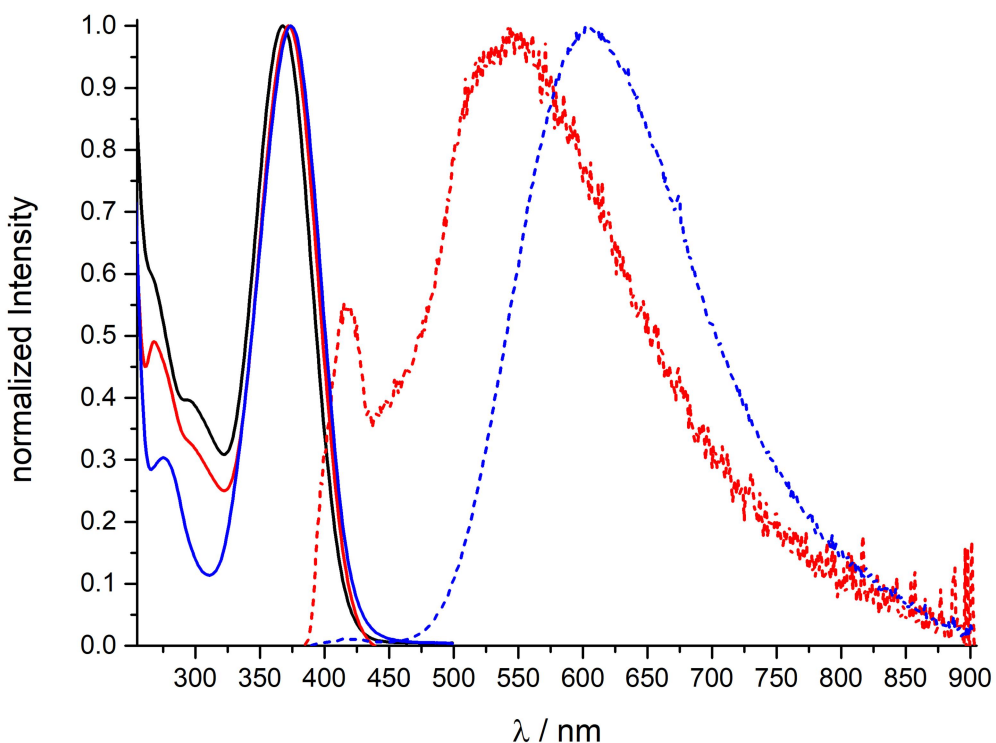


Figure 7.3.64. UV-vis absorption spectra (solid lines, in THF) of $\mathbf{1}^{\text{Mes}}$ (black), $\mathbf{1}^{\text{Tip}}$ (red) and $\mathbf{1}^{\text{Mes}^*}$ (blue) and fluorescence spectra (dashed lines, in THF) of $\mathbf{1}^{\text{Tip}}$ (red) and $\mathbf{1}^{\text{Mes}^*}$ (blue).

Cartesian coordinates (Å) and total energies (a.u.) of optimized stationary points

1^{Mes.}:

Total energy (B3LYP-D3(BJ)/def2-SV(P)): -1527.012730

C 3.158423 0.831135 -1.343643
C 2.229900 0.535368 -0.320678
C 2.747667 0.247601 0.962312
C 4.120336 0.249383 1.209386
C 5.019634 0.526826 0.171957
C 4.535084 0.816306 -1.107767
B 0.710915 0.510092 -0.675786
C 0.162066 1.261198 -1.947279
C -0.156451 0.573051 -3.139074
C -0.686652 1.275690 -4.228300
C -0.924020 2.653977 -4.171803
C -0.599965 3.327428 -2.987304
C -0.054441 2.658572 -1.884131
C 0.039068 -0.920718 -3.239140
C -1.477154 3.397593 -5.363532
C 0.281978 3.430401 -0.628094
P -0.576739 -0.135963 0.517309
C -2.078702 -0.710973 -0.348723
C -2.789030 0.177679 -1.179122
C -3.927198 -0.251778 -1.863535
C -4.395064 -1.562091 -1.711339
C -3.713787 -2.440343 -0.863379
C -2.563915 -2.021007 -0.187363

C	-0.054057	-1.492511	1.639771
C	-0.400358	-1.372490	3.007941
C	0.005274	-2.367977	3.906878
C	0.740898	-3.482639	3.492226
C	1.054310	-3.595021	2.132396
C	0.671641	-2.626350	1.196405
C	-1.208034	-0.203382	3.524148
C	1.046854	-2.827736	-0.249586
C	1.198242	-4.529791	4.477606
H	2.784334	1.074786	-2.342922
H	5.232952	1.039418	-1.921193
H	6.097562	0.521601	0.363702
H	4.494071	0.029936	2.214611
H	2.062943	0.021587	1.783737
H	-0.929421	0.727807	-5.145800
H	-0.774611	4.407268	-2.920844
H	1.351353	3.325335	-0.369372
H	0.062434	4.505172	-0.744998
H	-0.289741	3.055929	0.240754
H	-0.067892	-1.271746	-4.279609
H	1.036168	-1.227939	-2.877420
H	-0.711089	-1.453789	-2.626961
H	-2.036264	-2.719010	0.468085
H	-4.074304	-3.465285	-0.728800
H	-5.291294	-1.893611	-2.244733
H	-4.456082	0.448827	-2.517361

H -2.444755 1.207026 -1.300424
 H -2.045242 4.292486 -5.054495
 H -0.664313 3.741409 -6.032766
 H -2.145357 2.757231 -5.965834
 H 1.612459 -4.471142 1.784801
 H -0.265386 -2.269038 4.963325
 H 1.397126 -3.859104 -0.422875
 H 0.194249 -2.634882 -0.918977
 H 1.857302 -2.141052 -0.550336
 H -0.697148 0.757721 3.338957
 H -2.189376 -0.137666 3.021217
 H -1.385814 -0.298666 4.608785
 H 0.634069 -4.470484 5.423946
 H 1.078620 -5.548698 4.068096
 H 2.270606 -4.402570 4.721603

1^{Tip}:

Total energy (B3LYP-D3(BJ)/def2-SV(P)): -1762.660440

C 0.108593 -0.210515 1.932021
 C 1.424248 -0.478668 2.394580
 C 2.492691 -0.399565 1.493605
 C 2.305996 -0.074191 0.147711
 C 1.001151 0.158574 -0.294697
 P -1.244997 -0.249051 3.180608
 C -1.985702 -1.915005 3.108111
 C -3.038768 -2.257962 3.978686

C	-3.604323	-3.532657	3.934188
C	-3.115215	-4.496816	3.046125
C	-2.046254	-4.175476	2.205393
C	-1.483693	-2.896469	2.235016
C	1.707259	-0.804510	3.858628
C	1.969834	0.485451	4.652575
C	3.487432	0.020929	-0.802579
C	3.651500	1.446518	-1.352090
C	-1.481596	0.318426	-0.046574
H	-2.191890	0.384218	0.784454
B	-2.515433	1.112707	3.032472
C	-3.945982	0.840646	3.627929
C	-4.964619	0.199121	2.887075
C	-6.201618	-0.061799	3.489038
C	-6.464490	0.286686	4.818701
C	-5.449769	0.924556	5.542415
C	-4.205386	1.213329	4.968874
C	-4.729654	-0.226933	1.459018
C	-7.810815	0.015064	5.441657
C	-3.139087	1.895743	5.793361
C	-2.097627	2.535442	2.547284
C	-3.107050	3.420605	2.112219
C	-2.798082	4.676674	1.586006
C	-1.465577	5.092887	1.512161
C	-0.446762	4.244071	1.961812
C	-0.760488	2.981097	2.461821

H	0.793255	-1.258669	4.273188
C	2.839568	-1.818884	4.057848
C	-1.582638	1.632192	-0.833279
C	-1.909380	-0.879783	-0.909048
C	3.387306	-1.008096	-1.938838
H	-4.151964	3.107821	2.185813
H	-3.597902	5.336924	1.240317
H	-1.219957	6.079677	1.110686
H	0.596429	4.566894	1.912836
H	0.049417	2.327979	2.790669
H	-6.979859	-0.561692	2.903854
H	-5.632286	1.207171	6.584058
H	-2.808771	2.834303	5.319160
H	-3.501426	2.132077	6.804546
H	-2.241456	1.262727	5.891326
H	-5.639296	-0.656169	1.014566
H	-4.415618	0.621160	0.828992
H	-3.936458	-0.988965	1.400432
H	-0.649819	-2.654955	1.573389
H	-1.646609	-4.923130	1.515035
H	-3.558961	-5.495065	3.016913
H	-4.431573	-3.774746	4.606436
H	-3.424517	-1.523756	4.686640
H	-7.730712	-0.132708	6.529788
H	-8.501436	0.861413	5.277717
H	-8.284262	-0.879132	5.007216

H	0.831698	0.396286	-1.347270
H	3.507369	-0.595472	1.846083
H	-2.928713	-0.727340	-1.299644
H	-1.234217	-1.012566	-1.770679
H	-1.906477	-1.813076	-0.327455
H	-2.626113	1.810005	-1.139481
H	-1.256300	2.489045	-0.227784
H	-0.972355	1.607519	-1.751170
H	2.892851	-2.118908	5.116464
H	2.678578	-2.725193	3.453344
H	3.824724	-1.403128	3.790938
H	2.148018	0.261903	5.717115
H	2.854555	1.012811	4.258725
H	1.108333	1.167817	4.591174
H	4.547382	1.520061	-1.990111
H	2.781208	1.740185	-1.961648
H	3.749022	2.178704	-0.535318
H	4.280975	-0.968303	-2.582834
H	3.294009	-2.031178	-1.542285
H	2.508647	-0.814322	-2.575682
H	4.391821	-0.216864	-0.216085
C	-0.104870	0.095415	0.561352

1^{Mes*}:

Total energy (B3LYP-D3(BJ)/def2-SV(P)): -1880.299031

C	-0.100327	1.139998	0.209375
---	-----------	----------	----------

C	-0.084143	0.360479	1.387324
C	1.179951	-0.059895	1.858777
C	2.358723	0.277672	1.194820
C	2.311897	1.052149	0.028946
C	1.075888	1.482648	-0.462281
B	-1.452325	0.024781	2.072760
C	-2.805055	0.552005	1.453982
C	-3.509952	-0.223942	0.506215
C	-4.717441	0.251029	-0.021137
C	-5.252417	1.487666	0.361760
C	-4.538787	2.252877	1.292955
C	-3.328743	1.806699	1.839702
C	-2.984106	-1.576249	0.085250
C	-6.539754	1.996819	-0.240693
C	-2.606049	2.651764	2.862497
P	-1.583464	-0.969699	3.586595
C	-3.152582	-1.364656	4.396171
C	-4.392697	-0.908146	3.905678
C	-5.577921	-1.234385	4.568318
C	-5.558888	-2.017435	5.726790
C	-4.332504	-2.475362	6.218749
C	-3.142851	-2.154780	5.563499
C	-0.217246	-1.731271	4.544953
C	0.383201	-1.011983	5.630273
C	1.354685	-1.675439	6.398948
C	1.762388	-2.983173	6.155972

C	1.175628	-3.647435	5.078056
C	0.200470	-3.075991	4.252255
C	0.083310	0.470854	6.027422
C	-0.310194	-3.958345	3.066937
C	2.819771	-3.699583	7.009269
H	-1.061453	1.482905	-0.184917
H	1.027773	2.088078	-1.373184
H	3.236615	1.318199	-0.493368
H	3.321504	-0.064618	1.587806
H	1.244781	-0.665543	2.765040
H	-5.258147	-0.363321	-0.749936
H	-4.937874	3.224510	1.605281
H	-1.553756	2.823189	2.572100
H	-3.091376	3.634362	2.989338
H	-2.583344	2.153962	3.848981
H	-3.572067	-1.995639	-0.748770
H	-1.928425	-1.516393	-0.234538
H	-3.019601	-2.297378	0.922023
H	-2.194452	-2.520954	5.962899
H	-4.297236	-3.090059	7.123870
H	-6.491064	-2.268855	6.241660
H	-6.527854	-0.866846	4.167515
H	-4.437522	-0.295857	3.006302
H	-7.068498	2.677632	0.449165
H	-6.348009	2.561285	-1.174155
H	-7.222925	1.167844	-0.496511

H	1.503329	-4.662905	4.882095
H	1.813336	-1.150017	7.226591
C	0.338049	-5.362791	3.067499
C	-1.833295	-4.211151	3.130094
C	0.076552	-3.317296	1.716554
C	0.499078	1.425801	4.887513
C	-1.397882	0.695183	6.407002
C	0.895141	0.915716	7.267043
C	3.345201	-2.817364	8.154476
C	2.198025	-4.972473	7.625445
C	4.014966	-4.090784	6.111821
H	-2.117135	-4.935453	2.345665
H	-2.124382	-4.633626	4.107517
H	-2.425681	-3.302873	2.965562
H	-0.058624	-5.931464	2.209404
H	1.434182	-5.322996	2.950242
H	0.099930	-5.936896	3.979730
H	-0.235088	-3.976851	0.886382
H	-0.401222	-2.342328	1.566023
H	1.169143	-3.174882	1.650104
H	-1.522130	1.716877	6.808493
H	-2.078988	0.594927	5.553039
H	-1.721121	-0.019278	7.183863
H	0.643403	1.966179	7.490869
H	0.653281	0.321491	8.165288
H	1.984418	0.873325	7.098046

H	0.334792	2.473371	5.198881
H	1.569178	1.303734	4.645770
H	-0.076523	1.255619	3.970290
H	4.789283	-4.609858	6.706021
H	3.709764	-4.765591	5.293750
H	4.473001	-3.194546	5.656593
H	2.944333	-5.505203	8.242916
H	1.337996	-4.716231	8.269618
H	1.842033	-5.672393	6.850212
H	4.095809	-3.376657	8.740466
H	3.832804	-1.901599	7.777016
H	2.537976	-2.518096	8.845704

2:

Total energy (B3LYP-D3(BJ)/def2-SV(P)): -3528.890661

C	-2.086708	0.980508	-4.591505
C	-1.285451	-0.124140	-4.153144
C	-1.889927	-1.409920	-3.932069
C	-3.262207	-1.532740	-4.176046
C	-4.066455	-0.480743	-4.614899
C	-3.455239	0.752956	-4.810282
P	0.517808	0.095968	-3.907185
C	1.384168	-0.237155	-5.457450
C	2.783148	-0.116309	-5.578749
C	3.410326	-0.385277	-6.796402
C	2.667195	-0.777019	-7.913919

C 1.279019 -0.897851 -7.800911
C 0.642194 -0.631894 -6.588661
C -1.164697 -2.687522 -3.398787
C -2.110907 -3.908576 -3.351241
C -5.566103 -0.714237 -4.848313
C -6.284690 0.553165 -5.337339
C -1.591450 2.447996 -4.804173
C -2.713250 3.360564 -5.350230
B 1.351197 0.580890 -2.368991
C 2.925504 0.687803 -2.405954
C 3.549699 1.919630 -2.698136
C 4.949057 2.002050 -2.729871
C 5.756048 0.886379 -2.483020
C 5.125139 -0.329950 -2.188753
C 3.732080 -0.443259 -2.137455
C 2.714440 3.139064 -3.003304
C 7.261067 0.981423 -2.507098
C 3.097625 -1.771262 -1.804258
C 0.572665 0.811532 -1.034589
C 1.319688 1.027866 0.144908
C 0.717939 1.074005 1.397811
C -0.675897 0.913247 1.553034
C -1.435103 0.804858 0.365126
C -0.830195 0.742028 -0.885725
B -1.415692 0.658682 2.907964
C -2.971907 0.880446 3.052598

C	-3.894275	-0.167848	2.836031
C	-5.268134	0.073335	2.978579
C	-5.763208	1.331455	3.336453
C	-4.840318	2.365489	3.542709
C	-3.463417	2.160194	3.404719
C	-3.416571	-1.553219	2.476111
C	-7.242750	1.580195	3.492301
C	-2.504310	3.295709	3.666874
P	-0.491957	0.027168	4.343713
C	1.298841	-0.352569	4.232488
C	2.241232	0.653776	4.629359
C	3.562055	0.538978	4.169150
C	3.994911	-0.491397	3.340375
C	3.081475	-1.504841	3.056217
C	1.751696	-1.497839	3.492424
C	1.929312	1.944276	5.453188
C	1.294381	3.006082	4.528270
C	5.405689	-0.541618	2.738166
C	6.277270	0.637763	3.197558
C	0.904834	-2.733200	3.051033
C	0.176280	-2.420173	1.728048
C	-1.287561	-0.562623	5.852549
C	-0.534286	-1.280685	6.800829
C	-1.124480	-1.738608	7.978347
C	-2.476488	-1.490289	8.234990
C	-3.229257	-0.771934	7.301024

C	-2.646569	-0.305692	6.121321
C	3.220958	2.569549	6.033607
C	1.018498	1.692778	6.671070
C	6.101447	-1.853646	3.157919
C	5.284234	-0.487678	1.200355
C	-0.105540	-3.199681	4.114620
C	1.810957	-3.962552	2.788927
C	-6.217709	-1.161860	-3.521985
C	-5.748509	-1.817813	-5.912181
C	-0.686740	-2.466208	-1.948380
C	0.014425	-3.116610	-4.297885
C	-0.444293	2.550301	-5.832603
C	-1.161791	3.062181	-3.454859
H	-2.522795	0.724217	0.435505
H	-1.462783	0.604746	-1.762474
H	2.405722	1.122690	0.075095
H	1.353312	1.204614	2.270652
H	-5.970830	-0.748220	2.808352
H	-5.204322	3.360593	3.818533
H	-1.753982	3.379780	2.864244
H	-3.029907	4.258516	3.750314
H	-1.946437	3.133460	4.604433
H	-4.260995	-2.236348	2.303475
H	-2.794928	-1.545198	1.566788
H	-2.794233	-1.980612	3.278143
H	0.522327	-1.477634	6.609947

H	-0.521594	-2.295140	8.700745
H	-2.938529	-1.851081	9.157108
H	-4.286125	-0.565502	7.488721
H	-3.248977	0.258053	5.410929
H	-7.484127	1.938484	4.507352
H	-7.594648	2.353582	2.788571
H	-7.828282	0.666897	3.309047
H	3.422432	-2.330912	2.441145
H	4.273394	1.308940	4.437640
H	3.383895	0.187772	-4.724337
H	-0.442215	-0.729537	-6.516773
H	0.682042	-1.202318	-8.664694
H	3.164824	-0.985598	-8.864126
H	4.496573	-0.284667	-6.866560
H	2.418760	-1.681715	-0.940548
H	3.856236	-2.531432	-1.565924
H	2.489974	-2.148075	-2.642096
H	2.165340	3.017121	-3.951690
H	3.334125	4.044150	-3.085805
H	1.956196	3.310686	-2.222369
H	5.737767	-1.213473	-1.983701
H	5.420423	2.963698	-2.955449
H	7.599184	1.983255	-2.811061
H	7.688133	0.770493	-1.511379
H	7.699548	0.248515	-3.204791
H	-4.071484	1.577155	-5.143389

H	-3.739213	-2.493034	-4.015669
H	-1.991979	3.037828	-2.732508
H	-0.312752	2.534858	-3.011669
H	-0.866247	4.113744	-3.600738
H	-2.303590	4.372249	-5.487400
H	-3.090585	3.022001	-6.327502
H	-3.562920	3.448228	-4.657190
H	0.491083	2.109073	-5.476641
H	-0.713115	2.056153	-6.778751
H	-0.243562	3.611542	-6.048969
H	-6.819838	-2.003763	-6.093003
H	-5.285670	-1.521813	-6.866958
H	-5.292045	-2.768397	-5.597632
H	-6.215273	1.371845	-4.604385
H	-5.874374	0.912978	-6.293715
H	-7.353137	0.337432	-5.493687
H	-5.773911	-2.095130	-3.144024
H	-6.092330	-0.391647	-2.744587
H	-7.297003	-1.335559	-3.663308
H	-0.307519	-3.236275	-5.343635
H	0.845686	-2.405681	-4.281768
H	0.405087	-4.085970	-3.949616
H	-2.956783	-3.759971	-2.663749
H	-2.506391	-4.172470	-4.344118
H	-1.543071	-4.775214	-2.981386
H	0.055991	-1.668829	-1.872058

H	-1.530327	-2.201795	-1.292946
H	-0.229465	-3.390188	-1.559501
H	1.172089	-4.843452	2.626123
H	2.431642	-3.855998	1.887874
H	2.471482	-4.176396	3.643752
H	0.888225	-2.098305	0.953666
H	-0.349696	-3.317326	1.362741
H	-0.557123	-1.619334	1.849644
H	0.393702	-3.423857	5.069071
H	-0.894918	-2.469402	4.307082
H	-0.596398	-4.122046	3.767176
H	4.694316	-1.327248	0.805367
H	4.794637	0.440652	0.869180
H	6.279970	-0.527989	0.730447
H	6.410436	0.648652	4.290706
H	7.276217	0.561222	2.740689
H	5.847391	1.604634	2.893296
H	7.116153	-1.902290	2.730227
H	6.187602	-1.919859	4.254189
H	5.550281	-2.739969	2.809507
H	-0.012178	1.454891	6.396044
H	1.403790	0.874141	7.297421
H	0.982434	2.602305	7.290776
H	1.967600	3.245085	3.690418
H	0.340512	2.662772	4.112330
H	1.107200	3.934583	5.092357

H	3.793371	1.846299	6.635252
H	3.885206	2.982540	5.261178
H	2.942848	3.407701	6.689751

3:

Total energy (B3LYP-D3(BJ)/def2-SV(P)): -3528.892479

C	-5.365214	-0.442354	4.534892
C	-5.089670	-0.246018	3.163763
C	-6.198719	-0.130672	2.295891
C	-7.507504	-0.205419	2.769090
C	-7.750999	-0.400925	4.133812
C	-6.673830	-0.519883	5.016296
B	-3.594973	-0.172791	2.710291
C	-2.411863	-0.269040	3.750904
C	-1.795466	-1.510703	4.029356
C	-0.692064	-1.561375	4.889043
C	-0.173088	-0.407008	5.490175
C	-0.812090	0.811887	5.234033
C	-1.918790	0.897063	4.378185
C	-2.294677	-2.773911	3.371420
C	1.051662	-0.480281	6.367322
C	-2.544304	2.239806	4.087380
P	-3.087881	0.062439	0.981515
C	-1.362359	0.123966	0.459950
C	-1.054750	0.114444	-0.915063
C	0.260593	0.106711	-1.366494
C	1.335833	0.112058	-0.456278

C	1.028158	0.174398	0.917244
C	-0.287024	0.179094	1.368795
P	3.061740	0.031044	-0.972403
B	3.575282	-0.228416	-2.695492
C	5.071889	-0.325823	-3.138003
C	5.354559	-0.508873	-4.509483
C	6.665203	-0.605511	-4.981936
C	7.737437	-0.520945	-4.089538
C	7.486794	-0.339287	-2.724145
C	6.176024	-0.244048	-2.260149
C	-4.120437	0.184092	-0.529223
C	-4.465164	1.477549	-1.039071
C	-5.063064	1.546149	-2.307943
C	-5.335780	0.425412	-3.085097
C	-5.033513	-0.822897	-2.539631
C	-4.440788	-0.996615	-1.283978
C	-4.244407	2.837612	-0.302287
C	-4.200628	-2.470468	-0.825231
C	-5.945515	0.515117	-4.491510
C	4.099444	0.149365	0.535258
C	4.492822	1.438628	1.020219
C	5.133330	1.504684	2.268185
C	5.397446	0.386065	3.051486
C	5.032121	-0.858194	2.536658
C	4.399567	-1.030195	1.300091
C	4.286093	2.796587	0.275638
C	6.043073	0.478409	4.441754

C	4.105329	-2.503099	0.868930
C	2.399787	-0.320710	-3.744973
C	1.790177	-1.564229	-4.033819
C	0.694757	-1.615763	-4.902503
C	0.177035	-0.460517	-5.504704
C	0.806509	0.759640	-5.235171
C	1.906098	0.845713	-4.369288
C	2.287121	-2.826654	-3.372845
C	-1.020984	-0.543681	-6.417475
C	2.520660	2.190678	-4.065970
H	4.522829	-0.575719	-5.215237
H	6.851065	-0.747138	-6.050052
H	8.765300	-0.596038	-4.454636
H	8.319459	-0.272090	-2.018823
H	6.006860	-0.103611	-1.191787
H	0.225856	-2.583099	-5.110347
H	0.425844	1.672375	-5.704123
H	3.618133	2.161974	-4.155195
H	2.140105	2.970371	-4.742266
H	2.298697	2.503067	-3.031921
H	1.831374	-3.722524	-3.819847
H	3.381748	-2.919790	-3.453758
H	2.050136	-2.829322	-2.296503
H	1.829824	0.206653	1.655701
H	-0.467871	0.217650	2.439222
H	-1.856048	0.099352	-1.654289
H	0.441458	0.085885	-2.437200

H	-1.313338	0.448169	-6.793479
H	-0.817759	-1.188455	-7.289225
H	-1.890980	-0.975663	-5.895489
H	5.248439	-1.732562	3.139914
H	5.428267	2.473151	2.649428
H	-6.034891	0.019131	1.227799
H	-8.344131	-0.111664	2.071573
H	-8.777264	-0.460122	4.506148
H	-6.854308	-0.673010	6.083733
H	-4.529404	-0.534906	5.232996
H	-1.851421	-3.669999	3.830515
H	-3.390874	-2.858225	3.438996
H	-2.043534	-2.786647	2.298367
H	-0.219506	-2.527979	5.091286
H	-0.433889	1.723553	5.707131
H	1.967925	-0.575188	5.759308
H	1.160967	0.421797	6.988117
H	1.018058	-1.354903	7.036493
H	-3.640320	2.205413	4.191591
H	-2.158030	3.019787	4.760067
H	-2.338546	2.555848	3.050973
H	-5.266255	-1.699043	-3.134612
H	-5.314912	2.517961	-2.711088
C	-6.215026	1.966569	-4.918727
H	-6.645770	1.981799	-5.932007
H	-6.929928	2.465444	-4.246041
H	-5.290665	2.564358	-4.941345

C	-4.962992	-0.113365	-5.503250
H	-4.000060	0.420658	-5.497110
H	-4.761438	-1.170758	-5.274259
H	-5.376417	-0.063699	-6.523881
C	-7.282134	-0.256569	-4.519316
H	-7.996399	0.171831	-3.798467
H	-7.734301	-0.205328	-5.523210
H	-7.146699	-1.319066	-4.266949
C	-2.699436	-2.796245	-0.666706
H	-2.580000	-3.867857	-0.439989
H	-2.148094	-2.581607	-1.594727
H	-2.224645	-2.233581	0.142434
C	-4.958276	-2.758174	0.486657
H	-4.592879	-2.151968	1.318956
H	-6.034662	-2.561043	0.368364
H	-4.833771	-3.817194	0.764520
C	-4.738973	-3.488131	-1.855832
H	-4.217660	-3.424857	-2.823100
H	-4.574011	-4.502515	-1.463169
H	-5.819637	-3.376398	-2.031023
C	-5.006377	2.859258	1.039074
H	-6.084416	2.703735	0.878928
H	-4.652163	2.092476	1.733058
H	-4.872441	3.838108	1.527056
C	-2.745287	3.142507	-0.080442
H	-2.283130	2.488714	0.665831
H	-2.177063	3.036709	-1.017382

H	-2.630969	4.179735	0.273015
C	-4.794546	4.028722	-1.118907
H	-4.268638	4.162273	-2.076504
H	-5.872439	3.937841	-1.320495
H	-4.647646	4.949338	-0.534831
C	5.033662	2.794023	-1.074095
H	6.108386	2.608078	-0.925048
H	4.650874	2.035069	-1.761373
H	4.922143	3.775056	-1.563277
C	2.790276	3.124910	0.069390
H	2.298259	2.451864	-0.639380
H	2.239736	3.071807	1.021369
H	2.691484	4.148883	-0.325001
C	4.863829	3.985678	1.076073
H	5.945433	3.888011	1.253030
H	4.710491	4.905802	0.492878
H	4.360957	4.125289	2.045134
C	2.594255	-2.783020	0.715629
H	2.439968	-3.857433	0.526725
H	2.046825	-2.517317	1.632713
H	2.140449	-2.235351	-0.115236
C	4.853096	-2.839156	-0.437513
H	4.512088	-2.231416	-1.279142
H	5.936045	-2.681146	-0.320116
H	4.688641	-3.896666	-0.699801
C	4.608527	-3.520053	1.918032
H	4.094716	-3.415470	2.885833

H	4.401727	-4.534851	1.546950
H	5.693556	-3.448691	2.086448
C	5.004608	0.032930	5.494317
H	4.122937	0.692532	5.476335
H	4.658195	-0.995689	5.311145
H	5.439236	0.068510	6.506854
C	7.276108	-0.447352	4.508614
H	8.020641	-0.165032	3.747437
H	7.753796	-0.375764	5.499135
H	7.010592	-1.502302	4.344529
C	6.496618	1.907586	4.779770
H	7.230380	2.285190	4.050565
H	5.650366	2.610979	4.810405
H	6.973247	1.921446	5.772320

Erklärung zur Autorenschaft

"BNB-Doped phenalenyls – aromaticity switch upon one-electron reduction"

Merian Crumbach, Ozan Ayhan, Lars Fritze, Jan A. P. Sprenger, Ludwig Zapf, Malik Finze and Holger Hellen^{*}
Chem. Commun. **2021**, 57, 2408–2411.

Detaillierte Darstellung der Anteile an der Veröffentlichung (in %)
 Angabe Autoren/innen (ggf. Haupt- / Ko- / korrespondierende/r Autor/in) mit Vorname Nachname (Initialen)

Autor/in 1 (MC), Autor/in 2 (OA), Autor/in 3 (LF), Autor/in 4 (JAPS), Autor/in 5 (LZ), Autor/in 6 (MF), Autor/in 7 (HH)

Autor	A1	A2	A3	A4	A5	A6	A7	A8	A9	A10	A11	Σ in Prozent
Idee/Ideenentwicklung/Konzept	4 %	1 %							15 %			20 %
Synthesen	15 %											15 %
Analytik	9 %	2 %	2 %	2 %								15 %
Theoretische Berechnungen	10 %							1 %				11 %
												0%
												0%
												0%
												0%
Verfassen der Veröffentlichung	5 %								11 %			16 %
Korrektur der Veröffentlichung	2 %							2 %	4 %			8 %
Koordination der Veröffentlichung									15 %			15 %
Summe	45 %	1 %	2 %	2 %	2 %	2 %	2 %	2 %	46 %			100%

Erklärung zur Autorenschaft

"Dithiophene-Fused Oxadiborepins and Azadiborepins: A New Class of Highly Fluorescent Heteroaromatics"

Merian Crumbach, Jonas Bachmann, Lars Fritze, Andreas Helbig, Ivo Krummenacher, Holger Braunschweig, Holger Helten*,
Angew. Chem. Int. Ed. **2021**, *60*, 9290–9295.

Detaillierte Darstellung der Anteile an der Veröffentlichung (in %),
 Angabe Autoren/innen (ggf. Haupt- / Ko- / korrespondierende/r Autor/in) mit Vorname Nachname (Initialen)

Autor/in 1 (MC), Autor/in 2 (JB), Autor/in 3 (LF), Autor/in 4 (AH), Autor/in 5 (IK), Autor/in 6 (HB), Autor/in 7 (HH)

Autor	A1	A2	A3	A4	A5	A6	A7	A8	A9	A10	A11	Σ in Prozent
Idee/Ideenentwicklung/Konzept	5 %								15 %			20 %
Synthesen	15 %	1 %										16 %
Analytik	10 %		2 %					2 %				14 %
Theoretische Berechnungen	10 %											10 %
												0%
												0%
												0%
												0%
Verfassen der Veröffentlichung	5 %									11 %		16 %
Korrektur der Veröffentlichung	2 %						1 %		2 %	4 %		9 %
Koordination der Veröffentlichung										15 %		15 %
Summe	47 %	1 %	2 %	1 %	2 %	1 %	2 %	2 %	45 %			100%